Evidence-Based Complementary and Alternative Medicine

Complementary and Alternative Therapies for Inflammatory Disease

Lead Guest Editor: Xiang Liu
Guest Editors: Ying-Ju Lin and Yanhong Zhu

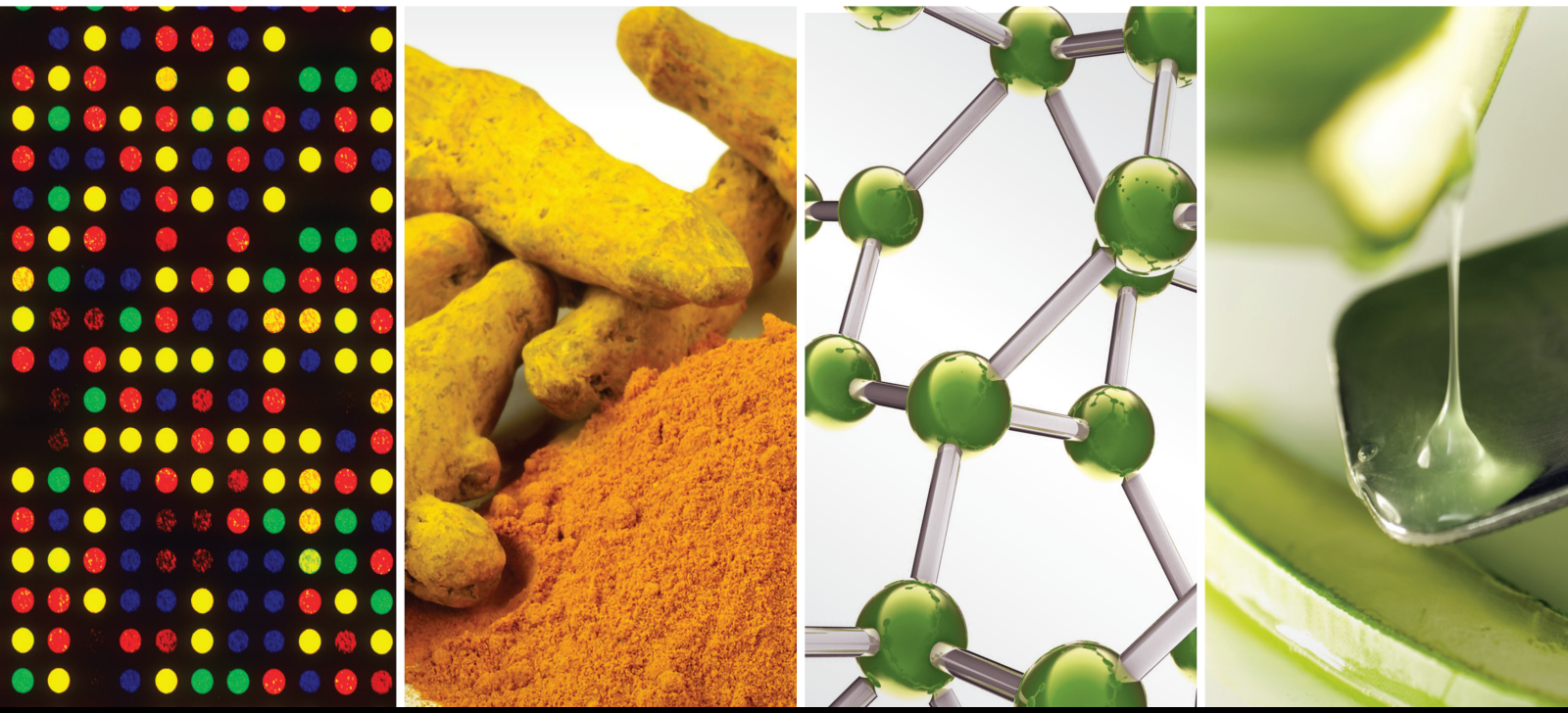

Complementary and Alternative Therapies for Inflammatory Disease

Evidence-Based Complementary and Alternative Medicine

Complementary and Alternative Therapies for Inflammatory Disease

Lead Guest Editor: Xiang Liu
Guest Editors: Ying-Ju Lin and Yanhong Zhu

Chief Editor

Associate Editors

Academic Editors

Contents

Contents

Hindawi
Evidence-Based Complementary and Alternative Medicine
Volume 2022, Article ID 5752803, 9 pages
https://doi.org/10.1155/2022/5752803

Research Article

Antiliver Fibrosis Formula of Fuzheng Huayu Alleviates Inflammatory Response

Qing-Qi Chang,[1] **Yi-Feng Pan**,[2] **Jia-Yi Yang**,[1] **Rong-Sheng Li**,[2] **Chun-Lu Yuan**,[1] **Ya-Fang Liao**,[1] **Dan-Dan Zhang**,[1] **and Cheng-Hai Liu**[3]

[1]*Institute of Interdisciplinary Integrative Medicine Research, Shanghai University of Traditional Chinese Medicine, Shanghai 201203, China*
[2]*Shanghai Huanghai Pharmaceutical Co. Ltd., Shanghai 200051, China*
[3]*Institute of Liver Diseases, Shuguang Hospital Affiliated to Shanghai University of Traditional Chinese Medicine, Shanghai 201203, China*

Correspondence should be addressed to Dan-Dan Zhang; izhangdd@126.com and Cheng-Hai Liu; chenghailiu@hotmail.com

Received 3 February 2022; Revised 14 August 2022; Accepted 24 August 2022; Published 12 November 2022

Academic Editor: Xiang Liu

Fuzheng Huayu's (FZHY) formula ameliorated liver fibrosis in clinical and experimental practice. Based on the close link between fibrosis and inflammation, its anti-inflammatory effect and related mechanisms were explored in this present study. With the aid of the inflammatory macrophage model, FZHY significantly blocked nitrite accumulation without observable cytotoxicity due to its suppression of inducible nitric oxide synthase (iNOS) gene and protein expressions in a concentration-depended manner. Proinflammatory mediators including IL-6, CD86, and CD40 were also restrained by FZHY. Interestingly, FZHY induced anti-inflammatory mediators heme oxygenase 1 (HO-1) and peroxisome proliferator-activated receptor γ (PPAR-γ) expressions simultaneously. Downregulation of iNOS and miR-155 and upregulation of PPAR-γ were also observed in CCl_4-induced liver fibrosis mice upon FZHY administration. Mechanically, FZHY strikingly eliminated the phosphorylation of STAT1 and MAPK. Taken together, FZYH regulated the balance of proinflammatory and anti-inflammatory mediators partially via modulating STAT1/MAPK pathways and the miR-155/PPAR-γ axis.

1. Introduction

Hepatic fibrosis is a chronic wound-healing response characterized by inflammation [1]. Genetic changes, hepatitis virus infections, excessive alcohol consumption, lipid metabolic disorders, and autoimmune diseases trigger continuous liver injury and subsequent chronic inflammation that lead to liver fibrosis [2, 3]. Understanding the underlined inflammatory mechanisms is critical to developing strategies to control fibrosis [4].

Hepatic macrophages are the primary immune cells, consisting of liver-resident macrophages, monocyte-derived macrophages, and Kupffer cells that trigger liver inflammatory response and also play a crucial role in the pathologic progress of fibrosis [5]. Traditionally, macrophages can be polarized into proinflammatory/M1 macrophages or anti-inflammatory/M2 macrophages upon different microenvironmental stimulations. M1 macrophages predominantly express inducible nitric oxide synthase (iNOS) and secrete classical proinflammatory cytokines such as interleukin (IL)-6 and IL-1β to exaggerate the inflammatory response induced by *T* helper (Th)-1 signals such as lipopolysaccharide (LPS) and interferon (IFN)-γ. Accumulating evidence strongly implies that iNOS-derived nitric oxide (NO) has been associated with the pathogenesis of liver diseases during inflammatory conditions. These inflammatory mediators also emerge as vital profibrotic hubs. IL-1β promotes liver fibrosis partially in an IL-17-dependent manner [6]. Thus, targeting macrophages and inhibition of M1 macrophage-led

inflammation development are approaches to interfere with fibrosis [7].

MicroRNAs (miRNAs) are small, noncoding RNAs that negatively control target gene expressions by promoting degradation or translational inhibition. miR-155 exerts a proinflammatory effect during the progress of hepatic fibrosis in immune cells [8]. PPAR-γ is involved in the progression of liver fibrosis as one of the target genes of miR-155 [9]. CCl_4 administration decreases the expression of PPAR-γ in liver tissue and the antifibrotic effect of crocin partly via enhancing PPAR-γ to mediate inflammatory response and fibrogenic events [10].

Fuzheng Huayu's formula (FZHY) was approved by the Chinese State Food and Drug Administration (SFDA) (No: Z20050546) as an antifibrotic medicine in 2002. FZHY is composed of six Chinese medicines, including *Radix Salvia Miltiorrhizae* (Danshen), *Cordyceps* (Chong Cao), *Semen Persicae* (Taoren), *Pollen Pini* (Song Huafen), *Gynostemma Pentaphyllammak* (Jiaogulan), and *Fructus Schisandrae chinensis* (Wuweizi), which is used to invigorate blood circulation, remove blood stasis, tonify essence, and nourish liver according to the theory of TCM. FZYH's antifibrotic effect has been confirmed in accumulating experimental and clinical evidence [11–20]. Current data showed FZHY alleviated inflammatory cytokines TNF-α and IL-6 and profibrotic genes VEGF and TGF-β1 in the liver fibrotic rat model [21]. However, its anti-inflammatory mechanisms remain to be elucidated.

Thus, in this present study, we evaluated the anti-inflammatory effect and relevant mechanisms of FZHY.

2. Materials and Methods

2.1. Materials. FZHY was obtained from Huanghai Pharmaceutical Co. (Shanghai, China). RPMI 1640 medium, fetal bovine serum (FBS), and 0.25% trypsin were purchased from Gibco (Rockville, MD, USA). BCA protein assay kit and TRIzol reagent were purchased from Invitrogen (Carlsbad, CA, USA). Special antibodies including p-JNK(#9251; 1:1000), T-JNK(#9252; 1:1000), p-ERK(#9101; 1:1000), T-ERK(#9102; 1:1000), p-P38(#9211; 1:1000), T-P38(#9212; 1:1000), p-STAT-1(#7649; 1:1000), T-STAT-1(#14994; 1:1000), and iNOS(#13120; 1:1000) were purchased from cell signaling technology (Beverly, MA, USA). Anti-HO-1 (ab68477; 1:10000), CD40 (ab252428; 1:1000), IL-6 (ab259341; 1:1000), and horseradish peroxidase-labeled goat antirabbit IgG were purchased from Abcam (Cambridge, UK). CD86 (13395-1-AP; 1:500) was purchased from ProteinTech Group (Chicago, IL, USA). Polyvinylidene difluoride (PVDF) membranes, western blotting detection reagent ECL, and murine recombinant IFN-γ were purchased from Millipore (Bedford, MA, USA). LPS, 1400W, Griess reagent, and MTT were purchased from Sigma-Aldrich (St. Louis, MO, USA). MicroRNA primers, transcription kits, and universal PCR master mix were obtained from GenePharma Company (Shanghai, China). Standard compounds sodium danshensu, salvianolic acid B, and adenosine were purchased from the National Institutes for Food and Drug Control (Beijing, China).

2.2. High-Performance Liquid Chromatography (HPLC) Assay. FZHY standardization was performed using HPLC fingerprinting with chemical standard compounds such as sodium danshensu, salvianolic acid B (two compounds isolated from *Radix Salvia Miltiorrhizae*), and adenosine (a compound isolated from Cordyceps) according to Chinese Pharmacopoeia (2015 edition).

2.3. Cell Culture. RAW 264.7 cells from the American Type Culture Collection (ATTC, Rockville, MD) were cultured in RPMI 1640 medium supplemented with 10% FBS. The cell passages below 10 were used, and three replicates were performed in each experiment.

2.4. Cell Viability. The effect of FZHY on the proliferation of RAW 264.7 cells was detected by the MTT assay. RAW 264.7 cells were incubated into 96-well plates at a density of 10000 cells/well and were allowed to adhere overnight. Cells were treated with FZHY in different concentrations (0, 12.5, 25, 50, 100, 200, 400, 800, and 1000 μg/mL) and under 1400W (50 μM), respectively. After 24 hours, 0.5 mg/ml MTT was added to each group and was incubated for additional 4 hours. The supernatant of each group was discarded and then the absorbance at 490 nm with formazan-DSMO dissolution was read. The cell availability of each group was calculated compared to the cell availability of the control group as 100%.

2.5. Nitrite Assay. RAW 264.7 cells were seeded into 96-well plates at a density of 100,000 cells/well and were divided into the control group, the model group, FZHY treatment groups (25, 50, 100, and 200 μg/mL), and the positive drug group 1400W (50 μM, a selective inhibitor of iNOS), respectively. After serum-free treatment for 24 h, the control group was treated with serum-free 1640 medium, and the model group was stimulated with LPS (100 ng/mL)/IFN-γ (100 U/mL), while the FZHY administration groups were treated with 25, 50, 100, and 200 μg/mL and stimulators LPS (100 ng/mL)/IFN-γ (100 U/mL). After 24 hours, 100 μL of the supernatant of each group was collected and added to 100 μL of Griess reaction reagent for 10 mins and then was read at 540 nm using a microplate reader. Then, the nitrite content in the cell supernatant was calculated using the nitrate standard curve.

2.6. Animal Experiment. The murine liver fibrosis model induced by CCl_4 and administration with or without FZHY was proceeded in a previous study [20], and preserved livers were used for further experiments to detect the inflammation-relevant mediators.

2.7. qPCR Analysis. RAW 264.7 cells were cultured and divided into the control, model, and FZHY treatment groups (100 and 200 μg/mL), respectively. After being allowed to adhere overnight, cells were treated with serum-free 1640 medium for 24 h. The samples of cells and liver tissues were collected, and the total RNA was extracted by the Trizol

method, and miR-155, iNOS, CD86, CD40, IL-6, PPAR-γ, and HO-1 were detected. The primers of qRT-PCR for iNOS, CD86, CD40, IL-6, PPAR-γ, and HO-1 are listed in Table 1.

2.8. Western Blot Analysis. RAW 264.7 cells were cultured in 30 mm culture dishes with 1×10^6 cells. The protein samples of each group were collected, and western blotting was performed after protein denaturation. The protein expressions of iNOS, HO-1, CD40, CD86, and IL-6 compared with β-actin and the phosphorylation levels of p38, JNK, ERK, and STAT1 compared with total p38, JNK, ERK, and STAT1 were determined.

2.9. Statistical Evaluation. Data were presented as the mean ± SD of results obtained from at least three experiments. Data were assessed by ANOVA analysis and the *t*-test. $P < 0.05$ was considered as statistically significant.

3. Results

3.1. FZHY Suppressed the Expression of Inducible Inflammatory Synthase iNOS In Vitro and In Vivo. To examine the cell viability, RAW 264.7 cells were incubated with FZHY at increasing concentrations (0, 12.5, 25, 50, 100, 200, 400, 800, and 1000 μg/mL) and with 1400W (50 μM) for 24 h. FZHY presented no significant influence on cell viability up to 200 μg/mL by the MTT assay as well as 1400w at the dosage of 50 μM (Figure 1(a)).

iNOS has been used as the major biomarker for the definition of M1 proinflammatory macrophages, so we further examined the effect of FZHY at dosages of 25, 50, 100, and 200 μg/mL on nitrite accumulation, the stable oxidative metabolite of nitric oxide, and in the supernatant from differently treated cells. FZHY inhibited nitrite accumulation induced by LPS plus IFN-γ in a concentration-dependent manner (Figure 1(b)). As expected, FZHY inhibited iNOS expressions at gene and protein levels in a concentration-dependent manner on inflammatory macrophages (Figures 1(c) and 1(d)). 1400W, a well-known inducible nitric oxide synthase (iNOS) selective inhibitor, reduced nitrite production by 97.45% at 50 μM compared to the model group induced by LPS plus IFN-γ.

Compared with the normal group, the infiltration of inflammatory cells and collagen deposition in the portal area were significantly increased in CCl_4-induced liver fibrosis mice, while FZHY presented the prevention and curing effects on CCl4-induced liver inflammation and fibrosis [20]. iNOS also altered its expression in liver fibrosis. iNOS deficiency improved liver inflammation and genes encoding collagen, leading to decrease fibrosis [22]. We continued to test iNOS in the liver tissues from CCl_4-induced liver fibrosis mice with and without FZHY administration. Results demonstrated that FZHY administration did reduce iNOS expression in liver tissues (Figures 1(e) and 1(f)).

Based on these results, FZHY strongly attenuated iNOS in inflammatory macrophages and liver tissues from CCl_4-induced liver fibrosis mice.

3.2. FZHY Enhanced Expression of Anti-Inflammatory Enzyme HO-1. HO-1 is the inducible and rate-limiting enzyme in heme catabolism and exhibits anti-inflammatory functions to resolve cellular oxidative stress and inflammatory cascade reaction. LPS failed to induce iNOS production in HO-1-overexpressing cells suggesting that HO-1 protected RAW 264.7 cells from inflammation damage [23]. Therefore, we examined the effect of FZHY on HO-1 using qPCR and western blot analysis on macrophages. Results showed that FZHY strikingly increased expressions of HO-1 at gene and protein levels (Figure 2).

3.3. FZHY Reduced Other Inflammatory Mediators. iNOS, CD86, CD40, and IL-6 are typical proinflammatory mediators in M1 macrophages [7]. Results showed CD86, CD40, and IL-6 mRNA and protein levels were augmented in LPS plus IFN-γ stimulated macrophages compared with the control group. The expressions of inflammatory mediator concentration dependently reduced after FZHY treatment. These findings suggested that FZHY restrained expressions of these proinflammatory mediators (Figure 3).

3.4. STAT1/MAPK Signaling Pathways Were Involved in the FZHY-Led Effect. The signal transducer and activator of transcription 1 (STAT1) were involved in the mediation of IFN-γ intracellular signaling [24]. Mitogen-activated protein kinases (MAPKs), including p38, extracellular signal-regulated kinase (ERK), and c-JunN-terminal kinases (JNK), played pivotal roles in inflammatory responses [25]. Activated STAT1/MAPK signal pathways led to the induction of iNOS and other proinflammatory cytokines.

Thus, we next investigated whether FZHY inhibited iNOS expression by regulating STAT1/MAPK pathways. LPS plus IFN-γ increased the phosphorylation levels of MAPK and STAT-1. FZHY treatment concentration dependently abrogated phosphorylation of STAT1 and MAPK (Figure 4).

These data suggested that STAT1/MAPK pathways were involved in the FZHY-led effect.

3.5. FZHY Modulated miR-155/PPAR-γ Axis. miR-155/PPAR-γ axis regulated the progress of inflammation and liver fibrosis [9]. Under the inflammation condition, the level of miR-155 was notably boosted. However, FZHY dramatically struck the elevated level of miR-155 and upregulated expression of its target gene PPAR-γ on macrophages and liver tissues from CCl_4-induced liver fibrosis mice (Figure 5).

3.6. Chemical Quality Control of FZHY by HPLC Analysis. We identified three compounds as the chemical quality control of FZHY by HPLC analysis (Figure 6). The content of sodium danshensu (8.3%), salvianolic acid B (13.25%), and adenosine (3.95%) in FZHY met the requirements of Chinese Pharmacopoeia.

Table 1: Primer sequences used for qRT-PCR amplification.

Gene	Sense sequence	Antisense sequence
iNOS	5′-GGAGCGAGTTGTGGATTGTC-3′	5′-GTGAGGGCTTGGCTGAGTGAG-3′
CD86	5′-GCACGGACTTGAACAACCAG-3′	5′-CCTTTGTAAATGGGCACGGC-3′
CD40	5′-ATTTGTGCCAGCCAGGAAGCCG-3′	5′-GCATCCGGGACTTTAAACCACAGA-3′
IL-6	5′-CCACTTCACAAGTCGGAGGCTTA-3′	5′-GTGCATCATCGCTGTTCATACAATC-3′
PPAR-γ	5′-AGACCACTCGCATTCCTTTGAG-3′	5′-GCAGGTTCTACTTTGATCGCACT-3′
HO-1	5′-CACAGATGGCGTCACTTCGTC-3′	5′-GTGAGGACCCACTGGAGGAG-3′
GAPDH	5′-AACGGATTTGGTCGTATTGGG-3′	5′-CAGGGGTGCTAAGCAGTTGG-3′

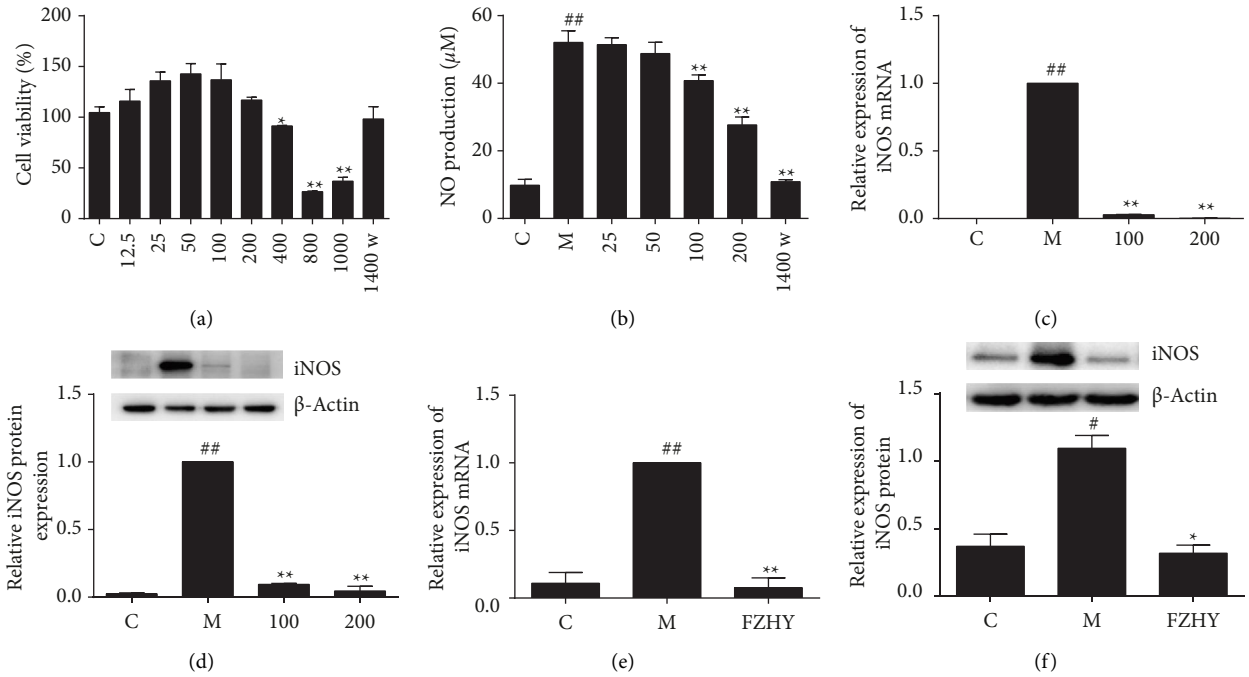

Figure 1: FZHY inhibited iNOS in inflammatory macrophages and mice CCl_4-treated liver tissues. (a) Cell viability was determined by MTT assay. (b) NO production was evaluated by Griess reaction following incubation with model group (LPS/IFN-γ), control group (vehicle control), and 25–200 μg/ml FZHY treatment groups for 24 h. (c) iNOS mRNA in each group from cells was assessed by qPCR. (d) iNOS protein in each group from cells was assessed by western blotting. (e) iNOS mRNAs from liver tissues were assessed by qPCR. (f) iNOS proteins from liver tissues were assessed by western blot. Values are presented as the mean ± SD (standard deviation) from at least three replicates. (C) Vehicle control of macrophages or control group mice; (M) model group (stimulation by LPS at 100 ng/mL and IFN-γ at 100 ng/mL or CCl_4 induced mice); 1400W (an iNOS selective inhibitor at 50 μM); 100: FZHY treatment group at the concentration of 100 μg/mL on macrophages; 200: FZHY treatment group at the concentration of 200 μg/mL on macrophages; FZHY : FZHY treatment group at the dosage of 5.6 g/kg/day for 6-week administration on CCl_4-induced mice; ##$P < 0.01$ versus C group; #$P < 0.05$ versus C group; **$P < 0.01$ versus M group; *$P < 0.05$ versus M group.

4. Discussion

Inflammation is a key component and a contributor to profibrogenic progress. Increasing evidence showed that anti-inflammatory therapy exerted its effect in the treatment of liver fibrosis [26]. Targeting chronic inflammation in the context of fibrogenesis might lead to potential antifibrotic therapies. Macrophages play a central role in the progression of liver inflammation and fibrosis progression [27]. M1 macrophages induced enzymes and secreted cytokines to regulate fibrogenesis [28]. Thus, controlling M1 macrophage polarization during fibrosis provides a crucial strategy.

LPS plus IFN-γ can activate M1 macrophages that exert a proinflammatory phenotype. iNOS is a significant marker of M1 macrophages. Excessive NO, a gas signal molecule with high reactive properties, produced by iNOS results in oxidative and nitroxidative stress under inflammatory conditions. These findings demonstrated that FZHY suppressed the expression of iNOS at gene and protein levels in a concentration-dependent manner. The accumulation of nitrite and the steady production of NO are also reduced by FZHY (Figure 1). Thus, FZHY's anti-inflammatory activity depends on its inhibition of NO and iNOS. Other M1 markers, including CD86, CD40, and IL-6, were also diminished upon FZHY administration (Figure 3).

Current evidence demonstrated that HO-1 presented a crucial role in anti-inflammatory response and antioxidant progress [29]. Induction of HO-1 in LPS stimulated

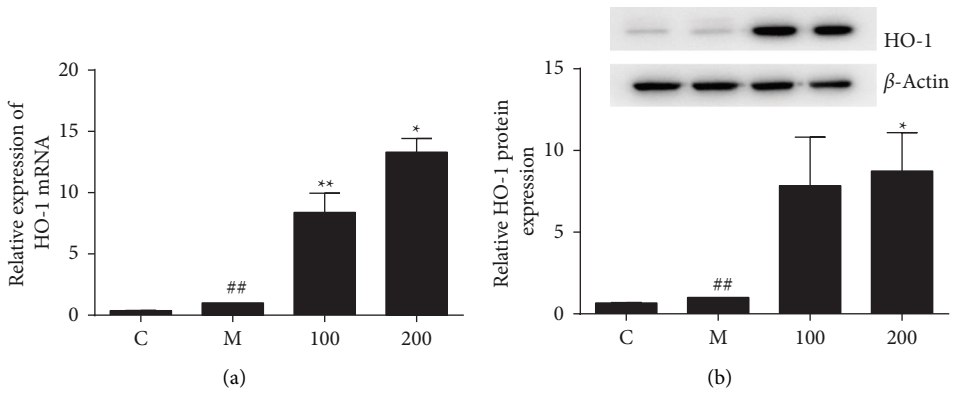

Figure 2: FZHY induced anti-inflammatory HO-1. (a) HO-1 mRNA in each group was assessed by qPCR. (b) HO-1 protein in each group was assessed by western blot. Values are presented as the mean ± SD of at least three replicates. ##$P < 0.01$ versus C group; **$P < 0.01$ versus M group; *$P < 0.05$ versus M group.

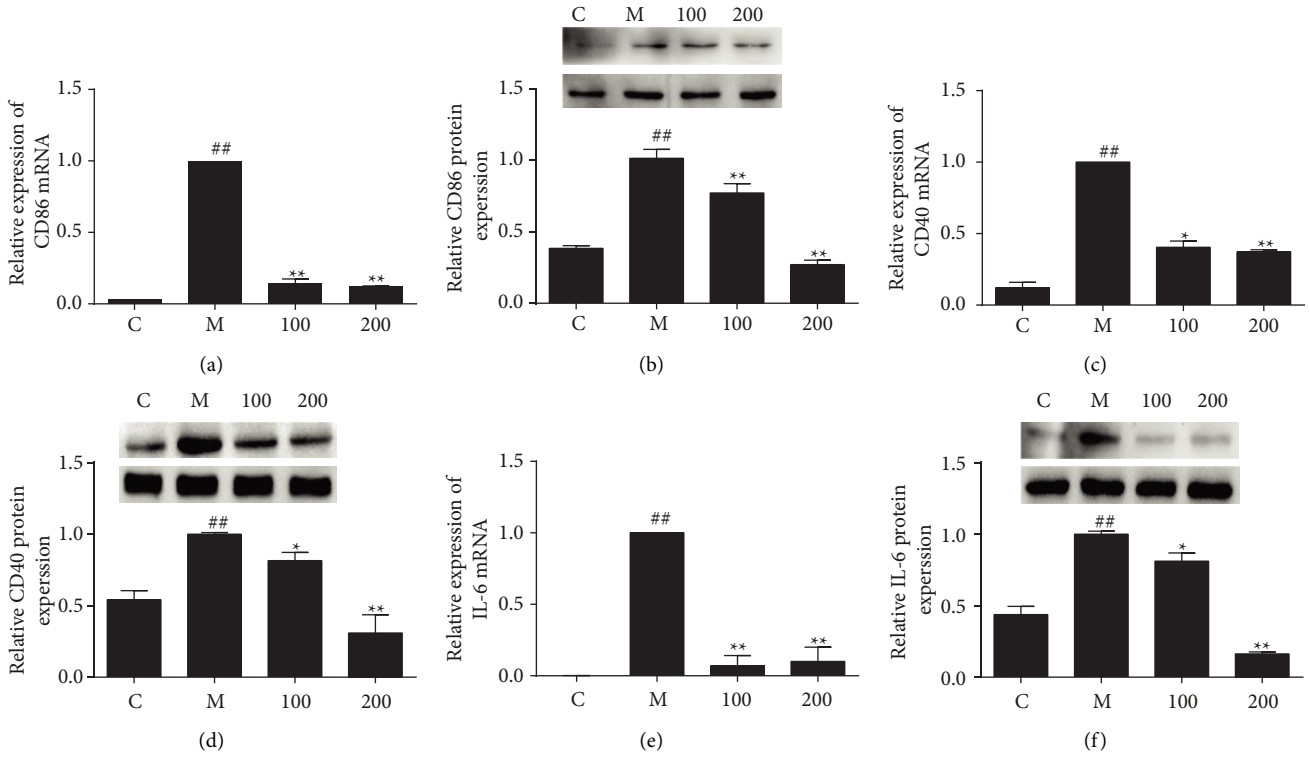

Figure 3: FZHY regulated the proinflammatory mediators. The mRNA and protein levels of markers including CD86 (a, b), CD 40 (c, d), and IL-6 (e, f) were detected by qPCR and western blotting. Values are presented as the mean ± SD of at least three replicates. ##$P < 0.01$ versus C group; **$P < 0.01$ versus M group. *$P < 0.05$ versus M group.

macrophages and suppressed the production of proinflammatory mediators, while deficiency of HO-1 presented an inflammatory phenotype [30]. Induction of HO-1 caused by the NO produced from iNOS attenuated iNOS expression and NO production [31]. There is a negative feedback loop between HO-1 and iNOS. A previous study showed that FZHY upregulated the antioxidative gene HO-1 in ameliorating nutritional fibrosing steatohepatitis [32]. Notably, FZHY also simultaneously induced antioxidative enzyme HO-1 expression to resolute inflammatory damage triggering a cellular protective mechanism (Figure 2). These data implied that the anti-inflammatory action of FZHY was partially attributed to the induction of HO-1.

The STAT1/MAPK signaling pathways were involved in the progression of inflammation [33]. Results suggested that the activation of STAT1/MAPK pathways was remarkably abolished by FZHY (Figure 4).

microRNAs (miRNAs) are crucial for the progression of inflammation and fibrosis. Accumulating studies suggested that proinflammatory miR-155 promoted liver fibrosis.

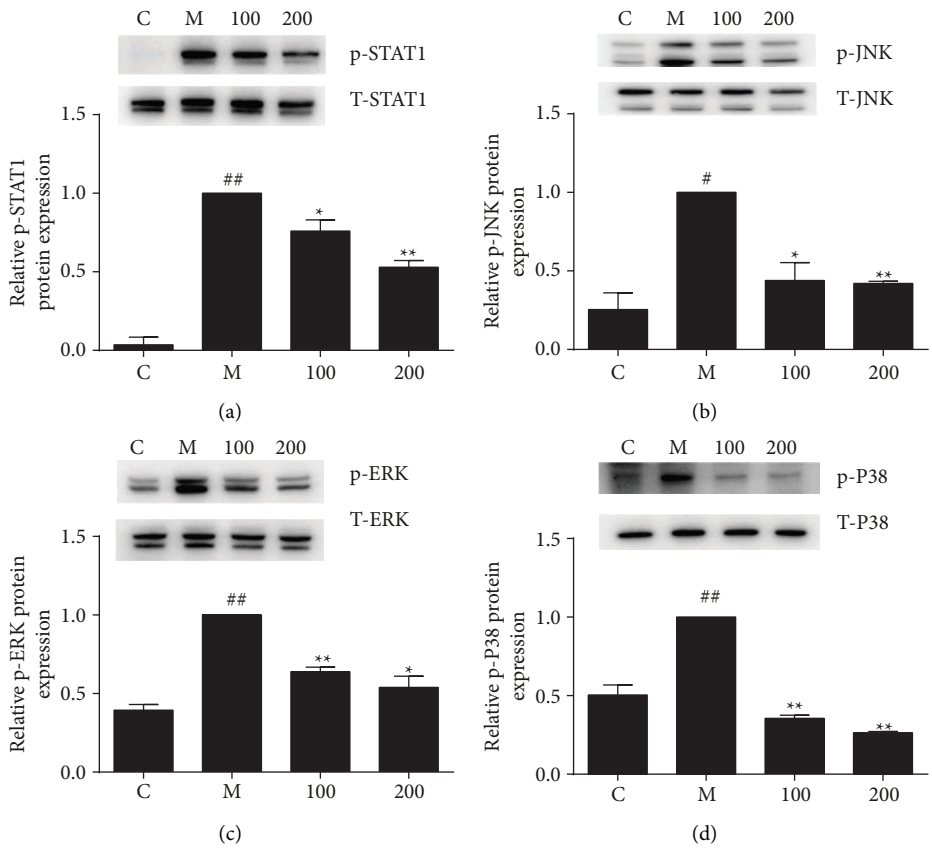

Figure 4: Effects of FZHY on STAT1/MAPKs signaling pathways. (a) p-STAT1 and STAT1, (b) p-JNK and JNK, (c) p-ERK and ERK, and (d) p-p38 and p38 protein expressions were assessed by western blotting and calculated using an imaging system. Values are presented as the mean ± SD of at least three replicates. $##P < 0.01$ versus C group; $#P < 0.05$ versus C group; $^{*}P < 0.05$ versus M group; $^{**}P < 0.01$ versus M group.

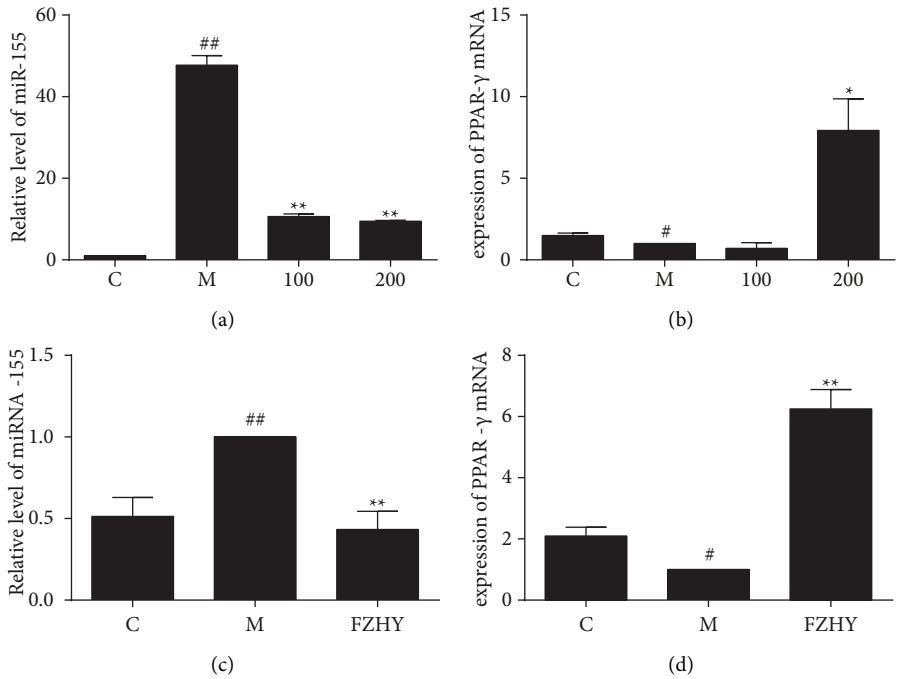

Figure 5: FZHY regulated miR-155/PPAR-γ axis. miR-155 and PPAR-γ mRNA in each group from macrophages (a, b) and liver tissues (c, d) were assessed by qPCR. Values are presented as the mean ± SD of at least three replicates. $##P < 0.01$ versus C group; $#P < 0.05$ versus C group; $^{**}P < 0.01$ versus M group; $^{*}P < 0.05$ versus M group.

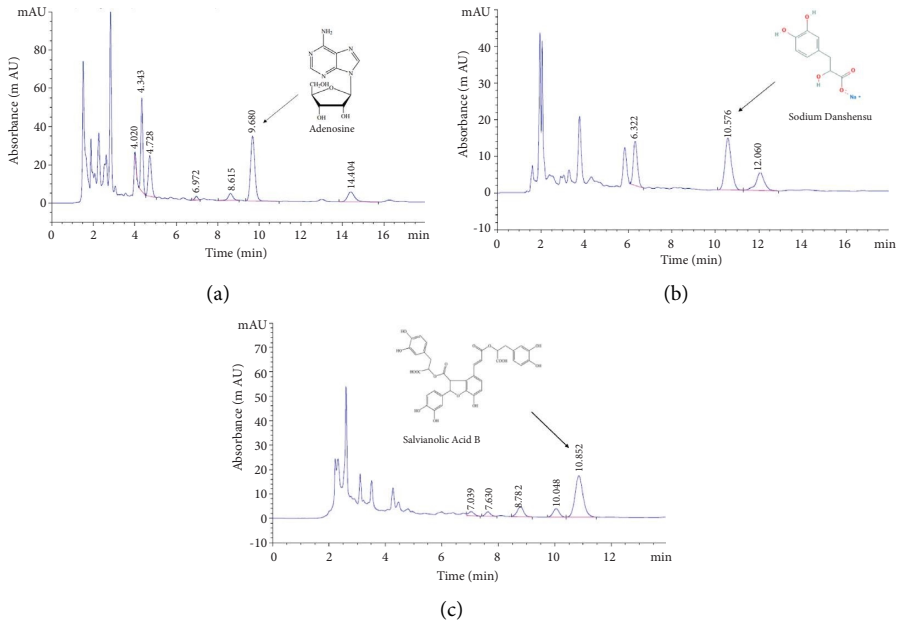

Figure 6: HPLC analysis of FZHY using three ingredients.

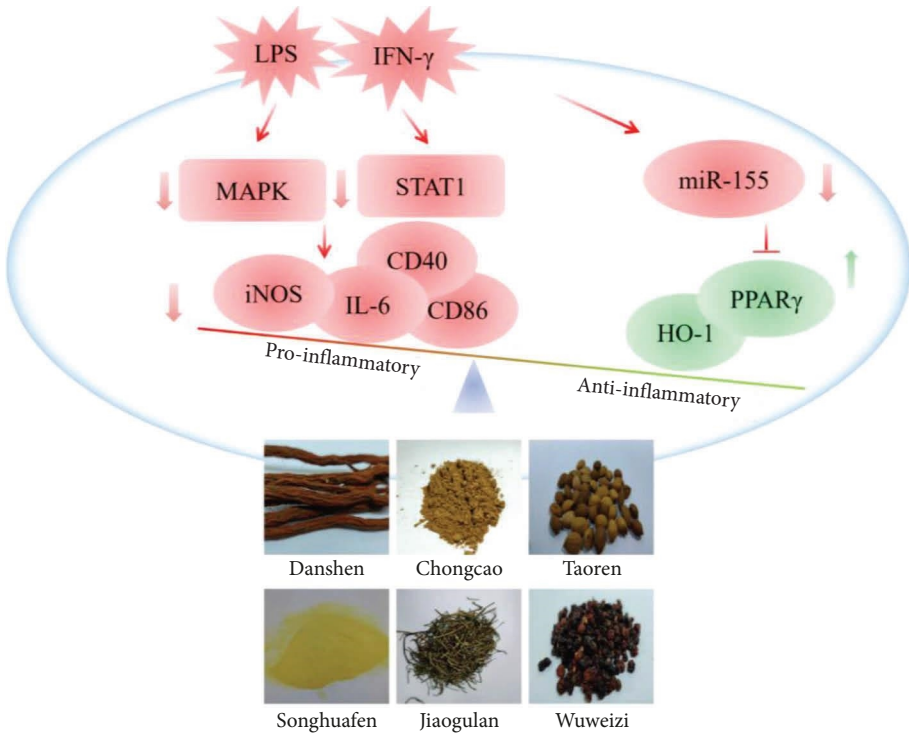

Figure 7: Anti-inflammatory mechanisms summary of FZHY.

Elevated miR-155 was observed in a mouse model of liver fibrosis and cirrhotic livers of alcoholic patients. Profibrotic genes by alcohol diet or CCl_4 treatment were reduced in miR-155 KO mice [9]. miR-155 targeted PPAR-γ, SMAD2/5, Snail1, and STAT3 to regulate fibrosis phenotype [34]. miR-155 inhibitor increased the expression of PPAR-γ in alcohol-treated macrophages. Activation of PPAR-γ suppressed iNOS expression in M1 macrophages and displayed anti-inflammatory properties. The tyrosine nitration of PPAR-γ by iNOS impaired its transcriptional activity and stability [35].

A network pharmacology approach and a cell-based assay revealed that schisandrin B, salvianolic acid A, and

kaempferol from FZHY could bind to PPAR-γ [19]. We found that proinflammatory miR-155 increased while its target gene PPAR-γ decreased upon stimulation by LPS in IFN-γ or CCl_4-induced liver fibrosis mice, while FZHY reduced the level of miR-155 and upregulated the expression of PPAR-γ (Figure 5).

5. Conclusions

Collectively, our findings demonstrated that FZHY exerted an anti-inflammatory effect on LPS plus IFN-γ -induced inflammation with modulation of proinflammatory and anti-inflammatory mediators via MAPK/STAT-1 signaling pathways and miR-155/PPAR-γ axis (Figure 7). Future studies are needed to elucidate active compounds from FZHY and core targets and pathways in depth underlying the relationship between inflammation and fibrosis.

Data Availability

The data used to support the findings of this study are included in the article.

Conflicts of Interest

The authors declare that they have no conflicts of interest.

Authors' Contributions

Qing-Qi Chang, Yi-Feng Pan, and Jia-Yi Yang contributed equally to this work.

Acknowledgments

This work was supported by the funds of Shanghai International Science and Technology Cooperation Project (18400731400), the National Natural Science Foundation of China (81730109, 81773946, 81573673, and 81001666), the Innovation Project for Undergraduates of Shanghai University of Traditional Chinese Medicine (2020SHUTCM152), and the National Science and Technology Major Project of China (2009ZX09311-003).

References

[1] Y. Koyama and D. A. Brenner, "Liver inflammation and fibrosis," *Journal of Clinical Investigation*, vol. 127, no. 1, pp. 55–64, 2017.

[2] M. Mack, "Inflammation and fibrosis," *Matrix Biology*, vol. 68-69, pp. 106–121, 2018.

[3] T. Kisseleva and D. Brenner, "Molecular and cellular mechanisms of liver fibrosis and its regression," *Nature Reviews Gastroenterology and Hepatology*, vol. 18, no. 3, pp. 151–166, 2021.

[4] E. Seki and RF. Schwabe, "Hepatic inflammation and fibrosis: functional links and key pathways," *Hepatology*, vol. 61, no. 3, pp. 1066–1079, 2015.

[5] F. Tacke, "Targeting hepatic macrophages to treat liver diseases," *Journal of Hepatology*, vol. 66, no. 6, pp. 1300–1312, 2017.

[6] RG. Gieling, K. Wallace, and YP. Han, "Interleukin-1 participates in the progression from liver injury to fibrosis," *American Journal of Physiology-Gastrointestinal and Liver Physiology*, vol. 296, no. 6, pp. G1324–G1331, 2009.

[7] Y. Wen, J. Lambrecht, C. Ju, and F. Tacke, "Hepatic macrophages in liver homeostasis and diseases-diversity, plasticity and therapeutic opportunities," *Cellular and Molecular Immunology*, vol. 18, no. 1, pp. 45–56, 2021.

[8] X. Wang, Y. He, B. Mackowiak, and B. Gao, "MicroRNAs as regulators, biomarkers and therapeutic targets in liver diseases," *Gut*, vol. 70, no. 4, pp. 784–795, 2021.

[9] S. Bala, T. Csak, B. Saha et al., "The pro-inflammatory effects of miR-155 promote liver fibrosis and alcohol-induced steatohepatitis," *Journal of Hepatology*, vol. 64, no. 6, pp. 1378–1387, 2016.

[10] J. Chhimwal, S. Sharma, P. Kulurkar, and V. Patial, "Crocin attenuates CCl4-induced liver fibrosis via PPAR-gamma mediated modulation of inflammation and fibrogenesis in rats," *Human & Experimental Toxicology*, vol. 39, no. 12, pp. 1639–1649, 2020.

[11] P. Liu, C. Liu, L. M. Xu et al., "Effects of Fuzheng Huayu 319 recipe on liver fibrosis in chronic hepatitis B," *World Journal of Gastroenterology*, vol. 4, no. 4, pp. 348–353, 1998.

[12] Z. X. Li, Z. M. Zhao, P. Liu, Q. Zheng, and C. Liu, "Treatment of HBV cirrhosis with fuzheng huayu tablet and entecavir: design of a randomized, double-blind, parallel and multicenter clinical trial," *Chinese Journal of Integrative Medicine*, vol. 27, no. 7, pp. 509–513, 2021.

[13] S. Dong, Q. L. Chen, and S. B. Su, "Curative effects of fuzheng huayu on liver fibrosis and cirrhosis: a meta-analysis," *Evidence-based Complementary and Alternative Medicine*, vol. 2015, Article ID 125659, 11 pages, 2015.

[14] X. Deng, J. Liang, Z. W. Liu, F. Wu, and X. Li, "Treatment of posthepatitic cirrhosis by Fuzheng Huayu Tablet for reinforcing qi and resolving stasis," *Chinese Journal of Integrative Medicine*, vol. 19, no. 4, pp. 289–296, 2013.

[15] Y. N. Song, J. J. Sun, Y. Y. Lu et al., "Therapeutic efficacy of fuzheng-huayu tablet based traditional Chinese medicine syndrome differentiation on hepatitis-B-caused cirrhosis: a multicenter double-blind randomized controlled trail," *Evidence-based Complementary and Alternative Medicine*, vol. 2013, Article ID 709305, 8 pages, 2013.

[16] L. Zhang and D. Schuppan, "Traditional Chinese Medicine (TCM) for fibrotic liver disease: hope and hype," *Journal of Hepatology*, vol. 61, no. 1, pp. 166–168, 2014.

[17] M. Wu, Y. Zhou, S. L. Qin et al., "Fuzheng huayu capsule attenuates hepatic fibrosis by inhibiting activation of hepatic stellate cells," *Evidence-based Complementary and Alternative Medicine*, vol. 2020, Article ID 3468791, 14 pages, 2020.

[18] X. Q. Hu, Y. N. Song, R. Wu et al., "Metabolic mechanisms of Fuzheng-Huayu formula against liver fibrosis in rats," *Journal of Ethnopharmacology*, vol. 238, Article ID 111888, 2019.

[19] X. Xing, S. Chen, L. Li et al., "The active components of fuzheng huayu formula and their potential mechanism of action in inhibiting the hepatic stellate cells viability - a network pharmacology and transcriptomics approach," *Frontiers in Pharmacology*, vol. 9, p. 525, 2018.

[20] M. Zhang, H. L. Liu, K. Huang et al., "Fuzheng huayu recipe prevented and treated CCl4-induced mice liver fibrosis through regulating polarization and chemotaxis of intrahepatic macrophages via CCL2 and CX3CL1," *Evidence-based Complementary and Alternative Medicine*, vol. 2020, Article ID 8591892, 12 pages, 2020.

[21] H. Xie, Y. Tao, J. Lv, P. Liu, and C. Liu, "Proteomic analysis of the effect of fuzheng huayu recipe on fibrotic liver in rats,"

Evidence-based Complementary and Alternative Medicine, vol. 2013, Article ID 972863, 10 pages, 2013.

[22] S. Becerril, A. Rodríguez, V. Catalán et al., "iNOS gene ablation prevents liver fibrosis in leptin-deficient ob/ob mice," *Genes*, vol. 10, no. 3, p. 184, 2019.

[23] J. Ren, L. Li, Y. Wang, J. Zhai, G. Chen, and K. Hu, "Gambogic acid induces heme oxygenase-1 through Nrf2 signaling pathway and inhibits NF-κB and MAPK activation to reduce inflammation in LPS-activated RAW264.7 cells," *Biomedicine & Pharmacotherapy*, vol. 109, pp. 555–562, 2019.

[24] R. Dai, R. A. Phillips, E. Karpuzoglu, D. Khan, and S. A Ahmed, "Estrogen regulates transcription factors STAT-1 and NF-κB to promote inducible nitric oxide synthase and inflammatory responses," *The Journal of Immunology*, vol. 183, no. 11, pp. 6998–7005, 2009.

[25] E. K. Kim and E. J. Choi, "Compromised MAPK signaling in human diseases: an update," *Archives of Toxicology*, vol. 89, no. 6, pp. 867–882, 2015.

[26] H. Kawaratani, K. Moriya, T. Namisaki et al., "Therapeutic strategies for alcoholic liver disease: focusing on inflammation and fibrosis (Review)," *International Journal of Molecular Medicine*, vol. 40, no. 2, pp. 263–270, 2017.

[27] O. Krenkel, T. Puengel, O. Govaere et al., "Therapeutic inhibition of inflammatory monocyte recruitment reduces steatohepatitis and liver fibrosis," *Hepatology*, vol. 67, no. 4, pp. 1270–1283, 2018.

[28] T. A. Wynn and L. Barron, "Macrophages: master regulators of inflammation and fibrosis," *Seminars in Liver Disease*, vol. 30, no. 03, pp. 245–257, 2010.

[29] N. K. Campbell, H. K. Fitzgerald, and A. Dunne, "Regulation of inflammation by the antioxidant haem oxygenase 1," *Nature Reviews Immunology*, vol. 21, no. 7, pp. 411–425, 2021.

[30] K. D. Poss and S. Tonegawa, "Reduced stress defense in heme oxygenase 1-deficient cells," *Proceedings of the National Academy of Sciences*, vol. 94, no. 20, pp. 10925–10930, 1997.

[31] K. Srisook and Y. N. Cha, "Super-induction of HO-1 in macrophages stimulated with lipopolysaccharide by prior depletion of glutathione decreases iNOS expression and NO production," *Nitric Oxide*, vol. 12, no. 2, pp. 70–79, 2005.

[32] Y. H. Jia, R. Q. Wang, H. M. Mi et al., "Fuzheng Huayu recipe prevents nutritional fibrosing steatohepatitis in mice," *Lipids in Health and Disease*, vol. 11, no. 1, p. 45, 2012.

[33] Y. T. Yeung, F. Aziz, A. Guerrero-Castilla, and S. Arguelles, "Signaling pathways in inflammation and anti-inflammatory therapies," *Current Pharmaceutical Design*, vol. 24, no. 14, pp. 1449–1484, 2018.

[34] E. Karkeni, J. Astier, F. Tourniaire et al., "Obesity-associated inflammation induces microRNA-155 expression in adipocytes and adipose tissue: outcome on adipocyte function," *Journal of Clinical Endocrinology and Metabolism*, vol. 101, no. 4, pp. 1615–1626, 2016.

[35] C. Jennewein, A. von Knethen, T. Schmid, and B. Brune, "MicroRNA-27b contributes to lipopolysaccharide-mediated peroxisome proliferator-activated receptor γ (PPARγ) mRNA destabilization," *Journal of Biological Chemistry*, vol. 285, no. 16, pp. 11846–11853, 2010.

Hindawi
Evidence-Based Complementary and Alternative Medicine
Volume 2022, Article ID 9152201, 18 pages
https://doi.org/10.1155/2022/9152201

Research Article

The Pharmacological Mechanism of Xiyanping Injection for the Treatment of Novel Coronavirus Pneumonia (COVID-19): Based on Network Pharmacology Strategy

Liang-jing Xia,[1,2] Liang-ming Zhang,[1] Kun Yang,[1,3] Tong Chen,[4] Xian-wen Ye,[5] and Zi-jun Yan[1,4]

[1]*Department of Pharmacy, Panzhihua Central Hospital, Panzhihua 617067, China*
[2]*School of Pharmacy and Pharmaceutical Sciences (Institute of Pharmaceutical Sciences), Shandong First Medical University (Shandong Academy of Medical Sciences), Jinan 250117, China*
[3]*School of Pharmacy, Dali University, Dali 671000, China*
[4]*School of Pharmaceutical Sciences and Yunnan Key Laboratory of Pharmacology for Natural Products, Kunming Medical University, Kunming 650500, China*
[5]*Centre of TCM Processing Research, Beijing University of Chinese Medicine, Beijing 102488, China*

Correspondence should be addressed to Zi-jun Yan; swallowyzj@163.com

Received 16 February 2022; Accepted 15 June 2022; Published 8 July 2022

Academic Editor: Xiang Liu

Purpose. The possible mechanism of Xiyanping injection treatment COVID-19 is discussed through the network pharmacology. *Methods*. Obtaining the chemical structure of Xiyanping injection through the patent application and obtaining control compounds I, II, III, IV, V, Yanhuning injection (VI, VII), Chuanhuning injection (VIII, IX), 10 compounds were analyzed by D3Targets-2019-nCoV. The human anti-COVID-19 gene in COVID-19 DisGeNET was intersected with the CTD Andrographolide target gene and then combined with D3Targets-2019-nCoV, resulting in 93 genes, using the Venny 2.1 platform. The PPI network was constructed by the String platform and Cytoscape 3.8.2 platform. The GO, KEGG, and tissue of the target were analyzed using the Metascape platform and DAVID platform. The gene expression in the respiratory system was analyzed using the ePlant platform. The CB-Dock is used for the docking verification and degree values of the first 20 genes. *Results*. Finally, 1599 GO and 291 KEGG results were obtained. GO is mostly associated with the cell stress response to chemicals, the cell response to oxidative stress, and the cell response to reactive oxygen species. In total, 218 KEGG pathway concentrations were related to infection and other diseases and 73 signaling pathways mostly related to inflammation and immune pathways, such as TNF signaling pathway and MAPK signaling pathway. The molecular docking results show that Xiyanping injection, compound III, has a good docking relationship with 20 target proteins such as HSP90AA1. Tissue has 22 genes that are pooled in the lungs. *Conclusion*. Xiyanping injection may inhibit the release of various inflammatory factors by inhibiting intracellular pathways such as MAPK and TNF. It acts on protein targets such as HSP90AA1 and plays a potential therapeutic role in COVID-19. Thus, compound III may be treated as a potential new drug for the treatment of COVID-19 and the Xiyanping injection may treat patients with COVID-19 infection.

1. Introduction

According to expert consensus, Xiyanping injection belongs to Chinese medicine injections, primarily composed of *sodium((1R, 2R, 4aR, 8aS)-2-hydroxy-5-((E)-2-((S)-4-hydroxy-2-oxodihydrofuran-3(2H)- ylidene) ethyl)-1,4a,6-trimethyl-1,2,3,4,4a,7,8,8a-octahydronaphthalen-1-yl)methyl sulfate* ($C_{20}H_{29}O_5{\cdot}SO_3Na$). It mainly has anti-inflammatory, antibacterial, anticough, and other effects and enhances the body's immunity, [1]. In the "2019 Novel Coronavirus Diagnosis and Treatment Program" (Trial 6th Edition) implemented by the State Health and Construction

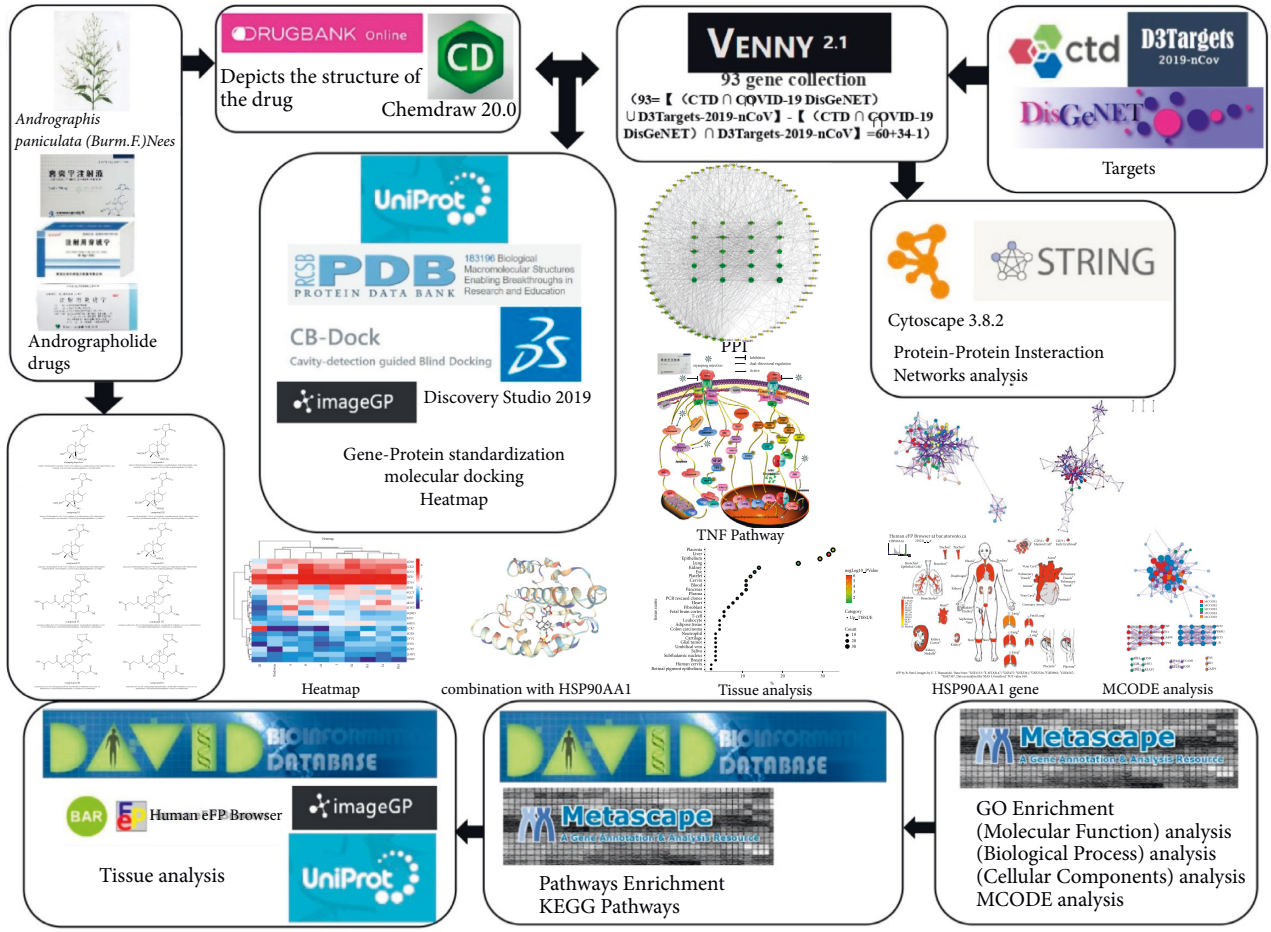

Figure 1: Technological roadmap of Xiyanping injection.

Commission of China, the virus infection is heavy and critical or combined with mild bacterial infection, and the treatment of Xiyanping injection is recommended with Chinese medicine injection. The recommended usage is as follows: 0.9% sodium chloride injection 250 mL plus Xiyanping injection 100 mg b.i.d. [2]. The drug has been on the market for more than 30 years. In 2016, Xiyanping injection ranked in the top three in the market for Chinese medicine injections in the clear-heat detoxification category, with market size of about 2.6 billion yuan, often used in pediatrics [3].

Coronaviruses (CoVs) consist of a single positive-chain RNA virus that belongs to the coronavirus group and can develop into respiratory, intestinal, nervous, reproductive, and other diseases in infected animals and humans [4]. In 2019, some hospitals in Wuhan City, Hubei Province, have found several cases of unexplained pneumonia with a history of exposure to the South China seafood market, which has been confirmed as a new type of coronavirus infection caused by acute respiratory infections. The World Health Organization has named the virus "COVID-19" [5]. Similar to the pathological mechanism of Severe Acute Respiratory Syndrome (SARS), SARS-CoV-2 infections disrupt the epithelial-endothelial barrier in the bronchial and alveoli, causing alveoli-capillary oxygen transfer dysfunction and impaired oxygen diffusion. In patients with severe COVID-19, severe coagulation dysfunction and thrombosis and sepsis further lead to multiple organ failures [6]. Zhong Nanshan's team reported in the literature that 63.4% of COVID-19 patients had a fever and lung abnormalities in chest CT scans; experimental studies have shown that patients with COVID-19 have lymphocyte reduction and increased levels of reactive protein (CRP) [7].

Recently, network pharmacology has been widely used in the study of Chinese medicine anti-SARS-CoV-2 [8]. The emerging network pharmacology technology can be widely used to explore the possible mechanism of Chinese medicine to treat diseases through multicomponent, multitarget, and multichannel levels and to explore potential therapeutic drugs [9]. The Chinese medicine injections in the New Coronary Virus Pneumonia Treatment Programme (Trial 7) [10] are included in the recommended SARS-CoV-2 treatment options, such as Xiyanping injection, Xuebijing injection, Reduning, Tanreqing injection, Xingnaoling injection, Shenfu injection, Shenmai injection, and Shengmai injection. This has also raised awareness and acceptance of Chinese medicine injections. In Wuhan Jinyintan Hospital, Wuhan Lung Hospital, Huazhong University of Science, and Technology Tongji Medical College affiliated Concord Hospital, seriously ill patients by the Chinese and

Table 1: 93 genes collected.

UniProt ID	Gene names
P07900	HSP90AA1
Q9Y243	AKT3
P62937	PPIA
Q2M2I8	AAK1
Q9Y2I7	PIKFYVE
P31751	AKT2
P35613	BSG
Q99720	SIGMAR1
Q16774	GUK1
P27823	PGA5
P27824	CANX
P09651	HNRNPA1
P42684	ABL2
Q4KMQ2	ANO6
O15393	TMPRSS2
P09958	FURIN
P07711	CTSL
P01031	C5
P78536	ADAM17
P31749	AKT1
P51636	CAV2
P53779	MAPK10
P30530	AXL
Q9H2X3	CLEC4M
O76074	PDE5A
P68104	EEF1A1
Q02127	DHODH
P45983	MAPK8
P05121	SERPINE1
P06400	RB1
P26447	S100A4
P48506	GCLC
Q16236	NFE2L2
P40763	STAT3
P08670	VIM
P04040	CAT
P12830	CDH1
Q15910	EZH2
P35968	KDR
P28482	MAPK1
P27361	MAPK3
P04637	TP53
P15336	ATF2
P10415	BCL2
P11802	CDK4
P10145	CXCL8
P20711	DDC
P49327	FASN
P00441	SOD1
P01375	TNF
P13500	CCL2
P29279	CCN2
Q9NSE2	CISH
P19875	CXCL2
P11712	CYP2C9
P08684	CYP3A4
P08246	ELANE
P17948	FLT1
P02751	FN1
P01100	FOS
P24298	GPT
P08721	SPP1
P15692	VEGFA
P05231	IL6
P42574	CASP3
P09601	HMOX1
Q14790	CASP8
P55957	BID
P05177	CYP1A2
P25445	FAS
P48023	FASLG
P05305	EDN1
P08253	MMP2
P14780	MMP9
P05164	MPO
P16284	PECAM1
P37231	PPARG
P04049	RAF1
P59594	ACE2
Q16665	HIF1A
P01137	TGFB1
Q14145	KEAP1
P13647	KRT5
O14733	MAP2K7
P45984	MAPK9
P01024	C3
P60842	EIF4A1
P00390	GSR
P00738	HP
P05412	JUN
P49841	GSK3B
P01033	TIMP1
P19320	VCAM1

Western Medical Federation, more patients used Chinese medicine injections, achieved good results. Professor Zhangboli said "for patients with mild illness, a large number of practices have proved that Chinese medicine can improve symptoms, shorten the course of treatment, and promote healing" [11]. Mild patients often present with fever, dry cough, and fatigue symptoms mainly. Some patients have wheezing, and lungs scattered in the oozing symptoms; Chinese medicine has detoxification, cough relief, and other good therapeutic effects. He led the clinical study of the Wuhan Fire Line project. The phase analysis shows that the first batch of 52 patients in Hubei Province combined with Western medicine hospital clinical control study: including 34 cases of Chinese and Western medicine combined treatment group, 18 cases of the simple Western medicine treatment group. The data analysis results show that compared with the Western medicine group, the clinical symptoms of the combination group of Chinese and Western medicine were shortened by 2 days. The normal temperature was reduced by 1.7 days. The average number of hospital days was shortened by 2.2 days. The CT image improvement rate was increased by 22%, and the clinical cure rate was increased by 33% [11].

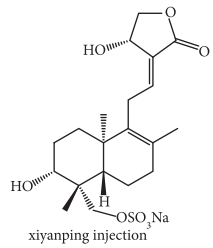

xiyanping injection

sodium ((1*R*,2*R*,4a*R*,8a*S*)-2-hydroxy-5-((*E*)-2-((*S*)-4-hydroxy-2-oxodihydrofuran-3(2*H*)-ylidene)ethyl)-1,4a,6-trimethyl-1,2,3,4,4a,7,8,8a-octahydronaphthalen-1-yl)methyl sulfate

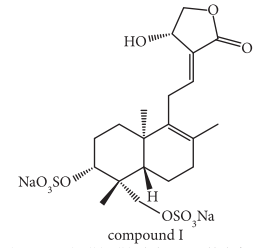

compound I

sodium (1*R*,2*R*,4a*R*,8a*S*)-5-((*E*)-2-((*S*)-4-hydroxy-2-oxodihydrofuran-3(2*H*)-ylidene)ethyl)-1,4a,6-trimethyl-1-((sulfonatooxy)methyl)-1,2,3,4a,7,8,8a-octahydronaphthalen-2-yl sulfate

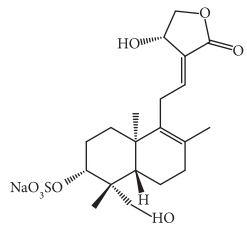

compound II

sodium ((1*R*,2*R*,4a*R*,8a*S*)-5-((*E*)-2-((*S*)-4-hydroxy-2-oxodihydrofuran-3(2*H*)-ylidene)ethyl)-1-(hydroxymethyl)-1,4a,6-trimethyl-1,2,3,4,4a,7,8,8a-octahydronaphthalen-2-y1 sulfate

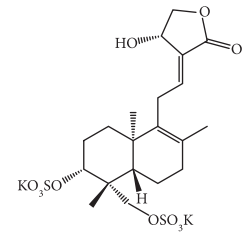

compound III

potassium (1*R*,2*R*,4a*R*,8a*S*)-5-((*E*)-2-((*S*)-4-hydroxy-2-oxodihydrofuran-3(2*H*)-ylidene)ethyl)-1,4a,6-trimethyl-l-((sulfonatooxy)methyl)-1,2,3,4,4a,7,8,8a-octahydronaphthalen-2-y1 sulfate

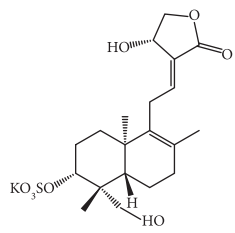

compound IV

potassium (1*R*,2*R*,4a*R*,8a*S*)-5-((*E*)-2-((*S*)-4-hydroxy-2-oxodihydrofuran-3(2*H*)-ylidene)ethyl)-1-(hydroxymethyl)-1,4a,6-trimethyl-1,2,3,4,4a,7,8,8a-octahydronaphthalen-2-y1 sulfate

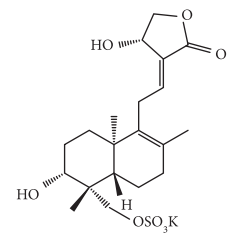

compound V

potassium ((1*R*,2*R*,4a*R*,8a*S*)-2-hydroxy-5-((*E*)-2-((*S*)-4-hydroxy-2-oxodihydrofuran-3(2*H*)-ylidene)ethyl)-1,4a,6-trimethyl-1,2,3,4,4a,7,8,8a-octahydronaphthalen-1-yl)methyl sulfate

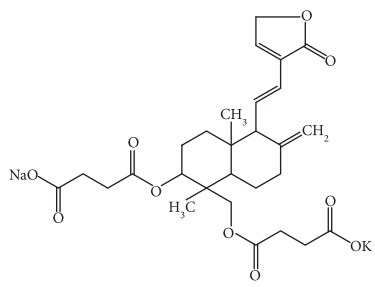

compound VI

potassium sodium (*E*)-4-((2-((3-carboxylatopropanoyl)oxy)-1,4a-dimethyl-6-methylene-5-(2-(2-oxo-2,5-dihydrofuran-3-yl)vinyl)decahydronaphthalen-1-yl)methoxy)-4-oxobutanoate

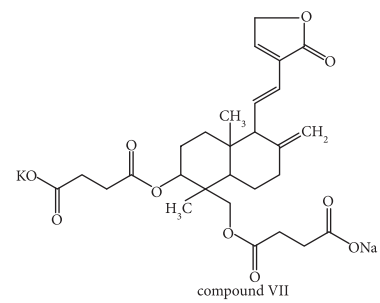

compound VII

potassium sodium (*E*)-4-((2-((3-carboxylatopropanoyl)oxy)-1,4a-dimethyl-6-methylene-5-(2-(-oxo-2,5-dihydrofuran-3-yl)vinyl)decahydronaphthalen-1-yl)methoxy)-4-oxobutanoate

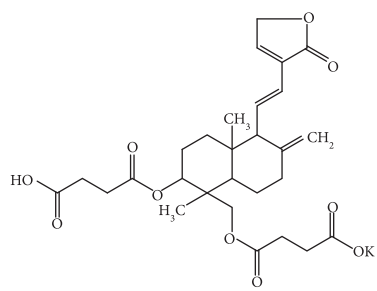

compound VIII

potassium (*E*)-4-((2-((3-carboxypropanoyl)oxy)-1,4a-dimethyl-6-methylene-5-(2-(2-oxo-2,5-dihydrofuran-3-yl)vinyl)decahydronaphthalen-1-yl)methoxy)-4-oxobutanoate

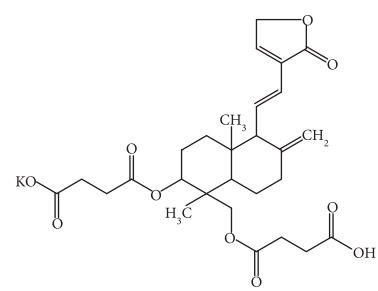

compound IX

potassium (*E*)-4-((1-(((3-carboxypropanoyl)oxy)methyl)-1,4a-dimethyl-6-methylene-5-(2-(2-oxo-2,5-dihydrofuran-3-yl)vinyl)decahydronaphthalen-2-yl)oxy)-4-oxobutanonate

Figure 2: The structure of the compound.

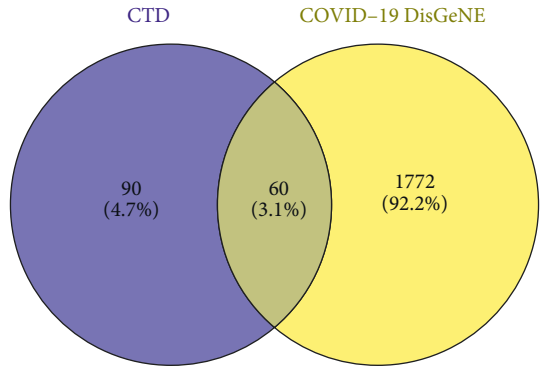

Figure 3: 60 genes.

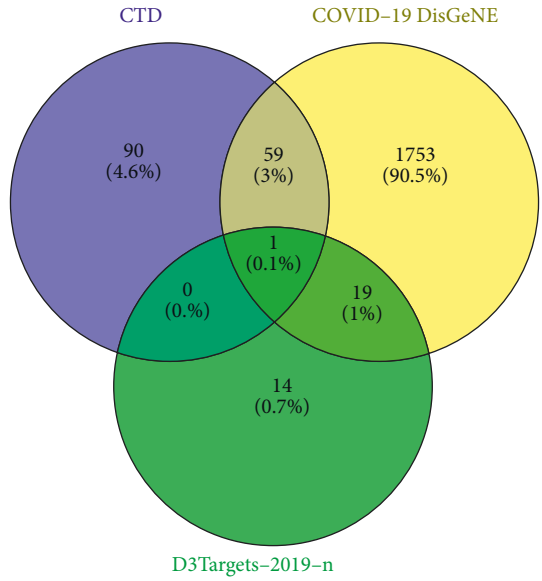

Figure 4: 93 genes.

Based on clinical data, this article uses network pharmacology to explore the possible mechanism of Xiyanping injection anti-SARS-CoV-2, while andrographolide, compound III, can be used as a potential new anti-SARS-CoV-2 drug (Figure 1).

2. Materials and Methods

2.1. Collection of Target Compounds. We obtained the chemical structures of six andrographolide salts, including Xiyanping injection and other andrographolide salts synthesized in process production, through the contents in the patent book of pharmaceutical companies. These five compounds were derived from the production process of Xiyanping injection, but they were not produced in the market as the objects of subsequent pharmacodynamic development, and there were no related clinical studies: I, II, III, IV, and V. We obtained similar andrographolide Chinese medicine injections via the DrugBank [12] platform (https://go.drugbank.com/): Yanhuning injection compounds: VI and VII; Chuanhuning injection compounds: VIII and IX. Ten compounds are drawn and saved in SDF format via ChemDraw 20.0 software [13].

2.2. Screening of Disease Targets. Based on the D3Targets-2019-nCoV platform [14] (https://www.d3pharma.com/D3Targets-2019-nCoV/index.php), the Xiyanping injection anti-COVID-19-related target genes were docked. We obtained human gene targets related to andrographolide based on the CTD platform [15] (https://ctdbase.org/). The CTD platform [15]captures the set of genetic targets that andrographolide acts on in humans; the Human anti-COVID-19 gene dataset on the COVID-19 DisGeNET platform [16] (https://ctdbase.org/) takes the target intersection collection of these two gene sets through the Venny 2.1 platform (https://bioinfogp.cnb.csic.es/tools/venny/). The collection is then merged with the human anti-COVID-19 target obtained by the D3Targets-2019-nCoV platform [14]. Finally, a target set of the andrographolide drug Xiyanping injection anti-

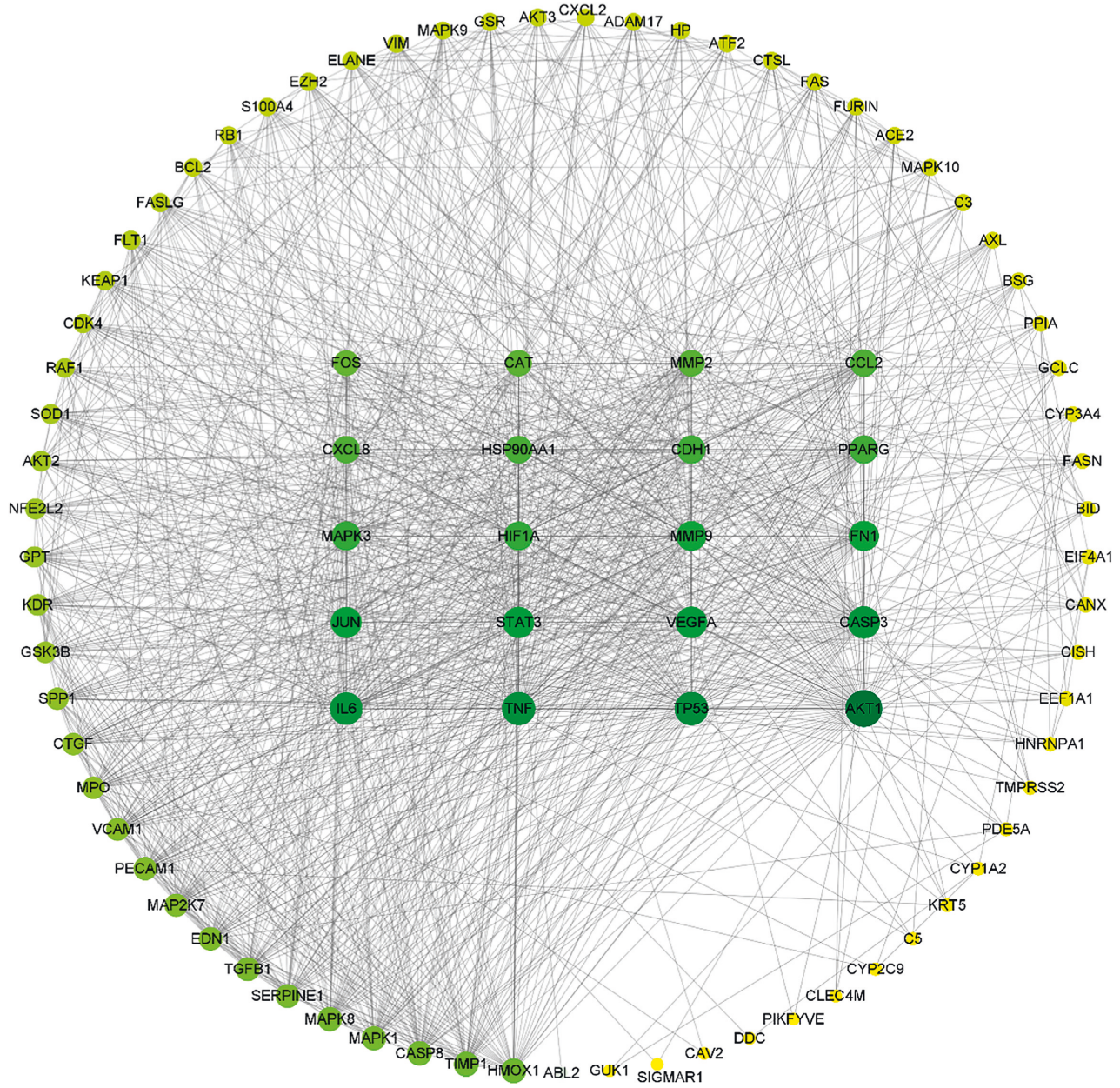

Figure 5: The PPI networks for 89 genes.

COVID-19 was obtained [(CTD ∩ COVID-19 DisGeNET)∪ D3Targets-2019-nCoV]−[(CTD ∩ COVID-19 DisGeNET)∩ D3Targets-2019-nCoV].

2.3. Target Gene Network Construction and Analysis. The target protein is converted into the corresponding gene name through the UniProt platform [17] (https://www.uniprot.org/), and the target protein interaction network (PPI network) is built through the String platform [18] (https://www.string-db.org/). Finally, a compound-target PPI network is built using the Cytoscape 3.8.2 software platform [19].

2.4. GO and KEGG Pathway Enrichment Analysis. To further analyze the function of the target, the target is uploaded to the Metascape platform [20] (https://metascape.org/); the species is limited to "*H. sapiens*," the threshold $P < 0.05$, and its GO biofunction (biological process (BP), molecular function (MF), and cell composition (CC)) enrichment analysis is carried out. At the same time, KEGG signal path enrichment analysis and tissue structural analyses are carried out through the DAVID platform [21] (https://david.ncifcrf.gov/), and Enrichment Plot is drawn through the image GP platform (http://www.ehbio.com/).

2.5. Drug Ingredients: Protein Targets' Molecular Docking. Download the Human Target Protein (Table 1) in the Top 20 Degrees from the PDB platform [22] (https://www.rcsb.org/): 20 target macromolecules, hydrogenation, removal of water

Table 2: The top 20 genes for the degree value.

PDB ID	Target gene	Degree	UniProt ID	Protein name
6CCY	AKT1	75	P31749	RAC-alpha serine/threonine-protein kinase
4KVP	TP53	65	P04637	Cellular tumor antigen p53
4TWT	TNF	64	P01375	Tumor necrosis factor
4ZS7	IL6	62	P05231	Interleukin-6
6CKZ	CASP3	61	P42574	Caspase-3
6D3O	VEGFA	59	P15692	Vascular endothelial growth factor A
6QHD	STAT3	58	P40763	Signal transducer and activator of transcription 3
6MFA	JUN	57	P05412	Transcription factor AP-1
5J6Z	FN1	55	P02751	Fibronectin
2OW1	MMP9	54	P14780	Matrix metalloproteinase-9
6GES	MAPK3	51	P27361	Mitogen-activated protein kinase 3
4H6J	HIF1A	51	Q16665	Hypoxia-inducible factor 1-alpha
2O72	CDH1	49	P12830	Cadherin-1
2VV1	PPARG	49	P37231	Peroxisome proliferator-activated receptor gamma
4U93	HSP90AA1	47	P07900	Heat shock protein HSP 90-alpha
3IFD	CCL2	46	P13500	C-C motif chemokine 2
5D14	CXCL8	46	P10145	Interleukin-8
1CK7	MMP2	44	P08253	72 kDa type IV collagenase
7P8W	CAT	43	P04040	Catalase
1FOS	FOS	41	P01100	FOS G0S7

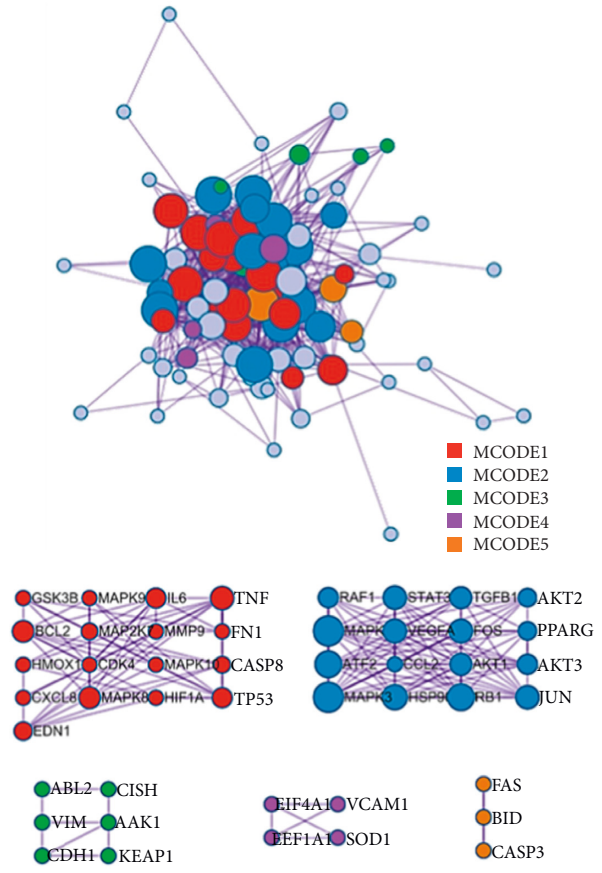

Figure 6: The targets analysis.

molecules, removal of ligands, etc., through Discovery Studio 2019 Client software [23]. The target component and macromolecules are uploaded to the CB-Dock platform [24] (https://clab.labshare.cn/cb-dock/php/) for molecular docking to bind the energy ≤ −5.0 kcal/mol as the basis for molecular-target interactions [25]. The docking results are mapped to heatmap via the image GP platform, and the binding sites and patterns of ligand drugs and target proteins

Table 3: Network and annotation.

Network	Annotation
MyList	hsa05161|Hepatitis B|−41.7; R-HSA-1280215|Cytokine Signaling in Immune system|−39.3; ko04933|AGE-RAGE signaling pathway in diabetic complications|−38.8
MyList_MCODE_ALL	hsa05161|Hepatitis B|−47.8; hsa05200|Pathways in cancer |−46.3; WP4666|Hepatitis B infection|−42.3
MyList_SUB1_MCODE_1	hsa05161|Hepatitis B|−22.8; hsa05200|Pathways in cancer |−20.8; ko04933|AGE-RAGE signaling pathway in diabetic complications|−20.5
MyList_SUB1_MCODE_2	hsa05200|Pathways in cancer|−24.0; hsa05161|Hepatitis B|−23.3; ko05212|Pancreatic cancer|−22.9
MyList_SUB1_MCODE_3	R-HSA-194315|Signaling by Rho GTPases|−3.5; R-HSA-1280215|Cytokine Signaling in Immune system|−3.5; R-HSA-9716542|Signaling by Rho GTPases, Miro GTPases, and RHOBTB3|−3.5
MyList_SUB1_MCODE_4	R-HSA-1280215|Cytokine Signaling in Immune system|−4.2
MyList_SUB1_MCODE_5	WP384|Apoptosis modulation by HSP70|−9.6; WP2507|Nanomaterial induced apoptosis|−9.5; M197|PID HIV NEF PATHWAY|−8.8

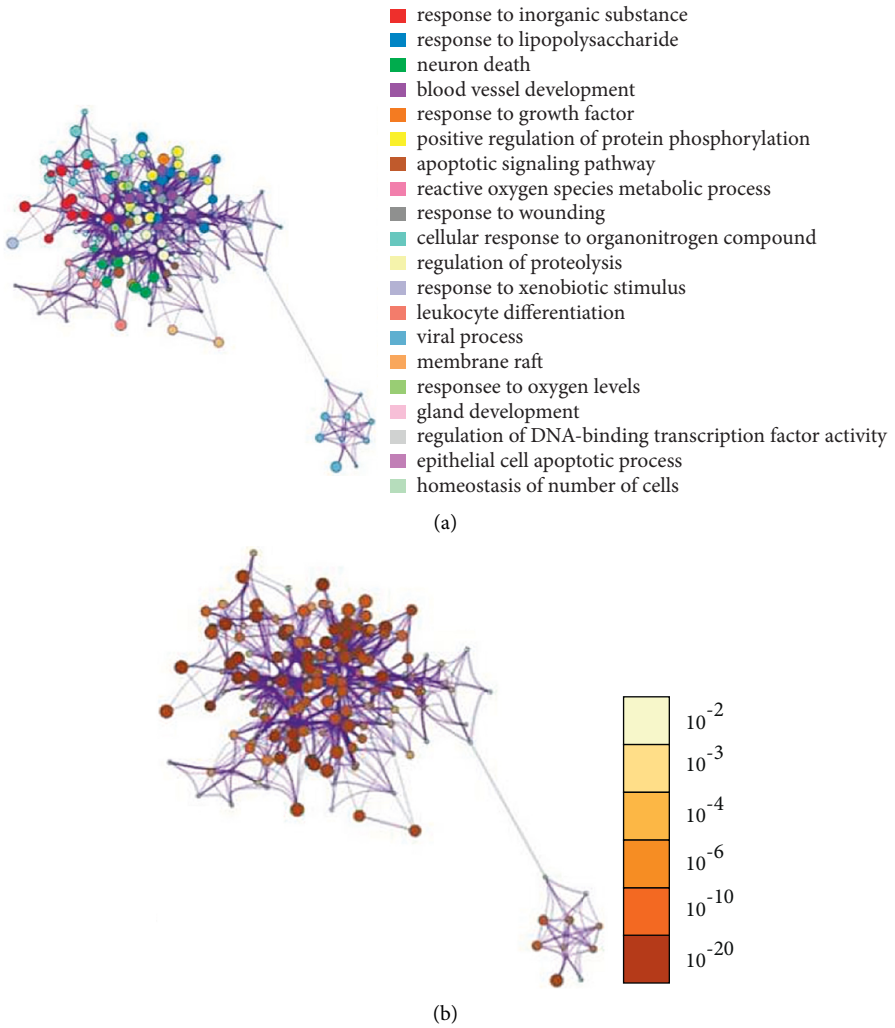

Figure 7: (a) GO color by cluster; (b) GO color by p-value.

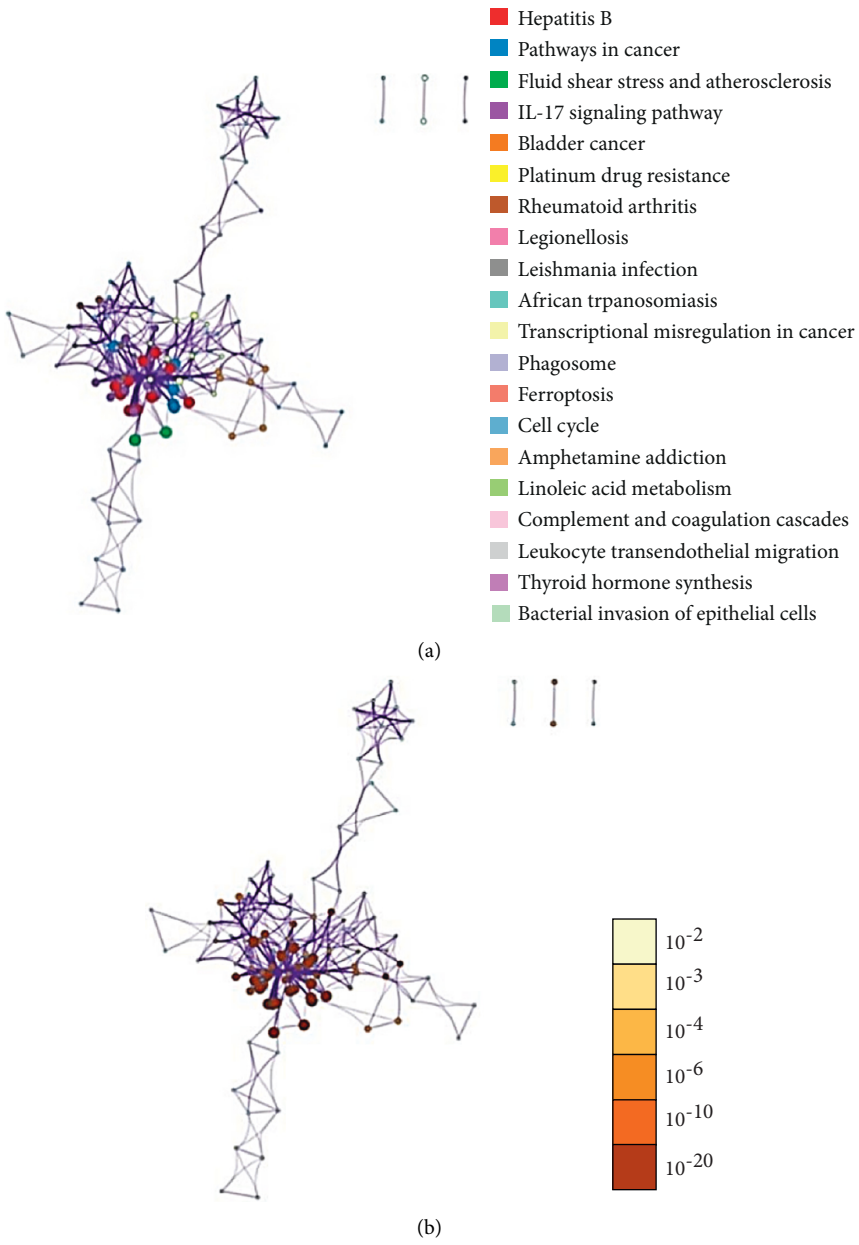

Figure 8: (a) KEGG color by cluster; (b) KEGG color by cluster.

are observed through Discovery Studio 2019 Client software [23].

2.6. Organizing Enrichment Analysis. We performed organizational analysis via the DAVID platform [21], analysis of Xiyanping injection Vina scores of higher HSP90AA1, CAT gene target and compound III Vina score of higher TNF, and FOS gene target and observed the relationship between genes and tissues, using the Human eFP Browser platform [26].

3. Results

3.1. Screening of Active Compounds. We obtained the chemical structure of andrographolide-sulfonate: Xiyanping injection, I, II, III, IV, and V through a patent application for Jiangxi Qingfeng Pharmaceuticals [27]. The DrugBank Platform has similar andrographolide Chinese injections: Yanhuning injection compounds: VI and VII; Chuanhuning injection compounds: VIII and IX (Figure 2).

3.2. Target Gene Network Analysis. D3Targets-2019-nCoV platform database [14] was used to collect 34 human genes. The 1812 human genes associated with COVID-19 in the DisGeNET platform [16] were intersected with 150 *Homo sapiens* target genes in the CTD platform [15]. For andrographolide, 60 genes (Figure 3) were collected through the Venny 2.1 platform. The genetic results of the D3Targets-2019-nCoV platform [14] were combined to obtain 93 genes

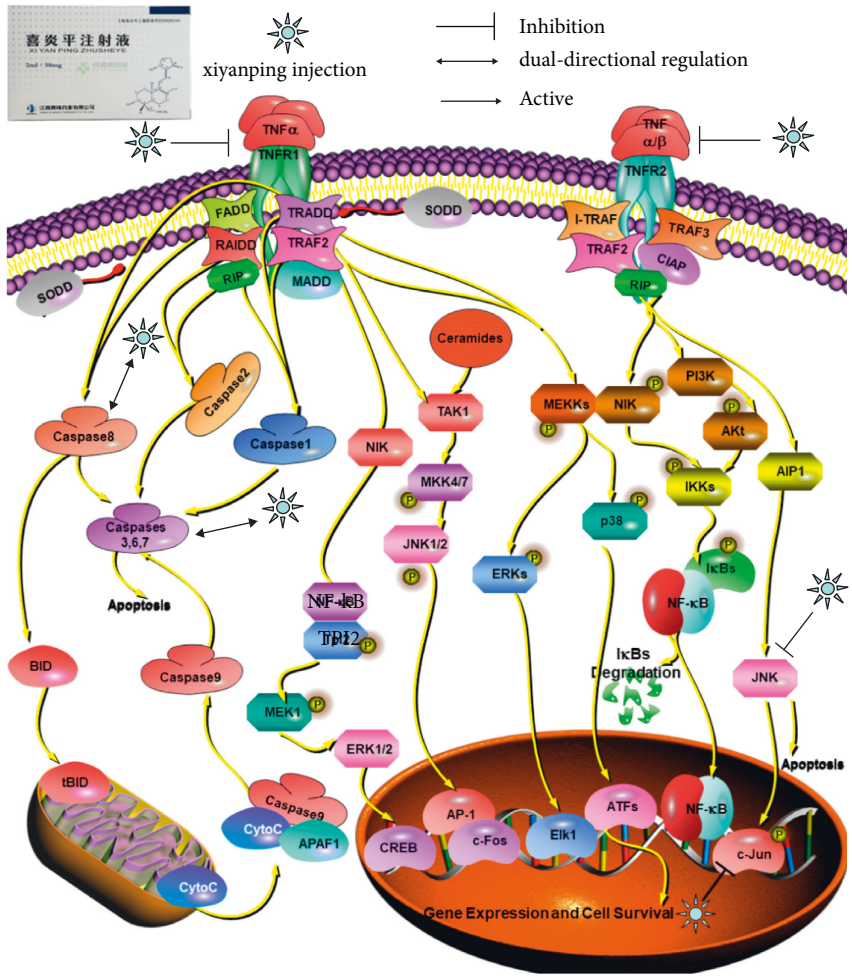

Figure 9: TNF pathway.

(Table 1, Figure 4). We standardized the 93 target genes obtained with the UniProt platform [17]. By analyzing 93 genes through the String platform [18], the number of nodes of the network graph was 93, 1174 edges, and the PPI rich P-value: $<1.0e-16$, which is considered to have strong biological significance. The target PPI network was built using the Cytoscape 3.8.2 platform [19], in which 89 gene nodes were associated, average degree value of 26.38. The circle is the target gene, and the base color with the degree value less than the average value is yellow, and the larger the degree value is, the closer it is to green and the larger the shape is (Figure 5). The top 20 degree values in the PPI network diagram are used as the core targets, in which 20 targets, such as target AKT1 (Degree: 75.0), TP53 (Degree: 65.0), and TNF (Degree: 64.0), are all greater than the average of 1.5 times. These targets are considered to be the main target points for the anti-COVID-19 by the andrographolide drugs (Table 2).

3.3. GO and KEGG Signal Path Enrichment Analysis. GO Enrichment 2343 items through the Metascape platform, which can be clustered into five items by their target properties (Figure 6). The most significant category of items is the mitogen-activated protein kinase MAPK family (MAPK1, MAPK2, MAPK8, etc.), which has the function of regulating cell growth, differentiation, stress adaptation to the environment, inflammatory response, and other important cellular physiological and pathological processes [28]. Studies have also shown an unexpected mechanical link between MAPK signals and inflammatory network control during reprogramming caused by tumor therapy [29]. As can be seen from (Table 3), Cytokine Signaling in Immune system, Nanomaterial induced apoptosis, and PID HIV NEF PATHWAY may be Xiyanping injection anti-SARS-CoV-2 important biologic processes. In total, there are1599 GO biofunctions, of which 1447 are biological processes (BP), 61 are cell compositions (CC), and 91 are molecular functions (MF) (Figures 7(a), 7(b)). Most of the top 20 GO features are related to the reaction of response to an inorganic substance, cellular response to chemical stress, response to oxidative stress, and response to reactive oxygen species. We obtained 291 KEGG path enrichment features (Figures 8(a), 8(b)): 218 were related to infection and other diseases and 73 signaling pathways are mostly related to inflammation and immune pathways. Enriched by the DAVID platform [21] to 107

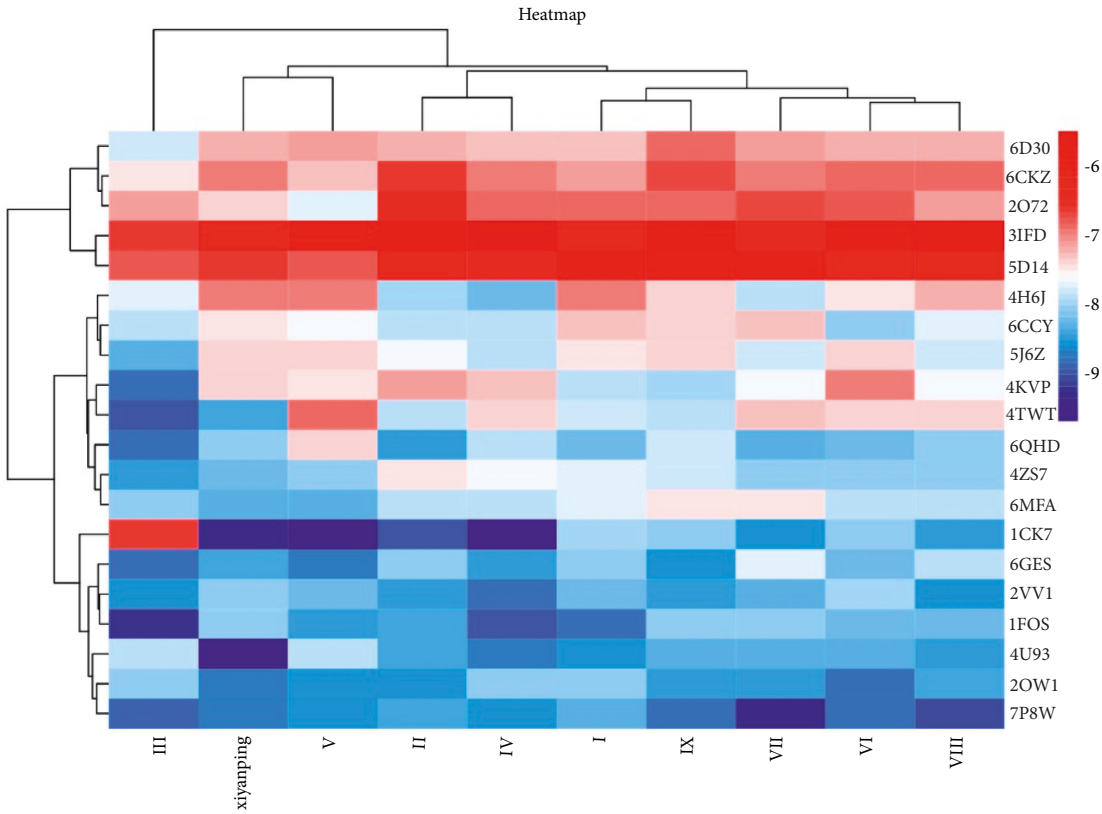

Figure 10: Binding energy heatmap of some compounds with a target protein.

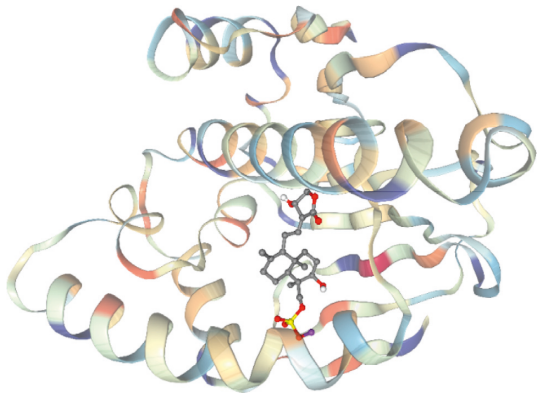

Figure 11: Xiyanping injection in combination with HSP90AA1.

KEGG results, 47 correspond to a variety of diseases such as Hepatitis B, Chagas disease (American trypanosomiasis), colorectal cancer, and influenza A, tubeless. There are 60 pathways, the first three of which are TNF signaling pathways, the Toll-like receptor signaling pathway, and the HIF-1 signaling pathway, most of which are related to immune and inflammatory pathways, and we concluded that injection may be anti-SARS-CoV-2 through inflammation and immune pathways. Showing the TNF pathway (Figure 9), the sunflower represents Xiyanping injection, and the three arrows represent inhibition, dual-directional regulation, and active.

3.4. Analysis of Molecular Docking Results. It is generally believed that the smaller the binding energy of the ligand to the receptor, the greater the likelihood of its interaction and the easier the binding [30]. Andrographolide sulfonates include the following: Xiyanping injection, compound I, compound II, compound III, compound IV, and compound V; Yanhuning injection: VI and VII; Chuanhuning injection: VIII and IX. The degree value of the top 20 target proteins (Table 2) was selected for molecular docking with the above compounds. As can be seen from the molecular docking results, the binding energy of the target compound with the 20 target protein macromolecules is less than −5.0 k·J/mol

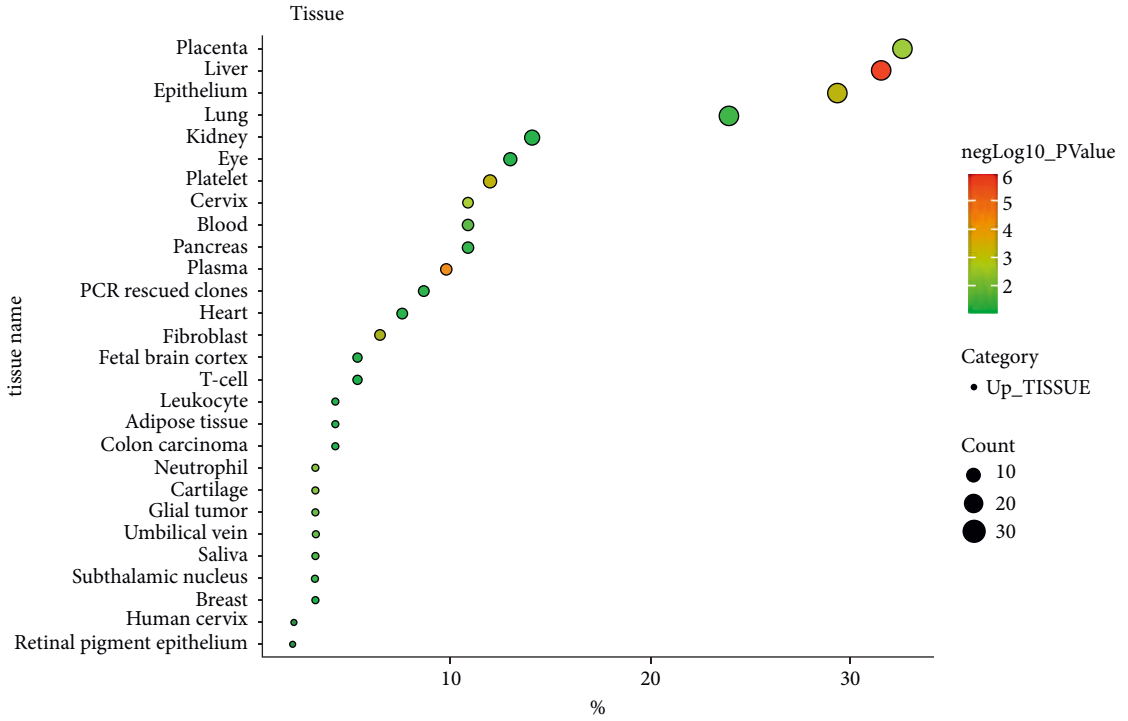

Figure 12: Organizational enrichment differences.

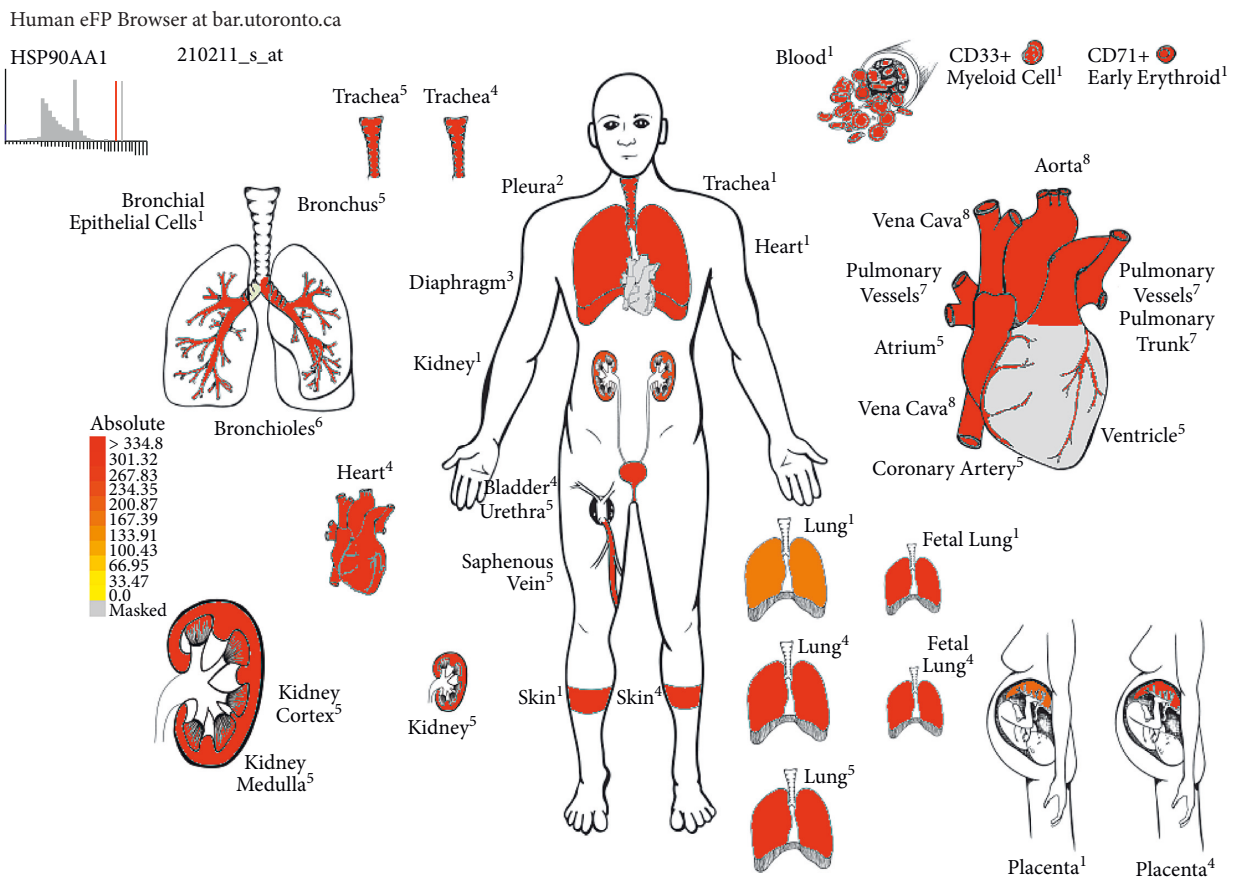

eFP by R. Patel. Images by E. T. Hamanishi. Data from: [1]GSE1133; [2]E-MTAB-47; [3]GSE475; [4]GSE2361; [5]GSE3526; [6]GSE8961; [7]GSE4567;. [8]GSE7307. Data normalized by MAS 5.0 method. TGT value 100.

Figure 13: Expression of HSP90AA1 in the human respiratory and circulatory system.

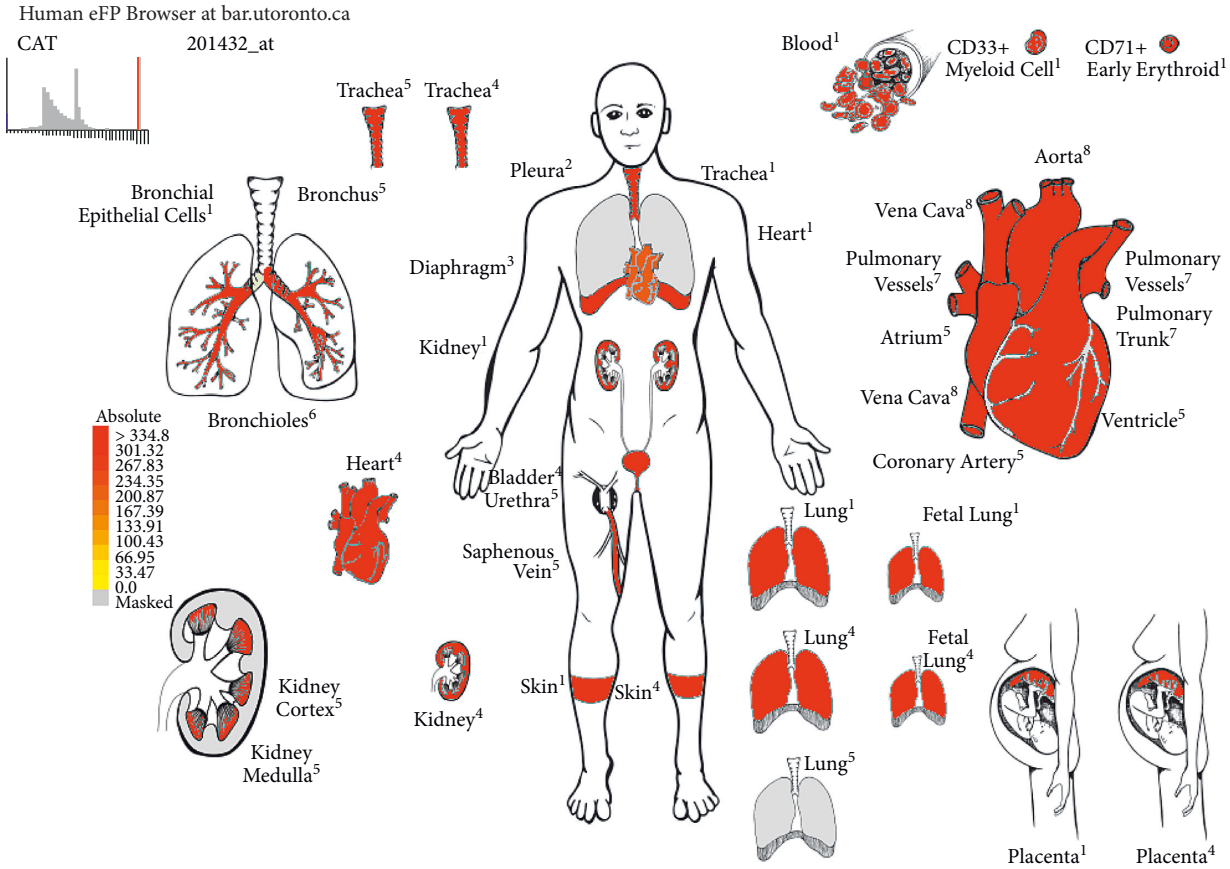

eFP by R. Patel. Images by E. T. Hamanishi. Data from: [1]GSE1133; [2]E-MTAB-47; [3]GSE475; [4]GSE2361; [5]GSE3526; [6]GSE8961; [7]GSE4567;. [8]GSE7307. Data normalized by MAS 5.0 method. TGT value 100.

Figure 14: Expression of CAT in the human respiratory and circulatory system.

[25]. Studies suggest that these ingredients may have anti-SARS-CoV-2 effects [2], and the results indicate that compounds III and Xiyanping injection have a good binding ability with target proteins. See heatmap for molecular docking binding energy (Figure 10). Colors range from red to blue. The bluer the color, the smaller the binding energy, the stronger the binding ability, and the better the docking results. Xiyanping injection and gene: HSP90AA1 (target protein: 3U93) has the highest Vina score of −9.7, Xiyanping injection, and HSP90AA1 (target protein: 3U93) docking mode (Figure 11).

3.5. Organizing Enrichment Analysis. The differential expression of 93 gene targets in human tissue was analyzed using DAVID platform [21] Tissue Enrichment. As can be seen from (Figure 12), the redder the *P*-value circle, the greater the enrichment value, and the larger the count circle shape, the more enriched the gene. It can be seen that in tissues, placenta, liver, epithelial, lung, and other common target expressions are significant, of which the number of lung targets is 22. Among them, the results of molecular docking show that the high scores of Xiyanping injection Vina are HSP90AA1 and CAT gene target, and TNF and FOS gene target have higher compound III Vina scores. The expression of the above four genes in the respiratory and circulatory system was analyzed by the Human eFP Browser platform [26], and the distribution and absoluteness of the genes in the human body were analyzed (Figures 13–16). The higher the absolute, the redder the color, and the higher the gene expression. Human HSP90AA1 and other targets are believed to be effective potential therapeutics.

4. Discussion

According to the clinical trials of Zhang XY, Lv L, and Zhou YL, it can be proved that Xiyanping has the effect of treating COVID-19 [31]. Zhang XY, Lv L, Zhou YL, and others recruited 130 consecutive COVID-19 patients with mild-to-moderate symptoms from five research sites and randomly assigned them to receive Xiyanping injection combined with standard treatment or standard support treatment alone at a 1 : 1 ratio. The results showed that Xiyanping injection significantly reduced the time of cough relief, fever regression, and virus clearance. No serious adverse events were reported during the study. The above clinical trials can prove that Xiyanping has the effect of treating COVID-19, which is worthy of clinical promotion.

The main component of Xiyanping injection is andrographolide, which is the main effective component of

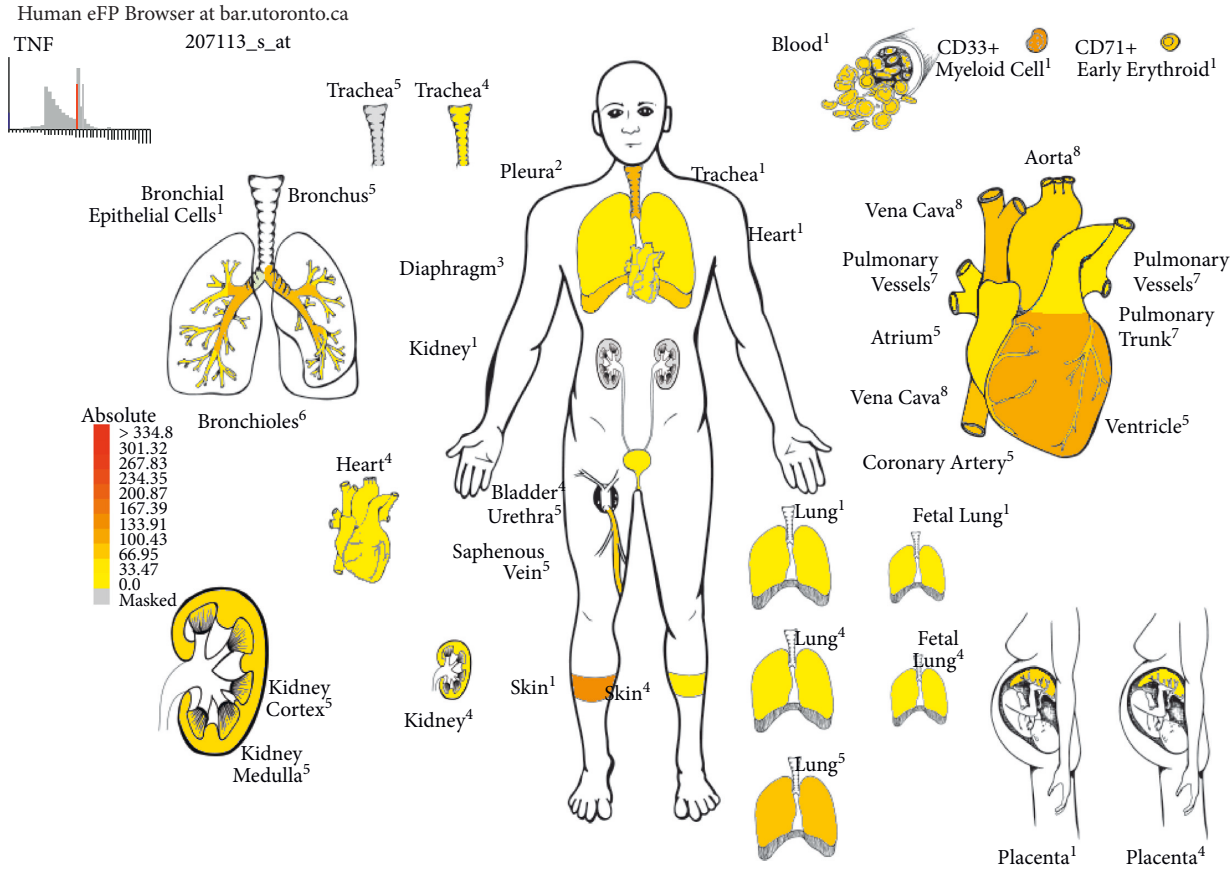

eFP by R. Patel. Images by E. T. Hamanishi. Data from: [1]GSE1133; [2]E-MTAB-47; [3]GSE475; [4]GSE2361; [5]GSE3526; [6]GSE8961; [7]GSE4567;. [8]GSE7307. Data normalized by MAS 5.0 method. TGT value 100.

Figure 15: Expression of TNF in the human respiratory and circulatory system.

the natural plant *Andrographis paniculata*. It has the effects of dispelling heat and detoxification, anti-inflammatory, and analgesic. It has special effects on bacterial and viral upper respiratory tract infections and dysentery and is known as a natural antibiotic drug [32]. In clinical application of the product, its side effects are small. The median lethal dose of alcohol extracts of *Andrographis paniculata* in mice was 13.19 g/kg (calculated by andrographolide). The modern injection has adverse reactions because it directly enters the internal circulation without passing through the liver metabolism of the digestive system. The adverse reactions of andrographolide injections—Yanhuning injection and Chuanhuning injections—are more serious; therefore, they should be used with caution in children. China's National Medical Products Administration has reported security issues with Yanhuning injection/Chuanhuning injection and noted that Yanhuning injection/Chuanhuning injection was used cautiously for children [33]. In the consensus of experts on the clinical application of Xiyanping injection (Child Edition) in 2019, experts believed that Xiyanping injection can be used in children and has good clinical efficacy [1]. Xiyanping injection was recommended by multiple pediatric diseases guidelines/consensuses, and the adverse reactions were much smaller than those of similar drugs. In 2010, Xiyanping injection was recommended in the new editions of Hand, Foot and Mouth Disease Diagnosis and Treatment Guidelines, Influenza A (H1N1) Diagnosis and Treatment Programme, and Fever with Thrombocytopenia Prevention and Treatment Guidelines issued by the Ministry of Health (Table 4).

Excessive TNF can cause tissue damage, which is one of the core cytokines of an "inflammatory storm" caused by infection. TNF can induce cells to release cytokines, but in some cases, it can also induce apoptosis or programmed cell necrosis [34]. After Xiyanping injection enters the patient, its anti-inflammatory effect may be related to the TNF pathway, triggering many TNF pathway reactions: inhibiting TNFR1 and TNFR2 in the TNF pathway. At the same time, Xiyanping injection can regulate Caspase-3 and Caspase-8 in the Caspase family involved in the TNF pathway and mediate cell apoptosis. The activation of NFB JNK protein kinase-mediated by TRAF is inhibited by Xiyanping injection. Xiyanping injection inhibits the extracellular MAPK inflammatory pathway (inhibition of MAPK1, MAPK3, inhibition of MAP production), inhibits NF-κB and other pathways in the nucleus through various pathways, inhibits the release of various inflammatory factors, and plays a role in the treatment of COVID-19.

Target gene HSP90AA1: HSP90AA1 is an important regulator of inflammation because HSP90AA1 is currently

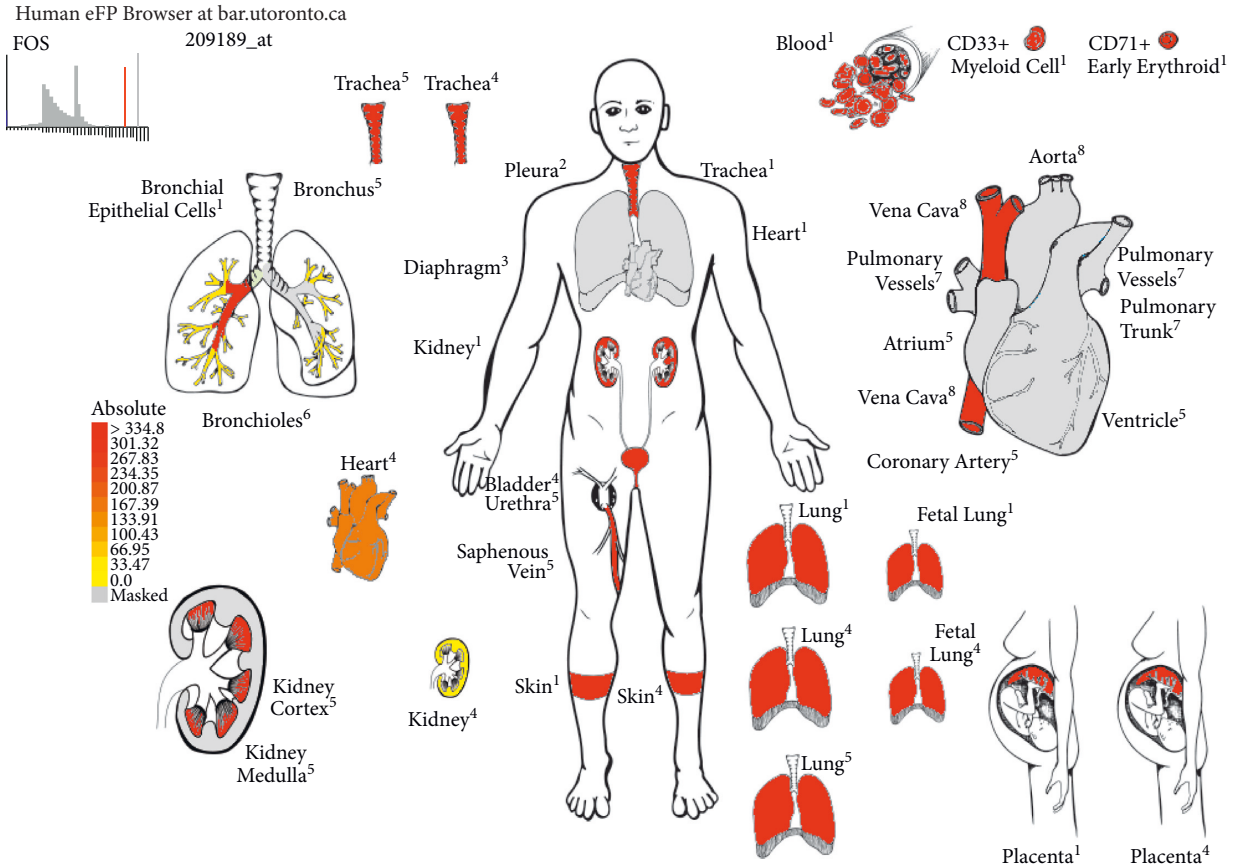

eFP by R. Patel. Images by E. T. Hamanishi. Data from: [1]GSE1133; [2]E-MTAB-47; [3]GSE475; [4]GSE2361; [5]GSE3526; [6]GSE8961; [7]GSE4567;. [8]GSE7307. Data normalized by MAS 5.0 method. TGT value 100.

Figure 16: Expression of FOS in the human respiratory and circulatory system.

Table 4: Xiyanping injection has been included in the guide/expert consensus list.

Serial number	Guideline/expert consensus name	Release year	Guidelines/expert consensus/formulation bodies
1	Hand-foot-mouth disease diagnosis and treatment guidelines (2010 edition)	**2010**	National Health Commission of the People's Republic of China
2	Guidelines for the diagnosis and treatment of viral pneumonia in children in TCM	**2011**	World Federation of Chinese Medicine societies
3	Expert consensus on integrated traditional Chinese and Western medicine treatment of acute fever in children	**2011**	Ma Rong, Wang Xuefeng, etc.
4	Guideline for clinical diagnosis and treatment of pediatrics of traditional Chinese medicine hand-foot-mouth disease (revised)	**2016**	China Association of Chinese Medicine
5	Clinical Diagnosis and Treatment Guidelines for Pediatrics of Traditional Chinese Medicine · Varicella (Revised)	**2016**	China Association of Chinese Medicine
6	Chinese medicine pediatric clinical diagnosis and treatment guidelines bacillary dysentery (formulation)	**2017**	China association of Chinese medicine
7	Expert Consensus on Diagnosis and Treatment of Mycoplasma Pneumoniae Pneumonia in Children by Integrated Traditional Chinese and Western Medicine (2017)	**2017**	China Association of Chinese Medicine of Pediatric Pneumonia Alliance
8	Expert Consensus on Clinical Application of Xiyanping Injection (for Children)	**2019**	Institute of Basic Research In Clinical Medicine/China Academy Of Chinese Medical Sciences
9	The new diagnosis and treatment scheme for coronavirus pneumonia (trial version 4)	**2020**	National Health Commission of the People's Republic of China / National Administration of Traditional Chinese Medicine

Table 4: Continued.

Serial number	Guideline/expert consensus name	Release year	Guidelines/expert consensus/formulation bodies
10	The new diagnosis and treatment scheme for coronavirus pneumonia (trial version 5)	**2020**	National Health Commission of the People's Republic of China/National Administration of Traditional Chinese Medicine
11	The new diagnosis and treatment scheme for coronavirus pneumonia (trial version 6)	**2020**	National Health Commission of the People's Republic of China/National Administration of Traditional Chinese Medicine
12	The diagnosis and treatment scheme of new coronavirus pneumonia (trial version 7)	**2020**	National Health Commission of the People's Republic of China/National Administration of Traditional Chinese Medicine
13	New coronavirus pneumonia diagnosis and treatment plan (trial version 8)	**2020**	National Health Commission of the People's Republic of China/National Administration of Traditional Chinese Medicine

understood as an extracellular agent secreted in wound healing and inflammation. Extracellular HSP90 + induces inflammation by activating NF-κB (RELA) and STAT3 transcription procedures, including proinflammatory cytokines IL-6 and IL-8 [35]. In addition, it has an intracellular anticancer effect and induces autophagy. The anti-inflammatory mechanism of Xiyanping injection may be highly related to this target.

Target gene CAT: CAT gene occurs in almost all aerobic breathing organisms, which helps protect cells from the toxic effects of hydrogen peroxide. It promotes cell growth, including T cells, B cells, bone marrow leukemia cells, melanoma cells, breast cells, and normal and transformed fibroblasts [36]; Xiyanping injection may act on this target, anti-inflammatory effect.

Target gene TNF: TNF gene induces VEGF production by cooperating with IL1B and IL6 [37], plays an anti-inflammatory role, and plays a role in angiogenesis.

Target gene FOS: FOS is considered to play an important role in signal transduction, cell proliferation, and cell differentiation. In growth cells, phospholipid synthesis may be activated by CDS1 and PI4K2A [38]. This activity requires Tyr dephosphorization and association with the endoplasmic retina [38].

From the molecular docking Vina data, it was found that the overall score of compound III was better than that of Xiyanping injection. This also indicates the possibility of a potential new drug, with compound III having better water solubility than Xiyanping injection.

5. Conclusions

In this study, through network pharmacology, molecular docking, target analysis, and tissue analysis, it can be concluded that Xiyanping injection and andrographolide sulfonates such as compound III in the treatment of COVID-19 mainly act on HSP90AA1, CAT, TNF, FOS, and other targets. At the same time, Xiyanping injection inhibits the release of a variety of inflammatory factors by inhibiting intracellular MAPK, TNF, and other pathways and inhibiting NF-κB and other pathways in the nucleus, thus playing a role in the treatment of COVID-19. Compound III is a potential new drug for the treatment of COVID-19. Xiyanping injection can achieve a therapeutic effect in patients with infectious pneumonia, which is in line with the "*Chinese Association of Traditional Chinese Medicine Expert Consensus* (literature reports)" [1] conclusion. In summary, Xiyanping injection is effective and safe in treating COVID-19, which is an important method for the treatment of COVID-19 in integrative medicine. The clinical practice and popularization and application are of far-reaching significance.

Data Availability

All data used to support the findings of the study are included within the article.

Conflicts of Interest

No potential conflicts of interest were reported by the authors.

Acknowledgments

All the authors of the manuscript are immensely grateful to their respective universities and institutes for their technical assistance and valuable support in the completion of this research project. This research was partially supported by grants from the National Natural Science Foundation of China (81760698), the Seventh Batch of Yunnan Specialty Plant Polysaccharide Engineering Research Center Construction Plan ([2019]-57), the General Project of the Department of Science and Technology of Yunnan Province (202001BA070001-041), and the Administration of Traditional Chinese Medicine of Sichuan Province (2020JC0086).

References

[1] Z. F. Wang, P. Rong, R. Ma et al., "Experts consensus statement on Xiyanping Injection in clinical practice(children)," *Zhongguo Zhongyao Zazhi*, vol. 44, no. 14, pp. 2932–2936, 2019.

[2] National Health Commission National Administration of Traditional Chinese Medicine, "Diagnosis and treatment of new coronavirus pneumonia (trial sixth edition)," *Chinese Journal of Viral Diseases*, vol. 10, pp. 81–85, 2020.

[3] Z. F. Wang, X. Chen, W. Zhang, and Y. M. Xie, "Literature review on premarketing and postmarketing evidence of xiyanping injection," *Zhongguo Zhongyao Zazhi*, vol. 39, no. 18, pp. 3637–3640, 2014.

[4] A. Zumla, J. F. W. Chan, E. I. Azhar, D. S. C. Hui, and K. Y. Yuen, "Coronaviruses-drug discovery and therapeutic options," *Nature Reviews Drug Discovery*, vol. 15, no. 5, pp. 327–347, 2016.

[5] X. W. Ye, Y. L. Deng, X. Zhang et al., "Study on the mechanism of treating COVID-19 with shenqi wan based on network pharmacology," *Drug Development and Industrial Pharmacy*, vol. 4, pp. 1–22, 2021.

[6] W. J. Wiersinga, A. Rhodes, A. C. Cheng, S. J. Peacock, and H. C. Prescott, "Pathophysiology, transmission, Diagnosis, and treatment of coronavirus disease 2019 (COVID-19): a review," *JAMA*, vol. 324, no. 8, p. 782, 2020.

[7] L. Fu, B. Wang, T. Yuan et al., "Clinical characteristics of coronavirus disease 2019 (COVID-19) in China: a systematic review and meta-analysis," *Journal of Infection*, vol. 80, no. 6, pp. 656–665, 2020.

[8] X. W. Ye, Y. L. Deng, L. T. Xia, H. Ren, and J. Zhang, "Uncovering the mechanism of the effects of paeoniae radix alba on iron-deficiency anaemia through a network pharmacology-based strategy," *BMC Complement Med Ther*, vol. 20, no. 1, p. 130, 2020 28.

[9] Y. Deng, X. Ye, Y. Chen et al., "Chemical characteristics of platycodon grandiflorum and its mechanism in lung cancer treatment," *Frontiers in Pharmacology*, vol. 11, Article ID 609825, 2020.

[10] "Diagnosis and treatment protocol for novel coronavirus pneumonia (trial version 7)," *Chinese Medical Journal*, vol. 133, no. 9, pp. 1087–1095, 2020.

[11] X. Li, C. Wang, B. Zhang, and B. Yang, "Editorial for the special issue on COVID-19," *Engineering (Beijing)*, vol. 6, no. 10, pp. 1057–1060, 2020.

[12] D. Probst and J. L. Reymond, "Exploring drugbank in virtual reality chemical space," *Journal of Chemical Information and Modeling*, vol. 58, no. 9, pp. 1731–1735, 2018.

[13] Z. Li, H. Wan, Y. Shi, and P. Ouyang, "Personal experience with four kinds of chemical structure drawing software: review on ChemDraw, ChemWindow, ISIS/Draw, and ChemSketch," *Journal of Chemical Information and Computer Sciences*, vol. 44, no. 5, pp. 1886–1890, 2004.

[14] Y. Shi, X. Zhang, K. Mu et al., "D3Targets-2019-nCoV: a webserver for predicting drug targets and for multi-target and multi-site based virtual screening against COVID-19," *Acta Pharmaceutica Sinica B*, vol. 10, no. 7, pp. 1239–1248, 2020.

[15] A. P. Davis, C. J. Grondin, R. J. Johnson et al., "Comparative toxicogenomics database (CTD): update 2021," *Nucleic Acids Research*, vol. 49, no. D1, pp. D1138–D1143, 2021.

[16] J. Piñero, À. Bravo, N. Queralt-Rosinach et al., "DisGeNET: a comprehensive platform integrating information on human disease-associated genes and variants," *Nucleic Acids Research*, vol. 45, no. D1, pp. D833–D839, 2017.

[17] UniProt Consortium, "UniProt: the universal protein knowledgebase in 2021," *Nucleic Acids Research*, vol. 49, no. D1, pp. D480–D489, 2021.

[18] C. von Mering, L. J. Jensen, B. Snel et al., "STRING: known and predicted protein-protein associations, integrated and transferred across organisms," *Nucleic Acids Research*, vol. 33, pp. D433–D437, 2004.

[19] P. Shannon, A. Markiel, O. Ozier et al., "Cytoscape: a software environment for integrated models of biomolecular interaction networks," *Genome Research*, vol. 13, no. 11, pp. 2498–2504, 2003.

[20] Y. Zhou, B. Zhou, L. Pache et al., "Metascape provides a biologist-oriented resource for the analysis of systems-level datasets," *Nature Communications*, vol. 10, no. 1, p. 1523, 2019.

[21] D. W. Huang, B. T. Sherman, and R. A. Lempicki, "Systematic and integrative analysis of large gene lists using DAVID bioinformatics resources," *Nature Protocols*, vol. 4, no. 1, pp. 44–57, 2009.

[22] S. K. Burley, H. M. Berman, G. J. Kleywegt, J. L. Markley, H. Nakamura, and S. Velankar, "Protein data bank (PDB): the single global macromolecular structure archive," *Methods in Molecular Biology*, vol. 1607, pp. 627–641, 2017.

[23] E. P. Raman, T. J. Paul, R. L. Hayes, and C. L. Brooks, "Automated, accurate, and scalable relative protein-ligand binding free-energy calculations using lambda dynamics," *Journal of Chemical Theory and Computation*, vol. 16, no. 12, pp. 7895–7914, 2020.

[24] Y. Liu, M. Grimm, W. T. Dai, Mc. Hou, Z. X. Xiao, and Y. Cao, "CB-Dock: a web server for cavity detection-guided protein-ligand blind docking," *Acta Pharmacologica Sinica*, vol. 41, no. 1, pp. 138–144, 2020.

[25] Y. C. Chen, "Beware of docking," *Trends in Pharmacological Sciences*, vol. 36, no. 2, pp. 78–95, 2015.

[26] R. V. Patel, E. T. Hamanishi, and N. J. Provart, "A human "eFP" browser for generating gene expression anatograms," *PLoS One*, vol. 11, no. 3, Article ID e0150982, 2016.

[27] C. Tang, W. Ye, Y. Hu, and X. Yang, "Sulfonated derivative of andrographolide and combination of medication," *China Unexamined Application. Open to Public Inspection CN20051038561*, 2005.

[28] M. Burotto, V. L. Chiou, J. M. Lee, and E. C. Kohn, "The MAPK pathway across different malignancies: a new perspective," *Cancer*, vol. 120, no. 22, pp. 3446–3456, 2014.

[29] J. Brägelmann, C. Lorenz, S. Borchmann et al., "MAPK-pathway inhibition mediates inflammatory reprogramming and sensitizes tumors to targeted activation of innate immunity sensor RIG-I," *Nature Communications*, vol. 12, no. 1, p. 5505, 2021.

[30] L. Pinzi and G. Rastelli, "Molecular docking: shifting paradigms in drug discovery," *International Journal of Molecular Sciences*, vol. 20, no. 18, p. 4331, 2019.

[31] X. Y. Zhang, L. Lv, Y. L. Zhou et al., "Efficacy and safety of Xiyanping injection in the treatment of COVID-19: a multicenter, prospective, open-label and randomized controlled trial," *Phytotherapy Research*, vol. 35, no. 8, pp. 4401–4410, 2021.

[32] S. G. S. Kandanur, N. Tamang, N. R. Golakoti, and S. Nanduri, "Andrographolide: a natural product template for the generation of structurally and biologically diverse diterpenes," *European Journal of Medicinal Chemistry*, vol. 176, pp. 513–533, 2019.

[33] National Medical Products Administration, "Adverse drug reaction information circular (No. 23) concerned about the safety of Chuanhuning injection and Yanhuning injection," https://www.nmpa.gov.cn/xxgk/yjjsh/ypblfytb/20090901120001886.html.

[34] R. Zhang, T. Xue, A. Shao et al., "Bclaf1 regulates c-FLIP expression and protects cells from TNF-induced apoptosis and tissue injury," *EMBO Reports*, vol. 23, no. 1, Article ID e52702, 2022.

[35] J. E. Bohonowych, M. W. Hance, K. D. Nolan, M. Defee, C. Parsons, and J. Isaacs, "Extracellular Hsp90 mediates an

NF-κB dependent inflammatory stromal program: implications for the prostate tumor microenvironment," *The Prostate*, vol. 74, no. 4, pp. 395–407, 2014.

[36] A. Takeuchi, T. Miyamoto, K. Yamaji et al., "A human erythrocyte-derived growth-promoting factor with a wide target cell spectrum: identification as catalase," *Cancer Research*, vol. 55, no. 7, pp. 1586–1589, 1995.

[37] H. Nakahara, J. Song, M. Sugimoto et al., "Anti-interleukin-6 receptor antibody therapy reduces vascular endothelial growth factor production in rheumatoid arthritis," *Arthritis & Rheumatism*, vol. 48, no. 6, pp. 1521–1529, 2003.

[38] G. Bossis, C. E. Malnou, R. Farras et al., "Down-regulation of c-Fos/c-Jun AP-1 dimer activity by sumoylation," *Molecular and Cellular Biology*, vol. 25, no. 16, pp. 6964–6979, 2005.

Hindawi
Evidence-Based Complementary and Alternative Medicine
Volume 2022, Article ID 4593201, 15 pages
https://doi.org/10.1155/2022/4593201

Research Article

Wound Healing Effects of *Dracontomelon dao* on Bacterial Infection Wounds in Rats and Its Potential Mechanisms under Simulated Space Environment

Jianxia Wen,[1,2] **Zhuo Xu**,[2,3] **Xiao Ma**,[3] **and Yanling Zhao**[2]

[1]*School of Food and Bioengineering, Xihua University, Chengdu, China*
[2]*Department of Pharmacy, Chinese PLA General Hospital, Beijing, China*
[3]*School of Pharmacy, Chengdu University of Traditional Chinese Medicine, Chengdu, China*

Correspondence should be addressed to Yanling Zhao; zhaoyl2855@126.com

Received 13 January 2022; Accepted 30 April 2022; Published 24 June 2022

Academic Editor: Yanhong Zhu

Dracontomelon dao (*D. dao*) is the leaves of *Dracontomelon duperreanum* Pierre (*D. dao* auct. non (Blanco) Merr. and Rolfe; *D. sinense* Stopf.). As a valuable traditional Chinese medicine from Anacardiaceae, *D. dao* has a long history of treating bedsores, skin ulcers, and other infection diseases. In addition, the volatile oil from *D. dao* leaves exhibits antitumor effects. However, these reported studies only focused on evaluating the antimicrobial efficacy on model strains *in vitro*, without paying attention to the antimicrobial activity and anti-inflammatory effects *in vivo*. This study was aimed to provide evidence of antimicrobial activity and anti-inflammatory and proangiogenesis activities of *Dracontomelon dao* (*D. dao*) on the skin of rats under simulated space environment. The weightlessness model of rats in space environment was established. Then, rats were given *D. dao* for 15 days. Wound healing effects of *D. dao* on histopathology and inflammatory cytokines in *E. coli*-induced wound infection in weightless rats were analyzed. Furthermore, the molecular biology technology was performed to evaluate the wound healing effects of *D. dao* on the relative protein level of NF-κB as well as PI3K/Akt signaling pathways. Immunohistochemistry was used for the protein expression of VEGFA. The wound healing effects of *D. dao* on bacterially infected wounds in rats were manifested by lowering the size of the wound and significantly increasing the shrinkage rate of the wound. *D. dao* had effect on alleviating histological damage of skin tissue and downregulation inflammatory cytokines level. In addition, the results indicated that *D. dao* has a regulatory effect on inflammation and angiogenesis and could regulate the relative protein level of MAPK/NF-κB as well as PI3K/AKT signaling pathways. The current study highlighted the crucial role of *D. dao* in relieving skin tissue injury in *E. coli*-induced wound infection in weightless rats by regulating the MAPK/NF-κB as well as PI3K/AKT signaling pathways. This study could provide a new agent for the treatment of bacterial infected wounds in simulated space environment.

1. Introduction

People have developed a strong interest in manned spaceflight due to the efforts of private and government agencies [1]. Living in such an extreme environment will result in reduced immune status and profound changes in the human bacterial community. Under microgravity conditions, the efficacy of antibiotics decreases and the mutation rate of microorganisms increases significantly [2, 3]. Assuming that there is no obvious microbial contamination in the structure of the spacecraft or its air, food, and water supply, any infection of the crew members will be caused by endogenous human and animal flora carried at the time of departure, which may limit the types of infection encountered in a predictable manner [4, 5]. It is reported that the microflora of bacteria was found after a short flight, which may be related to diet, mainly intestinal microflora, such as *Escherichia coli* (*E. coli*) [6, 7]. Microgravity environment makes its mutation more resistant [8]. The negative effects of space travel on immune function, especially cellular immunity, will result in the increase of the chances of bacteria building infection lesions [9]. These factors will affect

effective treatment and infection diseases will occur. Trauma, such as tearing and open fractures, is likely to occur during the long-term mission in the space station [10]. Once infection wounds occur, it will pose a direct threat to the lives of astronauts and even result in the failure of space missions. Therefore, effective antibiotics are needed to prevent serious wound infections. Many studies have indicated that plant products are potential wound healing and effective antimicrobial agents and are largely more popular because of their wide availability and unnecessary side effects [11–13].

Dracontomelon dao (*D. dao*) is the leaves of *Dracontomelon duperreanum* Pierre (*D. dao auct. non* (Blanco) Merr. And Rolfe; *D. sinense* Stopf.). As a valuable traditional Chinese medicine from Anacardiaceae, *D. dao* has a long history of treating bedsores, skin ulcers, and other infection diseases [14, 15]. In addition, the volatile oil from *D. dao* leaves exhibits antitumor effects [16]. Our previous studies [17–19] have shown that different extracts of *D. dao* leaves show different antimicrobial activities, especially the ethyl acetate (EtOAc) extract containing flavonoids and phenolic acids, and exhibit effective antimicrobial activity against *Escherichia coli* (*E. coli*), *Pseudomonas aeruginosa* (*P. aeruginosa*), and *Staphylococcus aureus* (*S. aureus*). However, these reported studies only focused on evaluating the antimicrobial efficacy on model strains *in vitro*, without paying attention to the antimicrobial activity and anti-inflammatory effects *in vivo*. In order to fully imitate the status and living conditions of astronauts in the space capsule, tail-suspended hindlimb-unloaded rats in simulation capsules have been widely performed on for simulating the effects of microgravity. Moreover, this model could lead to body fluids moving to the neck as well head area and induces postural muscle unloading under microgravity condition.

In this study, we investigated the healing of infection wounds in tail-suspended hindlimb-unloaded rats by topical application of *D. dao* under simulated weightlessness environment of space and tried to explore its molecular mechanism. The results indicated that topical application of *D. dao* could not only improve the healing of infection wounds by reducing the expression level of proinflammatory factors, including interleukin-6 (IL-6), interleukin-1β (IL-1β), and tumor necrosis factor-α (TNF-α), but also increase angiogenesis by increasing the expression level of growth factors, such as vascular endothelial growth factor A (VEGFA) and transforming growth factor-β (TGF-β1), thereby shortening healing time. In order to determine the target pathway of *D. dao*, the effects on signaling pathways of nuclear factor kappa-B (NF-κB), phosphoinositide 3-kinase (PI3K), and mitogen-activated protein kinase (MAPK) were subsequently studied to elucidate its related molecular mechanisms.

2. Materials and Methods

2.1. Ethic Statement. This study was performed in line with the recommendation of the Guidelines for the Care and Use of Laboratory Animals of the Ministry of Science and Technology of China. All breeding and experiments were undertaken with review and approval from the Animal Ethical and Experimental Committee of the Chinese PLA General Hospital. The Approval ID is IACUC-2020-0027.

2.2. Preparation of the D. dao Extracts. The leaves of *D. dao* (batch number: 20141013) were obtained from the Chinese herbal medicine market in Guangdong Province, China. The leaves were dried in a cool place and stored at room temperature. *D. dao* leaves were roughly grinded in a chalking machine, sifted (60 mesh), and stored in the sealed containers. 540 g of *D. dao* leaves powder was accurately weighed and refluxed with 12 times 80% ethanol for 2 h, which was repeated three times. Then, the extracts were combined, filtered, and evaporated. In addition, they could be dissolved in proper amount of ultrapure water. Finally, the EtOAc extract was obtained by repeated extraction with EtOAc in the ratio of 1 : 1.5 (H_2O : EtOAc = 1 : 1.5) for 5 times. Finally, the weight ratio of *D. dao* leaves was 12.65%. The extract was dried at low temperature and stored at 4°C for further study.

2.3. Animals Handling. A total of 84 healthy inbred Sprague Dawley rats (190–210 g) of both sexes were obtained from SPF Biotechnology Co., Ltd., Beijing, China. They were individually housed and were periodically weighed once a week. All the animals were closely observed for any infection. Rats showing signs of infection would be isolated and excluded from the study. They were maintained in a temperature-controlled room (23 ± 2°C) and kept on a 12 h/12 h light/dark illumination cycle (lights on at 06 : 00 am) and humidity of 45–50% in an air-conditioned room. Rats had free access to food and water. Rats were handled after adapting to the laboratory environment and observation for 7 days.

2.4. Weightlessness Model in the Simulated Space Environment. The tails of the rats were connected to a rotating suspension device mounted on top of a custom-designed plexiglass cage (length = 45 cm, width = 45 cm, height = 45 cm). After washing with 75% ethanol, the tails were fixed with a tail strap that raised the hindlimbs of rats off the cage floor by a 30° head-down angle with their hindlimbs being unloaded [20–22]. They were caged separately and fed on tap water and chow ad libitum (Figures 1(a) and 1(b)). The cages containing rats were placed on a platform outfitted with an oscillator to simulate the capsule's ascent. The vibration conditions were listed as follows: frequency of 91.5 HZ, vibration time of 58 s, and amplitude of 1 G. Subsequently, all animals were fed with a standard laboratory food and raised in the simulated capsule platform of the China Astronaut Research and Training Centre (Beijing, China). The conditions of the platform are shown in Figure 1(c). The simulated space station environment was kept at 18–25°C and 90 ± 1 Kpa on a 45 : 90 min light/dark cycle. The weightless rats were observed for 14 days before the creation of wound. The system is stable and reliable when

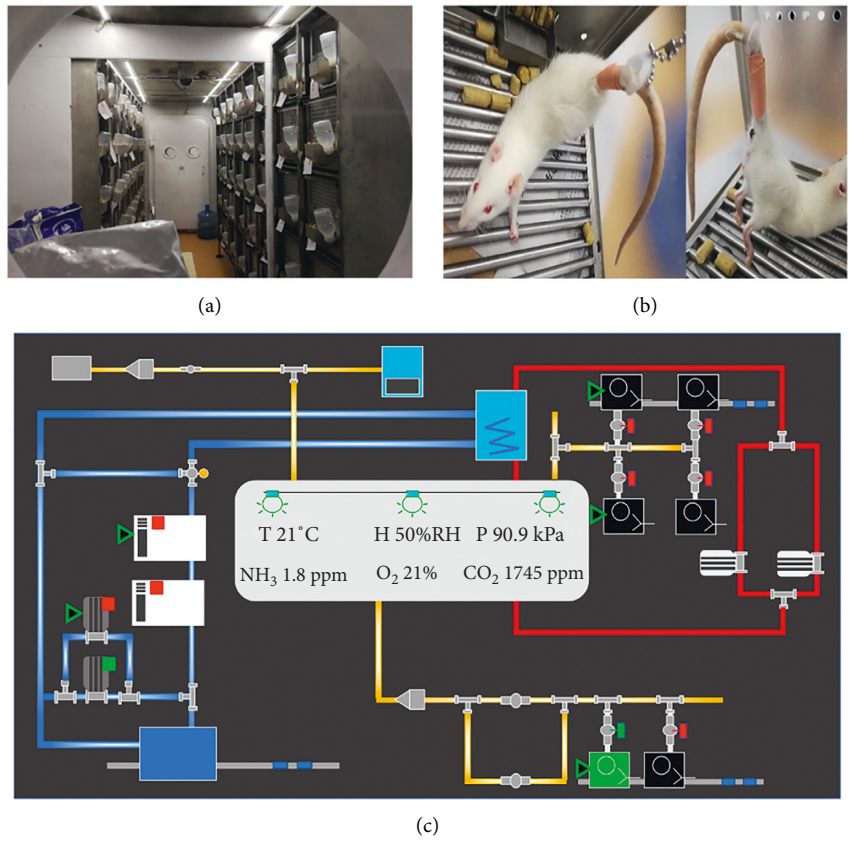

(a) (b) (c)

Figure 1: Simulated animal experiment scene in space environment and spacecraft drug screening platform. (a) The scene of animal experiments under the simulated space environment. (b) Hindlimb-suspended rats. (c) Simulated spacecraft drug screening platform.

creating a model of weightlessness in a simulated space environment in this study.

2.5. Creation of Wound Infection in Weightless Rats. The weightless rats were depilated on the back after anesthesia with urethane (30%, 0.7 ml/100 g). Two excised wounds were created by cutting a full-thickness skin with a diameter of 1.5 cm from a predetermined area on both sides of the dorsal region of the midline to the depth of loose subcutaneous tissue [23]. The *E. coli* suspension (ATCC 25922, 10^8 cfu/ml) was dropped via pipette to induce skin infection [24, 25]. 1 ml of the suspension was used for each wound except the uninfected group. The wound was covered with medical transparent film, wrapped, and fixed with sterile antilicking gauze.

2.6. Grouping and Administration. The rats were randomly assigned to four groups, each of which contained 21 animals. The dose of the drug was consistent with the results of the previous experimental study [26]:

(1) Infection group (IG): the infection wound administered vehicle (30% glycerine) only

(2) Low-dosage group (LDG): the infection wound treated with 0.08 g/ml *D. dao* (with 30% glycerine as vehicle)

(3) High-dosage group (HDG): the infection wound treated with 0.8 g/ml *D. dao* (with 30% glycerine as vehicle)

(4) Uninfection group (UIG): uninfected wound administered vehicle only

After the successful establishment of the skin infection model, the rats were given normal saline for debridement treatment. Each wound was smeared to administer 100 μL corresponding drug liquid once a day for 15 days. Rats had free access to food and water throughout the whole experiment. The doses of *D. dao* used in this research were proved to have no toxic reactions in rats. Subsequently, the wounds were left undressed and placed in an open environment.

2.7. Wound Contraction Evaluation. At 0, 3, 5, 10, and 15 days after inflicting the wounds, the wound area was metered by tracing the outline with transparent paper. If the moist granulation tissue was no longer visible and the wound was covered by new epithelial tissue, the wound was supposedly closed (completely healed). The area within each tracing boundary was scanned by a scanner and analyzed by the image analysis software Image-Pro Plus 6.0 (Media Cybernetics, Inc., Bethesda, MD, USA) and expressed as the percentage of wound shrinkage. These values were expressed as a percentage of the 0-day measurement value and were

evaluated by Wilson's formula [27]. The formula was as follows:

$$\%\text{wound contraction} = \frac{\text{wound area on 0 day}-\text{wound area on particular day}}{\text{wound area on 0 day}} \times 100\%. \quad (1)$$

2.8. Tissue and Blood Collection. Seven rats in each subgroup were selected randomly to collect tissue and blood samples on days 5, 10, and 15. After anesthesia, the rats were punctured at the abdominal aorta to collect blood samples, which were centrifuged to obtain serum. Then, the serum was dispensed into tubules and stored in a refrigerator at −80°C. Next, the granulation tissue and/or healing tissue was collected. One portion of the tissue was preserved in 10% neutral buffered formalin for tissue histopathological and immunohistochemical analysis. The other section was stored at −80°C for further use.

2.9. Histopathologic Evaluation. Hematoxylin-eosin staining (HE) was used to detect the histopathological changes of excised wounds in rats. Different concentrations of ethanol were used to hydrate the wound tissue. The excised wound tissue was fixed and sectioned, and the xylene solution was deparaffinized and transparent. Subsequently, the embedded granulation tissue is sliced into thin slices, which were five-micron-thick slices of the epidermis, dermis, and subcutaneous pannus on the glass slide. After dewaxing, the sample was rehydrated with distilled water and stained with hematoxylin and eosin. The sample was placed under a microscope for microscopic examination, and images were collected and analyzed.

2.10. Detection of Inflammatory Cytokines. The serum samples of rats were taken out and rethawed in a refrigerator at 4°C. Serum biochemical indices were measured respectively by the Synergy H1 Hybrid Reader (Biotech, USA). The corresponding enzyme-linked immunosorbent assay (ELISA) kits were used to detect the content of serum inflammation cytokines, including TNF-α, IL-1β, and IL-6. The ELISA kits were purchased from Shanghai MLBIO biotechnology Co., Ltd. (Shanghai, China). The operation process was carried out in strict accordance with the requirements of the ELISA kit instructions. The results were averaged and expressed as pg/mL protein.

2.11. Western Blotting for the Protein Expression. The western blotting method was performed to investigate the effect of *D. dao* on the relative protein expression of NF-κB, MAPK, and PI3K/Akt signaling pathways and growth factors. The granulation tissues of rats were homogenized and subsequently analyzed by tissue lyser (Shanghai Jingxin Industrial Development Co., Ltd., Shanghai, China) supplemented with radio immunoprecipitation assay (RIPA) buffer containing phenylmethylsulfonyl fluoride (PMSF). Protein concentration was calculated by the bicinchoninic acid assay (BCA) protein assay kit (Beyotime Biotechnology, Shanghai, China). The samples were separated electrophoretically on 10% SDS-PAGE gels for fractionation at 80 V for the first time and then at 120 V. After fractionation, the protein was transferred to a polyvinylidene difluoride (PVDF) membrane (Millipore, Bedford, MA, USA) at 200 mA for 2 h. These membranes were then blocked in 5% skimmed milk powder in TBS containing 0.1% Tween 20 (TBST) for 1 h at room temperature and then incubated at 4°C overnight with different primary antibodies. The primary antibodies were anti-p65 (#8242, 1 : 1000, Cell Signaling Technology (CST), Inc., Danvers, MA, USA), p-P65 (#3033, 1 : 1000, CST), p-IκBα (#9246, 1 : 1000, CST), p-IKKα/β (#2697, 1 : 1000, CST), p-MEK (#9154, 1 : 1000, CST), MEK (ab178876, 1 : 20000, Abcam, United states), p-ERK (#3958, 1 : 1000, CST), ERK (#4695, 1 : 1000, CST), p-JNK (#9255, 1 : 1000, CST), JNK (#9252, 1 : 1000, CST), p38MAPK (AM065-1, 1 : 1000, Beyotime, Shanghai, China), p-AKT (#4060, 1 : 2000, CST), AKT (#4691, 1 : 1000, CST), VEGFA (ab1316, 1 : 100, Abcam), TGF-β_1 (21898-1-AP, 1 : 600, Proteintech), and GAPDH (10494-1-AP, 1 : 10,000, Proteintech). After washing with TBST for 3 times, the membranes were incubated with horseradish peroxidase-conjugated secondary antibody (goat anti-rabbit IgG or goat anti-mouse IgG) for 1 h at room temperature. Finally, the immunoreactivity bands were detected by the enhanced chemiluminescence (ECL; Amersham Biosciences, Little Chalfont, UK) agent. The band intensities were analyzed using the Image J software. The protein expression of GAPDH was used as an internal control to normalize the data.

2.12. Immunohistochemistry Analysis of VEGFA Expression. Immunohistochemistry was performed to detect the protein expression level of VEGFA to determine the formation of new blood vessels at different days after injury. The operation process was as follows: the wound tissue section is kept at 60°C for 2 h and then deparaffinized and dehydrated. Thereafter, 3% H_2O_2 in methanol was used to prevent endogenous peroxidase activity. The section was added to anti-mouse VEGFA monoclonal antibody (ab1316, 1 : 200, Abcam) and incubated overnight at 4°C. After washing the sections with phosphate buffered saline, they were treated with horseradish peroxidase-conjugated secondary antibody (Wuhan Servicebio Technology Co., Ltd., China) at room temperature for 50 minutes. The section was examined under a microscope (100x magnification) to determine the positive expression of VEGFA in the wound. Then, the highest expression areas were observed under a microscope (400x magnification).

After being washed with phosphate buffered saline, the sections were treated with the secondary antibody conjugated with horseradish peroxidase (Wuhan Servicebio Technology Co., Ltd., China) at room temperature for 50 min. After staining with 3, 3′-diaminobenzidine (DAB)/H_2O_2 and hematoxylin, the sections were dehydrated, cleared, and mounted for viewing. For VEGFA analysis, the sections were examined under a microscope (100x magnification) to identify the highest positive expression in the wound. Then, the highest expression areas were observed under a microscope (400x magnification).

2.13. Statistical Analysis. The results were expressed as mean ± standard deviation (SD). The statistical significance of the detected differences was calculated by one-way analysis of variance (ANOVA) followed by Dunnett's multiple comparison test. Data analysis was performed by using SPSS 20.0 (SPSS Inc., Chicago, IL, USA) statistical package program. $P < 0.05$ was considered statistically significant, and $P < 0.01$ was considered highly significant.

3. Results

3.1. Effect of D. dao on Wound Closure and Percent Wound Contraction. Early formation and shedding of scab, as well as wound closure, in *D. dao*-treated groups was characterized in comparison with IG (model) group. On the fifth day, local vasoconstriction created the local wound, most of which was filled with blood. The granular granulation tissue was not observed macroscopically. The normal wound group was moist and clean, with fresh particles around. On the 10th day, most of the wounds in the model group were covered by gray granulation tissue, the crust was hard, the depression was in the center of the wound, the recovery remained not ideal. The granulation tissue fully filled the bottom of the wound, and the epithelial tissue of the outer edge of the wound grew vigorously. On the 15th day, the wounds of the high-dose group of the traditional Chinese medicine group and the normal-wound group of the traditional Chinese medicine group were overall healed, and the rats exhibited a good condition. The wounds of the infection-wound group and the low-dose group of Chinese medicine were covered by scar tissue. Gross evaluation of wound suggested that topical *D. dao* application downregulated the wound size (Figure 2(a)) with significant percentage of increase in wound contraction (Figure 2(b)), as compared with IG group.

3.2. Effect of D. dao in Histopathology of Skin Tissue. On the fifth day, considerable inflammatory factors infiltrated in each group, the tissue structure was necrotic, and the skin appendage disappeared. On the 10th day, the normal-wound group and the traditional Chinese medicine group showed the epidermis hyperplasia, the acanthosis was thickened, and the wound was attached to inflammatory cells. The number turned smaller, and the infective-wound group still showed significant inflammatory cell infiltration. On the 15th day, most of the epithelial tissues of the normal group and the traditional Chinese medicine group were well formed, and the epidermis was differentiated largely, close to the normal epithelium. The infective-wound group exhibited thicker epidermis than the normal epidermis, which was still accompanied by inflammatory cell infiltration. Low magnification (x10) images of wounds are shown in Figure 3(a) and the high magnification (x40) images are shown in Figure 3(b).

3.3. Effect of D. dao on Proinflammatory Mediators (pg/ml protein). Serum levels of TNF-α, IL-1β, and IL-6 were measured in this study. As shown in Figure 4, the serum levels of TNF-α (Figure 4(a)), IL-1β (Figure 4(b)), and IL-6 (Figure 4(c)) were significantly increased in the IG group compared with the UIG group ($P < 0.01$).Conversely, compared with the IG group, the *D. dao* high-dose group and low-dose group could dramatically decrease the serum levels of TNF-α, IL-1β, and IL-6 ($P < 0.05$ or $P < 0.01$) on day 5, day 10, and day 15.

3.4. Effect of D. dao on Growth Factors. The representative western blot bands of GAPDH, VEGFA, and TGF-β_1 are given in Figure 5(a). In HDG group, the protein levels of VEGFA (Figure 5(b)) and TGF-β_1 (Figure 5(c)) significantly increased on day 5 (1.00 ± 0.12-fold for VEGFA, 1.49 ± 0.33-fold for TGF-β_1), day 10 (1.00 ± 0.12-fold for VEGFA, 0.62 ± 0.13-fold for TGF-β_1), and day 15 (1.00 ± 0.12-fold for VEGFA, 0.56 ± 0.08-fold for TGF-β_1); these levels increased in LDG group on day 5 (0.77 ± 0.13-fold for VEGFA, 1.07 ± 0.24-fold for TGF-β_1), day 10 (0.94 ± 0.08-fold for VEGFA, 0.53 ± 0.16-fold for TGF-β_1), and day 15 (0.51 ± 0.02-fold for VEGFA, 0.46 ± 0.06-fold for TGF-β_1) after wounding in comparison with those of IG group.

Moreover, immunohistochemistry microscopy was performed to verify whether treatment with *D. dao* could upregulate VEGFA expression. Low-magnification (x10) images of wounds are shown in Figure 6(a) and the high-magnification (x40) images are shown in Figure 6(b). On day 5, VEGFA-related expression was observed everywhere in inflammatory cells, neutrophils, and lymphocytes, and in endothelial cells and fibroblasts; VEGFA expression in IG group was found significantly lower than that in other groups. On days 10 and 15, it was observed that VEGFA expression in endothelial cells and fibroblasts was significantly reduced.

3.5. Effect of D. dao on NF-κB Signaling. Whether *D. dao* affected NF-κB signaling was examined. *D. dao* effectively inhibited degradation of the inhibitory proteins IκBα and p-IκBα in a dose-dependent manner (Figure 7(a)). Likewise, the phosphorylation of both p–NF–κB p65 and NF-κB p65 was inhibited by *D. dao* in a dose-dependent manner (Figure 7(b)). The phosphorylation status of IKKα/β proteins was also examined, namely, the upstream of the p-IκBα/NF-κB complex. IKKα/β protein phosphorylation was dramatically upregulated by infection stimulation, and this phosphorylation was significantly inhibited through

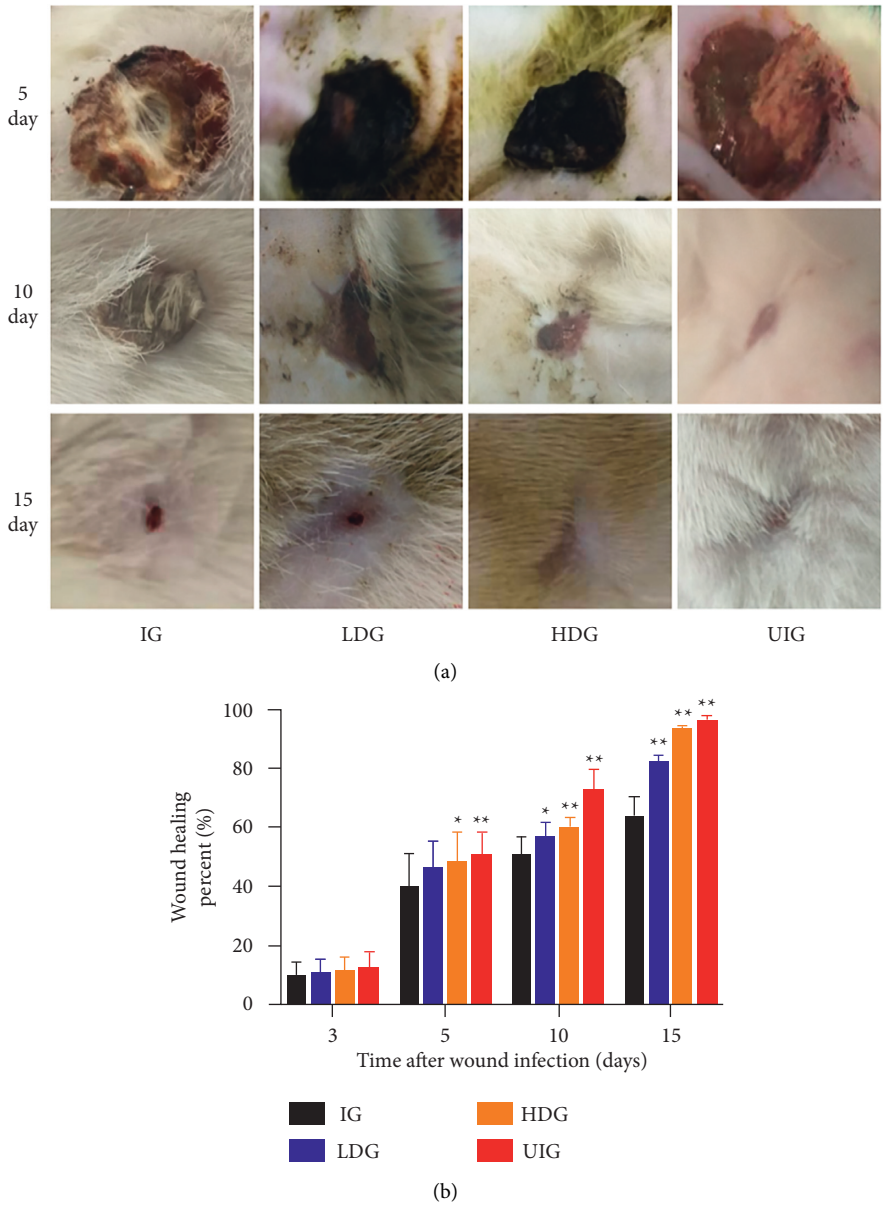

Figure 2: Effect of *D. dao* on gross appearance of healing wound and percentage of wound contraction (calculated in respect to day 0) on days 5, 10, and 15 after wounding in rats. (a) The other groups showed progressively better wound closure, as compared to the IG group. (b) Percentage of wound contraction in the other groups was greater, as compared to control. All values are represented as mean ± SD, $n = 6$ animals in each group. Significance was determined by ANOVA followed by Dunnett's test. $^{*}P < 0.05$ and $^{**}P < 0.01$ vs. IG group.

rhododendrin treatment [28] (Figures 7(c)and 7(d)). These results imply that the NF-κB signaling pathway is affected by *D. dao*, rendering it a useful anti-inflammatory therapy.

3.6. Effect of D. dao on MAPK and PI3K/Akt Signaling. Whether *D. dao* could inhibit MAPK (Figures 8(a) and 8(b)) and PI3K/Akt (Figures 9(a) and 9(b)) signaling pathways, which were also activated by infection stimulation, was determined as well. In terms of MAPK signaling, *D. dao* effectively inhibited phosphorylation of ERK1/2, MEK, p38, JNK, and Akt in HDG group. These results imply that *D. dao* can inhibit MAPK and PI3K/Akt signaling, as well as NF-κB signaling.

4. Discussion

This study aims to investigate the antimicrobial activity and anti-inflammatory effects of *D. dao* on the *E. coli*-treated wound skins under the simulated space environment. The results show that *D. dao* could significantly increase the healing rate of infectious wounds in rats, thereby shortening healing time, promoting the growth of granulation tissue, reducing inflammatory factor infiltration, promoting epidermal division, and exerting antibacterial effects. This study establishes an infectious wound model in rats on the simulation space environmental drug screening platform, which provides a reference for preparing a diseased animal model that is more fitted with the aerospace environment. The

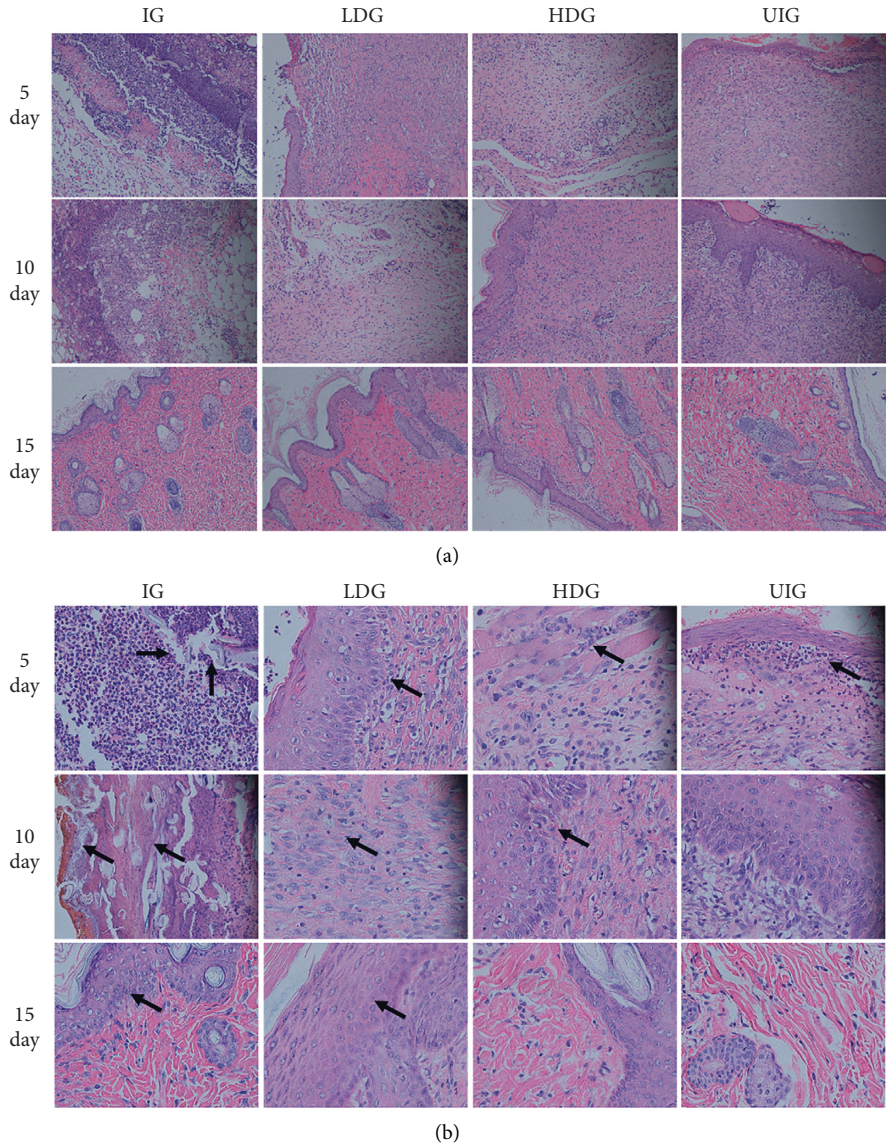

Figure 3: Representative images of H&E-stained histologic wound sections of IG, LDG, HDG, and UIG groups on days 5, 10, and 15 after wounding (x10 magnification shown in (a) and x40 magnification shown in (b)). H&E staining sections at 5, 10, and 15 days show that the other groups accelerated to the recovery of epidermis and reconstruction of skin appendage as compared to the IG group.

results of the experimental research revealed the antimicrobial activity and anti-inflammatory effects, as well as possible mechanism, of *D. dao* on bacterial infection wounds in rats under simulated space environment. This study provides an experimental basis for the development of *D. dao* as a bacterial infectious disease drug in the state of the simulated space environment.

Trauma may occur during long-term missions in the space station, such as tearing and open fractures. Wound healing is a process of simultaneous interaction of various cytokines and growth factors, disorder and change of which will result in damage to wound healing [29]. Normal wound healing consists of four stages: hemostasis, inflammation, proliferation, and remodeling. Bacterial infection is one of the main complex factors affecting wound healing by affecting several inflammatory and growth factors [30, 31].

D. dao is a traditional Chinese medicine with a long history for treating bedsore, ulcer, skin ulcer, and other infection diseases, main active ingredients of which are flavonoids and phenolic acids, which have significant antimicrobial, anti-inflammatory, and anti-infective activities [18]. In this study, we demonstrated that topical application of *D. dao* under simulated space environment can correct disordered infection wound healing by balancing the expression of various inflammatory mediators and growth factors during healing. Figure 2(b) shows that, compared with IG group, the wound healing rate of HDG group increased significantly from 5th day to 15th day. The results showed that the wound healing rate was significantly accelerated after *D. dao* application. On day 15, the wound almost completely healed. Compared with IG group, the expression of angiogenesis-related factors such as VEGFA

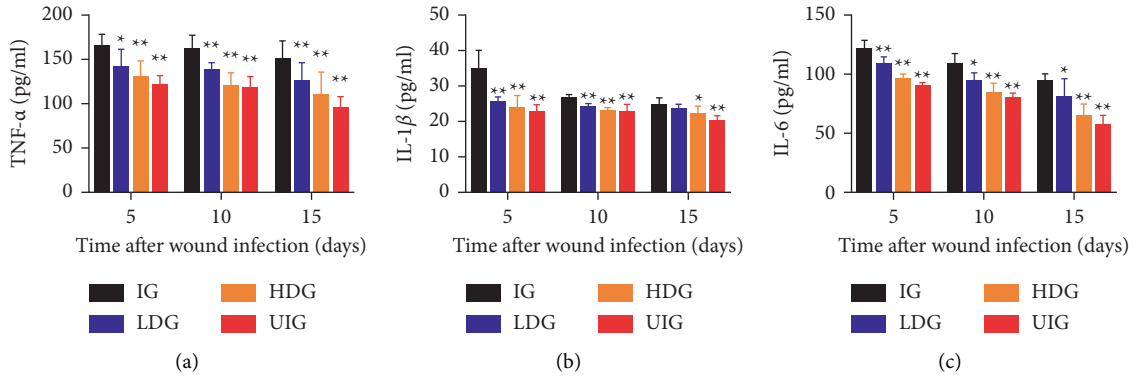

FIGURE 4: *D. dao* inhibits proinflammatory mediator expression and production in granulation/healing tissue of rats on days 5, 10, and 15 after wounding. (a) The expression of TNF-α. (b) The expression of IL-1β. (c) The expression of IL-6. Data were expressed as mean ± SD ($n = 6$). Significance was determined by ANOVA followed by Dunnett's test. $^{*}P < 0.05$ and $^{**}P < 0.01$ vs. IG group.

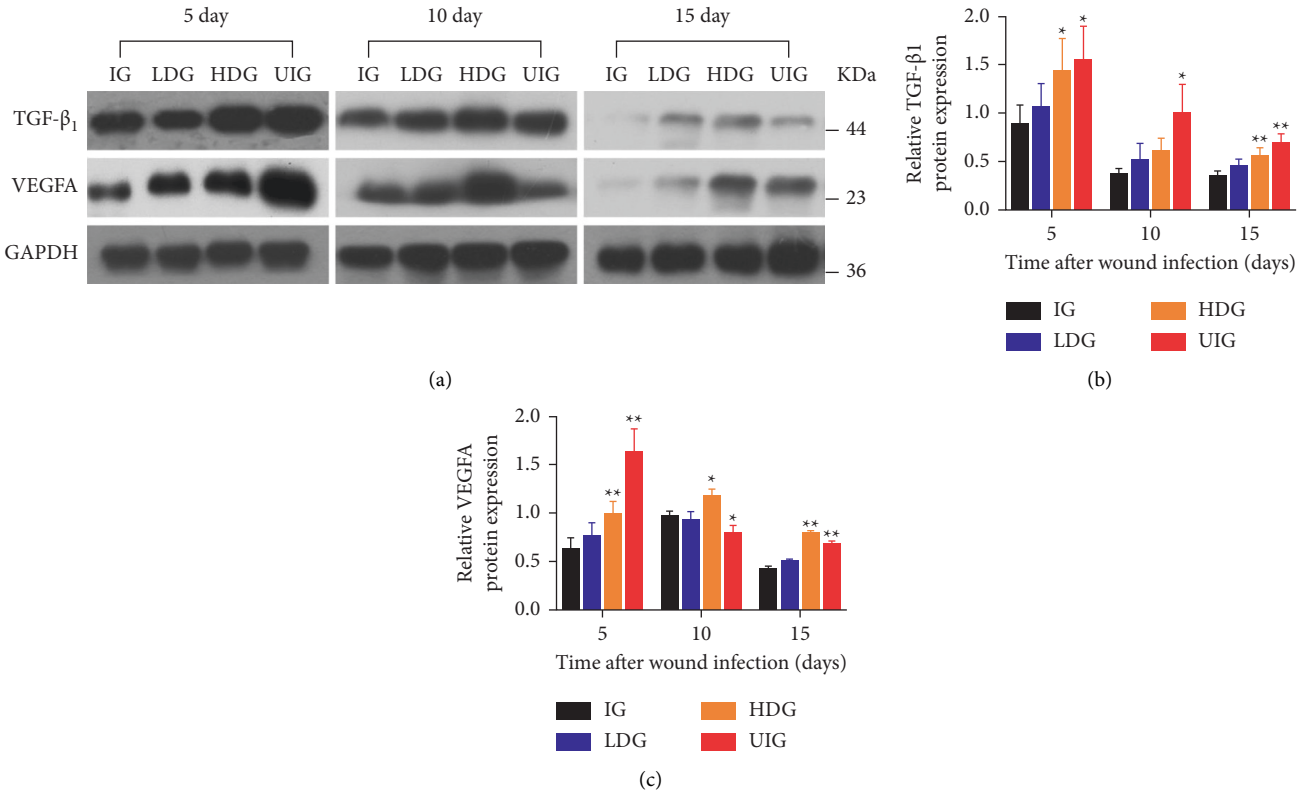

FIGURE 5: Effects of *D. dao* on the protein expression of TGF-β1 and VEGFA. (a) The western blot bands of TGF-β1 and VEGFA. (b) The relative protein expression of TGF-β1. (c) The relative protein expression of VEGFA. These proteins were normalized by GAPDH at each time point and values are expressed as relative change compared to IG group. Data were expressed as mean ± SD ($n = 3$). Significance was determined by ANOVA followed by Dunnett's test. $^{*}P < 0.05$ and $^{**}P < 0.01$ vs. the IG group.

and TGF-β1 was upregulated in HDG group, while the expression of inflammatory factors (TNF-α, IL-6, and IL-1β) was downregulated.

Granulation tissue is the basis for the formation of appropriate healing matrix, which is an immature type composed of inflammatory cells, angioblasts, fibroblasts, collagen fibers, and new blood vessels in the early stage [32, 33]. This immature granulation tissue becomes more mature and durable in the later stage, which is the basic feature of appropriate wound repair [34]. In addition to the formation of ECM during healing, its progressive degradation and remodeling must form mature wound healing tissues in a regulatory manner. The formation and programmed degradation of different cells and components in granulation tissue are influenced by different cytokines (such as TNF-α, IL-6, and IL-1β) and growth factors (such as TGF-β_1 and VEGFA) [35]. Therefore, there should be a sufficient balance between synthesizers and degradants. Collagen is

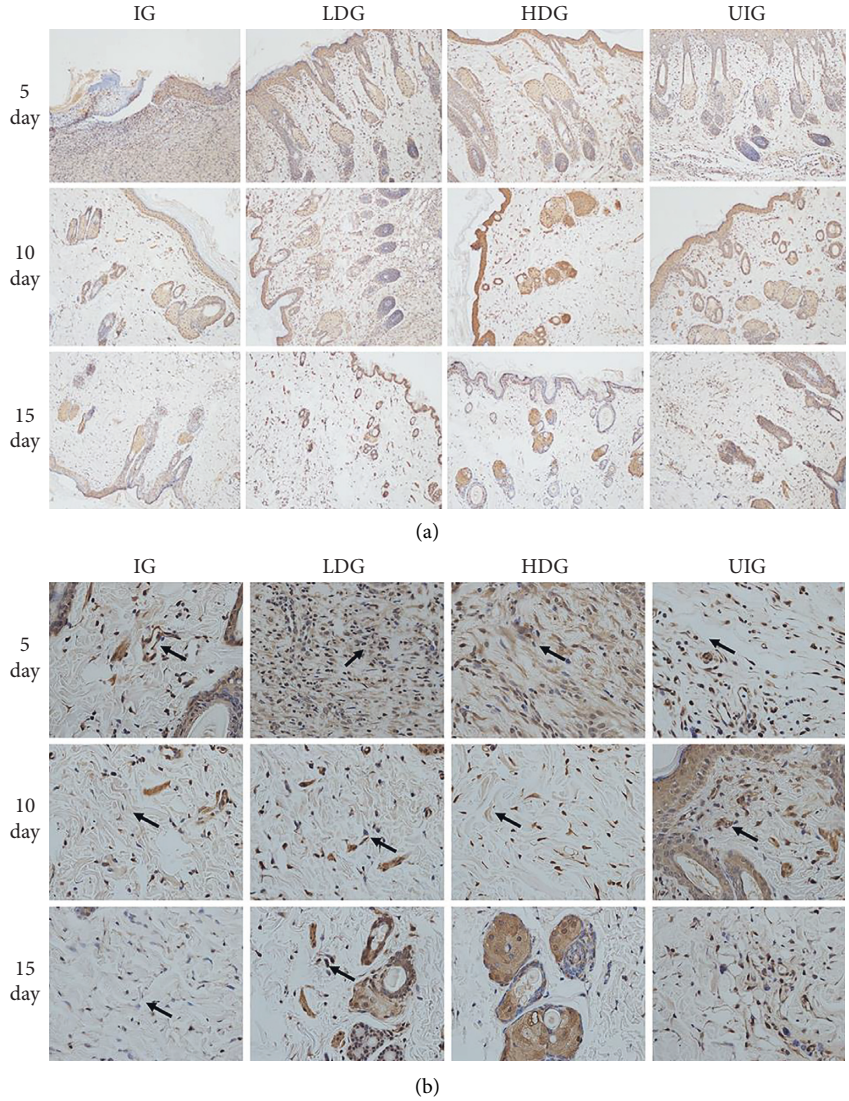

Figure 6: Representative images of immunohistochemistry analysis of the effect of *D. dao* on the expression of VEGFA in IG, LDG, HDG, and UIG groups on days 5, 10, and 15 after wounding (x10 magnification shown in (a) and x40 magnification shown in (b)).

the main component of granulation tissue. The collagen synthesized by fibroblasts depends on TGF-β1, which is very important for wound healing [36]. It is reported that the application of TNF-α reduced the expression of collagen and the tensile strength of wounds [37]. Therefore, the increase of TNF-α level in later stage is harmful to granulation tissue. However, TGF-β_1 is an important factor in the formation of high-quality granulation tissue. If the wound is filled with high-quality granulation tissue, the epithelium begins to form, because the granulation tissue provides a bed for laying the epithelium. Reepithelialization contributes to wound closure by transforming the keratinocytes from stationary phenotypes to migratory and proliferative phenotypes, which are impaired in bacterial infections. This may result from poor-quality granulation tissue and/or failure of keratinocytes transformation. The application of *D. dao* in infection wounds increased the expression of TGF-β_1 (Figure 5(a)) and decreased the expression of TNF-α (Figure 4(b)), which were beneficial to increase collagenous fiber to form granulation tissue and accelerate epithelial regeneration during wound healing.

Angiogenesis is a part of the proliferative phase in wound healing, which involves the migration and proliferation of endothelial cells and angiogenesis. This process begins as early as the third day after injury [37]. VEGFA is a key regulator of many wound healing events, including angiogenesis, epithelialization, and collagen deposition [38]. In addition, it induces vasodilation, endothelial cell migration, and endothelial cell proliferation [39]. Here, we report that, after *D. dao* treatment, the expression of VEGFA in the wound was strongly induced on the 5th day due to bacterial proliferation. However, the expression of VEGFA ©n IG group was significantly lower than that in other groups. Compared with the ^{5t}h day, inflammatory cells in LDG and HDG groups were mainly absorbed by wound tissue, and significant reductions in VEGFA expression were also observed in endothelial cells and fibroblasts on the 1^{0t}h and 1^{5t}h day (Figures 5(a) and 5(c)). The results of WB

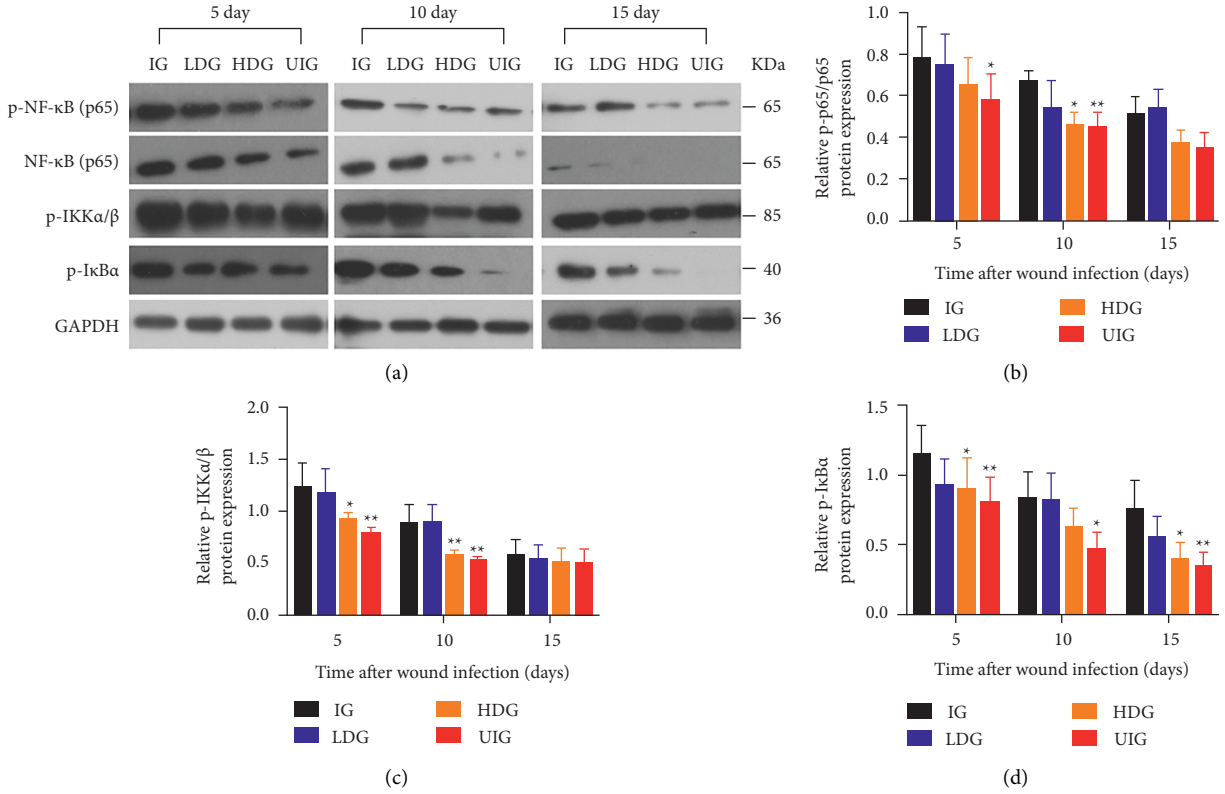

Figure 7: *D. dao* inhibits NF-κB signaling pathway. (a) The western blot bands of p–NF–κB (p65), NF-κB (p65), p-IKKα/β, and p-IκBα. (b) The relative protein expression of p-p65/p65. (c) The relative protein expression of p-IKKα/β. (d) The relative protein expression of p-IκBα. Data were expressed as mean ± SD ($n = 3$). Significance was determined by ANOVA followed by Dunnett's test. $^{*}P < 0.05$ and $^{**}P < 0.01$ vs. IG group.

protein banding expression were consistent with those of immunohistochemistry.

Several cytokines (IL-1β, TNF-α, and IL-6) have been recognized as representative proinflammatory cytokines in wound healing. TNF-α in the inflammatory stage of wound healing can stimulate the chain reaction of inflammation by inducing and activating the expression and production of inflammatory cytokines such as IL-1 and IL-6 [40]. It participates in the initiation of early wound healing response. In wound healing, it can improve tissue repair by promoting the activation of inflammatory cells and regulating immune function as well as accelerating the migration and proliferation of keratinocytes. However, overexpression and imbalance of the relationship with other cytokines will cause a series of inflammatory damage. IL-1β is also a proinflammatory factor produced by macrophage activation, which can stimulate the effect of heat production and promote wound growth and healing and plays a key role in inflammatory response [40]. As the earliest and most important cytokine in inflammation, TNF-α can promote the formation of IL-1, and IL-1 can also induce the release of TNF-α. IL-6 is a multicellular cytokine with a wide range of biological activities, which participates in immune response, inflammatory response, and anti-infection defense. IL-6 promotes gene expression in the nucleus of inflammatory cells, as well as activation and aggregation of neutrophils, and induces the production of acute reactive protein in liver tissue through binding to receptors to activate the signal transduction pathway of MAPK, which is an important indicator reflecting the severity of inflammation and tissue injury, and its expression is positively correlated with the degree of trauma [41]. The level of IL-6 in patients with severe multiple trauma increased significantly, especially in patients with coinfection, so it can be used as one of the indicators to judge the degree of inflammation [31]. The results of this study showed that proinflammatory factors showed dynamic changes in the process of wound healing. Longitudinal comparison showed a downward trend at three time points, indicating that the inflammatory state was intrinsically related to wound healing. In the course of the disease, proinflammatory factors, such as TNF-α, IL-6, and IL-1β, showed synergy, which may be related to the abovementioned inflammatory chain reaction. The expression of TNF-α, IL-6, and IL-1β in IG group was significantly higher than that in normal group at each time points, which was negatively correlated with wound healing time, indicating that pathological inflammation caused by high expression of proinflammatory factors was one of the causes of delayed healing of infection wounds. The expression of TNF-α, IL-6, and IL-1β in the two groups intervened by *D. dao* decreased significantly than that in IG group, and the healing rate increased significantly at the same time point, suggesting that the regulation of proinflammatory factors could affect the wound healing rate. In addition, the wound treated

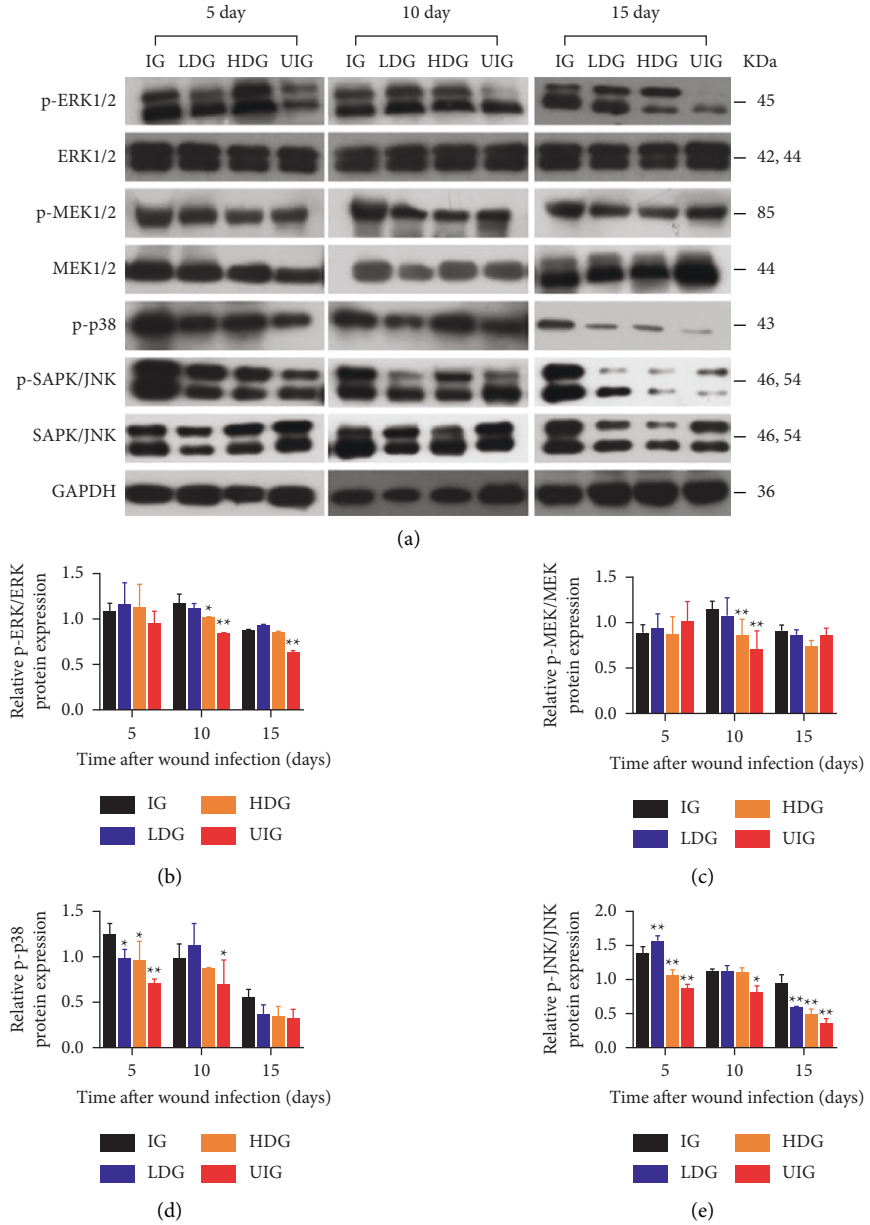

Figure 8: *D. dao* inhibits MAPK signaling pathway. (a) The western blot bands of p-ERK1/2, ERK1/2, p-MEK, MEK, p-p38, and JNK. (b) The relative protein expression of p-ERK/ERK. (c) The relative protein expression of p-MEK/MEK. (d) The relative protein expression of p-p38. (e) The relative protein expression of p-JNK/JNK. Data were expressed as mean ± SD ($n = 3$). Significance was determined by ANOVA followed by Dunnett's test. $^{*}P < 0.05$ and $^{**}P < 0.01$ vs. the IG group.

by *D. dao* regenerated epithelial layer in a short time due to the lower level of inflammation and the increased fibroblasts (H&E staining, Figure 3(a)), eventually resulting in faster wound closure.

To clarify the target pathway of *D. dao* therapy, we first studied the NF-κB signaling pathway, namely, a major therapeutic target pathway activated by common inflammatory diseases. The binding of TNF-α to TNF receptor (TNFR) activates the NF-κB pathway and induces chronic inflammatory diseases such as rheumatoid arthritis, inflammatory bowel disease, multiple sclerosis, and atherosclerosis [42, 43]. *D. dao* treatment reduced the degradation and phosphorylation of IκBα and NF-κB p65 and inhibited the phosphorylation of upstream signal protein IKKα/β, suggesting that *D. dao* affected the formation of IKK complex in the NF-κB signaling pathway (Figure 7). Because inflammation is a complex network involved in multiple signal cascades, we also studied the effects of *D. dao* on other signaling pathways. It effectively inhibits signal transduction pathway of MAPK and PI3K/Akt (Figures 8 and 9). The signal pathways were summarized and presented in Figure 10. Our results suggest that *D. dao* is related to the inhibition of proinflammatory mediators, the enhancement of growth factor expression, and the inhibition of NF-kappa

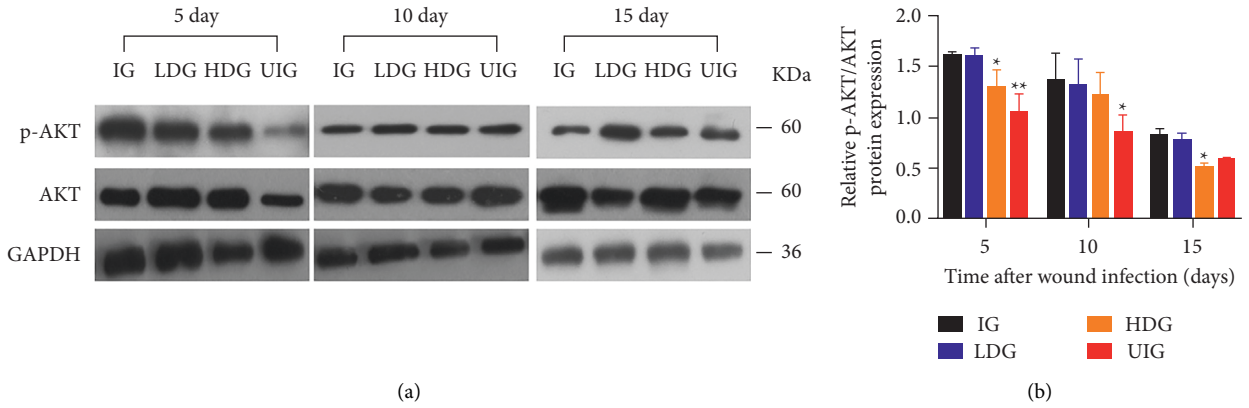

FIGURE 9: *D. dao* inhibits PI3K/Akt signaling pathway. (a) The western blot images of p-Akt and Akt. (b) The relative protein quantification in granulation/healing tissue of rats on days 5, 10, and 15 after wounding. These proteins were normalized by GAPDH at each time point and values are expressed as relative change compared to IG group. Data were expressed as mean ± SD ($n = 3$). Significance was determined by ANOVA followed by Dunnett's test. $^{*}P < 0.05$ and $^{**}P < 0.01$ vs. the IG group.

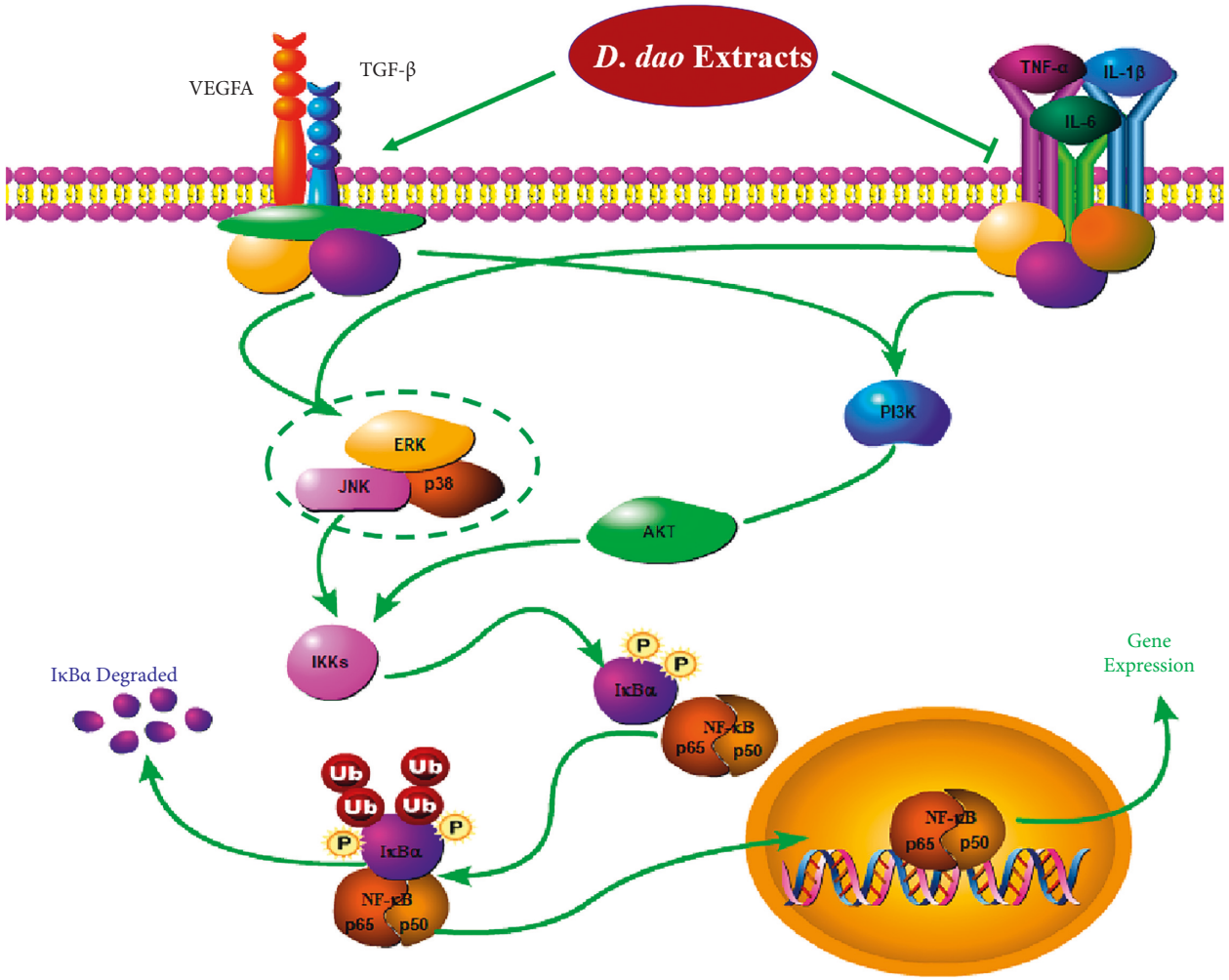

FIGURE 10: The summarized action pathways of *D. dao* on the infected wound.

B, MAPK, and PI3K/Akt signaling pathways. In conclusion, these results support the potential use of *D. dao* as a novel local anti-inflammatory agent for wound infection (Figure S1: preliminary phytochemical study of *D. dao*. The mass spectrum of L-epicatechin (a), syringic acid (b), catechin hydrate (c), quercetin (d), gallic acid (e), methyl gallate (f), ethyl gallate (g), apigenin (h), and naringenin (i)).

5. Conclusion

The results reveal that *D. dao* application accelerates the timely progression of infective wound healing by regulating the expression of a number of cytokines and growth factors, including TNF-α, IL-6, IL-1β, VEGFA, and TGF-β_1. It reduces inflammation and angiogenesis and improves maturation of infective wound. The mechanistic studies demonstrate that *D. dao* inhibits NF-κB signaling as well as MAPK and PI3K/Akt signaling pathways. In conclusion, *D. dao* has shown potential in the treatment of cutaneous wounds in infective wound and it could be envisioned as a new agent for accelerating infective wound healing in the space station.

Abbreviations

D. dao: *Dracontomelon dao*
EtOAc: Ethyl acetate
E. coli: *Escherichia coli*
P. aeruginosa: *Pseudomonas aeruginosa*
S. aureus: *Staphylococcus aureus*
IL-6: Interleukin-6
IL-1β: Interleukin-1β
TNF-α: Tumor necrosis factor-α
VEGFA: Vascular endothelial growth factor A
TGF-β1: Transforming growth factor-β
NF-κB: Nuclear factor kappa-B
PI3K: Phosphoinositide 3-kinase
MAPK: Mitogen-activated protein kinase
IG: Infection group
LDG: Low-dosage group
HDG: High-dosage group
UIG: Uninfection group
HE: Hematoxylin-eosin
ELISA: Enzyme-linked immunosorbent assay
PMSF: Phenylmethylsulfonyl fluoride
BCA: Bicinchoninic acid assay
PVDF: Polyvinylidene difluoride
SD: Standard deviation
ANOVA: One-way analysis of variance.

Data Availability

The datasets used and/or analyzed in this study can be obtained from the corresponding author upon reasonable request.

Ethical Approval

The Chinese PLA General Hospital approved this project.

Conflicts of Interest

The authors declare that there are no conflicts of interest.

Authors' Contributions

J.-x. Wen conceived the study and wrote the manuscript. Z. Xu prepared the samples. X. Ma checked the data. Y.-l. Zhao designed the study and amended the paper. All data were generated in-house, and no paper mill was used. All authors agree to be accountable for all aspects of work ensuring integrity and accuracy.

Acknowledgments

This work was financially supported by the National Major Drug Discovery Project of China (Grant no. 2015ZX09J15102-004), Science Foundation of Sichuan Education Department (18ZA0186), and Xihua University Talent Introduction Project (Z211060).

Supplementary Materials

Supplemental File 1: preliminary phytochemical study of *D. dao.* (*Supplementary Materials*)

References

[1] S. S. Panesar, J. C. Fernandez-Miranda, M. Kliot, and K. Ashkan, "Neurosurgery and manned spaceflight," *Neurosurgery*, vol. 86, no. 3, pp. 317–324, 2020.
[2] G. Senatore, F. Mastroleo, N. Leys, and G. Mauriello, "Effect of microgravity & space radiation on microbes," *Future Microbiology*, vol. 13, pp. 831–847, 2018.
[3] L. Zea, M. Larsen, F. Estante et al., "Phenotypic changes exhibited by *E. coli* cultured in space," *Frontiers in Microbiology*, vol. 8, 2017.
[4] D. P. Engelhart, J. Patton, E. Plis et al., "Space environment simulation and sensor calibration facility," *Review of Scientific Instruments*, vol. 89, Article ID 023301, 2018.
[5] S. Grover, "Skin in aviation and space environment," *Indian Journal of Dermatology, Venereology and Leprology*, vol. 77, no. 4, pp. 413–417, 2011.
[6] P. Mehta and D. Bhayani, "Impact of space environment on stability of medicines: challenges and prospects," *Journal of Pharmaceutical and Biomedical Analysis*, vol. 136, pp. 111–119, 2017.
[7] Y. Zhang, M. Moreno-Villanueva, S. Krieger, G. Ramesh, S. Neelam, and H. Wu, "Transcriptomics, NF-κB pathway, and their potential spaceflight-related health consequences," *International Journal of Molecular Sciences*, vol. 18, no. 6, 2017.
[8] H. W. Kim and M. S. Rhee, "Influence of low-shear modeled microgravity on heat resistance, membrane fatty acid composition, and heat stress-related gene expression in *Escherichia coli* O157:H7 ATCC 35150, ATCC 43889, ATCC 43890, and ATCC 43895," *Applied and Environmental Microbiology*, vol. 82, no. 10, pp. 2893–2901, 2016.
[9] C. Liu, "The theory and application of space microbiology: China's experiences in space experiments and beyond," *Environmental Microbiology*, vol. 19, no. 2, pp. 426–433, 2017.
[10] A. P. Taylor and Sommer, "Towards rational treatment of bacterial infections during extended space travel,"

International Journal of Antimicrobial Agents, vol. 26, no. 3, pp. 183–187, 2005.

[11] A. N. Aziz, H. Ibrahim, D. Rosmy Syamsir, M. Mohtar, J. Vejayan, and K. Awang, "Antimicrobial compounds from Alpinia conchigera," *Journal of Ethnopharmacology*, vol. 145, no. 3, pp. 798–802, 2013.

[12] Y. D. Boakye, C. Agyare, G. P. Ayande, N. Titiloye, E. A. Asiamah, and K. O. Danquah, "Assessment of wound-healing properties of medicinal plants: the case of Phyllanthus muellerianus," *Frontiers in Pharmacology*, vol. 9, no. 9, 2018.

[13] J. Choi, Y. G. Park, M. S. Yun, and J. W. Seol, "Effect of herbal mixture composed of Alchemilla vulgaris and Mimosa on wound healing process," *Biomedicine and Pharmacotherapy*, vol. 106, pp. 326–332, 2018.

[14] S. Liu, Y. Zhao, N. Zeng et al., "Anti-bacterial effect of four extracts from leaves of Dracontomelon dao on *Escherichia coli* growth using microcalorimetry coupled with principal component analysis," *Journal of Thermal Analysis and Calorimetry*, vol. 116, no. 1, pp. 491–497, 2013.

[15] Y. Yuniati, N. Hasanah, S. Ismail, S. Anitasari, and S. Paramita, "Antibacterial activity of dracontomelon dao extracts on methicillin-resistant S. Aureus (mrsa) and *E. coli* multiple drug resistance (mdr)," *African Journal of Infectious Diseases*, vol. 12, pp. 62–67, 2018.

[16] M. R. Khan and A. D. Omoloso, "Antibacterial and antifungal activities of Dracontomelon dao," *Fitoterapia*, vol. 73, no. 4, pp. 327–330, 2002.

[17] Y. Li, H. Xia, M. Wu et al., "Evaluation of the antibacterial effects of flavonoid combination from the leaves of dracontomelon dao by microcalorimetry and the quadratic rotary combination design," *Frontiers in Pharmacology*, vol. 8, 2017.

[18] M. Wu, F. Qu, Y. Zhao et al., "Microcalorimetry and turbidimetry to investigate the anti-bacterial activities of five fractions from the leaves of Dracontomelon dao on *P. aeruginosa*," *Journal of Thermal Analysis and Calorimetry*, vol. 123, no. 3, pp. 2367–2376, 2015.

[19] Y. Zhao, S. Liu, F. Qu et al., "Calorimetry, Microcalorimetry coupled with principal component analysis for investigating the anti- *Staphylococcus aureus* effects of different extracted fractions from Dracontomelon dao," *Journal of Thermal Analysis and Calorimetry*, vol. 120, no. 1, pp. 913–920, 2015.

[20] J. P. He, X. Feng, J. f. Wang et al., "Icariin prevents bone loss by inhibiting bone resorption and stabilizing bone biological apatite in a hindlimb suspension rodent model," *Acta Pharmacologica Sinica*, vol. 39, no. 11, pp. 1760–1767, 2018.

[21] H. Kang, Y. Fan, P. Zhao, C. Ren, Z. Wang, and X. Deng, "Regional specific modulation of the glycocalyx and smooth muscle cell contractile apparatus in conduit arteries of tail-suspended rats," *Journal of Applied Physiology*, vol. 120, no. 5, pp. 537–545, 2016.

[22] W.-Y. Li, X.-Y. Li, Y. H. Tian et al., "Pulsed electromagnetic fields prevented the decrease of bone formation in hindlimb-suspended rats by activating sAC/cAMP/PKA/CREB signaling pathway," *Bioelectromagnetics*, vol. 39, no. 8, pp. 569–584, 2018.

[23] V. F. Suzuki-Banhesse, F. F. Azevedo, E. P. Araujo et al., "Effect of atorvastatin on wound healing in rats," *Biological Research for Nursing*, vol. 17, no. 2, pp. 159–168, 2015.

[24] Z. Deng, F. Liu, and C. Li, "Therapeutic effect of ethylenediaminetetraacetic acid irrigation solution against wound infection with drug-resistant bacteria in a rat model: an animal study," *Bone and Joint Research*, vol. 8, no. 5, pp. 189–198, 2019.

[25] N. Tatiya-Aphiradee, W. Chatuphonprasert, and K. Jarukamjorn, "Anti-inflammatory effect of Garcinia mangostana Linn. pericarp extract in methicillin-resistant Staphylococcus aureus-induced superficial skin infection in mice," *Biomedicine and Pharmacotherapy*, vol. 111, pp. 705–713, 2019.

[26] Z. Xu, H. Li, X. Qin et al., "Antibacterial evaluation of plants extracts against ampicillin-resistant *Escherichia coli* (*E. coli*) by microcalorimetry and principal component analysis," *AMB Express*, vol. 9, no. 1, p. 101, 2019.

[27] M. Ram, V. Singh, S. Kumawat et al., "Deferoxamine modulates cytokines and growth factors to accelerate cutaneous wound healing in diabetic rats," *European Journal of Pharmacology*, vol. 764, pp. 9–21, 2015.

[28] Y. J. Jeon, B. H. Kim, S. Kim et al., "Rhododendrin ameliorates skin inflammation through inhibition of NF-κB, MAPK, and PI3K/Akt signaling," *European Journal of Pharmacology*, vol. 714, pp. 7–14, 2013.

[29] M. Ram, V. Singh, S. Kumawat, V. Kant, S. K. Tandan, and D. Kumar, "Bilirubin modulated cytokines, growth factors and angiogenesis to improve cutaneous wound healing process in diabetic rats," *International Immunopharmacology*, vol. 30, pp. 137–149, 2016.

[30] Y. Kim, Y.-S. Lee, J.-Y. Yang, S.-H. Lee, Y.-Y. Park, and M.-N. Kweon, "The resident pathobiont Staphylococcus xylosus in Nfkbiz-deficient skin accelerates spontaneous skin inflammation," *Scientific Reports*, vol. 7, no. 1, p. 6348, 2017.

[31] S. E. Moghadam, M. Moridi Farimani, S. Soroury, S. N. Ebrahimi, and E. Jabbarzadeh, "Hypermongone C accelerates wound healing through the modulation of inflammatory factors and promotion of fibroblast migration," *Molecules*, vol. 24, 2019.

[32] S. K. Dev, P. K. Choudhury, R. Srivastava, and M. Sharma, "Antimicrobial, anti-inflammatory and wound healing activity of polyherbal formulation," *Biomedicine and Pharmacotherapy*, vol. 111, pp. 555–567, 2019.

[33] A. Russo, E. Concia, F. Cristini et al., "Current and future trends in antibiotic therapy of acute bacterial skin and skin-structure infections," *Clinical Microbiology and Infections*, vol. 22, pp. S27–S36, 2016.

[34] V. Kant, A. Gopal, D. Kumar et al., "Curcumin-induced angiogenesis hastens wound healing in diabetic rats," *Journal of Surgical Research*, vol. 193, no. 2, pp. 978–988, 2015.

[35] Y. S. Wu and S. N. Chen, "Apoptotic cell: linkage of inflammation and wound healing," *Frontiers in Pharmacology*, vol. 5, no. 1, 2014.

[36] A. D. Kandhare, J. Alam, M. V. K. Patil, A. Sinha, and S. L. Bodhankar, "Wound healing potential of naringin ointment formulation via regulating the expression of inflammatory, apoptotic and growth mediators in experimental rats," *Pharmaceutical Biology*, vol. 54, no. 3, pp. 419–432, 2015.

[37] T. Tang, L. Yin, J. Yang, and G. Shan, "Emodin, an anthraquinone derivative from Rheum officinale Baill, enhances cutaneous wound healing in rats," *European Journal of Pharmacology*, vol. 567, no. 3, pp. 177–185, 2007.

[38] H. H. Jeon, Q. Yu, Y. Lu et al., "FOXO1 regulates VEGFA expression and promotes angiogenesis in healing wounds," *The Journal of Pathology*, vol. 245, no. 3, pp. 258–264, 2018.

[39] M. N. Salim, D. Masyitha, A. Harris et al., "Anti-inflammatory activity of Jatropha curcas Linn. latex in cream formulation on CD68 expression in mice skin wound," *Veterinary World*, vol. 11, no. 2, pp. 99–103, 2018.

[40] M. Rodrigues, N. Kosaric, C. A. Bonham, and G. C. Gurtner, "Wound healing: a cellular perspective," *Physiological Reviews*, vol. 99, no. 1, pp. 665–706, 2019.

[41] H. H. Arab, S. A. Salama, and I. A. Maghrabi, "Camel milk ameliorates 5-fluorouracil-induced renal injury in rats: targeting MAPKs, NF-κB and PI3K/Akt/eNOS pathways," *Cellular Physiology and Biochemistry*, vol. 46, no. 4, pp. 1628–1642, 2018.

[42] D. S. El-Agamy, K. M. El-Harbi, S. Khoshhal et al., "Pristimerin protects against doxorubicin-induced cardiotoxicity and fibrosis through modulation of Nrf2 and MAPK/NF-κB signaling pathways," *Cancer Management and Research*, vol. 11, pp. 47–61, 2019.

[43] S. Qi, Y. Xin, Y. Guo et al., "Ampelopsin reduces endotoxic inflammation via repressing ROS-mediated activation of PI3K/Akt/NF-κB signaling pathways," *International Immunopharmacology*, vol. 12, no. 1, pp. 278–287, 2012.

Hindawi
Evidence-Based Complementary and Alternative Medicine
Volume 2022, Article ID 5769555, 11 pages
https://doi.org/10.1155/2022/5769555

Research Article

Efficacy of *Acacia nilotica* Linn. Pod's Sitz Bath plus Vaginal Pessary in Syndromic Management of Abnormal Vaginal Discharge: A Randomized Controlled Trial

Rushda Saeedi,[1] **Arshiya Sultana**,[1] **Khaleequr Rahman**,[2] **Md Belal Bin Heyat**,[3,4,5] **Mohammad Amjad Kamal**,[6,7,8,9] **and Mumuni Ishawu**[10]

[1]*Department of Amraze Niswan wa Ilmul Qabalat, National Institute of Unani Medicine, Ministry of AYUSH, Government of India, Bengaluru 560091, Karnataka, India*
[2]*Department of Ilmul Saidla, National Institute of Unani Medicine, Ministry of AYUSH, Government of India, Bengaluru 560091, Karnataka, India*
[3]*IoT Research Center, College of Computer Science and Software Engineering, Shenzhen University, Shenzhen, Guangdong 518060, China*
[4]*International Institute of Information Technology, Hyderabad, Telangana 500032, India*
[5]*Department of Science and Engineering, Novel Global Community Educational Foundation, Hebersham, NSW 2770, Australia*
[6]*Institute for Systems Genetics, Frontier Science Center for Disease-related Molecular Network, West China Hospital, Sichuan University, Chengdu 610041, Sichuan, China*
[7]*King Fahd Medical Research Center, King Abdulaziz University, Saudi Arabia*
[8]*Department of Pharmacy, Faculty of Allied Health Sciences, Daffodil International University, Bangladesh*
[9]*Enzymoics, Novel Global Community Educational Foundation, Hebersham, NSW 2770, Australia*
[10]*Faculty of Business and Management Studies, Koforidua Technical University, Koforidua, Ghana*

Correspondence should be addressed to Arshiya Sultana; drarshiya@yahoo.com and Mumuni Ishawu; ishawu.mumuni1975@gmail.com

Received 3 January 2022; Accepted 4 May 2022; Published 25 May 2022

Academic Editor: Yanhong Zhu

Objectives. Abnormal vaginal discharge (*Sayalan al-Rahim*) is a common public health problem that significantly disrupts the health-related quality of life (HRQoL). Syndromic management infers the concurrent treatment of two or more infections. Hence, a comparative, single-blind study was planned to determine the efficacy of *Acacia* (*Acacia nilotica* Linn.) pod's sitz bath (*Abzan*) plus vaginal pessary (*Farzaja*) vs. placebo in abnormal vaginal discharge syndromic management, its associated symptoms, and women's HRQoL. *Methods*. Diagnosed patients ($n = 66$) were randomly divided into *Acacia* ($n = 33$) and placebo ($n = 33$) group. *Acacia* group received Sitz bath with *Acacia* pod powder (30g) solution followed by vaginal cotton pessary (5 ml of the same solution) once daily for 10 days. The placebo group received palm sugar powder (30g) solution for Sitz bath plus vaginal cotton pessary same as the *Acacia* group. Primary outcomes included clinical cure assessed with VAS for symptoms and Modified McCormack Pain Scale (McPS) for pelvic tenderness. The secondary outcomes included were the EQ-5D-5 L questionnaire, TSQM questionnaire, sachet count, and microbiological cure. Overall, therapeutic cure included clinical and microbiological cure after treatment. *Results*. The overall therapeutic cure for bacterial vaginosis, cervicitis, and uncomplicated pelvic inflammatory disease was 100% ($n = 7/7$), 45.45% ($n = 10/22$), and 71.42% ($n = 5/7$), respectively, in the *Acacia* group, while in the placebo group none of the patients had responded. The VAS score for symptoms was significantly reduced in *Acacia* than in the placebo group. At each follow-up, the improvement in the EQ-5D-5 L level of HRQoL was significantly higher in the *Acacia* group than in the placebo group. *Conclusion*. *Acacia* would be an effective and safe alternative in syndromic management of abnormal vaginal discharge, associated symptoms, and improved women's HRQoL. *Trial registration*. This trial was registered in the Clinical Trials Registry of Indian Trials Website and given the identification no. CTRI/2018/02/012175 (dated: 27/02/2018).

1. Introduction

Abnormal vaginal discharge (*Sayalan al-Rahim*) is the commonest gynaecological problem in women [1] reported (21.8%) in reproductive tract infection (RTI) after abnormal uterine bleeding (AUB). Almost ten million clinical visits each year are ascribed to vaginal discharge complaints. It is more common in women in developing countries, and available evidence suggests that about one-fourth of these women are having this complaint [2]. The ICMR conducted a hospital-based study in Delhi and reported the prevalence of abnormal vaginal discharge (AVD) is about 30% in women with RTIs. *Gardnerella vaginalis*, *Trichomonas vaginalis*, *Candida*, aerobic and anaerobic microbes, viruses, *Chlamydia*, etc. are various organisms that cause RTIs [1]. Lower reproductive tract infections are more common in Indian reproductive age women [3]. These infections can lead to long-term complications in women such as infertility, ectopic pregnancy, pelvic inflammatory disease, and propensity towards neoplasia with noteworthy morbidity that affects the quality of life and leads to a substantial burden on the healthcare system [4]. Abnormal white/vaginal discharge in women is associated with various other symptoms such as pruritus vulvae, backache, dysuria, and burning micturition. The syndromic approach (WHO 2005) is employed to manage vaginal infections by healthcare providers. Syndromic management is established on the patient's symptoms and infers the concurrent treatment of two or more infections [5]. Clinically, depending on the pathogenic infection, the first choice to treat infective vaginal discharge is antibiotics. To cure or prevent infections, no single broad-spectrum formulations are currently available for intravaginal use. Most of the drugs used to treat infective vaginal discharge cause side effects. Furthermore, antimicrobial resistance is increasing, rendering some regimens ineffective in several infections [3]. In the current scenario, adverse drug reactions of a chemical drug are one of the reasons for an increased drive observed towards the consumption of herbal drugs in many disease conditions. One of the suggested herbal drugs is *Acacia* (*Acacia nilotica* Linn.) pod for abnormal vaginal discharge.

A. arabica is a moderate-sized, spiny evergreen tree. It is a popular ornamental multipurpose avenue tree from the family Fabaceae and is commonly known as *kikar*. In India, its parts are used in ethnomedicinal practice for the prevention and treatment of various illnesses for many years [6]. In classical Unani medical texts, it has been mentioned that *A. arabica* pods are useful in abnormal vaginal discharge as it possesses anti-inflammatory (*Muhallil al-Waram*), astringent (*Qabiz*), and antiseptic (*Daf'-i-Taffun*) properties [6,7]. Satish et al. (2008) demonstrated the activity of pod *A. arabica* against a few strains of bacteria and fungi [8]. Kalaivani and Methew (2010) also demonstrated the maximum activity of *A. arabica* against *Candida albicans* and anaerobic bacteria [9]. Pharmacologically, this medicinal plant is proven for astringent, antimicrobial, anti-inflammatory, analgesic, antioxidant, and diuretic properties [10–14]. Although a few studies have been carried out on complementary and alternative medicines for abnormal vaginal discharge, bacterial vaginosis and cervicitis are available [3,5,15–20]. However, to date, none of the studies has determined the efficacy of *Acacia* pod's Sitz bath and vaginal pessary in syndromic management of abnormal vaginal discharge, associated symptoms, and women's health-related quality of life (HRQoL). Hence, this study was planned to validate its efficacy.

2. Materials and Methods

2.1. Trial Design. A parallel, single-blind, prospective, single-centre, simple randomized, placebo-controlled trial was carried out with approval from Institutional Ethical Committee (IEC No.NIUM/IEC/2016-17/014/ANQ/06). The study was conducted based on the GCP guidelines, Ministry of AYUSH, Govt. of India, and the Helsinki Declaration. All randomized patients received written and verbal information about the aims and procedures of the research and then signed a consent form to participate in the study. Patients at any point in time had the option to withdraw from the study.

2.2. Participants. Sixty-six patients with abnormal vaginal discharge were recruited from the outpatients and inpatients of our hospital

2.2.1. Inclusion and Exclusion Criteria. Married women between 18 and 50 years of age who had abnormal vaginal discharge and/or associated with low backache, burning micturition, lower abdomen pain, dysuria, dyspareunia, vulvar itching, and irritation were eligible for inclusion.

Patients were excluded from the study, who had undiagnosed uterine or vaginal bleeding, ulceration, vaginal douches, and genital malignancies. Pregnant, lactating, and unmarried women who were suspicious or clinically manifested with venereal disease were also excluded.

2.2.2. Demographic and Clinical Assessment. A general questionnaire including demographic characteristics and relevant history was completed for each patient. The patient's socio-economic status was recorded as per Kuppuswamy's socio-economic scale. At visit 1 (Day 0), the VAS score was calculated for abnormal vaginal discharge and its associated symptoms. The per speculum and vaginum examination were performed to note the Modified McCormack tenderness scale for pelvic pain, the nature, colour, quantity, and consistency of vaginal discharge and other associated clinical features of infections (vaginitis, cervicitis, cervical ectopy, and uncomplicated pelvic inflammatory disease (uPID). A vaginal wet mount test to diagnose bacterial vaginosis, candidiasis and trichomoniasis, and uPID was performed. All laboratory procedures were performed in the pathological laboratory of the National Institute of Unani Medicine. BV was diagnosed with Amsel criteria.

Cervicitis was diagnosed with the presence of congestion, hypertrophy, erosion of the cervix along with the presence of uterine/cervical motion tenderness, thick yellowish or greyish discharge, and the presence of >10 WBC per HPF on saline microscopy. Uncomplicated PID (uPID) was diagnosed as per CDC guidelines the presence of at least one of the following, i.e., uterine tenderness, cervical motion tenderness, or adnexal tenderness, and one or more of the following additional criteria, i.e., abnormal cervical or vaginal thick discharge; the presence of >10 WBCs per HPF or abundant number of WBCs with saline microscopy of vaginal fluid and elevated erythrocyte sedimentation rate were noted. The severity of cervical ectopy was graded as 2a (1/3rd) if it was involved 1/3rd portion of the cervix around the os and 2b (2/3rd) if the involved portion was 2/3rd of the cervix. Routine investigations at baseline were performed to exclude general diseases and sexually transmitted diseases. Wet mount and pap's smears were done at visit 1 (Day 0) and postintervention (days 11–13) for the assessment of the efficacy of the test drug. Pelvic ultrasonography was performed to exclude genital malignancies and other pathologies, respectively, at baseline.

2.3. Intervention. After a thorough literature survey, *Acacia* pod's Sitz bath plus vaginal cotton pessary for abnormal vaginal discharge was selected from the classical Unani literature based on its Unani and pharmacological properties such as antimicrobial, anti-inflammatory, and astringent. The pharmacognosist, Dr S. Noorunnisa Begum (Senior Assistant Professor, Centre for Repository of Medicinal Resources, Trans-Disciplinary University, Bengaluru), authenticated and identified the test drug as pods of *Acacia nilotica* Linn. belonging to the family Fabaceae with specimen number FRLHT Acc. No. 5008. The common name is *Acacia*. The test drug has been deposited in the Department of Pharmacology of our Institute with voucher specimen number 56/UQ/Res/2019 for future reference [Figure 1]

2.3.1. Extract Preparation. Joshanda of pods was modified into dry powder. Dried pods of *A. arabica* Linn. were coarsely powdered and sieved under aseptic precautions. To obtain the extract, the sieved powder was soaked in water (at the ratio of 1 : 4) and boiled at 100°C for an hour and filtered. The filtrate was dried in a hot air oven for four hours at 60°C, and the dry powder was obtained. All procedures were carried out in our pharmacy under the direct supervision of the pharmacist from our research team.

2.3.2. Dispensing of Drugs. To avoid exposure to humidity, 30g extract powder or placebo (palm sugar powder) was packed and dispensed in airtight aluminium sachets. Ten aluminium sachets were dispensed to each patient. One placebo capsule filled with edible cellulose (250 mg) was administered orally in the morning after meal for 10 days in both groups to increase the compliance of the patients.

2.3.3. Dosage and Methods. Patients were advised for a Sitz bath with powder followed by per vaginum cotton pessary soaked in 5 ml of the same solution once daily for 10 days in both groups. Patients were taught verbally how to use their medication for sitz bath and vaginal pessary insertion. All patients were instructed to add and mix the powder of one sachet in 250 ml of lukewarm water, and from this, 5 ml of solution was kept aside for the vaginal pessary and the remaining solution was added in 5 litres of water in a sitz bath for 20 min. After the sitz bath, patients were instructed to insert a vaginal pessary per vagina soaked in 5 ml of solution (which was kept aside) and to remove it the next morning.

2.4. Follow-Up. To minimize the dropout rate, patients were instructed to visit the hospital on Day 3 and days 11–14 during treatment and two follow-ups on days 30–34 and Day 45 without treatment. If patients were not able to visit on Day 3, they were called on mobile to enquire regarding the clinical features and compliance of the research drug. Moreover, they were asked to deliver empty and unused sachets. The side effects were assessed by the researcher, who determined whether the event was study related or not.

2.5. Outcomes. The primary outcomes (clinical and symptomatic response) included a change in VAS score for symptoms (abnormal vaginal discharge, lower abdominal pain, dysuria, burning micturition, dyspareunia, vulvar irritation, and itching) and Modified McCormack Pain Scale for abdominal pain and rebound tenderness at Day 11 and Day 45 from baseline.

The secondary outcome included changes in quality of life assessed by the EQ-5D-5 L health survey questionnaire from baseline to days 11–14, days 30–34, and Day 45. Treatment Satisfaction Questionnaire for Medication (TSQM), Ver II for satisfaction with medications, sachets count for compliance were assessed on days 11–14 after completion of the treatment and microbiological cure (vaginal wet mount test, pH and Pap's smear) was assessed on days 11–14 from baseline.

2.6. Sachet's Count. All patients were given ten sachets at baseline. Patients were instructed to return any unused and empty sachets, and the number of unused sachets returned was counted and recorded on days 11–14. A measure of patch adherence was calculated as the number of sachets dispensed minus the number returned, divided by 10 (i.e., the total number of prescribed doses). If a patient dropped out of the treatment and failed to return dispensed sachets, the sachets were assumed not to have been used and were treated in the same way as returns. For the patient who dropped out of treatment in the first postrandomization of the study and never returned any sachets, this variable was coded as 0% adherence. This method of data collection for the measurement of sachet adherence is similar to pill count [21].

(a) (b) (c)

Figure 1: Depiction of test drug (*Acacia nilotica*): (a) tree, (b) pod, (c) powder of aqueous extract.

2.7. Overall Therapeutic Cure. Overall, the therapeutic cure was defined as meeting the criteria for both clinical and microbiological cure/investigational cure after treatment on days 11–14 from baseline. The microbiological test included vaginal saline wet mount test, pH determination, pus cell count, and whiff test with 10% KOH to confirm bacterial vaginosis with Amsel criteria, trichomoniasis, candidiasis, and uPID.

Clinical cure was defined as a patient who had normal vaginal discharge, negative KOH test, normal p^H, and no uterine/cervical motion. Microbiological/investigational cure were defined as a normal vaginal cytology on vaginal smear and normal Pap smear report.

2.8. Randomization, Allocation, and Masking. A simple random sampling was used to randomly assign the patients into two groups. The allocation sequence was generated by random allocation software (RAS) with a single block with an allocation ratio of 1 : 1. An open list of random numbers was used through the order of randomization and until the interventions were assigned to the patient, it was concealed from the first researcher. The matching and masking were done by supplying the medicine in the same aluminium sachets.

2.9. Sample Size. The sample size of a total of 67 participants ($n1 = 33$, $n2 = 34$) was required that was calculated based on the proportion of cure 34% and 50% obtained from the previous study [22]. Hence, the sample size was taken as 66 including 10% dropout.

2.10. Statistical Analysis. For analysis of the data, the statistical software SPSS 22.0 ver 3.2.2 were used. Mean ± SD was used for results from continuous measurements and number (%) for categorical measurements. For all statistical tests, the test of significance was 5%, 95% confidence interval, and 80% power of the study, a two-sided p value. The Chi-square test or Fisher's tests were utilized for comparison of the proportions. For intragroup comparisons, a paired Student's t-test or Wilcoxon matched paired test depends on the skewness of data. The intergroup comparison using Student's t-test and Mann–Whitney U test for normally distributed data and skewed data, respectively, was performed. The ITT principle was performed for all efficacy variables using data from all randomized subjects with at least one postrandomization outcome measure. The last observation carried forward method was used to impute the missing data.

3. Results

3.1. Recruitment and Follow-Up. The recruitment of patients was initiated on 1 March 2018 and completed on 8 November 2018. Initially, a total of 130 patients were screened, of which 64 were excluded (31 were ineligible, and 33 patients refused to participate). Thus, 33 patients were randomly allocated to each group. The flowchart for the enrolment of patients is shown in Figure 2.

3.2. Participant. The majority of the patients (96.96%) in each group were from an urban area. The mean age was 28.66 ± 5.76 and 30.57 ± 5.47 years in the *Acacia* and placebo group. The socio-demographic and reproductive characteristics are summarized in Table 1.

3.3. Primary Outcomes

3.3.1. VAS Score of Abnormal Vaginal Discharge (AVD) and Its Associated Symptoms. Acacia group showed improvement in the mean VAS score for AVD and its associated symptoms after treatment. The intergroup comparison at each follow-up was statistically significant, $p < 0.0001$ (Table 2).

3.3.2. Modified McCormack Pain Scale for Abdominal Pain and Rebound Tenderness. The mean score for the Modified McCormack Pain Scale (McPS) for abdominal pain and rebound tenderness on Day 11 was 1.06 ± 1.36 in the acacia and 1.96 ± 1.28 in the placebo group ($P = 0.01$, statistically significant) (Table 2).

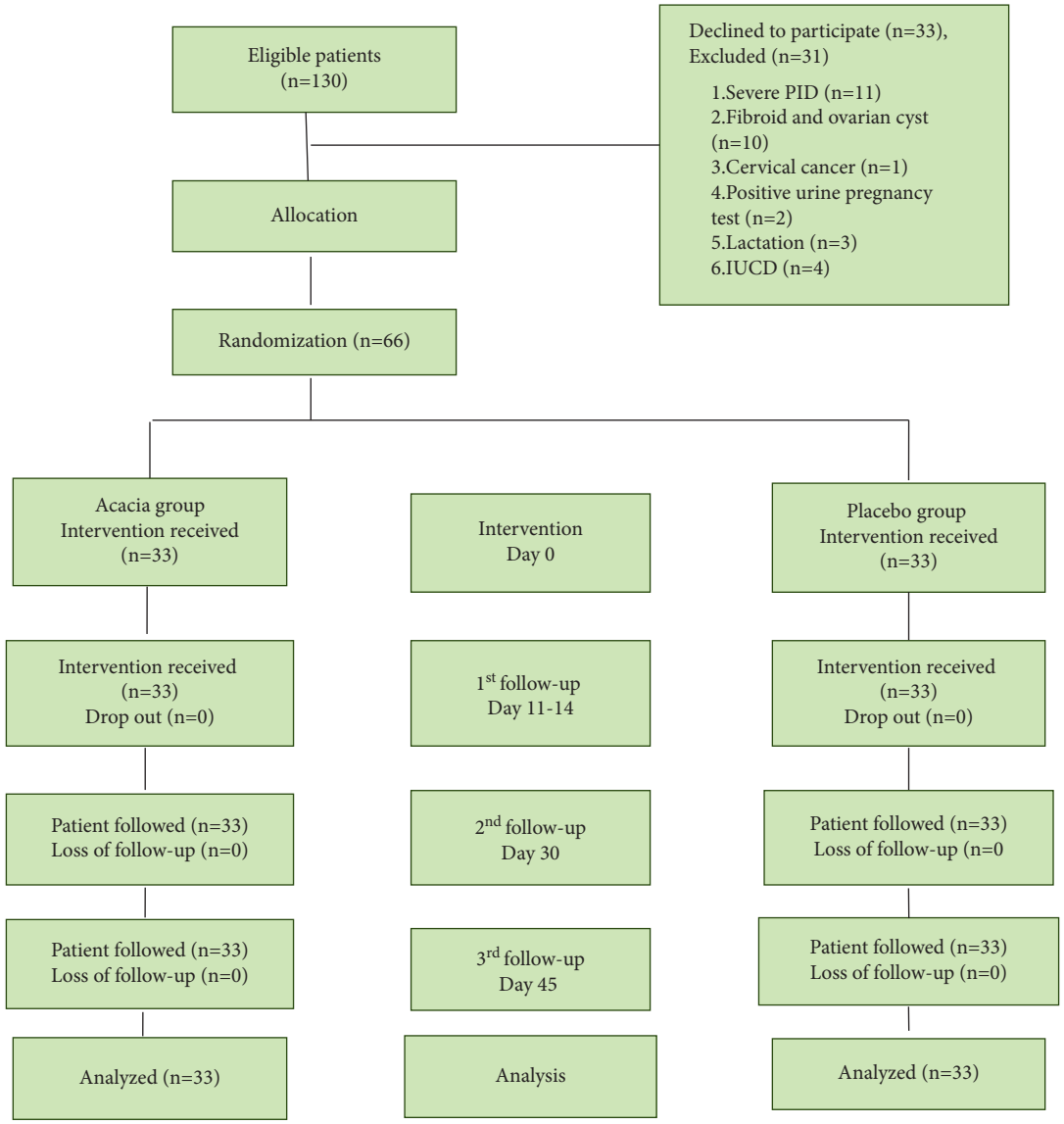

Figure 2: Flow chart of patients through the study according to consort statement.

Table 1: Baseline and socio-economic characteristics.

Variables	*Acacia* group ($n = 33$)	Placebo group ($n = 33$)	p value
Age (year)	28.66 ± 5.76	30.57 ± 5.47	0.17[c]
Urban	32 (96.96)	32(96.96)	1.00[a]
Past menstrual cycle			0.282[a]
Irregular	6(18.18)	3(9.09)	
Regular	27(81.81)	30(90.90)	
Duration of abnormal Vaginal discharge (days)	15.51 ± 11.85	14.72 ± 13.74	0.65[b]
Socio-economic status			0.71[a]
Upper middle (II)	13 (39.39)	16(48.48)	
Lower middle (III)	13 (39.39)	12(36.36)	
Upper lower (IV)	7 (21.21)	5(15.15)	
Height(cm)	156.28 ± 5.40	154.22 ± 4.73	0.051[c]
Weight(Kg)	61.09 ± 13.42	26.2 ± 5.89	0.714[c]
BMI (kg/m2)	24.98 ± 5.19	26.2 ± 5.89	0.376[c]

Data presented were as follows: mean ± SD or no (%); $p > 0.05$, considered not significant; tests used were as follows: [a]Fisher's exact test; [b]Chi-squared test; [c]Mann–Whitney U test.

Table 2: Primary Outcome: VAS scoring of symptoms and the Modified McCormack Pain Scale in the *Acacia* and the control group.

Primary outcome	*Acacia* group ($n = 33$)	Placebo group ($n = 33$)	p value
VAS for LAP and LBA			
Day 0	4.66 ± 1.68	5.18 ± 1.26	0.26
Days 11–14	1.36 ± 1.72	5.06 ± 1.27	<0.0001
Day 45	0.63 ± 1.02^{a}	4.90 ± 1.33^{b}	<0.0001
VAS for abnormal vaginal discharge			
Day 0	6.39 ± 0.70	6.12 ± 0.59	0.39
Days 11–14	1.51 ± 2.04	6 ± 0.61	<0.0001
Day 45	0.60 ± 1.19^{a}	6 ± 0.61^{b}	<0.0001
VAS for dyspareunia			
Day 0	1.54 ± 2.32	1.75 ± 2.34	0.83
Days 11–14	0.15 ± 0.44	1.72 ± 2.34	0.02
Day 45	0.03 ± 0.17^{a}	1.60 ± 2.20^{b}	0.007
VAS for dysuria			
Day 0	1.69 ± 2.43	1.84 ± 2.43	0.74
Days 11–14	1.69 ± 2.43	1.81 ± 2.39	0.04
Day 45	0.09 ± 0.29^{a}	1.66 ± 2.21^{b}	0.008
VAS for burning micturition			
Day 0	3.48 ± 2.48	3 ± 2.44	0.38
Days 11–14	0.75 ± 1.03	2.84 ± 2.34	0.0007
Day 45	0.33 ± 0.64^{a}	2.69 ± 2.24^{b}	0.0001
VAS for vulvar irritation			
Day 0	3.18 ± 2.55	3 ± 2.72	0.94
Days 11–14	0.87 ± 1.34	2.87 ± 2.64	0.003
Day 45	0.18 ± 0.46^{a}	2.84 ± 2.60^{b}	<0.0001
VAS for vulvar itching			
Day 0	4.63 ± 2.14	3.90 ± 2.45	0.18
Days 11–14	1.42 ± 1.73	3.78 ± 2.23	<0.0001
Day 45	0.39 ± 0.65^{a}	3.63 ± 2.35^{b}	<0.0001
Modified McCormack Pain Scale (McPS) for abdominal tenderness			
Day 0	2.36 ± 1.43	2.36 ± 1.43	0.43
Days 11–14	1.06 ± 1.36	1.96 ± 1.28	0.01
Day 45	0.33 ± 0.76^{a}	1.93 ± 1.24^{b}	<0.0001

Data presented were as follows: mean ± SD; $^{a}p < 0.0001$ considered extremely significant on Day 11 and Day 30 from Day 0 in the *Acacia* group. $^{b}p > 0.05$ considered not significant on days 11–14 and Day 45 from Day 0 in the placebo group; tests used were as follows: Wilcoxon matched paired test VAS : visual analogue scale; LAP : lower abdominal pain; LBA : low backache.

3.4. Secondary Outcome Measures

3.4.1. EQ-5D-5L Health Questionnaire for HRQoL. At baseline, index level in the *Acacia* and placebo group was statistically insignificant ($p = 0281$). The *Acacia* group showed statistically significant improvement than the placebo group in EQ-5D-5L ($p < 0.001$). The *Acacia* group showed a statistically significant difference at posttreatment compared to baseline ($p < 0.001$), whereas it was insignificant in the placebo group ($p > 0.05$). The tests used were Mann–Whitney U test and Wilcoxon matched paired test for intergroup and intragroup comparison, respectively (Figure 3).

3.4.2. Treatment Satisfaction Questionnaire for Medication (TSQM). On Day 11, the mean score of TSQM was 53.51 ± 4.34 and 41.96 ± 3.64 in the *Acacia* and placebo groups, respectively, statistically extremely significant ($p < 0.001$) in the *Acacia* group (Figure 3).

3.4.3. Sachet's Count for Compliance. The compliance in both groups was 100%

3.4.4. Microbiological Test. The microbiological test on Day 11 was statistically significant ($p < 0.0001$) when compared to Day 0 in the *Acacia* group; however, in the placebo group, it was insignificant ($p > 0.05$) (Table 3).

3.4.5. Overall Therapeutic Outcome. In the *Acacia* group, the therapeutic cure for bacterial vaginosis, cervicitis, and PID was 100% ($n = 7/7$), 45.45% ($n = 10/22$), and 71.42% ($n = 5/7$), respectively, whereas in the control group none of the patients had responded to the treatment (Table 4).

Data presented were as follows: no (%) or mean ± SD; $^{a}p < 0.0001$ considered extremely significant on Day 11 from Day 0 in the *Acacia* group; $^{b}p > 0.05$ considered not significant on Day 11 from Day 0 in the placebo group; tests used were as follows: Fisher's exact test and Wilcoxon matched paired test.

4. Discussion

4.1. Major Findings. This study is the first of its kind as none of the studies until date as per the researcher's knowledge has conducted a trial on sitz bath and vaginal pessary of *A. arabica* pod powder in abnormal vaginal discharge

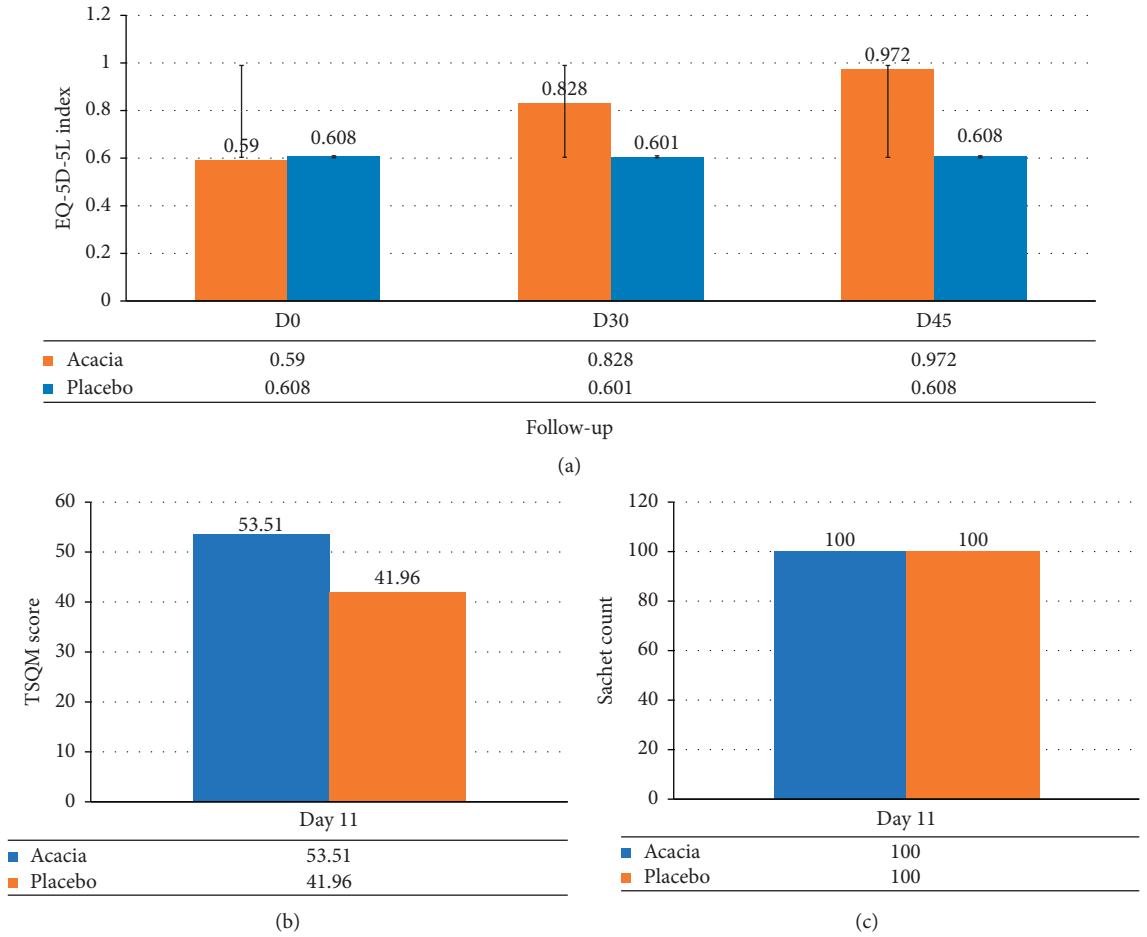

Figure 3: Depiction of secondary outcomes: (a) EQ-5D-5 L score, (b) TSQM score, and (c) Sachet count.

Table 3: Microbiological evaluation in the *Acacia* and placebo groups.

Investigation	*Acacia* group ($n = 33$)		p value	Placebo group ($n = 33$)		p value
	Day 0	Day 11–14		Day 0	Day 11-14	
			Amsel's criteria			
Whiff test			0.02			1.00
Negative	24 (72.72)	31 (93.93)		25 (75.75)	25 (75.75)	
Positive	9 (27.27)	2 (6.06)		8 (24.24)	8 (24.24)	
Clue cells			0.02			1
Negative	24 (72.72)	31 (93.93)		24 (72.72)	24(72.72)	
Positive	9 (27.27)	2 (6.06)		9 (27.27)	9 (27.27)	
Vaginal pH	4.54 ± 0.46	3.93 ± 0.48[a]	<0.0001	4.57 ± 0.47	4.59 ± 0.44[b]	0.78
			Vaginal wet mount test for microscopic investigation of vaginal discharge			
KOH slide for hyphae			1.00			1.00
Present	0 (0)	0 (0)		1 (3.03)	1 (3.03)	
Absent	33 (100)	33 (100)		32 (96.96)	32 (96.96)	
Normal saline test for trichomonas			1.00			1.00
Absent	33 (100)	33 (100)		33 (100)	33(100)	
Present	0	0		0	0	
Pus cells (hpf)			<0.001			0.93
<10	3 (9.09)	24 (72.72)		5 (15.15)	5 (15.15)	
11–20	6 (18.18)	6 (18.18)		8 (24.24)	7 (21.21)	
21–30	21 (63.63)	2 (6.06)		15 (45.45)	14 (42.42)	
>30	3 (9.09)	1 (3.03)		5 (15.15)	7 (21.21)	

Table 3: Continued.

Investigation	*Acacia* group ($n = 33$)		p value	Placebo group ($n = 33$)		p value
	Day 0	Day 11–14		Day 0	Day 11-14	
Pus cells (hpf)	22.96 ± 8.48	8.21 ± 7.85	<0.001	23.15 ± 7.32	22.15 ± 8.7	0.47
Pap smear						
Normal	4 (12.12)	20 (60.60)	<0.001	4 (12.12)	8 (24.24)	0.63
Inflammatory	22 (66.66)	11 (33.33)		22 (66.66)	18 (54.54)	
BV	7 (21.21)	2 (6.06)		6 (18.18)	6 (18.18)	
Candidiasis	0(0)	0(0)[a]		1 (3.03)	1(3.03)[b]	

Data presented were as follows: no (%) or mean ± SD; [a]$P < 0.0001$ considered extremely significant on day 11 from day 0 in the Acacia group; [b]$P > 0.05$ considered not significant on day 11 from day 0 in the Placebo group; Tests used were as follows: fisher's exact test and Wilcoxon matched paired test.

Table 4: Overall therapeutic outcome (clinical cure, microbiological cure, and therapeutic cure in both groups).

Variables		Bacterial vaginosis		Candidiasis		Cervicitis		uPID	
Groups		AG	PG	AG	PG	AG	PG	AG	PG
No. of Pt		7(100)	6(100)	0	1(100)	22(100)	22(100)	7(100)	14(100)
Clinical cure									
Colour of discharge									
D0	White	7(100)	4(66.6)	0	1(100)	4(66.6)	6(27.27)	2(28.57)	4(28.57)
	Greyish	0(0)	0			15(68.18)	14(63.63)	2(28.57)	6(42.85)
	Yellowish	0(0)	2(33.33)			3(13.63)	2(9.09)	3(42.85)	4(28.57)
	Greenish	0(0)	0(0)			0(0)	0(0)	0(0)	0(0)
D11-14	Responded	7(100)	0	0	0	17(77.27)	0	5(71.42)	0
Odour of discharge									
D0	No-smell	0(0)	0(0)	—	0(0)	0(0)	0(0)	0(0)	0(0)
	Foul-smell	7(100)	0(0)	—	1(100)	19(86.36)	21(95.45)	5(71.42)	8(57.14)
	Fishy	0(0)	6(100)			3(13.63)	1(4.54)	2(28.57)	6(42.85)
D11-14	Responded	7(100)	0	0	0	20(90.90)	0	7(100)	0
Amount of discharge									
D0	Present	7(100)	6(100)	—	1(100)	22(100)	22(100)	7(100)	14(100)
D11-14	Responded	7(100)	0	—	0	10(45.45)	0	5(71.42)	0
D0	Ut. motion tenderness	—	—	—	—	17(77.27)	18(81.81)	7(100)	14(100)
D11-14	Responded	—	—	—	—	10(58.82)	0	5(71.42)	0
D0	McPS	—	—	—	—	—	—	7(100)	14(100)
D11	Responded	—	—	—	—	—	—	5(71.42)	0
Microbiological and investigational cure (vaginal smear, pH, pap smear)									
D0	pH > 4.5	6(85.7)	5(83.33)	—	—	—	—	—	—
D11-14	Responded	6(100)	0						
	Clue cells	7(100)	6(100)						
D0	Hyphae	—	—	—	1(100)	—	—	—	—
	Pus cells >10					22(100)	21 (95.45)	6(85.71)	13(92.8)
D11-14	Responded	7(100)	0		0	13(59.09)	0	6	7(100)
D0	Whiff test	7(100)	6(100)	—	—	—	—	—	7(100)
D11-14	Responded	7(100)	0	—	—	—	—	—	7(100)
D0	Pap smear	7(100)	6(100)	-	1(100)	22(100)	22(100)		7(100)
D11-14	Responded	7(100)	0	—	—	10(45.45)	0		7(100)
Therapeutic cure		7(100)	0	0	0	10(45.45)	0	5(71.42)	0

Data presented were as follows: no (%); AG : *Acacia* group; PG : placebo group; McPS : Modified McCormack Pain Scale; Pt : patient; uPID (uncomplicated pelvic inflammatory disease)

syndromic management, its associated symptoms, and improving women's health-related quality of life (HRQoL). The interpretation of the results supports that there was a significant reduction in abnormal vaginal discharge, its associated symptoms, and improvement in HRQoL in patients in the *Acacia* group. The present study showed a significant reduction in all symptoms in the *Acacia* group; similarly, Salhan et al. also reported a significant reduction in lower abdominal pain, dysuria, and vaginal itching with Praneem vaginal tablets [3]. In the *Acacia* group, the therapeutic cure for bacterial vaginosis, cervicitis, and PID was 100% ($n = 7/7$), 45.45% ($n = 10/22$), and 71.42% ($n = 5/7$), respectively, and none had trichomoniasis and a significant reduction in the symptoms. Likewise, Patel et al. showed that Ginlac-V pessary showed 100% efficacious in bacterial vaginosis and overall symptomatic relief was 82%

in symptomatic vaginal discharge [17] and Motlagh et al. reported a 94% response with oral metronidazole plus *Prangos ferulacea* vaginal cream [19]. The present study showed a significant decrease in VAS score for low backache, vaginal discharge, and lower abdominal pain in the *Acacia* group; similarly, Bhat and Begum (2017) also reported a significant reduction in VAS score of symptoms for syndromic management of abnormal vaginal discharge with Unani formula [5].

4.2. Interpretation and Justification. Abnormal vaginal discharge is the commonest symptom for women in India to pursue care. *Acacia* pod extract was efficacious in the syndromic management of AVD, its associated symptoms, and improved HRQoL as it has anti-inflammatory (*Muhallil al-Waram*), astringent (*Qabiz*), and antiseptic (*Daf'-i-Taffun*) properties [6, 7]. Furthermore, *in vitro* and *in vivo* pharmacological studies have also proven anti-inflammatory [10, 11, 14], analgesic [10, 11], antimicrobial [23, 24], antispasmodic [25], diuretics [11], antioxidant properties [9, 13, 26], and antiseptic properties [10–14] of the pods. The aforementioned pharmacological properties are credited to the presence of phytoconstituents such as tannins, alkaloids, organic acids, flavonoids, polyphenolic compounds, volatile oils, glycosides, and coumarins [8, 9, 11, 13]. The methanolic pod extract of *A. arabica* showed significant inhibition against Gram-positive and Gram-negative species *in vitro* study [23]. Similarly, Satish et al. also reported antibacterial and antifungal activity of the methanolic extracts of *A. arabica* pods, and the highest activity was against *S. aureus*, *E. coli,* and *A. Niger* [8]. Another study also showed that the methanolic extract of pods had inhibitory activity against *P. aeruginosa*, *E. coli*, and *S. aureus* [24]. A study showed that the antimicrobial activity of the *Acacia* pods is probably due to polyphenolic compounds, and/or volatile oils cause inhibition of various microorganisms [8]. Phenol is established as a chemical antiseptic. The astringent effect of the pods is due to the presence of tannins [11]. Another study reported that the antioxidant and antibacterial activities are attributed to the presence of proteins and/or flavonoids and high total phenolic content [27]. The pods contain phytochemicals such as catechin, catechin 5-O-gallate, gallic acid, methyl gallate, 1-O-galloyl-β-D-glucose, gallocatechin 5-O-gallate, 1-6-di-O-galloyl-β-D-glucose, and digallic acid [28]. These phytochemicals are possibly accountable for the experiential activity. For example, tannins therapeutically have antiseptic properties and their precipitating activity is used in detecting alkaloids, proteins, and gelatin. Flavonoids and phenolic compounds are frequently found effective *in vitro* as antimicrobial substances against various microorganisms. They are plant metabolites with at least one hydroxyl group. Gallic acid by the mechanism of action in *E. coli, S. aureus, P. aeruginosa, and Listeria monocytogenes* led to "permanent changes in membrane properties through the decrease of negative surface charge, hydrophobicity changes, and pore formation in the cell membranes or local rupture with resulting leakage of essential intracellular constituents." Oladous et al. (2019) reported that although gallic acid and methyl gallate have better activity than the crude extract, catechin was the most active compound against *S. aureus, E. coli, P. aeruginosa,* and clinical isolates of *K. pneumonia, Candida albicans, S. typhi,* and *B. subtilis* organisms [29].

The infective vaginal discharge not only affects women's routine physical and social activities but also their mental health and all aspects of a woman's life, thereby affecting HRQoL negatively. The positive effect of *A. arabica* pods on mood, headache, fatigue, and energy level is due to its antioxidant properties [9, 13, 26]. Furthermore, to explain that the reduction of associated symptoms may be attributed to its reported scientifically proven pharmacological activities such as astringent, anti-inflammatory, analgesic, and diuretic properties [8–14]. The *Acacia* group did not show any adverse effects during and after the completion of this trial.

4.3. Strengths of the Study. This is the first of its kind single-blind, randomized, placebo-controlled study using traditional regimen methods, sitz bath, and vaginal pessary of *Acacia* pods were efficacious for abnormal vaginal discharge syndromic management, its associated symptoms, and women's HRQoL. There were good patient's retention and compliance with the protocol. Overall therapeutic cure for the disease was also seen.

4.4. Limitations and Future Recommendations. Because of time constraints and lack of infrastructure, laboratory tests such as vaginal and cervical swab culture, nucleic acid amplification test (NAAT), and endometrial biopsy to verify the efficacy of the results were not possible. Furthermore, double-blind, phase IV clinical trials with larger samples are recommended.

5. Conclusion

The result of this study indicates that an *Acacia* pod's sitz bath and vaginal pessary were effective for syndromic management of abnormal vaginal discharge, its associated symptoms, and improving women's HRQoL. Furthermore, it is safe, well-accepted, and tolerated by the patients.

Data Availability

The research is approved by the Institutional Ethics Committee (same has been added in the manuscript). The findings of this study are available from the corresponding author upon request.

Disclosure

No competing financial interests exist.

Conflicts of Interest

The authors declared that they have no conflicts of interest.

Authors' Contributions

All authors equally contributed in drafting, designing, critically reviewing, analysing the data, and proofreading the manuscript.

Acknowledgments

The authors are thankful to the Director of our Institute for providing all the best facilities and resources to accomplish this research work. This research was supported by the fund from the Ministry of AYUSH as an unrestricted grant for the dissertation work. UN and Hindawi under Research4Life policy have financially supported for publication.

References

[1] A. M. Farhan, E. A. Eldesouky, E. A. Gaballah, and M. E. Soltan, "Comparison of visual, clinical, and microbiological diagnosis of symptomatic vaginal discharge in the reproductive age group," *Benha Medical Journal*, vol. 34, no. 1, pp. 43–48, 2017.

[2] S. Venugopal, K. Gopalan, A. Devi, and A. Kavitha, "Epidemiology and clinico-investigative study of organisms causing vaginal discharge," *Indian Journal of Sexually Transmitted Diseases and AIDS*, vol. 38, no. 1, pp. 69–75, 2017.

[3] S. Salhan, V. Tripathi, R. Sehgal, G. Kumar, G. P. Talwar, and A. Chatterjee, "A phase II randomized controlled trial to evaluate the safety and efficacy of Praneem polyherbal vaginal tablets compared with betadine vaginal pessary in women with symptoms of abnormal vaginal discharge," *Asia-Pacific Journal of Public Health*, vol. 21, no. 4, pp. 461–468, 2009.

[4] S. Valsangkar, D. Selvaraju, R. Rameswarapu, and S. Kamutapu, "Impairment of quality of life in symptomatic reproductive tract infection and sexually transmitted infection," *Journal of Reproduction and Infertility*, vol. 15, no. 2, pp. 87–93, 2014.

[5] K. A. Rabiu, A. A. Adewunmi, F. M. Akinlusi, and O. I. Akinola, "Female reproductive tract infections: understandings and care seeking behaviour among women of reproductive age in Lagos, Nigeria," *BMC Women's Health*, vol. 10, no. 1, pp. 8–7, 2010.

[6] L. J. Rather, S. Salam, and F. Mohammad, "Acacia arabica (L.): a review of its traditional uses, phytochemistry, and pharmacology," *Sustainable Chemistry and Pharmacy*, vol. 2, 2015.

[7] C. P. Khare, *Indian Medicinal Plants (an illustrated dictionary)*, Springer Publishers, Berlin, Germany, 2007.

[8] S. Satish, M. P. Raghavendra, and K. A. Raveesha, "Evaluation of the antibacterial potential of some plant plants against human pathogenic bacteria," *Advances in Biological Research*, vol. 2, no. 3-4, pp. 44–48, 2008.

[9] T. Kalaivani and L. Mathew, "Free radical scavenging activity from leaves of Acacia arabica (L.) Wild. ex Delile, an Indian medicinal tree," *Food and Chemical Toxicology*, vol. 48, 2010.

[10] S. D. Sokeng, J. Koubé, F. Dongmo et al., "Acute and chronic anti-inflammatory effects of the aqueous extract of *Acacia arabica* (L.) Del. (Fabaceae) pods," *Academia Journal of Medicinal Plants*, vol. 1, no. 1, pp. 1–5, 2013.

[11] M. Abeer, A. Haj, and S. O. Yagoub, "Anti-microbial activity *of Acacia arabica* extracts against some bacteria isolated from clinical specimens," *Research Journal of Medicinal Plant*, vol. 1, no. 1, pp. 25–28, 2007.

[12] V. K. Bansal and R. K. Goel, "Gastroprotective effect of *Acacia arabica* young seedless pod extract: role of polyphenolic constituents," *Asian Pacific Journal of Tropical Medicine*, vol. 5, no. 7, pp. 523–528, 2012.

[13] B. N. Singh, B. R. Singh, R. L. Singh, D. Prakash, B. K. Sarma, and H. B. Singh, "Antioxidant and anti-quorum sensing activities of green pod of *Acacia arabica* L," *Food and Chemical Toxicology*, vol. 47, no. 4, pp. 778–786, 2009.

[14] L. A. Alli, M. O. Nafiu, A. A. Adesokan, M. A. Akanji, A. Y. Tijani, and Q. A. Salawu, "Antipyretic and analgesic activities of aqueous extract of *Acacia arabica* root," *Biokemistri*, vol. 26, no. 2, pp. 55–62, 2014.

[15] M. Simbar, Z. Azarbad, F. Mojab, and H. Alavi Majd, "A comparative study of the therapeutic effects of the *Zataria multiflora* vaginal cream and metronidazole vaginal gel on bacterial vaginosis," *Phytomedicine*, vol. 15, no. 12, pp. 1025–1031, 2008.

[16] T. A. Bhat and W. Begum, "Efficacy of *Tamarindus indicus, Melia azadirach* and *Santalum album* in syndromic management of abnormal vaginal discharge: a single-blind randomised controlled trial," *Journal of Complementary and Integrative Medicine*, vol. 15, no. 2, pp. 1–8, 2018.

[17] Y. Patel, S. Gopalan, R. Bagga, M. Sharma, S. Chopra, and S. Sethi, "A randomized trial comparing a polyherbal pessary (a complementary and alternative medicine) with Ginlac-V pessary (containing clotrimazole, tinidazole and lactobacilli) for treatment of women with symptomatic vaginal discharge," *Archives of Gynecology and Obstetrics*, vol. 278, no. 4, pp. 341–347, 2008.

[18] J. A. Balogun and F. E. Okonofua, "Management of chronic pelvic inflammatory disease with shortwave diathermy: a case report," *Physical Therapy*, vol. 68, no. 10, pp. 1541–1545, 1988.

[19] A. Azadpour Motlagh, M. Dolatian, F. Mojab et al., "The effect of *Prangos Ferulacea* vaginal cream on accelerating the recovery of Bacterial Vaginosis: a randomized controlled clinical trial," *International Journal of Community Based Nursery and Midwifery*, vol. 6, no. 2, pp. 100–110, 2018.

[20] X. Mao, R. Zhao, R. Yao et al., "Chinese herbal formula Feilin vaginal gel prevents the cervicitis in mouse model," *Evidence Based Complementart Alternative Medicine*, vol. 2019, Article ID 4168126, 10 pages, 2019.

[21] W. Y. Lam and P. Fresco, "Medication adherence measures: an overview," *BioMed Research International*, vol. 2015, pp. 1–12, 2015.

[22] P. Moghtadaei, F. Sardari, and S. Esmaeilian, "Comparison of ceftriaxone plus weekly azithromycin or daily ofloxacin for outpatient treatment of pelvic inflammatory disease: a randomized clinical trial," *Journal of Family and Reproductive Health*, vol. 2, no. 2, pp. 87–94, 2008.

[23] S. M. Gmaraldeen, A. A. Magzoub, A. M. Badri, M. I. Garbi, and M. Saleh, "Antibacterial activity of *Acacia nilotica* fruits extract against pathogenic bacteria," *Int J Appl Res*, vol. 2, no. 6, pp. 103–106, 2016.

[24] P. Oladosu, N. R. Isu, K. Ibrahim et al., "Time kill-kinetics antibacterial study of *Acacia nilotica*," *African Journal of Microbiology Research*, vol. 7, no. 46, pp. 5248–5252, 2013.

[25] R. Chaubal, P. V. Pawar, G. D. Hebbalkar et al., "Larvicidal activity of *Acacia nilotica* extracts and isolation of D- Pinitol-A bioactive carbohydrate," *Chemistry and Biodiversity*, vol. 2, pp. 684–688, 2005.

[26] O. A. Abuelgassim, "Antioxidant potential of date palm leaves and *Acacia nilotica* fruit in comparison with other four common Arabian medicinal plants," *Life Science Journal*, vol. 10, no. 4, pp. 3405–3410, 2013.

[27] M. B. Sadiq, W. Hanpithakpong, J. Tarning, and A. K. Anal, "Screening of phytochemicals and in vitro evaluation of antibacterial and antioxidant activities of leaves, pods and bark extracts of *Acacia nilotica* (L.) Del," *Industrial Crops and Products*, vol. 77, pp. 873–882, 2015.

[28] A. A. Karim and A. Azlan, "Fruit pod extracts as a source of nutraceuticals and pharmaceuticals," *Molecules*, vol. 17, no. 10, pp. 11931–11946, 2012.

[29] O. P. Oladosu, N. R. Isu, I. M. Aboh, S. E. Okhale, A. T. Orishadipe, and H. O. Egharevba, "Antibacterial activity of bioflavonoid from fruit pulps of *Acacia nilotica* Willd," *Microbiology Research Journal International*, vol. 1, pp. 1–12, 2019.

Hindawi
Evidence-Based Complementary and Alternative Medicine
Volume 2022, Article ID 6404588, 11 pages
https://doi.org/10.1155/2022/6404588

Research Article

Resveratrol Ameliorates Lipopolysaccharide-Induced Sudden Sensorineural Hearing Loss in *In Vitro* Model through Multitarget Antiapoptotic Mechanism Based on Network Pharmacology and Molecular Docking

Shiming Ye,[1,2] **Jing Liu**,[1,3] **Qi Dong**,[4] **Xinxin Wang**,[2] **and Wandong She**[1,3,4]

[1]*Department of Otolaryngology-Head and Neck Surgery, Nanjing Drum Tower Hospital Clinical College of Traditional Chinese and Western Medicine, Nanjing University of Chinese Medicine, Nanjing 210008, China*
[2]*Department of Otolaryngology, Yizheng People's Hospital, Yangzhou 211400, Jiangsu, China*
[3]*Department of Otolaryngology Head and Neck Surgery, Nanjing Drum Tower Hospital, The Affiliated Hospital of Nanjing University Medical School, Nanjing 210008, China*
[4]*Department of Otolaryngology-Head and Neck Surgery, Nanjing Drum Tower Hospital, Medical College of Southeast University, Nanjing 210008, China*

Correspondence should be addressed to Wandong She; shewandong@163.com

Received 25 January 2022; Revised 8 April 2022; Accepted 19 April 2022; Published 19 May 2022

Academic Editor: Vijaya Anand

Objective. To explore the effects of resveratrol (RSV) on hair cell apoptosis caused by sudden sensorineural hearing loss (SSNHL) and its effect on lipopolysaccharide-induced apoptosis of HEI-OC1 cells. *Methods*. We used the network pharmacology method to screen molecules related to RSV for the treatment of SSNHL and analyzed these molecules and their enriched biological processes and signaling pathways through Kyoto Encyclopedia of Genes and Genomes (KEGG) and Gene Ontology (GO) analysis. We selected hub genes related to apoptosis using protein-protein interaction (PPI) analysis for *in vitro* and molecular docking verification. *Results*. Eighty overlapping genes were identified as potential targets for RSV treatment of SSNHL. Further GO analysis showed that the biological processes were mainly related to toxicity, cell proliferation, and lipopolysaccharide reactions. KEGG analysis showed that the AGE-RAGE signaling pathway in diabetic complications, Kaposi's sarcoma-associated herpesvirus infection, FoxO signaling pathway, PI3K-Akt signaling pathway, and other inflammatory signaling pathways were concentrated. *AKT1, STAT3, JUN, TNF, TP53, MAPK3, CASP3*, and *VEGFA* were screened as HUB genes using PPI analysis. The apoptosis-related proteins TNF, CASP3, AKT1, and TP53 were selected for *in vitro* experiments, which showed that mRNA was significantly different before and after RSV intervention, confirming that the corresponding protein receptors could bind well with RSV. *Conclusion*. RSV mainly affects the prognosis of SSNHL through anti-inflammatory effects and may improve hair cell apoptosis caused by inflammatory factors through multitargeted interventions involving TNF, CASP3, AKT1, and TP53.

1. Introduction

Although sudden sensorineural hearing loss (SSNHL) is an acute sensorineural hearing loss of unknown etiology, our recent studies have shown that inflammatory factors may represent a common pathological basis for SSNHL caused by various elements [1]. Apoptosis is considered to be the main pathogenic manifestation of SSNHL [2], along with age-related deafness [3] and autoimmune inner-ear disease [4]. Apoptosis of cochlear sensory hair cells has been observed in SSNHL animal models, *in vitro* models, and lipopolysaccharide (LPS) models of the middle ear [5–7]. At present, SSNHL still involves glucocorticoid-based comprehensive treatment [8, 9], but certain treatments are still ineffective

even if the dosage of glucocorticoids is timely and sufficient [10]. Under the traditional concept of "one disease, one gene, one drug," no specific treatment has been found. Therefore, multitargeted natural products involving a broad range of pharmacological activities are most likely to show potential superiority [11].

Resveratrol (RSV) is a polyphenolic organic compound widely found in a variety of herbaceous plants and is a bioactive component of wine and grape juice [12]. It has extensive anti-inflammatory, antioxidant, neuroprotective, and cardiovascular protective effects [13]. Its molecular weight (MW = 228.25) is low and has good blood-brain barrier (BBB = −1) permeability, which obeys Lipinski's five laws, including a MW between 180 and 500 Da, an octanol-water partition coefficient (Alog P = 3.01) below 5, the number of possible receptors (Hacc = 3) < 10, and hydrogen bond donors (Hdon = 3) < 5 [14]. We speculated that RSV might also play a therapeutic role in sensorineural hearing loss (SHL) through the blood-labyrinth barrier. Many studies have found that RSV exhibits good outcomes in the treatment of SHL, such as age-related deafness [3], cisplatin-induced hearing loss [15], and noise-induced hearing loss [16]. However, RSV has not been reported in SSNHL.

In the present study, we used the network pharmacology method to screen RSV- and SSNHL-related molecules and analyzed these molecules and their enriched biological processes and signaling pathways using Kyoto Encyclopedia of Genes and Genomes (KEGG) and Gene Ontology (GO) analysis. Moreover, we selected hub genes related to apoptosis through protein-protein interaction (PPI) analysis for molecular docking verification and further verified the results in an *in vitro* model of LPS-induced acute hearing loss. Our results suggested that RSV plays a protective role in cochlear cells by regulating key factors involved in the apoptotic pathway. The current study lays a foundation for future *in vivo* validation and clinical application to improve the prognosis of patients with refractory SSNHL. The flowchart of such analysis is presented in Figure 1.

2. Materials and Methods

2.1. RSV-Related Target Genes Screening. The Traditional Chinese Medicine System Pharmacology (TCMSP) database is based on the framework of Traditional Chinese Medicine System Pharmacology [17]. We used the TCMSP (http://tcmspw.com/tcmsp.php) database to search for RSV-related targets and used the UniProt [18] (https://www.uniprot.org) database to convert the obtained target proteins into the corresponding genes (the species was defined as human). All database searches were conducted in March 2021.

2.2. Acquisition of Target Genes Related to SSNHL. We used the DisGeNET [19] (http://www.disgenet.org) database to search the pathogenesis of SSNHL-related target genes. The DisGeNET database is a comprehensive platform integrating and specifying disease-related genes and provides variation data from the scientific literature and multiple sources.

2.3. Potential Drug-Disease Target Gene Screening. We used the online tool Venny2.1 to analyze intersecting genes (https://bioinfogp.cnb.csic.es/tools/venny) [20], identify potential RSV-SSNHL target genes, and save the Venn diagram.

2.4. GO Function Enrichment and KEGG Analysis. The RSV-SSNHL cross genes whose names were modified to formal gene symbols were introduced into David 6.8 [21] (https://david.ncifcrf.gov/home.jsp) and KEGG pathway [22] (https://www.genome.jp/kegg/pathway.html) databases. The species was defined as "human," and the exclusion criteria were set as p value < 0.05 and q value < 0.05.

2.5. PPI Analysis of Potential Target Genes and Screening of Hub Genes. Potential drug-disease target genes were imported into the online database STRING [23] (https://string-db.org/) to conduct PPI analysis (selecting high confidence 0.7), and the results were input into Cytoscape software. We selected the top-eight degrees as hub genes. Hub genes related to apoptosis were selected for further *in vitro* verification.

2.6. Cell Culture and Treatments

2.6.1. CCK-8 Analysis. HEI-OC1 cells, donated by Professor Chai Renjie's Laboratory (Medical College of Southeast University, Nanjing, China), were cultured in DMEM containing 10% fetal bovine serum (FBS) and 100 U/mL penicillin. Cells were seeded into 96-well microplates at a density of 5×10^3 cells/well for 24 h. The cells were then divided into three groups. The first group was cultured with various concentrations (0, 2, 5, 10, 25, and 50 μg/mL) of LPS (L2630, Sigma) in a high-glucose DMEM culture medium for 24 h. A CCK-8 kit (A311-01/02, Vazyme, Nanjing, China) was used to determine the optimal concentration. The second group (RSV + LPS group) was pretreated with different concentrations (0, 5, 10, 20, and 40 μmol) of RSV (HY-16561, MCE) for 12 h and then treated with the optimum concentration of LPS for 24 h. The third group was a solvent control cohort. All experiments were repeated three times.

2.6.2. Apoptosis Analysis Using FITC/PI. Cells were collected, digested with EDTA-free trypsin, and washed twice with precooled PBS. The cells were gently blown into a single-cell suspension with 100 μL of 1 × binding buffer. Annexin V-FITC (5 μL of) and 5 μL propidium iodide (PI) staining solutions were added to the binding buffer. Cells were incubated in the dark for 10 min at room temperature, gently mixed with 400 μL of 1 × binding buffer, and subjected to flow cytometry within 1 h. The total apoptotic rate is calculated as follows: Q2+Q3.

2.6.3. RT-qPCR Analysis. To examine differentially expressed mRNAs in HEI-OC1 cells in the different treatment groups, total RNA was extracted using TRIzol (R401-

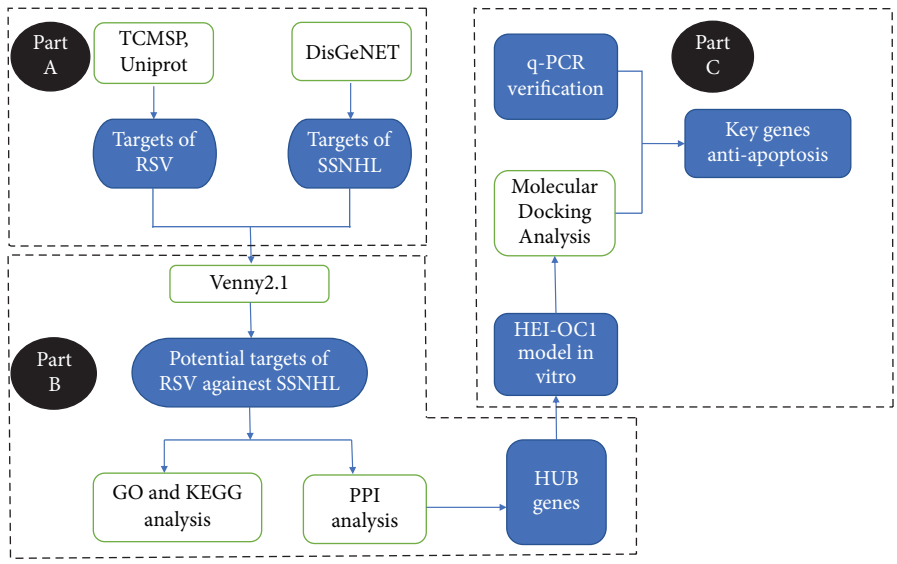

Figure 1: Flowchart of analysis. (a) Target search using TCMSP, Uniprot, and DisGeNET. (b) Target analysis using Venny2.1, GO, and KEGG with PPI. (c) Key target verification in HEI-OC1 cells.

01, Vazyme) and cDNA was generated using the HiScriptII 1st Strand cDNA Synthesis Kit (R211-01/02,Vazyme). RT-qPCR was performed using ChamQ SYBR qPCR Master Mix (Q311-02/03, Vazyme), according to the manufacturer's instructions. PCR primers were synthesized by TSINGKE Biotechnology Co., Ltd. (Beijing, China) and were purified by oligonucleotide purification cartridge (OPC). The results are shown in Table 1. The samples underwent initial denaturation at 95°C for 30 s, and then 40 cycles were performed at 95°C for 10 s and 60°C for 30 s. Finally, melting curves were obtained under the conditions of 95°C for 15 s, 60°C for 60 s, and 95°C for 15 s, repeated three times for each gene. Changes in expression were calculated using the $2^{-\Delta\Delta CT}$ method.

2.6.4. Molecular Docking Analysis. Molecular docking can be used to model the interactions between a small molecule and protein structures at the atomic level. Molecular docking analysis was used to predict the binding of apoptosis-related proteins to RSV. We obtained the RSV three-dimensional structure from the PubChem database (https://pubchem.ncbi.nlm.nih.gov/) and the three-dimensional structures of apoptosis-related hub protein receptors from the RCSB Protein Data Bank (PDB) database (http://www.rcsb.org/). Molecular docking simulations of the target protein receptor and RSV were performed using AutoDock Tool (v.1.5.6) and AutoDock Vina 1.1.2 (Molecular Graphics Laboratory, Scripps Institute, 2011) and displayed using the PyMOL molecular graphics system (v.2.4.0, Schrödinger, LLC) [24].

2.7. Statistical Analysis. Data are presented as means ± standard deviation (SD). All statistical analyses were performed using Microsoft Excel and GraphPad Prism, v.7. Two-tailed unpaired Student's *t*-test was used for analysis involving two groups. One-way analysis of variance (ANOVA) was used among multiple groups (> two groups), p values < 0.05 were considered statistically significant.

3. Results

3.1. Screening Results of RSV Target Genes. A total of 151 RSV target proteins were obtained from TCMSP and back-translated into their corresponding genes using UniProt. The species selected was humans. The results are presented in Table S1.

3.2. Screening Results of Target Genes Related to SSNHL. A total of 2,342 corresponding target genes were obtained from the DisGeNET database by inputting the disease name of sudden sensorineural hearing loss. The results are presented in Table S2.

3.3. Potential Drug-Disease Target Gene Screening Results. We obtained a total of 80 drug-disease cross genes using the online tool Venny2.1 (Figure 2).

3.4. GO Functional Enrichment and KEGG Analysis Results. GO analysis showed that toxic reactions, cell proliferation, response to LPS, oxidative stress, inflammation, and aging were mainly involved in cytokine receptor, receptor ligand activity, receptor regulator activity, cytokine activity, and protein dimerization activity. The cell composition mainly included membrane rafts, membrane microdomains, membrane regions, nuclear chromosomes, and transcription factor complexes (Figure 3).

KEGG analysis indicated that 80 potential target genes were enriched involving 92 signaling pathways, of which the 10 most important pathways included the AGE-RAGE signaling pathway in diabetic complications, Kaposi's sarcoma-associated herpesvirus infection, FoxO signaling

Table 1: Primer list for mRNA expression of apoptosis-related genes.

Primers for mRNA expression of apoptosis-related genes (5′-3′)		
Primers	Forward	Reverse
Caspase-3	GAAACTCTTCATCATTCAGGCC	GCGAGTGAGAATGTGCATAAAT
Tnf	ATGTCTCAGCCTCTTCTCATTC	GCTTGTCACTCGAATTTTGAGA
Akt1	TGCACAAACGAGGGGAATATAT	CGTTCCTTGTAGCCAATAAAGG
Tp53	TGGAAGGAAATTTGTATCCCGA	GTGGATGGTGGTATACTCAGAG
Gapdh	AGGTCGGTGTGAACGGATTTG	TGTAGACCATGTAGTTGAGGTCA

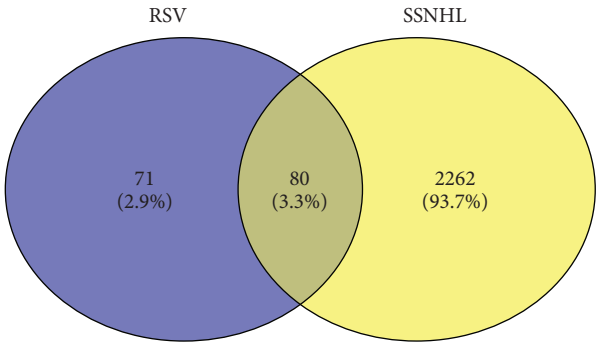

Figure 2: Venny analysis of RSV-SSNHL potential target genes. Eighty RSV-SSNHL cross genes were found by this analysis.

pathway, PI3K-Akt signaling pathway, proteoglycan in cancer, small molecule ribonucleic acids in cancer, human cytomegalovirus infection, hepatitis B, MAPK signaling pathway, fluid shear stress, and atherosclerosis (Figure 4).

3.5. PPI Analysis of Potential Target Genes Related to Apoptosis of Top Ten Genes. We used the online STRING database to analyze differential genes PPI and imported the results into Cytoscape software to analyze 2,416 related nodes (Figure 5(a)). According to the number of nodes ≥70, *AKT1, STAT3, JUN, TNF, TP53, MAPK3, CASP3*, and *VEGFA* were screened (Table S3). Among these hub genes, *TNF, CASP3, AKT1*, and *TP53* are involved in the apoptosis pathway both outside and inside the cell. We speculated that this might play a protective role in hair cells by regulating the apoptosis pathway involving TNF, CASP3, AKT1, and TP53 (Figure 5(b)). We used the STRING database to further analyze the relationship among TNF, CASP3, AKT1, and TP53 (Figure 5(c)).

3.5.1. CCK-8 Analysis Results. CCK-8 screening showed that LPS (2 μg/mL) could induce apoptosis in HEI-OC1 cells after 24 h of treatment (Figure 6(a)). Therefore, we chose a concentration of 2 μg/mL for subsequent experiments. We found that 10 μmol RSV exerted a significant protective effect against LPS-induced apoptosis in HEI-OC1 cells in a dose-dependent manner (Figure 6(b)).

3.5.2. FITC/PI Analysis Results. FITC/PI analysis showed that there was a significant difference in apoptotic rates in HEI-OC1 cells among the different groups. Compared with the control group, the apoptosis rate in the LPS intervention group significantly increased, whereas there was no significant difference in the apoptosis rate in the RSV + LPS intervention group (Figure 7).

3.5.3. RT-qPCR Analysis Results. RT-qPCR results showed that the mRNA expression levels of apoptosis-related genes in the different groups were statistically different: the AKT1, TNF, caspase3, and TP53 levels in the LPS group were higher than those in the control group, and this difference was statistically significant, while there was no significant difference in the RSV + LPS group (Figure 8).

3.5.4. Molecular Docking Results. We obtained the three-dimensional structure of RSV from the PubChem database and the three-dimensional structure of apoptosis-related protein target receptors from the RCSB PDB database. Molecular docking potential simulation of target proteins and RSV was generated using AutoDock Tool and AutoDock Vina software. Finally, combinations of the target and equivalent component were verified through molecular docking, and the combination relationship between the target and equivalent component was established using the PyMOL molecular graphics system. We designated TNF-RSV, caspase-3-RSV, AKT1-RSV, and P53-RSV for verification. Among the four docking simulations, the minimum affinity was −7.8 kcal/mol, −7.4 kcal/mol, −6.2 kcal/mol, and −5.5 kcal/mol (Table 2). The grid centers are shown in Table 2, and distances to the best mode were 0.000 rmsd l.b. and 0.000 rmsd u.b. (Figure 9).

4. Discussion

The etiology of SSNHL remains unclear, which may be related to hair cell apoptosis and damage caused by inflammatory responses, viral infection, microcirculation disturbance, and other factors, because inflammation can result in microvascular damage [25], atherosclerosis [26], and cochlear immune responses [27]; *in vivo* experiments have shown that LPS-stimulated guinea pigs have severe cochlear microcirculation disturbance [28]. Therefore, inflammation is considered to be an important cause of SSNHL. We identified 151 potential RSV targets from TCMSP and 2,342 SSNHL-related genes from the DisGeNET database. Venny analysis identified 80 overlapping genes as potential targets for RSV treatment of SSNHL. Furthermore, GO analysis revealed that the potential targets are mainly involved in toxic reactions, cell proliferation, and LPS reactions. The molecular functions involved were

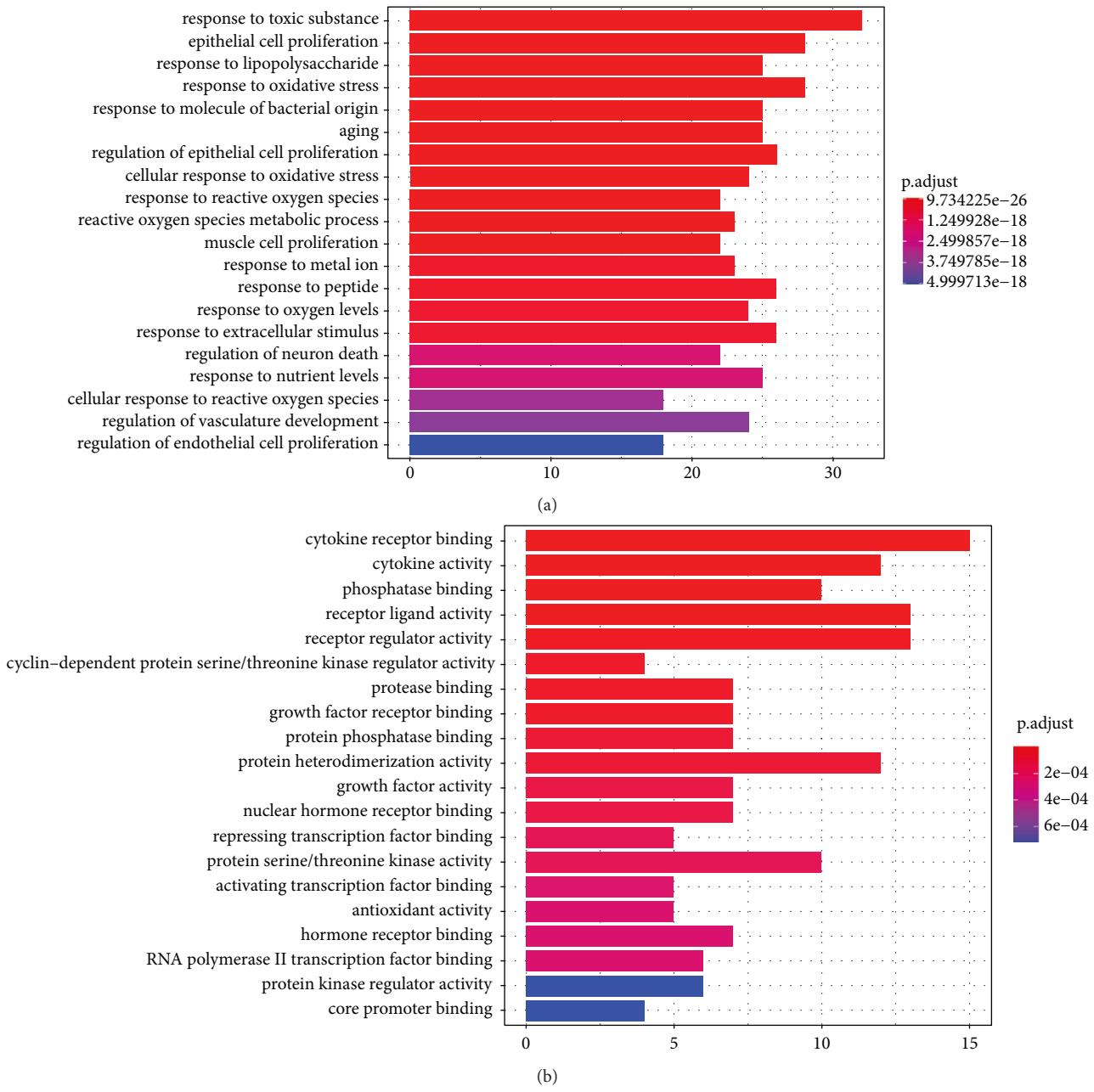

Figure 3: Continued.

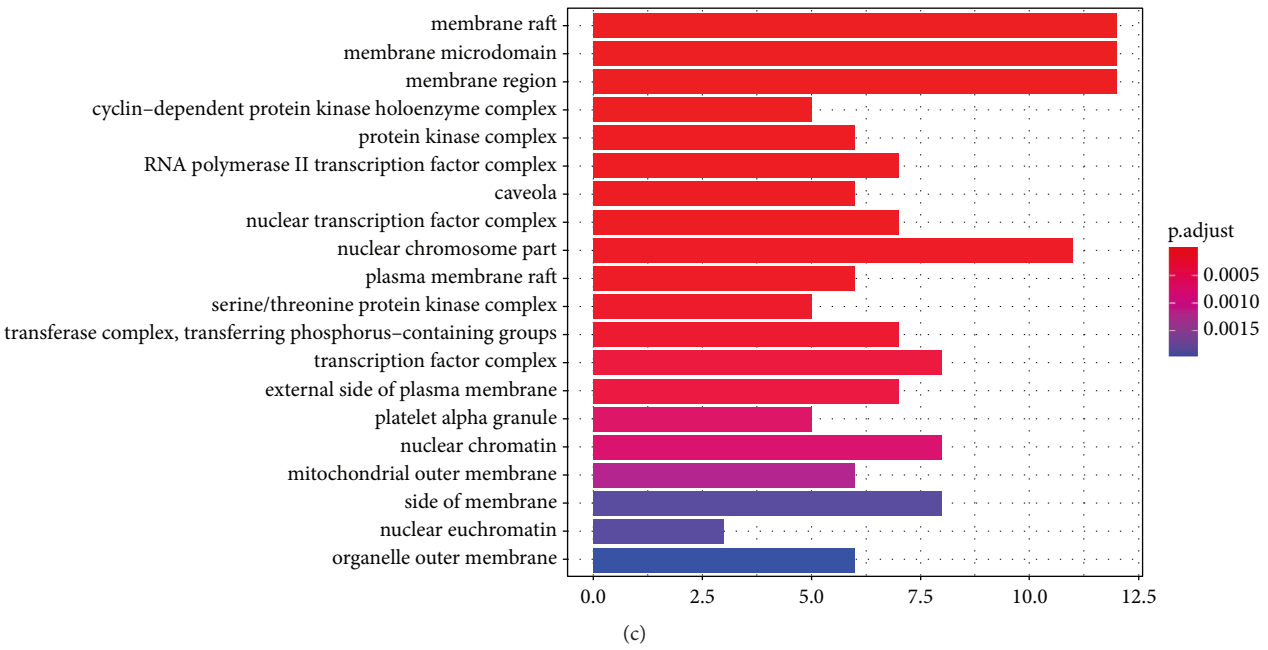

Figure 3: GO enrichment analysis of potential targets. (a) Molecular function enrichment analysis. (b) Cell composition enrichment analysis. (c) Bioprocess enrichment analysis. p value gradually increases as the color changes from dark red to blue.

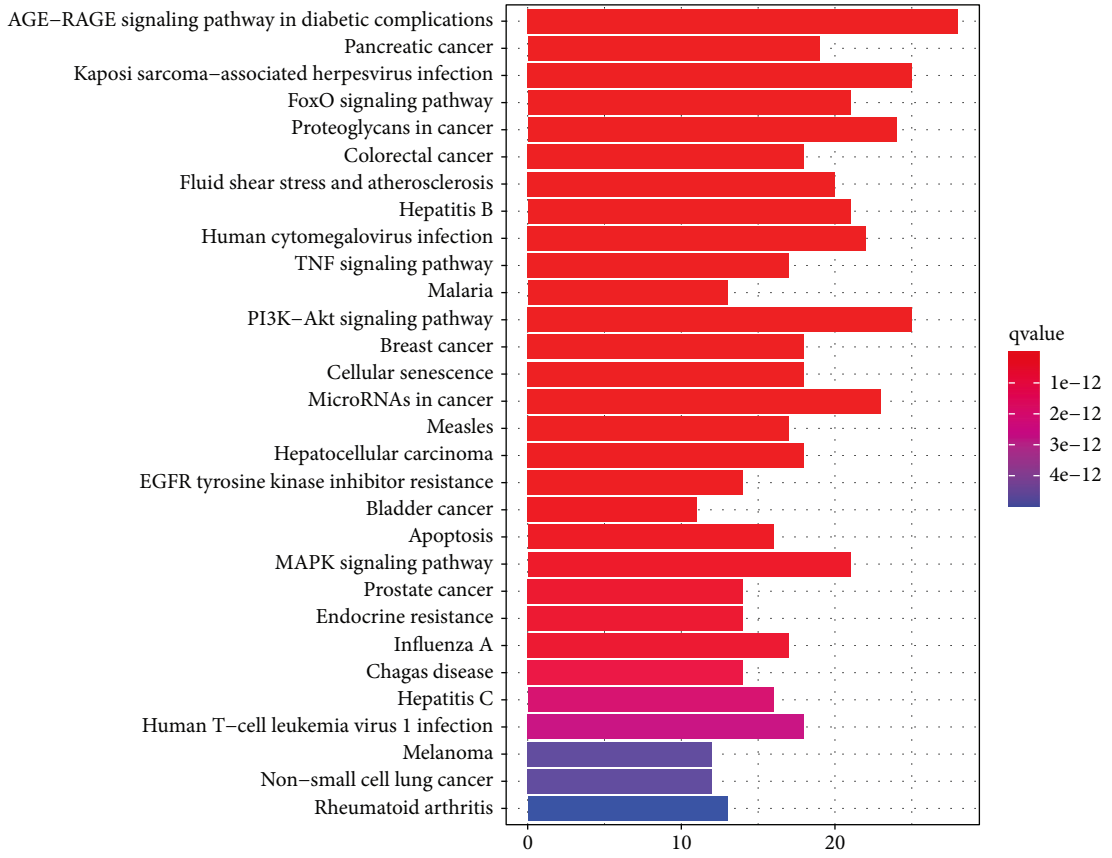

Figure 4: KEGG enrichment analysis of potential targets. q value is the adjusted p value, and q value gradually increases as the colors change from dark red to blue.

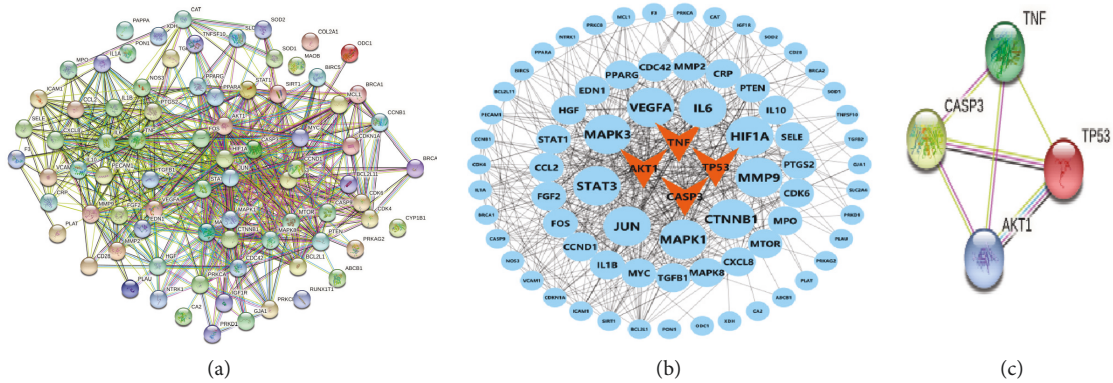

(a) (b) (c)

Figure 5: PPI analysis and target genes antiapoptosis screening results. (a) The string analysis of all genes resveratrol-SSNHL. (b) Cytoscape mapping results by degree values and apoptosis-related genes. (c) The relationship of four apoptosis-related genes based on STRING database analysis, edges represent protein-protein associations: green lines mean textmining; wine red lines mean experimentally determined; pale yellow lines mean from curated databases; black lines mean co-expression.

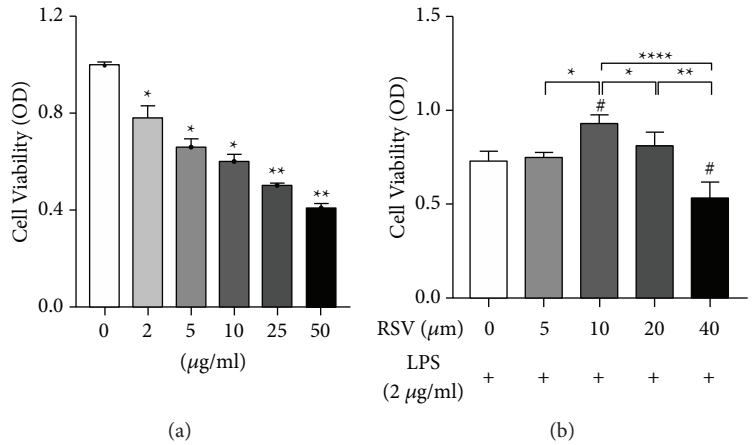

(a) (b)

Figure 6: CCK-8 analysis results. (a) CCK-8 analysis results for HEI-OC1 cells exposed to different concentrations of LPS. All concentrations of LPS induced significant apoptosis in HEI-OC1 cells versus the control group ($^{*}p < 0.05$ or $^{**}p < 0.01$). (b) Protective effects of RSV against LPS-induced apoptosis in HEI-OC1 cells. $\#p < 0.05$ versus the control group (0 μmol of RSV). 10 μmol RSV administration showed significant protection versus the control group (0 μmol of RSV). 5 and 20 μmol of RSV did not exhibit a significant protective effect. 40 μmol of RSV even reduced the activity compared to that in the control group ($^{*}p < 0.05$, $^{**}p < 0.01$, or $^{****}p < 0.001$).

mainly cytokine receptors and cellular components, including membrane rafts. KEGG analysis also focused on the AGE-RAGE signaling pathway in diabetic complications, Kaposi's sarcoma-associated herpesvirus infection, FoxO signaling pathway, PI3K-AKT signaling pathway, and other inflammatory and apoptosis-related signaling pathways. To further understand relationships among potential targets, we screened *AKT1, STAT3, JUN, TNF, TP53, MAPK3, CASP3*, and *VEGFA* as hub genes using PPI analysis. Among these hub genes, *TNF, CASP3, AKT1*, and *TP53* are involved in intracellular or extracellular apoptotic pathways. We verified that RSV could improve LPS-induced HEI-OC1 cell apoptosis by TNF, CASP3, AKT1, and TP53 multitargeted intervention *in vitro*. Molecular docking studies also identified that these central targets exhibited good affinity for RSV.

Glucocorticoids are currently recognized as the primary treatment for various types of SSNHL. Studies have shown that dexamethasone can play a protective role in TNF-α-induced apoptosis by activating signaling pathways such as PI3K/AKT and NF-kB [29] and revealed the protective effect of tunicamycin in HEI-OC1 cells by inhibiting endoplasmic reticulum stress [30]. However, certain patients remain insensitive to hormone therapy, which may play a beneficial role through multitargeted intervention involving traditional Chinese medicine.

RSV is a natural polyphenol with a stilbene skeleton that has many beneficial properties such as anti-inflammatory, antioxidant, and neuroprotective activities [13]. Studies have shown that RSV can be used to treat neurodegenerative (ND) diseases through multitargeted treatment [31]. In this study, we selected *TNF, CASP3, AKT1,* and *TP53* as hub genes related to apoptosis by PPI analysis. TNF-α is closely related to the occurrence and development of nervous disorders. Previous studies have shown that TNF-α inhibits glucocorticoid receptor function, *TNF-α* mutant mice are prone to high-frequency hearing loss during early development stages [32], and targeted

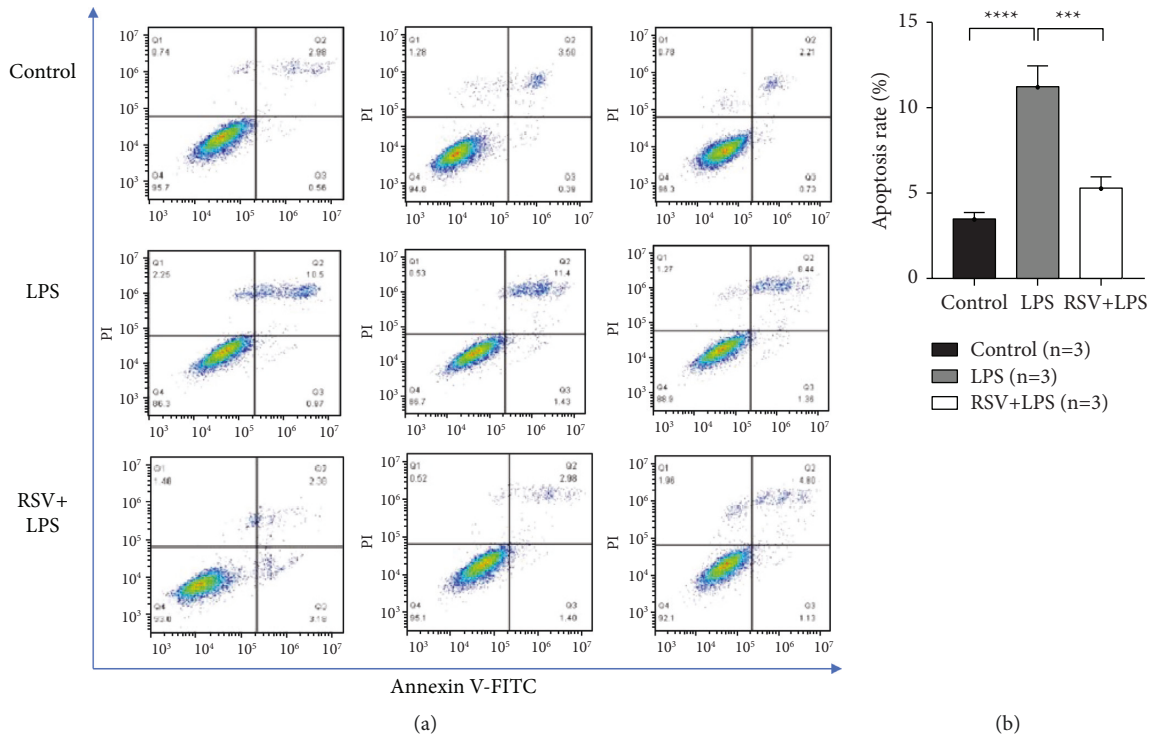

Figure 7: Results of FITC/PI analysis. (a) Examples of FITC/PI flow cytometric analysis results of three groups. (b) Statistical analysis results of FITC/PI flow cytometry apoptosis rates among groups. **** $p < 0.0001$ versus the control group and *** $p < 0.001$ versus the RSV + LPS group.

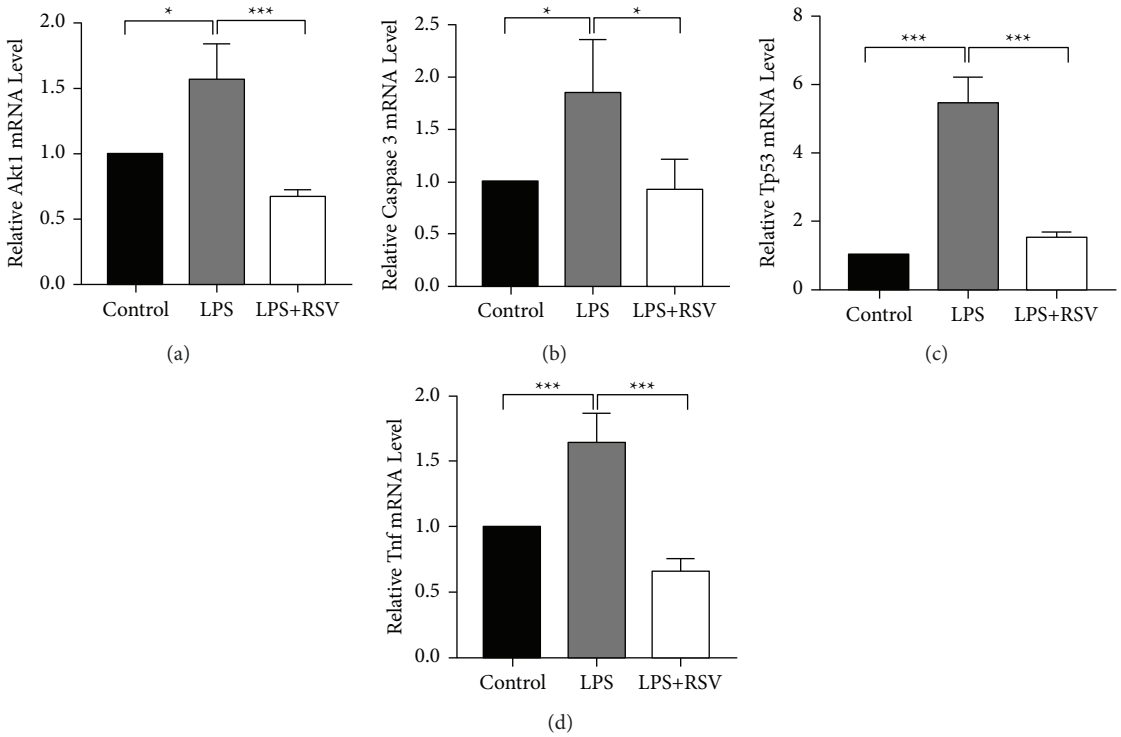

Figure 8: mRNA expression of apoptosis-related genes among groups. (a) The AKT1 mRNA expression. (b) The caspase-3 mRNA expression. (c) The TP53 mRNA expression. (d) The TNF mRNA expression. Compared to the control group, the AKT1, TNF, caspase-3, and TP53 levels in the LPS group significantly increased (* $p < 0.05$ or *** $p < 0.001$) while no significant changes were observed in the RSV + LPS group ($p > 0.05$).

Table 2: The minimum binding energy of resveratrol and apoptosis-related key receptors.

Drug	Target	The minimum binding energy (kcal/mol)	Grid center (X/Y/Z)
Resveratrol	TNF	−7.8	20.083/49.892/39.738
	Caspase-3	−7.4	26.71/22.591/37.128
	AKT1	−6.2	21.62/14.471/9.976
	P53	−5.5	52.103/−12.611/45.156

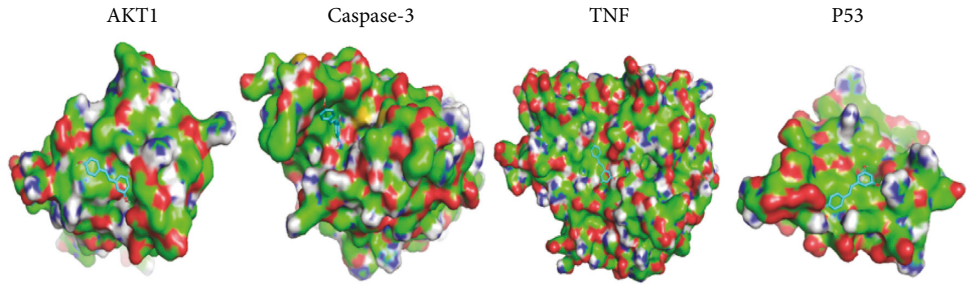

Figure 9: Diagram of structural interactions between resveratrol and apoptosis-related key receptors.

silencing of TNF-α is beneficial to prevent NIHL [33]. Exogenous and endogenous pathways focus on the activation of executors such as caspase-3 and ultimately the physical execution of apoptotic cell death [34]. Studies have shown that inhibiting caspases can prevent or delay hair cell death induced by noise or aminoglycosides [35]. In a hypoxia-induced SSNHL *in vitro* model, the level of cleaved-caspase-3 significantly increased [2]. AKT1 promotes cell proliferation by regulating cyclins and inhibits apoptosis by p53 [36]. Studies have also shown that age-related cochlear hair cell apoptosis is related to miR-34a/SIRT1/p53 signal transduction, which may represent a potential target for the treatment of age-related hearing loss [3]. Our results showed that RSV regulates *TNF, CASP3, AKT1*, and *TP53* mRNA levels and may play a protective role in LPS-induced apoptosis of hair cells through multitarget regulation. Molecular docking further confirmed the good docking performance of the target protein structures with RSV.

We may have chosen a relatively single database in the early stage of network pharmacological analysis, but TCMSP and DisGeNET databases selected in this study are the most representative databases. Among them, TCMSP contains 29,384 species of 499 Chinese herbal medicines, 3,311 targets, and 837 related diseases registered with the Chinese Pharmacopoeia [17]. The DisGeNET release in 2019 covers over 24,000 diseases and features, 17,000 genes, and 117,000 genomic variations, covering the full spectrum of human diseases and normal and abnormal features [19]. In the process of *in vitro* verification, we found that apoptosis of HEI-OC1 cells increased after LPS treatment, and flow cytometric analysis showed that the apoptosis rate was significantly higher than that of the control group. The apoptosis rate of the RSV + LPS group decreased, and there was no significant difference compared to that of the control cohort. We verified binding involving target proteins corresponding to key genes and RSV through molecular docking studies. Moreover, we found that TNF had the lowest minimum binding energy (-7.8 kcal/mol) among the four key apoptosis-related proteins, which further verified the close relationship between the pathogenesis of SSNHL and inflammation. Consistent with previous studies [1, 37–39], we speculate that RSV might play a protective role in hair cell apoptosis mainly through anti-inflammatory effects.

5. Conclusion

In summary, RSV is expected to be a safe and effective multitarget drug treatment for SSNHL therapy. Our network pharmacological analysis involving RSV predicted that the therapeutic effect of RSV is mediated by the regulation of apoptosis-related pathways involving TNF, CASP3, AKT1, and TP53. It will be necessary to explore the main mechanisms of RSV action through further *in vivo* verification experiments.

Data Availability

Data can be obtained from authors upon reasonable request.

Conflicts of Interest

The authors declare that there are no conflicts of interest.

Authors' Contributions

Design scheme were contributed by WS and SY. Execution experiment and analysis results were contributed by SY and JL. Network pharmacology analysis and mapping were carried out by SY, QD, and XXW. Writing and revision of the papers were done by SY and WS.

Acknowledgments

The authors thank researchers who created and shared databases and online analysis platforms. This work was supported by Medical Science and Technology Development Foundation Nanjing Department of Health (ZKX21012).

Supplementary Materials

Table S1. Targets of resveratrol from the TCMSP database (151 resveratrol target proteins were obtained and transformed into corresponding differential genes). *Table S2*. Targets of SSNHL from the DisGeNET database (2342 corresponding target genes were obtained). *Table S3*. RSV-SSNHL potential targets and Cytoscape analysis results (a total of 2416 nodes were obtained by PPI analysis, and the number of nodes was selected as greater than or equal to 70). (*Supplementary Materials*)

References

[1] M. Hiramatsu, M. Teranishi, Y. Uchida et al., "Polymorphisms in genes involved in inflammatory pathways in patients with sudden sensorineural hearing loss," *Journal of Neurogenetics*, vol. 26, no. 3-4, pp. 387–396, 2012.

[2] L. Xie, Q. Zhou, X. Chen et al., "Elucidation of the Hdac2/Sp1/miR-204-5p/Bcl-2 axis as a modulator of cochlear apoptosis via in vivo/in vitro models of acute hearing loss," *Molecular Therapy - Nucleic Acids*, vol. 23, pp. 1093–1109, 2021.

[3] H. Xiong, J. Pang, H. Yang et al., "Activation of miR-34a/SIRT1/p53 signaling contributes to cochlear hair cell apoptosis: implications for age-related hearing loss," *Neurobiology of Aging*, vol. 36, no. 4, pp. 1692–1701, 2015.

[4] L. Chai, Y. Gao, Z. Y. Gu, and D. F. Ni, "Apoptosis and apoptosis-related genes in experimental autoimmune inner ear disease," *Zhonghua er bi yan hou tou jing wai ke za zhi*, vol. 40, no. 8, pp. 561–565, 2005.

[5] S. Esaki, F. Goshima, H. Kimura et al., "Auditory and vestibular defects induced by experimental labyrinthitis following herpes simplex virus in mice," *Acta Oto-Laryngologica*, vol. 131, no. 7, pp. 684–691, 2011.

[6] N. Amarjargal, N. Andreeva, J. Gross et al., "Differential vulnerability of outer and inner hair cells during and after oxygen-glucose deprivation in organotypic cultures of newborn rats," *Physiological Research*, vol. 58, no. 6, pp. 895–902, 2009.

[7] K. i. Watanabe, K. Jinnouchi, A. Hess, O. Michel, and T. Yagi, "Detection of apoptotic change in the lipopolysaccharide (LPS)-treated cochlea of Guinea pigs," *Hearing Research*, vol. 158, no. 1-2, pp. 116–122, 2001.

[8] Editorial Committee of Chinese Journal of Otorhinolaryngology head and Neck Surgery OHaNSBoCMA, "Guideline of diagnosis and treatment of sudden deafness (2015)," *Zhonghua er bi yan hou tou jing wai ke za zhi*, vol. 50, no. 6, pp. 443–447, 2015.

[9] S. S. Chandrasekhar, B. S. Tsai Do, S. R. Schwartz et al., "Clinical practice guideline: sudden hearing loss (update) executive summary," *Otolaryngology - Head and Neck Surgery*, vol. 161, no. 2, pp. 195–210, 2019.

[10] C. Mirian and T. Ovesen, "Intratympanic vs systemic corticosteroids in first-line treatment of idiopathic sudden sensorineural hearing loss: a systematic review and meta-analysis," *JAMA Otolaryngol Head Neck Surg*, vol. 146, no. 5, pp. 421–428, 2020.

[11] R. Kaur, A. Sood, D. K. Lang et al., "Natural products as sources of multitarget compounds: advances in the development of ferulic acid as multitarget therapeutic," *Current Topics in Medicinal Chemistry*, vol. 22, no. 5, pp. 347–365, 2022.

[12] X. Meng, J. Zhou, C. N. Zhao, R. Y. Gan, and H. B. Li, "Health benefits and molecular mechanisms of resveratrol: a narrative review," *Foods*, vol. 9, no. 3, p. 340, 2020.

[13] T. Farkhondeh, S. L. Folgado, A. M. Pourbagher-Shahri, M. Ashrafizadeh, and S. Samarghandian, "The therapeutic effect of resveratrol: focusing on the Nrf2 signaling pathway," *Biomedicine & Pharmacotherapy*, vol. 127, p. 110234, 2020.

[14] C. M. Chagas, S. Moss, and L. Alisaraie, "Drug metabolites and their effects on the development of adverse reactions: revisiting Lipinski's Rule of Five," *International Journal of Pharmaceutics*, vol. 549, no. 1-2, pp. 133–149, 2018.

[15] C. H. Lee, K. W. Kim, S. M. Lee, and S. Y. Kim, "Dose-dependent effects of resveratrol on cisplatin-induced hearing loss," *International Journal of Molecular Sciences*, vol. 22, no. 1, p. 113, 2020.

[16] M. D. Seidman, W. Tang, V. U. Bai et al., "Resveratrol decreases noise-induced cyclooxygenase-2 expression in the rat cochlea," *Otolaryngology - Head and Neck Surgery*, vol. 148, no. 5, pp. 827–833, 2013.

[17] J. Ru, P. Li, J. Wang et al., "TCMSP: a database of systems pharmacology for drug discovery from herbal medicines," *Journal of Cheminformatics*, vol. 6, no. 1, p. 13, 2014.

[18] UniProt, "A worldwide hub of protein knowledge," *Nucleic Acids Research*, vol. 47, no. D1, pp. D506–d515, 2019.

[19] J. Piñero, J. M. Ramírez-Anguita, J. Saüch-Pitarch et al., "The DisGeNET knowledge platform for disease genomics: 2019 update," *Nucleic Acids Research*, vol. 48, no. D1, pp. D845–D855, 2020.

[20] L. Sun, S. Dong, Y. Ge et al., "DiVenn: an interactive and integrated web-based visualization tool for comparing gene lists," *Frontiers in Genetics*, vol. 10, p. 421, 2019.

[21] da W. Huang, B. T. Sherman, and R. A. Lempicki, "Systematic and integrative analysis of large gene lists using DAVID bioinformatics resources," *Nature Protocols*, vol. 4, no. 1, pp. 44–57, 2009.

[22] M. Kanehisa, M. Furumichi, M. Tanabe, Y. Sato, and K. Morishima, "KEGG: new perspectives on genomes, pathways, diseases and drugs," *Nucleic Acids Research*, vol. 45, no. D1, pp. D353–D361, 2017.

[23] D. Szklarczyk, A. L. Gable, D. Lyon et al., "STRING v11: protein-protein association networks with increased coverage, supporting functional discovery in genome-wide experimental datasets," *Nucleic Acids Research*, vol. 47, no. D1, pp. D607–d613, 2019.

[24] O. Trott and A. J. Olson, "AutoDock Vina: improving the speed and accuracy of docking with a new scoring function, efficient optimization, and multithreading," *Journal of Computational Chemistry*, vol. 31, no. 2, pp. 455–461, 2010.

[25] M. Hoffman, A. Blum, R. Baruch, E. Kaplan, and M. Benjamin, "Leukocytes and coronary heart disease," *Atherosclerosis*, vol. 172, no. 1, pp. 1–6, 2004.

[26] P. Libby, "Inflammation in atherosclerosis-No longer a theory," *Clinical Chemistry*, vol. 67, no. 1, pp. 131–142, 2021.

[27] M. Masuda, S. Kanzaki, S. Minami et al., "Correlations of inflammatory biomarkers with the onset and prognosis of idiopathic sudden sensorineural hearing loss," *Otology & Neurotology*, vol. 33, no. 9, pp. 1692–1150, 2012.

[28] B. G. Weiss, S. Freytag, B. Kloos et al., "Cannabinoid receptor 2 agonism is capable of preventing lipopolysaccharide induced decreases of cochlear microcirculation - a potential approach for inner ear pathologies," *Otology & Neurotology*, vol. 42, no. 9, pp. e1396–e1401, 2021.

[29] S. M. Haake, C. T. Dinh, S. Chen, A. A. Eshraghi, and T. R. Van De Water, "Dexamethasone protects auditory hair

cells against TNFα-initiated apoptosis via activation of PI3K/Akt and NFκB signaling," *Hearing Research*, vol. 255, no. 1-2, pp. 22–32, 2009.

[30] Z. Liu, B. Fei, L. Xie et al., "Glucocorticoids protect HEI-OC1 cells from tunicamycin-induced cell damage via inhibiting endoplasmic reticulum stress," *Open Life Sciences*, vol. 16, no. 1, pp. 695–702, 2021.

[31] W. Wang, S. Wang, T. Liu et al., "Resveratrol: multi-targets mechanism on neurodegenerative diseases based on network pharmacology," *Frontiers in Pharmacology*, vol. 11, p. 694, 2020.

[32] N. Oishi, J. Chen, H. W. Zheng, K. Hill, J. Schacht, and S. H. Sha, "Tumor necrosis factor-alpha-mutant mice exhibit high frequency hearing loss," *Journal of the Association for Research in Otolaryngology*, vol. 14, no. 6, pp. 801–811, 2013.

[33] J. C. Rodrigues, A. L. L. Bachi, G. A. V. Silva et al., "New insights on the effect of TNF alpha blockade by gene silencing in noise-induced hearing loss," *International Journal of Molecular Sciences*, vol. 21, no. 8, p. 2692, 2020.

[34] S. Christgen, R. E. Tweedell, and T. D. Kanneganti, "Programming inflammatory cell death for therapy," *Pharmacology & Therapeutics*, vol. 232, Article ID 108010, 2022.

[35] A. G. Cheng, L. L. Cunningham, and E. W. Rubel, "Mechanisms of hair cell death and protection," *Current Opinion in Otolaryngology & Head and Neck Surgery*, vol. 13, no. 6, pp. 343–348, 2005.

[36] N. Hinz and M. Jücker, "Distinct functions of AKT isoforms in breast cancer: a comprehensive review," *Cell Communication and Signaling*, vol. 17, no. 1, p. 154, 2019.

[37] M. Svrakic, S. Pathak, E. Goldofsky et al., "Diagnostic and prognostic utility of measuring tumor necrosis factor in the peripheral circulation of patients with immune-mediated sensorineural hearing loss," *Archives of Otolaryngology - Head and Neck Surgery*, vol. 138, no. 11, pp. 1052–1058, 2012.

[38] E. Demirhan, N. P. Eskut, Y. Zorlu, I. Cukurova, G. Tuna, and F. G. Kirkali, "Blood levels of TNF-α, IL-10, and IL-12 in idiopathic sudden sensorineural hearing loss," *The Laryngoscope*, vol. 123, no. 7, pp. 1778–1781, 2013.

[39] J. G. Doo, D. Kim, Y. Kim et al., "Biomarkers suggesting favorable prognostic outcomes in sudden sensorineural hearing loss," *International Journal of Molecular Sciences*, vol. 21, no. 19, p. 7248, 2020.

Hindawi
Evidence-Based Complementary and Alternative Medicine
Volume 2022, Article ID 5524107, 8 pages
https://doi.org/10.1155/2022/5524107

Research Article

Anti-Inflammatory and Antioxidant Effects of the Indole-Derived N-Salicyloyltryptamine on Peritonitis and Joint Disability Induced by Carrageenan in Rodents

B. P. Sousa-Neto,[1] **F. V. M. Cunha**,[1] **Daniel Barbosa Nunes**,[1] **B. S. Gomes**,[1] **Layane Valeria Amorim**,[1] **Everton Moraes Lopes**,[1] **S. J. C. Gutierrez**,[2] **F. R. C. Almeida**,[1,3] **D. D. R. Arcanjo**,[1,4] **M. F. V. Souza**,[5] **and F. A. Oliveira**[1,3]

[1]*Medicinal Plants Research Center, Federal University of Piaui, Av. Universitária s/n, Campus Ministro Petrônio Portella, SG-15, Ininga, 64049-550 Teresina, PI, Brazil*
[2]*Faculty of Pharmacy, Federal University of Piauí, Av. Universitária s/n, Campus Ministro Petrônio Portella, Ininga, 64049-550 Teresina, PI, Brazil*
[3]*Department of Biochemistry and Pharmacology, Federal University of Piauí, Av. Universitário s/n, Campus Ministro Petrônio Portella, SG-08, Ininga, 64049-550 Teresina, PI, Brazil*
[4]*Department of Biophysics and Physiology, Federal University of Piauí, Av. Universitária s/n, Campus Ministro Petrônio Portella, Ininga, 64049-550 Teresina, PI, Brazil*
[5]*Federal University of Paraíba, Coordinator of the Graduate Program in Development and Technological Innovation of Drugs. (Association UFRN/UFPB/UFRPE/UFC), 64049-550 Teresina, PI, Brazil*

Correspondence should be addressed to D. D. R. Arcanjo; daniel.arcanjo@ufpi.edu.br

Received 5 February 2022; Accepted 26 April 2022; Published 13 May 2022

Academic Editor: Xiang Liu

Purpose. To investigate the anti-inflammatory and antioxidant activities of N-salicyloyltryptamine (NST) in experimental models of carrageenan (Cg)-induced peritonitis in mice, and evaluation of the effects of NST on Cg-induced joint disability in rats. *Methods*. Female Swiss mice were submitted to Cg-induced peritonitis in mice or Cg-induced joint disability in rats after intraperitoneal injection of NST (100 or 200 mg/kg). Total leukocyte count, total protein concentration, myeloperoxidase (MPO) and catalase (CAT) activities, and nitrite (NO_2^-) and thiobarbituric acid reactive species (TBARS) levels were determined. *Results*. NST significantly decrease the migration of leukocytes to peritoneal exudate. Cg induces inflammatory responses mediated by expression of reactive oxygen species (ROS). The results further showed that NST significantly decreased MPO and CAT activities, as well as reduced NO_2^- and TBARS levels, compared with the vehicle group. Animals treated with NST significantly reduced paw elevation time (PET) on the first hour after induction of joint injury, and this effect was sustained throughout the analysis. *Conclusion*. NST presented anti-inflammatory and antioxidant effects in experimental models of carrageenan-induced peritonitis and joint disability in mice and rats, respectively, which may be related to the modulation of neutrophils migration as well as the involvement of antioxidant mechanisms.

1. Introduction

The indole nucleus is part of many natural and synthetic molecules with important biological activities [1]. Among the indolic derivatives, benzoyltryptamine, whose structures are related to N-benzoyltryptamine, is previously obtained from the species *Myrtopsis myrtoidea* (Baill.) Guillaumin, a plant of the family Rutaceae [2]. These derivatives include the compounds N-N-dimethyltryptamine and 5-methoxy-NN-dimethyltryptamine, which possess psychotomimetic

activity [3]. N-Salicyloyltryptamine or (2-hydroxy-N-[2-(1H-indol-3-yl)ethyl]-benzamide) exhibited anticonvulsant, hypnotic, and muscle relaxant activities [4].

An in vitro study has shown that NST negatively modulates expression of both TNF-α and IL-1β, inhibits the phosphorylation of ERK1/2 and IκBα, and reduces the concentrations of reactive oxygen (ROS) and nitrogen (RNS) species in macrophages, thus contributing to the reversal of inflammatory response [5]. The presence of oxidizing agents has been associated with cardiovascular diseases [6], diabetes [7], cancer, [8], rheumatoid arthritis, and arthrosis [9]. The study shows that NST exerts antiedematogenic activity in in vivo models induced by different phlogistic agents [10]. However, no studies have been found in the literature showing the antioxidant activity of NST in vivo protocols.

One of the main oxidizing agents present in the inflammatory process is nitric oxide (NO) [11], produced mainly by activated macrophages; when reacted with oxygen, it forms peroxynitrite ($ONOO^-$), a powerful protein oxidant. $ONOO^-$ can then be protonated in the presence of ionic hydrogen (H^+), giving rise to a highly reactive and toxic radical, hydroxyl (HO^-), effectively potentiating the toxic action of NO and O^{-2} [12]. This radical favor vasodilation due to a synergistic effect with PGI_2, relaxing like muscle cells, allows the movement of leukocyte cells through the endothelium [13]. However, $ONOO^-$ also produces harmful effects on the organism, such as tissue damage, DNA deamination, and activating nuclear signaling pathways for the transcription of proinflammatory agents [14, 15].

The most reasonable alternative to inhibit ROS is supplementation with antioxidant agents. However, it has often not been possible to attenuate the progress of the disease, reducing the life expectancy [16]. Oxidative disorders produced by ROS or RNS are underlying several inflammation-related pathophysiological processes by the production of proinflammatory cytokines and suppression of the antioxidant defense systems and characteristic edema formation [17]. In diseases such as rheumatoid arthritis and arthrosis, which normally occur in the joints, free radicals are produced primarily by macrophages and activated neutrophils in the synovial membrane and chondrocytes [9]. In this sense, there is a need for discoveries of new compounds with both anti-inflammatory and antioxidant potentials.

Therefore, considering that reports of the anti-inflammatory and antioxidant effects of NST in vivo assays involving the inhibition of reactive oxygen species are lacking, the present study aims to investigate the anti-inflammatory and antioxidant effects induced by NST in experimental models of peritonitis and articular disability in experimental models in rodents.

2. Materials and Methods

2.1. Drugs and Reagents. The NST 2-hydroxy-N-[2-(1H-indol-3-yl)-ethyl]-benzamide was obtained by "in house" synthesis as previously reported (João Pessoa, PB, Brazil; patent document: BR 200304393-A) in Laboratory of Pharmaceutical Chemistry, UFPI (Teresina, PI, Brazil) [5]. Carrageenan, acetic acid, Triton X-100, L-methionine, hydroxylamine chloride, riboflavin, thiobarbituric acid (TBA), Griess reagent, sodium dodecylsulfate, O-dianisidine, hexadecyltrimethylammonium bromide (HTAB), sodium phosphate, 5,5′-dithiobis-(2-nitrobenzoic acid) (DTNB), and sodium nitrite were purchased from Sigma-Aldrich (Saint Louis, MO, USA). Indomethacin (Indocid®), sodium phosphate, zinc sulfate, hydrogen peroxide, Tris base, sodium hydroxide, and trichloroacetic acid were purchased from Merck (Darmstadt, Germany). Turk's solution was purchased from Newprov (Pinhais, PR, Brazil).

2.2. Animals. Female Wistar rats (170–230 g) and Swiss mice (27–32 g) ($n = 6$ per group) were used in experiments. The animals were maintained at $23 \pm 1^{\circ}C$ and 12–12 h dark/light cycles, and they had free access to food and tap water. After experimental protocols, the animals were euthanized by intraperitoneal administration of thiopental sodium (150 mg/kg, i.p.). The conduction of all experimental protocols using animals was authorized by the Animal Use Ethics Committee (CEUA) from Universidade Federal do Piauí (permission no. 082/14; date of approval: 24-Nov-2014), as well as they followed internationally recommended guidelines.

2.3. Effect of NST on Carrageenan-Induced Peritonitis in Mice. Female Swiss mice (25–30 g) were treated intraperitoneally with vehicle (0.9% NaCl + 5.0% Tween 80), NST at doses of 50, 100, and 200 mg/kg), or indomethacin at dose of 10 mg/kg. After 30 minutes, carrageenan (0.05 mL at 1.0%) was administered into the peritoneal cavity [18]. Then, after 4 hours, euthanasias were carried out, and then, peritoneal cavities were washed with 5 mL of heparinized (10 IU/mL) PBS solution [19]. Additional exudate aliquot was collected to analyze the activities of myeloperoxidase (MPO), catalase (CAT), nitrite (NO_2^-), and thiobarbituric acid reactive species (TBARS).

2.4. Total Leukocyte Counting in the Peritoneal Exudate. A sample of 0.380 mL of the Turk's solution (1/20) was added to 0.02 ml of peritoneal exudate, and the number of leukocytes was counted using a Neubauer chamber under the optical microscope. Numbers of total leukocytes were determined according to the following formula: cells/$mm^3 = N \times 20 \times 2.5$, where N represents the number of cells, 20 is the dilution factor of Turk's solution, and 2.5 is the total volume into the Neubauer chamber. Results were expressed as total leukocytes/mm^3 [20].

2.5. Measurement of Proteins in the Peritoneal Exudate. Proteins were quantified using specific protein dosing kits [21]. Biuret reagent, potassium hydroxide solution (KOH), and copper sulfate ($CuSO_4$), associated with sodium and potassium tartrate ($KNaC_4H_4O_6{\cdot}4H_2O$), were used to dose proteins. After centrifugation of the exudate, the supernatants were collected and transferred to specific cuvettes and placed in a Labtest®'s automatic biochemical analyzer,

serial number 1208.26 (Lagoa Santa, MG, Brazil), according to manufacturer's recommendations.

2.6. Evaluation of Myeloperoxidase Activity (MPO) in the Peritoneal Exudate. The MPO activity was assayed according with the method [21]. Briefly, 400 μL of the peritonitis exudate was centrifuged at 4000 g for 7 min at 4°C. Then, 100 μl of supernatant was collected and added to 1 ml of 0.5% HTAB buffer, pH 6.0 (hexadecyltrimethylammonium bromide), and centrifuged at 4500 $\times g$ and 4°C for 10 min. Then, 10 μl of the supernatant was withdrawn and incubated with 200 μl of the reading solution (0.167 mg/mL O-dianisidine and 1.0% H_2O_2 in phosphate buffer pH 6.0). After 5 min, the MPO activity was determined at 450 nm and expressed in units of MPO per microliter (U MPO/μL).

2.7. Evaluation of Catalase Activity (CAT) in the Peritoneal Exudate. Briefly, samples (20 μL) were incubated with 50 mM phosphate buffer, pH 7.0 (1.2 mL). Right after, 1.0 mL of 30 mM H_2O_2 was added, and absorbances were measured at 240 nm every 2 min for 6 min. CAT activity was expressed in μmols of H_2O_2 decomposed/min/μL of peritoneal exudate [22].

2.8. Determination of Nitrite (NO_2^-) Content in the Peritoneal Exudate. Briefly, 20 μL of the peritoneal exudate was added in distilled water (1 : 4 v/v) and submitted to deproteinization by incubation of 300 g/L zinc sulfate (1 : 20 v/v), followed by centrifugation for 15 min at 1000 $\times g$ [23]. Afterwards, 100 μL of Griess' reagent was added to 100 μL of supernatant. After 10 minutes, absorbances were read at 550 nm [24]. A standard curve was obtained for $NaNO_2$ solution (sodium nitrite) to determine nitrite concentration. Results are expressed in terms of μmol/mL of peritoneal exudate.

2.9. Determination of Thiobarbituric Acid Reactive Species (TBARS) Content in the Peritoneal Exudate. For thiobarbituric acid reactive species (TBARS) determination, twenty microliters of the exudate were added to 0.5% TBA (600 μL) and 20% acetic acid pH 3.5 (350 μL). Then, samples were heated at 100°C and boiled for 45 minutes, followed by ice bath for 15 minutes. Afterwards, fifty microliters of 8.1% sodium dodecyl sulfate (SDS) were added, and samples were centrifuged at 12,000 $\times g$ for 15 minutes at 25°C. Absorbances were read at 420, 490, and 550 nm filters. A standard curve was obtained for malondialdehyde (MDA) to determine the TBARS content. Results were expressed as nmol MDA/mL of peritoneal exudate [25].

2.10. Assessment of NST-Induced Effects on Carrageenan-Induced Joint Disability in Rats. In parallel with the carrageenan-induced peritonitis, the effects of NST on joint motor disability degree were evaluated. After setting for 30 minutes and immediately prior to the induction of carrageenan joint disability, the animals were submitted to the joint disability test for 60 seconds at the speed of 3 revolutions per minute (RPM), and the results were recorded as a control measure [26]. The animals were then treated intraperitoneally with vehicle (0.9% NaCl + 5.0% Tween80), NST at doses of 50, 100, and 200 mg/kg, or indomethacin at dose of 10 mg/kg. After 30 minutes, the animals received intraarticular administration of 100 μL (300 μg) of carrageenan into tibiofemoral joint of right paws. Measurements were performed for 60 seconds every hour until the sixth hour and one reading after 24 hours.

2.11. Statistical Analysis. The results were expressed as mean ± SEM. One-way ANOVA followed by Tukey's post-test or two-way ANOVA followed by Bonferroni's post-test were applied. Differences were considered at significance level when $p < 0.05$. Statistical analyses and graphs plotting were performed using GraphPad Prism® software version 6.01 for Windows (GraphPad Software, La Jolla California USA, https://www.graphpad.com).

3. Results

3.1. Effect of NST on the Total Number of Leukocytes in Carrageenan-Induced Peritonitis Exudate in Mice. Pretreatment of animals with NST (100 and 200 mg/kg) was able to significantly reduce the migration of total leukocytes (1.37 ± 0.07 and 0.59 ± 0.05, respectively) to the peritoneal exudate, as well as for indomethacin (10 mg/kg) (0.5 ± 0.1), when compared with the vehicle group (2.56 ± 0.11). NST at the dose of 50 mg/kg was not effective in this protocol (Figure 1).

3.2. Measurement of Total Proteins in the Peritoneal Exudate. Both NST at doses of 100 and 200 mg/kg or indomethacin (10 mg/kg) markedly reduced the concentration of total proteins in the peritoneal exudate when compared with the vehicle group. NST at 50 mg/kg was not effective in this protocol (Figure 2).

3.3. Effect of NST on Myeloperoxidase (MPO) Activity. Myeloperoxidase activity decreased in animals treated with NST (1.38 ± 0.20 and 1.43 ± 0.24 at doses of 100 and 200 mg/kg, respectively) or indomethacin (1.09 ± 0.20) when compared with the vehicle group (3.90 ± 0.31). No significant results were observed in the group treated with NST 50 mg/kg (Figure 3).

3.4. Effect of NST on Catalase (CAT) Activity. In NST-treated groups (100 and 200 mg/kg), CAT activity significantly decreased (0.93 ± 0.10 and 0.71 ± 0.15, respectively) when compared with the vehicle group (1.84 ± 0.27). Treatment with indomethacin (10 mg/kg) significantly decreased catalase activity (0.69 ± 0.04) when compared with the vehicle group (1.84 ± 0.27) (Figure 4).

3.5. Effect of NST on Nitrite (NO_2^-) Concentration. The NST at doses of 100 and 200 mg/kg promoted a significant decrease in the concentration of nitrite (14.09 ± 1.17 and

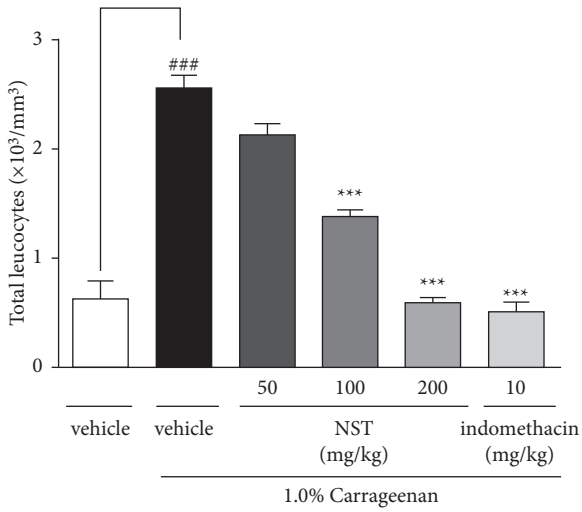

Figure 1: Effects of NST (50, 100, or 200 mg/kg, i.p.), vehicle (0.9% NaCl + 5% Tween 80, i.p.), and indomethacin (10 mg/kg, i.p.) on the total number of leukocytes in the peritoneal exudate of mice after administration of 1.0% carrageenan. Values are expressed as mean ± S.E.M. $^{###}P < 0.001$ when compared with only vehicle; $^{***}p < 0.001$ when compared with vehicle plus 1.0% carrageenan. One-way ANOVA was followed by Tukey's post hoc test.

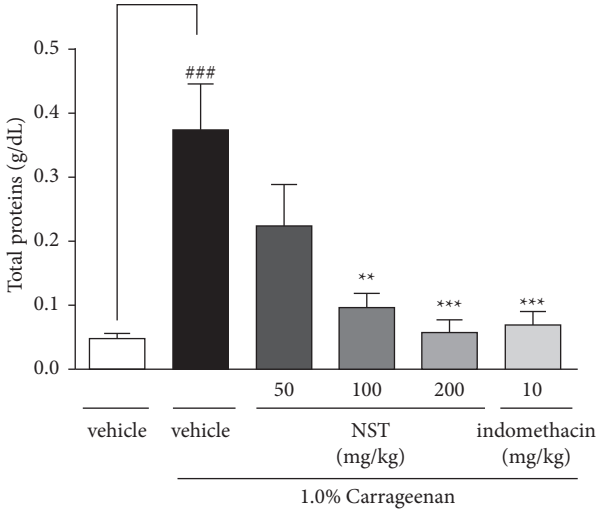

Figure 2: Effects of NST (50, 100, or 200 mg/kg, i.p.), vehicle (0.9% NaCl + 5% Tween 80, i.p.), and indomethacin (10 mg/kg, i.p.) on the concentration of total proteins in the peritoneal exudate of mice after administration of 1.0% carrageenan. Values are expressed as mean ± S.E.M. $^{###}P < 0.001$ when compared with only vehicle; $^{**}p < 0.01$ and $^{***}p < 0.001$ when compared with vehicle plus 1.0% carrageenan. One-way ANOVA was followed by Tukey's post hoc test.

13.02 ± 1.51, respectively) in peritoneal exudate when compared with the vehicle group (33.05 ± 3.57). Likewise, animals treated with indomethacin (10 mg/kg) also showed a significant reduction of NO_2^- concentration. On the other hand, NST 50 mg/kg did not present any significant effect (Figure 5).

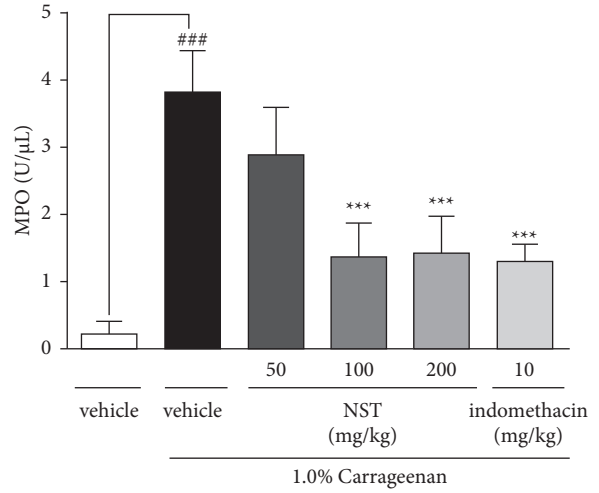

Figure 3: Effects of NST (50, 100, or 200 mg/kg, i.p.), vehicle (0.9% NaCl + 5% Tween 80, i.p.), and indomethacin (10 mg/kg, i.p.) on the myeloperoxidase (MPO) activity in the peritoneal exudate of mice after administration of 1.0% carrageenan. Values are expressed as mean ± S.E.M. $^{###}P < 0.001$ when compared with only vehicle; $^{***}p < 0.001$ when compared with vehicle plus 1.0% carrageenan. One-way ANOVA was followed by Tukey's post hoc test.

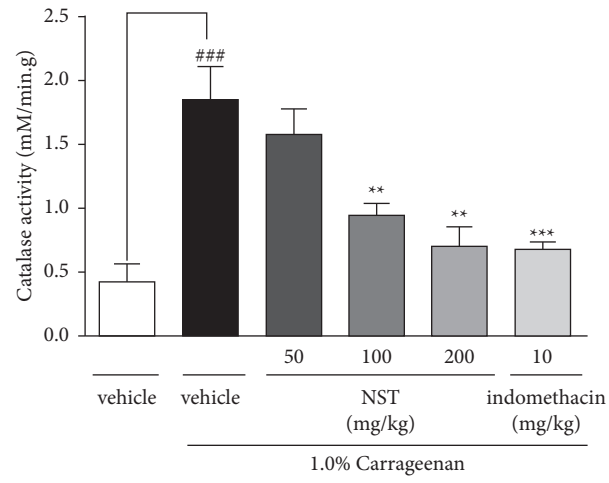

Figure 4: Effects of NST (50, 100, or 200 mg/kg, i.p.), vehicle (0.9% NaCl + 5% Tween 80, i.p.), and indomethacin (10 mg/kg, i.p.) on the catalase (CAT) activity in the peritoneal exudate of mice after administration of 1.0% carrageenan. Values are expressed as mean ± S.E.M. $^{###}P < 0.001$ when compared with only vehicle; $^{**}p < 0.01$ and $^{***}p < 0.001$ when compared with vehicle plus 1.0% carrageenan. One-way ANOVA was followed by Tukey's post hoc test.

3.6. Effect of NST on the Concentration of TBARS. NST (100 and 200 mg/kg) was able to decrease concentrations of thiobarbituric acid reactive species (3.10 ± 0.53 and 2.40 ± 0.24, respectively) when compared with the vehicle group (4.68 ± 0.32). Likewise, indomethacin (10 mg/kg) decreased TBARS concentration (2.94 ± 0.32). On the other hand, any significant results were observed for NST at the lowest dose of 50 mg/kg (Figure 6).

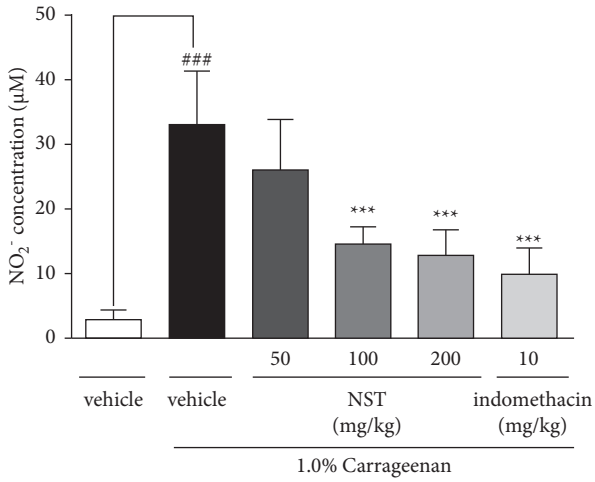

Figure 5: Effects of NST (50, 100, or 200 mg/kg, i.p.), vehicle (0.9% NaCl + 5% Tween 80, i.p.), and indomethacin (10 mg/kg, i.p.) on nitrite (NO_2^-) concentration in the peritoneal exudate of mice after administration of 1.0% carrageenan. Values are expressed as mean ± S.E.M. $^{###}P < 0.001$ when compared with only vehicle; $^{***}p < 0.001$ when compared with vehicle plus 1.0% carrageenan. One-way ANOVA was followed by Tukey's post hoc test.

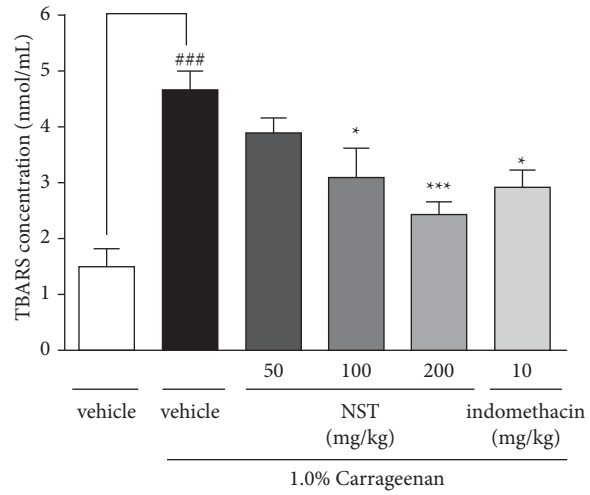

Figure 6: Effects of NST (50, 100, or 200 mg/kg, i.p.), vehicle (0.9% NaCl + 5% Tween 80, i.p.), and indomethacin (10 mg/kg, i.p.) on TBARS concentration in the peritoneal exudate of mice after administration of 1.0% carrageenan. Values are expressed as mean ± S.E.M. $^{###}P < 0.001$ when compared with only vehicle; $^{*}p < 0.05$ and $^{**}p < 0.01$ when compared with vehicle plus 1.0% carrageenan. One-way ANOVA was followed by Tukey's post hoc test.

3.7. Effect of NST on Carrageenan-Induced Joint Disability. Injection of carrageenan (300 μg per 100 μL of total volume) into the tibiofemoral joint of the animals caused articular disability evidenced by an increase in paw elevation time in the vehicle group. In the present study, NST (100 and 200 mg/kg) and indomethacin (10 mg/kg) showed a marked significant decrease in paw elevation time (PET) during 4 h of observation, which remained up to the 24th hour after carrageenan injection. NST (50 mg/kg) showed no significant inhibition during the observed period (Figure 7).

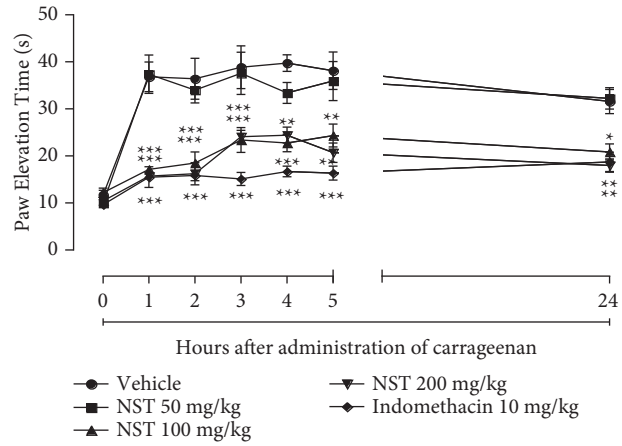

Figure 7: Effect of NST (50, 100 or 200 mg/kg, i.p.), vehicle (0.9% NaCl + 5% Twee n80, i.p.), and indomethacin (10 mg/kg, i.p.) on the carrageenan-induced joint disability 100 μL (300 μg) in female rats. Values are expressed as mean ± S.E.M. $^{**}p < 0.01$ and $^{***}p < 0.001$ vs. vehicle control. One-way ANOVA was followed by Bonferroni's post hoc test.

4. Discussion

Compounds that contain the indole nucleus are related to the metabolism of tryptophan and may exhibit ligands in different regions of the indolic core [27]. The indole ring has a heterocyclic structure described in 1866, which is present in a considerable number of natural compounds derived mainly from plants [28]. NST consists of an N-benzoyl-tryptamine-related chemical structure, an isolated alkaloid from the plant species *Myrtopsis myrtoidea* (Baill) Guillaumin [2]. Furthermore, a recent study demonstrated no sign of apparent toxicity and no animal deaths after intraperitoneal administration of NST at 2000 mg/kg followed by 14 days of observation [10].

Indolic derivative compounds present in biological tissue such as tryptophan, melatonin, and serotonin are potent hydroxyl radical sequesters, preventing cellular oxidative damage and mitigating leukocyte migration [27]. Therefore, the carrageenan-induced acute peritonitis in mice was chosen for investigation of mechanisms underlying both antioxidant and anti-inflammatory effects of NST. When administered intraperitoneally, carrageenan was able to increase capillary permeability, which causes leukocyte infiltration, extravasation of proteins into the tissue, or exudate and release of cytokines. These events are important in triggering inflammatory processes [29]. In this context, this experimental model allows to quantify migrated cells towards peritoneal cavity, which involves roles of inflammatory cytokines and chemokines [30].

Considering the cellular events, the evaluation of the presence of leukocytes is important to assess the installation of an inflammatory response. Neutrophils play important and crucial roles in several inflammatory conditions [31]. In this study, animals pretreated with NST showed a marked reduction in both number of leukocytes and total proteins in

peritoneal exudate. This may contribute to the recovery from the inflammatory process.

Then, the NST modulating activity on important enzymatic complexes such as myeloperoxidase (MPO), catalase (CAT), and nitrite (NO) concentrations and thiobarbituric acid reactive species were analyzed. MPO can be released after activation of leukocytes in phagosomes or in the extracellular space. When released, it reacts with the hydrogen peroxide formed by NADPH oxidase and increases the toxic potential of this oxidant [32]. A previous study has shown that substances that inhibit MPO activity may exhibit important anti-inflammatory activity [33]. In this study, similar results were observed in groups treated with NST or indomethacin, where MPO concentration was decreased, suggesting an anti-inflammatory activity of NST in this process.

The activity of the catalase in the peritoneal exudate was then evaluated. This enzyme catalyzes the reduction of H_2O_2 into H_2O eliminating ROS as such this contributes efficiently to combat inflammatory processes [34]. The decrease in catalase activity was observed in the study. This may be related to the decrease of leukocyte cells in the peritoneal exudate, since part of this antioxidant enzyme is produced by mitochondria, mainly leukocytes [35]. This study shows that catalase activity is reduced in patients with decreased myeloid lineage cell; however, patients with leukocytosis from chronic myeloid leukemia had high catalase activity [36].

Later, the NST activity on nitrite concentrations in the peritoneal exudate was analyzed. NO-2 is a relatively short-lived reactive species which underlies several biological processes. As nitric oxide (NO), it has role as an important endothelium-derived relaxing factor and is responsible for regulating vascular blood flow promoting vasodilation [37]. Considering the involvement of NO in inflammation-related cellular and molecular events, the decrease of biosynthesis of this radical using NO synthase inhibitors, such as L-NAME, has been investigated as a potential treatment of inflammatory conditions [38]. Therefore, we investigated the action of NST on the concentration of nitrite in carrageenan-induced peritonitis in mice. Factors such as low concentration and extreme short half-life hinder the dosing of NO in biological samples [39]. Thus, the indirect determination can be made by plasma nitrate and nitrite dosage [40]. Animals intraperitoneally treated with NST promoted a significant reduction of nitrite concentrations at doses of 100 and 200 mg/kg. Interestingly, extraction fractions obtained from *Alstonia scholaris* L. containing alkaloids such as picrinine, valesamine, and escolaricin, which contain the indolic nucleus in their structures, also displayed the anti-inflammatory effect by inhibition of NO and PGE_2 biosyntheses [41].

The antioxidant activity of NST on lipid peroxidation was also investigated; it is known that this phenomenon is quite harmful to the organism because it favors free radical reaction increasing cellular damage [42]. Scientific literature reports that the lipids peroxidation is directly associated with the onset of diseases such as atherosclerosis, rheumatoid arthritis, and Alzheimer's disease [43, 44]. The assessment of damages caused by lipid peroxidation on oxidative stress and inflammation was performed by determining thiobarbituric acid reactive species (TBARS) in experimental groups. In this sense, animals treated with NST showed significant lower concentrations of TBARS at doses of 100 or 200 mg/kg when compared with the vehicle group. Studies show that indole alkaloids such as 16-formyl-alpha-methoxystrictamine tubotaivine and picralinal inhibited exudation in xylene-induced mice ear edema. These alkaloids inhibited the concentrations of inflammation-related mediators, such as TBARS, PGE_2, NO_2^-, and malondialdehyde in the experimental model of carrageenan-induced air pouch in mice [45].

Previous studies show that the presence of the oxidizing agent in the articular synovial fluid favors lipid peroxidation and induces chondrocyte degradation and cartilage peroxidation. These events represent a primary risk factor for the development of arthritis [46]. In parallel, neutrophil depletion in uric acid crystal-induced gout is important for reversal of the inflammatory process [47]. Thus, considering the involvement of the migration of neutrophils and decrease of oxidative stress, the effects of NST on carrageenan-induced joint disability in mice were evaluated. This test is based on the joint disability using the loss of functionality through the inflammatory process as a measure (functio laesa). This technique is widely used for screening of possible analgesic and anti-inflammatory drugs [48–50].

The induction of arthritis by intraarticular injection of carrageenan presents a pattern of development similar to carrageenan-induced mouse paw edema. The administration of carrageenan in the joint cavity promotes in the first hours the liberation of inflammation-related mediators which induce edema and fast infiltration of polymorphonuclear granulocytes, leading to disablement due to joint sensitization manifested by limb withdrawal when the inflamed joint is pressed (mechanical hyperalgesia) [51]. In this model of carrageenan-induced joint disability, NST was effective in reducing the paw elevation time (PET). NST-treated animals showed a decrease in joint disability from the first hour after administration of carrageenan.

Chemical compounds containing indole nucleus presented antinematode and anti-inflammatory activities by acting as inhibitors of 5-lipoxygenase and cyclooxygenase enzymes, which convert arachidonic acid to leukotrienes and prostaglandins, respectively [52]. Studies have reported that indole alkaloids have exhibited a wide range of biological activities, such as anti-inflammatory activity, because they inhibit superoxide anion generation and the release of human neutrophil elastase [50–53]. They also possess anticonvulsive, cardiovascular, and antibacterial properties [45]. Thus, the present study corroborates the previous findings, since we found that NST decreases the paw elevation time when compared with the vehicle group.

5. Conclusion

In this regard, the present study supports evidences of the anti-inflammatory action of NST and its possible benefits in treatment of joint disability. Furthermore, nonclinical and clinical studies may be relevant regarding its potential application as an effective anti-inflammatory drug and to ensure its safety for therapeutic purposes.

Data Availability

The data used to support the findings of this study are available from the corresponding author upon request.

Conflicts of Interest

The authors declare that they have no conflicts of interest.

Authors' Contributions

Francisco A. Oliveira and Stanley J. G. Gutierrez conceptualized the study. Benedito P. Sousa Neto, Francisco V. M. Cunha, Daniel B. Nunes, Bruno S. Gomes, Layane V. Amorim, and Everton M. Lopes developed methodology. Benedito P Sousa Neto, Fernanda R. C. Almeida, and Francisco A. Oliveira performed formal analysis and investigated the study. Benedito P. Sousa Neto, Daniel B. Nunes, and Daniel D. R. Arcanjo wrote the original draft. Maria F. V. Sousa, Fernanda R. C. Almeida, and Francisco A. Oliveira wrote and reviewed the article. Stanley J. G. Gutierrez, Maria F. V. Sousa, and Francisco A. Oliveira collected resources. Francisco A. Oliveira supervised the study.

Acknowledgments

This work was supported by the CAPES (Coordenação de Aperfeiçoamento de Pessoal de Nível Superior, Brazil) (master's scholarship) and CNPq (Conselho Nacional de Desenvolvimento Científico e Tecnológico, Brazil) (Chamada Universal–MCTI/CNPq no. 14/2014).

References

[1] E. J. Barreiro and V. d. S. Bolzani, "Biodiversidade: fonte potencial para a descoberta de fármacos," *Química Nova*, vol. 32, no. 3, pp. 679–688, 2009.

[2] M. S. Hifnawy, J. Vaquette, T. Sévenet, J.-L. Pousset, and A. Cavé, "Produits neutres et alcaloides de Myrtopsis macrocarpa, M. myrtoidea, M. novae-caledoniae et M. sellingii," *Phytochemistry*, vol. 16, no. 7, pp. 1035–1039, 1977.

[3] X.-L. Jiang, H.-W. Shen, and A.-M. Yu, "Modification of 5-methoxy-N, N-dimethyltryptamine-induced hyperactivity by monoamine oxidase A inhibitor harmaline in mice and the underlying serotonergic mechanisms," *Pharmacology*, vol. 68, pp. 608–615, 2016.

[4] F. A. Oliveira, R. N. de Almeida, M. d. F. V. Sousa, J. M. Barbosa-Filho, S. A. Diniz, and I. A. de Medeiros, "Anticonvulsant properties of N-salicyloyltryptamine in mice," *Pharmacology Biochemistry and Behavior*, vol. 68, no. 2, pp. 199–202, 2001.

[5] J. Gasparotto, M. A. de Bittencourt Pasquali, N. Somensi et al., "Effect of N-salicyloyltryptamine (STP), a novel tryptamine analogue, on parameters of cell viability, oxidative stress, and immunomodulation in RAW 264.7 macrophages," *Cell Biology and Toxicology*, vol. 29, no. 3, pp. 175–187, 2013.

[6] H. N. Siti, Y. Kamisah, and J. Kamsiah, "The role of oxidative stress, antioxidants and vascular inflammation in cardiovascular disease (a review)," *Vascular Pharmacology*, vol. 71, pp. 40–56, 2015.

[7] S. Tangvarasittichai, "Oxidative stress, insulin resistance, dyslipidemia and type 2 diabetes mellitus," *World Journal of Diabetes*, vol. 6, no. 3, pp. 456–480, 2015.

[8] C. Karaaslan and S. Suzen, "Antioxidant properties of melatonin and its potential action in diseases," *Current Topics in Medicinal Chemistry*, vol. 15, no. 9, pp. 894–903, 2015.

[9] R. A. Roberts, R. A. Smith, S. Safe, C. Szabo, R. B. Tjalkens, and F. M. Robertson, "Toxicological and pathophysiological roles of reactive oxygen and nitrogen species," *Toxicology*, vol. 276, no. 2, pp. 85–94, 2010.

[10] B. P. Sousa-Neto, B. S. Gomes, F. V. M. Cunha et al., "Antiedematogenic activity of the indole derivative N-salicyloyltryptamine in animal models," *Anais da Academia Brasileira de Ciências*, vol. 90, no. 1, pp. 185–194, 2018.

[11] J. W. Little, T. Doyle, and D. Salvemini, "Reactive nitroxidative species and nociceptive processing: determining the roles for nitric oxide, superoxide, and peroxynitrite in pain," *Amino Acids*, vol. 42, no. 1, pp. 75–94, 2012.

[12] G.-C. Yen, P.-D. Duh, D.-W. Huang, C.-L. Hsu, and T. Y.-C. Fu, "Protective effect of pine (Pinus morrisonicola Hay.) needle on LDL oxidation and its anti-inflammatory action by modulation of iNOS and COX-2 expression in LPS-stimulated RAW 264.7 macrophages," *Food and Chemical Toxicology*, vol. 46, no. 1, pp. 175–185, 2008.

[13] Y. Hellsten, M. Nyberg, L. G. Jensen, and S. P. Mortensen, "Vasodilator interactions in skeletal muscle blood flow regulation," *The Journal of Physiology*, vol. 590, no. 24, pp. 6297–6305, 2012.

[14] D. Salvemini, J. W. Little, T. Doyle, and W. L. Neumann, "Roles of reactive oxygen and nitrogen species in pain," *Free Radical Biology and Medicine*, vol. 51, no. 5, pp. 951–966, 2011.

[15] I.-T. Lee and C.-M. Yang, "Role of NADPH oxidase/ROS in pro-inflammatory mediators-induced airway and pulmonary diseases," *Biochemical Pharmacology*, vol. 84, no. 5, pp. 581–590, 2012.

[16] A. R. Mendelsohn and J. W. Larrick, "Paradoxical effects of antioxidants on cancer," *Rejuvenation Research*, vol. 17, no. 3, pp. 306–311, 2014.

[17] A. A. M. Abd-allah, N. A. M. N. El-deen, W. M. Mohamed, and F. M. Naguib, "Mast cells and pro-inflammatory cytokines roles in assessment of grape seeds extract anti-inflammatory activity in rat model of carrageenan-induced paw edema," *Iranian Journal of Basic Medical Sciences*, vol. 21, pp. 97–107, 2018.

[18] R. Vinegar, J. F. Truax, and J. L. Selph, "Some quantitative temporal characteristics of carrageenin-induced pleurisy in the rat," *Experimental Biology and Medicine*, vol. 143, no. 3, pp. 711–714, 1973.

[19] G. E. P. Sousa and S. H. Ferreira, "Blockade by anti-macrophage serum of the migration of PMN neutrophils into the inflammed peritoneal cavity," *Agents & Actions*, vol. 17, pp. 1–5, 1985.

[20] A. A. Muller, S. A. Reiter, K. G. Heider, and H. Wagner, "Plan-derived acetophenones with antiasthmatic and antiinflammatory properties: inhibitory effects in chemotaxis, right angle scatter and actin polimeryzation of polymorphonucleare granulocytes," *Planta Medica*, vol. 65, pp. 97–103, 2001.

[21] M. M. G. Pinheiro, S. B. O. Fernandes, C. E. Fingolo, F. Boylan, and P. D. Fernandes, "Anti-inflammatory activity

of ethanol extract and fractions from Couroupita guianensis Aublet leaves," *Journal of Ethnopharmacology*, vol. 146, no. 1, pp. 324–330, 2013.

[22] S. Takahara, H. B. Hamilton, J. V. Neel, T. Y. Kobara, Y. Ogura, and E. T. Nishimura, "Hypocatalasemia: a new genetic carrier state," *Journal of Clinical Investigation*, vol. 39, no. 4, pp. 610–619, 1960.

[23] F. Romitelli, S. A. Santini, E. Chierici et al., "Comparison of nitrite/nitrate concentration in human plasma and serum samples measured by the enzymatic batch Griess assay, ion-pairing HPLC and ion-trap GC-MS: the importance of a correct removal of proteins in the Griess assay," *Journal of Chromatography B*, vol. 851, no. 1-2, pp. 257–267, 2007.

[24] L. C. Green, D. A. Wagner, J. Glogowski, P. L. Skipper, J. S. Wishnok, and S. R. Tannenbaum, "Analysis of nitrate, nitrite, and [15N]nitrate in biological fluids," *Analytical Biochemistry*, vol. 126, no. 1, pp. 131–138, 1982.

[25] H. Ohkawa, N. Ohishi, and K. Yagi, "Assay for lipid peroxides in animal tissues by thiobarbituric acid reaction," *Analytical Biochemistry*, vol. 95, no. 2, pp. 351–358, 1979.

[26] C. R. Tonussi and S. H. Ferreira, "Mechanism of diclofenac analgesia: direct blockade of inflammatory sensitization," *European Journal of Pharmacology*, vol. 251, no. 2-3, pp. 173–179, 1994.

[27] A. Cano, O. Alcaraz, and M. B. Arnao, "Free radical-scavenging activity of indolic compounds in aqueous and ethanolic media," *Analytical and Bioanalytical Chemistry*, vol. 376, no. 1, pp. 33–37, 2003.

[28] J. E. Williams, "Review of antiviral and immunomodulating properties of plants of the peruvian rainforest with a particular emphasis on Uña de Gato and Sangre de Grado," *Alternative Medicine Review*, vol. 6, pp. 567–579, 2001.

[29] S. Pitchford, D. Pan, and H. C. E. Welch, "Platelets in neutrophil recruitment to sites of inflammation," *Current Opinion in Hematology*, vol. 24, no. 1, pp. 23–31, 2017.

[30] K. Sun, X. Song, R. Y. Jia, Z. Yin, Y. Zou, and L. Li, "Evaluation of analgesic and anti-inflammatory activities of water extract of Galla Chinensis in vivo models," *Evidence-Based Complementary and Alternative Medicine*, vol. 2018, Article ID 6784032, 7 pages, 2018.

[31] E. Kolaczkowska and P. Kubes, "Neutrophil recruitment and function in health and inflammation," *Nature Reviews Immunology*, vol. 13, no. 3, pp. 159–175, 2013.

[32] J. Arnhold and J. Flemmig, "Human myeloperoxidase in innate and acquired immunity," *Archives of Biochemistry and Biophysics*, vol. 500, no. 1, pp. 92–106, 2010.

[33] G. F. Passos, E. S. Fernandes, F. M. da Cunha et al., "Anti-inflammatory and anti-allergic properties of the essential oil and active compounds from Cordia verbenacea," *Journal of Ethnopharmacology*, vol. 110, no. 2, pp. 323–333, 2007.

[34] J. Yao, Y. Cheng, M. Zhou et al., "ROS scavenging Mn_3O_4 nanozymes for in vivo anti-inflammation," *Chemical Science*, vol. 9, no. 11, pp. 2927–2933, 2018.

[35] E. Cadenas and K. J. A. Davies, "Mitochondrial free radical generation, oxidative stress, and aging11This article is dedicated to the memory of our dear friend, colleague, and mentor Lars Ernster (1920-1998), in gratitude for all he gave to us," *Free Radical Biology and Medicine*, vol. 29, no. 3-4, pp. 222–230, 2000.

[36] C. Kidson, "Variations in catalase activity in human leukocytes," *Blood*, vol. 19, no. 1, pp. 82–88, 1962.

[37] J. Davignon and P. Ganz, "Role of endothelial dysfunction in atherosclerosis," *Respiration and Circulation*, vol. 109, no. (23 Suppl 1), pp. III-27–III-32, 2004.

[38] L. Li, A. Hsu, and P. K. Moore, "Actions and interactions of nitric oxide, carbon monoxide and hydrogen sulphide in the cardiovascular system and in inflammation - a tale of three gases!" *Pharmacology & Therapeutics*, vol. 123, no. 3, pp. 386–400, 2009.

[39] M. Grau, U. B. Hendgen-Cotta, P. Brouzos et al., "Recent methodological advances in the analysis of nitrite in the human circulation: nitrite as a biochemical parameter of the l-arginine/no pathway," *Journal of Chromatography B*, vol. 851, no. 1-2, pp. 106–123, 2007.

[40] J. Sun, X. Zhang, M. Broderick, and H. Fein, "Measurement of nitric oxide production in biological systems by using Griess reaction assay," *Sensors*, vol. 3, no. 8, pp. 276–284, 2003.

[41] R. N. Alolga, S. W. Amadi, V. Onoja, A. G. Assanhou, M. Muyaba, and S. A. Kassim, "Anti-inflammatory and antipyretic properties of Kang 601 Heji, a traditional Chinese oral liquid dosage form," *Asian Pacific Journal of Tropical Biomedicine*, vol. 5, no. 11, pp. 921–927, 2015.

[42] A. Catalá, "Lipid peroxidation of membrane phospholipids generates hydroxy-alkenals and oxidized phospholipids active in physiological and/or pathological conditions," *Chemistry and Physics of Lipids*, vol. 157, pp. 1–11, 2009.

[43] E. Niki, "Lipid peroxidation: physiological levels and dual biological effects," *Free Radical Biology and Medicine*, vol. 47, no. 5, pp. 469–484, 2009.

[44] M. Arimon, S. Takeda, K. L. Post, S. Svirsky, B. T. Hyman, and O. Berezovska, "Oxidative stress and lipid peroxidation are upstream of amyloid pathology," *Neurobiology of Disease*, vol. 84, pp. 109–119, 2015.

[45] J.-H. Shang, X.-H. Cai, T. Feng et al., "Pharmacological evaluation of *Alstonia scholaris*: anti-inflammatory and analgesic effects," *Journal of Ethnopharmacology*, vol. 129, no. 2, pp. 174–181, 2010.

[46] A.-R. Phull, B. Nasir, I. u. Haq, and S. J. Kim, "Oxidative stress, consequences and ROS mediated cellular signaling in rheumatoid arthritis," *Chemico-Biological Interactions*, vol. 281, pp. 121–136, 2018.

[47] V. Fattori, F. A. Amaral, and W. A. Verri-Jr, "Neutrophils and arthritis: Role in disease and pharmacological perspectives," *Pharmacological Research*, vol. 112, pp. 84–98, 2006.

[48] J.-J. Chen, C.-Y. Chung, T.-L. Hwang, and J.-F. Chen, "Amides and benzenoids from zanthoxylum ailanthoides with inhibitory activity on superoxide generation and elastase release by neutrophils," *Journal of Natural Products*, vol. 72, no. 1, pp. 107–111, 2009.

[49] F. V. M. Cunha, B. d. S. Gomes, B. d. S. Neto et al., "Ferulic acid ethyl ester diminished Complete Freund's Adjuvant-induced incapacitation through antioxidant and anti-inflammatory activity," *Naunyn-Schmiedeberg's Archives of Pharmacology*, vol. 389, no. 1, pp. 117–130, 2016.

[50] B. S. Gomes, B. P. S. Neto, E. M. Lopes et al., "Anti-inflammatory effect of the monoterpene myrtenol is dependent on the direct modulation of neutrophil migration and oxidative stress," *Chemico-Biological Interactions*, vol. 273, pp. 73–81, 2017.

[51] V. Santer, A. Sriratana, and D. A. Lowther, "Carrageenin-induced arthritis: V. a morphologic study of the development of inflammation in acute arthritis," *Seminars in Arthritis and Rheumatism*, vol. 13, no. 2, pp. 160–168, 1983.

[52] C. M. M. Santos, D. Ribeiro, A. M. S. Silva, and E. Fernandes, "2,3-diarylxanthones as potential inhibitors of arachidonic acid metabolic pathways," *Inflammation*, vol. 40, no. 3, pp. 956–964, 2017.

[53] J.-J. Chen, Y.-T. Luo, T.-L. Hwang, P.-J. Sung, T.-C. Wang, and I.-S. Chen, "A new indole alkaloid and anti-inflammatory constituents from Strychnos cathayensis," *Chemistry and Biodiversity*, vol. 5, no. 7, pp. 1345–1352, 2008.

Hindawi
Evidence-Based Complementary and Alternative Medicine
Volume 2022, Article ID 6072286, 9 pages
https://doi.org/10.1155/2022/6072286

Research Article

Correlation Analysis of Umbilical Cord Blood Metabolic Phenotype and Inflammation in Patients with Gestational Diabetes Mellitus Complicated with Overweight and Obesity

Qiuling Chen, Wenxia Li, Yanxia Deng, Yongqi Li, Le Huang, Liping Zhao, and Hua Li

Department of Obstetrics, Changsha Hospital for Maternal & Child Health Care Affiliated to Hunan Normal University, Changsha 417000, Hunan, China

Correspondence should be addressed to Hua Li; qiuqiu1632021@163.com

Received 17 January 2022; Revised 15 April 2022; Accepted 22 April 2022; Published 13 May 2022

Academic Editor: Xiang Liu

Background. Gestational diabetes mellitus (GDM) is a common metabolic disorder in pregnancy. The incidence rate is increasing year by year, which seriously threatens the safety of maternal and infant. Obesity is a vital factor in inducing GDM. Pregnant women with GDM account for a large proportion of overweight and obese pregnant women. Our study aimed to explore the potential mechanism of differential metabolites on inflammation and find the intervention and management methods for GDM in overweight and obese pregnant women. *Methods*. Umbilical cord blood samples and placenta were collected from normal weight pregnant women with GDM (control group) and overweight and obese pregnant women with GDM (obesity group) for a comparative study. Serum inflammatory factors IL-10, TNF-α, IL-6, lipopolysaccharide (LPS), and TLR4 expression were detected by ELISA. The expression levels of BCL-2 and caspase-3 were measured by Western blot. TUNEL staining was used to observe the apoptosis of placental villi. KEGG combined with metabolomics was used to compare the differences of metabolic maps between the two groups. *Results*. Compared with the control group, the level of anti-inflammatory factor IL-10 in the cord blood was decreased in the obesity group, while the levels of proinflammatory factors TNF-α, IL-6, and LPS were increased. In the placental tissues, the obesity group had higher concentrations of LPS, TLR4, and caspase-3 and lower concentration of BCL-2. Placental villi in the obesity group were more likely to undergo apoptosis than the control group. Correlation analysis showed that the above metabolite concentrations were negatively correlated with TNF-α or LPS. *Conclusion*. Metabolites could control obesity in the process of controlling the occurrence and development of inflammation.

1. Introduction

Gestational diabetes mellitus (GDM) is a complication of pregnancy unique to women. The incidence of pregnancy-induced hypertension, eclampsia, and other diseases in GDM pregnant women is increasing, and the possibility of excessive fetal growth is also increasing. Infants are also more likely to develop various neonatal diseases including hyperbilirubinemia, hypocalcemia, erythema, and respiratory distress syndrome [1]. It can be seen that GDM has serious short-term or long-term harm to the mother and her offspring.

The etiology of GDM has a strong epidemiological correlation with physiological changes during pregnancy, obesity, individual genes, fetal maternal GDM exposure, and other environmental factors [2]. Among these factors, obesity is considered to be the most variable and important risk factor associated with GDM [3, 4], which can increase the risk of adverse pregnancy outcomes in pregnant women and their offspring, and independently contribute to the occurrence and development of GDM in pregnant women [5]. The increasing obesity worldwide has led to an upward trend in the incidence of GDM and perinatal complications related to the disease. People have gradually realized that it is important to strengthen the attention and research related to obesity and GDM [6]. Therefore, it is imminent to reduce the prevalence of GDM in pregnant women through weight management.

Studies have shown that GDM may affect the incidence of diseases in offspring through cord blood. The offspring of GDM showed demethylation, which was related to the risk of autism spectrum disorder, type 1/2 diabetes, and other diseases [7, 8]. Furthermore, the content of most fatty acids in GDM pregnant women and GDM infants was lower than those in the healthy pregnant women group [9]. The above studies have shown that cord blood is an important bridge between mothers and fetuses. However, the phenotypic characteristics of the overall metabolic profile of cord blood still need to be further understood.

In the pregnancy complications of obesity and GDM, placental inflammation had been observed to play a central role in the fetal environment [10]. Some bacteria could create a local anti-inflammatory environment in the placenta and transform it into a maintenance effect on the GDM state. However, compared with normal GDM pregnant women, the content of related bacteria was reduced in the placenta of overweight and obese GDM pregnant women. The anti-inflammatory effect was reduced, and it was not conducive to the progress of the metabolism that can easily lead to a more unfavorable inflammatory phenotype [11]. The correlation between the metabolism and inflammation provides a feasible path for us to intervene overweight and obese GDM pregnant women.

This study intended to collect cord blood and placental tissue samples from normal weight, overweight, and obese pregnant women who were clinically diagnosed with GDM. Metabolomics was used to analyze the differences in cord blood metabolism profiles between the two groups and screen out significantly different metabolites. We combined the changes in the levels of inflammatory factors in cord blood to explore the potential correlation between different metabolites and inflammation, in order to provide a theoretical basis for the intervention and management of GDM in overweight and obese pregnant women.

2. Methods

2.1. Source and Grouping of Subjects. This study was approved by the Clinical Research Ethics Committee of Changsha Maternal and Child Health Hospital (Approval No.: 2021013). During the experiment, all subjects informed consent to the conduct of this experiment. The test procedure was in line with the Declaration of Helsinki.

A total of 16 pregnant women with normal weight and 7 overweight and obese GDM pregnant women were included in the study. The subjects were all pregnant women who attended Changsha Maternity and Child Health Hospital from May 2020 to June 2021. The experiment was set as the control group and obesity group (pregnant women who were overweight or obese) according to the BMI classification standard. The cord blood had been collected from 16 cases in the control group and 7 cases in the obesity group, 23 cases in total, 2 copies for each case. Placental tissues were collected, with 5 cases in each group and 10 cases in total. The clinical characteristics of the subjects are given in Table 1.

Inclusion criteria: age 25–40; BMI standard was defined as overweight or obesity; and using the diagnostic criteria of the International Association of Diabetes and Pregnancy Research Groups (IADPSG), oral glucose tolerance test (OGTT), and blood glucose level 0 h ≥ 5.1 mmol/L, 1 h ≥ 10.0 mmol/L, and 2 h ≥ 8.5 mmol/L.

Exclusion criteria: pre-GDM: glycosylated hemoglobin (HbA1c) was more than 6.5% or fasting blood glucose (FBG) was more than 7 mmol/L or 2 h blood glucose level (OGTT) was more than 11.1 mmol/L; multiple pregnancy; suffering from chronic diseases such as metabolic and gastrointestinal health (such as inflammatory bowel disease); and diagnosis or history of clotting disorders.

2.2. Enzyme-Linked Immunosorbent Assay (ELISA). The whole blood sample was placed overnight at 4°C and centrifuged at 1000 g at 2–8°C for 15 min, and the supernatant was taken out for later use. 25 μL each of the protein sample was tested and the diluted BSA standard (Saibao, Yancheng, China) was added to the enzyme-labeled reaction wells of IL-10 (KE00170, Proteintech, USA), TNF-α (KE00068, Proteintech, USA), IL-6 (KE00139, Proteintech, USA), and LPS (CSB-E09945 h, Wuhan Huamei Biological Engineering Co., Ltd., China) kits at the same time, and then, BCA was added to work liquid complete quantitative detection. Subsequently, the absorbance value of each sample and BSA standard was measured with a microplate reader in the range of 540–590 nm.

2.3. Western Blot. We took 3–5 mL sample and washed them with PBS. Then, RIPA solution was added to lyse and centrifuged to obtain serum or tissue supernatant. The BCA method was used to quantitatively detect the protein concentration, and then, appropriate amount of protein supernatant was added according to the protein quantitative results for electrophoresis separation. The diluted primary antibody TLR4 (19811-1-AP, 1 : 5000, Proteintech, USA) was added to serum, and the diluted primary antibody BCL-2 (12789-1-AP, 1 : 2000, Proteintech, USA), caspase-3 (#9661, 1 : 1000, CST, USA), and the internal reference protein β-actin (66009-1-Ig, 1 : 5000, Proteintech, USA) were added to the tissue supernatant and incubated overnight at 4°C. Then, the samples were incubated with HRP-labeled secondary antibodies HRP goat anti-mouse IgG (SA00001-1, 1 : 5000, Proteintech, USA) or HRP goat anti-rabbit IgG (SA00001-2, 1 : 5000, Proteintech, USA) for 1.5 h at room temperature. ECL was used for color development and exposure imaging, and Quantity One professional gray analysis software was used to observe the intensity of protein bands.

2.4. TUNEL. We followed the instructions of the TUNEL kit (40306ES50, Shanghai Yisheng Bio, China). After the two groups of placental tissues were sliced, they were washed with PBS (pH = 7.2–7.6, Abiowell, China) for 3 times, and equilibration buffer was added and placed at room temperature for 10–30 min. Subsequently, 50 μL of TdT enzyme incubation buffer was added to the sectioned tissues and incubated at 37°C in the dark for 30 min. The nuclei were

Table 1: Basic information of subjects.

	Control	Obesity	Significance
n	7	7	
Age (year)	30.43 ± 2.97	33.43 ± 3.77	ns
Height (cm)	157.57 ± 3.86	161.14 ± 3.27	ns
Prepregnancy weight (kg)	48.17 ± 1.99	77.07 ± 5.49	*
Postpartum weight (kg)	58.74 ± 3.73	86.64 ± 9.66	*
Prepregnancy BMI (%)	19.68 ± 1.28	29.65 ± 1.42	*
Body fat percentage (%)	26.54% ± 2.24%	39.20% ± 3.49	*
Fasting blood glucose (mmol/L)	4.49 ± 0.26	5.11 ± 0.39	*
HbA1c (%)	4.97% ± 0.18%	5.48% ± 0.43%	*

ns, no significance. $^*P < 0.05$ vs. the control group.

stained with DAPI working solution (Abiowell, China) for 10 min at the same temperature and rinsed with PBS. Buffered glycerol (Abiowell, China) was used to seal slices, and slices were observed under the ×400 field of view of the fluorescence microscope (BA410 T, Motic, China). If the nucleus was stained brown, it was a positive apoptotic cell.

2.5. Nontargeted Metabolite Analysis. Seven cases were selected from cord blood of 16 in the control group, and the LC-MC analysis was performed together with cord blood of 7 in the obesity group. After the sample was diluted with water and rethawed, it was centrifuged for 15 min. The supernatant was taken for testing, and the data were preprocessed as required. PLS-DA analysis was used to investigate the sample quality, and the metabolites were screened for differences in genes between groups. At the same time, MetaboAnalyst 4.0 in conjunction with the Kyoto Encyclopedia of Genes and Genomes (KEGG) and Human Metabolome Database (HMDB) were used to conduct enrichment pathway analysis of metabolites in the two sets of cord blood.

2.6. Statistical Analysis. GraphPad Prism 8.0 was used for statistical analysis and drawing of all data in this study. The measurement data conforming to the normal distribution were expressed as the mean ± standard deviation, and the comparison of the means between the two groups was performed by the *t*-test. Spearman correlation analysis was applied to conduct correlation study. $P < 0.05$ indicated a statistically significant difference.

3. Results

3.1. Inflammatory Factor Levels in Cord Blood. First, ELISA was used to detect the concentrations of anti-inflammatory factor IL-10 and proinflammatory factors TNF-α, IL-6, and LPS in cord blood of the two groups. The results of the measurement are shown in Figure 1. The level of IL-10 in the obesity group was much lower than that in the control group (Figure 1(a)), while the levels of TNF-α, IL-6, and LPS showed a significant upward trend (Figures 1(b), 1(c), and 1(d)). At the same time, the ELISA method was used to detect TLR4 expression, which showed that the content in the obesity group was significantly higher than that in the control group (Figure 1(e)). These results showed that the inflammatory factors and LPS in cord blood of the obesity group were released in large quantities, TLR4 was activated, and the proinflammatory response was triggered.

3.2. Changes in Umbilical Cord Blood Metabolism Atlas. Next, nontargeted metabolic was applied to test cord blood of two groups. PLS-DA was used to analyze the differences in metabolites between the two groups: the respective regions of the two groups in the figure were clearly separated, and there were obvious differences in metabolomics components (Figure 2(a)). The results of the heat map analysis showed that compared with the control group, the obesity group had significantly higher levels of propylparaben, pyrroloquinoline Q, medroxyprogesterone, and anisic acid in cord blood. On the contrary, glutamine, azelate, histidine, and hesperidin and other metabolites levels were decreased (Figure 2(b)). *P* value was used to screen the metabolites with significant differences. The volcano chart clearly showed the upregulation or downregulation of metabolites: compared with the control group, the four metabolites of hesperidin, taurine, N-acetyl-L-tryptophan, and 3-indolepropionic acid were significantly downregulated in the obesity group, and their content was significantly reduced (Figure 2(c)).

3.3. Functional Changes of Differential Metabolites in Umbilical Cord Blood. The overview map of metabolome enrichment showed that metabolite enrichment was mainly concentrated in 5 metabolic pathways. Among them, the differential metabolites in the D-glutamine and D-glutamate metabolism pathways were the most enriched, followed by the nitrogen metabolism, taurine and hypotaurine metabolism, arginine biosynthesis, and alanine, aspartate, and glutamate metabolism (Figure 3).

3.4. Changes in Placental Tissue Inflammation. The concentration of LPS in the placenta tissues was detected by ELISA, and the concentration of LPS in the obesity group was much higher than that in the control group (Figure 4(a)). Western blot was applied to detect the TLR4 level, which showed higher concentration in the obesity group (Figure 4(b)). TUNEL staining was used to observe placental villi apoptosis, which showed that the villi apoptosis of the obesity group was significantly increased than

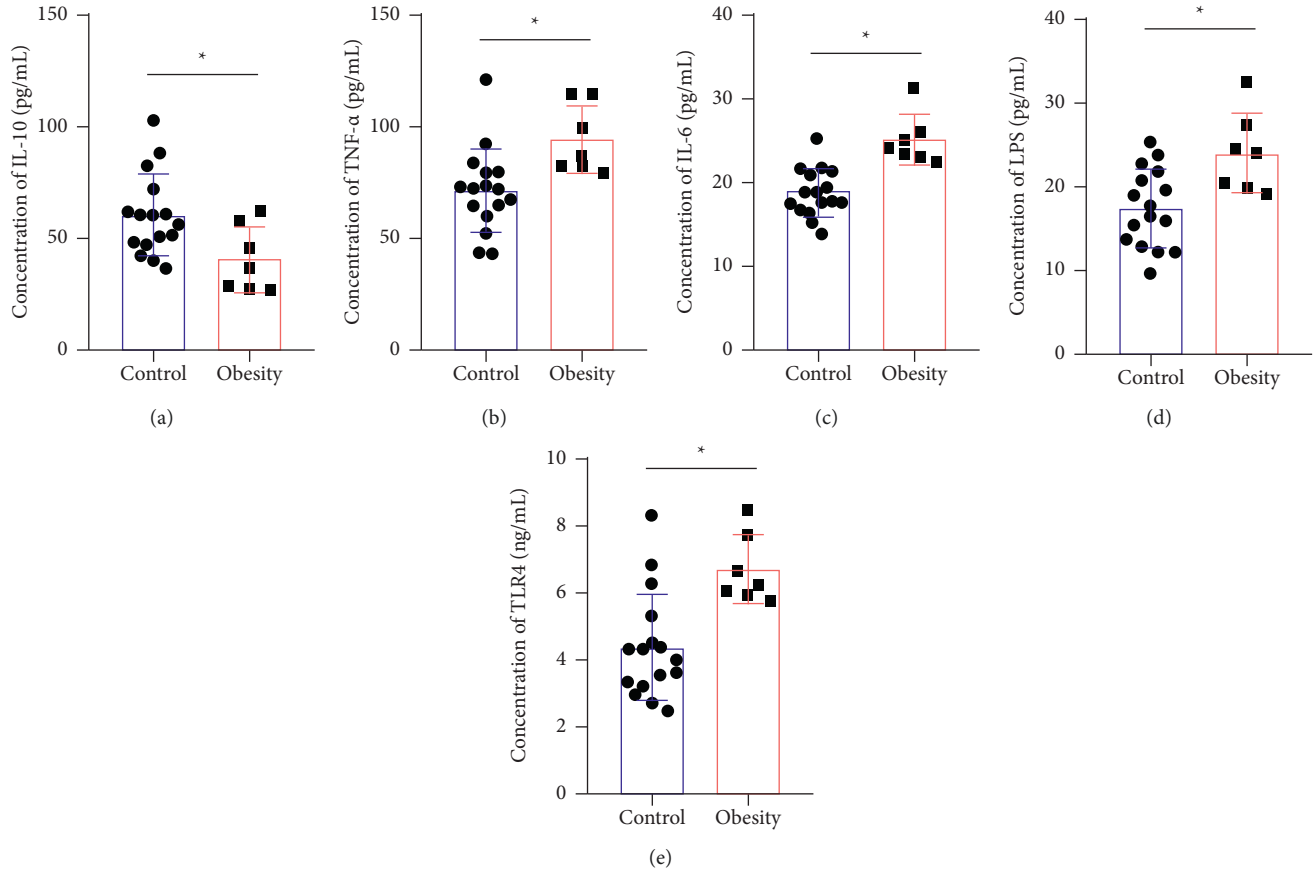

Figure 1: Inflammatory factor levels in cord blood. ELISA was used to detect the levels of IL-10 (a), TNF-α (b), IL-6 (c), LPS (d), and TLR4 (e) in cord blood of pregnant women with GDM. $^*P < 0.05$ vs. the control group.

that of the control group (Figure 4(c)). At the same time, Western blot was applied to detect BCL-2 and caspase-3 levels. Compared with the control group, BCL-2 in the obesity group showed a lower level, but caspase-3 showed a higher level (Figures 4(d) and 4(e)).

3.5. Correlation between Inflammation and Changes in Metabolite Concentration. We performed correlation analysis on the difference metabolites with significant changes in the content of the two groups in the above metabolic analysis and inflammatory factors. The change of hesperidin was significantly correlated with the content of proinflammatory factor TNF-α. Three metabolites of taurine, N-acetyl-L-tryptophan, and 3-indolepropionic acid were related to the change of LSP (Figure 5(a)). The reduction of the above four metabolites would lead to a significant increase in TNF-α or LPS (Figures 5(b)–5(e)). It could be considered that changes in the concentration of certain metabolites were indeed related to the occurrence of inflammation, and the lower the concentration of metabolites, the more likely inflammation will occur.

4. Discussion

The incidence of GDM in overweight and obese pregnant women is getting higher and higher, and it is an inevitable trend to continuously explore its treatment methods. GDM mostly reduces the risk from nutrient intervention and drug therapy [12, 13]. Studies have shown that women who supplemented with 600 μg of folic acid before pregnancy can reduce the risk of GDM by about 30% than women who have not supplemented with folic acid [14]. Taking probiotics during pregnancy can effectively prevent GDM by regulating gut microbiota [15]. However, when overweight and obese women took probiotics during pregnancy, it was found that probiotics did not play a role in preventing GDM in overweight and obese pregnant women [16, 17]. It can be considered that exogenous nutrient intervention can reduce the risk of disease in GDM patients, but its effect on overweight and obese GDM pregnant women is unknown. The drug treatment may have an adverse effect on the offspring and lack long-term safety [12]. How to effectively intervene or treat GDM in overweight and obese pregnant women still needs further research.

Alan R. Saltiel et al. explored the inflammatory mechanism related to obesity and many metabolic diseases and confirmed the potential of anti-inflammatory therapy in the treatment of obesity-related diseases [18, 19]. The results of our study showed that the level of anti-inflammatory factor in the obesity group in cord blood and placental tissues was significantly lower than that in the control group, while the levels of various proinflammatory factors and LPS were

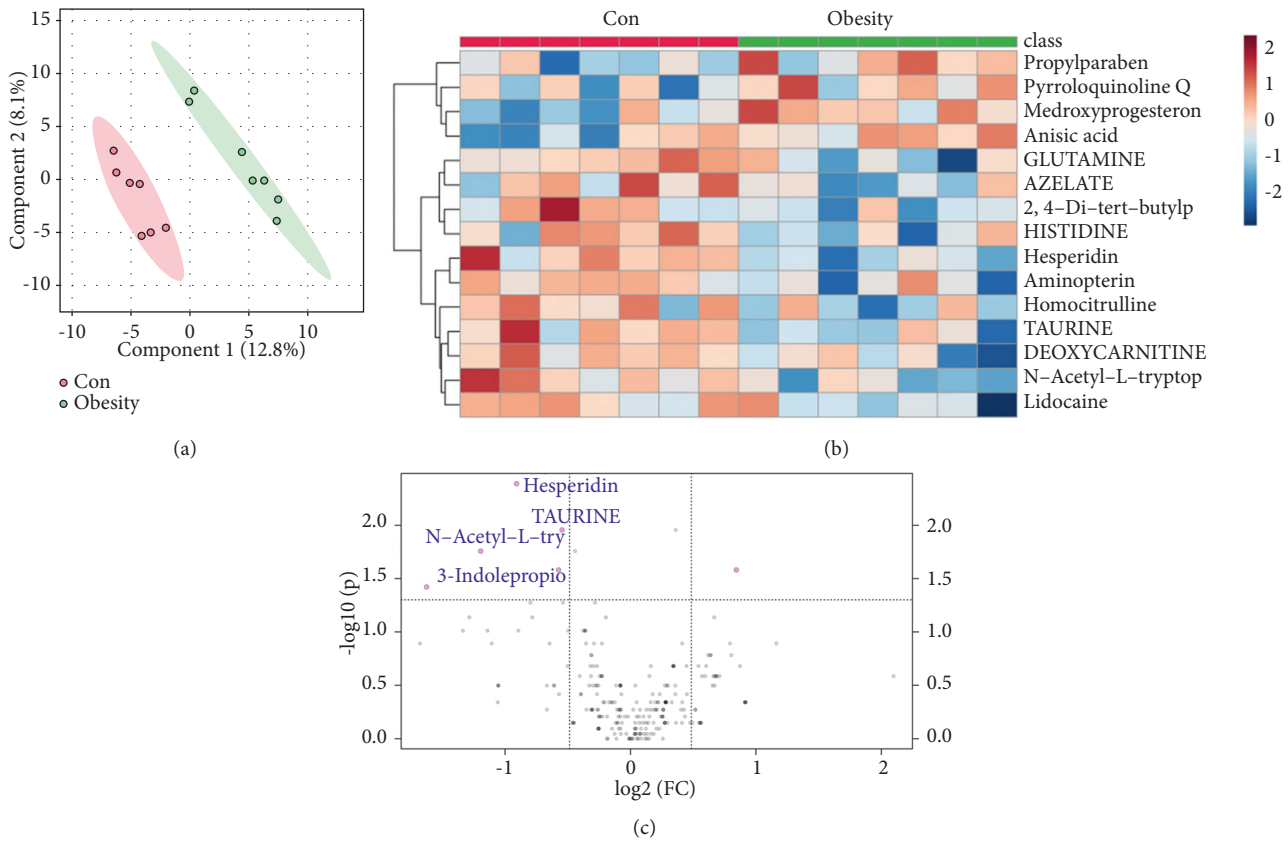

Figure 2: Changes in umbilical cord blood metabolism Atlas. (a) PLS-DA used to analyze the difference levels of metabolites between the two groups. (b) Heat map showing the enrichment of metabolites between the groups. (c) The volcano map showing metabolites with significant differences.

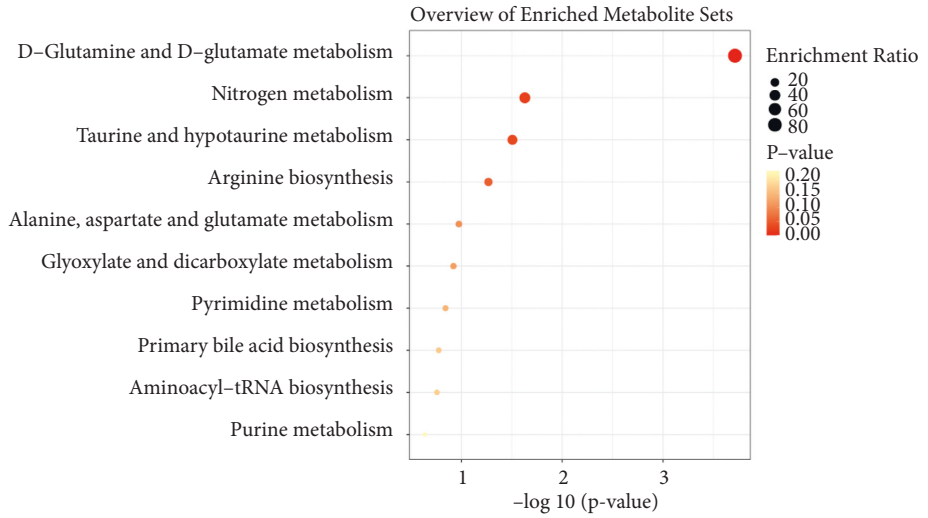

Figure 3: Functional changes of differential metabolites in cord blood. The enrichment analysis chart showed the main enrichment metabolic pathways of different metabolites.

significantly higher than those in the control group. We also verified that there was a certain correlation between obesity and inflammation, and the goal of controlling obesity could be achieved by inhibiting the occurrence and development of inflammation. The levels of related inflammatory factors had similar changes in cord blood and placental tissues. It could be considered that the mother's body affected the structure and function of the placenta through cord blood. Therefore, this study intended to reduce the prevalence of obese GDM mothers through changes in the content of

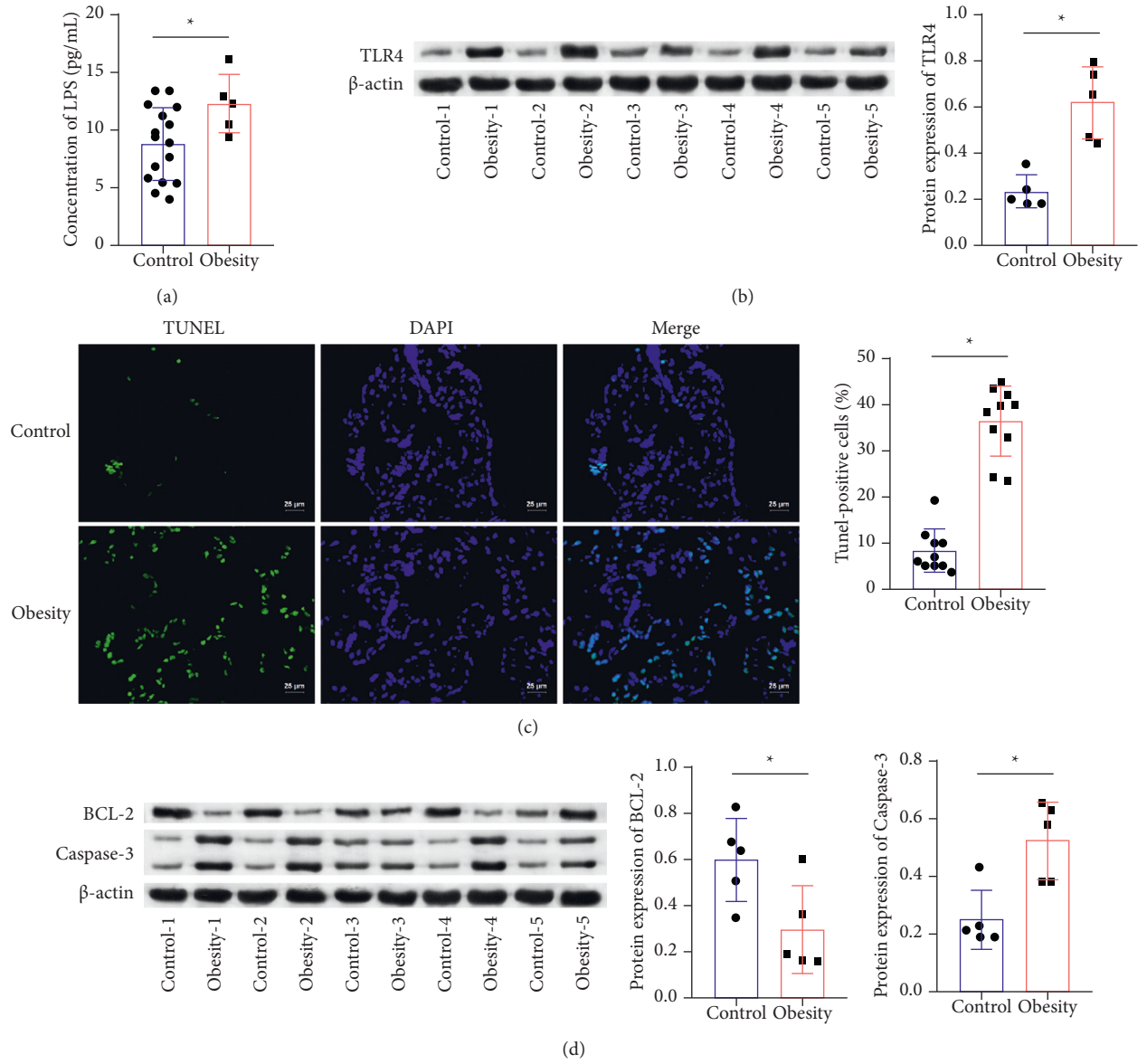

FIGURE 4: Changes in placental tissue inflammation. (a) ELISA applied to detect LPS concentration. (b) Western blot used to measure TLR4 content. (c) TUNEL staining performed to observe placental villi apoptosis (TUNEL, ×400, scale bar = 25 μm). (d)-(e) Western blot applied to measure BCL-2 and caspase-3 proteins expression. $^*P < 0.05$ vs. the control group.

differential metabolites in umbilical cord blood, while reducing the harm of GDM to the offspring.

The results of metabolomics analysis showed that hesperidin, taurine, N-acetyl-L-tryptophan, 3-indolepropionic acid, and other metabolites were significantly downregulated in the obesity group. Haijun Xiong et al. found that hesperidin can effectively alleviate the inflammation caused by hyperglycemia and hyperlipidemia and participate in the inhibition of adipogenesis to achieve the therapeutic effect on obesity [20, 21]. Tawar Qaradakhi et al. found that taurine is also involved in the process of the fat metabolism and has a good anti-inflammatory effect on cardiovascular diseases [22]. The metabolites of N-acetyl-L-tryptophan and 3-indolepropionic acid could alleviate or inhibit many inflammatory reactions [23]; 3-indolepropionic acid had been found to prevent steatohepatitis [24]. The above studies showed that four metabolites whose concentrations were significantly decreased in this differential metabolite analysis had a certain degree of the inflammation inhibitory effect, further illustrating that hesperidin and taurine were involved in the control process of obesity.

Our analysis of the correlation between differential metabolites and inflammation also showed that the above four metabolites were significantly related to TNF-α or LPS, and the lower the metabolite concentration, the more likely inflammation will occur. Hesperidin could improve colitis by reducing TNF-α [25], and taurine could slow down the occurrence of many diseases induced by LPS [26, 27]. However, the predecessors have not discussed the interaction mechanism of N-acetyl-L-tryptophan, 3-indolepropionic

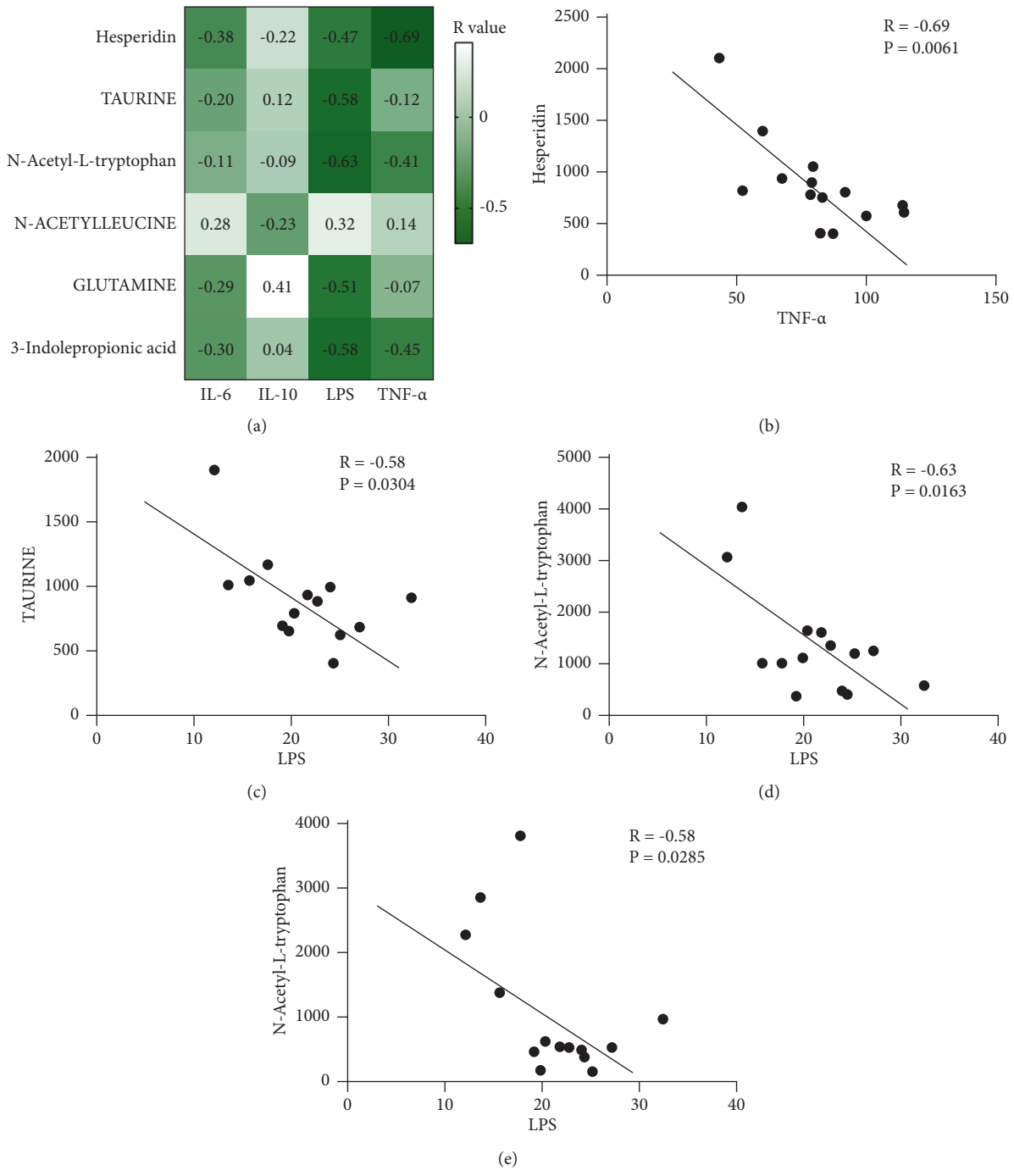

Figure 5: Correlation between inflammation and changes in metabolite concentration. (a) Correlation analysis between different metabolites and inflammatory factors. (b)–(e) The concentration of inflammatory factors varied with the content of metabolites. *Metabolites have a significant correlation with inflammatory factors.

acid, and LPS. The above issues can be explored in the follow-up, and it is hoped that more breakthroughs in the treatment of inflammatory diseases can be achieved.

The above studies showed that we can mediate the occurrence and development of inflammation by regulating the content of related metabolites in overweight and obese GDM pregnant women, providing strong evidence for effective intervention and management of overweight and obese GDM. However, how to implement the theory in clinical operation and what kind of treatment effect will be obtained in the end still requires a lot of verification and practice by researchers. At the same time, due to the limitation of samples, we need to spend more time collecting samples of normal weight with GMD and overweight or obese with no GMD. The association between overweight and GDM was further confirmed by comparing the four

groups: normal weight no GMD, normal weight with GMD, overweight or obese with no GMD, and overweight or obese with GMD.

In conclusion, metabolites controlled the occurrence and development of inflammation, so as to achieve the purpose of controlling obesity. This study explored the theoretical basis for intervention and management of overweight and obese GDM pregnant women from metabolomics.

Data Availability

The data used to support the findings of this study are available from the corresponding author upon request.

Disclosure

Qiuling Chen and Wenxia Li are the co-first authors.

Conflicts of Interest

The authors declare that they have no conflicts of interest.

Authors' Contributions

Qiuling Chen, Wenxia Li, Yanxia Deng, Yongqi Li, Le Huang, LiPing Zhao, and Hua Li designed the study, performed the research, analysed data, wrote the article, revised it critically for important intellectual content, and gave final approval of the version to be submitted. Qiuling Chen and Wenxia Li contributed equally to this study.

Acknowledgments

This work was supported by Hunan Province clinical medical technology innovation guide project (2020SK53101), and Science Foundation of Hunan Province (2021JJ70059).

References

[1] E. M. Alfadhli, "Gestational diabetes mellitus," *Saudi Medical Journal*, vol. 36, no. 4, pp. 399–406, 2015.

[2] E. C. Johns, F. C. Denison, J. E. Norman, and R. M. Reynolds, "Gestational diabetes mellitus: mechanisms, treatment, and complications," *Trends in Endocrinology and Metabolism*, vol. 29, no. 11, pp. 743–754, 2018.

[3] M. Lende and A. Rijhsinghani, "Gestational diabetes: overview with emphasis on medical management," *International Journal of Environmental Research and Public Health*, vol. 17, no. 24, Article ID 9573, 2020.

[4] M. Farren, N. Daly, A. C. O'Higgins, A. McKeating, P. J. Maguire, and M. J. Turner, "The interplay between maternal obesity and gestational diabetes mellitus," *Journal of Perinatal Medicine*, vol. 43, no. 3, pp. 311–317, 2015.

[5] C. Wang, Y. Wei, X. Zhang et al., "A randomized clinical trial of exercise during pregnancy to prevent gestational diabetes mellitus and improve pregnancy outcome in overweight and obese pregnant women," *American Journal of Obstetrics and Gynecology*, vol. 216, no. 4, pp. 340–351, 2017.

[6] U. Schaefer-Graf, A. Napoli, and C. J. Nolan, "Diabetes in pregnancy: a new decade of challenges ahead," *Diabetologia*, vol. 61, no. 5, pp. 1012–1021, 2018.

[7] C. G. Howe, B. Cox, R. Fore et al., "Maternal gestational diabetes mellitus and newborn DNA methylation: findings from the pregnancy and childhood epigenetics consortium," *Diabetes Care*, vol. 43, no. 1, pp. 98–105, 2020.

[8] I. Floris, B. Descamps, A. Vardeu et al., "Gestational diabetes mellitus impairs fetal endothelial cell functions through a mechanism involving microRNA-101 and histone methyltransferase enhancer of zester homolog-2," *Arteriosclerosis, Thrombosis, and Vascular Biology*, vol. 35, no. 3, pp. 664–674, 2015.

[9] H. Ortega-Senovilla, U. Schaefer-Graf, and E. Herrera, "Pregnant women with gestational diabetes and with well controlled glucose levels have decreased concentrations of individual fatty acids in maternal and cord serum," *Diabetologia*, vol. 63, no. 4, pp. 864–874, 2020.

[10] P. Pantham, I. L. Aye, and T. L. Powell, "Inflammation in maternal obesity and gestational diabetes mellitus," *Placenta*, vol. 36, no. 7, pp. 709–715, 2015.

[11] J. Bassols, M. Serino, G. Carreras-Badosa et al., "Gestational diabetes is associated with changes in placental microbiota and microbiome," *Pediatric Research*, vol. 80, no. 6, pp. 777–784, 2016.

[12] E. D. Szmuilowicz, J. L. Josefson, and B. E. Metzger, "Gestational diabetes mellitus," *Endocrinology and Metabolism Clinics of North America*, vol. 48, no. 3, pp. 479–493, 2019.

[13] I. Silva-Zolezzi, T. M. Samuel, and J. Spieldenner, "Maternal nutrition: opportunities in the prevention of gestational diabetes," *Nutrition Reviews*, vol. 75, no. suppl 1, pp. 32–50, 2017.

[14] M. Li, S. Li, J. E. Chavarro et al., "Prepregnancy habitual intakes of total, supplemental, and food folate and risk of gestational diabetes mellitus: a prospective cohort study," *Diabetes Care*, vol. 42, no. 6, pp. 1034–1041, 2019.

[15] A. Homayouni, N. Bagheri, S. Mohammad-Alizadeh-Charandabi et al., "Prevention of gestational diabetes mellitus (GDM) and probiotics: mechanism of action: a review," *Current Diabetes Reviews*, vol. 16, no. 6, pp. 538–545, 2020.

[16] L. K. Callaway, H. D. McIntyre, H. L. Barrett et al., "Probiotics for the prevention of gestational diabetes mellitus in overweight and obese women: findings from the SPRING double-blind randomized controlled trial," *Diabetes Care*, vol. 42, no. 3, pp. 364–371, 2019.

[17] O. Pellonperä, K. Mokkala, N. Houttu et al., "Efficacy of fish oil and/or probiotic intervention on the incidence of gestational diabetes mellitus in an at-risk group of overweight and obese women: a randomized, placebo-controlled, double-blind clinical trial," *Diabetes Care*, vol. 42, no. 6, pp. 1009–1017, 2019.

[18] M. F. Gregor and G. S. Hotamisligil, "Inflammatory mechanisms in obesity," *Annual Review of Immunology*, vol. 29, no. 1, pp. 415–445, 2011.

[19] A. R. Saltiel and J. M. Olefsky, "Inflammatory mechanisms linking obesity and metabolic disease," *Journal of Clinical Investigation*, vol. 127, no. 1, pp. 1–4, 2017.

[20] H. Xiong, J. Wang, Q. Ran et al., "Hesperidin: a therapeutic agent for obesity," *Drug Design, Development and Therapy*, vol. 13, pp. 3855–3866, 2019.

[21] S. Tejada, S. Pinya, M. Martorell et al., "Potential anti-inflammatory effects of Hesperidin from the genus citrus," *Current Medicinal Chemistry*, vol. 25, no. 37, pp. 4929–4945, 2019.

[22] T. Qaradakhi, L. K. Gadanec, K. R. McSweeney, J. R. Abraham, V. Apostolopoulos, and A. Zulli, "The anti-

inflammatory effect of taurine on cardiovascular disease," *Nutrients*, vol. 12, no. 9, Article ID 2847, 2020.

[23] J. Wang, S. Yu, J. Li et al., "Protective role of N-acetyl-l-tryptophan against hepatic ischemia-reperfusion injury via the RIP2/caspase-1/IL-1β signaling pathway," *Pharmaceutical Biology*, vol. 57, no. 1, pp. 385–391, 2019.

[24] X. Zhang, O. O. Coker, E. S. Chu et al., "Dietary cholesterol drives fatty liver-associated liver cancer by modulating gut microbiota and metabolites," *Gut*, vol. 70, no. 4, pp. 761–774, 2021.

[25] J. Zhang, H. Lei, X. Hu, and W. Dong, "Hesperetin ameliorates DSS-induced colitis by maintaining the epithelial barrier via blocking RIPK3/MLKL necroptosis signaling," *European Journal of Pharmacology*, vol. 873, Article ID 172992, 2020.

[26] Y. Liu, F. Li, L. Zhang, J. Wu, Y. Wang, and H. Yu, "Taurine alleviates lipopolysaccharide-induced liver injury by anti-inflammation and antioxidants in rats," *Molecular Medicine Reports*, vol. 16, no. 5, pp. 6512–6517, 2017.

[27] S. H. Cheong, S. H. Lee, Y. J. Jeon, and D. S. Lee, "Mussel (*Mytilus coruscus*) water extract containing taurine prevents LPS-induced inflammatory responses in zebrafish model," *Advances in Experimental Medicine & Biology*, vol. 975 Pt 2, pp. 931–942, 2017.

Hindawi
Evidence-Based Complementary and Alternative Medicine
Volume 2022, Article ID 1588786, 16 pages
https://doi.org/10.1155/2022/1588786

Research Article

Zengye Decoction Attenuated Severe Acute Pancreatitis Complicated with Acute Kidney Injury by Modulating the Gut Microbiome and Serum Amino Acid Metabolome

Xiao-Yu Dai, Qian Hu, Jia-Qi Yao, Xiao-Jia Wu, Yi-Fan Miao, Juan Li, Mei-Hua Wan, and Wen-Fu Tang

Department of Integrated Traditional Chinese and Western Medicine, West China Hospital, Sichuan University, Chengdu 610041, Sichuan Province, China

Correspondence should be addressed to Wen-Fu Tang; hxtangwenfu@126.com

Received 27 December 2021; Accepted 17 February 2022; Published 9 May 2022

Academic Editor: Yanhong Zhu

Objective. To explore the effect and underlying mechanism of Zengye decoction (ZYD), a traditional formula from China, on the severe acute pancreatitis (SAP) rat model with acute kidney injury (AKI). *Methods*. The SAP-AKI model was induced by 3.5% sodium taurocholate. Rats were treated with normal saline or ZYD twice and sacrificed at 36 h after modeling. Amylase, lipase, creatinine, blood urea nitrogen, kidney injury molecule 1(KIM-1), and multiple organs' pathological examinations were used to assess the protective effect of ZYD. Gut microbiome detected by 16S rRNA sequencing analysis and serum amino acid metabolome analyzed by liquid chromatography-mass spectrometry explained the underlying mechanism. The Spearman correlation analysis presented the relationship between microflora and metabolites. *Results*. ZYD significantly decreased KIM-1($P < 0.05$) and the pathological score of the pancreas ($P < 0.05$), colon ($P < 0.05$), and kidney ($P < 0.05$). Meanwhile, ZYD shifted the overall gut microbial structure (β-diversity, ANOSIM $R = 0.14$, $P = 0.025$) and altered the microbial compositions. Notably, ZYD reduced the potentially pathogenic bacteria—Bacteroidetes, Clostridiales vadin BB60 group, and uncultured_Clostridiales_bacterium, but promoted the short-chain fatty acid (SCFA) producers—Erysipelotrichaceae, Bifidobacterium, Lactobacillus, and *Moryella* (all $P < 0.05$). Moreover, principal component analysis (PCA), partial least squares-discriminant analysis (PLS-DA), and hierarchical clustering analysis (HCA) presented a remarkable change in amino acid metabolome after SAP-AKI induction and an apparent regulation by ZYD treatment (R2Y 0.878, $P = 0.01$; Q2 0.531, $P = 0.01$). Spearman's correlation analysis suggested that gut bacteria likely influenced serum metabolites levels (absolute $r > 0.4$ and FDR $P < 0.02$). *Conclusions*. ZYD attenuated SAP-AKI by modulating the gut microbiome and serum amino acid metabolome, which may be a promising adjuvant treatment.

1. Introduction

Severe acute pancreatitis (SAP) is a changeable and possibly lethal disease with multiple organ dysfunctions [1]. Acute kidney injury (AKI) is a frequent complication of SAP with extremely high mortality [2]. Metabolic reprogramming is a part of accepted pathologies underlying SAP-AKI, but the exact mechanism remains unclear [3]. Meanwhile, unique treatment for SAP-AKI is still under exploration [4].

Recently, the gut microbiome-modulating endogenous metabolism has aroused many interests [5]. More and more research studies have indicated that gut bacterial dysbiosis plays a vital role in the pathological mechanism of acute pancreatitis (AP) and AKI [6, 7]. Also, reports have demonstrated that improving gut microbiota could protect against SAP [8, 9]. However, rare studies investigated the effect of modulating microbiome on SAP-AKI. The serum metabolome is responsive to the gut microbiome variation [10], and metabolomics is a powerful tool to explore potential pathogenesis and effective drugs for diseases [11]. Amino acids serve as major nutrients and signaling molecules to regulate various physiological processes [12].

Nevertheless, AP and AKI cause distinct disorders in the amino acid metabolic profile [13, 14]. Several studies presented that regulating the overall serum metabolome may protect AP [15–17], but very little is known about the effect of regulating the amino acid metabolome in SAP-AKI.

Zengye decoction (ZYD), a traditional Chinese medicine, consists of *Scrophulariae* (Xuanshen), *Ophiopogonis* (Maidong), and *Rehmannia* (Shengdi), which has been widely used in many Asian countries for thousands of years [18]. Research studies have reported that ZYD can ameliorate metabolic disorders like diabetes [19, 20]. Remarkably, Liu et al. proved that ZYD could regulate the gut microbiota and amino acid metabolism pathway to cure constipated rats [21]. To our knowledge, no report has explored the application of ZYD on SAP or AKI. Thus, we hypothesized that ZYD could protect SAP-AKI by modulating the gut microbiome and serum amino acid metabolome. This study may provide a novel therapeutic method for SAP-AKI and elucidate the potential underlying mechanisms.

2. Materials and Methods

2.1. Animals. Twenty-one male Sprague Dawley rats (weight: 220 ± 10 g, clean grade) were obtained from Dashuo Experimental Animal Co., Ltd (Chengdu, China) (certificate no. 512003500015140; license no. SCXK (Sichuan) 2020–030). After one week of acclimation, the animals fasted but were free to access water 24 h ahead of the experiment. The experimental protocol passed the ethics of the West China Hospital of Sichuan University and was approved by the Animal Ethics Committee (protocol number: 2020234A, Chengdu, China).

2.2. ZYD Preparation. ZYD decoction is composed of Scrophulariae, Ophiopogonis, and Rehmannia. According to the Chinese Pharmacopoeia, the appropriate daily dose of these crude drugs for an adult (60 kg) is 15 g, 12 g, and 12 g, respectively. Besides, the frequently used administration of this decoction is 3 times a day. Thus, a single dose per kilogram of body weight is about 0.21 g/kg (=0.021 g/100 g). In line with the experimental methodology of pharmacology written by Xu et al. [22], a 6.3-fold dose of an adult is reasonable for Sprague Dawley rats, which is about 0.13 g/100 g body weight.

These crude drugs were obtained from the Affiliated Hospital of Chengdu University of Traditional Chinese Medicine (Chengdu, China), where they were processed to spray-dried particles by professionals in the pharmacy department after identification. Afterward, we reconstituted the spray powder with 40°C distilled water at 0.13 g/ml and treated the ZYD group experimental animals by intragastric administration (1 ml/100 g body weight).

2.3. Experimental Design. Sprague Dawley rats were randomly separated into the control group (C, $N = 7$) with sham operation, SAP model group (MG, $N = 7$), and ZYD treatment group (ZYD, $N = 7$). All rats were anesthetized with pentobarbital sodium solution (2%) by intraperitoneal injection (50 mg/kg) [23]. The subsequent operation is similar as Zhang et al. described in their research [24]. In brief, the biliopancreatic duct was found and carefully cannulated, and then, a microvascular clamp was applied to temporarily close the hepatic duct. Next, 3.5% sodium taurocholate (1 ml/kg body weight) induced the SAP model by infusion at a speed of 6 ml/h. Finally, we replaced the pancreas and cautiously closed the abdomen. ZYD decoction was applied to experimental rats at 12 h and 24 h after SAP induction by intragastric injection, respectively. At the same time, the C and MG were administered equivalent volumes of saline. Rats were sacrificed at 36 h after the SAP model establishment. Blood samples stood for 2 h before centrifugation (1,300 g, 10 min, 4°C), and serum samples were stored at −80°C until analysis. Fresh tissues, including pancreas, colon, and kidney, were fixed with paraformaldehyde at room temperature and sent to Lilai Biotechnology Company for embedding by paraffin and section. Fresh fecal samples taken from the colon were rapidly preserved in a liquid nitrogen container and maintained at −80°C until analysis.

2.4. Laboratory Tests. The concentrations of amylase, lipase, creatine (Cr), and blood urea nitrogen (BUN) in serum were detected by Roche Cedex C501 automatic biochemical analyzer (Switzerland). Serum kidney injury molecule 1 (KIM-1) level was measured by ELISA Kit (Cat. No. ZC-37184) from Zhuo Cai Technology Company (Shanghai, China) in line with the instructions from the manufacturer.

2.5. Histopathologic Examination. The paraffin-embedded pancreas, colon, and kidney tissues from each group, after sliced (5 μm), dewaxed, and stained with hematoxylin and eosin (H&E), were observed under an upright microscope (Zeiss, Germany) by two professional pathologists in a blind manner. The pancreas (×200) and kidney (×200) were scored, respectively, for edema, neutrophil infiltration, necrosis, and hemorrhage on a 0 (none) to 4 (severe) scale [25]; then, the composite scores were calculated. The colon (×200) was scored for inflammation-associated histological changes using an established scoring system with a scale from 0 to 4 [26]. Random ten fields of each section were counted, and the average of the composite scores for each field was presented as the final pathological injury score.

2.6. 16S rRNA Sequencing Analysis of Gut Microbiome

2.6.1. DNA Extraction. The stools were sent to OE Biotech (Shanghai, China) to perform the 16S rRNA analysis. According to the instructions from the manufacturer, overall genomic DNA was extracted through DNeasy PowerSoil Kit (QIAGEN, cat. no. 12888, USA). NanoDrop (Thermo Fisher 2000, USA) and agarose gel examined the concentration of DNA. Then, they were applied for PCR amplification with the aid of barcoded primers and Tks Gflex DNA Polymerase (Takara, cat. no. R060B, Japan).

Amplifying the particular regions (V3–V4) of 16S rRNA genes helped the bacterial diversity analysis and the widespread primers: 343F (5′-TACGGRAGGCAGCAG-3′) and 798R (5′- AGGGTATCTAATCCT-3′) were used in this study. After surveying the quality utilizing gel, purified by AMPure XP beads (Agencourt, USA), the PCR products were amplified for PCR again. Then, the final amplicon was acquired by purifying again and quantified utilizing the Qubit dsDNA assay kit (Thermo Fisher, cat. no. Q32854, USA). In the end, these amplicons were merged at equal amounts for subsequent sequencing.

2.6.2. Bioinformatic Analysis. Unprocessed sequencing data were saved in the FASTQ format. Trimmomatic software (version 0.35) was applied to preprocess the paired-end reads for detecting and cutting off blurred bases (N) [27]. The sliding window trimming method helped cut out the low-quality sequences (average quality score <20). Then, Flash software (version 1.2.11) assembled paired-end reads [28]. Parameters in the assembly were as follows: 10 bp–200 bp of overlapping and 20% of maximum mismatch rate. QIIME software (version 1.8.0) assisted in further denoising of sequences as below: abandoning reads with sequences that were blurred, homologous, or below 200 bp; retaining reads whose 75% bases are above Q20. Then, reads with chimera were explored and deleted [29]. With the help of VSEARCH software (version 2.4.2), operational taxonomic units (OTUs) were generated from the clean reads, which were derived from primer sequence removal and clustering (similarity cutoff: 97%) [30]. The representative read of each OTU was picked by the QIIME package. Analysis for α-diversity, such as Shannon index, Simpson index, Chao 1 index, and observed species, was detailed in previous research [31]. Linear discriminant analysis (LDA) of effect size (LEfSe) was performed according to Zhu et al. [32]. Nonmetric multidimensional scaling (NMDS) based on Bray-Curtis distance, analysis of similarities (ANOSIM), and Kyoto Encyclopedia of Genes and Genomes (KEGG) pathway analysis was described in the research implemented by Lei et al. [33, 34]. Ribosomal Database Project (RDP) classifier was utilized to annotate all typical reads against the SILVA database (version 123) with a 70% confidence threshold [35].

2.7. Serum Amino Acid Metabolome Detection. For metabolomic analysis, twenty-one serum samples were sent to the West China-Washington Mitochondria and Metabolism Research Center. A merged method for targeted analysis of amino acids and untargeted profiling was implemented in this study [36]. The UltiMate 3000 rapid separation liquid chromatography (Thermo Fisher Scientific, USA) equipped with a BEH Amide column (100 × 2.1 mm, 1.7 μm, Waters, USA) coupled with *Q* Exactive Plus quadrupole-Orbitrap high-resolution mass spectrometry (Thermo Fisher Scientific, USA) performed this measurement. Detailed procedures from reagent preparation to liquid chromatography-tandem mass spectrometry (LC-MS/MS) data analysis were depicted in the research reported by Zhang et al. [37]. Special parameters in this study were as follows. The column temperature was 35°C, and the elution gradient linearly changed: 0–2 min, 100% B; 2–4 min, 100%–95% B; 4–9 min, 95%–85% B; 9–14 min, 85%–50% B; 14–17 min, 50%–50% B; 17–17.1 min, 50%–100% B; and 17.1–25 min, 100% B. Differentially expressed metabolites were screened under these conditions: 1. Kruskal-Wallis test $P < 0.05$; 2. variable importance for the projection (VIP) score >1. R software (version 4.1.0) was used for statistical data analysis, such as Kruskal-Wallis test, hierarchical clustering analysis (HCA), principal component analysis (PCA), partial least squares-discriminant analysis (PLS-DA), and pathway analysis against the database KEGG [38].

2.8. Spearman's Correlation Analysis. The cor.test (R software 4.1.0) performed Spearman's correlation analysis between serum metabolite concentration and genera abundance. The *P*-value of multiple comparisons was corrected by Benjamin-Hochberg false discovery rate (FDR), and the association was considered statistically significant if absolute r value > 0.4 and adjusted $P < 0.2$ [39].

2.9. Statistical Analysis. Data (mean ± standard error of mean (SEM)) were analyzed by SPSS26.0 (Chicago, IL, USA). The type of parametric distribution was examined using the Shapiro-Wilk test. One-way ANOVA with post hoc least significant difference (LSD) test was carried out for three groups with standard distribution data. Mann-Whitney *U* test for two groups and Kruskal-Wallis test for three groups were used to compare continuous variables. $P < 0.05$ was regarded as statistically significant.

3. Results

3.1. ZYD Showed a Protective Effect against SAP-AKI. In this experiment, we established the SAP-AKI model by a refusion of 3.5% sodium taurocholate and sacrificed rats at 36 h after modeling to observe the effect of ZYD. Serum amylase ($P < 0.05$), lipase ($P < 0.05$), and KIM-1 ($P < 0.05$) levels significantly increased after SAP induction. Conversely, ZYD decreased the serum concentration of amylase and lipase and significantly reduced KIM-1 ($P < 0.05$) (Figure 1(a)). There was no distinct difference in Cr and BUN among the three groups (data not shown).

The MG group showed severe morphological injuries like edema and acinar cell necrosis in the pancreas, neutrophil infiltration in the colon, and hemorrhage in the kidney compared to the C group ($P < 0.05$, Figure 1(b)). In contrast, a significant injury amelioration of the pancreas ($P < 0.05$), colon ($P < 0.05$), and kidney ($P < 0.05$) was presented in the ZYD group (Figure 1(b)). In brief, these results suggest a protective effect from ZYD on SAP-AKI.

3.2. ZYD Modulated the Gut Microbiome in SAP-AKI. To detect the effect of ZYD on gut microflora in rats with SAP-AKI, we analyzed 21 fecal samples using the 16S rRNA gene sequencing method. OTUs, clustered from the high-quality amplicon sequence variants from the gut bacterial gene V3-V4 region, were the basis for gut microbiome comparison. A

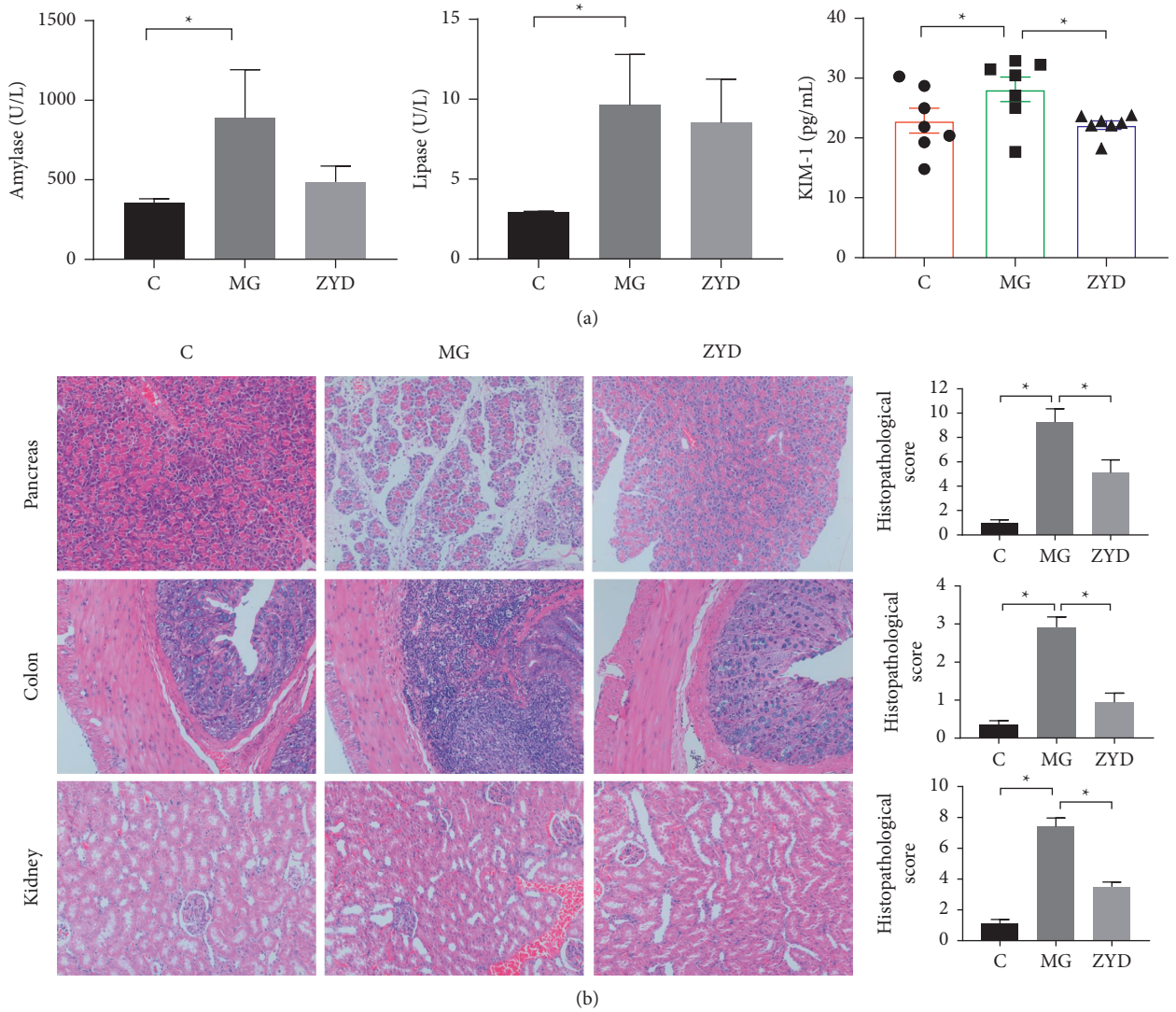

Figure 1: ZYD protects against SAP-AKI. (a) Comparison of amylase, lipase, and kidney injury molecule 1(KIM-1) in serum. *: $P < 0.05$ (amylase and lipase decided by the Mann-Whitney test, KIM-1 decided by the one-way ANOVA followed LSD test). (b) Pathological picture and scores of the pancreas, colon, and kidney. Scale bar: 100 μm (×200). *: $P < 0.05$ (one-way ANOVA followed LSD test). (c) Healthy control group with the sham operation, MG: severe acute pancreatitis model group, and ZYD: Zengye decoction treatment group. $n = 7$ (per group). Data are presented as the mean ± SEM.

total of 3,083 OTUs overlapped among the three groups, with 143, 157, and 117 OTUs specifically detected in the C, MG, and ZYD groups, respectively (Supplementary Figure 1(a)). The species accumulation curves tended to flatten out as the number of samples increased, which meant adequate sequencing in this experiment (Supplementary Figure 1(b)). Interestingly, four α-diversity indices among the three groups were comparable, revealing that ZYD did not significantly affect intrasample species richness and diversity (Supplementary Figure 1(c)).

The β-diversity analysis (NMDS based on Bray-Curtis distance) displays the similarity of the overall bacterial structure [34]. Although the cluster of samples in MG could not be separated from the C, ZYD dramatically shifted microbial structure from SAP-AKI status (ANOSIM $R = 0.14$, $P = 0.025$) (Figure 2(a)). The LDA of effect size (LEfSe) identified 10, 10, and 14 predominant bacterial taxa in the C, MG, and ZYD, respectively (from phyla to genera, LDA > 3, and $P < 0.05$) (Figure 2(b), Supplementary Figure 1(d)), which suggests a different microbial composition among the three groups. In addition, potentially pathogenic bacteria [40], such as *Bacteroidetes*, were over-represented in the MG. At the same time, short-chain fatty acid (SCFA) producers—*Erysipelotrichaceae*, *Bifidobacterium*, and *Lactobacillus*—were predominant in the ZYD [41, 42].

Next, the alterations of microbial compositions were assessed by the Mann-Whitney *U* test. At the phylum level, SAP-AKI increased the abundance of *Bacteroidetes*, but ZYD decreased it ($P < 0.05$) (Figure 2(c)). At the family level, the Clostridiales vadin BB60 group was increased by SAP-AKI ($P < 0.05$) but was decreased by ZYD ($P < 0.05$) (Figure 2(d)). At the genus level, 12 genera were shifted by

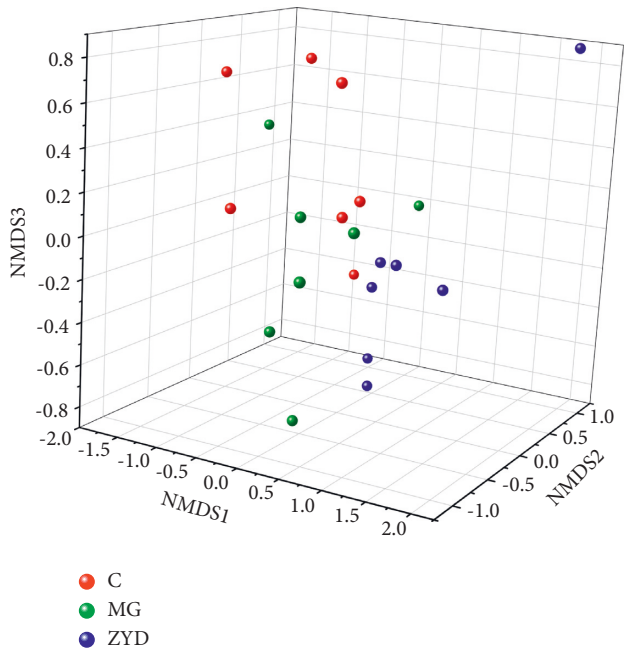

(a)

Figure 2: Continued.

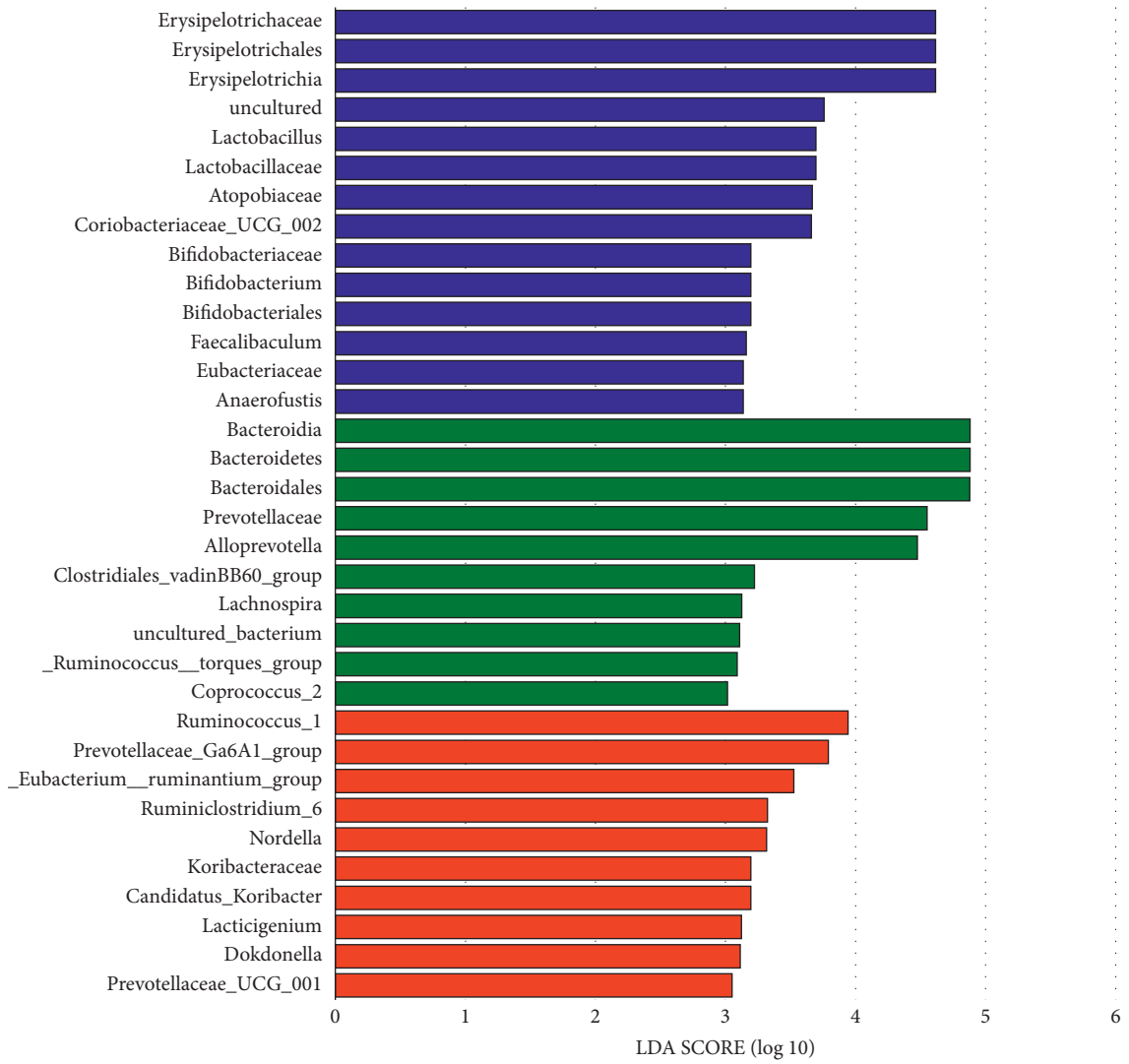

(b)

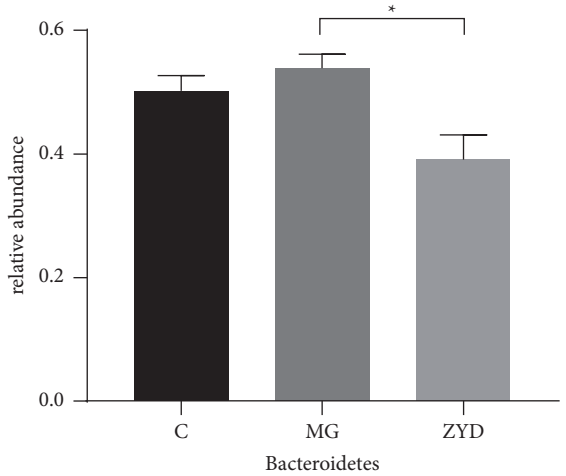

(c)

Figure 2: Continued.

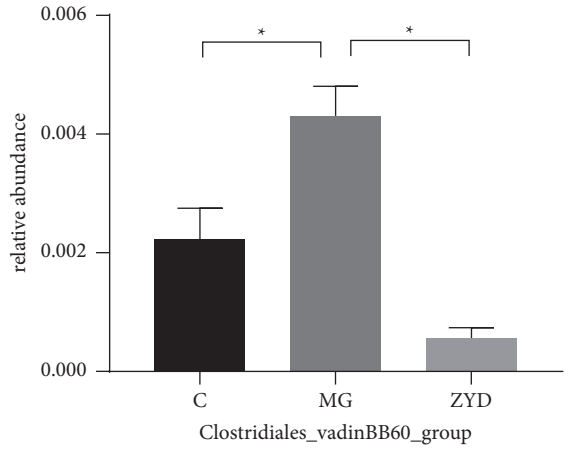

(d)

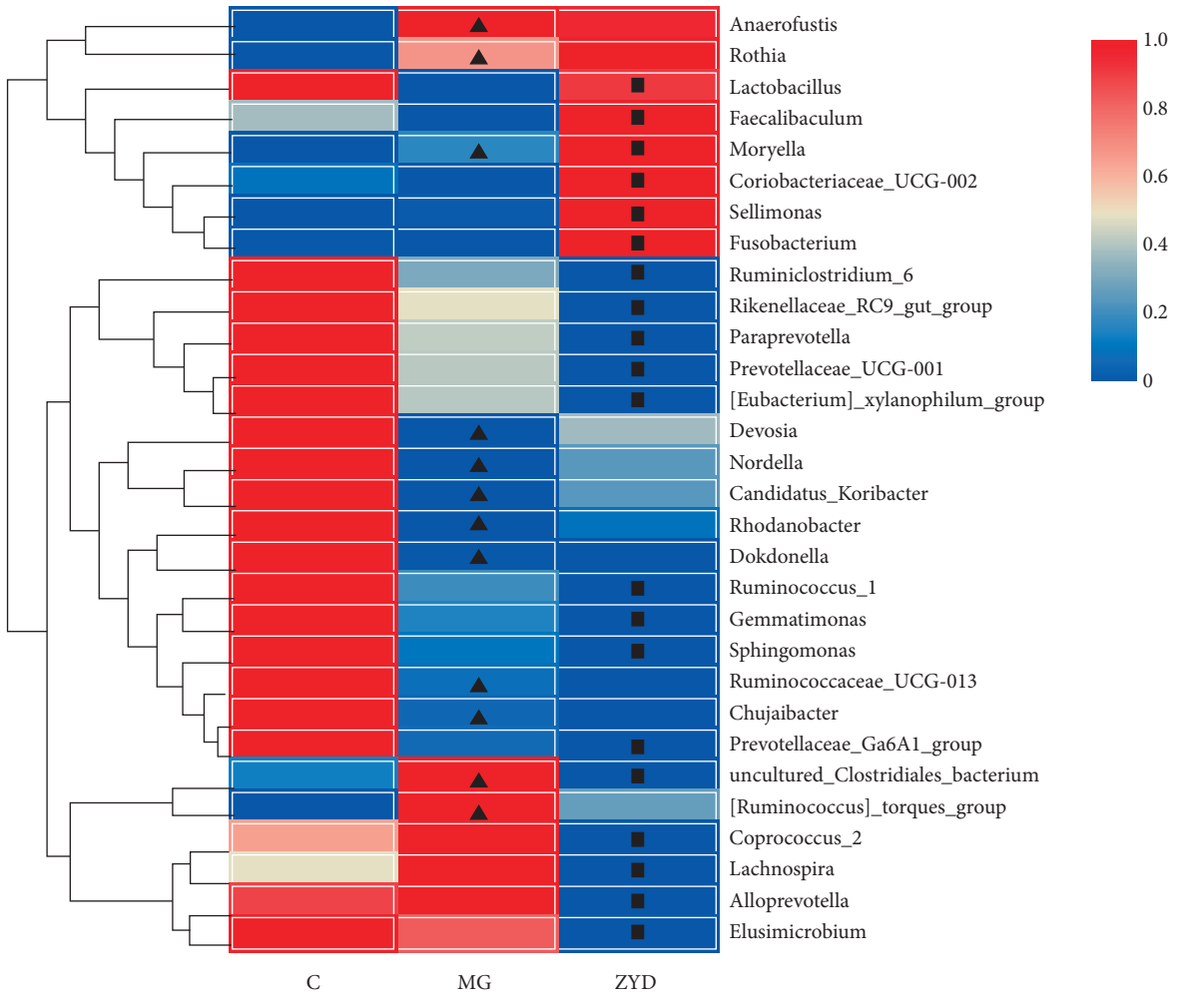

(e)

Figure 2: Continued.

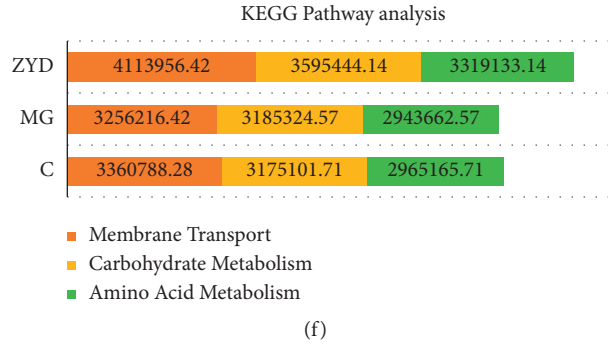

(f)

Figure 2: ZYD modulated the gut microbiome in SAP-AKI. (a) Nonmetric multidimensional scaling (NMDS) based on Bray-Curtis distance compared gut microbial structure among the three groups. (b) Linear discriminant analysis (LDA) analysis identified the predominant bacterial taxa among the three groups. (c) ZYD decreased Bacteroidetes (*: $P < 0.05$, Mann-Whitney U test). $n = 7$ (per group). Data are presented as the mean ± SEM. (d) The variation trend of Clostridiales vadin BB60 group (*: $P < 0.05$, Mann-Whitney U test). $n = 7$ (per group). Data are presented as the mean ± SEM. (e) Heatmap showed the abundance change in 30 genera across the three groups, ▲: C vs. MG, $P < 0.05$, Mann-Whitney test; ■: MG vs. ZYD, $P < 0.05$, Mann-Whitney U test. $n = 7$ (per group). Data are presented as the mean ± SEM. (f) KEGG pathway analysis of the gut microbiota functional gene. C: Healthy control group with the sham operation, MG: severe acute pancreatitis model group, and ZYD: Zengye decoction treatment group.

SAP-AKI status ($P < 0.05$), and 20 genera were regulated by ZYD ($P < 0.05$) (Figure 2(e)). Notably, ZYD increased *Lactobacillus* ($P < 0.05$) and *Moryella* ($P < 0.05$) while decreasing uncultured_Clostridiales_bacterium ($P < 0.05$). Collectively, these results pointed to a significant modulation effect by ZYD treatment on the gut microbial profile.

Furthermore, KEGG pathway analysis showed that the gut microflora functional gene of amino acid metabolism was more abundant in the ZYD group, implying that the amino acid metabolome may be regulated by ZYD (Figure 2(f)).

3.3. ZYD Regulated the Serum Amino Acid Metabolome in SAP-AKI. To explore the effect of ZYD on the serum amino acid metabolome, we performed the metabolomic analysis by LC-MS/MS. Totally, 814 metabolites were identified from the 21 serum samples. Unsupervised method PCA presented the variation trend in the data and detected the potential outlier of serum samples [43]. The PCA scatter plot (Figure 3(a)) showed that the first principal component (PC1) covered 14.59% of the variation and separated the SAP-AKI status and healthy control group (except one outlier in the MG). The second principal component (PC2) covered 12.68% of the variation and distinctly divided the MG and ZYD group. Furthermore, the supervised method PLS-DA was applied to characterize the global metabolic difference across groups [43]. According to the group, distinguished clusters were shaped in the PLS-DA plot, indicating that the metabolic phenotype was dramatically changed by SAP-AKI and ZYD (Figure 3(b)). Correspondingly, permutation test showed a good interpretability and predictability of this PLS-DA model (R2Y 0.878, $P = 0.01$; Q2 0.531, $P = 0.01$) (Figure 3(c)) [43]. Thus, the subsequent analysis could be implemented.

The 53 metabolites with statistical significance across groups were selected by Kruskal-Wallis test ($P < 0.05$) and variable importance for the projection score (VIP >1). HCA is an effective algorithm to sort similar samples based on the relative areas of characteristic peaks detected by LC-MS/MS [44]. Combining the HCA and heatmap visualization helps discover the variation trend of these differential metabolites [45]. Figure 3(d) presented a remarkable abundance change in these metabolites after SAP-AKI modeling and ZYD treatment. Plus, twenty-one serum samples were clustered into three categories (except one outlier), and the cluster of ZYD was closer to the control group than MGs. It can be inferred that ZYD can regulate the disturbed metabolic profile of amino acids in SAP-AKI.

To explore the underlying protective mechanism of ZYD, we next performed the KEGG pathway enrichment analysis of these metabolites. As the bubble chart showed, multiple pathways were enriched by these metabolites (Figure 3(e)). Among them, the KEGG pathway of alanine, aspartate, and glutamate metabolism ($P < 0.01$, Impact = 0.5) may play a critical role during the ZYD therapy for SAP-AKI. These results collectively presented a remarkable change in amino acid metabolome after SAP-AKI induction and an apparent regulation by ZYD treatment.

3.4. Correlation between the Differential Genera and Metabolites. Spearman's correlation analysis was performed on the 30 genera and 53 metabolites with a statistical difference (Kruskal-Wallis test, $P < 0.05$) across the three groups. Interestingly, significant interactions were identified (absolute $r > 0.4$ and FDR $P < 0.2$) among these genera and metabolites, indicating that gut bacteria likely induced the change in serum metabolite level (Figure 4).

4. Discussion

SAP-AKI raises the risk of developing chronic kidney disease and the mortality of patients, but the exact pathological mechanism remains unclear and unique treatments are urgently needed [46]. This study successfully established the SAP-AKI rat model and observed a disturbance in the gut

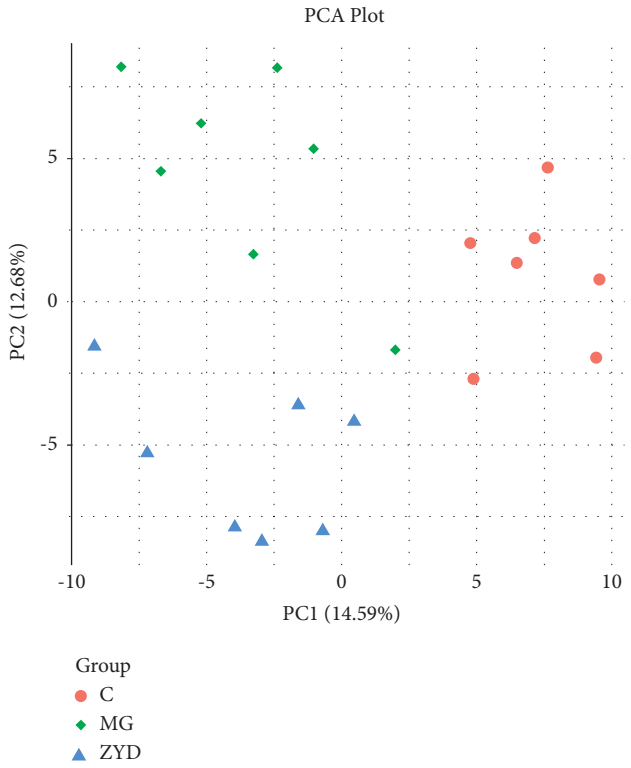

(a)

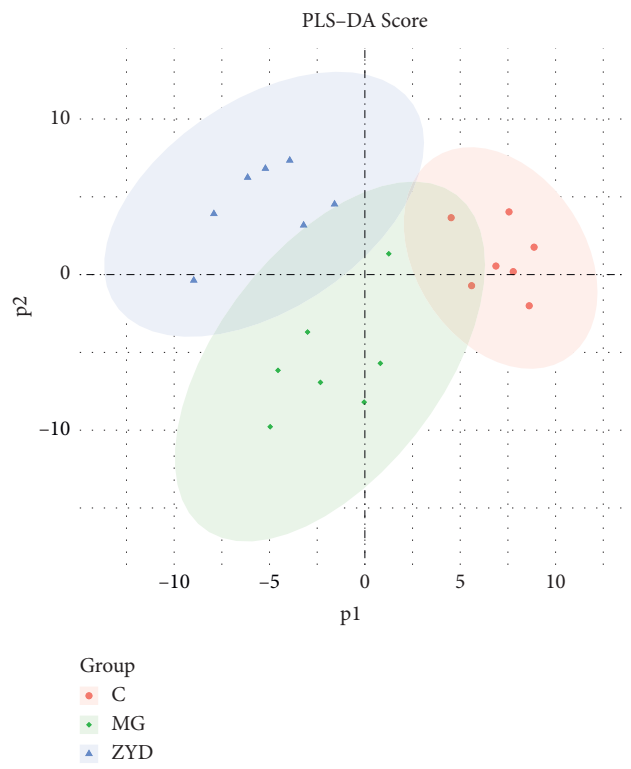

(b)

Figure 3: Continued.

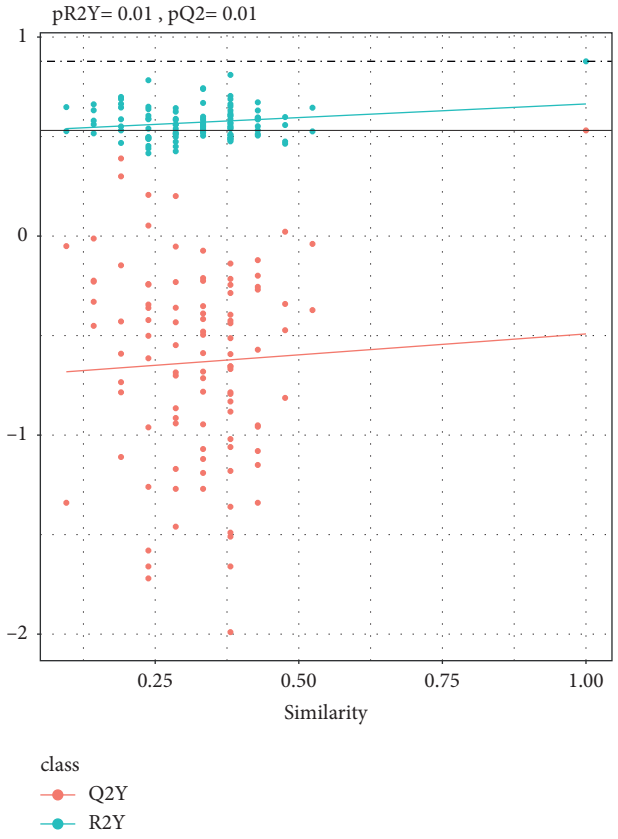

(c)

Figure 3: Continued.

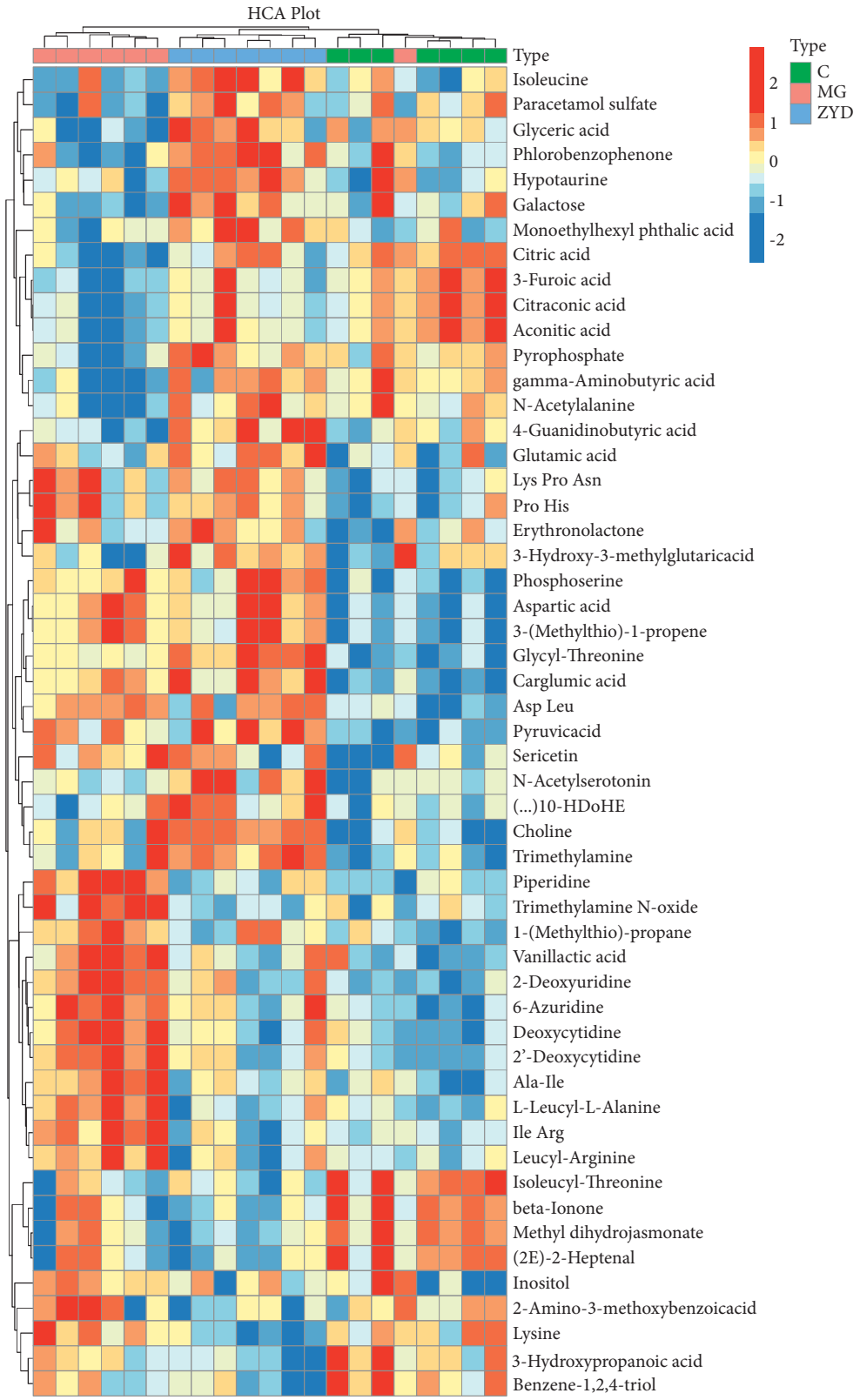

(d)

Figure 3: Continued.

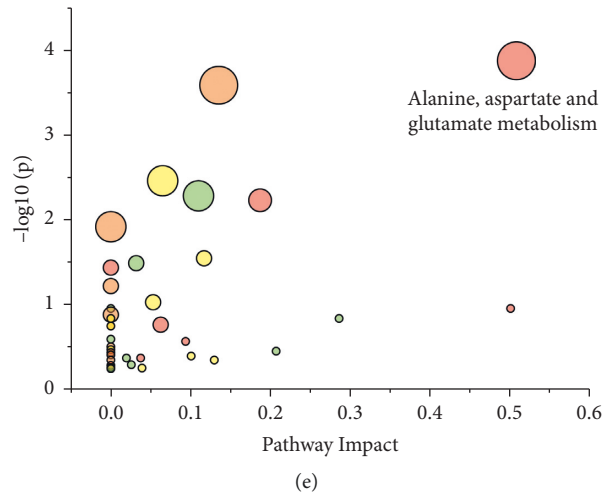

(e)

Figure 3: ZYD regulated the serum amino acid metabolome. (a) Principal component analysis (PCA) of the amino acid metabolites among the three groups. (b) The partial least squares-discriminant analysis (PLS-DA) compared the metabolic profile across groups. (c) Permutation test of this PLS-DA model. (d) The heatmap and hierarchical clustering analysis (HCA) detailed the variation of the three groups' 53 differential metabolites (Kruskal-Wallis test, $P < 0.05$). The correlation of samples was decided by Euclidean distance. (e) KEGG pathway enrichment analysis of the 53 differential metabolites. C: Healthy control group with the sham operation, MG: severe acute pancreatitis model group, and ZYD: Zengye decoction treatment group. $n = 7$ (per group).

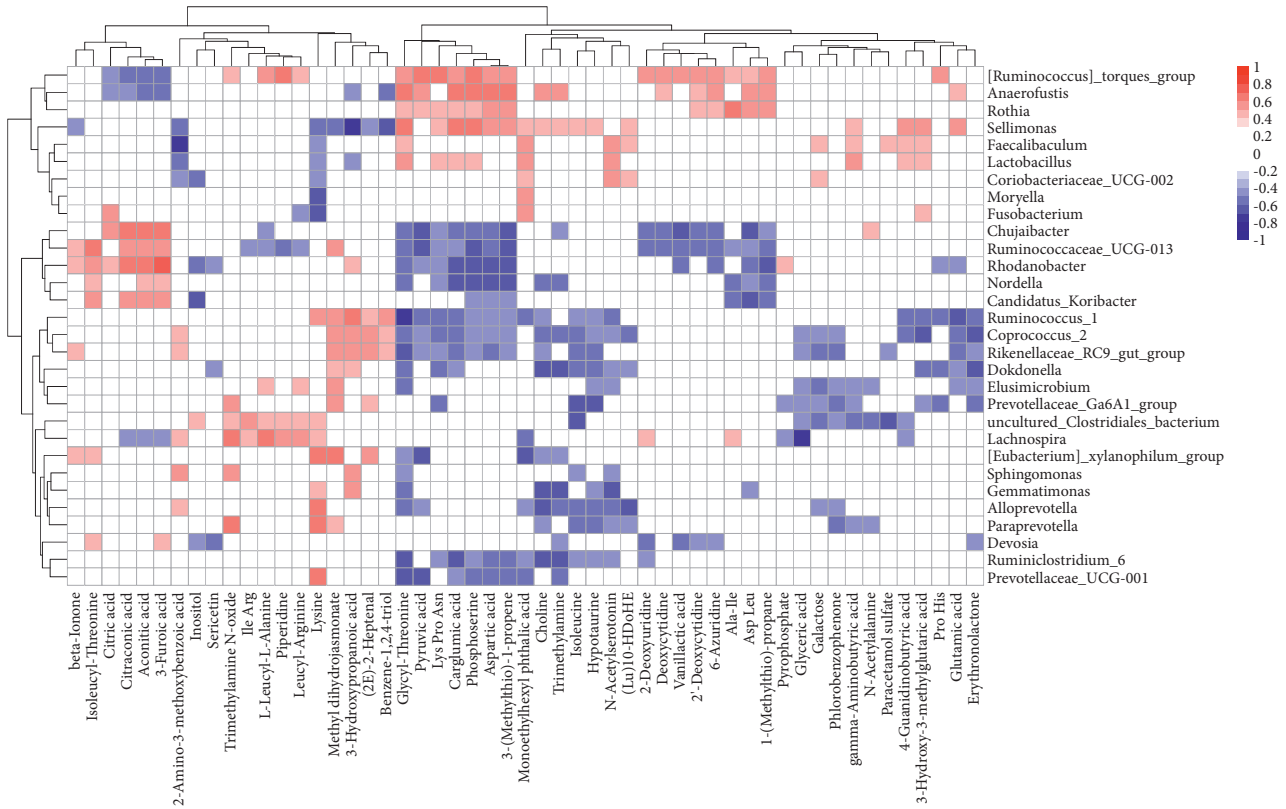

Figure 4: Correlation between the gut microbiota and serum metabolites. The heatmap detailed the positive (red) and negative (blue) correlation between the differential genera (row) and serum amino acid metabolites (column) across groups. This significant correlation was decided by Spearman's correlation analysis (absolute r value > 0.4 and FDR $P < 0.2$).

microbiome and serum metabolome. Our results presented that ZYD reshaped the landscape of the gut microflora, conferred resistance to amino acid metabolic imbalance, and showed a protective effect against SAP-AKI.

Secretion of amylase and lipase is an important function of pancreatic acinar cells. When pancreatic acinar cells are damaged, a mass of amylase and lipase will directly enter the circulatory system rather than the digestive duct [47, 48].

Thus, amylase and lipase are the globally recommended biomarkers for assessing acute pancreatitis severity [49]. In this study, the significant increase in both indices and histopathological scores suggested a successful SAP model establishment. As expected, ZYD decreased serum amylase and lipase to a large extent, though not reached statistical significance, which also implied the protective effect of ZYD to pancreatic acinar cells during SAP. This speculation was also supported by our histopathological results, in which the pathological injury of acinar cells was obviously reduced by ZYD treatment. At present, the diagnosis of AKI complicating from SAP depends on the dynamic increase in serum Cr [49]. BUN is usually used to evaluate kidney function in clinical practice [50]. However, both do not accurately reflect kidney injury severity, especially in early-stage SAP [51]. Therefore, the changes in Cr and BUN in this study were slight and insignificant. One preliminary study proved the diagnostic value of urinary KIM-1 concentration for SAP-AKI patients, which showed the shortcomings like lasting a short time and the need for frequent monitoring [52]. A rare study explored the serum KIM-1 value for SAP-AKI severity assessment [51]. But Chang et al. discovered a significant increase in serum KIM-1 in the hemorrhagic shock rat model with AKI [53]. Consistent with the literature, we found that serum KIM-1 was significantly lifted in the 36 h SAP-AKI rat model but approached normal after ZYD treatment. So, this result suggests the diagnostic value of serum KIM-1 for SAP-AKI in the early stage. More research studies are needed to elucidate this point.

Emerging research indicated that gut microbiota plays an essential role in the progression of acute pancreatitis [45, 46], implying that modulating gut microbial structure could be an efficient therapy for SAP. An earlier study reported that chitosan oligosaccharides attenuated SAP by modulating the β-diversity and predominant composition of gut bacteria [54]. Partly in line with previous research [9], ZYD also showed the capability to shift the gut bacterial structure from SAP-AKI, as evidenced by NMDS and LDA-LEfSe. Thus, we speculate that ZYD improves SAP-AKI via the modulation of gut microflora. The *Bacteroidetes* (phylum), potentially pathogenic bacteria [55], were a dominant gut bacterial member in the SAP-AKI. Similarly, the Clostridiales vadin BB60 group (family) and uncultured_Clostridiales_bacterium (genus), both belonging to the opportunistically pathogenic Clostridiales (order) [56], significantly increased in the SAP-AKI status. However, our results demonstrated that these pathogenic bacteria were effectively decreased by ZYD treatment. So, it can be inferred that reducing pathogenic microbiota may be closely related to the protective mechanism of ZYD. Alteration of gut microbial composition contributes to the variation of bacterial metabolites, which may influence the progression of SAP [57]. SCFAs, a widely studied metabolite of bacteria, showed good performance in maintaining intestinal homeostasis [58]. Research studies also indicated that supplements of SCFAs helped ameliorate organ injuries in SAP [59, 60]. In this study, SCFA-producing strains—*Erysipelotrichaceae*, *Bifidobacterium*, *Lactobacillus*, and *Moryella*, were more abundant in ZYD than MG [42, 61]. It suggests that ZYD protects SAP-AKI by increasing these bacteria to indirectly supplement SCFAs. In a word, our results imply that ZYD ameliorates SAP-AKI by modulating the gut microbiome, including reducing pathogenic bacteria and improving SCFA-producing strains.

Amino acids are a substantial energy source to fuel the body [62]. In acute pancreatitis, systemic inflammation causes a hypercatabolic state, contributing to increased energy requirements and disrupting the metabolism of amino acids [13, 63]. For critical patients with AKI, the hypercatabolic condition also negatively affects protein degradation and amino acid conversions [64]. So, regulating the metabolism of amino acids may serve as a potential therapy for SAP-AKI. The previous study has elucidated the capability of Chinese medicine to treat acute pancreatitis by altering the metabolic profile [16]. As expected, the unique metabolic phenotypes of amino acids in SAP-AKI and after ZYD treatment are presented in the scatter plot of PCA and PLS-DA. Moreover, the variation of the 53 differential metabolites across groups revealed that the ZYD could alter the metabolic profile of amino acids toward healthy status. In short, these results imply that ZYD attenuates SAP-AKI by regulating the amino acid metabolome. One unexpected finding was an outlier from the MG group, but we considered it due to a lesser degree of illness after SAP-AKI modeling. In addition, KEGG analysis demonstrated that ZYD might affect multiple pathways to therapy for SAP-AKI, but the way of alanine, aspartate, and glutamate metabolism significantly enriched by multiple metabolites is worth great attention. Alanine, aspartate, and glutamate play an essential role in protein structure and energy supplement through the tricarboxylic cycle [62]. Our result showed that SAP bothered the metabolism of these metabolites in this pathway, and ZYD significantly regulated most of them and notably increased glutamic acid (glutamate). The supply of glutamine, which can be hydrolyzed to glutamate, could improve gut permeability, oxidative stress, and reduce the complication rate in SAP patients [65]. Thus, it can be inferred that ZYD could regulate energy supplements by influencing the pathway of alanine, aspartate, and glutamate metabolism to protect SAP-AKI, but more research studies are needed to elucidate it.

The metabolome is responsive to the physiological condition and gut microflora variation [66, 67]. Amino acids have emerged as critical signaling metabolites to regulate metabolism and inflammation through the relationship with microbiota and host receptors [68]. Correspondingly, in this study, significant correlations were identified between gut bacteria and amino acids, which were also modulated by SAP-AKI and ZYD. Therefore, we speculate that the interaction of gut microbiota and serum metabolome was related to the underlying mechanism of ZYD protection.

There are several limitations to this study. First, these experimental data come from a small number of SAP-AKI animal models. Second, the current developing level of the methodology may limit the detection of the gut microbiome and metabolome in serum. However, this study provided a new therapy to SAP-AKI and preliminary elucidated the

underlying mechanism. Our findings may be helpful for further comprehension of the SAP-AKI pathology and appropriate clinical application for ZYD.

5. Conclusions

ZYD attenuated SAP-AKI by modulating the gut microbiome and serum amino acid metabolome, which may be a promising adjuvant treatment.

Data Availability

The datasets used and/or analyzed during the current study are available from the corresponding author upon reasonable request.

Disclosure

The funder had no role in study design, data collection and analysis, the decision to publish, and the preparation of the manuscript.

Conflicts of Interest

The authors declare that they have no conflicts of interest.

Authors' Contributions

Wen-fu Tang designed the research and obtained funding; Xiao-yu Dai, Qian Hu, Jia-qi Yao, and Xia-jia Wu performed the experiment; Xiao-yu Dai analyzed the data and drafted the paper; Yi-fan Miao, Juan Li, and Mei-hua Wan made critical revisions of the manuscript.

Acknowledgments

The authors would like to thank Liang Ge, Zhang Lu, and Zheng Wen (West China-Washington Mitochondria and Metabolism Research Center, West China Hospital, Sichuan University) for metabolomic data acquisition and analysis. This work was supported by the National Natural Science Foundation of China (grant no. 81873203).

Supplementary Materials

The supplementary figures were uploaded with the original manuscript. (*Supplementary Materials*)

References

[1] L. Boxhoorn, R. P. Voermans, S. A. Bouwense et al., "Acute pancreatitis," *The Lancet*, vol. 396, no. 10252, pp. 726–734, 2020.

[2] S. Uchino, J. A. Kellum, R. Bellomo et al., "Acute renal failure in critically ill Patients a multinational, multicenter study," *JAMA*, vol. 294, no. 7, pp. 813–818, 2005.

[3] S. Peerapornratana, C. L. Manrique-Caballero, H. Gómez, and J. A. Kellum, "Acute kidney injury from sepsis: current concepts, epidemiology, pathophysiology, prevention and treatment," *Kidney International*, vol. 96, no. 5, pp. 1083–1099, 2019.

[4] R. Bellomo, J. A. Kellum, C. Ronco et al., "Acute kidney injury in sepsis," *Intensive Care Medicine*, vol. 43, no. 6, pp. 816–828, 2017.

[5] M. G. Rooks and W. S. Garrett, "Gut microbiota, metabolites and host immunity," *Nature Reviews Immunology*, vol. 16, no. 6, pp. 341–352, 2016.

[6] M. E. Cen, F. Wang, Y. Su, W. J. Zhang, B. Sun, and G. Wang, "Gastrointestinal microecology: a crucial and potential target in acute pancreatitis," *Apoptosis : An International Journal on Programmed Cell Death*, vol. 23, no. 7-8, pp. 377–387, 2018.

[7] H. Rabb, J. Pluznick, and S. Noel, "The microbiome and acute kidney injury," *Nephron*, vol. 140, no. 2, pp. 120–123, 2018.

[8] X. Piao, B. Liu, X. Sui et al., "Picroside II improves severe acute pancreatitis-induced intestinal barrier injury by inactivating oxidative and inflammatory TLR4-dependent PI3K/AKT/NF-κB signaling and improving gut microbiota," *Oxidative Medicine and Cellular Longevity*, vol. 2020, Article ID 3589497, 9 pages, 2020.

[9] S. Takauji, H. Konishi, M. Fujiya et al., "Polyphosphate, derived from Lactobacillus brevis, modulates the intestinal microbiome and attenuates acute pancreatitis," *Digestive Diseases and Sciences*, vol. 66, no. 11, pp. 3872–3884, 2021.

[10] F. Chen, X. Dai, C. C. Zhou et al., "Integrated analysis of the faecal metagenome and serum metabolome reveals the role of gut microbiome-associated metabolites in the detection of colorectal cancer and adenoma," *Gut*, vol. 0, pp. 1–11, 2021.

[11] O. Fiehn, "Metabolomics - the link between genotypes and phenotypes," *Functional Genomics*, vol. 48, no. 1-2, pp. 155–171, 2002.

[12] Z. Dai, Z. Wu, S. Hang, W. Zhu, and G. Wu, "Amino acid metabolism in intestinal bacteria and its potential implications for mammalian reproduction," *Molecular Human Reproduction*, vol. 21, no. 5, pp. 389–409, 2015.

[13] P. Sandstrom, L. Trulsson, T. Gasslander, T. Sundqvist, U. von Dobeln, and J. Svanvik, "Serum amino acid profile in patients with acute pancreatitis," *Amino Acids*, vol. 35, no. 1, pp. 225–231, 2008.

[14] Q. Wei, X. Xiao, P. Fogle, and Z. Dong, "Changes in metabolic profiles during acute kidney injury and recovery following ischemia/reperfusion," *PLoS One*, vol. 9, no. 9, Article ID e106647, 2014.

[15] Y. He, J. Dai, M. Niu et al., "Inhibition of nicotinamide phosphoribosyltransferase protects against acute pancreatitis via modulating macrophage polarization and its related metabolites," *Pancreatology*, vol. 21, no. 5, pp. 870–883, 2021.

[16] J. Li, S. F. Zhu, X. L. Zhao et al., "Metabolomic profiles illuminate the efficacy of Chinese herbal Da-Cheng-Qi decoction on acute pancreatitis in rats," *Pancreatology: Official Journal of the International Association of Pancreatology (IAP)*, vol. 15, no. 4, pp. 337–343, 2015.

[17] W. Huang, H. Liu, Y. Li, and G. Mai, "The effects of rhein and honokiol on metabolic profiles in a mouse model of acute pancreatitis," *Medical Science Monitor: International Medical Journal of Experimental and Clinical Research*, vol. 26, Article ID e925727, 2020.

[18] C.-y. Li, S.-l. Wu, L.-x. Sun, T.-t. Yan, and Y. Wang, "Protective effect of Zengye decoction (增液汤) on submandibular glands in nonobese diabetic mice," *Chinese Journal of Integrative Medicine*, vol. 25, no. 1, pp. 45–50, 2019.

[19] Z. Liu, W. Kuang, X. Xu et al., "Putative identification of components in Zengye Decoction and their effects on glucose consumption and lipogenesis in insulin-induced insulin-

resistant HepG2 cells," *Journal of Chromatography B*, vol. 1073, pp. 145–153, 2018.

[20] M. Wang, S.-Q. Chang, Y.-S. Tian, G.-Q. Zhang, and J. Qi, "Zengye decoction ameliorates insulin resistance by promoting glucose uptake," *Rejuvenation Research*, vol. 23, no. 5, pp. 367–376, 2020.

[21] D. Liu, L. Lin, Y. Lin et al., "Zengye decoction induces alterations to metabolically active gut microbiota in aged constipated rats," *Biomedicine & Pharmacotherapy*, vol. 109, pp. 1361–1371, 2019.

[22] S. Xu, R. Bian, and X. Chen, *Experimental Methodology of Pharmacology*, People's Sanitary Publishing Press, Geneva, 3rd edition, 2002.

[23] X. L. Yi, J. Hu, Q. T. Wu et al., "Effect of different-volume fluid resuscitation on organ functions in severe acute pancreatitis and therapeutic effect of poria cocos," *Evidence Based Complement Alternative Medicine*, vol. 2020, Article ID 6408202, 2020.

[24] Q. Zhang, X. Tao, S. Xia et al., "Emodin attenuated severe acute pancreatitis via the P2X ligand-gated ion channel 7/NOD-like receptor protein 3 signaling pathway," *Oncology Reports*, vol. 41, no. 1, pp. 270–278, 2019.

[25] L. Yuan, L. Zhu, Y. Zhang et al., "Effect of Da-Cheng-Qi decoction for treatment of acute kidney injury in rats with severe acute pancreatitis," *Chinese Medicine*, vol. 13, no. 1, p. 38, 2018.

[26] S. Wirtz, V. Popp, M. Kindermann et al., "Chemically induced mouse models of acute and chronic intestinal inflammation," *Nature Protocols*, vol. 12, no. 7, pp. 1295–1309, 2017.

[27] A. M. Bolger, M. Lohse, and B. Usadel, "Trimmomatic: a flexible trimmer for Illumina sequence data," *Bioinformatics*, vol. 30, no. 15, pp. 2114–2120, 2014.

[28] D. Reyon, S. Q. Tsai, C. Khayter, J. A. Foden, J. D. Sander, and J. K. Joung, "FLASH assembly of TALENs for high-throughput genome editing," *Nature Biotechnology*, vol. 30, no. 5, pp. 460–465, 2012.

[29] J. G. Caporaso, J. Kuczynski, J. Stombaugh et al., "QIIME allows analysis of high-throughput community sequencing data," *Nature Methods*, vol. 7, no. 5, pp. 335-336, 2010.

[30] T. Rognes, T. Flouri, B. Nichols, C. Quince, and F. Mahé, "VSEARCH: a versatile open source tool for metagenomics," *Peer Journal*, vol. 4, Article ID e2584, 2016.

[31] N. Huang, D. Hua, G. Zhan et al., "Role of Actinobacteria and Coriobacteriia in the antidepressant effects of ketamine in an inflammation model of depression," *Pharmacology Biochemistry and Behavior*, vol. 176, pp. 93–100, 2019.

[32] B. Zhu, J. Shen, R. Jiang et al., "Abnormalities in gut microbiota and serum metabolites in hemodialysis patients with mild cognitive decline: a single-center observational study," *Psychopharmacology*, vol. 237, no. 9, pp. 2739–2752, 2020.

[33] Y. Lei, L. Tang, S. Liu et al., "Parabacteroides produces acetate to alleviate heparanase-exacerbated acute pancreatitis through reducing neutrophil infiltration," *Microbiome*, vol. 9, no. 1, 115 pages, 2021.

[34] A. M. Boukerb, C. Noël, E. Quenot et al., "Comparative analysis of fecal microbiomes from wild waterbirds to poultry, cattle, pigs, and wastewater treatment plants for a microbial source tracking approach," *Frontiers in Microbiology*, vol. 12, Article ID 697553, 2021.

[35] Q. Wang, G. M. Garrity, J. M. Tiedje, and J. R. Cole, "Naïve bayesian classifier for rapid assignment of rRNA sequences into the new bacterial taxonomy," *Applied and Environmental Microbiology*, vol. 73, no. 16, pp. 5261–5267, 2007.

[36] T. Teav, H. Gallart-Ayala, V. Van der Velpen, F. Mehl, H. Henry, and J. Ivanisevic, "Merged targeted quantification and untargeted profiling for comprehensive assessment of acylcarnitine and amino acid metabolism," *Analytical Chemistry*, vol. 91, no. 18, pp. 11757–11769, 2019.

[37] L. Zhang, W. Zheng, X. Li et al., "A merged method for targeted analysis of amino acids and derivatives using parallel reaction monitoring combined with untargeted profiling by HILIC-Q-Orbitrap HRMS," *Journal of Pharmaceutical and Biomedical Analysis*, vol. 203, Article ID 114208, 2021.

[38] D. Wang, S. Guo, H. He, L. Gong, and H. Cui, "Gut microbiome and serum metabolome analyses identify unsaturated fatty acids and butanoate metabolism induced by gut microbiota in patients with chronic spontaneous urticaria," *Frontiers in Cellular and Infection Microbiology*, vol. 10, p. 24, 2020.

[39] Y. Minamoto, C. C. Otoni, S. M. Steelman et al., "Alteration of the fecal microbiota and serum metabolite profiles in dogs with idiopathic inflammatory bowel disease," *Gut Microbes*, vol. 6, no. 1, pp. 33–47, 2015.

[40] H. J. Flint and S. H. Duncan, "Bacteroides and prevotella," in *Encyclopedia of Food Microbiology, (Second Edition)*, C. A. Batt and M. L. Tortorello, Eds., Oxford: Academic Press, Oxford, UK, pp. 203–208, 2014.

[41] M. Waluga, "Biomarkers of irritable bowel syndrome," in *A Comprehensive Overview of Irritable Bowel Syndrome*, J. Fichna, Ed., Academic Press, Cambridge, UK, pp. 107–127, 2020.

[42] E. N. Bermingham, P. Maclean, D. G. Thomas, N. J. Cave, and W. Young, "Key bacterial families (Clostridiaceae, Erysipelotrichaceae and Bacteroidaceae) are related to the digestion of protein and energy in dogs," *Peer Journal*, vol. 5, Article ID e3019, 2017.

[43] T. Feng, H. Ding, J. Wang, W. Xu, Y. Liu, and Á. Kenéz, "Alterations of serum metabolites and fecal microbiota involved in Ewe follicular cyst," *Frontiers in Microbiology*, vol. 12, Article ID 675480, 2021.

[44] T. Tullis, B. Alber, L. Zhao et al., "Machine learning algorithms identify clinical subtypes and cancer in Anti-TIF1-gamma+ myositis: a longitudinal study of 87 patients," *Frontiers in Immunology*, vol. 13, p. 802499, 2022.

[45] G. Liang, J. Yang, T. Liu et al., "A multi-strategy platform for quality control and Q-markers screen of Chaiqin chengqi decoction," *Phytomedicine*, vol. 85, Article ID 153525, 2021.

[46] J. A. Kellum, P. Romagnani, G. Ashuntantang, C. Ronco, A. Zarbock, and H.-J. Anders, "Acute kidney injury," *Nature Reviews Disease Primers*, vol. 7, no. 1, p. 52, 2021.

[47] Q. Zhang, C. Zhao, L. Zhang et al., "Escin sodium improves the prognosis of acute pancreatitis via promoting cell apoptosis by suppression of the ERK/STAT3 signaling pathway," *Oxidative Medicine and Cellular Longevity*, vol. 2021, Article ID 9921839, 20 pages, 2021.

[48] Z. Zhou, Y. Chen, W. Dong, R. An, K. Liang, and X. Wang, "Da cheng qi decoction alleviates cerulein-stimulated AR42J pancreatic acinar cell injury via the JAK2/STAT3 signaling pathway," *Evidence-Based Complementary and Alternative Medicine: eCAM*, vol. 2021, Article ID 6657036, 12 pages, 2021.

[49] P. A. Banks, T. L. Bollen, C. Dervenis et al., "Classification of acute pancreatitis-2012: revision of the Atlanta classification and definitions by international consensus," *Gut*, vol. 62, no. 1, pp. 102–111, 2013.

[50] E. Razmpoosh, S. Safi, N. Abdollahi et al., "The effect of Nigella sativa on the measures of liver and kidney parameters:

a systematic review and meta-analysis of randomized-controlled trials," *Pharmacological Research*, vol. 156, Article ID 104767, 2020.

[51] J. Wajda, P. Dumnicka, M. Maraj, P. Ceranowicz, M. Kuźniewski, and B. Kuśnierz-Cabala, "Potential prognostic markers of acute kidney injury in the early phase of acute pancreatitis," *International Journal of Molecular Sciences*, vol. 20, no. 15, p. 3714, 2019.

[52] J. Wajda, P. Dumnicka, W. Kolber et al., "The marker of tubular injury, kidney injury molecule-1 (KIM-1), in acute kidney injury complicating acute pancreatitis: a preliminary study," *Journal of Clinical Medicine*, vol. 9, no. 5, p. 1463, 2020.

[53] S. Y. Chang, R. Q. Sun, M. Feng, Y. X. Li, H. L. Wang, and Y. M. Xu, "BML-111 inhibits the inflammatory response and apoptosis of renal tissue in rats with hemorrhagic shock by inhibiting the MAPK pathway," *European Review for Medical and Pharmacological Sciences*, vol. 22, no. 11, pp. 3439–3447, 2018.

[54] Q.-x. Mei, J.-h. Hu, Z.-h. Huang et al., "Pretreatment with chitosan oligosaccharides attenuate experimental severe acute pancreatitis via inhibiting oxidative stress and modulating intestinal homeostasis," *Acta Pharmacologica Sinica*, vol. 42, no. 6, pp. 942–953, 2021.

[55] X. Hu, H. Li, X. Zhao et al., "Multi-omics study reveals that statin therapy is associated with restoration of gut microbiota homeostasis and improvement in outcomes in patients with acute coronary syndrome," *Theranostics*, vol. 11, no. 12, pp. 5778–5793, 2021.

[56] K. E. Bach Knudsen, M. L. Hartvigsen, M. S. Hedemann, and K. Hermansen, "Mechanisms whereby whole grain cereals modulate the prevention of type 2 diabetes," in *Molecular Nutrition and Diabetes*, D. Mauricio, Ed., Academic Press, San Diego, pp. 87–103, 2016.

[57] Y. Zhu, Q. Mei, Y. Fu, and Y. Zeng, "Alteration of gut microbiota in acute pancreatitis and associated therapeutic strategies," *Biomedicine & Pharmacotherapy*, vol. 141, Article ID 111850, 2021.

[58] D. Parada Venegas, M. K. De la Fuente, G. Landskron et al., "Short chain fatty acids (SCFAs)-Mediated gut epithelial and immune regulation and its relevance for inflammatory bowel diseases," *Frontiers in Immunology*, vol. 10, p. 277, 2019.

[59] X. Pan, X. Fang, F. Wang et al., "Butyrate ameliorates caerulein-induced acute pancreatitis and associated intestinal injury by tissue-specific mechanisms," *British Journal of Pharmacology*, vol. 176, no. 23, pp. 4446–4461, 2019.

[60] T. Zhang, M. Xia, Q. Zhan, Q. Zhou, G. Lu, and F. An, "Sodium butyrate reduces organ injuries in mice with severe acute pancreatitis through inhibiting HMGB1 expression," *Digestive Diseases and Sciences*, vol. 60, no. 7, pp. 1991–1999, 2015.

[61] J. P. Carlier, G. K'Ouas, and X. Y. Han, "Moryella indoligenes gen. nov., sp. nov., an anaerobic bacterium isolated from clinical specimens," *International Journal of Systematic and Evolutionary Microbiology*, vol. 57, no. Pt 4, pp. 725–729, 2007.

[62] D. B. Lindsay, "Amino acids as energy sources," *Proceedings of the Nutrition Society*, vol. 39, no. 1, pp. 53–59, 1980.

[63] M. Bhatia, "Acute pancreatitis as a model of SIRS," *Frontiers in Bioscience*, vol. 14, pp. 2042–2050, 2019.

[64] I. F. Btaiche, R. A. Mohammad, C. Alaniz, and B. A. Mueller, "Amino Acid requirements in critically ill patients with acute kidney injury treated with continuous renal replacement therapy," *Pharmacotherapy: The Journal of Human Pharmacology and Drug Therapy*, vol. 28, no. 5, pp. 600–613, 2008.

[65] M. Arutla, M. Raghunath, G. Deepika et al., "Efficacy of enteral glutamine supplementation in patients with severe and predicted severe acute pancreatitis- A randomized controlled trial," *Indian Journal of Gastroenterology*, vol. 38, no. 4, pp. 338–347, 2019.

[66] P. Takis, A. Taddei, R. Pini et al., "Fingerprinting acute digestive diseases by untargeted NMR based metabolomics," *International Journal of Molecular Sciences*, vol. 19, no. 11, p. 3288, 2018.

[67] R. W. McGarrah, S. B. Crown, G.-F. Zhang, S. H. Shah, and C. B. Newgard, "Cardiovascular metabolomics," *Circulation Research*, vol. 122, no. 9, pp. 1238–1258, 2018.

[68] T. Wu, F. Xu, C. Su et al., "Alterations in the gut microbiome and cecal metabolome during Klebsiella pneumoniae-induced pneumosepsis," *Frontiers in Immunology*, vol. 11, p. 1331, 2020.

Hindawi
Evidence-Based Complementary and Alternative Medicine
Volume 2022, Article ID 3166416, 17 pages
https://doi.org/10.1155/2022/3166416

Research Article

Chinese Herb Injections in the Adjuvant Treatment for Ulcerative Colitis: A Network Meta-Analysis of Randomized Controlled Trials

Ziyang Zhou,[1] Hao Chen,[1] Yingkai Shen,[1] and Hailiang Huang[2]

[1]*College of Traditional Chinese Medicine, Shandong University of Traditional Chinese Medicine, Jinan 250355, China*
[2]*College of Rehabilitation Medicine, Shandong University of Traditional Chinese Medicine, Jinan 250355, China*

Correspondence should be addressed to Hailiang Huang; 06000031@sdutcm.edu.cn

Received 1 January 2022; Revised 21 March 2022; Accepted 3 April 2022; Published 22 April 2022

Academic Editor: Xiang Liu

Ulcerative colitis refers to an inflammatory disease lasting for a long time, which affects the colon. In China, injections of traditional Chinese herbs have been generally combined with traditional Western medicines such as mesalazine and sulfasalazine to treat ulcerative colitis. Nevertheless, the safety and efficacy exhibited by different CHIs for treating UC remains controversial. Therefore, a network meta-analysis method was employed in this study for the assessment of the effect and safety exhibited by CHI for treating UC. Seven English and Chinese databases were searched for relevant randomized controlled trials (RCTs) from the time of database creation to December 30, 2021. An assessment was conducted for the included RCTs' quality with the use of the Cochrane risk offset assessment device, and this study processed the data with the use of Review Manager 5.3 or Stata16.0 software. On the whole, 42 literature with data on 3668 patients were included. The overall response rate, inflammatory factors, recurrence rate, and adverse reactions were evaluated. In comparison with traditional Western medicines-based treatment, CHI integrated with traditional Western medicines presented an overall response rate ($P < 0.05$) and could better reduce the TNF-α ($P < 0.05$), IL-6($P < 0.05$), and IL-8 level rate ($P < 0.05$) while better increasing the IL-10 level rate ($P < 0.05$). Besides, adverse reactions of CHI integrated with traditional Western medicine had a lower incidence ($P < 0.05$), and no significant distinction was identified in recurrence rate levels between the two interventions. CHI has some efficacy for treating UC. Xiangdan injection, Shenmai injection, Shengmai injection, and Danshen injection may be the most effective CHI. Nevertheless, more multicenter randomized controlled double-blind trials with great quality and large samples are required for research confirmation. Trial Registration: the registration was made for the protocol of this network meta-analysis in PROSPERO with ID CRD42021251429.

1. Introduction

Ulcerative colitis refers to an idiopathic disease-causing inflammation that lasts for a long time and impacts the colon. Adults with the age from 30 to 40 years most suffer from ulcerative colitis, which causes their disability [1, 2]. Epidemiological data demonstrate that ulcerative colitis does not show sex predominance [3–5]. The onset of ulcerative colitis happens most significantly between the ages of 30 and 40 years. [4, 6]. Ulcerative colitis has rising incidence and prevalence over time in the globe [7]. Most patients with ulcerative colitis receive treatment by using pharmacological therapy for initially inducing remission and subsequently maintaining corticosteroid-free remission. In terms of mild-to-moderate UC, oral and rectal 5-aminosalycilates have been extensively applied. In accordance with moderate-to-severe colitis, medication types comprise the Janus kinase inhibitor with small molecules, biological agents that target tumor necrosis factor and integrin, and thiopurine [8]. Nevertheless, many traditional drugs for treating UC produce adverse reactions or complications while exerting efficacy. For instance, mesalamine can effectively induce and keep remission [9]. On the other hand, this drug has more severe adverse reactions. Representative negative influence exerted by mesalamine cover paradoxical reaction worsening diarrhea and drug-induced interstitial nephritis with 0.2% risk [10]. Though corticosteroids can effectively induce remission, they have correlations to many complications, many of which are often irreversible [11, 12]. Therefore, it is urgent to discover a treatment for UC with good safety and efficacy.

For treating UC, the main advantage of traditional Chinese medicine is that it can maintain remission for a long time and reduce the recurrence rate [13]. Chinese herbal injection (CHI) refers to a type of novel preparation exhibiting great biological availability and great curative influence [14]. It is an innovative application of dosage, combining traditional Chinese medicine theory with modern scientific technology. At present, CHI integrated with traditional Western medicine is extensively employed to clinically treat UC and has achieved good efficacy. Samuel Wei et al. [15] carried out the meta-analysis for the safety and effect exhibited by Danshen injection integrated to sulfasalazine or mesalazine for treating UC. The results reflected that Danshen injection could significantly improve the clinical effective rate of UC and reduce the recurrence rate compared with Western medicine. Moreover, it can better improve coagulation function, control the inflammatory response, and down-regulate TNF-α, IL-8, and IL-6 serum levels in patients. The clinical observation of Liang Xuan [16] revealed that Shengmai injection integrated with mesalazine, compared with mesalazine alone, was more effective and could better reduce the scores of abdominal pain, diarrhea, bloody stools, and tenesmus. Zhu Bingxi [17] discovered that Danshen injection had a protective effect on the mucosa of ulcerative colitis triggered by acetic acid within rats, and the mechanism may be achieved by up-regulating superoxide dismutase (SOD) and downregulating the biological level of malondialdehyde (MDA), indicating that Danshen injection can help scavenge oxygen free radicals. Although various CHIs have acceptable efficacy for treating UC, the effects and safety exhibited by a single CHI integrated to traditional drugs for treating UC were only reported in currently published literature. To date, no meta-analysis comparing different CHIs in combination with traditional drugs for treating UC has been published. Therefore, this paper has an aim at drawing an indirect comparison of the effects and safety exhibited by various CHIs integrated with traditional drugs for treating UC with a network meta-analysis method to lay a more solid basis for clinically treating UC.

We present the following article in accordance with the checklist of the PRISMA extension for network meta-analysis.

2. Materials and Methods

2.1. Eligibility Standards

2.1.1. Inclusion Standards

(1) Study type. It was a randomized controlled trial of CHI integrated with traditional Western medicine for treating UC. Publication languages were limited to Chinese and English.

(2) Study subjects. For patients definitely diagnosed with ulcerative colitis, the diagnostic standards indicate the Consensus Opinions on the Diagnosis and Treatment of Inflammatory Bowel Disease issued by the Chinese Medical Association in 2018 [18] without limiting their nationality, age, gender, ethnicity, and course of the disease.

(3) Intervention measures. The control received the treatment by using traditional western medicine. The experimental group received the treatment by using CHI or CHI integrated with traditional western medicine. All the covered literature should report any one of the primary or secondary outcome indicators. The primary outcome indicator was the overall response rate. The secondary outcome indicators were as follows: inflammatory factors, recurrence rate, and incidence of adverse reactions.

2.1.2. Exclusion Standards

(1) The treatment group is CHI integrated with other treatment methods other than traditional Western medicine

(2) Repeated publication of literature

(3) Unable to extract data or missing data of literature conference literature

(4) Non-RCT literature, such as network meta-analysis, meta-analysis, systematic reviews, reviews, theoretical literature, famous medical practices, animal experiments, case-control literature, and cohort literature

2.2. Types of Outcome Measures. In this study, primary and secondary outcome indicators were identified under the guidance of this strategy, based on four versions [18–21] of domestic and international clinical guidelines and expert consensus on ulcerative colitis, combined with the frequency of outcome indicators in the articles.

The main outcome measures were as follows: (1) the overall response rate, which refers to the Chinese Medical Association 2018 Consensus Opinions on the Diagnosis and Treatment of Inflammatory Bowel Disease [18]. The main reference standards included the following: (1) significantly effective: the clinical symptom disappeared, and colonoscopy suggested the mucosa to be approximately normal or no active inflammation; (2) effective: the clinical symptoms basically disappeared, and colonoscopy demonstrated mild mucosal inflammation; and (3) ineffective: rare enhancement in clinical symptom or colonoscopy reexamination. Overall response rate = (number of significantly effective cases + number of effective cases)/(total number of cases) × 100%. The secondary outcome measures were as follows: (2) inflammatory factor (interleukin-10 (IL-10), interleukin-8 (IL-8), interleukin-6 (IL-6), and tumor necrosis factor-α (TNF-α)); (3) recurrence rate; and (4) incidence of adverse reactions.

2.3. Search Strategies. Computerized searches were performed on the databases of CNKI, WAN FANG DATA, VIP, CBM, the Cochrane Library, Embase, PubMed, and Web of Science to obtain published randomized controlled trials (RCTs) of CHI in Ulcerative Colitis (UC) from its inception to December 30, 2021.

A search strategy of subject headings plus free words was used.

Supplementary Table 1 lists the search strategy for the respective database.

2.4. Literature Screening and Data Extraction. Relevant literature was searched, and bibliographies were exported in accordance with the search strategy. Endnote X9 software was used to eliminate repeated literature and literature inconsistent with the inclusion standards. The full text of the literature that might meet the inclusion standards was downloaded for determining if it complied with the inclusion standards.

Two authors (Ziyang Zhou and Hao Chen) independently screened, extracted, and cross-checked the literature in accordance with the including and excluding standards. Disagreement was addressed through a discussion with a third investigator (Yingkai Shen).

The data extraction standards included the following: first author, publication time, sample size, gender ratio, mean age, mean disease duration, the number of cases, intervention measures in the test group, intervention measures in the control, course of treatment, outcome measures, and adverse reactions.

2.5. Bias Risk Assessment. By complying with the risk of bias tool (Risk of Bias) in Review Manager 5.3 software, two evaluators (Ziyang Zhou and Hao Chen) independently performed a quality assessment for each study from seven perspectives: the blind method for subjects and participants, allocation concealment, random sequence generation, the blind method for result assessment, selective report, incomplete result data, and other deviations. The literature quality was evaluated at three levels, namely, "unclear" (lack of relevant information or uncertain bias), "high" (high bias), and "low" (low bias). Disagreements were resolved by discussing them with a third investigator (Yingkai Shen). The visualization was conducted for risk bias assessment results of the covered literature using Review Manager 5.3 software.

2.6. Statistical Investigation. This study employed Review Manager 5.3 software for traditional meta-analysis and literature quality assessment. The odds ratio (OR) and 95% CI acted as effect size indicators for dichotomous variables (overall response rate, recurrence rate, and incidence of adverse reactions). Mean difference (MD) and 95% CI were regarded as effect size indicators for continuous variables (inflammatory factors). All the included literature in this study involved pairwise comparisons, without forming a closed loop. The heterogeneity test was mainly determined by I^2. If there was no heterogeneity between the study results ($I^2 \leq 50\%$), this study employed the fixed-effect model in terms of meta-analysis. If there was heterogeneity among the study results ($I^2 > 50\%$), the heterogeneity source was further analyzed. After the exclusion of effects exerted by significant clinical heterogeneity, the random-effects model was employed for the meta-analysis. Under a frequency-based random-effects model, STATA16.0 software was adopted for performing a network meta-analysis, in which the study outcome measures were network-analyzed by group commands. Besides, data processing, network evidence plots, funnel plots, forest plots, and ranking of the area under the curve (SUCRA) were completed in turn. The overall ranking of treatments was estimated by calculating the area under the cumulative ranking probability plot (SUCRA) for each method. Moreover, the advantages and disadvantages of the interventions were ranked in accordance with the size of SUCRA. SUCRA = 1 indicated that the interventions were absolutely effective, while SUCRA = 0 suggested that the interventions were absolutely ineffective. The publication bias of the involved literature was evaluated with a funnel plot.

3. Results

3.1. Literature Search and Screening. There were 961 articles initially searched. After the layer-by-layer screening, 42 articles were finally included. The screening of literature is illustrated in Figure 1.

3.2. Basic Characteristics of Involved Literature. On the whole, 42 pieces of literature [19, 21–61] which included 3668 patients. Supplementary Material Table 2 gives the basic information of the involved literature.

3.3. Bias Risk Assessment of Involved Literature. Regarding random sequence generation, seven pieces of literature employed a random number table for random allocation. One study used the single and double number method for randomization, one study applied randomization in accordance with the date of admission, and two literature studies did not mention randomization. Additionally, no specific method of randomization was reported in the remaining 31 pieces of literature. Concerning randomization concealment, none of the literature mentioned the use of any allocation concealment method, nor the use of the blind method about blinding of the subjects to interventionalists. In terms of blinding the evaluators of the results, one study used a double-blind of pathological findings, while the use of the blind method for the evaluators of the results was not presented in the remaining 41 pieces of literature. For incomplete result data, four pieces of literature had dropout/withdrawal cases, which may affect the true results. Particularly, there was no missing outcome data for the remaining 38 pieces of literature. All literature reported all prespecified outcome measures given selective reporting.

None of the literature reported other sources of bias. The risk of bias assessment of the involved literature is illustrated in Figure 2.

3.4. Outcome Indicators

3.4.1. Total Effectiveness Rate

(1) Evidence Network. Thirty-seven pieces of literature reported overall response rates involving 17 CHI treatment

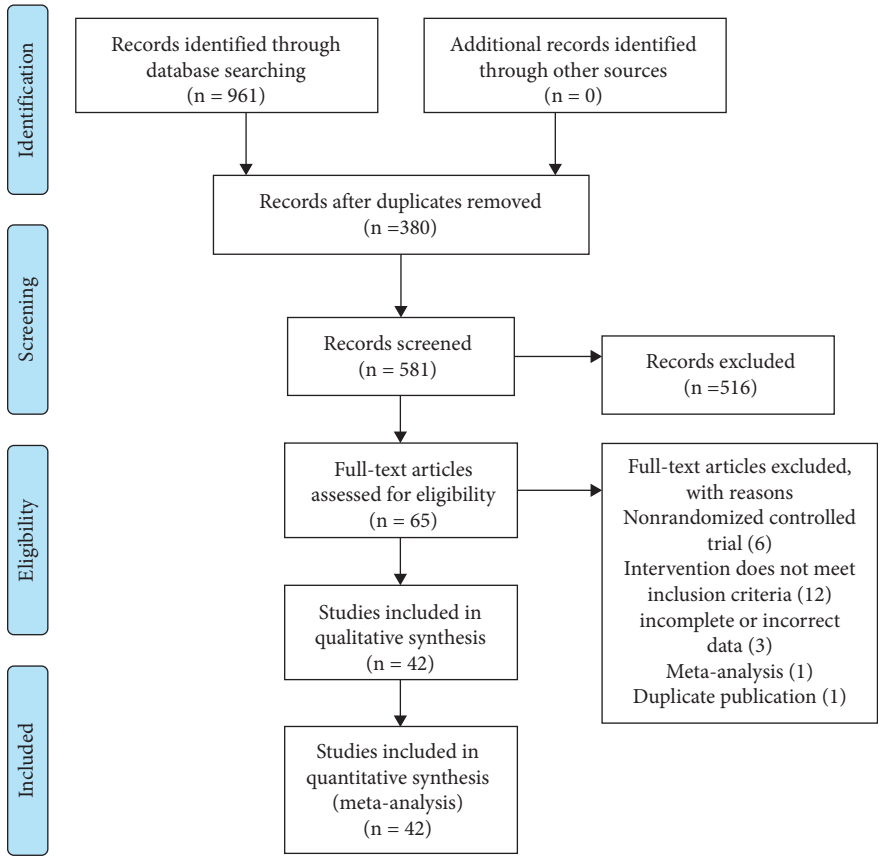

Figure 1: The process of literature filtering.

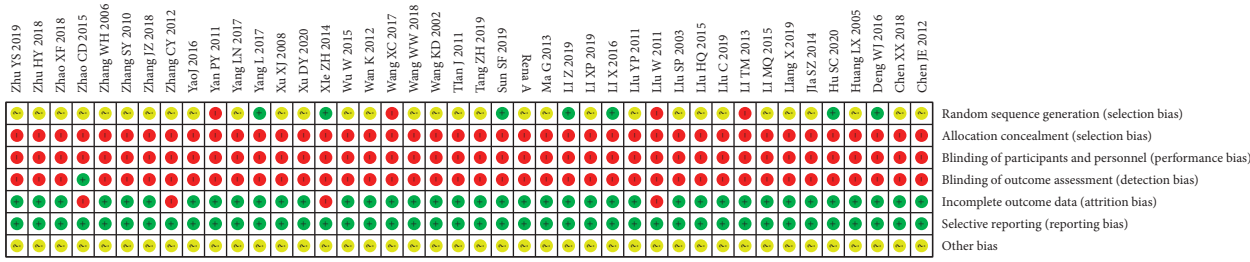

Figure 2: Risk of bias for all RCTs included in this study.

regimens. The dot size indicates the sample size using the intervention, the line thickness represents the number of RCTs using the two-point treatment intervention, all 17 CHIs denote direct comparisons, and there is no closed-loop formation. The network evidence of the overall response rate is exhibited in Figure 3.

(2) Publication Bias. The funnel plot of this study revealed that most of the scatter points were located on both sides of the vertical line. They were basically symmetrical and may have had a certain degree of publication bias. The funnel plot of the overall response rate of 17 CHIs integrated with traditional Western medicine for treating UC is presented in Figure 4.

(3) Network Meta-analysis. Thirty-seven pieces of literature reported overall response rates involving 17 CHIs. Network comparison was conducted in 17 CHIs, yielding a total of 136 pairwise comparisons, nine of which were statistically significant. Compared with traditional Western medicine, OR and 95% CI of traditional west medicine integrated with Xiangdan injection, traditional Western medicine integrated with Shengmai injection, traditional Western medicine integrated with Danshen injection, traditional Western medicine integrated with Danshen powder injection, traditional Western medicine integrated with Xuesaitong powder injection, traditional Western medicine integrated with Shuxuening injection, and traditional Western medicine integrated with *Astragalus* injection were 12.25 and [1.50, 99.80], 4.91 and [1.74, 13.85], 4.24 and [2.81, 6.40],3.65 and [2.09, 6.37], 3.47 and [1.13, 10.68], 3.41 and [1.72, 6.76], and 3.16 and [1.65, 6.06], respectively. The specific results are shown in Figure 5.

(4) SUCRA Probability Ranking. In accordance with the area under the curve diagram of SUCRA (Figure 6), the overall response rates of 17 CHI and traditional west medicine were ranked probabilistically from high to low as follows: C + XD

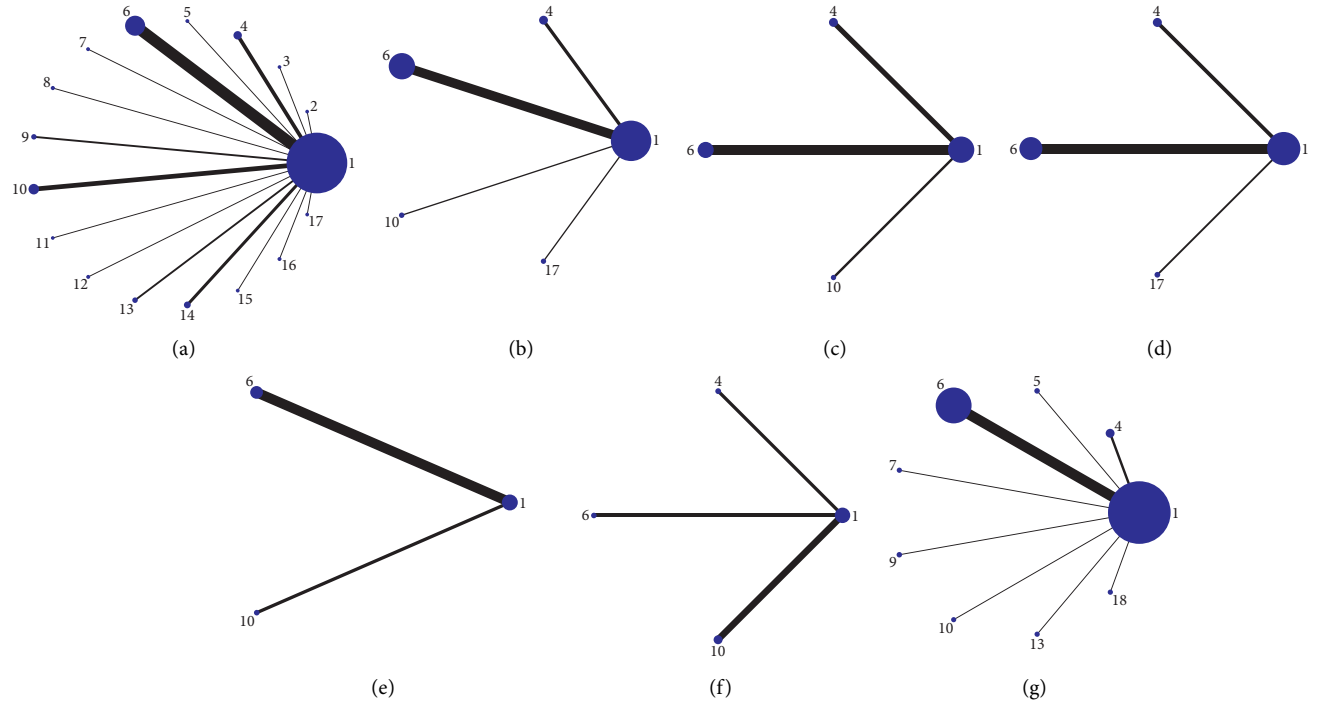

Figure 3: Network diagrams of outcome indicators. (a) Overall response rate; (b)TNF-α; (c)IL-6; (d)IL-8; (e)IL-10; (f) recurrence rate; (g) adverse reaction rate. 1: Conventional western medicine, 2: conventional Western medicine + Shenfu injection, 3: conventional Western medicine + Shenqi Fuzheng injection, 4: conventional Western medicine + Danshen powder injection, 5: conventional Western medicine + compound Danshen injection, 6: conventional Western medicine + Danshen injection, 7: conventional Western medicine + compound Kushen injection, 8: conventional Western medicine + Guanxinning injection, 9: conventional Western medicine + Safflower injection, 10: conventional Western medicine + *Astragalus* injection, 11: conventional Western medicine + Shenmai injection, 12: conventional Western medicine + Acanthopanax injection, 13: conventional Western medicine + Shengmai injection, 14: conventional Western medicine + Shuxuening injection, 15: conventional Western medicine + Xiangdan injection, 16: conventional Western medicine + Xuesaitong powder injection, 17: conventional Western medicine + Houttuynia injection, and 18: conventional Western medicine + Angelica injection.

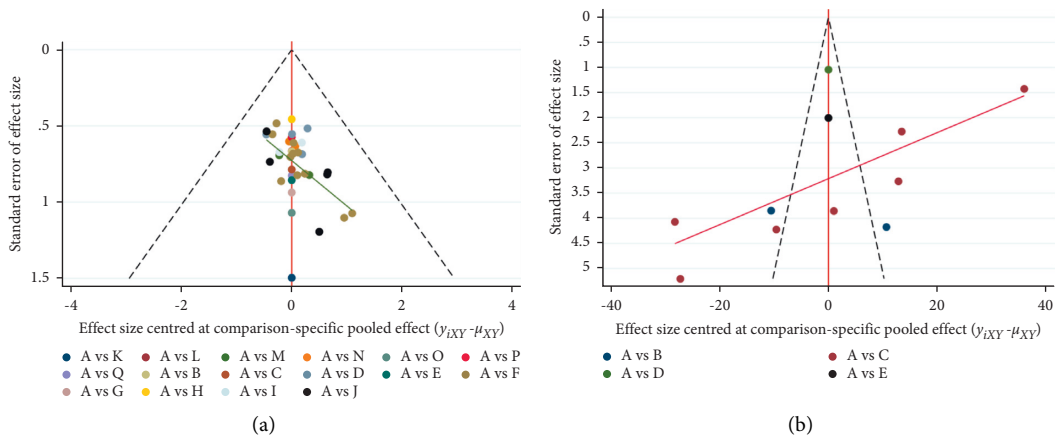

Figure 4: Continued.

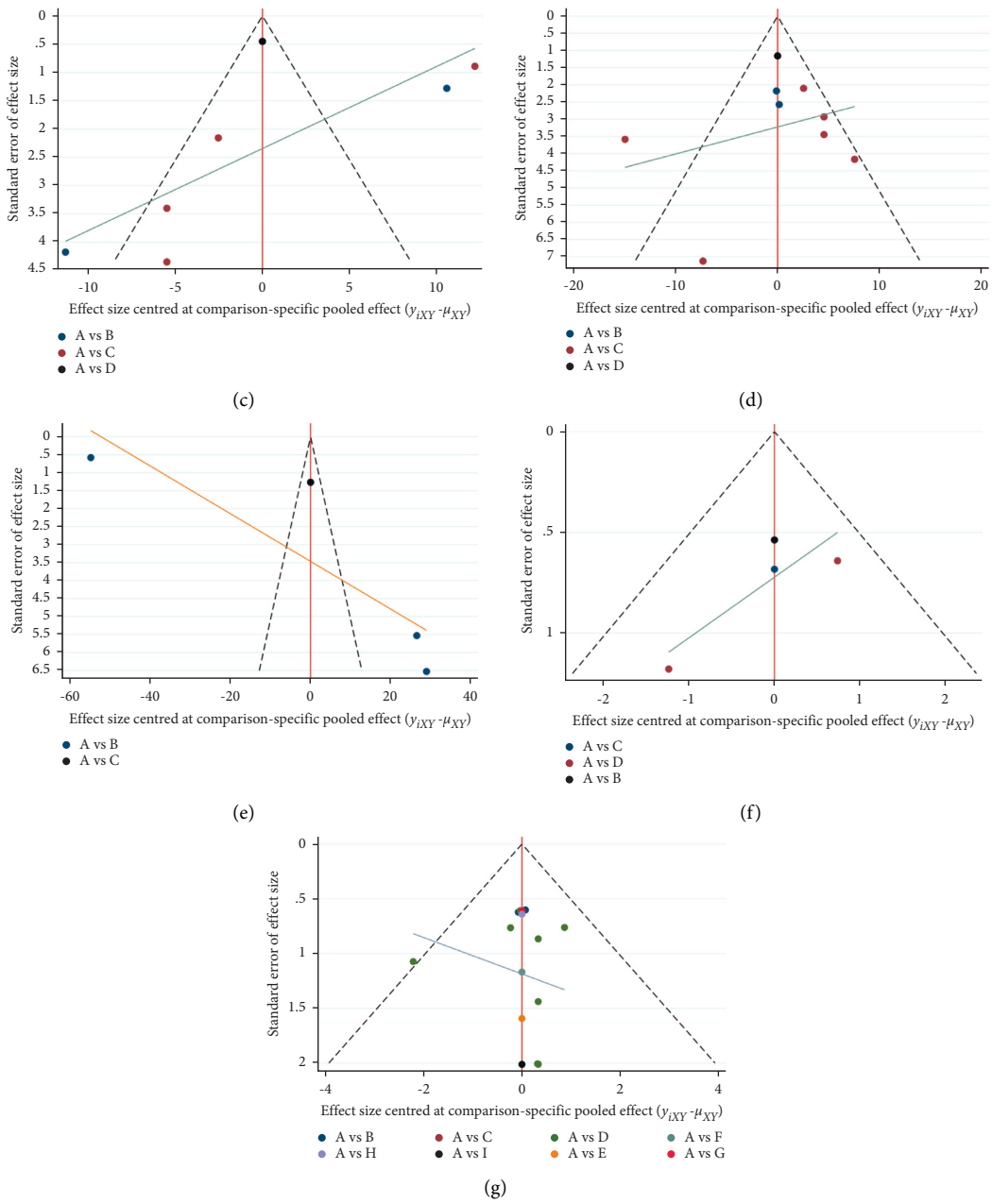

Figure 4: Funnel plot of outcome indicators. (a) Overall response rate; (b) TNF-α; (c) IL-6; (d) IL-8; (e) IL-10; (f) recurrence rate; (g) adverse reaction rate. A : Conventional Western medicine, B : conventional Western medicine + Shenfu injection, C : conventional Western medicine + Shenqi Fuzheng injection, D : conventional Western medicine + Danshen powder injection, E : conventional Western medicine + compound Danshen injection, F : conventional Western medicine + Danshen injection, G : conventional Western medicine + compound Kushen injection, H:conventional Western medicine + Guanxinning injection, I : conventional Western medicine + Safflower injection, J : conventional Western medicine + *Astragalus* injection, K : conventional Western medicine + Shenmai injection, L : conventional Western medicine + Acanthopanax injection, M : conventional Western medicine + Shengmai injection, N : conventional Western medicine + Shuxuening injection, O : conventional Western medicine + Xiangdan injection, P : conventional Western medicine + Xuesaitong powder injection, and Q : conventional Western medicine + Houttuynia injection.

(83.8%) > C + SM1 (78.8%) > C + SM2 (66.1%) > + C + DS (62.9%) > C + YXC (62.1%) > C + FFDS (58.7%) > C + FFKS (57.1%) > C + DSFZ (53.8%) > C + XSTF (50.9%) > C + SXN (50.0%) > C + HQ (46.0%) > C + HH (42.6%) > C + SF (42.6%) > C + GXN (40.0%) > C + SQFZ (34.6%) > C + CWJ (14.8%) > C (5.1%).

3.4.2. Inflammatory Factors

(1) Tumor necrosis Factor-Alpha (TNF-α) Evidence Network. 11 pieces of literature reported TNF-α, involving 4 CHI treatment regimens. The dot size indicates the sample size using the intervention, the line thickness represents the

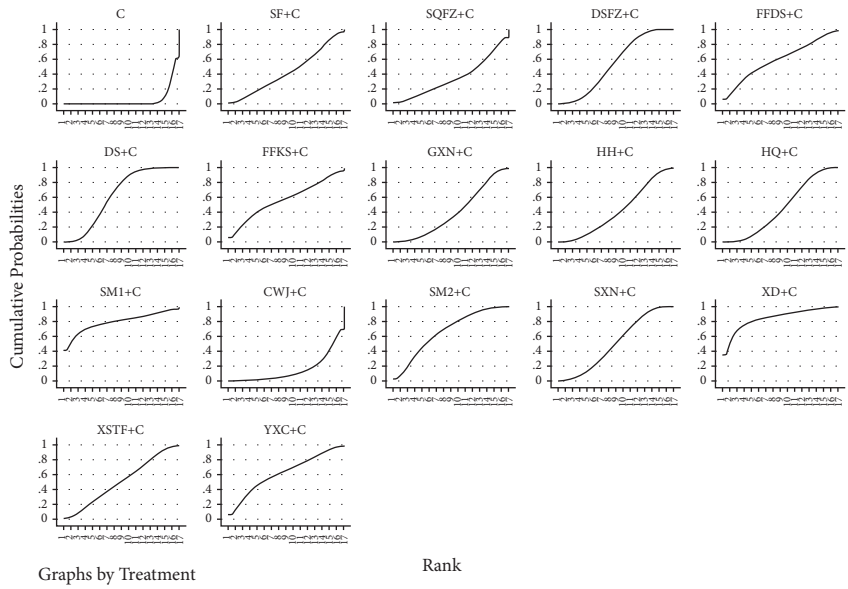

(a)

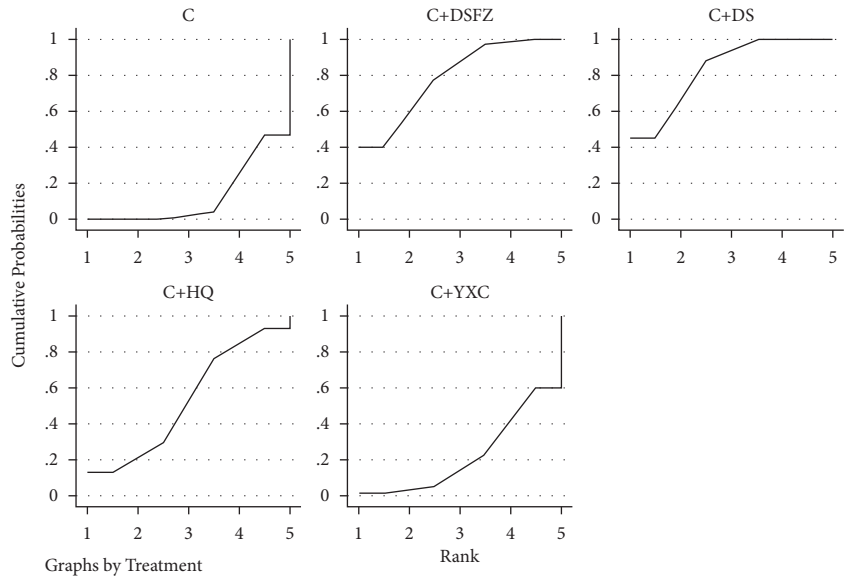

(b)

Figure 5: Continued.

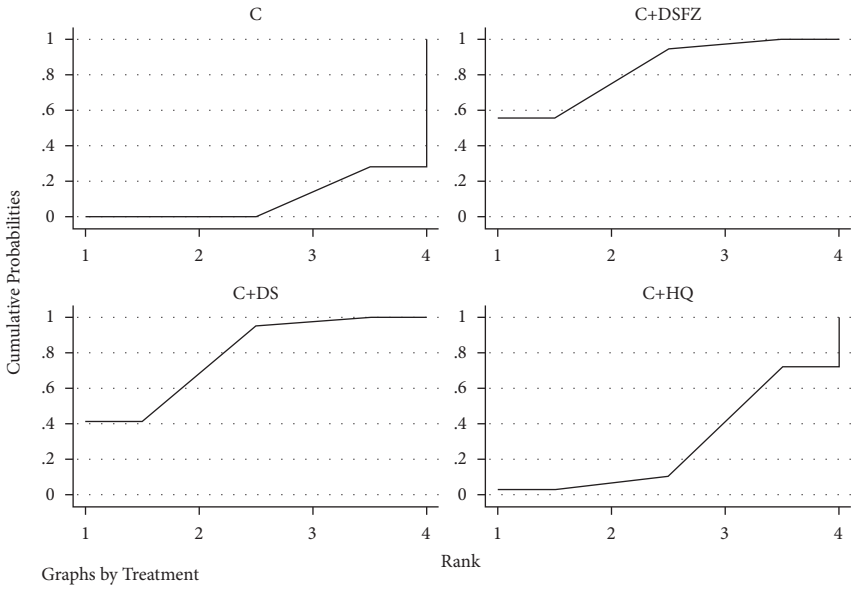

(c)

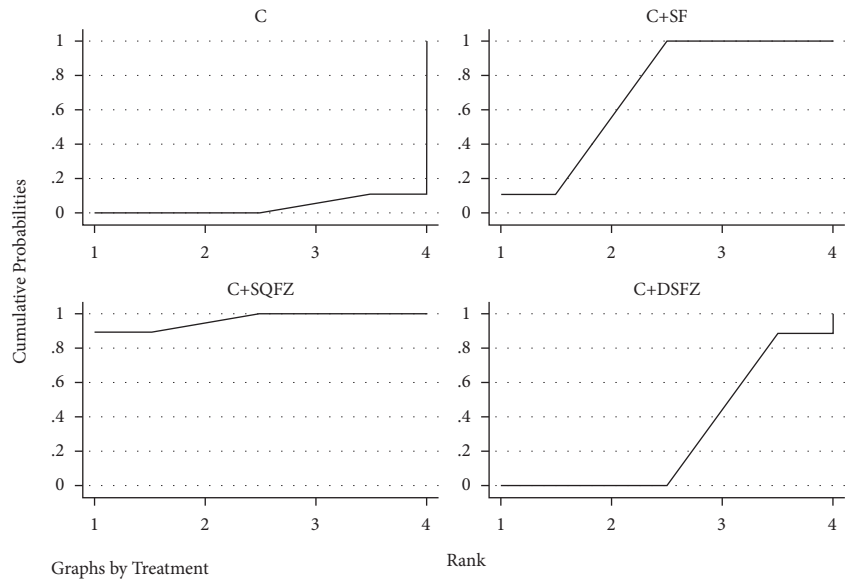

(d)

Figure 5: Continued.

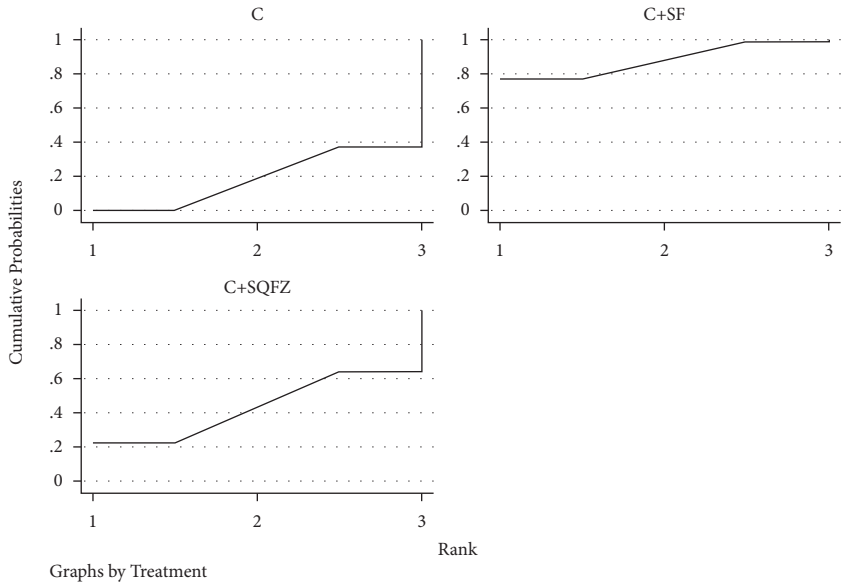

(e)

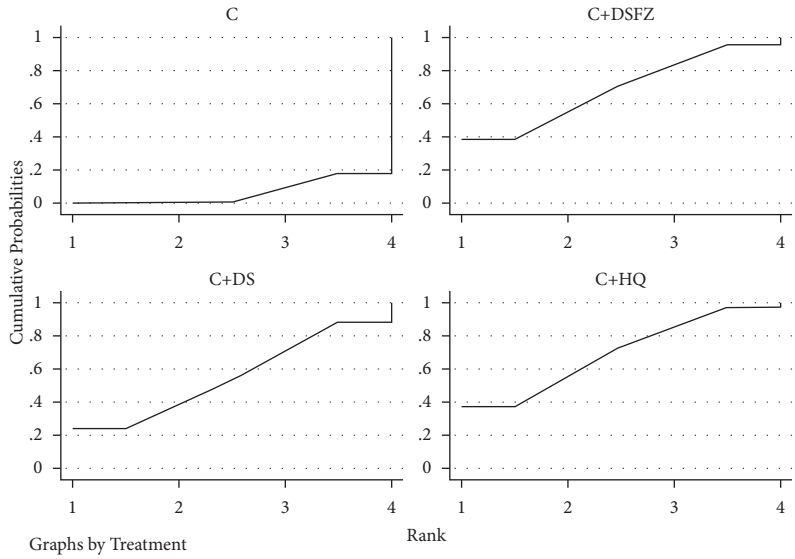

(f)

Figure 5: Continued.

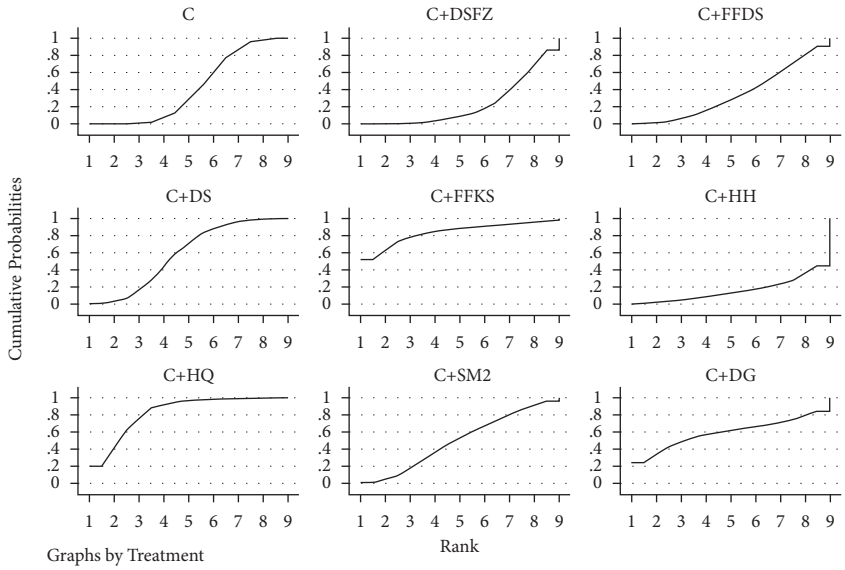

(g)

Figure 5: Curve diagram of SUCRA of outcome indicators. (a) Overall response rate; (b) TNF-α; (c) IL-6; (d) IL-8; (e) IL-10; (f) recurrence rate; (g) adverse reaction rate. C : Conventional Western medicine, SF:Shenfu injection, SQFZ: Shenqi Fuzheng injection, DSFZ: Danshen powder injection, FFDS: compound Danshen injection, DS: Danshen injection, FFKS: compound Kushen injection, GXN: Guanxinning injection, HH: Safflower injection, HQ: *Astragalus* injection, SM1 : Shenmai injection, CWJ: Acanthopanax injection, SM2 : Shengmai injection, SXN: Shuxuening injection, XD:Xiangdan injection, XSTF: Xuesaitong powder injection, YXC: Houttuynia injection, and DG: Angelica injection.

number of RCTs using the two-point treatment intervention, all 4 CHIs denote direct comparisons, and there is no closed-loop formation. The network evidence of the TNF-α is exhibited in Figure 3.

Publication Bias. The funnel plot of this study revealed that most of the scatter points were located on both sides of the vertical line. They were basically symmetrical and may have a certain degree of publication bias. The funnel plot of the TNF-α of 4 CHIs integrated with traditional Western medicine for treating UC is presented in Figure 4.

Network Meta-analysis. 11 pieces of literature reported TNF-α involving 4 CHIs. Network comparison was conducted in 4 CHIs, yielding a total of 20 pairwise comparisons, two of which were statistically significant. Compared with traditional Western medicine, MD and 95% CI of traditional Western medicine integrated with Danshen powder injection and traditional Western medicine integrated with Danshen injection, were −47.76 and [−78.83, −16.69] and −49.77 and [−66.34, −33.21], respectively. The specific results are shown in Figure 7(a).

SUCRA Probability Ranking. In accordance with the area under the curve diagram of SUCRA (Figure 5), the reduced TNF-α rate of 4 CHI and traditional west medicine were ranked probabilistically from high to low as follows: C + DS (83.2%) > C + DSFZ(78.8%) > C + HQ (53.1%) > C + YXC (22.4%) > C (12.7%).

3.4.3. Interleukin-6 (IL-6)

(1) Evidence Network. Thirty-seven pieces of literature reported IL-6, involving 3 CHI treatment regimens. The dot size indicates the sample size using the intervention, the line thickness represents the number of RCTs using the two-point treatment intervention, all 3 CHIs denote direct comparisons, and there is no closed-loop formation. The network evidence of the IL-6 is exhibited in Figure 3.

(2) Publication Bias. The funnel plot of this study revealed that most of the scatter points were located on both sides of the vertical line. They were basically symmetrical and may have a certain degree of publication bias. The funnel plot of the IL-6 of 3 CHIs integrated with traditional Western medicine for treating UC is presented in Figure 4.

(3) Network Meta-analysis. 7 pieces of literature reported IL-6, involving 3 CHIs. Network comparison was conducted in 3 CHIs, yielding a total of 12 pairwise comparisons, two of which were statistically significant. Compared with traditional west medicine, MD and 95% CI of traditional Western medicine integrated with Danshen powder injection and traditional west medicine integrated with Danshen injection, were−25.50 and [−40.54, −10.46] and −23.75 and [−34.35, −13.14], respectively. The specific results are shown in Figure 6.

(4) SUCRA Probability Ranking. In accordance with the area under the curve diagram of SUCRA (Figure 5), the reduced IL-6pa rate of 3 CHI and traditional west medicine were ranked probabilistically from high to low as follows: C + DSFZ (83.7%) > +C + DS (78.8%) > C + HQ (28.6%) > C (9.3%).

3.4.4. Interleukin-8 (IL-8) Evidence Network. 9 pieces of literature reported IL-8, involving 3 CHI treatment regimens. The dot size indicates the sample size using the

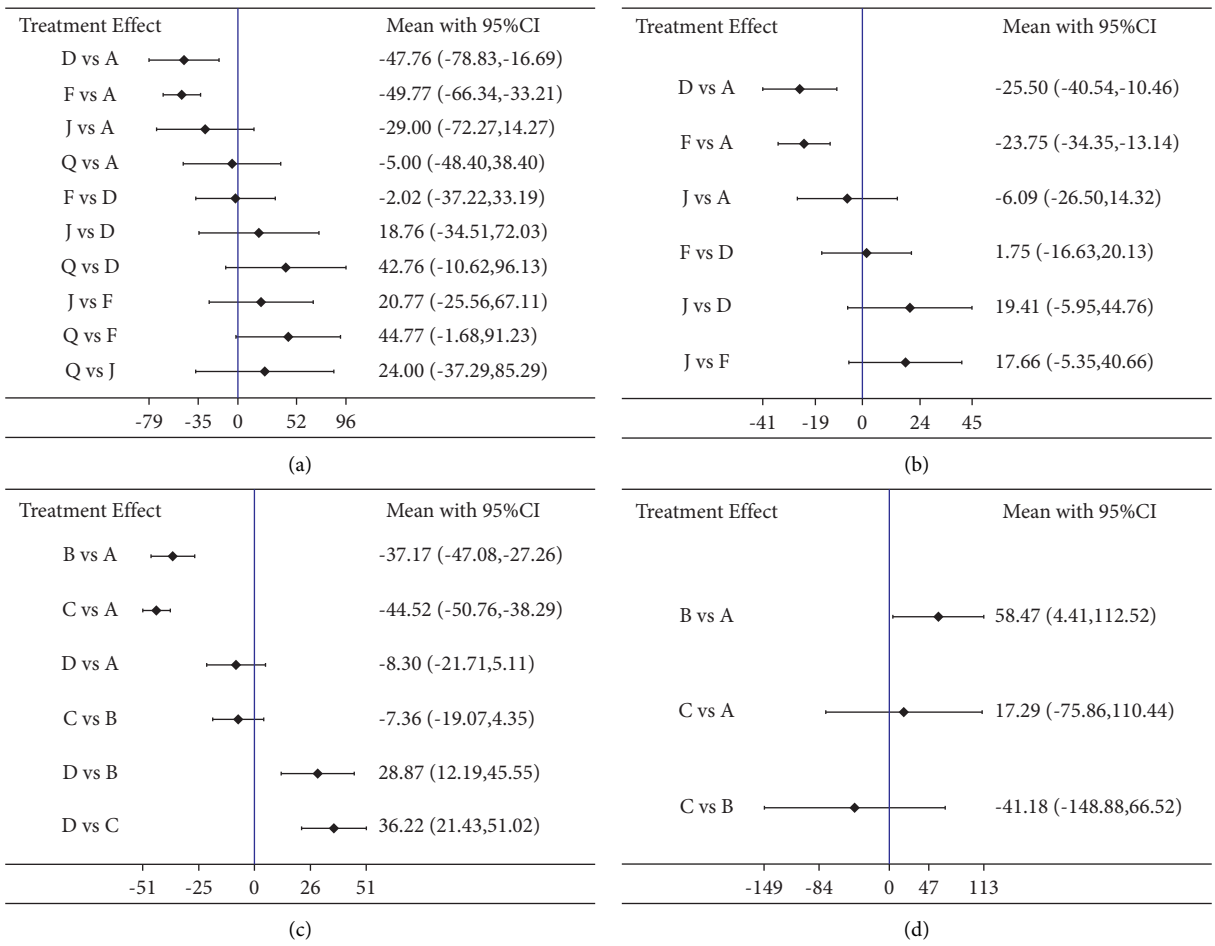

Figure 6: Pairwise comparison forest graph of outcome indicators. (a)TNF-α; (b) IL-6; (c) IL-8; (d) IL-10. A : Conventional Western medicine, B : conventional Western medicine + Shenfu injection, C : conventional Western medicine + Shenqi Fuzheng injection, D : conventional Western medicine + Danshen powder injection, E : conventional Western medicine + compound Danshen injection, F : conventional Western medicine + Danshen injection, G : conventional Western medicine + compound Kushen injection, H:conventional Western medicine + Guanxinning injection, I : conventional Western medicine + Safflower injection, J : conventional Western medicine + *Astragalus* injection, K : conventional Western medicine + Shenmai injection, L : conventional Western medicine + Acanthopanax injection, M : conventional Western medicine + Shengmai injection, N : conventional Western medicine + Shuxuening injection, O : conventional Western medicine + Xiangdan injection, P : conventional Western medicine + Xuesaitong powder injection, and Q : conventional Western medicine + Houttuynia injection.

intervention, the line thickness represents the number of RCTs using the two-point treatment intervention, all 3 CHIs denote direct comparisons, and there is no closed-loop formation. The network evidence of the IL-8 is exhibited in Figure 3.

(1) Publication Bias. The funnel plot of this study revealed that most of the scatter points were located on both sides of the vertical line. They were basically symmetrical and may have a certain degree of publication bias. The funnel plot of the IL-8 of 3 CHIs integrated with traditional west medicine for treating UC is presented in Figure 4.

(2) Network Meta-analysis. 9 pieces of literature reported IL-8, involving 3 CHIs. Network comparison was conducted in 3 CHIs, yielding a total of 12 pairwise comparisons, two of which were statistically significant. Compared with traditional Western medicine, MD and 95% CI of traditional Western medicine integrated with Shenfu injection and traditional west medicine integrated with Shenqi Fuzheng injection, were −37.17 and [−47.08, −27] and −44.52 and [−50.76, −38.29], respectively. The specific results are shown in Figure 6.

(3) SUCRA Probability Ranking. In accordance with the area under the curve diagram of SUCRA (Figure 5), the reduced IL-8 rate of 3 CHI and traditional Western medicine were ranked probabilistically from high to low as follows: C + SQFZ (96.3%) > C + SF (70.2%) > +C + DSFZ (29.5%) > C (3.8%).

3.4.5. Interleukin-10 (IL-10)

(1) Evidence Network. 4 pieces of literature reported IL-10, involving 2 CHI treatment regimens. The dot size indicates the sample size using the intervention, the line thickness represents the number of RCTs using the two-point treatment

C+XD															
0.97 (0.03,35.53)	C+SM1														
2.50 (0.24,25.93)	2.59 (0.12,58.07)	C+SM2													
2.89 (0.34,24.51)	2.99 (0.15,57.89)	1.16 (0.38,3.54)	C+DS												
2.58 (0.18,36.50)	2.67 (0.09,76.18)	1.03 (0.15,7.07)	0.89 (0.17,4.74)	C+YXC											
2.80 (0.19,41.09)	2.90 (0.10,85.12)	1.12 (0.16,8.07)	0.97 (0.17,5.45)	1.09 (0.11,11.18)	C+FFDS										
2.94 (0.18,47.76)	3.05 (0.10,96.95)	1.18 (0.14,9.71)	1.02 (0.15,6.68)	1.14 (0.10,13.19)	1.05 (0.09,12.63)	C+FFKS									
3.36 (0.38,29.42)	3.48 (0.18,68.87)	1.34 (0.41,4.37)	1.16 (0.58,2.32)	1.30 (0.23,7.22)	1.20 (0.20,7.03)	1.14 (0.17,7.78)	C+DSFZ								
3.53 (0.33,38.20)	3.66 (0.16,84.71)	1.42 (0.31,6.54)	1.22 (0.37,4.05)	1.37 (0.19,9.84)	1.26 (0.17,9.52)	1.20 (0.14,10.36)	1.05 (0.30,3.69)	C+XSTF							
3.59 (0.40,32.64)	3.72 (0.18,75.66)	1.44 (0.41,4.99)	1.24 (0.56,2.77)	1.39 (0.24,8.08)	1.28 (0.21,7.86)	1.22 (0.17,8.67)	1.07 (0.44,2.59)	1.02 (0.27,3.80)	C+SXN						
3.88 (0.43,34.87)	4.02 (0.20,81.05)	1.55 (0.46,5.29)	1.34 (0.62,2.90)	1.50 (0.26,8.61)	1.38 (0.23,8.38)	1.32 (0.19,9.26)	1.15 (0.49,2.72)	1.10 (0.30,4.03)	1.08 (0.42,2.78)	C+HQ					
4.20 (0.43,40.96)	4.35 (0.20,93.21)	1.68 (0.43,6.59)	1.45 (0.55,3.86)	1.63 (0.26,10.32)	1.50 (0.23,10.01)	1.43 (0.19,10.98)	1.25 (0.44,3.56)	1.19 (0.28,4.98)	1.17 (0.38,3.58)	1.08 (0.36,3.25)	C+HH				
4.32 (0.36,51.25)	4.48 (0.18,111.20)	1.73 (0.33,9.21)	1.50 (0.38,5.90)	1.68 (0.21,13.45)	1.54 (0.18,12.97)	1.47 (0.15,14.02)	1.29 (0.31,5.34)	1.22 (0.22,6.88)	1.20 (0.27,5.27)	1.11 (0.26,4.81)	1.03 (0.21,5.00)	C+SF			
4.46 (0.46,43.64)	4.62 (0.22,99.24)	1.79 (0.45,7.03)	1.54 (0.58,4.13)	1.73 (0.27,11.00)	1.59 (0.24,10.67)	1.52 (0.20,11.70)	1.33 (0.46,3.81)	1.26 (0.30,5.32)	1.24 (0.40,3.83)	1.15 (0.38,3.48)	1.06 (0.30,3.74)	1.03 (0.21,5.04)	C+GXN		
5.44 (0.40,73.50)	5.64 (0.21,154.95)	2.18 (0.34,13.98)	1.88 (0.38,9.29)	2.11 (0.23,19.74)	1.94 (0.20,18.97)	1.85 (0.17,20.35)	1.62 (0.31,8.35)	1.54 (0.23,10.38)	1.52 (0.28,8.18)	1.40 (0.26,7.48)	1.30 (0.22,7.66)	1.26 (0.17,9.51)	1.22 (0.21,7.24)	C+SQFZ	
9.83 (0.83,116.16)	10.19 (0.41,252.24)	3.94 (0.74,20.84)	3.40 (0.87,13.35)	3.81 (0.48,30.47)	3.51 (0.42,29.38)	3.34 (0.35,31.78)	2.93 (0.71,12.08)	2.78 (0.50,15.57)	2.74 (0.63,11.93)	2.53 (0.59,10.88)	2.34 (0.48,11.31)	2.27 (0.36,14.42)	2.20 (0.45,10.70)	1.81 (0.24,13.59)	C+CWJ
12.25 (1.50,99.80)	12.69 (0.68,238.39)	**4.91 (1.74,13.85)**	**4.24 (2.81,6.40)**	4.75 (0.94,23.98)	4.38 (0.82,23.42)	4.17 (0.66,26.14)	**3.65 (2.09,6.37)**	**3.47 (1.13,10.68)**	**3.41 (1.72,6.76)**	**3.16 (1.65,6.06)**	**2.91 (1.20,7.07)**	2.83 (0.77,10.49)	**2.74 (1.12,6.71)**	2.25 (0.48,10.50)	1.25 (0.34,4.59)	C

(a)

C+ HH			
1.00 (0.05,20.21)	C+ DSFZ		
0.63 (0.03,14.32)	0.63 (0.02,17.05)	C+ DS	
0.15 (0.02,1.07)	0.15 (0.02,1.39)	0.23 (0.02,2.54)	C

(b)

C+FFKS							
0.51 (0.02,14.55)	C+HQ						
0.30 (0.00,46.19)	0.59 (0.01,36.44)	C+DG					
0.20 (0.01,4.80)	0.39 (0.10,1.51)	0.66 (0.01,35.66)	C+DS				
0.18 (0.01,5.08)	0.34 (0.06,1.95)	0.58 (0.01,36.42)	0.88 (0.22,3.59)	C+SM2			
0.14 (0.01,3.24)	**0.28 (0.08,0.93)**	0.47 (0.01,24.40)	0.72 (0.38,1.34)	0.81 (0.23,2.87)	C		
0.12 (0.00,3.36)	0.23 (0.04,1.26)	0.39 (0.01,24.20)	0.60 (0.16,2.30)	0.68 (0.12,3.83)	0.83 (0.25,2.74)	C+FFDS	
0.09 (0.00,2.30)	0.18 (0.04,0.77)	0.30 (0.01,16.93)	0.46 (0.16,1.31)	0.52 (0.11,2.35)	0.63 (0.27,1.48)	0.76 (0.18,3.30)	C+DSFZ
0.05 (0.00,2.21)	0.09 (0.01,1.20)	0.15 (0.00,14.57)	0.23 (0.02,2.49)	0.26 (0.02,3.58)	0.32 (0.03,3.19)	0.39 (0.03,5.13)	0.51 (0.04,5.85)	C+HH

(c)

Figure 7: (a–c) Results from the NMA showing the effect of each of the interventions. (a) ORs with 95% CIs of the overall response rates. (b) ORs with 95% CIs of the recurrence rate. (c)ORs with 95% CIs of the adverse reactions. The values in bold font represent statistically significant differences.

intervention, all 2 CHIs denote direct comparisons, and there is no closed-loop formation. The network evidence of IL-10 is exhibited in Figure 3.

(2) Publication Bias. The funnel plot of this study revealed that most of the scatter points were located on both sides of the vertical line. They were basically symmetrical and may have had a certain degree of publication bias. The funnel plot of the IL-10 of 2 CHIs integrated with traditional Western medicine for treating UC is presented in Figure 4.

(3) Network Meta-analysis. 4 pieces of literature reported IL-10, involving 2 CHIs. Network comparison was conducted in 2 CHIs, yielding a total of 6 pairwise comparisons, two of which were statistically significant. Compared with traditional Western medicine, the MD and 95% CI of traditional Western medicine integrated with Shenfu injection were 4.41 and [112, 52]. The specific results are shown in Figure 6.

(4) SUCRA Probability Ranking. In accordance with the area under the curve diagram of SUCRA (Figure 5), the increased IL-10 rate of 3 CHI and traditional Western medicine were ranked probabilistically from high to low as follows: C + SF (87.8%) > C + SQFZ (43.4%) > + C (18.8%).(43.4%) > + C (18.8%).

3.4.6. Recurrence Rate Evidence Network. 4 pieces of literature reported a recurrence rate, involving 3 CHI treatment regimens. The dot size indicates the sample size using the intervention, the line thickness represents the number of RCTs using the two-point treatment intervention, all 3 CHIs denote direct comparisons, and there is no closed-loop formation. The network evidence of the recurrence rate is exhibited in Figure 3.

(1) Publication Bias. The funnel plot of this study revealed that most of the scatter points were located on both sides of the vertical line. They were basically symmetrical and may have had a certain degree of publication bias. The funnel plot of the recurrence rate of 3 CHIs integrated with traditional Western medicine for treating UC is presented in Figure 4.

(2) Network Meta-analysis. 4 pieces of literature reported a recurrence rate, involving 3 CHIs. A network comparison was conducted in 3 CHIs, yielding a total of 6 pairwise comparisons. The results showed that no significant difference was identified in the recurrence rate between the 4 interventions. The specific results are shown in Figure 7(b).

(3) SUCRA Probability Ranking. In accordance with the area under the curve diagram of SUCRA (Figure 5), the reduced recurrence rate of 3 CHI and traditional Western medicine were ranked probabilistically from high to low as follows: C + HQ (69.6%) > C + DSFZ (68.6%) > C + DS (55.4%) > C (6.4%).

3.4.7. Incidence of Adverse Reactions

(1) Evidence Network. 4 pieces of literature reported an incidence of adverse reactions involving 8 CHI treatment regimens. The dot size indicates the sample size using the intervention, the line thickness represents the number of RCTs using the two-point treatment intervention, all 8 CHIs denote direct comparisons, and there is no closed-loop formation. The network evidence of the incidence of adverse reactions is exhibited in Figure 3.

(2) Publication Bias. The funnel plot of this study revealed that most of the scatter points were located on both sides of the vertical line. They were basically symmetrical and may have had a certain degree of publication bias. The funnel plot of the incidence of adverse reactions of 8 CHIs integrated with traditional Western medicine for treating UC is presented in Figure 4.

(3) Network Meta-analysis. 4 pieces of literature reported an incidence of adverse reactions involving 8 CHIs. Network comparison was conducted in 8 CHIs, yielding a total of 36 pairwise comparisons, two of which were statistically significant. Compared with traditional Western medicine, the OR and 95% CI of traditional Western medicine integrated with *Astragalus* injection and traditional Western medicine integrated with Danshen powder injection were 0.28 and [0.08, 0.93] and 0.18 and [0.04, 0.77], respectively. The specific results are shown in Figure 7(c).

(4) SUCRA Probability Ranking. In accordance with the area under the curve diagram of SUCRA (Figure 5), the reduced Incidence of adverse reactions of 8 CHI and traditional Western medicine were ranked probabilistically from high to low as follows: C + FFKS (83.4%) > C + HQ (83%) > C + DG (59.1%) > C + DS (58.4%) > C + SM2 (50.4%) > C (41.5%) > C + FFDS (35.3%) > C + DSFZ (23%)>C + HH (15.8%).

4. Discussion

With the increasing number of published clinical studies of CHI for UC, clinical reports of different CHIs combined with conventional therapies for the adjuvant treatment of UC are also on the rise. However, no definitive conclusion has been reached as to which of the different CHI adjuvant therapies has the best adjuvant effect on UC. We believe that traditional meta-analyses limited only by a two-by-two comparison no longer provide valid methodological support for the selection of the optimal intervention for the treatment of CSR. In contrast, network meta-analysis allows for comparisons between multiple interventions. Therefore, this study is the first to compare the efficacy and safety of different CHI adjuvant treatments for UC using a network meta-analysis based on a frequency-based framework, with the aim of synthesizing direct versus indirect comparisons and providing a more credible evidence-based medical basis for the clinical treatment of UC.

The ranking results demonstrated that regarding the probability of overall clinical response rate, the efficacy ranking was Xiangdan injection > Shenmai injection > -Shengmai injection > Danshen injection > Houttuynia injection > Compound Danshen injection > Compound Kushen

injection > Danshen powder injection > Xuesaitong powder injection > Shuxuening injection > *Astragalus* injection > Safflower injection > Shenfu injection > Guanxinning injection > Shenqi Fuzheng injection > Acanthopanax senticosus injection > traditional Western medicine; in terms of the reduced TNF-αlevels, the probability ranking was Danshen injection > Danshen powder injection > *Astragalus* injection > Houttuynia injection > traditional Western medicine; concerning the reduced IL-6 levels, the probability ranking was Danshen powder injection > Danshen injection > *Astragalus* injection > traditional Western medicine; for the reduced IL-8 levels, the probability ranking was Shenqi Fuzheng Injection > Shenfu Injection > Danshen Powder Injection > traditional Western medicine; with respect to the increased IL-10 levels, the probability ranking was Shenfu injection > Shenqi Fuzheng injection > traditional Western medicine; as for the reduced recurrence rate, the probability ranking was *Astragalus* injection > Danshen powder injection > Danshen injection > traditional west medicine; respecting the reduced adverse reactions, the probability ranking was compound Kushen injection > *Astragalus* injection > Angelica sinensis injection > Danshen injection > Shengmai injection > traditional west medicine > compound Danshen injection > Danshen powder injection > Safflower injection.

The results suggested that Xiangdan injection, Shenmai injection, Shengmai injection, and Danshen injection integrated with traditional Western medicine treatment possessed the greatest possibility to be the optimal regimen. In the multiple-group comparison of the above overall response rate, inflammatory factors, recurrence rate, and outcome measures of the incidence of adverse reactions, the performance of traditional Western medicine alone ranked low. Thus, a combination of traditional Chinese and Western medicine was superior to traditional Western medicine alone.

In summary, Xiangdan injection, Shenmai injection, Shengmai injection, and Danshen injection integrated with traditional Western medicine treatment ranked first regarding effective rate. Besides, it was most likely to be the optimal regimen among the above interventions included. The top interventions could be selected for patients with different goals.

Through extensive comparisons with previous studies, we found that the top four herbal injections in terms of efficacy have had a certain number of relevant experimental animal studies published. These studies are expected to add credibility to the findings of the current study from the perspective of basic research and shed more light on the mechanism of action of CHI for UC.

The main ingredient of Xiangdan injection is the extract of the Chinese herbal medicine Dan, which is involved in descending incense. Salvia miltiorrhiza has the function of activating blood circulation, relieving pain, clearing the heart, relieving irritation, cooling the blood, and eliminating carbuncles. Radix *Rehmanniae* has the ability to resolve blood stasis and stop bleeding, regulate Qi, and relieve pain. A large number of animal experimental studies have shown [62–65] that cryptotanshinone, tanshinone IIA, and dihydrotanshinone I, the main natural compound components in Xiangdan injection, intervene in mice with ulcerative colitis to accelerate the speed of microcirculatory blood flow and improve mesenteric microcirculation, which is conducive to accelerating the repair of injured intestinal mucosa and promoting the healing of ulcerated surfaces.

Ginseng and maitake injection is mainly composed of red ginseng and maitake, which have the function of tonifying qi and consolidating essence, nourishing yin and generating fluid. A considerable number of published animal experiments have shown [66–68] that red ginseng extract, the main ingredient in ginseng and wheat injection, can significantly improve the structure of the intestinal microbiota of rats with ulcerative colitis and alleviate the symptoms of ulcerative colitis in vivo. And it can alleviate macroscopic lesions such as shortened colons, blood in stool and weight loss in mice with dextran sodium sulfate (DSS)-induced ulcerative colitis.

The main ingredient of Shengvei injection is the extract of Chinese herbal medicine, Red Ginseng, Mai Dong, and Wu Wei Zi, which has the effect of benefiting Qi and nourishing Yin, restoring the pulse and fixing detachment. An animal experimental study by Juan Lu, Yue Yu et al. [69] showed that raw vein injection had a protective effect on the intestinal mucosa of mice and was able to significantly improve the survival rate in a mouse model of inflammation.

The main ingredient of Danshen injection is the extract of the Chinese medicine Danshen. It has the efficacy of activating blood circulation, removing blood stasis, opening the veins, and nourishing the heart.

A related animal experimental study [70] showed that the combination of total phenolic acid of Danshen stem leaves, the main component of Danshen injection, and tanshinone significantly improved the symptoms of ulcerative colitis in mice by inhibiting the TLR4/PI3K/AKT/mTOR signaling pathway and exerting a protective effect on the intestinal mucosa of mice with dextran sulfate sodium (DSS)-induced ulcerative colitis.

5. Limitation

In this study, the safety and efficacy of various CHIs for treating UC were compared by network meta-analysis, providing a certain reference for clinical practice. However, there are still some limits here. First, the methodological quality of the involved literature was small on the whole. Among the 42 pieces of involved literature, 31 did not specify the random sequence generation method. None of the literature employed a random allocation concealment method. Besides, selectivity bias may exist during subject selection. None of the literature involved the blind method between subjects and interventionalists, and only one study used pathological result double-blind for the assessment of the results, making it a potential source of bias in the assessment of results. Four pieces of literature had dropouts/withdrawals. Moreover, patient age, drug dosage, and treatment process differed between the literature with some clinical heterogeneity. Additionally, there may be some small sample effects, leading to publication bias in the study. Combined

with related basic research, we found that there are still some gaps in the research of direct intervention of CHI in UC animal experiments. Further relevant in vivo or in vitro model validation is pending. At the same time, it is recommended that more standardized randomized controlled double-blind trials with good quality, large samples, and multicenter participation are needed in the future to provide a stronger basis for the safety and efficacy of integrating CHI with conventional drugs for UC.

6. Conclusion

The result of the network meta-analysis indicated that CHI integrated with traditional drugs is likely to be effective for treating UC. For treating UC, the overall response rate of CHI integrated with traditional drugs, which could better reduce TNF-α, IL-6, and IL-8 levels and better increase IL-10 levels, was higher than that of traditional treatment. Besides, CHI integrated with traditional Western medicine can better reduce the incidence of adverse reactions, and there is no significant difference in the recurrence rate. In our involved literature, Xiangdan injection, Shenmai injection, Shengmai injection, and Danshen injection may be the most effective CHI. Nevertheless, more high-quality, large sample, and multi-center randomized controlled double-blind trials are still required for research confirmation.

Data Availability

All the data in this study are available within the manuscript.

Additional Points

The authors have completed the PRISMA reporting checklist.

Disclosure

All authors have completed the ICMJE uniform disclosure form.

Conflicts of Interest

The authors have no conflicts of interest to declare.

Authors' Contributions

Ziyang Zhou and Hailiang Huang conceptualized the study; Hao Chen and Yingkai Shen curated the data; Ziyang Zhou and Hao Chen contributed to the investigation of the study; Ziyang Zhou and Hao Chen contributed to the methodology; Hailiang Huang contributed to the supervision; Ziyang Zhou contributed to the writing of the original draft; and Ziyang Zhou contributed to the review and editing of the manuscript.

Acknowledgments

The current study was financially supported by the Preliminary Mechanism and Efficacy Assessment by the excellent scientific research and innovation teams at Shandong University of Traditional Chinese Medicine for treating major diseases (No. 220316).

Supplementary Materials

Literature search strategy. Supplementary Table 2: basic situation of the included studies. Supplementary Table 3: checklist of the PRISMA extension for network meta-analysis. (*Supplementary Materials*)

References

[1] M. L. Hoivik, B. Moum, I. C. Solberg, M. Henriksen, M. Cvancarova, and T. Bernklev, "Work disability in inflammatory bowel disease patients 10 years after disease onset: results from the IBSEN Study," *Gut*, vol. 62, no. 3, pp. 368–375, 2013.

[2] J. Torres, V. Billioud, D. B. Sachar, L. Peyrin-Biroulet, and J. F. Colombel, "Ulcerative colitis as a progressive disease: the forgotten evidence," *Inflammatory Bowel Diseases*, vol. 18, no. 7, pp. 1356–1363, 2012.

[3] C. N. Bernstein, A. Wajda, L. W. Svenson et al., "The epidemiology of inflammatory bowel disease in Canada: a population-based study," *American Journal of Gastroenterology*, vol. 101, no. 7, pp. 1559–1568, 2006.

[4] J. Cosnes, C. Gower-Rousseau, P. Seksik, and A. Cortot, "Epidemiology and natural history of inflammatory bowel diseases," *Gastroenterology*, vol. 140, no. 6, pp. 1785–1794, 2011.

[5] E. V. Loftus Jr., "Clinical epidemiology of inflammatory bowel disease: incidence, prevalence, and environmental influences," *Gastroenterology*, vol. 126, no. 6, pp. 1504–1517, 2004.

[6] J. M. Shapiro, H. Zoega, S. A. Shah et al., "Incidence of crohn's disease and ulcerative colitis in Rhode Island: report from the ocean state crohn's and colitis area registry," *Inflammatory Bowel Diseases*, vol. 22, no. 6, pp. 1456–1461, 2016.

[7] N. A. Molodecky, I. S. Soon, D. M. Rabi et al., "Increasing incidence and prevalence of the inflammatory bowel diseases with time, based on systematic review," *Gastroenterology*, vol. 142, no. 1, pp. 46–54, 2012.

[8] J. D. Feuerstein, A. C. Moss, and F. A. Farraye, "Ulcerative colitis," *Mayo Clinic Proceedings*, vol. 94, no. 7, pp. 1357–1373, 2019.

[9] G. B. Feagan and and K. J. MacDonald, "Once daily oral mesalamine compared to conventional dosing for induction and maintenance of remission in ulcerative colitis: a systematic review and meta-analysis," *Inflammatory Bowel Diseases*, vol. 18, 2012.

[10] Claude and Eugene, "Ulcerative colitis practice guidelines in adults," *Clinics & Research in Hepatology & Gastroenterology*, vol. 36, no. 1, pp. 10–12, 2012.

[11] R. P. Perrillo, R. Gish, and Y. T. Fa Lck-Ytter, "American gastroenterological association institute technical review on prevention and treatment of hepatitis B virus reactivation during immunosuppressive drug therapy," *Gastroenterology*, vol. 148, no. 1, pp. 221–244, 2015.

[12] G. R. Lichtenstein, M. T. Abreu, R. Cohen, and W. Tremaine, "American Gastroenterological Association Institute technical review on corticosteroids, immunomodulators, and infliximab in inflammatory bowel disease," *Gastroenterology*, vol. 130, no. 3, pp. 935–939, 2006.

[13] X. Wu, D. Xia, K. Fang, G. Chen, and X. Dong, "Progress in clinical research on treatment of ulcerative colitis with traditional Chinese and western medicine," *Research of Integrated Traditional Chinese and Western Medicine*, vol. 13, no. 02, pp. 118–121, 2021.

[14] J. Gao, G. Chen, H. He et al., "Therapeutic effects of breviscapine in cardiovascular diseases: a review," *Frontiers in Pharmacology*, vol. 8, p. 289, 2017.

[15] Z. W. Liao, J. M. Gu, J. Yan, Y. Xu, and B. Ye, "A systematic review of the efficacy and safety of Danshen injection in the auxiliary treatment of ulcerative colitis," *Chinese Archives of Traditional Chinese Medicine*, vol. 38, no. 01, pp. 51–57, 2020.

[16] X. Liang, Y. H. Qv, and L. L. Gu, "Clinical observation of Shengmai injection on ulcerative colitis," *Journal of Hubei University of Chinese Medicine*, vol. 21, no. 05, pp. 58–60, 2019.

[17] B. X. Zhu, Y. M. Lv, and S. M. Ye, "Study on protective effect of salvia miltiorrhiza on mucosa of rats with acetic ulcerative colitis," *Chinese Journal of Integrated Traditional and Western Medicine on Digestion*, no. 04, pp. 214-215, 2000.

[18] K. C. Wu, J. Liang, Z. H. Liang et al., "Chinese consensus on diagnosis and treatment of inflammatory bowel disease (Beijing, 2018)," *Chinese Journal of Practical Internal Medicine*, vol. 38, no. 09, pp. 796–813, 2018.

[19] Chinese Society of Traditional Chinese Medicine Branch of Spleen and Gastrointestinal Diseases, "Expert consensus opinion on the treatment of ulcerative colitis in Chinese medicine (2017)," *Chinese Journal of Traditional Chinese Medicine*, vol. 32, no. 8, pp. 3585–3589, 2017.

[20] B. Bressler, J. k. Marshall, C. N. Bernstein et al., "Clinical Practice Guidelines for the Medical Management of Non-Hospitalized Ulcerative Colitis: Toro," *Gastroenterology*, vol. 148, no. 5, pp. 1035–1058, 2015.

[21] M. Harbord, R. Eliakim, D. Bettenworth et al., "European crohn's and colitis organisation[ECCO]. third euro-pean evidence-based consensus on diagnosis and manage-ment of ulcerative colitis Part 2: current management," *Journal of Crohns Colitis*, vol. 11, no. 7, pp. 769–784, 2017.

[22] K. D. Wang, "Clinical observation on 38 cases of ulcerative colitis treated by Shenfu injection," *Chinese Journal of Integrative Medicine on Cardio-Cerebrovascular Disease*, vol. 04, p. 10, 2002.

[23] C. D. Zhao, X. J. Zhang, L. Zhang et al., "Effect of Shenqi Fuzheng injection on CX3CR1 of large intestine mucosa in patients with ulcerative colitis," *Chongqing Medicine*, vol. 44, no. 29, 2015.

[24] X. P. Li, "The effect of Danshen powder injection in the treatment of ulcerative colitis and its influence on the levels of Hcy and inflammatory factors in patients," *Clinical Research and Practice*, vol. 4, no. 02, pp. 26-27, 2019.

[25] W. W. Wang, S. C. Wei, and W. T. Xing, "The effect of Danshen powder injection on D-dimer, PT, FIB and PLT in subjects with ulcerative colitis," *Journal of Clinical and Experimental Medicine*, vol. 17, no. 08, pp. 834–838, 2018.

[26] J. Z. Zhang, Y. Zhang, Y. X. Hao, and H. B. Qi, "The effect and significance of Danshen injection on the content of D-dimer in patients with ulcerative colitis," *Modern Journal of Integrated Traditional Chinese and Western Medicine*, vol. 32, pp. 4968-4969, 2018.

[27] L. X. Huang, "Effect of danshen injection on hypercoagulable state of ulcerative colitis," *Chinese Archives of Traditional Chinese Medicine*, vol. 10, pp. 1901-1902, 2005.

[28] J. Y. J. Wang, R. Sun, and Z. Yang, "Observation on the efficacy of Danshen injection combined with ornidazole in the treatment of ulcerative colitis," *Modern Journal of Integrated Traditional Chinese and Western Medicine*, vol. 25, no. 34, pp. 3864-3865, 2016.

[29] C. Liu, J. Yang, F. C. Zhu, X. L. Li, and J. Ma, "Evaluation of the efficacy of Danshen injection combined with compound lactic acid bacteria capsules in the treatment of ulcerative colitis," *Hebei Medical Journal*, vol. 41, no. 13, 2012.

[30] L. Yang, "Effect of Danshen injection combined with Bacillus subtilis double live bacteria enteric-coated capsules on intestinal mucosal function in patients with ulcerative colitis," *Heilongjiang Medicine and Pharmacy*, vol. 06, pp. 153-154, 2016.

[31] Y. S. Zhu, "The therapeutic effect of Danshen injection combined with mesalazine on patients with ulcerative colitis," *Heilongjiang Journal of Traditional Chinese Medicine*, vol. 48, no. 02, pp. 249-250, 2019.

[32] X. X. Chen, S. H. Liang, and F. Q. Ma, "The effect of Danshen injection combined with mesalazine on serum HIF-1α and inflammatory cytokine levels in patients with mild to moderate active ulcerative colitis," *Shanghai Journal of Traditional Chinese Medicine*, vol. 52, no. 07, pp. 55–58, 2018.

[33] X. C. Wang, L. L. Zhang, and Z. K. Guo, "Efficacy of Danshen injection combined with mesalazine in the treatment of ulcerative colitis and its influence on inflammatory factors and coagulation indexes," *Evaluation and Analysis of Drug-Use in Hospitals of China*, vol. 17, no. 03, p. 344, 2017.

[34] L. N. Yang and J. Wang, "Observation of therapeutic effect of danshen injection combined with mesalazine on ulcerative colitis," *Clinical Medicine*, vol. 37, no. 04, pp. 117–119, 2017.

[35] G. Ma and W. J. Dai, "Effect of danhong injection on CD62p in patients with ulcerative colitis," *Journal Of Wannan Medical College*, vol. 32, no. 06, pp. 471–473, 2013.

[36] S. P. Liu, W. G. Dong, S. C. Liu, and J. F. He, "Effect of Angelica injection on the function of platelet in patients with ulcerative colitis and its significance," *Journal of Chinese Physician*, vol. 07, pp. 904–906, 2003.

[37] J. Tian, D. Li, L. Ge, W. Cheng, and Y. J. Xu, "Comparative observation on the efficacy of compound kushen injection combined with routine enema in treating ulcerative colitis," *China Modern Doctor*, vol. 49, no. 20, pp. 77-78, 2011.

[38] S. Y. Zhang, Y. L. Wei, and Y. F. Pan, "The efficacy of coronarin injection combined with mesalazine in the treatment of ulcerative colitis," *Chinese Journal of Clinical Rational Drug Use*, vol. 3, no. 08, p. 39.

[39] W. Wu and Z. Li, "Clinical observation of honghua injection in adjuvant treatment of ulcerative colitis," *Medicine*, vol. 000, no. 008, p. 83, 2015.

[40] P. Y. Yan, J. G. Liu, M. L. Zhu, and J. M. Li, "Clinical observation of honghua injection in adjuvant treatment of ulcerative colitis," *Modern Medicine Journal of China*, vol. 13, no. 01, p. 48, 2011.

[41] S. Z. Jia, "Observation on therapeutic effect of huangqi injection intravenously combined with enema in treating ulcerative colitis," *Journal of Bingtuan Medicine*, vol. 39, no. 01, pp. 30-31, 2014.

[42] M. Q. Li, J. Zhao, X. Guo, J. liu, and M. J. Liu, "Observation on therapeutic effect of huangqi injection intravenously on ulcerative colitis," *Journal of Yanan University(Medical Science Edition)*, vol. 01, pp. 29-30, 2005.

[43] Y. P. Liu and S. Y. Zhou, "Astragalus injection combined with mesalazine in the treatment of 42 cases of ulcerative colitis," *China Pharmaceuticals*, vol. 20, no. 10, pp. 77-78, 2011.

[44] T. M. Li, "Observation on the effect of astragalus injection combined with mesalazine in the treatment of ulcerative

colitis," *Journal of Medical Information*, vol. 26, no. 30, p. 80, 2013.

[45] S. C. Hu and M. Li, "Clinical effect of huangqi injection on ulcerative colitis," *Guizhou Medical Journal*, vol. 44, no. 11, pp. 1772-1773, 2020.

[46] Z. Li, "Analysis of the effect of Shenmai injection on patients with ulcerative colitis," *Chinese Journal of Modern Drug Application*, vol. 13, no. 21, pp. 97–99, 2019.

[47] D. Y. Xu, "Application of mesalazine combined with Danshen injection in the treatment of ulcerative colitis," *Chinese Community Doctors*, vol. 36, no. 20, pp. 76-77, 2020.

[48] J. E. Chen, "Clinical study of sulfasalazine, hydrocortisone, acanthopanax injection combined with enema in the treatment of ulcerative colitis," *Journal of Hebei Medical University*, vol. 33, no. 06, pp. 629–631, 2012.

[49] W. J. Deng, Y. C. Ma, and L. L. Ma, "Efficacy of mesalazine combined with Danshen injection in the treatment of ulcerative colitis and its influence on inflammatory factors and coagulation indexes in patients," *World Chinese Journal of Digestology*, vol. 24, no. 03, pp. 462–466, 2016.

[50] X. Li, "Clinical efficacy of mesalazine combined with Danshen injection in the treatment of ulcerative colitis and its influence on inflammatory factors and coagulation indexes in patients," *The Journal of Medical Theory and Practice*, vol. 29, no. 12, pp. 1591-1592, 2016.

[51] S. S. Sun, "Clinical analysis of mesalazine combined with Danshen injection in the treatment of ulcerative colitis," *Guide of China Medicine*, vol. 17, no. 04, pp. 60-61, 2019.

[52] H. Y. Zhu, "Analysis of the effect of mesalazine combined with Danshen injection on inflammatory factors in patients with ulcerative colitis," *Contemporary Medicine*, vol. 24, no. 01, pp. 100-101, 2018.

[53] X. J. Xu, K. Zhang, and Y. Wang, "Shengmai injection assisted treatment of 50 cases of ulcerative colitis," *Chinese Journal of Integrated Traditional and Western Medicine on Digestion*, no. 05, pp. 343-344, 2008.

[54] R. Abu, "Analysis of shuxuening injection combined with routine therapy to improve the inflammatory state of patients with active ulcerative colitis," *Modern Medicine and Health Research Electronic Journal*, vol. 1, no. 06, 2017.

[55] Z. H. Xie, T. J. Wang, Y. X. Zheng, F. F. Huang, and Z. M. Wang, "Analysis of shuxuening injection combined with routine therapy to improve the inflammatory state of patients with active ulcerative colitis," *Chinese Journal of Integrated Traditional and Western Medicine*, vol. 34, no. 10, pp. 1164–1167, 2014.

[56] H. Q. Liu and Y. H. Wang, "Observation on the curative effect of Shuxuening injection combined with mesalazine in the treatment of ulcerative colitis," *Jilin Medical Journal*, vol. 36, no. 12, pp. 2576-2577, 2015.

[57] K. Wan, L. Z. Qi, and Y. Yu, "Observation of therapeutic effect of shuxuening injection on ulcerative colitis," *China Practical Medicine*, vol. 7, no. 32, pp. 145-146, 2012.

[58] W. H. Zhang and B. Ren, "Observation on the effect of xiangdan injection on ulcerative colitis," *Journal of Qilu Nursing*, vol. 09, p. 844, 2006.

[59] Z. F. Tang, W. Y. Wang, Y. Z. Zhang, and X. J. Zheng, "Clinical application of Xuesaitong injection in ulcerative colitis," *Chinese Community Doctors*, vol. 30, no. 09, pp. 69-70, 2014.

[60] X. F. Zhao, "Analysis of serum IL-8 and TNF-α levels in patients with ulcerative colitis treated with Yuxingcao injection assisted by conventional western medicine," *World Latest Medicine Information*, vol. 18, no. 74, p. 157, 2018.

[61] W. Liu, Y. Liu, C. Y. Zhang, X. Zhang, L. He, and L. Li, "The effect of Danshen powder injection for injection on coagulation in patients with ulcerative colitis," *Chinese Archives of Traditional Chinese Medicine*, vol. 29, no. 10, pp. 2304-2305, 2011.

[62] A. Bai, N. Lu, Y. Guo, and X. Fan, "Tanshinone IIA ameliorates trinitrobenzene sulfonic acid (TNBS)-Induced murine colitis," *Digestive Diseases and Sciences*, vol. 53, no. 2, pp. 421–428, 2008.

[63] X. Liu, H. He, T. Huang et al., "Tanshinone IIA protects against dextran sulfate sodium- (DSS-)induced colitis in mice by modulation of neutrophil infiltration andactivation," *Oxidative Medicine and Cellular Longevity*, vol. 2016, Article ID 7916763, 10 pages, 2016.

[64] Y. Guo, X. Wu, Q. Wu, Y. Lu, J. Shi, and X. Chen, "Dihydrotanshinone I, a natural product, ameliorates DSS-induced experimental ulcerative colitis in mice," *Toxicology and Applied Pharmacology*, vol. 344, pp. 35–45, 2018.

[65] X. Min, X. Zeng, W. Zhao et al., "Cryptotanshinone protects dextran sulfate sodium-induced experimental ulcerative colitis in mice by inhibiting intestinal inflammation," *Phytotherapy Research*, vol. 34, no. 10, pp. 2639–2648, 2020.

[66] M. Guo, S. Ding, C. Zhao et al., "Red Ginseng and Semen Coicis can improve the structure of gut microbiota and relieve the symptoms of ulcerative colitis," *Journal of Ethnopharmacology*, vol. 162, pp. 7–13, 2015.

[67] E. Saba, Y. Y. Lee, M. Kim et al., "A novel herbal formulation consisting of red ginseng extract and Epimedium koreanum Nakai-attenuated dextran sulfate sodium-induced colitis in mice," *Journal of Ginseng Research*, vol. 44, no. 6, pp. 833–842, 2020.

[68] E. Saba, Y. Y. Lee, M. H. Rhee, and S.-D. Kim, "Alleviation of ulcerative colitis potentially through th1/th2 cytokine balance by a mixture of rg3-enriched Korean red ginseng extract and persicaria tinctoria," *Molecules*, vol. 25, no. 22, p. 5230, 2020.

[69] J. Lu, Y. Yu, X.-j. Wang et al., "Mechanism of Shengmai injection (生脉注射液) on anti-sepsis and protective activities of intestinal mucosal barrier in mice," *Chinese Journal of Integrative Medicine*, 2021, 10.1007/s11655-021-3292-y.

[70] K. Y. Peng, J. F. Gu, S. L. Su et al., "Salvia Miltiorrhiza Stems and Leaves Total Phenolic Acids Combination with Tanshinone Protect against DSS-Induced Ulcerative Colitis through Inhibiting TLR4/PI3K/AKT/mTOR Signaling Pathway in Mice," *Journal of Ethnopharmacol*, vol. 264, 2021.

Hindawi
Evidence-Based Complementary and Alternative Medicine
Volume 2022, Article ID 3707647, 19 pages
https://doi.org/10.1155/2022/3707647

Research Article

Topical Formulation of Noscapine, a Benzylisoquinoline Alkaloid, Ameliorates Imiquimod-Induced Psoriasis-Like Skin Lesions

Fahimeh Nourbakhsh,[1] Seyed Hadi Mousavi,[1] Pouria Rahmanian-Devin,[2] Vafa Baradaran Rahimi,[3] Hassan Rakhshandeh,[2] and Vahid Reza Askari[2,4,5,6]

[1]*Medical Toxicology Research Centre, Faculty of Medicine, Mashhad University of Medical Sciences, Mashhad, Iran*
[2]*Pharmacological Research Center of Medicinal Plants, Mashhad University of Medical Sciences, Mashhad, Iran*
[3]*Department of Cardiovascular Diseases, Faculty of Medicine, Mashhad University of Medical Sciences, Mashhad, Iran*
[4]*Applied Biomedical Research Center, Mashhad University of Medical Sciences, Mashhad, Iran*
[5]*Department of Pharmaceutical Sciences in Persian Medicine, School of Persian and Complementary Medicine, Mashhad University of Medical Sciences, Mashhad, Iran*
[6]*Department of Persian Medicine, School of Persian and Complementary Medicine, Mashhad University of Medical Sciences, Mashhad, Iran*

Correspondence should be addressed to Vahid Reza Askari; askariv@mums.ac.ir

Received 6 January 2022; Revised 17 March 2022; Accepted 5 April 2022; Published 22 April 2022

Academic Editor: Xiang Liu

Psoriasis is considered an autoimmune inflammatory disease. The disease is spread and diagnosed by the infiltration of inflammatory mediators and cells into the epidermis. Recent theoretical developments have focused on the effectiveness of noscapine (NOS) as a potential alkaloid for being used as a valuable treatment for different diseases. In the present study, psoriasis-like dermatitis was induced on the right ear pinna surface of male *Balb/c* mice by topical application of imiquimod (IMQ) for ten consecutive days, which was treated with noscapine (0.3, 1, 3, and 10% w/v) or clobetasol (0.05% w/v) as a positive control. The levels of ear length, thickness, severity of skin inflammation, psoriatic itch, psoriasis area severity index (PASI) score, and body weight were measured daily. On the 10^{th} day of study, each ear was investigated for inflammation, fibrosis, proliferation, and apoptosis using histopathological (H&E and Masson's trichrome staining) and immunohistochemistry (Ki67 and p53 staining) assays. Furthermore, the levels of inflammatory biomarkers were characterized by an enzyme-linked immunosorbent assay (ELISA). The results confirmed IMQ-induced psoriasis for five consecutive days. In contrast, noscapine significantly reduced the ear length, thickness, severity of skin inflammation, psoriatic itch and body weight, tumor necrosis factor-α (TNF-α), transforming growth factor-β (TGF-β), interferon-gamma (IFN-γ), interleukin 6 (IL-6), IL-17, and IL-23p19 in a concentration-dependent manner ($P < 0.001$–0.05 for all cases). Overall, topical noscapine significantly ameliorated both the macroscopical and microscopical features of psoriasis. However, further clinical investigations are required to translate the effects to clinics.

1. Introduction

Inflammation is defined by a series of events beginning with an induction phase, progressing to a maximum of inflammation, and then ending with a resolution phase [1–3]. Acute inflammation allows for rapid and complete immune activation, which is necessary for successful innate immunity defense [1–4]. It starts with detecting exogenous and endogenous surface receptors caused by mechanically, chemically, or biologically induced tissue damage, followed by the recruitment of effector cells, which also orchestrates an inflammatory reaction defined by the release of lipid and protein-based mediators of inflammation [5].

Psoriasis is an autoimmune and chronic inflammatory disease in which keratinocytes are impressed with significant proliferation and abnormal differentiation [6]. The infiltration of inflammatory cells and related inflammatory mediators characterizes the disease into the epidermis and

causes severe changes in the vascular system of the dermis [7]. Patients typically describe scaling of the body surface, itching, erythema, burning, and bleeding as symptoms. The prevalence of this disease globally is reported by 2-3% (more than 125 million people in the world), which is probably the most common autoimmune skin disease [8]. Both genetics and environmental factors are contributing to the disease [9]. In this regard, family history has been reported in approximately 30% of psoriatic patients. These patients have also observed polymorphisms of genes that regulate angiogenesis and inflammation [10, 11]. The entry of various immune cells and the production of inflammatory and proinflammatory cytokines in the epidermis intensify the inflammation in this area and develop psoriasis lesions [12]. Studies have shown that $CD4^+$ and $CD8^+$ T-cells play a fundamental role in the pathogenesis of psoriasis, initiating inflammation, and keeping inflammation in place.

On the other hand, the critical role of T-cells in psoriasis has been proven [13]. Although the exact pathogenesis of this disease is not yet fully understood, there is growing evidence that interleukin (IL)-23/IL-17A has a significant impact on the pathogenesis of the disease. In addition, several studies have demonstrated that the primary source of IL-17A production in the skin is $\gamma\delta$-T cells producing IL-17A by stimulating IL-23 [14]. Many inflammatory cytokines, including IL-23, IL-17A, IL-20, IL-22, IL1-β, IL-6, and TNF-α (tumor necrosis factor-α), act as a complex in the disease development [14]. Imiquimod (IMQ), a ligand for toll-like receptors (TLRs)-7/8 and a potent activator of the immune system, is used to treat genital and anal warts (caused by human papillomaviruses, HPV) selected as a psoriasis experimental design [15, 16]. In this regard, experimental data have shown that IMQ causes human-like dermatitis similar to psoriasis in animal studies. It was demonstrated that IMQ used in the treatment of active warts and keratosis could activate dendritic cells, plasma dendritic cells (PDCs), natural killer (NK) cells, and T lymphocytes to produce inflammation by interferon (IFN)-γ and IL-17/IL-23 secretions [14]. The experimental validation of this model might pave the way for novel treatment approaches that target upstream processes in psoriasis etiology [17]. Due to the use of this drug on the skin of mice, it causes the rapid entry of PDCs into the site. In fact, this drug's antiviral and antitumor activity is mainly mediated by activation of TLR-7 and TLR-8 (expressed by monocytes, macrophages, and PDCs) [18]. Although low doses of methotrexate and other suggested treatments are used weekly for psoriasis, numerous adverse effects have been reported for these medications, including hematological and gastrointestinal disorders such as abdominal discomfort, stomach pain, nausea and vomiting, and drowsiness [19, 20]. Therefore, the use and findings of medicines that control the severity of psoriasis with the least amount of adverse effects are a priority in the treatment and alleviation of psoriasis.

Noscapine is a benzyl alkaloid isoquinoline found in dark poppy plants with no opioid-like adverse effects [21–23]. However, it has been reported to inhibit cell proliferation in a wide range of cancer cells, even in many drug-resistant species [23–25]. Furthermore, noscapine has been demonstrated to be safe and to have no toxic effects on humoral or cell-mediated immunity. Along with its antitussive and antistroke effects, these findings generated an interest in establishing other roles of noscapine. The pharmacology of noscapine, as well as its effects on cellular signaling pathways, the mitotic spindle, and centrosome clustering, as well as its use as an antimalarial and cough suppressant, and its exceptional potential as a treatment for polycystic ovarian syndrome, strokes, and a variety of malignancies, are all detailed [22, 23]. Moreover, it has been indicated that noscapine could reduce the levels of inflammatory cytokines, such as IL-2, TNF-α, and IL-6, in different *in vitro* and *in vivo* models [22–25]. Therefore, in this study, we tried to evaluate the effectiveness of topical administration of noscapine in the animal model of IMQ-induced psoriasis with several macroscopic (such as ear length, thickness, severity of skin inflammation, psoriatic itch, psoriasis area severity index (PASI) score, and body weight), histopathologic (Hematoxylin and eosin, H&E, for inflammation and inflammatory cells infiltration levels, and Masson's trichrome for the fibrosis level), immunohistochemistry (Ki-67 as a marker of cell proliferation and p53 as a marker of cell apoptosis), and molecular (cytokines production) methods.

2. Materials and Methods

2.1. Chemicals and Reagents. Noscapine powder (purity 99.5%) was of analytical grade and bought from FaranShimi® Company, Hamedan, Iran. Cold cream was of commercial grade and obtained from Farabi® Company, Tehran, Iran. Unless otherwise noted, all chemicals and reagents were acquired from Sigma-Aldrich (St. Louis, MO, USA). Furthermore, 5% w/w imiquimod propionate cream patches was prepared from Aldara, MEDA, Sweden. The cytokine chemical and reagent characterizations were acquired from the eBioscience® company (St. Louis, MO, USA). Enzyme-linked immunosorbent assay (ELISA) kits were obtained for TNF-α, TGF-β, IFN-γ, IL-10, IL-6, IL-17A, and IL-23p19. Immunohistochemical examination was performed using the antibodies against Ki-67 protein (ZYTOMED) and p53 protein (GenomeMe) based on the kit protocols.

2.2. Preparation of Noscapine Cream. To prepare noscapine cream in the lowest dose (0.3 %w/w), 300 mg of noscapine was levigated in 2 mL of glycerin and then mixed with cold cream to have the final mixture of 100 g. Similarly, further doses of 1%, 3%, and 10% w/w of noscapine cream were prepared with the same method and different levels of noscapine. The final cream had good stability and illustration and was in a smooth consistency.

2.3. Animal Husbandry and Ethical Statements. Forty-two male inbred *Balb/c* mice (weighing 25.2 ± 4.6 g) were obtained from the Faculty of Medicine Animal Laboratory, Mashhad University of Medical Sciences, Mashhad, Iran, and then randomly divided into six groups for this research

($n = 7$/group). Animals were housed in cages at $22 \pm 1^{\circ}$C along with temperature conditions of 19–26°C, relative humidity of 70–70%, the light intensity of 300 lux, and exposure of 12 light/dark cycles. All animals had free access to food and tap water. Three or four mice were housed in each cage at better condition, which measured $206 \times 365 \times 140$ mm. Moreover, the mice were acclimatized for one week before starting the study. In fact, all animal procedures were carried out in compliance with the National Institutes of Health's Guide for the Use and Care of Laboratory Animals guidelines of institutional guidelines. Moreover, the Mashhad University of Medical Sciences Ethical Committee approved all procedures involving animals based on the policies of animal experiments and care (Ethical approval code: 990587, Approval date: 2020–09–07, Approval ID: IR.MUMS.MEDICAL.REC.1399.463).

2.4. Psoriasis Induction and Experimental Protocol. To induce psoriasis from the first day, a certain amount of 5% w/w IMQ cream (10 mg/cm^2 of skin) was used on the right ear pinna of mice in each group. Daily photographs were taken to record changes in skin lesions and were scored based on PASI scores, inflammation, thickness, and redness of mice's right ear pinna. Doses of medication and treatment were used for ten days. *Balb/c* mice were grouped as follows.

Group I: sham group, received a daily topical cold cream application as the vehicle on the right ear pinna.

Group II: negative control group, received a daily topical dosage of 5% IMQ cream (10 mg/cm^2 of skin) on the right ear pinna (left ear pinna was untreated as the internal control), and after 30 min received a daily topical cold cream, as the vehicle, on the right ear pinna.

Group III: positive group, received a daily topical dosage of 5% IMQ cream on the right ear pinna (left ear pinna was untreated as the internal control), and after 30 min received a daily topical clobetasol cream (0.05 % w/w) on the right ear pinna.

Group IV: NOS 0.3% w/w, received a daily topical dosage of 5% IMQ cream on the right ear pinna (left ear pinna was untreated as the internal control), and after 30 min received a daily topical 0.3% w/w noscapine cream on the right ear pinna.

Group V: NOS 1% w/w, received a daily topical dosage of 5% IMQ cream on the right ear pinna (left ear pinna was untreated as the internal control), and after 30 min received a daily topical 1% w/w noscapine cream on the right ear pinna.

Group VI: NOS 3% w/w, received a daily topical dosage of 5% IMQ cream on the right ear pinna (left ear pinna was untreated as the internal control), and after 30 min received a daily topical 3% w/w noscapine cream on the right ear pinna.

Group VII: NOS 10% w/w, received a daily topical dosage of 5% IMQ cream on the right ear pinna (left ear pinna was untreated as internal control), and after 30 min received a daily topical 10% w/w noscapine cream on the right ear pinna.

All doses were calculated based on the preliminary study with a three-fold increment in dose. An illustration of the experimental procedures is shown in Table 1.

2.5. Scoring Severity of Skin Inflammation. The levels of erythema, thickness, and scaling on the afflicted ear pinna surface were used to calculate PASI (Psoriasis Area and Severity Index) scores. On a four-point scale, PASI was calculated for each mice (0 = none; 1 = slight; 2 = moderate; 3 = marked; 4 = extremely marked). The total score was measured by the combined scores (scaling, erythema, and thickness). Ear thickness and ear length were measured in both ears every day with digital calipers (BEC, China). These factors are the criteria for the amount of epidermal growth and inflammation was measured by the rise in ear thickness and inflammation [26].

2.6. Behavioural Tests of IMQ-Induced Psoriatic Itch. Mice were acclimated to a plexiglass recording arena twice for 60 minutes each time before being tested. In addition, mice were recorded from above for 60 minutes two hours following each topical administration. A scratch bout was characterized as one or faster back-and-forth hind paw motions aimed at and touching the treated region, culminating in toe licking or biting or planting of the hind paw on the floor. Grooming motions and posterior paw movement directed away from the treatment region (e.g., ear scratching) were not counted [27].

2.7. Evaluating the Mice's Spleen, Ear, and Body Weight. At the end of the study, animals were sacrificed, and the tissues were dissected and kept at −70°C. In this way, the spleen and ear of each mouse were isolated, weighed and then photographed, and stored in a freezer with −70°C or 10% v/v formalin for further examinations. In addition, the spleen and ear index were calculated by dividing the weight of the spleen or ear of each mouse by the bodyweight of the mouse on the last day.

2.8. Histopathological Examination. Right ear pinnas were selected as a tissue sample and then were fixed in 10% v/v neutral-buffered formalin. Samples were placed separately in 10% v/v formalin in a Falcon-tube and delivered to the pathology laboratory. The samples were immersed in paraffin blocks and finally cut to a thickness of 4 μm. Hematoxylin and eosin (H&E, evaluating inflammation and inflammatory cells infiltration levels) and Masson's trichrome (evaluating fibrosis level) stainings were considered for each sample and photographed with a digital camera microscope [28–30]. The ear was considered for H&E and Masson's trichrome stainings.

Moreover, the spleen and cervical spinal cord (C3–C4) was also selected for H&E staining investigation, including inflammation and cellular infiltrations. The stained tissues were photographed with a digital camera microscope

Table 1: Illustration of the experimental procedures.

Protocol	Groups		Treatment day
($n = 7$/each group) Psoriatic lesion and Noscapine therapy	Sham	Daily topical cold cream (10 mg/cm^2 of skin)	Day 1–10
	Control negative	Daily topical dosage of 5% IMQ cream (10 mg/cm^2 of skin)	
	Control positive	Daily topical dosage of 5% IMQ + Daily topical clobetasol cream (0.05 %w/w)	
	Treatment	Daily topical dosage of 5% IMQ + daily topical 0.3% w/w noscapine cream	
		Daily topical dosage of 5% IMQ + daily topical 1% w/w noscapine cream	
		Daily topical dosage of 5% IMQ + daily topical 3% w/w noscapine cream	
		Daily topical dosage of 5% IMQ + daily topical 10% w/w noscapine cream	

(Nikon, Eclipse E200). The pathologic changes in the ear pinna of various groups were included: acanthosis, parakeratosis, and thickening of the subepidermal layer. These factors were evaluated semi-quantitatively on a scale of 0–10 (0 = No clinical signs or change, 1 = Partial inflammation, 2 = Slight inflammation and tissue damage in mice, 3 = Increased levels of inflammation and tissue destruction of the right ear pinna, spinal cord and increased spleen leukocytes, 4 = Low increase in epidermis thickness and inflammation, 5 = Moderate inflammation, ear pinna thickness, and low parakeratosis 6 = Moderate inflammation, moderate ear pinna thickness, epidermal parakeratosis 7 = Increasing inflammation, ear pinna thickness, epidermal parakeratosis, and a low score of hyperplasia of the epidermis 8 = Ear pinna thickness and inflammation, marked areas of necrosis with vacuolization of cells, epidermal parakeratosis, 9 = Ear pinna thickness and inflammation, parakeratosis of the epidermal layer, 10 = Maximum inflammation, increased inflammatory infiltration and hyperplasia of the epidermis and acanthosis) [26, 31].

2.9. Immunohistochemistry Examination. Immunohistochemistry (IHC) [32] is the method for detection of a specific antigen in a tissue, cell, or particular phase of a cell life cycle based on antigen-antibody detection using light microscopy [33]. In the present study, we performed IHC for detecting the Ki-67 as a marker of cell proliferation and the p53 as a marker of cell apoptosis in the right ear pinnas based on their kits' manual [32, 33]. The basic steps of the IHC-P protocol are as follows: (1) Fixing and embedding the tissue, (2) cutting and mounting the section, (3) deparaffinizing and rehydrating the section, (4) antigen retrieval, (5) immunohistochemical staining, (6) counterstaining (if desired), (7) dehydrating and stabilizing with mounting medium, and (8) viewing the staining under the microscope. These factors were semi-quantitatively scaled of 0–10 (0 = no change from untreated ears to 10 = maximum).

2.10. Total Protein Measurement Method. The Bradford protein assay was carried out to quantify the total protein concentration in each sample [2, 3, 34, 35]. In this regard, first, the Coomassie brilliant blue G-250 dye (10 mg) was dissolved in 50 ml ethanol 96%. Then, phosphoric acid 85% v/v (10 ml) was added, and the volume of the solution was increased to 100 ml. Thereafter, bovine serum albumin (4 mg/ml) solution was prepared as a standard curve. Then, after sample pouring (20 μl), a Bradford reagent (200 μl) was added to the 96-well microplate. Finally, the light absorption was read at 595 nm with a microplate reader after 5 minutes [2, 3, 28, 35].

2.11. Cytokine Assessments. The right ear pinnas of the mice were excised and kept at −70°C to evaluate cytokine measurement in skin tissue. The skins were homogenized at 4°C in tissue protein lysis buffer. In the following, the supernatants were selected for measuring the concentration of cytokines such as TNF-α, TGF-β, IFN-γ, IL-10, IL-6, IL-17A, and IL-23p19. ELISA was performed under the manufacturer's instructions based on the kits' protocols [2, 3, 28, 35].

2.12. Statistical Analysis. Data were analyzed using GraphPad Prism ® software version 8 (GraphPad Software, San Diego, CA) and presented based on the natures of parametric or non-parametric as means ± SD or median ± range (for the pathological score, including acanthosis, parakeratosis, thickening of subepidermal, histology score), respectively. The normality test was done for parametric data, based on the Kolmogorov–Smirnov and Bartlett's tests that assess the homogeneity of variances. Thereafter, comparisons between groups were carried out using a two-way analysis of variance (ANOVA) followed by a Sidak's multiple comparisons *post hoc* test. Repeated measures two-way ANOVA was done with the following Dunnett-T_3 multiple comparisons *post hoc* test for clinical scores. Non-parametric data were analyzed using the Kruskal–Wallis and Dunn's post-hoc multiple comparisons tests. The Brown–Forsythe test was also used if the SD was not equal and the statistical test in the equality of group variances based on performing an analysis of variance. Noteworthy, when P values (P) ≤ 0.05, 0.01, and 0.001 were considered statistically significant [2, 3, 28, 35]. The data and statistical analysis complied with the recommendations on experimental design, analysis and data sharing, and presentation in preclinical pharmacology [36–38]. A summary of the statistical analysis is shown in Table 2.

Table 2: Summarized protocols of the present study.

ANOVAs table	Time F (DFn, DFd)	Number of columns (intervention)	Number of rows (time)	Time × intervention	ANOVAs test
Thickness	F (10, 60) = 147.7 $P < 0.0001$, $N = 11$	F (6, 42) = 471.7	307.4	F (60, 420) = 70.32	Two way ANOVA Dunnet
Erythema	F (10, 60) = 352.2 $P < 0.0001$, $N = 11$	F (6, 36) = 177.4	11	F (60, 360) = 25.42	Two way ANOVA Sidak
Scales	F (10, 60) = 409.3 $P < 0.0001$, $N = 11$	F (6, 36) = 124.4	11	F (60, 360) = 19.18	Two way ANOVA Sidak
Total score	F (10, 60) = 922.8 $P < 0.0001$, $N = 11$	F (6, 36) = 827.4	11	F (60, 360) = 72.62	Two way ANOVA Sidak
Ear length	F (10, 60) = 467.5 $P < 0.0001$, $N = 11$	F (6, 36) = 363.5	11	F (60, 360) = 53.04	Two way ANOVA Dunnet
Scratch bouts	F (10, 420) = 509.3 $P < 0.0001$, $N = 11$	F (6, 36) = 230.3	11	F (60, 360) = 31.27	Two way ANOVA Dunnet
Body weight	F (2.970, 17.82) = 15.12 $P < 0.0001$	7	7	F (6, 36) = 3.490	One-way ANOVA Dunnet
Spleen weight	F (6, 42) = 16.19 $P < 0.0001$	1	7	—	One-way ANOVA Dunnet
Ear index	F (6, 42) = 10.62 $P < 0.0001$	1	7	—	One-way ANOVA Dunnet
Spleen index	F (6, 42) = 21.30 $P < 0.0001$	1	7	—	One-way ANOVA Dunnet
TNF-ơ	F (6, 18) = 53.55 $P < 0.0001$	7	35	—	Brown Forsythe test Dunnet T3
IL-10	F (6, 15) = 45.19 $P < 0.0001$	7	35	—	Brown Forsythe test Dunnet T3
TGF-β	F (6, 22) = 49.82 $P < 0.0001$	7	35	—	Brown Forsythe test Dunnet T3
IL-6	F (6, 15) = 31.8 $P < 0.0001$	7	35	—	Brown Forsythe test Dunnet T3
INF-ɣ	F (6, 10) = 57.52 $P < 0.0001$	7	35	—	Brown Forsythe test Dunnet T3
INF-ɣ/IL-10	F (6, 5) = 31.18 $P < 0.0001$	7	35	—	Brown Forsythe test Dunnet T3
IL-17A	F (6, 14) = 52.85 $P < 0.0001$	7	35	—	Brown Forsythe test Dunnet T3
IL-23p19	F (6, 23) = 54.29 $P < 0.0001$	7	35	—	Brown Forsythe test Dunnet T3

3. Results

3.1. Effects of Noscapine on the Ear Thickness, Erythema, Scales, and Ear Length. The right ear pinna of the mice showed symptoms of erythema, scaling, and thickening a couple of days after commencing IMQ administration (Figure 1). In the IMQ group (II), the severity of psoriasis-like symptoms steadily increased until day ten compared to the sham group (Figures 1 and 2).

Our results showed that the IMQ 5% application significantly increased the ear thickness compared to the sham group ($P < 0.001$, Figure 2(a)). In contrast, all concentrations of NOS (0.3, 1, 3, and 10% w/w) significantly and concentration-dependently reduced the level of the ear thickness compared to the IMQ-treated alone group ($P < 0.001$ for all cases). Furthermore, the trend of thickness reduction in the treated groups was observed from day seven at 0.3, 1, and 3% w/w of noscapine concentrations ($P < 0.001$ for all cases, Figure 2(a)) and from day six in NOS 10% w/w ($P < 0.001$, Figure 2(a)).

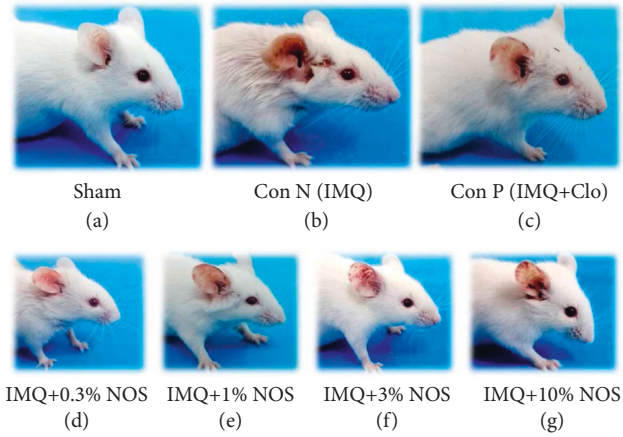

Figure 1: Severity of psoriasis-like symptoms in all groups for ten days was showing (a) sham group, (b) negative control group, (c) positive group, (d) sample group received IMQ plus 0.3% w/w NOS, (e) sample group received IMQ plus 1% w/w NOS, (f) sample group received IMQ plus 3% w/w NOS, and (g) sample group received IMQ plus 10% w/w NOS.

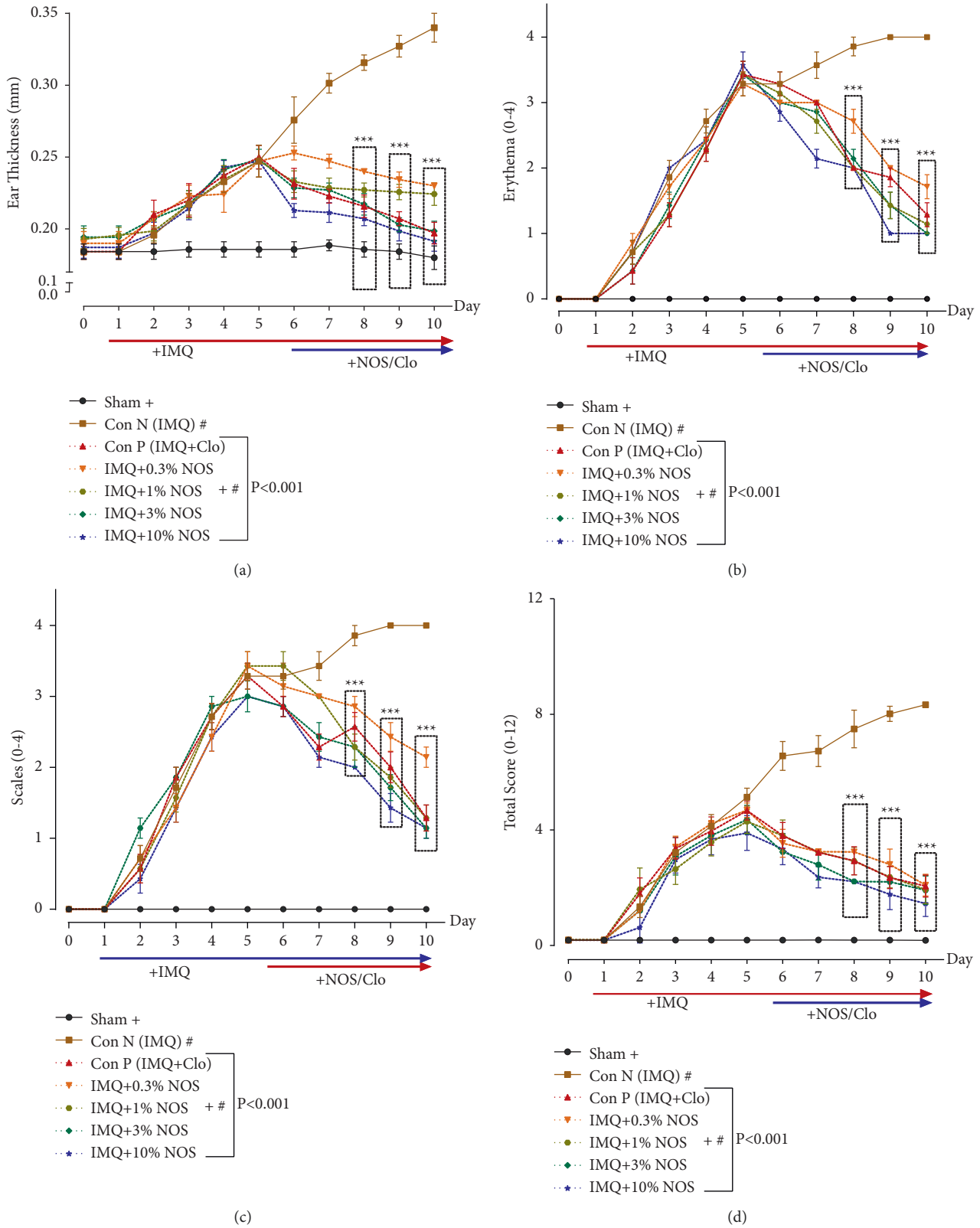

Figure 2: Continued.

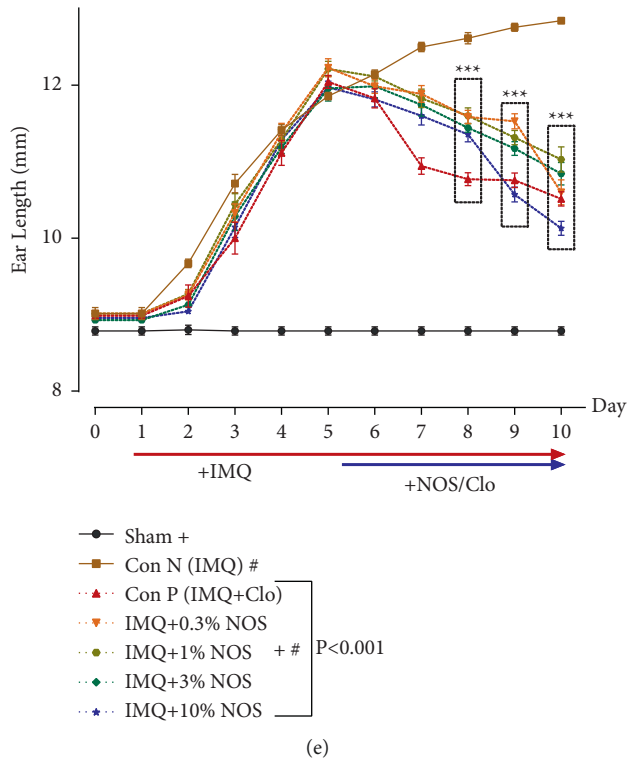

Figure 2: Phenotypical observations of ear pinna in treated mice groups. The symptoms of the thickness (a), erythema (b), scaling (c), the total score (d), and ear length (e) after commencing IMQ administration right ear pinna of the mice. The results are expressed as the mean ± SD ($n = 7$ in each group). The results indicate significant changes in the sham and negative control group ($^{***}P < 0.001$).

The results also showed an upward trend in inflammation and redness in all groups, up to day five of psoriasis induction. This study shows that all concentrations of NOS had a reducing effect on the amount of erythema compared to the IMQ-treated alone group ($P < 0.001$ for all cases, Figure 2(b)).

Scales (0–4) indicated the focal formation of inflamed and prominent plaques in different groups due to the overgrowth of skin epithelial cells. Scoring ranges are from zero to four based on each mouse's erythema, scaling, and thickening. Our results indicated that the application of different concentrations of NOS (0.3, 1, 3, and 10% w/w) significantly reduced the scale range from day eight compared to the control group ($P < 0.001$ for all cases, Figure 2(c)). However, NOS 3% w/w (2.429 ± 0.202, $P < 0.001$, Figure 2(c)) and NOS 10% w/w (2.143 ± 0.143, $P < 0.001$, Figure 2(c)) had a significant reduction effect on scales on the treatment groups from day seven (Figure 2(c)).

In addition, our findings also demonstrated that the total score in the control group received IMQ was significantly increased compared to the sham group ($P < 0.001$, Figure 2(d)). On the contrary, the application of different concentrations of NOS (0.3, 1, 3, and 10% w/w) and also Clo significantly diminished the total score from day eight compared to the control group ($P < 0.001$ for all cases, Figure 2(d)).

The results showed a significant increase in ear length during the use of IMQ compared to the sham group ($P < 0.001$, Figure 2(e)). In contrast, the application of different concentrations of NOS (0.3, 1, 3, and 10% w/w) significantly attenuated the ear length from day eight compared to the control group ($P < 0.001$ for all cases, Figure 2(e)).

3.2. Effect of Noscapine on the Spleen and Body Weight. The results showed that IMQ 5% w/w on the ear led to a significant increase in the body weight compared to the sham group ($P < 0.001$, Figure 3(a)). However, different concentrations of NOS (1, 3, and 10% w/w) meaningfully and concentration-dependently reduced the elevated body weight compared to the control group ($P < 0.001$ to 0.05 for all cases, Figure 3(a)).

The application of IMQ 5% w/w on the ear resulted in a significant elevation in the spleen weight compared to the sham group ($P < 0.001$, Figure 3(b)). The use of each Clo ($P < 0.05$), NOS 1% w/w ($P < 0.01$), NOS 1% w/w ($P < 0.001$), NOS 3% w/w ($P < 0.001$), or NOS 10% w/w ($P < 0.001$) notably reduced the elevated spleen weight compared to the control group (Figure 3(b)).

Ear (Figure 3(c)) and spleen (Figure 3(d)) indices were calculated by dividing the net weight of each respected organ by the body weight. As a result, both ear ($P < 0.001$, Figure 3(c)) and spleen ($P < 0.001$, Figure 3(d)) indices were increased in the IMQ control group compared to the sham group. Experimentally, using each Clo or NOS (0.3, 1, 3, and 10% w/w) notably reduced the elevated ear ($P < 0.001$–0.01

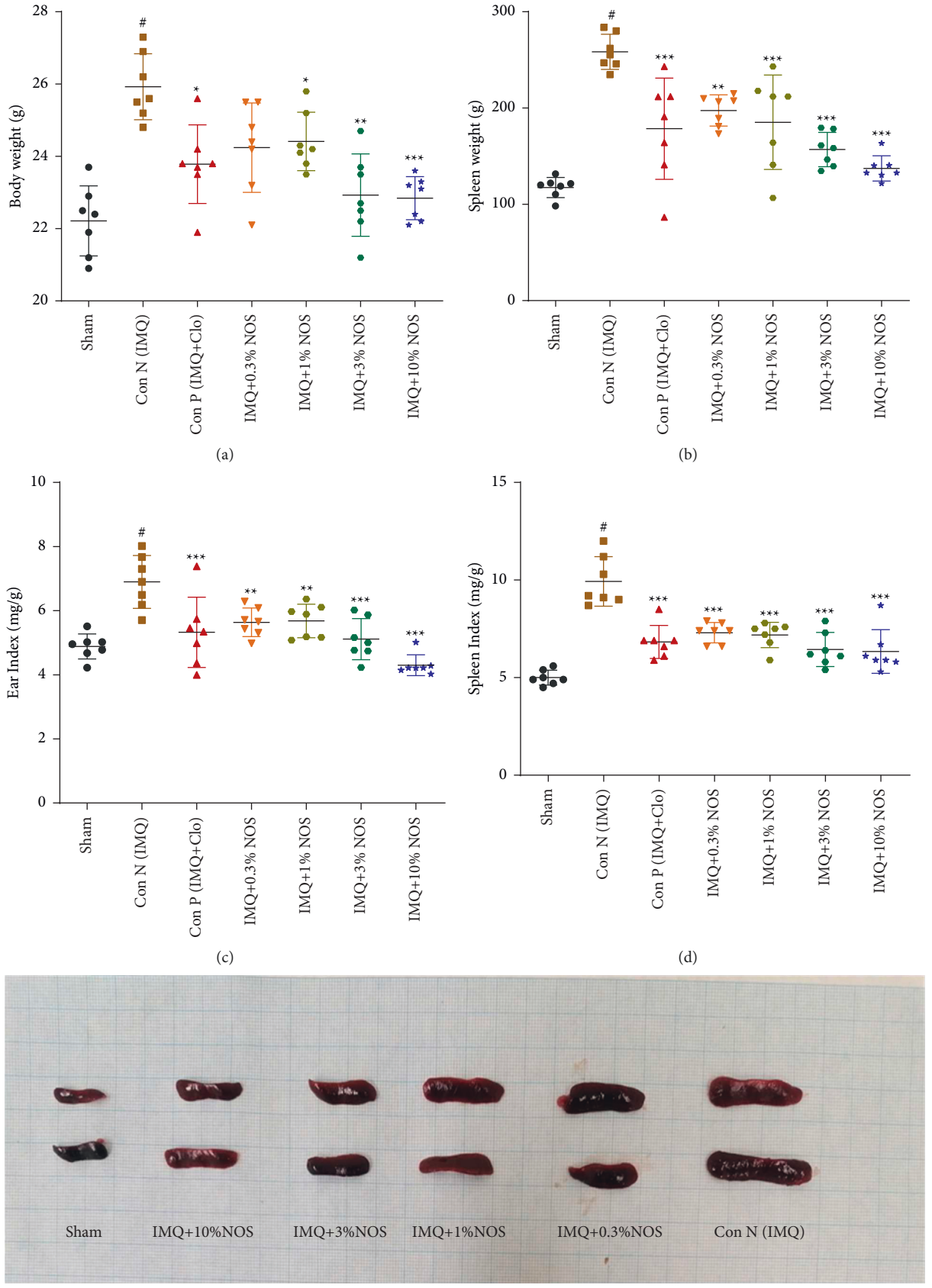

Figure 3: Continued.

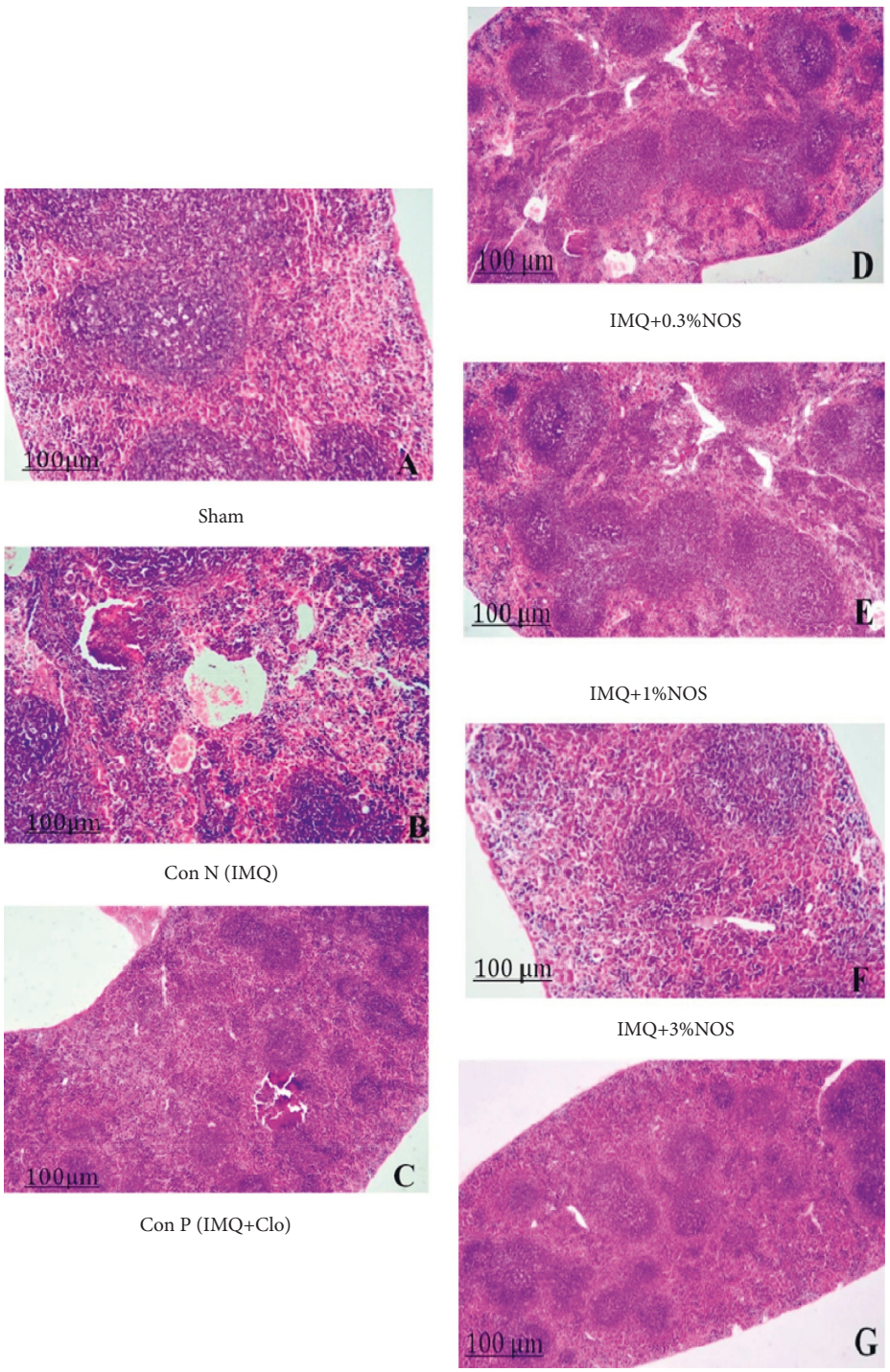

(f)

Figure 3: Investigation of mice in terms of body weight (a), the weight of the spleen (b), ear index (dividing weight of the ear to the bodyweight) (c), the spleen index (dividing weight of the spleen to the bodyweight) (d), representative photos of the spleen (e), and pathological investigation of the spleen (f), respectively showed in Figures 3(a)–3(f). The results are expressed as the mean ± SD ($n = 7$ in each group). The results indicate significant changes compared to the negative control group ($^{***}P < 0.001$, $^{**}P < 0.01$ and $^{*}P < 0.05$).

for all cases, Figure 3(c)) and spleen ($P < 0.001$ for all cases, Figure 3(d)) indices compared to the control group.

Additionally, Figure 3(e) represents the spleen length of each group, including A: negative control group, B: positive group, C: sample group received IMQ plus 0.3% w/w NOS, D: sample group received IMQ plus 1% w/w NOS, E: sample group received IMQ plus 3% w/w NOS, F: sample group received IMQ plus 10% w/w NOS. Moreover, Figure 3(f) shows the spleen's normal white pulp and abnormal red pulp in various groups.

3.3. Effect of Noscapine on the Scratching Behavior. The spontaneous scratch bouts were continuously greater in IMQ-treated mice than in control animals and steadily increased with time compared to the sham group ($P < 0.001$, Figure 4(a)). The rate of pruritus in the groups receiving IMQ increased sharply, while this rate increased significantly on days two to five and remained at its maximum until day five of psoriasis induction (Figure 4(a)). Reduction of pruritus was observed considerably in treated mice from day seven at doses of 1% w/w (255.7 ± 5.2), 3% w/w (248.5 ± 4.5), and 10% w/w NOS (196.2 ± 29.2) ($P < 0.001$ for all cases, Figure 4(a)). H&E staining of spinal cord sections revealed marked areas of necrosis with vacuolization of cells (Figure 4(b)).

3.4. Effect of Noscapine on the Concentration of the Cytokines. ELISA assays were used to assess inflammatory cytokines, essentials for inflammation in ear tissues of normal, IMQ-received, and NOS treated groups. In-ear skin samples from IMQ-received mice, levels of TNF-α-mediated cytokines, notably TGF-β, IL-6, IFN-γ, IL-17, and IL-23p19, were substantially increased compared to the sham group ($P < 0.001$ for all cases, Figures 5(a)–5(h)). In contrast, different concentrations of NOS (1, 3, and 10% w/w) significantly and concentration-dependently decreased in TNF-α, TGF-β, IFN-γ, IL-6, IFN-γ/IL-10, IL-17A, and IL-23p19 and also increased in the IL-10 expression in comparison to the control group ($P < 0.001$–0.05 for all cases, Figures 5(a)–5(h)).

3.5. Effect of Noscapine on the Histopathological Examination. H&E and Masson's trichrome staining (Figures 6(a) and 6(b)) of tissues were stained for each sample and photographed with a digital camera microscope (Nikon, Eclipse E200). Stained slices of IMQ-treated right ear pinnas were determined to match phenotypic findings and PASI score values. The pathologic changes in the ear pinna of various groups were acanthosis (Figure 6(c)), parakeratosis (Figure 6(d)) and thickening of the subepidermal layer (Figure 6(e)). These factors were evaluated semiquantitatively on a scale of 0–10 (0 = no change from untreated ears; 10 = maximum).

The IMQ-treated mice's right ear pinna sections revealed substantially enhanced acanthosis ($P < 0.001$, Figure 6(c)), parakeratosis, ($P < 0.001$, Figure 6(d)) and thickening of the subepidermal layer ($P < 0.001$, Figure 6(e)) in comparison to the control group (Figures 6(a) and 6(b)). The results also demonstrated that applying NOS (0.3, 1, 3, and 10% w/w), or Clo significantly reduced acanthosis ($P < 0.001$–0.01 for all cases, Figure 6(c)), parakeratosis ($P < 0.001$–0.01 for all cases, Figure 6(d)), and thickening of the subepidermal layer ($P < 0.001$ for all cases, Figure 6(e)) in comparison to the control group.

3.6. Effect of Noscapine on the Immunohistochemical Examination. Immunohistochemistry (IHC) staining was performed to detect p53 as a marker of cell apoptosis (Figure 7(a)) and Ki-67 as a cell proliferation marker (Figure 7(b)) based on the kit protocols by light microscopy. Positive p53 was presented in the subepidermal layer viewed by the brown nuclei of epidermal cells. Furthermore, positive Ki-67 was shown in the epidermis and considered by the brown nuclei of epidermal cells. Additionally, Figure 7(c) also presented a histopathological score of examined tissues semiquantitatively on a scale of 0–10 (0 = no change from untreated ears; 10 = maximum change in treated ears). In this regard, we found that the histology score was significantly increased in the IMQ-control group compared to the sham group ($P < 0.001$, Figure 7(c)). In contrast, applying NOS (0.3, 1, 3, and 10% w/w) or Clo significantly reduced the histology score compared to the control group ($P < 0.001$ for all cases, Figure 7(c)).

4. Discussion

To the best of our knowledge, this is the first study that evaluated the protective effects of noscapine against the IMQ-induced mouse model. As a result, we revealed that noscapine concentration-dependently and significantly reduced the inflammation and psoriatic manifestation of IMQ by lowering the ear thickness and length and modulating the apoptosis (p53) and cell proliferative (Ki-67) factors.

Since the prevalence of pruritus in patients with psoriasis has been reported to be 60%–90%, and many patients with psoriasis consider pruritus to be the most annoying symptom [39, 40], this study also examined and showed significant results of the therapeutic effects of noscapine in the pruritus induction model by IMQ. In line with the present investigation, numerous studies have evaluated the prevalence of pruritus in patients with psoriasis. Still, in general, only a focused treatment with a molecular signaling survey can relieve the itching associated with psoriasis [41]. Psoriasis is a chronic inflammatory and autoimmune disease in which epithelial cell proliferation increases compared to normal skin [42]. The effects of methotrexate and clobetasol on cell proliferation [43] and the impact of these drugs on the immune system justify the effectiveness of these drugs in this disease that some patients might be sensitive to during long-term treatment [44]. Noscapine as an old drug has significant clinical effects, including antitussive properties and cell proliferation. Hence, we tried to evaluate the effectiveness of topical administration noscapine in the animal model of psoriasis. Following the results of this research, it is possible to continue studies in the human phase [45].

The results showed that the reduction in thickness and skin inflammation occurred from day seven in all concentrations of noscapine. In fact, we found that noscapine can reduce fibrosis and also inflammation in the ear by reducing the inflammatory mediators (TNF-α, TGF-β, IFN-γ, IL-6,

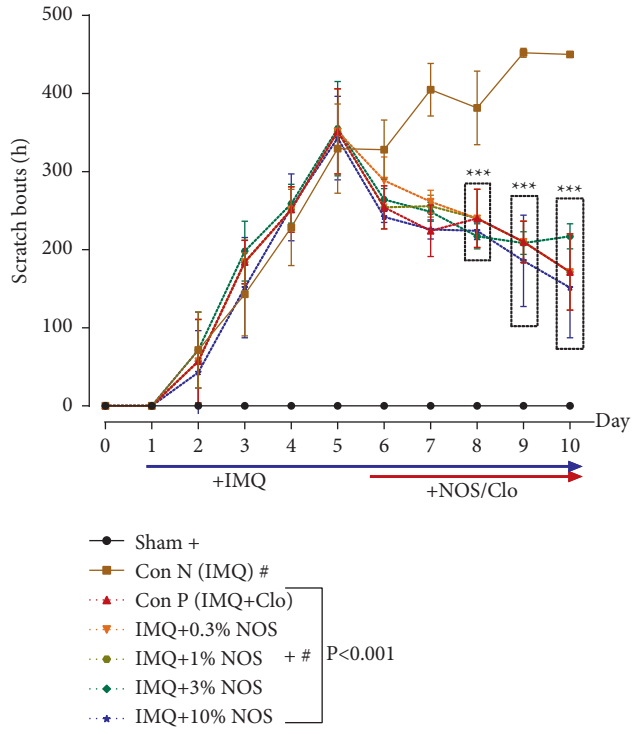

(a)

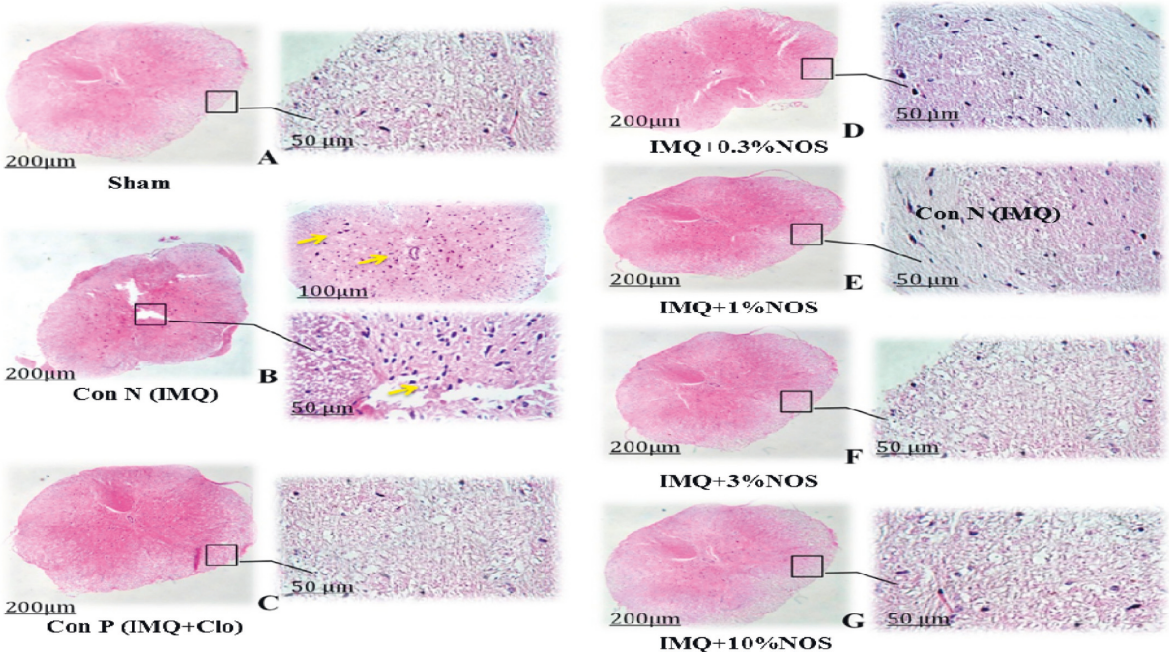

(b)

Figure 4: Number of scratching behavior in IMQ-induced psoriasis-like skin (a) and also H&E staining of cord sections revealed marked areas of necrosis with vacuolization of cells (b). The results are expressed as the mean ± SD ($n = 7$ in each group). The results indicate significant changes compared to the negative control group ($^{***}P < 0.001$).

IL-17, and IL-23p19), increasing IL-10 as an anti-inflammatory cytokine and modulating the apoptosis (p53) and cell proliferative (Ki-67) factors. The present study's findings were consistent with the results of other studies that indicated that topical administration of capsaicin significantly inhibited skin inflammation [46]. This reduction in thickness was not significant in the positive control group receiving the clobetasol from day six of treatment, indicating the superiority of the topical form of noscapine over the clobetasol application. Similar results were obtained in the therapeutic

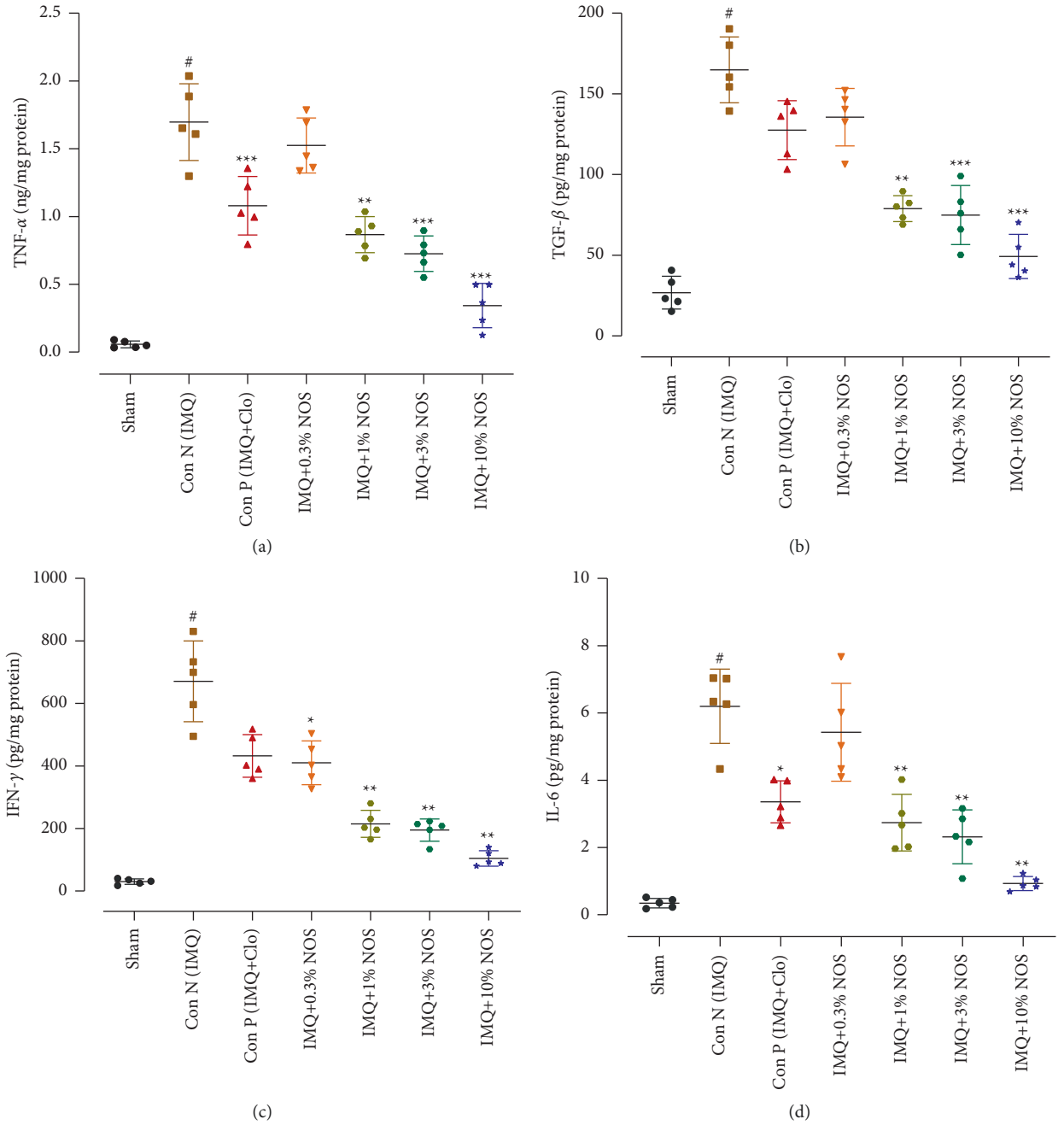

Figure 5: Continued.

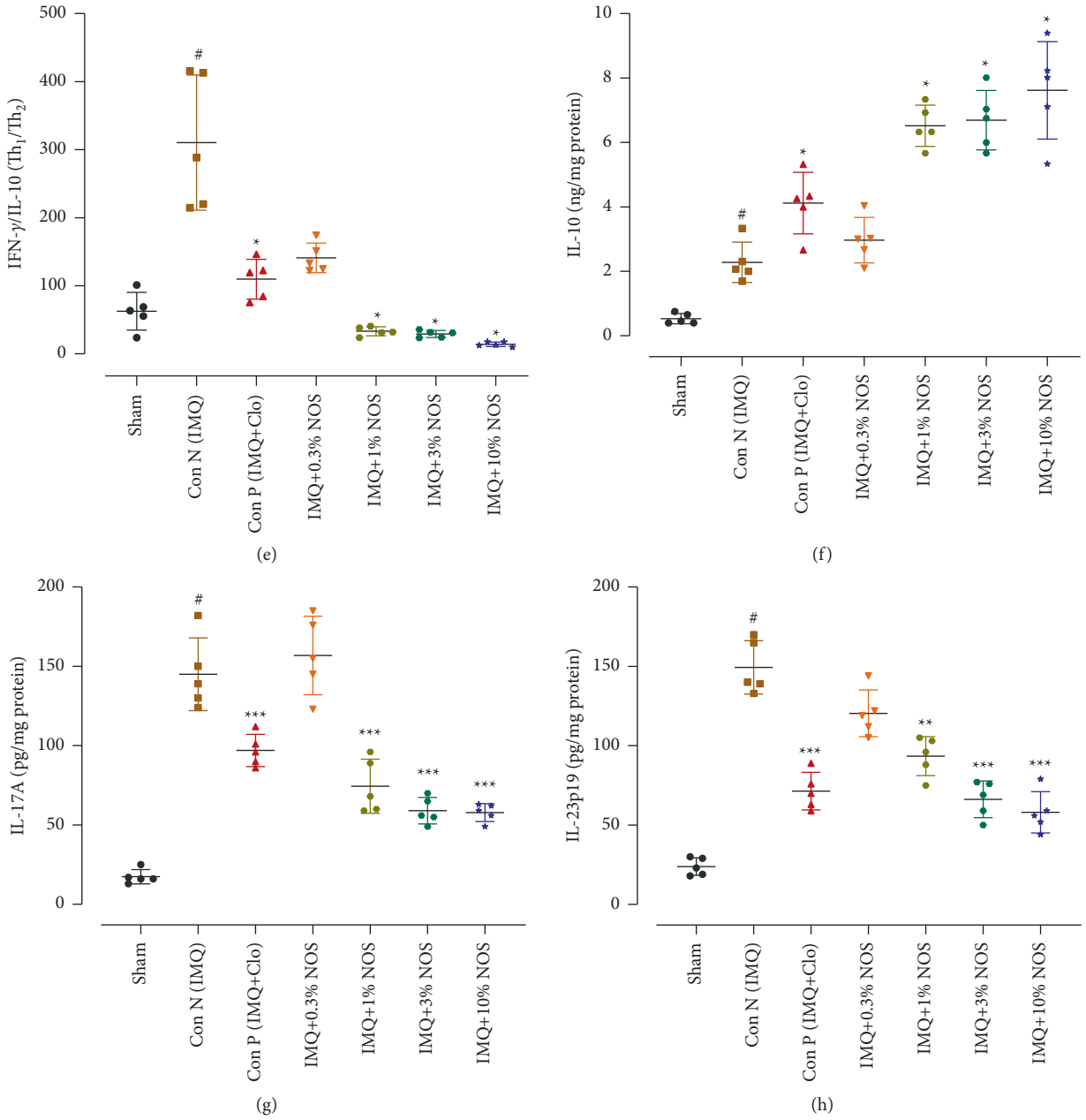

FIGURE 5: Concentration of cytokines levels such as TNF-α (a), TGF-β (b), IFN-γ (c), IL-6 (d), IFN-γ/IL-10 (e), IL-10 (f), IL-17A (g), and IL-23p19 (h), respectively, showed in Figure 5(a)–5(h). The results are expressed as the mean ± SD ($n = 7$ in each group). The results indicate significant changes compared to the negative control group ($^{***}P < 0.001$, $^{**}P < 0.01$, and $^{*}P < 0.05$).

effects of curcumin from day 6 of treatment in reducing inflammation and skin thickness in psoriasis-induced mice [47].

Numerous studies have reported the potent and significant antioxidant activity of noscapine [23, 48] in reducing the NF-κB expression, which leads to a decrease in cytokine production by T-cells [23, 49, 50]. Currently, we demonstrated that noscapine considerably inhibited the pro-inflammatory mediator productions such as TNF-α or IFNγ. Our evidence suggests that noscapine has high antioxidant activity and substantially decrease the transcription of the TNF-α signaling indicator, resulting in a reduction in T-cell cytokine production. It was shown that TNF-α-mediated cytokines, TGF-β, IL-6, and IFNγ were considerably reduced in the noscapine treated groups than the positive control group. Our results align with previous studies that pointed out the anti-inflammatory properties of noscapine, primarily via modulating the NF-κB signaling pathway in chemotherapeutic agents [23, 51]. Accordingly, noscapine treatment could impress the release of pro-inflammatory cells cytokines due to environmental stress and stress-activated protein kinases [52]. In this regard, similar researches show that TLR-mediated TNF-α and nitric oxide (NO) production in human and murine macrophages was inhibited by

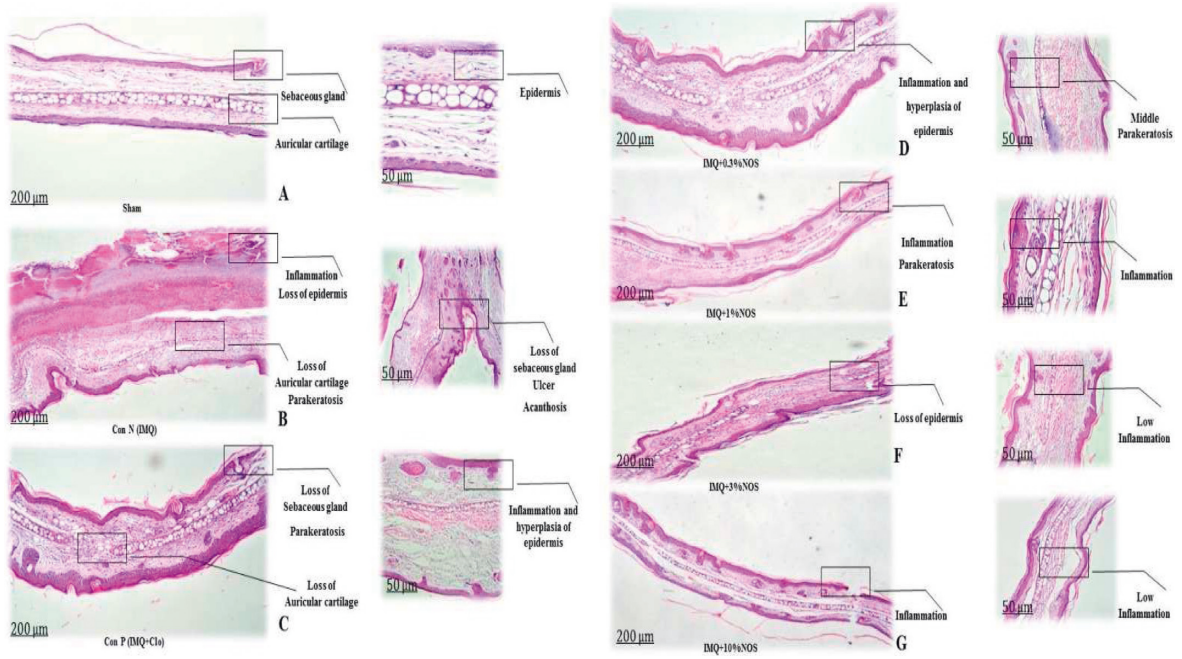

(a)

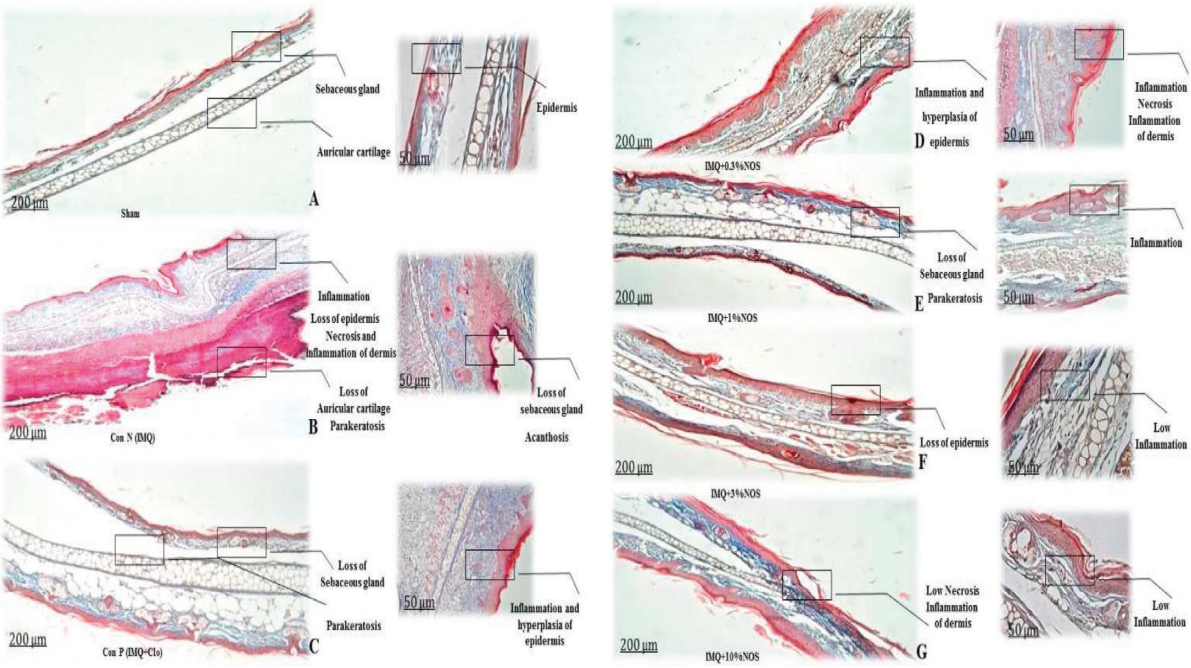

(b)

Figure 6: Continued.

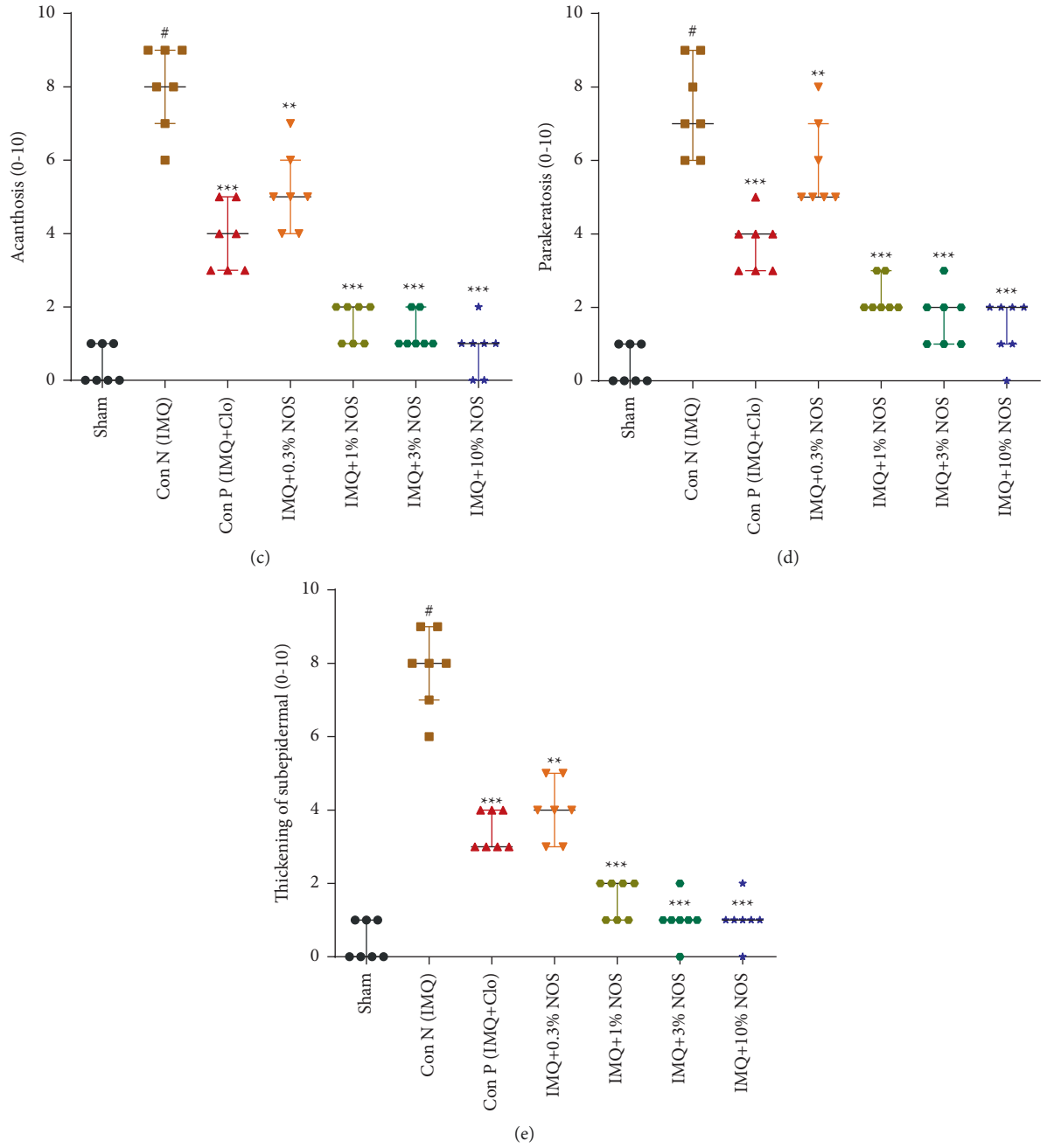

FIGURE 6: Hematoxylin and eosin (a) and trichrome staining (b) were presented for each sample. The pathologic changes in the ear pinna of various groups were included: acanthosis (c) parakeratosis (d) and thickening of the subepidermal layer (e) The data are expressed as the median ± IQR, ($n = 7$ in each group). The results also indicate significant changes compared to the negative control group ($^{***}P < 0.001$, $^{**}P < 0.01$ and $^{*}P < 0.05$).

brominated noscapine analogues (Br-nos and Red-Br-nos) with no indication of cellular damage [23]. Brominated noscapine analogs also reduced cytokine/chemokine (a non-TLR ligand)-induced sterile inflammation [23, 53].

It has been reported that IL-10 production has therapeutic benefits as common anti-psoriatic treatments on several cell types [54]. In this context, the present research results showed that treatment with all concentrations of noscapine except 0.3% NOS increases the level of IL-10. Furthermore, the current study results showed the effectiveness of a high concentration of noscapine (10%w/w) in regulating the expression of pro-inflammatory cytokines. Although definite mechanisms and signaling pathways in reducing these cytokines are indeterminate yet [23, 54], we believe that noscapine's antiproliferative and anti-inflammatory effects act through the suppression of TNF-α/IFNγ, which results in more severe inflammation and keratinocyte proliferation. These findings are inconsistent with previous research that the anti-psoriatic effects of the Wannachawee recipe significantly inhibited the TNF-α and IFNγ-

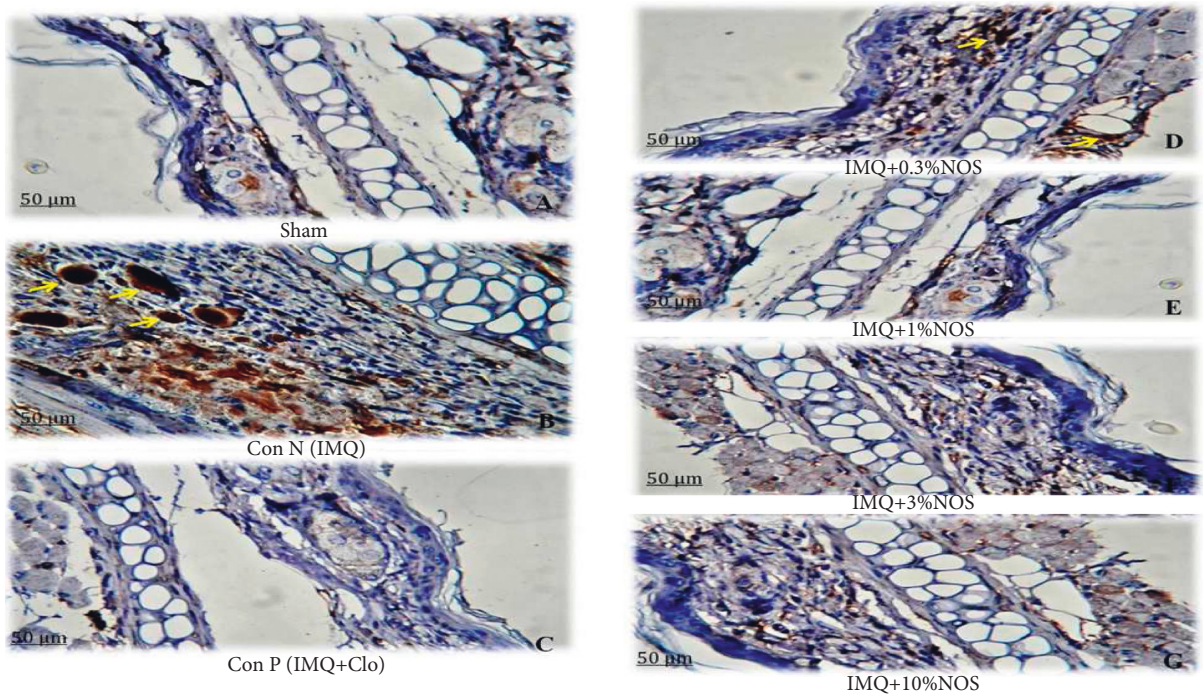

(a)

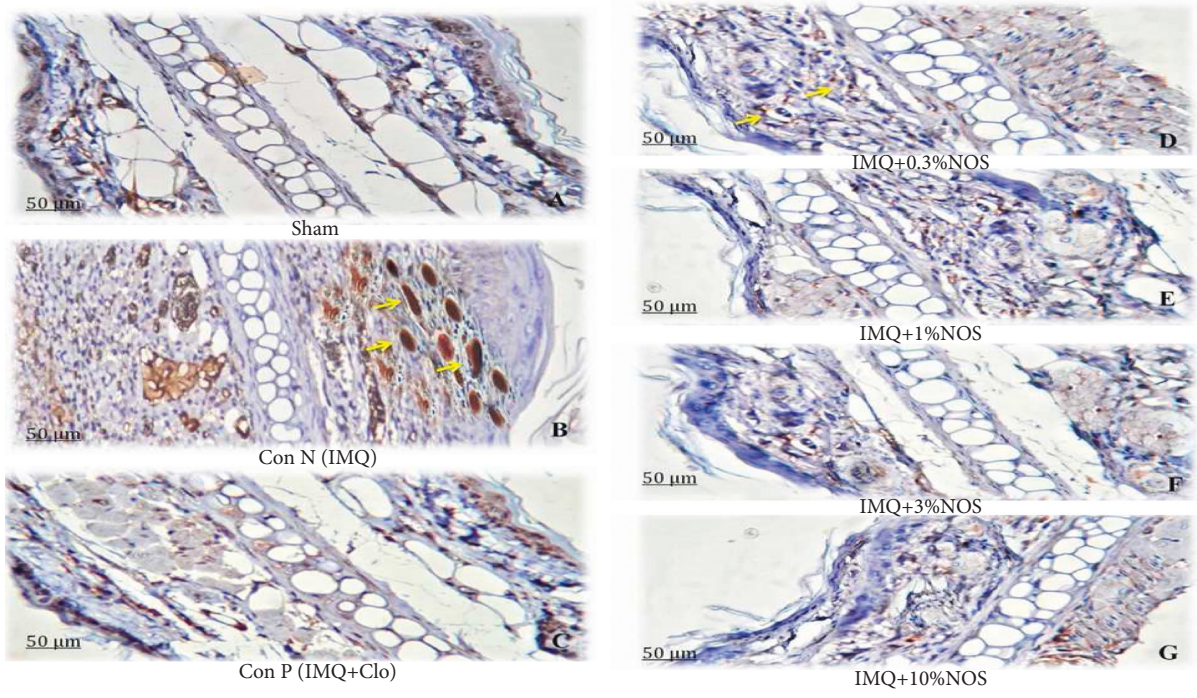

(b)

Figure 7: Continued.

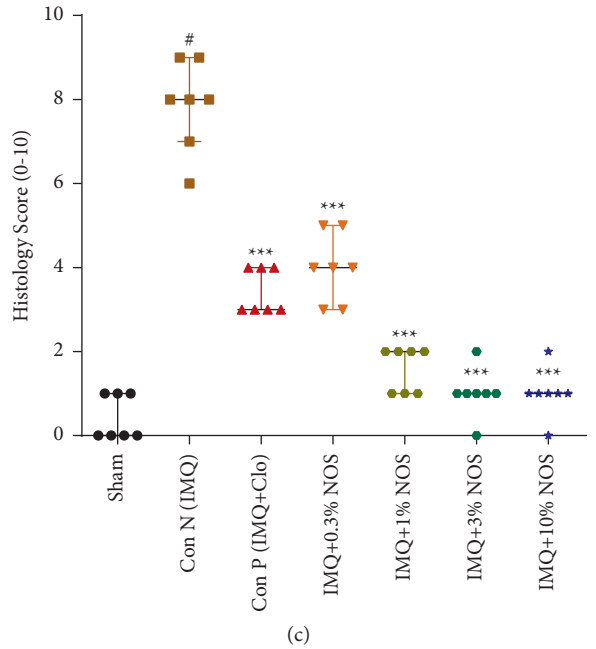

Figure 7: Immunohistochemistry (IHC) staining for p53 protein (a) and Ki-67 protein (b) as specific antigen in an ear tissue based on antigen-antibody reaction by light microscopy. The histopathological score of examined tissues (c) is expressed as the median ± IQR, ($n = 7$ in each group). The results also indicate significant changes compared to the negative control group ($^{***}P < 0.001$, $^{**}P < 0.01$ and $^{*}P < 0.05$).

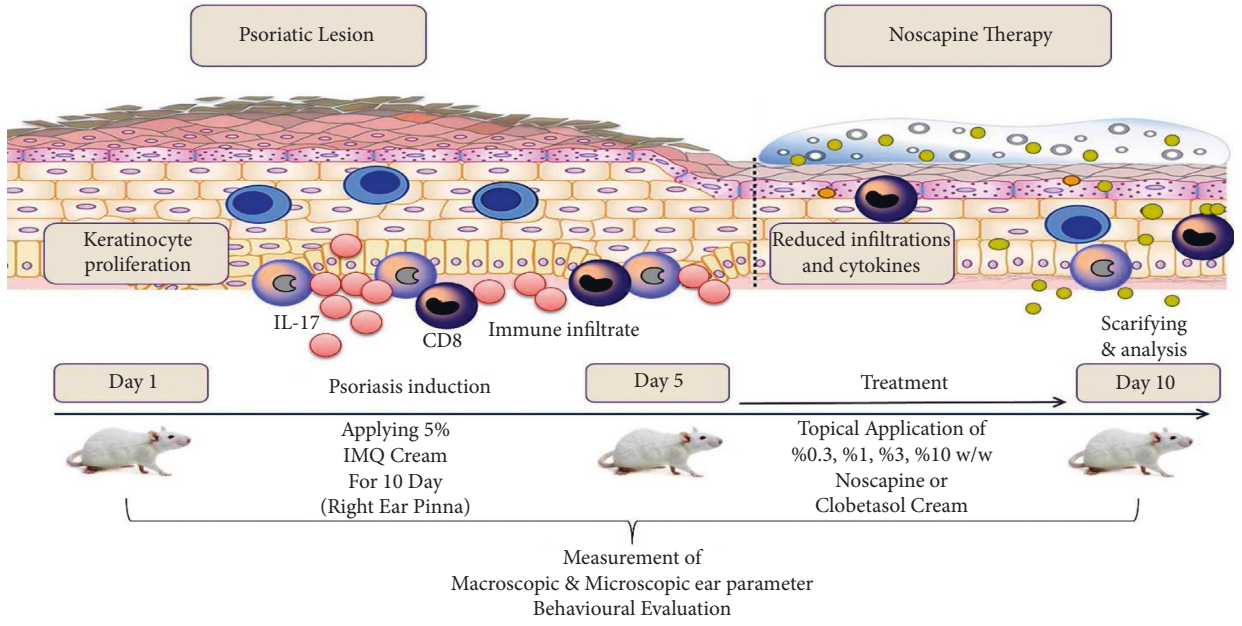

Figure 8: NOS alleviates IMQ-induced psoriasis-like skin lesions.

stimulated IL-17A, IL-22, and IL-23 secretion in HaCaT cells [26]. Although specific anti-inflammatory signaling pathways of noscapine in psoriasis induction are undefined, based on the current study results, we proposed that noscapine's antiproliferative and anti-inflammatory effect operates through the suppression of TNF-α/IFNγ/IL-23.

In conclusion, despite this investigation, it is well documented that noscapine can be considered as one of the therapeutic drugs in psoriasis disease and is widely evaluated in clinical trials studies. Figure 8 shows a graphical abstract of the procedure and possible protective mechanism of NOS against IMQ-induced psoriasis-like skin lesions.

Abbreviations

H and E: Hematoxylin and eosin
IFN-γ: Interferon-γ
IL-10: Interleukin 10
IL-17: Interleukin 17
IL-23p19: Interleukin 23p19
IL-6: Interleukin 6
IMQ: Imiquimod
NOS: Noscapine
PASI: Psoriasis area and severity index
PDCs: Plasmacytoid dendritic cell
TGF-β: Transforming growth factor-β
TLR: Toll-like receptor
TNF-α: Tumor necrosis factor-α.

Data Availability

The data used to support the findings of this study are available from the first author (F.N) upon reasonable request.

Ethical Approval

The study was conducted in compliance with ethical standards

Conflicts of Interest

The authors declare that they have no conflicts of interest.

Acknowledgments

The presented results in this paper were elicited from the PhD student project and research protocol (990587), which was supported financially by the vice-chancellor for research, Mashhad University of Medical Sciences, Mashhad, Iran.

References

[1] V. R. Askari, V. B. Rahimi, R. Zargarani, R. Ghodsi, M. Boskabady, and M. H. Boskabady, "Anti-oxidant and anti-inflammatory effects of auraptene on phytohemagglutinin (PHA)-induced inflammation in human lymphocytes," *Pharmacological Reports*, vol. 73, no. 1, pp. 154–162, 2021.

[2] V. R. Askari, V. Baradaran Rahimi, S. A. Tabatabaee, and R. Shafiee-Nick, "Combination of imipramine, a sphingomyelinase inhibitor, and β-caryophyllene improve their therapeutic effects on experimental autoimmune encephalomyelitis (EAE)," *International Immunopharmacology*, vol. 77, Article ID 105923, 2019.

[3] V. Baradaran Rahimi, V. R. Askari, and S. H. Mousavi, "Ellagic acid dose and time-dependently abrogates d-galactose-induced animal model of aging: investigating the role of PPAR-γ," *Life Sciences*, vol. 232, Article ID 116595, 2019.

[4] V. Baradaran Rahim, M. T. Khammar, H. Rakhshandeh, A. Samzadeh-Kermani, A. Hosseini, and V. R. Askari, "Crocin protects cardiomyocytes against LPS-Induced inflammation," *Pharmacological Reports*, vol. 71, no. 6, pp. 1228–1234, 2019.

[5] M. Boskabady, M. R. Khazdair, R. Bargi et al., "Thymoquinone ameliorates lung inflammation and pathological changes observed in lipopolysaccharide-induced lung injury," *Evidence-Based Complementary and Alternative Medicine*, vol. 2021, Article ID 6681729, 10 pages, 2021.

[6] M. Sticherling, "Psoriasis and autoimmunity," *Autoimmunity Reviews*, vol. 15, no. 12, pp. 1167–1170, 2016.

[7] T. Henseler and E. Christophers, "Disease concomitance in psoriasis," *Journal of the American Academy of Dermatology*, vol. 32, no. 6, pp. 982–986, 1995.

[8] R. Parisi, D. P. Symmons, C. E. Griffiths, and D. M. Ashcroft, "Global epidemiology of psoriasis: a systematic review of incidence and prevalence," *Journal of Investigative Dermatology*, vol. 133, no. 2, pp. 377–385, 2013.

[9] J. E. Gudjonsson and J. T. Elder, "Psoriasis: epidemiology," *Clinics in Dermatology*, vol. 25, no. 6, pp. 535–546, 2007.

[10] N. D. Loft, L. Skov, M. K. Rasmussen et al., "Genetic polymorphisms associated with psoriasis and development of psoriatic arthritis in patients with psoriasis," *PLoS One*, vol. 13, no. 2, Article ID e0192010, 2018.

[11] A. L. Neimann, S. B. Porter, and J. M. Gelfand, "The epidemiology of psoriasis," *Expert Review of Dermatology*, vol. 1, no. 1, pp. 63–75, 2006.

[12] F. Benhadou, D. Mintoff, and V. Del Marmol, "Psoriasis: keratinocytes or immune cells–which is the trigger?" *Dermatology*, vol. 235, no. 2, pp. 91–100, 2019.

[13] L. Flatz and C. Conrad, "Role of T-cell-mediated inflammation in psoriasis: pathogenesis and targeted therapy," *Psoriasis: Targets and Therapy*, vol. 3, pp. 1–10, 2013.

[14] Y. Deng, C. Chang, and Q. Lu, "The inflammatory response in psoriasis: a comprehensive review," *Clinical Reviews in Allergy & Immunology*, vol. 50, no. 3, pp. 377–389, 2016.

[15] A. Ueyama, M. Yamamoto, K. Tsujii et al., "Mechanism of pathogenesis of imiquimod-induced skin inflammation in the mouse: a role for interferon-alpha in dendritic cell activation by imiquimod," *The Journal of Dermatology*, vol. 41, no. 2, pp. 135–143, 2014.

[16] A. El Tawdy, I. M. Amin, R. Abdel Hay, A. S. Hassan, Z. S. Gad, and L. A. Rashed, "Toll-like receptor (TLR) 7 expression in mycosis fungoides and psoriasis: a case–control study," *Clinical and Experimental Dermatology*, vol. 42, no. 2, pp. 172–177, 2017.

[17] R. Rashmi, K. S. J. Rao, and K. H. Basavaraj, "A comprehensive review of biomarkers in psoriasis," *Clinical and Experimental Dermatology*, vol. 34, no. 6, pp. 658–663, 2009.

[18] A. K. Gupta, M. Browne, and R. Bluhm, "Imiquimod: a review," *Journal of Cutaneous Medicine and Surgery*, vol. 6, no. 6, pp. 554–560, 2002.

[19] M. Schön and M. Schön, "Imiquimod: mode of action," *British Journal of Dermatology*, vol. 157, pp. 8–13, 2007.

[20] S. Shen, T. O'Brien, L. M. Yap, H. M. Prince, and C. J. McCormack, "The use of methotrexate in dermatology: a review," *Australasian Journal of Dermatology*, vol. 53, no. 1, pp. 1–18, 2012.

[21] J. Seetharaman and S. Rajan, "Crystal and molecular structure of noscapine 1," *Zeitschrift für Kristallographie-Crystalline Materials*, vol. 210, no. 2, pp. 111–113, 1995.

[22] F. Nourbakhsh and V. R. Askari, "Biological and pharmacological activities of noscapine: focusing on its receptors and mechanisms," *BioFactors*, vol. 47, no. 6, pp. 975–991, 2021.

[23] P. Rahmanian-Devin, V. Baradaran Rahimi, M. R. Jaafari, S. Golmohammadzadeh, Z. Sanei-far, and V. R. Askari, "Noscapine, an emerging medication for different diseases: a mechanistic review," *Evidence-based Complementary and Alternative Medicine*, vol. 2021, Article ID 8402517, 16 pages, 2021.

[24] X. Chen, T.-T. T. Dang, and P. J. Facchini, "Noscapine comes of age," *Phytochemistry*, vol. 111, pp. 7–13, 2015.

[25] H. Singh, P. Singh, K. Kumari, A. Chandra, S. K Dass, and R. Chandra, "A review on noscapine, and its impact on heme metabolism," *Current Drug Metabolism*, vol. 14, no. 3, pp. 351–360, 2013.

[26] M. Na Takuathung, A. Wongnoppavich, A. Panthong et al., "Antipsoriatic effects of wannachawee recipe on imiquimod-induced psoriasis-like dermatitis in BALB/c mice," *Evidence-Based Complementary and Alternative Medicine*, vol. 2018, Article ID 7931031, 13 pages, 2018.

[27] K. Sakai, K. M. Sanders, M. R. Youssef et al., "Mouse model of imiquimod-induced psoriatic itch," *Pain*, vol. 157, no. 11, pp. 2536–2543, 2016.

[28] A. Jaafari, V. Baradaran Rahimi, N. Vahdati-Mashhadian et al., "Evaluation of the therapeutic effects of the hydro-ethanolic extract of *Portulaca oleracea* on surgical-induced peritoneal adhesion," *Mediators of Inflammation*, vol. 2021, Article ID 8437753, 18 pages, 2021.

[29] A. T. Feldman and D. Wolfe, "Tissue processing and hematoxylin and eosin staining," *Histopathology*, pp. 31–43, Springer, Berlin, Germany, 2014.

[30] N. C. Foot, "The masson trichrome staining methods in routine laboratory use," *Stain Technology*, vol. 8, no. 3, pp. 101–110, 1933.

[31] S. Y. Park, D. Gupta, R. Hurwich, C. H. Kim, and R. Dziarski, "Peptidoglycan recognition protein Pglyrp2 protects mice from psoriasis-like skin inflammation by promoting regulatory T cells and limiting Th17 responses," *The Journal of Immunology*, vol. 187, no. 11, pp. 5813–5823, 2011.

[32] F. M. Hofman and C. R. Taylor, "Immunohistochemistry," *Current Protocols in Immunology*, vol. 103, no. 1, p. 21, 2013.

[33] A.-A. Grosset, K. Loayza-Vega, É. Adam-Granger et al., "Hematoxylin and eosin counterstaining protocol for immunohistochemistry interpretation and diagnosis," *Applied Immunohistochemistry & Molecular Morphology*, vol. 27, no. 7, pp. 558–563, 2019.

[34] M. M. Bradford, "A rapid and sensitive method for the quantitation of microgram quantities of protein utilizing the principle of protein-dye binding," *Analytical Biochemistry*, vol. 72, no. 1-2, pp. 248–254, 1976.

[35] V. Baradaran Rahimi, A. Rajabian, H. Rajabi et al., "The effects of hydro-ethanolic extract of Capparis spinosa (C. spinosa) on lipopolysaccharide (LPS)-induced inflammation and cognitive impairment: evidence from in vivo and in vitro studies," *Journal of Ethnopharmacology*, vol. 256, Article ID 112706, 2020.

[36] M. J. Curtis, R. A. Bond, D. Spina et al., "Experimental design and analysis and their reporting: new guidance for publication in BJP," *British Journal of Pharmacology*, vol. 172, no. 14, pp. 3461–3471, 2015.

[37] C. H. George, S. C. Stanford, S. Alexander et al., "Updating the guidelines for data transparency in the British Journal of Pharmacology - data sharing and the use of scatter plots instead of bar charts," *British Journal of Pharmacology*, vol. 174, no. 17, pp. 2801–2804, 2017.

[38] S. P. H. Alexander, R. E. Roberts, B. R. S. Broughton et al., "Goals and practicalities of immunoblotting and immunohistochemistry: a guide for submission to the British Journal of Pharmacology," *British Journal of Pharmacology*, vol. 175, no. 3, pp. 407–411, 2018.

[39] A. G. Bahali, N. Onsun, O. Su et al., "The relationship between pruritus and clinical variables in patients with psoriasis," *Anais Brasileiros de Dermatologia*, vol. 92, no. 4, pp. 470–473, 2017.

[40] G. Yosipovitch, A. Goon, J. Wee, Y. Chan, and C. Goh, "The prevalence and clinical characteristics of pruritus among patients with extensive psoriasis," *British Journal of Dermatology*, vol. 143, no. 5, pp. 969–973, 2000.

[41] S. Kahremany, L. Hofmann, M. Harari, A. Gruzman, and G. Cohen, "Pruritus in psoriasis and atopic dermatitis: current treatments and new perspectives," *Pharmacological Reports*, vol. 73, no. 2, pp. 443–453, 2021.

[42] H. Valdimarsson, R. H. Thorleifsdottir, S. L. Sigurdardottir, J. E. Gudjonsson, and A. Johnston, "Psoriasis–as an autoimmune disease caused by molecular mimicry," *Trends in Immunology*, vol. 30, no. 10, pp. 494–501, 2009.

[43] N. Vincent, D. D. Ramya, and H. B. Vedha, "Progress in psoriasis therapy via novel drug delivery systems," *Dermatology Reports*, vol. 6, no. 1, 2014.

[44] P. Zwicky, S. Unger, and B. Becher, "Targeting interleukin-17 in chronic inflammatory disease: a clinical perspective," *Journal of Experimental Medicine*, vol. 217, no. 1, 2020.

[45] M. Mahmoudian and P. Rahimi-Moghaddam, "The anti-cancer activity of noscapine: a review," *Recent Patents on Anti-Cancer Drug Discovery*, vol. 4, no. 1, pp. 92–97, 2009.

[46] P. R. Desai, S. Marepally, A. R. Patel, C. Voshavar, A. Chaudhuri, and M. Singh, "Topical delivery of anti-TNFα siRNA and capsaicin via novel lipid-polymer hybrid nanoparticles efficiently inhibits skin inflammation in vivo," *Journal of Controlled Release*, vol. 170, no. 1, pp. 51–63, 2013.

[47] J. Sun, Y. Zhao, and J. Hu, "Curcumin inhibits imiquimod-induced psoriasis-like inflammation by inhibiting IL-1beta and IL-6 production in mice," *PLoS One*, vol. 8, no. 6, Article ID e67078, 2013.

[48] A. Shaghaghi, A. Alirezalu, E. Nazarianpour, A. Sonboli, and S. Nejad-Ebrahimi, "Opioid alkaloids profiling and anti-oxidant capacity of Papaver species from Iran," *Industrial Crops and Products*, vol. 142, Article ID 111870, 2019.

[49] B. Sung, K. S. Ahn, and B. B. Aggarwal, "Noscapine, a benzylisoquinoline alkaloid, sensitizes leukemic cells to chemotherapeutic agents and cytokines by modulating the NF-κB signaling pathway," *Cancer Research*, vol. 70, no. 8, pp. 3259–3268, 2010.

[50] S. A. Ebrahimi, "Noscapine, a possible drug candidate for attenuation of cytokine release associated with SARS-CoV-2," *Drug Development Research*, vol. 81, no. 7, pp. 765–767, 2020.

[51] V. Tomar, S. Kukreti, S. Prakash, J. Madan, and R. Chandra, "Noscapine and its analogs as chemotherapeutic agent: current updates," *Current Topics in Medicinal Chemistry*, vol. 17, no. 2, pp. 174–188, 2016.

[52] A. T. Funding, C. Johansen, K. Kragballe et al., "Mitogen-and stress-activated protein kinase 1 is activated in lesional psoriatic epidermis and regulates the expression of pro-inflammatory cytokines," *Journal of Investigative Dermatology*, vol. 126, no. 8, pp. 1784–1791, 2006.

[53] S. Zughaier, P. Karna, D. Stephens, and R. Aneja, "Potent anti-inflammatory activity of novel microtubule-modulating brominated noscapine analogs," *PLoS One*, vol. 5, no. 2, Article ID e9165, 2010.

[54] K. Kingo, S. Koks, H. Silm, and E. Vasar, "IL-10 promoter polymorphisms influence disease severity and course in psoriasis," *Genes and Immunity*, vol. 4, no. 6, pp. 455–457, 2003.

Hindawi
Evidence-Based Complementary and Alternative Medicine
Volume 2022, Article ID 8251344, 12 pages
https://doi.org/10.1155/2022/8251344

Research Article

In Vitro Immunomodulatory Effects of *Inonotus obliquus* Extracts on Resting M0 Macrophages and LPS-Induced M1 Macrophages

Dayue Shen,[1] **Yating Feng**,[1] **Xilan Zhang**,[1] **Jing Liu**,[1] **Le Gong**,[1] **Hui Liao**,[2] **and Rongshan Li**[3]

[1]*School of Pharmacy, Shanxi Medical University, Taiyuan 030001, China*
[2]*Department of Pharmacy, Fifth Hospital of Shanxi Medical University (Shanxi Provincial People's Hospital), Taiyuan 030012, China*
[3]*Department of Nephrology, Fifth Hospital of Shanxi Medical University (Shanxi Provincial People's Hospital), Taiyuan 030012, China*

Correspondence should be addressed to Hui Liao; huiliao@263.net and Rongshan Li; rongshanli13@163.com

Received 27 January 2022; Revised 4 April 2022; Accepted 11 April 2022; Published 21 April 2022

Academic Editor: Xiang Liu

Background. *Inonotus obliquus* (Chaga) is a parasitic fungus that is distributed mainly in northeast China. Our literature research showed chaga polysaccharides have bilateral effects on tumor necrosis factor (TNF)-α and interleukin (IL)-1β levels when they exert antitumor and antidiabetic activities. The current research tried to explore the influence of chaga extracts on inflammatory factors via macrophage polarization which has bilateral immune-regulation not only on healthy tissue homeostasis but also on pathologies. *Methods*. Chaga was extracted with 100°C water and precipitated with 80% ethanol. The extracts were studied on RAW264.7 macrophage at resting condition (M0) and lipopolysaccharide (LPS)-activated subtype (classic activated macrophage, M1). The IL-1β, TNF-α, nitric oxide (NO) level, and the protein expressions of M1 and alternative activated macrophage (M2) markers including IL-1β, inducible NO synthase (iNOS), mannose receptor (CD206), and arginase (Arg)-1 were compared. *Results*. The 100 g extracts contained 13.7 g polysaccharides and 1.9 g polyphenols. Compared with M0, the 50 μg/mL extracts increased NO level ($P < 0.05$) and decreased CD206 and Arg-1 expression significantly ($P < 0.05$). The extracts at 100–200 μg/mL increased NO and TNF-α level ($P < 0.05$), but increased iNOS and IL-1β expression significantly ($P < 0.05$). Compared with M1, the extracts decreased NO level at 25, 50, 100, and 200 μg/mL and decreased IL-1β and TNF-α level at 100–200 μg/mL significantly ($P < 0.05$). At 25–200 μg/mL, the extracts significantly increased CD206 and Arg-1 expression and decreased IL-1β and iNOS expression separately ($P < 0.05$). *Conclusions*. Our research suggested that the bilateral effects of the chaga extracts on iNOS, IL-1β, and NO level on M0/M1 macrophages might be related with chaga polysaccharides and chaga polyphenols. Some *in vivo* anticancer and antidiabetic research of purified chaga polysaccharides related to macrophage differentiation should be conducted further.

1. Introduction

Inonotus obliquus, also known as chaga, is a parasitic fungus that grows on birch trees and belongs to the Hymenochaetaceae family [1]. They are mainly distributed in northeast China and northern Russia [2]. Since the 16th century, this fungus has been used as food and medicine for the prevention and treatment of malignant tumors, diabetes, and cardiovascular diseases in Russia, Poland, and the Baltic countries [3]. Chaga has biologically active substances such as polysaccharides, polyphenols, and flavonoids, and has various biological activities such as antitumor, hypoglycemic, antioxidation, and immune stimulation [4, 5]. Based on PubMed, Scopus, Wanfang database (Wanfang), and China National Knowledge Infrastructure (CNKI), an extensive literature survey was conducted about the research of chaga

and its active substances on different diseases. Figure 1(a) shows that most of the articles of chaga were on antidiabetes research, followed by anticancer research over the last 10 years (2012–2021). As the two main active ingredients in chaga, Figures 1(b) and 1(c) show that polysaccharides have more research papers than polyphenols in antidiabetes and anticancer research.

Both cancer and diabetes are immunology-related diseases [6, 7]. Cancer immunology is the most rapidly expanding field in cancer research with the emerging importance of immunity in cancer pathogenesis [6]. A potential immune-regulatory factor in cancer immunology might represent an alternative target for the treatment of cancers [8]. In the development of type 2 diabetes mellitus (T2DM), chronic inflammation plays an important role, and the proinflammatory environment maintained by the innate immunity, including macrophages and related cytokines, can be influenced by adaptive immunity [7]. Our further literature research detailed the relationships between immune-regulatory signaling pathways of chaga polysaccharides and their antidiabetic [9–14] and antitumor activities [15–21] in Figure 2.

From Figure 2, it was interesting to see the bilateral effects of chaga polysaccharides on the following cytokines: protein kinase B (Akt) and matrix metalloprotein-9 (MMP-9) levels were increased in antidiabetic activities [10, 12], but decreased in anticancer effects [18, 19]. Conversely, chaga polysaccharides decreased reactive oxygen species (ROS), interleukin (IL)-1β, and tumor necrosis factor (TNF)-α level in antidiabetic activities [9] but increased ROS, IL-1β, and TNF-α level in anticancer effects [16, 17]. Our previous study showed that both IL-1β and TNF-α are the markers of a classic activated macrophage (M1), which is polarized from resting macrophage (M0) by lipopolysaccharide (LPS) [22, 23]. Based on the above literature research and our previous study, we were interested in investigating the effects of chaga on different macrophage conditions such as M0 and M1 and thus inflammatory factors such as IL-1β and TNF-α.

Macrophages are bone marrow-derived leukocytes that are key for healthy tissue homeostasis but can also contribute to pathologies such as metabolic syndrome [24]. Broadly, a macrophage is divided into three phenotypes: M0, M1-like, and alternative activated macrophage (M2)-like [23]. M1 and M2 have different transcription profiles and act by eliminating bacteria, viruses, and fungi from the host or repairing the damage triggered by inflammation, respectively [25]. In this research, the protein expressions of two markers of M1 differentiation including IL-1β and inducible nitric oxide synthase (iNOS), and two markers of M2 polarization, mannose receptor (CD206), and arginase (Arg)-1 were determined by Western blotting, and the levels of IL-1β, TNF-α, and nitric oxide (NO) were also tested.

2. Materials and Methods

2.1. Preparation of Samples. Chaga was collected from Lvliang Mountains in Shanxi province. The process for chaga extracts is shown in Figure 3 and described briefly as follows.

The chaga was cut into coarse particles with a grain size of about 2-3 mm. The 1 kg chaga particles were soaked into 10 L distilled water (w/w: 1 : 10) at room temperature for 3 h and then boiled at hot water (100°C) [26] for 1 h. The supernatants were removed and the residue was extracted another two times for 30 min, respectively. The total supernatants were collected and precipitated by 80% ethanol (v/v) [27] at 4°C for 12 h. The precipitates were collected and dried at 0.07 MPa vacuum and 55 ± 1°C to a constant weight. These dried samples were used for further research on the contents of polysaccharides and polyphenols.

2.2. Analyses of Polysaccharides Content

2.2.1. Standard Curve of Total Sugar. The total sugar was tested with phenol-sulfuric acid method using glucose as the standard [28]. About 1.0 mg/mL D-glucose (Solarbio, Beijing) stock solution was pipetted in deionized water at final concentrations of 25, 30, 35, 40, 45, 50, 55, and 60 μg/mL in 2 mL total volume and mixed with 2 mL of 5% phenol solution (v/v) and 10 mL of concentrated sulfuric acid (Shidande, Shanghai, P.R. China) separately. The mixture was placed in a water bath at 80°C and kept for 30 min. It was then cooled to room temperature, and the A values were measured at 486 nm using a spectrophotometer (Persee, Beijing). The standard curve of total sugar was obtained using the A value as the ordinate and the concentration as the abscissa.

2.2.2. Standard Curve of Reducing Sugar. The reducing sugar was determined by 3,5-dinitrosalicylic acid (DNS) assay [29]. 50 mg of glucose (Solarbio, Beijing) was weighed accurately and dissolved in 100 mL deionized water, and 0.5 mg/mL glucose standard solution was prepared. Then 0.0, 0.6, 0.8, 1.0, 1.2, and 1.4 mL of the prepared glucose standard solution were added to 2.0, 1.4, 1.2, 1.0, 0.8, 0.6 mL deionized water, respectively, and mixed with 1.5 mL DNS (Shidande, Shanghai, P.R. China) reagent separately. The mixtures were boiled in a water bath at 100°C for 5 min, then quickly cooled with running water, and diluted to 10 mL, and the absorbances were measured at a wavelength of 540 nm. A standard curve of reducing sugar was drawn using glucose concentration as the ordinate and absorbance as the abscissa.

2.2.3. Determination of Polysaccharide Content. The dried extract was accurately weighed and dissolved in deionized water, and 0.2 mg/mL solution of the extract was made separately. Then, 2 mL of the 0.2 mg/mL solution was mixed as aforementioned. The values of the total sugar and the reducing sugar were calculated according to the standard curve obtained above. Finally, the total polysaccharides content was calculated from the reducing sugar subtracted from the total sugar.

2.3. Analyses of Polyphenol Content. Polyphenol content was analyzed using Folin–Ciocalteu method, which was optimized by response surface methodology [30]. Briefly, 20 μL

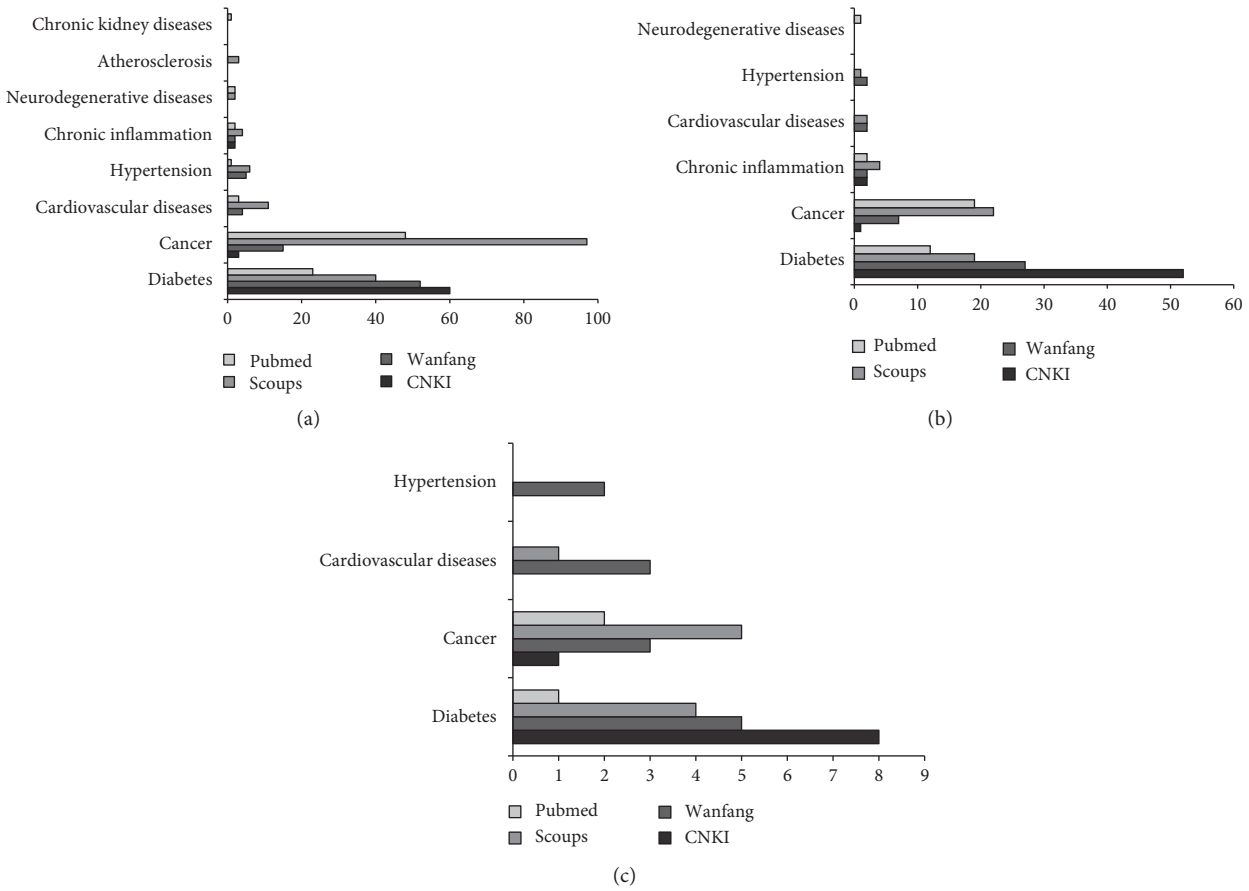

Figure 1: The articles of chaga and its active ingredients in the research of different diseases. (a) The articles of chaga. (b) The articles of chaga polysaccharides. (c) The articles of chaga polyphenols. Note: the literature survey was conducted over the last 10 years (2012–2021). Wanfang, Wanfang database; CNKI, China National Knowledge Infrastructure.

of 1 mg/mL extract was mixed with 100 μL of Folin–Ciocalteu's reagent and 1,580 μL of 50% EtOH. The above mixture was kept for 10 min in the dark. Then, 300 μL of an aqueous solution of 0.2 g/mL Na_2CO_3 was added and put back in the dark for 2 h with continuous stirring. Finally, the mixture was centrifuged at 10,000 g for 3 min and 200 μL of the extract was put in a Greiner microplate (Solarbio, Beijing). The absorbance was measured with the Infinite M200 PRO microplate spectrophotometer (Tecan Trading AG, Switzerland) at 765 nm. The polyphenol content was calculated according to a calibration curve made using gallic acid as the analytical standard.

2.4. Cell Source and Culture. The mouse macrophage RAW264.7 cell line was purchased from the Procell Life Science & Technology Co., Ltd. (Wuhan, China). According to the instructions, the cells were maintained in Dulbecco's modified Eagle's medium (DMEM, Solarbio Science & Technology, Beijing, China) supplemented with 10% fetal bovine serum (FBS, Gibco BRL, Gaithersburg, MD, USA), 100 U/mL penicillin, and 100 μg/mL streptomycin (Shanxi MiniBio Technology Co., Ltd, Shanxi, China) in a 5% CO_2 incubator at 37°C. The medium was replaced the next day.

2.5. Cytotoxicity of the Extracts with CCK-8 Assay. The relative survival rate of cells was detected and calculated by cell counting kit 8 (CCK-8) assay to indicate the cytotoxicity. RAW264.7 cells were seeded into 96-well plates at a density of 1×10^6 cells/mL and cultured in a 10% FBS DMEM for 24 h. Following another 24 h treatment with the extracts at 0, 25, 50, 100, 200, and 400 μg/mL, the supernatants were removed, and each well was washed with PBS before the addition of 10% FBS DMEM and 10 μL CCK-8 reagent (Shanxi MiniBio Technology Co., Ltd, Shanxi, China). Cell viability was determined by measuring the absorbance at 450 nm using a microporous plate reader (Model 550; Bio-Rad Laboratories, Inc., Hercules, CA, USA) after an incubation period of 2 h at 37°C. The average optical density was determined by examining six wells per group.

2.6. The Effects of the Extracts on CD206, Arg-1, IL-1β, and iNOS Protein Expressions on M0/M1 Macrophages. The normal medium-treated cells were the M0 macrophages (resting macrophages) and the LPS-treated cells were the M1 macrophages (classic activated macrophages). The iNOS, IL-1β, CD206, and Arg-1 protein expressions were tested by Western blotting after the chaga extracts (chaga crude polysaccharides) were used at 25, 50, 100, and

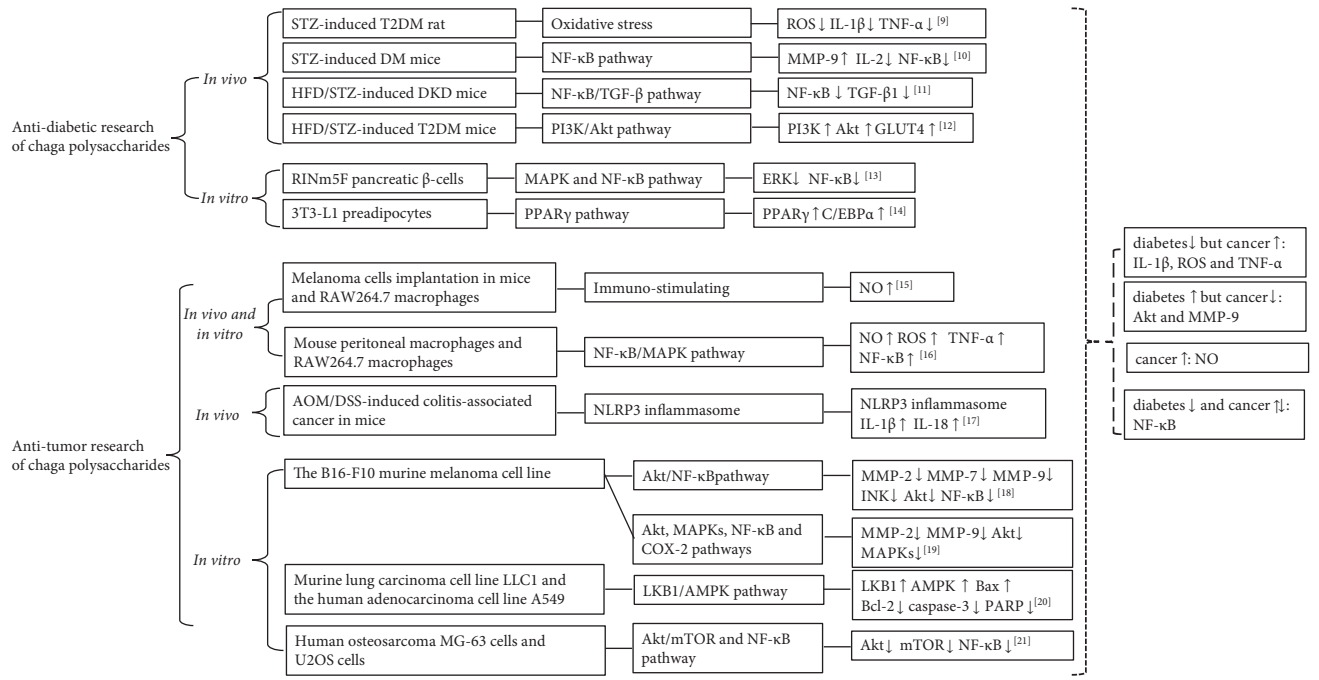

Figure 2: Antidiabetes and anticancer research of chaga polysaccharides based on immune-related signaling pathways. Abbreviations: AMPK, adenosine monophosphate-activated protein kinase; Akt, protein kinase B; AOM, azoxymethane; Bax, Bcl-2-associated X protein; Bcl-2, B-cell lymphoma 2; C/EBPα, CCAAT/enhancer-binding protein α; COX-2, cyclooxygenase-2; DKD, diabetic kidney disease; DM, diabetes mellitus; DSS, dextran sulfate sodium; ERK, extracellular signal-regulated kinase; GLUT4, glucose transporter protein 4; HFD, high fat diet; IL-1β, interleukin-1β; IL-2, interleukin-2; IL-18, interleukin-18; JNK, c-Jun N-terminal kinase; LKB1, liver kinase B 1; MAPK, mitogen-activated protein kinases; MMP-2, matrix metalloprotein-2; MMP-7, matrix metalloprotein-7; MMP-9, matrix metalloprotein-9; mTOR, mammalian target of rapamycin; NF-κB, nuclear factor κappa B; NLRP3, the nod-like receptor family protein 3; NO, nitric oxide; PARP, poly ADP-ribose polymerase; PI3K, phosphatidylinositol 3 kinase; PPARγ, peroxisome proliferator-activated receptors γ; T2DM, type 2 diabetes mellitus; TGF-β, transforming growth factor-β; TNF-α, tumor necrosis factor-α; STZ, streptozotocin.

200 μg/mL (CCP25, CCP50, CCP100, and CCP200) on M0 and M1 macrophages separately. The treated cells (1×10^6 cells/ml) were removed from the culture media and lysed with RIPA lysis buffer from Solarbio Science & Technology (Beijing, China) for 30 min. The protein concentrations were determined using a BCA Protein Assay Kit from Solarbio Science & Technology (Beijing, China). Samples containing 50 μg of protein were resolved by 10% SDS-PAGE electrophoresis and transferred to polyvinylidene fluoride membranes (Millipore, Shanghai, China) in a buffer tank with platinum wire electrodes. After immersing the membranes in 5% nonfat dried milk (diluted in 0.1% (v/v) Tween-20 PBS) for 2 h at room temperature to block the nonspecific binding, the membranes were incubated overnight with a primary antibody against iNOS (Catalog No. 18985-1-AP, Proteintech, Wuhan, China) at 1 : 2000 dilution, a primary antibody against IL-1β (Catalog No. bs-0812R, Bioss, Beijing, China) at 1 : 1000 dilution, a primary antibody against CD206 (Catalog No. bs-21473R, Bioss, Beijing, China) at 1 : 1000 dilution, and a primary antibody against Arg-1 (Catalog No. 16001-1-AP, Proteintech, Wuhan, China) at 1 : 5000 dilution at 4°C. The membranes were washed four times (15 min each) and then incubated with the corresponding secondary IgG conjugated to HRP antibody (Catalog No. SA00001-2, Proteintech, Wuhan, China) at room temperature for 1 h. The results were finally analyzed by the Quantity One analysis system (Bio-Rad, Hercules, CA, USA). GAPDH at a dilution of 1 : 5000 (Catalog No. 10494-1-AP, Proteintech, Wuhan, China) was used as the internal loading control.

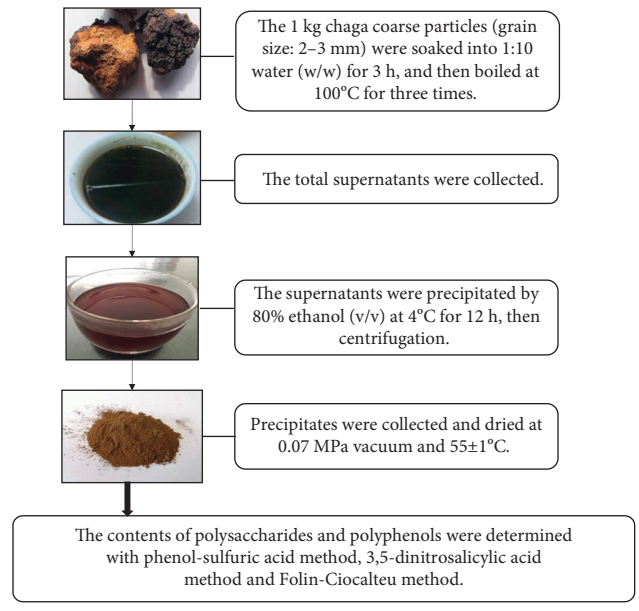

Figure 3: Extraction flowchart.

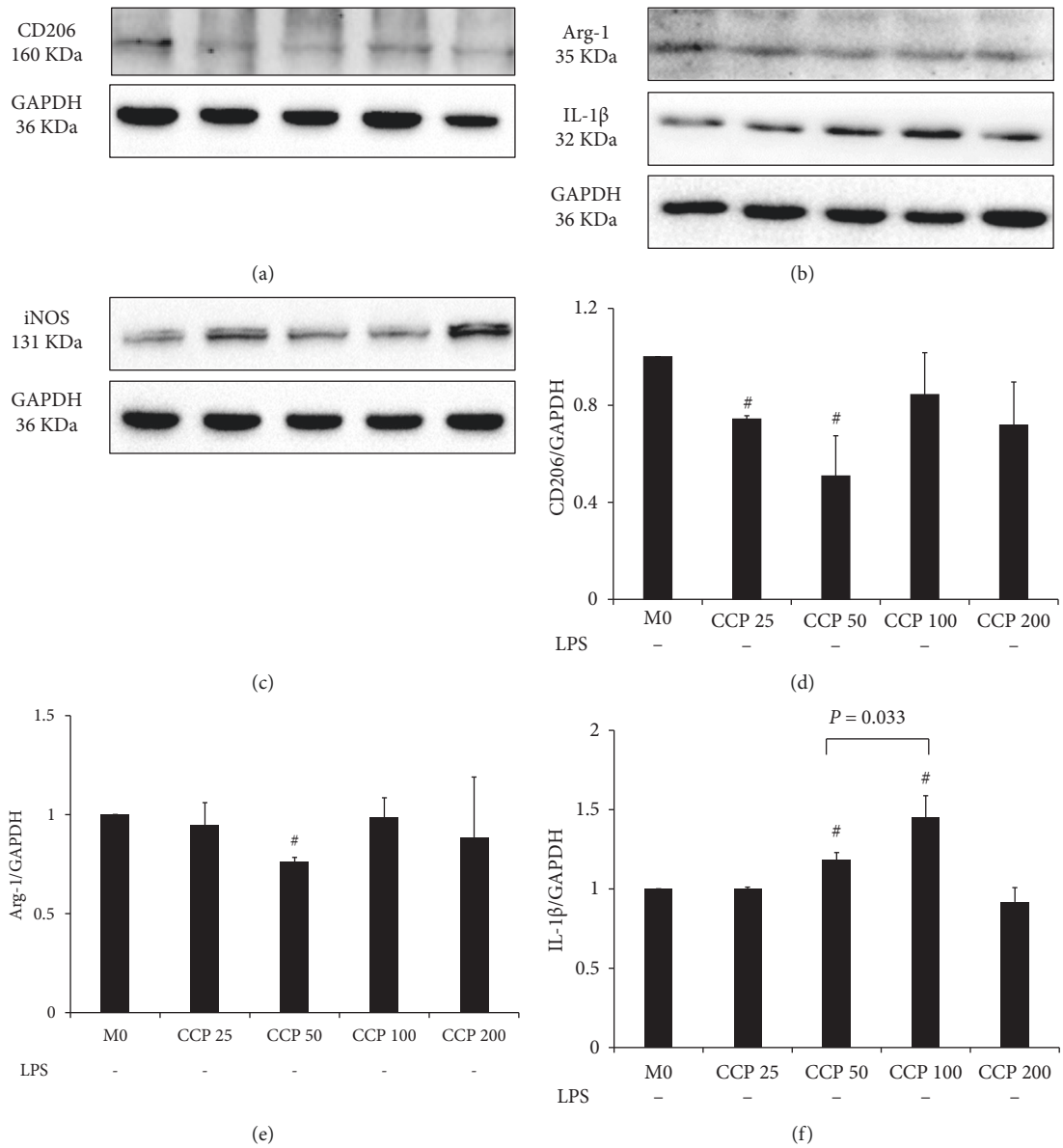

Figure 4: Continued.

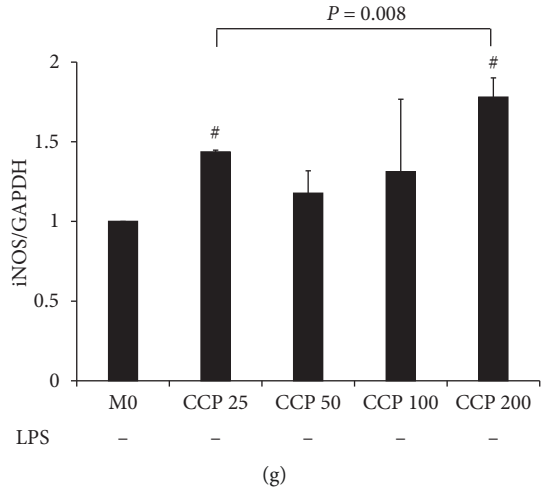

Figure 4: Effects of CCP on CD206, Arg-1, IL-1β, and iNOS protein expressions in M0 macrophages. (a) CD206 protein expressions. (b) Arg-1 and IL-1β protein expressions. (c) iNOS protein expression. The results of CD206, Arg-1, IL-1β, and iNOS protein expressions were represented in (d), (e), (f), and (g), respectively. All results were expressed as a ratio with respect to M0 and represented as the mean ± SD in triplicate. $^{\#}P < 0.05$, CCP versus M0. CCP, chaga crude polysaccharides; CCP 25, CCP at 25 μg/mL; CCP 50, CCP at 50 μg/mL; CCP 100, CCP at 100 μg/mL; CCP 200, CCP at 200 μg/mL; CD206, mannose receptor; Arg-1, arginase-1; IL-1β, interleukin-1β; iNOS, inducible nitric oxide synthase; M0, resting macrophages.

2.7. The Effects of the Extracts on IL-1β, TNF-α, and NO Levels on M0/M1 Macrophages. M0 macrophages (1×10^6 cells/mL) and M1 macrophages (1×10^6 cells/mL) were treated with CCP25, CCP50, CCP100, and CCP200 for 24 h separately. Cell supernatants were then harvested and centrifuged at 1,500 g for 10 min at 4°C. The IL-1β level was determined using an ELISA kit (Catalog No. MM-0040M1, Jiangsu Meimian Industrial Co., Ltd). The TNF-α level was determined using an ELISA kit (Catalog No. MM-0132M1, Jiangsu Meimian Industrial Co., Ltd). The absorbance was measured using a microplate reader (Model 550, Bio-Rad Laboratories, Inc.). Each sample underwent repeated testing three times.

The NO level was tested with the Griess assay. Nitrite, a stable end-product of NO metabolism, was measured using the Griess reaction. Culture media of the RAW 264.7 cells (100 μL) was mixed with an equal volume of Griess reagent (Yantai Science & Biotechnology Co. LTD, Yantai, China), followed by spectrophotometric measurement at 540 nm (Model 550, Bio-Rad Laboratories, Inc.). Nitrite concentrations in the culture media were determined by comparison with a sodium nitrite standard curve. All experiments were repeated three times.

2.8. Statistical Analysis. The SPSS 19.0 software (IBM, Armonk, NY, US) was used for statistical analysis. All the data were expressed as mean ± standard deviation (SD) of the mean. A two-sided Student's *t*-test was used to analyze the differences between the two groups. One-way analysis of variance with Bonferroni's posttest was used when more than two groups were present. A P value of <0.05 was considered statistically significant.

3. Results

3.1. The Polysaccharides and Polyphenol Content. A total of 112.5 g of extracts was obtained from 1 kg of chaga, with an extraction rate of 11.3%. Using the phenol-sulfuric acid method, the content of polysaccharides in the extract was measured to be 13.7%, i.e., 100 g of the extract contained 13.7 g of polysaccharides. With Folin–Ciocalteu method, the results showed that 100 g extracts contained 1.9 g polyphenol.

3.2. The Cytotoxicity Results. CCK-8 results showed that the extracts at 400 μg/mL inhibited the growth of RAW 264.7 cells (cell viability: (67.7 ± 4.7)%), which had a significant difference compared to the extracts at 0 μg/mL ((100.0 ± 3.9)%, $P < 0.001$) and was unsuitable for further tests. The cell viabilities of the CCP25, CCP50, CCP100, and CCP200 were (103.0 ± 4.6)%, (98.2 ± 5.8)%, (98.6 ± 6.2)%, and (97.3 ± 4.7)%, respectively, which had no significant difference compared to the extracts at 0 μg/mL and could be used for the following research.

3.3. The Results of the Extracts on CD206, Arg-1, IL-1β, and iNOS Protein Expressions in M0 Macrophages. Figures 4(a)–4(c) show the CD206, Arg-1, IL-1β and iNOS protein expression of CCP25, CCP50, CCP100, CCP200 on M0 macrophages. The analyses in Figures 4(d) and 4(e) indicated that compared to M0, CCP25 and CCP50 decreased CD206 expression significantly ($P < 0.001$ and $P = 0.007$), and CCP50 decreased Arg-1 expression significantly ($P < 0.001$). In Figures 4(f) and 4(g), we could see that compared to M0, CCP50 and CCP100 significantly

increased IL-1β expression ($P = 0.003$ and $P = 0.005$), and CCP 25 and CCP 200 increased iNOS expression significantly (both: $P < 0.001$).

Further analyses showed that the increased effect on IL-1β expression of CCP100 was better than CCP50 significantly ($P = 0.033$), and the increased effect on iNOS expression of CCP200 was better than CCP25 significantly ($P = 0.008$).

3.4. The Results of the Extracts on CD206, Arg-1, IL-1β, and iNOS Protein Expressions in M1 Macrophages. Figures 5(a)–5(d) show that the protein expression results of CD206, Arg-1, IL-1β, and iNOS after M1 macrophages were intervened with CCP. Compared with the M0 macrophages, CD206 and Arg-1 protein expression decreased ($P < 0.001$, $P = 0.001$) in Figures 5(e) and 5(f), while IL-1β and iNOS protein expression of M1 macrophages significantly increased ($P = 0.005$, $P < 0.001$) in Figures 5(g) and 5(h).

Compared with the M1 macrophages, significantly increasing effects of CCP50, CCP100, and CCP200 on CD206 expression could be seen in Figure 5(e) ($P = 0.002$, $P < 0.001$ and $P < 0.001$). Among the above three concentrations, CCP200 showed its best effects compared with CCP50 ($P = 0.003$) and CCP100 ($P = 0.008$).

Also compared with the M1 macrophages, CCP25, CCP100, and CCP200 increased Arg-1 expression significantly ($P = 0.001$, $P = 0.019$ and $P < 0.001$), and CCP200 was better than CCP25 ($P < 0.001$) and even better than M0 macrophages ($P < 0.001$).

Compared with the M1 macrophages again, CCP200 decreased IL-1β and iNOS expression significantly ($P = 0.037$ and $P < 0.001P < 0.001$) and CCP100 decreased iNOS significantly ($P = 0.004$). The decreasing effect on iNOS of CCP200 was better than CCP100 ($P = 0.010$).

3.5. The Results of the Extracts on IL-1β, TNF-α, and NO Levels in M0 Macrophages. Compared with the NO level of the M0 macrophages ((2.7 ± 0.6) μM), CCP50 ((9.3 ± 3.2) μM), CCP100 ((14.2 ± 3.5) μM), and CCP200 ((18.6 ± 2.1) μM) all showed significant increasing effects on NO production ($P = 0.025$, $P = 0.005$ and $P < 0.001$). The increased NO production of CCP200 was significantly higher than CCP50 ($P = 0.014$).

Compared with the TNF-α level of M0 macrophages ((452.9 ± 36.3) pg/mL), both CCP100 ((570.5 ± 21.0) pg/mL) and CCP200 ((606.5 ± 86.1) pg/ml) showed significant increasing effects on TNF-α level ($P = 0.008$ and $P = 0.047$).

3.6. The Results of the Extracts on IL-1β, TNF-α, and NO Levels in M1 Macrophages. Compared with the M0 macrophages, the NO production of M1 macrophages increased from (2.7 ± 0.6) μM to (86.9 ± 0.9) μM ($P < 0.001$), promoted IL-1β level in macrophages from (90.7 ± 6.7) pg/mL to (146.2 ± 7.9) pg/mL ($P < 0.001$), and elevated TNF-α content from (452.9 ± 36.3) pg/mL to (522.2 ± 45.7) pg/mL. Results are shown in Figures 6(a)–6(c).

In Figure 6(a), CCP25, CCP50, CCP100, and CCP200 all had significant effects on decreasing NO production in M1 macrophages (All: $P < 0.001$). The decreasing effects of CCP200 showed significantly better results compared with CCP25 ($P = 0.015$) and CCP50 ($P = 0.026$).

Compared with the IL-1β level of M1 macrophages in Figure 6(b), CCP at four tested concentrations all showed the decreasing effects, but only CCP100 ((109.5 ± 9.2) pg/mL) and CCP200 ((114.0 ± 10.0) pg/mL) showed significant effects ($P = 0.006$ and $P = 0.012$).

Finally, on TNF-α level in Figure 6(c), CCP200 showed its decreasing effects significantly ((350.8 ± 6.9) pg/mL, $P = 0.003$) when compared with M1 macrophages.

4. Discussion

Polysaccharides are among the most important members of the biopolymer family. They are natural macromolecules composed of monosaccharides. To date, more than 300 kinds of natural polysaccharide compounds have been identified. They are present in plants, microorganisms, and engage in a variety of physiological functions [31]. The crude extracts of the medicinal mushroom chaga have been used as effective traditional medicine to treat malicious tumors, gastritis, gastric ulcers, and other inflammatory conditions [32]. Our literature research in Figure 1 supported that among the extracts from chaga, polysaccharides are major bioactive components that possess antitumor, hypoglycemic, and anti-inflammation activities [33]. As we mentioned before, cancer and diabetes are both regarded as immunology-related diseases [6, 7]. Antitumor and hypoglycemic mechanisms related to immunomodulatory activities of chaga polysaccharides are further summarized in Figure 2.

Figure 2 shows that antitumor activities of chaga polysaccharides are achieved through multiple signals including but not limited to the activation of the nod-like receptor family protein 3 (NLRP3) inflammasome, nuclear factor κappa B(NF-κB)/mitogen-activated protein kinases (MAPK) pathway, liver kinase B 1(LKB1)/AMPK pathway, and the promoted effects on NO, TNF-α, and IL-1β level via above signals and immuno-stimulating effects [15–21]. Figure 2 also shows that *in vivo* hypoglycemic activities of chaga polysaccharides are confirmed by depressing oxidative stress, NF-κB/transforming growth factor (TGF)-β pathway, and PI3K/Akt pathway. Accordingly, their hypoglycemic activities are correlated with the inhibition of TNF-α, IL-1β, NF-κB, and ROS level [9–11]. Based on the above discussion, it seemed that chaga polysaccharides have bilateral immunomodulatory effects on TNF-α, IL-1β, etc. in the face of cancer and diabetes.

Water extraction and ethanol precipitation are popular methods to obtain crude polysaccharides from many fruiting bodies of mushrooms, such as *Coriolus versicolor* [34] and *Grifola frondosa* [35]. It was reported that *I. obliquus* polysaccharides could be initially purified via precipitation from an aqueous extract with 80% alcohol [36]. The chaga crude polysaccharides were obtained in our research with the above similar method and were further studied on macrophages at M0 resting condition and LPS-activated M1 subtype.

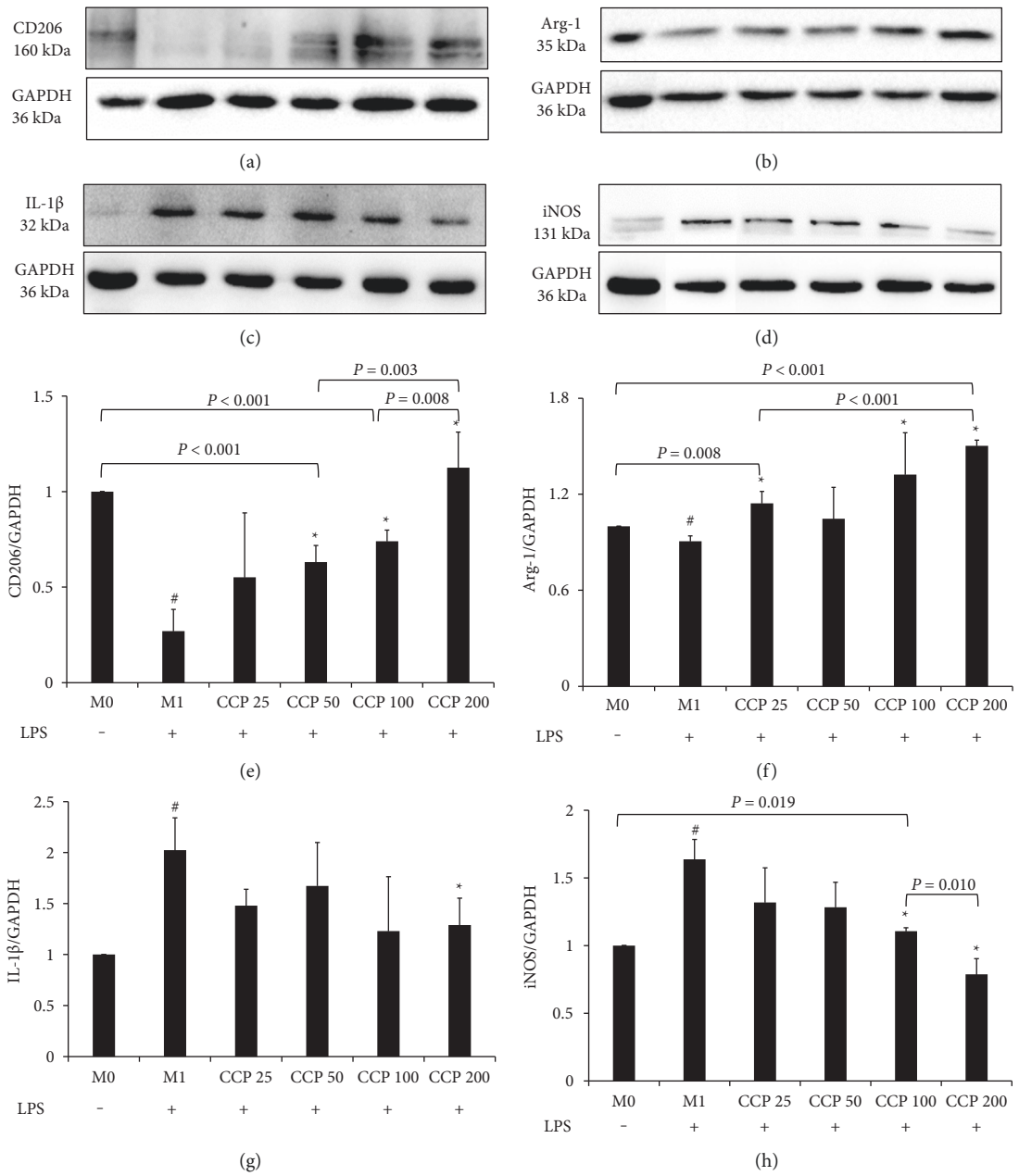

Figure 5: Effects of CCP on CD206, Arg-1, IL-1β, and iNOS protein expressions in M1 macrophages. (a) CD206 protein expressions. (b) Arg-1 protein expressions. (c) IL-1β protein expressions. (d) iNOS protein expression. The results of CD206, Arg-1, IL-1β, and iNOS were represented in (e), (f), (g), and (h), respectively. All results were expressed as a ration with respect to M0 control and represented as the mean ± SD in triplicate. $^{\#}P < 0.05$, M1 versus M0. $^{*}P < 0.05$, CCP versus M1. CCP, chaga crude polysaccharides; LPS, lipopolysaccharide; CCP 25, CCP at 25 μg/mL; CCP 50, CCP at 50 μg/mL; CCP 100, CCP at 100 μg/mL; CCP 200, CCP at 200 μg/mL; CD206, mannose receptor; Arg-1, arginase-1; IL-1β, interleukin-1β; iNOS, inducible nitric oxide synthase; M0, resting macrophages; M1, classic activated macrophages.

As pivotal immune stromal cells in the tumor microenvironment (TME), macrophages are extensively heterogeneous and exert both antitumor and protumor functions [37]. Tumor-associated macrophages (TAMs) are the critical components of tumors and play an important role in the development of the immunosuppressive TME. It was reported that the transition of TAMs from M2 to M1 is crucial for the immunotherapy of gastric cancer [38]. Some related research showed that polysaccharides isolated from the fruiting body of chaga was capable of promoting NO/ROS production, TNF-α secretion, and phagocytic uptake in macrophages RAW264.7 cells [16]. Figure 2 also shows that anticancer activities of chaga polysaccharides were related to increased NO, ROS, and TNF-α levels on macrophages [15, 16]. Our research confirmed for the first time *in vitro* that the elevated NO, TNF-α, and IL-1β levels of chaga crude polysaccharides might related to their activities in increasing M0 to M1 polarization and decreasing M2 polarization.

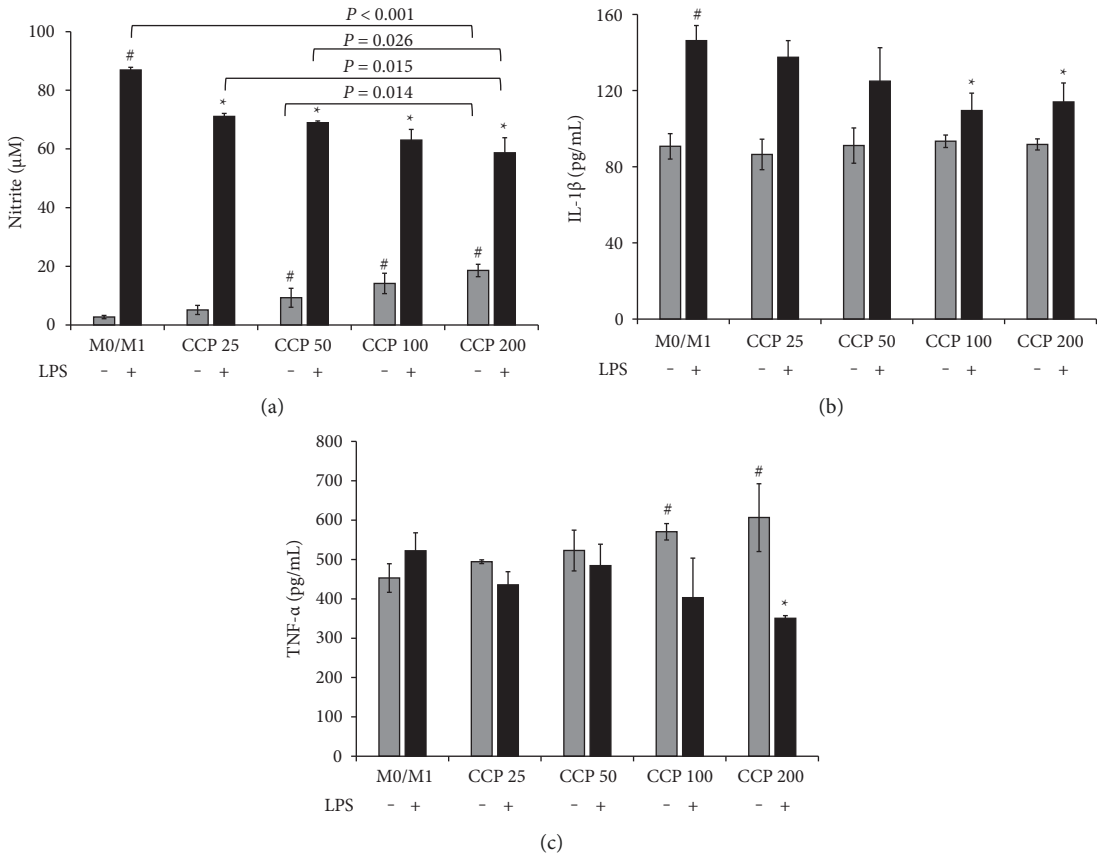

Figure 6: Effects of CCP on nitric oxide production, IL-1β, and TNF-α level in M0 and M1 macrophages. (a) Nitrite (nitric oxide production) levels. (b) IL-1β levels. (c) TNF-α levels. Values were expressed as the mean ± SD of the mean ($n = 3$). $^{\#}P < 0.05$, M1 versus M0. $^{*}P < 0.05$, CCP versus M1. CCP, chaga crude polysaccharides; LPS, lipopolysaccharide; CCP 25, CCP at 25 μg/mL; CCP 50, CCP at 50 μg/mL; CCP 100, CCP at 100 μg/mL; CCP 200, CCP at 200 μg/mL; IL-1β, interleukin-1β; TNF-α, tumor necrosis factor-α; M0, resting macrophages; M1, classic activated macrophages.

It was reported that the chaga polysaccharide can ameliorate azoxymethane/dextran sulfate sodium-induced colitis-associated cancer in mice [17]. Colon cancer is a common and deadly human digestive tract malignant tumor with a poor prognosis [39]. Triptolide is extracted from the traditional Chinese medicine *Tripterygium wilfordii*. Related research showed that triptolide-educated colon cancers retarded the macrophages' polarization to anti-inflammatory M2 status by decreasing the expression of Arg-1 and CD206, the markers of M2 polarization [39]. Could chaga polysaccharide exert its anticancer activity by promoting M0 to M1 subtype and decreasing M0 to M2 polarization? Further *in vivo* research should be conducted.

T2DM is characterized by low-grade chronic inflammation and metabolic dysfunction, which is observed in all tissues involved in energy homeostasis. A substantial body of evidence has established an important role for macrophages in these tissues during the development of T2DM [40]. Some related *in vivo* research demonstrated that hyperglycemia could polarize macrophages toward M1 via overproducing ROS under inflammatory condition [41]. An animal study showed that the mechanism of fasudil on the diabetic nephropathy progression might be associated with its induction of M2 polarization and the reduction of M1 polarization and inflammation [42]. A novel macrophage-regulating drug was reported to accelerate wound healing in a diabetic mouse model by decreasing M1 activity and enriching M2 populations. Furthermore, the efficiency of this macrophage-regulating medicine was confirmed in a multicenter, evaluator-blinded, phase 3 randomized clinical trial, which was performed across the US, China, and Taiwan [43].

In recent years, research on M1/M2 differentiation of chaga extract has been explored, such as inonotsuoxide B, a tetracyclic triterpenoid extracted from chaga, was reported to have a regulation effect on macrophage polarization [44]. To the best of our knowledge, our current work was the first study on the effect of chaga crude polysaccharides on regulating M1 to M2 phenotype. Our previous research showed that the protective effects of two safflower-derived compounds on hyperglycaemic stress-induced renal podocyte apoptosis via modulating macrophage M1 to M2 polarization [23]. We will try a study on M1/M2 subtype on diabetic animal model with chaga-purified polysaccharide in our following research.

In Table 1, it was interesting to see that when tested on resting the macrophage, CCP50 targeted both the markers of M1 and M2 including CD206, Arg-1, and IL-1β to produce NO. CCP200 increased iNOS expression to elevate NO and

Table 1: Comparison of CCP at different concentrations on M0 to M1/M2 and M1 to M2 regulation.

Regulation on macrophage polarization	The markers of M1 and M2	CCP25	CCP50	CCP100	CCP200
M0 to M1/M2 (CCP on M0 macrophages	CD206	#	#		
	Arg-1		#		
	IL-1β		#	#	
	iNOS	#			#
M1 to M2 (CCP on M1 macrophages)	CD206		*	*	*
	Arg-1	*		*	*
	IL-1β				*
	iNOS			*	*

Notes: # represented as a significant difference compared to M0 macrophages. *Represented as a significant difference compared to M1 macrophages. M0, resting macrophage; M1, classic activated macrophage; M2, alternative activated macrophage; CCP, chaga crude polysaccharides; LPS, lipopolysaccharide; CCP25, CCP at 25 μg/mL; CCP50, CCP at 50 μg/mL; CCP100, CCP at 100 μg/mL; CCP200, CCP at 200 μg/mL; CD206, mannose receptor; Arg-1, arginase-1; IL-1β, interleukin-1β; iNOS, inducible nitric oxide synthase.

TNF-α level. When tested on M1, CCP100 and CCP200 had effects on the markers of M1 and also M2, but CCP25 and CCP50 only increased the protein expressions of M2. The potential reason of the above results might be that the other active ingredients such as polyphenols and flavonoids also extracted simultaneously when aqueous extraction and alcoholic precipitation was used mainly for polysaccharides extraction [45]. Our research already confirmed that in addition to polysaccharides in the extracts, polyphenols were also present [46].

Some findings indicated that chaga polysaccharides exert immune-enhancing activity and other components in chaga also displayed antitumor activity [47]. Do different components have different effects on macrophage polarization? Further studies should probably focus on some purified compounds and their relationships with macrophage differentiation, such as inonotsuoxide B. The antitumor activity of inonotsuoxide B [48] and its regulation on macrophage polarization through sirtuin-1/endoplasmic reticulum stress axis [44] was explored.

In recent years, the structure determinations of chaga polysaccharides and their antitumor and antidiabetic research have already made some progress. The structure characterization and hypoglycaemic activities of two polysaccharides from *I. obliquus* were reported recently [49]. A novel water-soluble polysaccharide was isolated and purified from chaga. Its chemical characteristics and antitumor, immunoregulatory activity were also investigated [50]. With the help of experts in the chemical structure analysis, the structural characterization and immune activity screening of polysaccharides with different molecular weights [51] from chaga crude polysaccharides is being studied by our research team. The relationships of purified polysaccharides and their immunomodulatory roles related to macrophage polarization could have prospects.

5. Conclusions

Chaga, a parasitic fungus, has drawn more interest in recent years for its multiple pharmacological actions. According to our literature research, chaga polysaccharides play important roles in antitumor and antidiabetic activities. The resting macrophages can be polarized to M1 or M2 subtype, which play different immunomodulatory roles when macrophages exert anticancer and antidiabetic activities. Our current *in vitro* research suggested that the bilateral effects of the chaga extracts on TNF-α, IL-1β, and NO level on M0/M1 macrophages might be related to its contained polysaccharides and chaga polyphenols. Further anticancer and antidiabetic research of purified chaga polysaccharide and polyphenol related to macrophage polarization should be conducted *in vivo*.

Data Availability

The readers can access the data supporting the conclusions of the study from Figures 1–6 and Table 1. All those figures and tables are included within the manuscript. All authors declare that the data of the manuscripts can be verified from the results of the article, be replicated in the analysis, and be conducted in secondary analyses.

Ethical Approval

The authors declare there are no studies on human subjects, human data or tissue, or animals in this manuscript.

Conflicts of Interest

The authors declare there are no conflicts of interest.

Acknowledgments

This study was supported by Wu Jieping Medical Foundation (no. 320.6750.2021-08-10), Key R & D Project of Shanxi Province (International Scientific and Technological Cooperation, Independent Topics, no. 201903D421061), and Basic Research Program of Shanxi Province (no. 202103021224370).

References

[1] K. C. Duru, E. G. Kovaleva, I. G. Danilova, and P. Bijl, "The pharmacological potential and possible molecular mechanisms of action of *Inonotus obliquus* from preclinical studies," *Phytotherapy Research*, vol. 33, no. 8, pp. 1966–1980, 2019.

[2] Y. Wang, L. Guo, C. Liu, Y. Zhang, and S. Li, "Total triterpenoid extraction from *Inonotus obliquus* using ionic liquids and separation of potential lactate dehydrogenase inhibitors via ultrafiltration high-speed countercurrent

chromatography," *Molecules*, vol. 26, no. 9, pp. 2467–2514, 2021.

[3] J. Kim, S. C. Yang, A. Y. Hwang, H. Cho, and K. T. Hwang, "Composition of triterpenoids in *Inonotus obliquus* and their anti-proliferative activity on cancer cell lines," *Molecules*, vol. 25, no. 18, pp. 4066–4069, 2020.

[4] M. Wang, Z. Zhao, X. Zhou et al., "Simultaneous use of stimulatory agents to enhance the production and hypoglycaemic activity of polysaccharides from *Inonotus obliquus* by submerged fermentation," *Molecules*, vol. 24, no. 23, pp. 4400–4414, 2019.

[5] K. A. Szychowski, B. Skóra, T. Pomianek, and J. Gmiński, "*Inonotus obliquus*-from folk medicine to clinical use," *Journal of Traditional and Complementary Medicine*, vol. 11, no. 4, pp. 293–302, 2021.

[6] X. Fu, C. De Angelis, and R. Schiff, "Interferon signaling in estrogen receptor-positive breast cancer: a revitalized topic," *Endocrinology*, vol. 163, no. 1, pp. 1–15, 2022.

[7] S. Zhang, X. Gang, S. Yang et al., "The alterations in and the role of the Th17/Treg balance in metabolic diseases," *Frontiers in Immunology*, vol. 12, pp. 1–14, 2021.

[8] S. Rashid, D. Song, J. Yuan, B. H. Mullin, and J. Xu, "Molecular structure, expression, and the emerging role of siglec-15 in skeletal biology and cancer," *Journal of Cellular Physiology*, vol. 237, no. 3, pp. 1711–1719, 2022.

[9] B. Z. Diao, W. R. Jin, and X. J. Yu, "Protective effect of polysaccharides from *Inonotus obliquus* on streptozotocin-induced diabetic symptoms and their potential mechanisms in rats," *Evidence-based Complementary and Alternative Medicine*, vol. 2014, Article ID 841496, 5 pages, 2014.

[10] J. Wang, W. Hu, L. Li et al., "Antidiabetic activities of polysaccharides separated from *Inonotus obliquus* via the modulation of oxidative stress in mice with streptozotocin-induced diabetes," *PLoS One*, vol. 12, no. 6, Article ID e0180476, 2017.

[11] Y. J. Chou, W. C. Kan, C. M. Chang et al., "Renal protective effects of low molecular weight of *Inonotus obliquus* polysaccharide (LIOP) on HFD/STZ-induced nephropathy in mice," *International Journal of Molecular Sciences*, vol. 17, no. 9, pp. 1535–1617, 2016.

[12] J. Wang, C. Wang, S. Li et al., "Anti-diabetic effects of *Inonotus obliquus* polysaccharides in streptozotocin-induced type 2 diabetic mice and potential mechanism via PI3K-Akt signal pathway," *Biomedicine & Pharmacotherapy*, vol. 95, pp. 1669–1677, 2017.

[13] Y. C. Sim, J. S. Lee, S. Lee et al., "Effects of polysaccharides isolated from *Inonotus obliquus* against hydrogen peroxide-induced oxidative damage in RINm5F pancreatic β-cells," *Molecular Medicine Reports*, vol. 14, no. 5, pp. 4263–4270, 2016.

[14] J. I. Joo, D. H. Kim, and J. W. Yun, "Extract of chaga mushroom (*Inonotus obliquus*) stimulates 3T3-L1 adipocyte differentiation," *Phytotherapy Research*, vol. 24, no. 11, pp. 1592–1599, 2010.

[15] Y. O. Kim, H. W. Park, J. H. Kim, J. Y. Lee, S. H. Moon, and C. S. Shin, "Anti-cancer effect and structural characterization of endo-polysaccharide from cultivated mycelia of *Inonotus obliquus*," *Life Sciences*, vol. 79, no. 1, pp. 72–80, 2006.

[16] D. P. Won, J. S. Lee, D. S. Kwon, K. E. Lee, W. C. Shin, and E. K. Hong, "Immunostimulating activity by polysaccharides isolated from fruiting body of *Inonotus obliquus*," *Molecules and Cells*, vol. 31, no. 2, pp. 165–173, 2011.

[17] J. Li, C. Qu, F. Li et al., "*Inonotus obliquus* polysaccharide ameliorates azoxymethane/dextran sulfate sodium-induced colitis-associated cancer in mice via activation of the NLRP3 inflammasome," *Frontiers in Pharmacology*, vol. 11, pp. 1–11, 2021.

[18] K. R. Lee, J. S. Lee, S. Lee et al., "Polysaccharide isolated from the liquid culture broth of *Inonotus obliquus* suppresses invasion of B16-F10 melanoma cells via AKT/NF-κB signaling pathway," *Molecular Medicine Reports*, vol. 14, no. 5, pp. 4429–4435, 2016.

[19] K. R. Lee, J. S. Lee, Y. R. Kim, I. G. Song, and E. K. Hong, "Polysaccharide from *Inonotus obliquus* inhibits migration and invasion in B16-F10 cells by suppressing MMP-2 and MMP-9 via downregulation of NF-κB signaling pathway," *Oncology Reports*, vol. 31, no. 5, pp. 2447–2453, 2014.

[20] S. Jiang, F. Shi, H. Lin et al., "*Inonotus obliquus* polysaccharides induces apoptosis of lung cancer cells and alters energy metabolism via the LKB1/AMPK axis," *International Journal of Biological Macromolecules*, vol. 151, pp. 1277–1286, 2020.

[21] B. Su, X. Yan, Y. Li, J. Zhang, and X. Xia, "Effects of *Inonotus obliquus* polysaccharides on proliferation, invasion, migration, and apoptosis of osteosarcoma cells," *Analytical Cellular Pathology*, vol. 2020, Article ID 4282036, 7 pages, 2020.

[22] Y. Li, Y. Zhou, Y. Wang, R. Crawford, and Y. Xiao, "Synovial macrophages in cartilage destruction and regeneration-lessons learnt from osteoarthritis and synovial chondromatosis," *Biomedical Materials*, vol. 17, no. 1, pp. 012001–012009, 2022.

[23] Y. Li, D. Zheng, D. Shen, X. Zhang, X. Zhao, and H. Liao, "Protective effects of two safflower derived compounds, kaempferol and hydroxysafflor yellow A, on hyperglycaemic stress-induced podocyte apoptosis via modulating of macrophage M1/M2 polarization," *Journal of Immunology Research*, vol. 2020, Article ID 2462039, 11 pages, 2020.

[24] S. K. Wculek, G. Dunphy, I. Heras-Murillo, A. Mastrangelo, and D. Sancho, "Metabolism of tissue macrophages in homeostasis and pathology," *Cellular & Molecular Immunology*, vol. 19, no. 3, pp. 384–408, 2022.

[25] E. M. Melo, V. L. S. Oliveira, D. Boff, and I. Galvão, "Pulmonary macrophages and their different roles in health and disease," *The International Journal of Biochemistry & Cell Biology*, vol. 141, pp. 106095–106098, 2021.

[26] J. Fang, S. Gao, R. Islam, Y. Teramoto, and H. Maeda, "Extracts of phellinus linteus, bamboo (*Sasa senanensis*) leaf and chaga mushroom (*Inonotus obliquus*) exhibit antitumor activity through activating innate immunity," *Nutrients*, vol. 12, no. 8, pp. 2279–2312, 2020.

[27] A. Smith, S. Javed, A. Barad et al., "Growth-inhibitory and immunomodulatory activities of wild mushrooms from north-central british columbia (Canada)," *International Journal of Medicinal Mushrooms*, vol. 19, no. 6, pp. 485–497, 2017.

[28] H. Liao, D. Jia, X. Zhao, D. Zheng, Y. Li, and R. Li, "Effects of chaga medicinal mushroom *Inonotus obliquus* (Agaricomycetes) extracts on NOS-cGMP-PDE5 pathway in rat penile smooth muscle cells," *International Journal of Medicinal Mushrooms*, vol. 22, no. 10, pp. 979–990, 2020.

[29] H. T. Song, Y. Gao, Y. M. Yang et al., "Synergistic effect of cellulase and xylanase during hydrolysis of natural lignocellulosic substrates," *Bioresource Technology*, vol. 219, pp. 710–715, 2016.

[30] C. Fanali, V. Gallo, S. Della Posta et al., "Choline hloride-lactic acid-based NADES as an extraction medium in a response surface methodology-optimized method for the extraction of phenolic compounds from Hazelnut skin," *Molecules*, vol. 26, no. 9, pp. 1–15, 2021.

[31] M. Yin, Y. Zhang, and H. Li, "Advances in research on immunoregulation of macrophages by plant polysaccharides," *Frontiers in Immunology*, vol. 10, pp. 1–9, 2019.

[32] Y. Zhao and W. Zheng, "Deciphering the antitumoral potential of the bioactive metabolites from medicinal mushroom *Inonotus obliquus*," *Journal of Ethnopharmacology*, vol. 265, 2021.

[33] Y. Lu, Y. Jia, Z. Xue, N. Li, J. Liu, and H. Chen, "Recent developments in *Inonotus obliquus* (chaga mushroom) polysaccharides: isolation, structural characteristics, biological activities and application," *Polymers*, vol. 13, no. 9, pp. 1441–1521, 2021.

[34] X. Zhang, Z. Cai, H. Mao, P. Hu, and X. Li, "Isolation and structure elucidation of polysaccharides from fruiting bodies of mushroom coriolus versicolor and evaluation of their immunomodulatory effects," *International Journal of Biological Macromolecules*, vol. 166, pp. 1387–1395, 2021.

[35] A. Zhang, J. Deng, S. Yu, F. Zhang, R. J. Linhardt, and P. Sun, "Purification and structural elucidation of a water-soluble polysaccharide from the fruiting bodies of the *Grifola frondosa*," *International Journal of Biological Macromolecules*, vol. 115, pp. 221–226, 2018.

[36] Y. Han, S. Nan, J. Fan, Q. Chen, and Y. Zhang, "*Inonotus obliquus* polysaccharides protect against Alzheimer's disease by regulating Nrf2 signaling and exerting antioxidative and antiapoptotic effects," *International Journal of Biological Macromolecules*, vol. 131, pp. 769–778, 2019.

[37] W. Li, X. Wang, C. Li, T. Chen, and Q. Yang, "Exosomal noncoding RNAs: emerging roles in bilateral communication between cancer cells and macrophages," *Molecular Therapy*, vol. 30, no. 3, pp. 1036–1053, 2022.

[38] Y. Yang, Y. Yang, M. Chen et al., "Injectable shear-thinning polylysine hydrogels for localized immunotherapy of gastric cancer through repolarization of tumor-associated macrophages," *Biomaterials Science*, vol. 9, no. 19, pp. 6597–6608, 2021.

[39] X. Jiang, G. Cao, G. Gao, W. Wang, J. Zhao, and C. Gao, "Triptolide decreases tumor-associated macrophages infiltration and M2 polarization to remodel colon cancer immune microenvironment via inhibiting tumor-derived CXCL12," *Journal of Cellular Physiology*, vol. 236, no. 1, pp. 193–204, 2021.

[40] S. Russo, M. Kwiatkowski, N. Govorukhina, R. Bischoff, and B. N. Melgert, "Meta-inflammation and metabolic reprogramming of macrophages in diabetes and obesity: the importance of metabolites," *Frontiers in Immunology*, vol. 12, pp. 1–17, 2021.

[41] B. Zhang, Y. Yang, J. Yi, Z. Zhao, and R. Ye, "Hyperglycemia modulates M1/M2 macrophage polarization via reactive oxygen species overproduction in ligature-induced periodontitis," *Journal of Periodontal Research*, vol. 56, no. 5, pp. 991–1005, 2021.

[42] F. Xie, J. Lei, M. Ran et al., "Attenuation of diabetic nephropathy in diabetic mice by fasudil through regulation of macrophage polarization," *Journal of Diabetes Research*, vol. 2020, Article ID 4126913, 11 pages, 2020.

[43] Y. Y. Huang, C. W. Lin, N. C. Cheng et al., "Effect of a novel macrophage-regulating drug on wound healing in patients with diabetic foot ulcers: a randomized clinical trial," *JAMA Network Open*, vol. 4, no. 9, Article ID e2122607, 2021.

[44] N. Du, K. Wu, J. Zhang et al., "Inonotsuoxide B regulates M1 to M2 macrophage polarization through sirtuin-1/endoplasmic reticulum stress axis," *International Immunopharmacology*, vol. 96, pp. 107603–107609, 2021.

[45] J. Ding, H. Zhang, Y. Tian, P. F. H. Lai, H. Xu, and L. Ai, "Rheological properties of *Prunus persica* exudate: potential effects of proteins and polyphenols," *International Journal of Biological Macromolecules*, vol. 133, pp. 831–838, 2019.

[46] Y. Wang, F. Ouyang, C. Teng, and J. Qu, "Optimization for the extraction of polyphenols from *Inonotus obliquus* and its antioxidation activity," *Preparative Biochemistry & Biotechnology*, vol. 51, no. 9, pp. 852–859, 2021.

[47] H. He, Y. Li, M. Fang, T. Li, Y. Liang, and Y. Mei, "Carbon source affects synthesis, structures, and activities of mycelial polysaccharides from medicinal fungus *Inonotus obliquus*," *Journal of Microbiology and Biotechnology*, vol. 31, no. 6, pp. 855–866, 2021.

[48] T. Nakata, T. Yamada, S. Taji et al., "Structure determination of inonotsuoxides A and B and in vivo anti-tumor promoting activity of inotodiol from the sclerotia of *Inonotus obliquus*," *Bioorganic & Medicinal Chemistry*, vol. 15, no. 1, pp. 257–264, 2007.

[49] P. Liu, J. Xue, S. Tong, W. Dong, and P. Wu, "Structure characterization and hypoglycaemic activities of two polysaccharides from *Inonotus obliquus*," *Molecules*, vol. 23, no. 8, pp. 1948–2015, 2018.

[50] Y. Chen, Y. Huang, Z. Cui, and J. Liu, "Purification, characterization and biological activity of a novel polysaccharide from *Inonotus obliquus*," *International Journal of Biological Macromolecules*, vol. 79, pp. 587–594, 2015.

[51] K. Li, Y. X. Cao, S. M. Jiao, G. H. Du, Y. G. Du, and X. M. Qin, "Structural characterization and immune activity screening of polysaccharides with different molecular weights from astragali radix," *Frontiers in Pharmacology*, vol. 11, pp. 1–18, 2020.

Hindawi
Evidence-Based Complementary and Alternative Medicine
Volume 2022, Article ID 6211215, 13 pages
https://doi.org/10.1155/2022/6211215

Research Article

Artemisinin Alleviates Intestinal Inflammation and Metabolic Disturbance in Ulcerative Colitis Rats Induced by DSS

Xuemei Jia,[1] **Yunxiao Gao**,[1] **Liran Liu**,[1] **Yuxi Guo**,[1] **Jie Wang**,[1] **Hongyu Ma**,[1,2] **Runyuan Zhao**,[3] **Bolin Li**,[4] **Yao Du**,[4] **and Qian Yang**[4]

[1]*Hebei University of Chinese Medicine, Shijiazhuang, Hebei 050091, China*
[2]*Department of Traditional Chinese Medicine, Hebei General Hospital, Shijiazhuang, Hebei 050051, China*
[3]*Department of Gastroenterology, The First Affiliated Hospital of Guangzhou University of Chinese Medicine, Guangdong, Guangzhou 510405, China*
[4]*Department of Gastroenterology, The First Affiliated Hospital of Hebei University of Chinese Medicine, Shijiazhuang, Hebei 050011, China*

Correspondence should be addressed to Yao Du; 609661917@qq.com and Qian Yang; yang0311qian@126.com

Received 25 January 2022; Accepted 8 March 2022; Published 19 April 2022

Academic Editor: Xiang Liu

Objective. This study is aimed to reveal the possible mechanisms of artemisinin in the treatment of ulcerative colitis (UC) through bioinformatics analysis and experimental verification in UC model rats. *Methods*. Firstly, we searched two microarray data of the Gene Expression Omnibus (GEO) database to explore the differentially expressed genes (DEGs) between UC samples and normal samples. Then, we selected DEGs for gene ontology (GO) function enrichment analysis and Kyoto Encyclopedia of Genes and Genomes (KEGG) pathway enrichment analysis. The acute UC model of rats was established by using 3.5% dextran sulfate sodium (DSS) for 10 days to verify the core pathway. Finally, we evaluated the therapeutic effect of artemisinin at the molecular level and used metabonomics to study the endogenous metabolites in the rat serum. *Results*. We screened in the GEO database and selected two eligible microarray datasets, GSE36807 and GSE9452. We performed GO function and KEGG pathway enrichment analyses of DEGs and found that these DEGs were mainly enriched in the inflammatory response, immune response, and IL-17 and NF-κB signaling pathways. Finally, we verified the IL-17 signaling pathway and key cytokines, and ELISA and immunohistochemical results showed that artemisinin could downregulate the expression of proinflammatory cytokines such as IL-1β and IL-17 in the IL-17 signaling pathway and upregulate the expression of the anti-inflammatory cytokine PPAR-γ. Metabolomics analysis showed that 33 differential metabolites were identified in the artemisinin group (AG) compared to the model group (MG). Differential metabolites were mainly involved in alanine, aspartate, and glutamate metabolism and synthesis and degradation of ketone bodies. *Conclusion*. In this study, we found that artemisinin can significantly inhibit the inflammatory response in UC rats and regulate metabolites and related metabolic pathways. This study provides a foundation for further research on the mechanism of artemisinin in the treatment of UC.

1. Introduction

Ulcerative colitis (UC) is a chronic nonspecific intestinal inflammation characterized by abdominal pain, diarrhea, and blood in the stool [1]. The pathogenesis of UC is not completely clarified and may be related to immune, environmental, and genetic factors. The anti-UC drugs mainly include 5-aminosalicylic acid, hormones, immunosuppressive agents, etc. But UC cannot be cured completely and greater side effects were left in UC patients [2]. With the development of industrialization and urbanization, the number of diagnosed UC patients in China has increased sharply, with 1.2 cases per 100,000 people, and this number is still increasing [3]. About half of UC is classified as a chronic recurrent disease [4]. The long course and recurrent episodes often afflict the mental and psychological state of patients, and the prolonged course also leads to an increased risk of colorectal cancer [5].

The exact pathogenesis of UC is unknown. Studies have shown that bioinformatics technology can help us understand the pathogenesis of UC more clearly by identifying different genes in UC microarray data [6, 7].

Compared with chemical drugs, traditional Chinese medicines have the advantage of fewer side effects, and currently attract researchers' attention to the treatment of gastrointestinal diseases [8]. Artemisinin is a semiterpene lactone compound, which has been listed by the World Health Organization as a first-line drug for the treatment of malaria [9]. In addition to antimalarial, artemisinin also has anti-inflammatory, antibacterial, antitumor, antifibrosis, and immune regulation effects [10]. Studies have found that artemisinin can treat immune diseases by inducing the production of regulatory T cells and inhibiting the phosphorylation of AKT [11], and it can play an anti-inflammatory role by inhibiting the activation of NLRP3 inflammasome [12]. According to reports, artemisinin can ameliorate inflammation-driven lymphangiogenesis via VEGF-C/VEGFR-3 signaling pathway [13], and it can also induce the expression of CYP3A by activating PXR [14], thereby preventing inflammatory bowel disease. The treatment of artemisinin in immune and inflammatory diseases inspired us to explore the treatment of ulcerative colitis.

In recent years, metabolomics is widely used to discover the pathogenesis of diseases and the potential mechanism of action of drugs [15]. Metabolomics is a discipline that simultaneously qualitatively and quantitatively analyzes all low-molecular-weight metabolites of a certain organism or cell in a specific physiological period, and it can more accurately reflect the state of the biological system of small molecule metabolites in the treatment process from the overall level, which conforms to the holistic, dynamic, and dialectical views of Chinese medicine [16–18]. It has been confirmed that UC will cause metabolic disorders [19]. However, there are few studies on the metabolic changes of artemisinin in the treatment of UC. Therefore, it is meaningful to study whether artemisinin can reduce colon inflammation by reversing metabolism.

In this study, we applied two datasets from the Gene Expression Omnibus (GEO) database to identify the differentially expressed genes (DEGs) of UC and performed gene ontology (GO) functional and Kyoto Encyclopedia of Genes and Genomes (KEGG) pathway enrichment analyses on DEGs. Then, we constructed an acute UC model induced by dextran sulfate sodium (DSS) and verified the core pathways. Finally, we evaluated the therapeutic effect of artemisinin at the molecular level and used metabonomics to study the endogenous metabolites in the rat serum. The therapeutic effect of artemisinin on UC is provided on a theoretical basis.

2. Materials and Methods

2.1. Bioinformatics Analysis

2.1.1. Data Resource. We searched in the GEO database (http://www.ncbi.nlm.nih.gov/geo/) and collected the gene expression data of GSE36807 and GSE9452 in colon mucosal tissues from healthy individuals and UC patients. Microarray data included in GSE36807 and GSE9452 were obtained from GPL570-55999 platforms. GSE36807 included 7 healthy human colon tissue samples and 15 UC patients' colon tissue samples. GSE9452 included 5 healthy human colon tissue samples and 21 UC patients' colon tissue samples.

2.1.2. Data Preprocessing. The *R* language packages "Affy" and "affyPLM" were applied for background correction and normalization of the raw data. Then, according to the platform annotation information, each probe ID was converted into a gene ID. Subsequently, gene IDs were converted into gene symbols and saved. The *R* software "limma" package was used to screen DEGs between patients with UC and healthy human colon tissues, and the DEGs data of the intersection between the two were visualized with online software Venn diagram.

2.1.3. Gene Ontology and KEGG Pathway Enrichment Analyses. Both GO and KEGG enrichment analyses of the DEGs were performed using the *R* package clusterProfiler (version 4.0.3). The results of the analysis were expressed in the form of bar graphs and bubble graphs.

2.2. Experimental Verification

2.2.1. Drugs and Reagents. DSS was purchased from Meilun Biotechnology Co., Ltd. (Dalian, China). Mesalazine was purchased from Losan Pharma GmbH (Freiburg im Breisgau, Germany). Artemisinin was purchased from TCI Development Co., Ltd. (Shanghai, China). ELISA kits for IL-1β, IL-13, IL-33, and ST2 were purchased from Jiangsu Enzyme Immune Industrial Co., Ltd. (Jiangsu, China). ELISA kit for IL-17 was purchased from Shanghai Senxiong Technology Industry Co., Ltd. (Shanghai, China). ELISA kit for IL-23 was purchased from Shanghai XiTang Biological Technology Co., Ltd., (Shanghai, China).

2.2.2. Animal. A total of 40 SPF male Wistar rats (age, 8 weeks; weight, 200 ± 20g) were provided by the Animal Experiment Center of Hebei Medical University. All rats were kept in a special pathogen-free (SPF) room at a temperature of 23–25°C, in a 12-hour light and 12-hour dark cycle. They had free access to water and food and acclimatized for one week to enter the experiment. This experiment was approved by the Ethics Committee and Animal Experiment Committee of Hebei Academy of Traditional Chinese Medicine.

2.2.3. Experimental Design. DSS was used to induce the acute UC model. According to the random number table method, 40 rats were divided into a normal group (NG, $n = 10$) and a control group ($n = 30$). The NG rats were given normal drinking water, and the control group rats were given 3.5% DSS solution for 10 consecutive days to establish acute UC model rats. After 10 days, 3 rats were selected

randomly and sacrificed from the control group for pathological evaluation. Pathological changes such as congestion, edema, erosion, and ulcer appeared in the colon tissue, indicating that the model was successful. Three rats died during the modeling period. The successful control rats were randomly divided into three groups, model group (MG, $n = 8$), western medicine group (WG, $n = 8$), and artemisinin group (AG, $n = 8$). The WG was administered with 0.315 g/kg/d of mesalazine suspension, and AG was administered with 100 mg/kg/d of artemisinin suspension. NG and MG were given the same dose of 0.9% saline. After 14 days of treatment, the rats were fasted for 24 hours. Rats were injected intraperitoneally with 1% sodium pentobarbital (50 mg/kg).

2.2.4. Disease Activity Index (DAI). According to the DAI scoring standard established by Murano et al. [20], DAI = (weight loss score + stool trait score + stool blood score)/3 (Table 1).

2.2.5. Histopathological Evaluation. For hematoxylin-eosin (HE) staining, the paraffin sections of colon tissue that have been fixed and sectioned were soaked in xylene for dewaxing, hydrated in absolute ethanol, soaked in different gradients of ethanol, fully stained with hematoxylin staining solution, rinsed with distilled water, differentiated with hydrochloric acid and ethanol, rinsed with double distilled water, fully immersed in eosin staining solution, dehydrated with different gradients of ethanol, immersed in xylene, air dried, sealed with neutral gum, and observed under a microscope.

2.2.6. Immunohistochemistry. According to the immunohistochemical process, the contents of NF-κB and PPAR-γ in colon tissue were detected. The colon tissue sections were deparaffinized and hydrated, washed three times with PBS buffer, and then boiled with 0.01 M sodium citrate buffer for antigen retrieval. Endogenous peroxidase and biotin were inactivated with 3% hydrogen peroxide. Sections were blocked with 5% BSA, rabbit antirat NF-κB polyclonal antibody and rabbit antirat PPAR-γ polyclonal antibody were incubated overnight at 4°C, and secondary antibodies (1:500; Abcam, MA, US) at room temperature for 1 hour. Analysis was performed using the HMIAS-2000 imaging system, and NF-κB and PPAR-γ positive areas were observed under a microscope (Olympus, Tokyo, Japan).

2.2.7. Serum Sample Preparation. The anesthetized rat was placed on the operating table, of which 3–5 ml of blood was taken from the heart. Blood specimens were collected and centrifuged at 3000r/min at 4°C for 15 min. Then, separated serum samples were stored in −80°C refrigerator until testing.

2.2.8. Biochemical Analysis. The levels of IL-1β, IL-17, IL-23, IL-13, IL-33, and ST2 were measured by ELISA kit.

Table 1: The standard of DAI score.

Score	Decline in body weight (%)	Stool	Hematochezia
0	Naught	Normal	Negative
1	1–5	—	—
2	5–10	Semi-loose	BLD (+)
3	10–15	—	—
4	>15	Loose	Bloody eye

2.2.9. Metabolite Extraction. All serum samples were melted at 4°C, 100 μL serum was accurately pipetted into a 2 mL centrifuge tube, 100 μL internal standard mixture and 400 μL methanol (−20°C) were added, vortexed for 1 min; centrifuged at 12000 rpm and 4°C for 10 min, and 500 μL of the supernatant was placed in a 2 ml centrifuge tube and concentrated and dried in vacuo. About 150 μL of 80% methanol solution was reconstituted, and after mixing, centrifuged at 12000 rpm and 4°C for 10 min, and the supernatant was taken as the sample to be tested. About 20 μL is taken from each sample to be tested and mixed into a QC sample, and the remaining samples were used for LC-MS testing.

2.2.10. Liquid Chromatography-Mass Spectrometry (LC-MS) Analysis. Chromatographic separation was performed on a Thermo Vanquish system with an ACQUITY UPLC® HSS T3 (150 × 2.1 mm, 1.8 μm, Waters) column maintained at 40°C. The autosampler temperature was maintained at 8°C. The analyte was gradient eluted with 0.1% formic acid aqueous solution (A1) and 0.1% formic acid acetonitrile (B1) or 5 mM ammonium formate aqueous solution (A3) and acetonitrile (B3) at a flow rate of 0.25 mL/min. The gradient elution program was 0–1 min, 2% B1/B3; 1–9 min, 2%–50% B1/B3; 9–12 min, 50%–98% B1/B3; 12–13.5 min, 98% B1/B3; 13.5–14 min, 98%–2% B1/B3; 14–20 min, 2% B1-positive mode (14–17 min, 2% B3-negative mode).

Using the Thermo Q Exactive mass spectrometer, the ESI-MSn experiments were performed in positive and negative modes with the spray voltage of 3.8 kV and −2.5 kV, respectively. Sheath gas and auxiliary gas were set at 30 and 10 arbitrary units, respectively. The capillary temperature was 325°C, the full scan was carried out with a resolution of 70,000, and the scanning range was m/z 81–1,000. Data-dependent acquisition (DDA) MS/MS experiments were acquired with an HCD scan, and the normalized collision energy was 30 eV. Dynamic exclusion was performed to remove unnecessary MS/MS information.

2.2.11. Metabolite Identification and Statistical Analysis. The obtained original data were converted to mzXML format (xcms input file format) by Proteowizard software (v3.0.8789). R's XCMS package (v3.3.2) was used for peaks identification, peaks filtration, and peaks alignment. The main parameters were bw = 2, ppm = 15, peakwidth = c(5, 30), mzwid = 0.015, mzdiff = 0.01, and method = centWave. The peak areas of data of different magnitudes were normalized in batches. In order to obtain more reliable and intuitive results, the data were performed unit variance

scaling (UV) before multivariate statistical analysis. Principal component analysis (PCA), partial least-squares discriminant analysis (PLS-DA), and orthogonal partial least-squares discriminant analysis (OPLS-DA) were used to analyze all sample compounds. Metabolites with p value ≤ 0.05 + VIP ≥1; p value ≤ 0.05 + fold_change ≥1.5 or ≤0.667; one-way ANOVA p value ≤ 0.05 and VIP ≥1; two-way ANOVA p value ≤ 0.05 were considered differential metabolites. The identification of metabolites was first confirmed by the exact molecular weight of the metabolite (molecular weight error <15 ppm), then the fragment information was obtained according to the MS/MS model and annotated in the Metlin (http://metlin.scripps.edu) and MoNA (https://mona.fiehnlab.ucdavis.edu//) databases to obtain accurate metabolite information. Significantly altered metabolite data were performed using MetaboAnalyst (https://www.metaboanalyst.ca) for metabolic pathway analysis. HMDB (Human Metabolome Database, http://www. hmdh. ca) and KEGG (Kyoto Encyclopedia of Genes and Genomes, https://http://www.kegg.jp) were used to annotate differential metabolism and enrich related metabolic pathways.

3. Results

3.1. Results of Bioinformatics Analysis

3.1.1. Core Differential Genes. According to the screening conditions, the GSE36807 database contained a total of 484 DEGs, including 109 upregulated genes and 375 downregulated genes; the GSE9452 database contained 581 DEGs, including 173 upregulated genes and 408 downregulated genes. Venn software (version 2.1.0) was used to generate Venn diagrams of overlapping DEGs in 2 databases (Figure 1(a)), including 32 upregulated genes and 138 downregulated genes (Table S1).

3.1.2. GO and KEGG Enrichment Analyses. GO function and KEGG pathway enrichment analyses were performed on 170 common DEGs using *R* language software. GO function enrichment analysis includes the biological process (BP), cellular component (CC), and molecular function (MF).

According to the adjustment order of P value from small to large, the first 15 items were selected for analysis. Among them, BP was mainly related to functions such as leukocyte migration, humoral immune response, and cell response to lipopolysaccharide; CC was mainly associated with the extracellular matrix, cytoplasmic vesicle lumen, and collagen-containing extracellular matrix; MF mainly related to the chemokine activity, cytokine activity, *G* protein-coupled receptor binding, and other functions (Figure 1(b)). A total of 32 signal pathways were obtained through KEGG enrichment analysis (adjusted $p < 0.01$). The data were screened according to the P value, and the first 20 entries were selected for enrichment analysis, including the IL-17 signal pathway, NF-κB signal pathway, and chemokine signal pathway (Figure 1(c) and Table S2).

3.2. Results of Experimental Verification

3.2.1. Artemisinin Can Significantly Reduce Colon Injury and Disease Activity in UC. In order to explore the effect of artemisinin on the histological changes of DSS-induced UC model rats, we used HE staining to observe the rat colon tissue. As shown in Figure 2(a), the morphology of the colon of the rats in the NG was normal, the glands were neatly arranged, the crypts were normal, and there were no inflammatory cell infiltration, congestion, and edema. In the MG, the structure of the colonic mucosa was damaged obviously, the crypt structure was disordered, the goblet cells were reduced, the neutrophils were infiltrated, and there were crypt abscesses. After the intervention of mesalazine and artemisinin, the colon mucosa of the rats was relatively complete, the glands were arranged regularly, and there were slight congestion, edema, and inflammatory cell infiltration.

Compared with the NG, the DAI score of rats in the MG increased significantly, and after the intervention of artemisinin, the DAI score decreased significantly (Figure 2(b)). The above results indicated that artemisinin can significantly reduce colon injury and disease activity in UC rats.

3.2.2. Artemisinin Downregulated Proinflammatory Cytokines and Upregulated Anti-Inflammatory Cytokine in the IL-17 Signaling Pathway. In order to verify the effect of artemisinin on inflammation in UC rats, we selected the IL-17 signaling pathway and key cytokines for detection. The ELISA results showed that compared with the NG, the levels of serum IL-1β, IL-17, IL-23, IL-13, IL-33, and ST2 in the MG were significantly increased ($P < 0.05$). However, artemisinin treatment significantly decreased the expression levels of them in UC rats (Figure 3).

The results of immunohistochemistry showed that the expression level of PPAR-γ in the MG was significantly downregulated than that in the NG, and artemisinin administration significantly increased the expression level of PPAR-γ (Figures 4(a) and 4(c)). Different from this result, the expression level of NF-κB in the MG was significantly upregulated than that in the NG, and artemisinin administration significantly reduced the expression level of NF-κB (Figures 4(b) and 4(d)). These results indicated that artemisinin may inhibit the colonic inflammatory response in UC rats.

3.2.3. Liquid Chromatography-Mass Spectrometry (LC-MS) Method Verification. To obtain reliable and high-quality metabolomics data, we carried out quality control (QC) and quality assurance (QA). As shown in Figures 5(a) and 5(b), the PCA score plot showed that the QC samples were clustered together, which indicated that the data were reliable and reproducible.

3.2.4. Multivariate Statistical Analysis of Metabolites of Artemisinin in the Treatment of UC. In order to study the effect of artemisinin on the metabolic profile of UC rats'

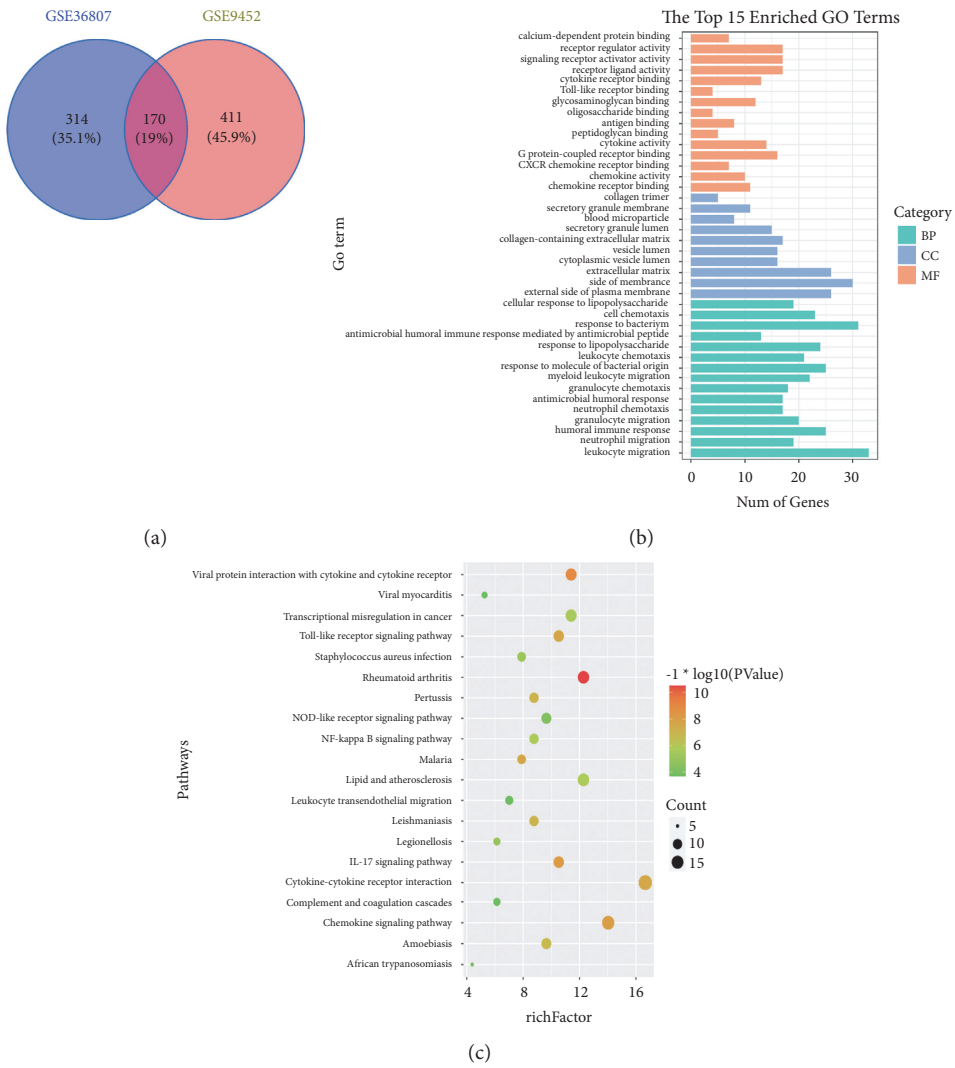

Figure 1: Identification of DEGs in two databases (GSE36807 and GSE9452) and GO analysis and KEGG pathway analysis of DEGs in UC. (a) Venn diagram between the common targets of two microarray data. (b) GO function analysis of intersection DEGs (top 15). (c) KEGG pathway bubble diagram of the intersection DEGs (top 20).

serum samples, we used PCA and PLS-DA for pattern recognition of the metabolite profiles in NG, MG, WG, and AG serum samples. The PCA score chart was established. In the positive and negative ion modes, the NG and the MG were significantly separated, indicating that DSS-induced UC rats had significant changes in physiology and metabolism (Figures 5(c) and 5(d)). The MG was significantly different from the AG (Figures 5(e) and 5(f)). It indicated that the overall metabolism of rats after the intervention of artemisinin was significantly different from that of the MG.

The OPLS-DA supervised pattern recognition method was employed to identify the different metabolites between each group. In the PLS-DA permutation experiment plots (Figure 5), the results of R^2 and Q^2 values generated by any random permutation on the left were lower than the origin on the right, which proved that the model had not been excessively fitting, and the results had high reliability.

The results of OPLS-DA analysis showed that the NG and the MG were significantly separated under the positive and negative ion modes, indicating that the metabolism of DSS-induced model rats had significantly changed compared with healthy rats (Figures 6(a) and 6(b)). The NG, MG, and AG were significantly separated, and the AG was located between the NG and the MG, indicating that after the treatment of artemisinin, the metabolism of DSS-induced model rats tended to improve to a normal state (Figures 6(e) and 6(f)).

3.2.5. Identification of Potential Biomarkers. The VIP value and p value were applied to show the importance of metabolites. VIP>1 and $p < 0.05$ were used as the criteria to screen differential metabolites. Compared with the NG, there were 17 metabolites significantly increased in the MG, mainly including pyrrolidonecarboxylic acid, L-malic acid, L-carnitine, isocitric acid, indoleglycerol phosphate, dethiobiotin, gluconic acid, and phenylacetic acid, and 16 metabolites were significantly reduced,

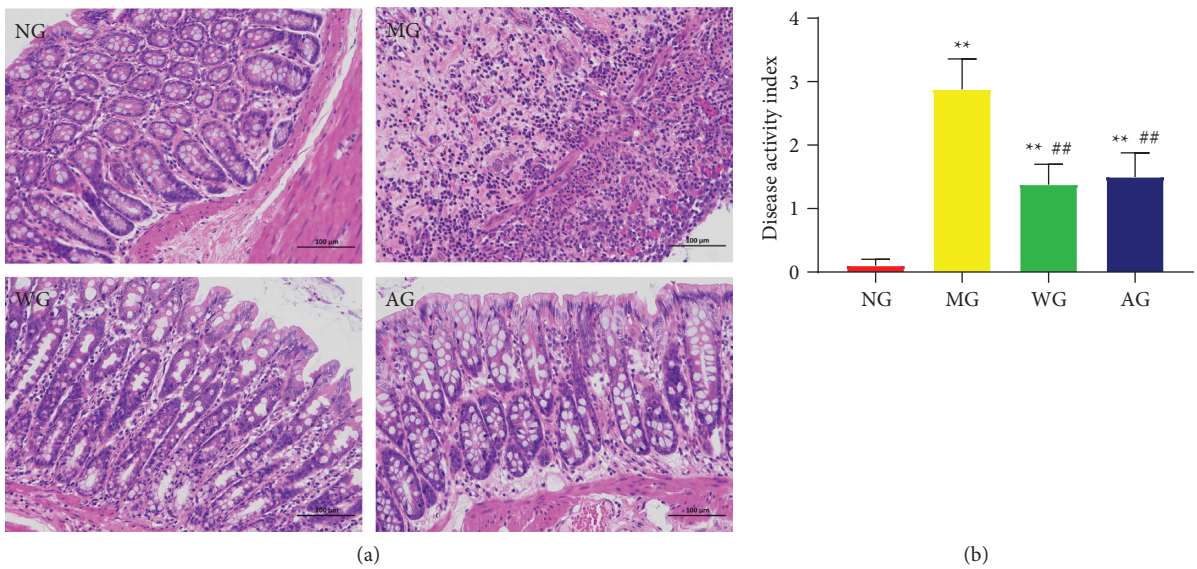

Figure 2: Artemisinin attenuates colonic inflammation induced by DSS. (a) HE staining (×200) of colon tissue in each group. (b) Disease activity index (DAI) in each group. NG: normal group; MG: model group; WG: western medicine group; AG: artemisinin group. $^{**}P < 0.05$ vs NG. $^{\#\#}P < 0.01$ vs MG.

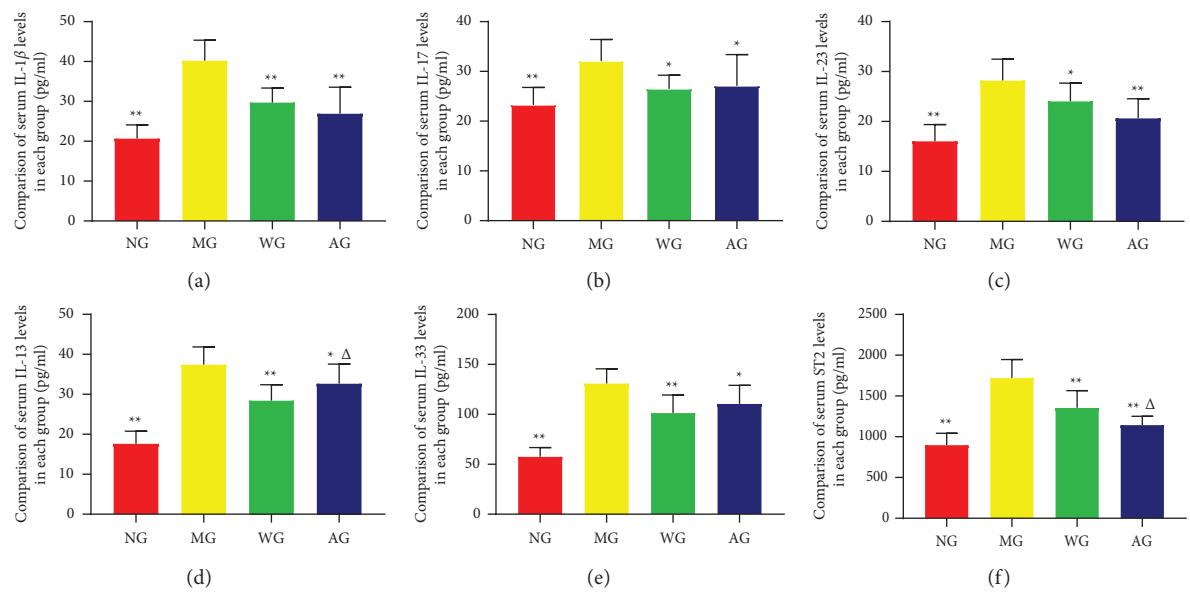

Figure 3: Effects of artemisinin on IL-17 signaling pathway and serum inflammatory factor expression in UC rats (n = 8 or 10). (a) IL-1β levels. (b) IL-17 levels. (c) IL-23 levels. (d) IL-13 levels. (e) IL-33 levels. (f) ST-2 levels. $^{*}P < 0.05$. $^{**}P < 0.01$ vs MG. $^{\Delta}P < 0.05$ vs WG.

mainly including jasmonic acid, homovanillin, gentisic acid, pyrimidodiazepine, cysteine-S-sulfate, 1H-indole-3-acetamide, 5-methylcytosine, and p-aminobenzoic acid. After the intervention of artemisinin, these biomarkers showed a significant reversal (Table 2).

3.2.6. Metabolic Pathway Analysis. Metabolic pathways of potential biomarkers identified in UC rats were analyzed using KEGG and MetPA databases. The impact value > 0.1 was considered as a significant difference. We imported the above 33 metabolites related to the occurrence of UC into the MetPA database to explore the potential pathways of artemisinin in the treatment of UC. The results showed that artemisinin treatment of UC was mainly related to four metabolic pathways: renal cell carcinoma, alanine, aspartate, and glutamate metabolism, synthesis and degradation of ketone bodies, and central carbon metabolism in cancer (Figure 7 and Table S3). Among these pathways, alanine, aspartate, and glutamate metabolism, and synthesis and degradation of ketone bodies were related to the development of UC. The above results indicated that artemisinin changed these biomarkers and related metabolic pathways to play a therapeutic effect on UC.

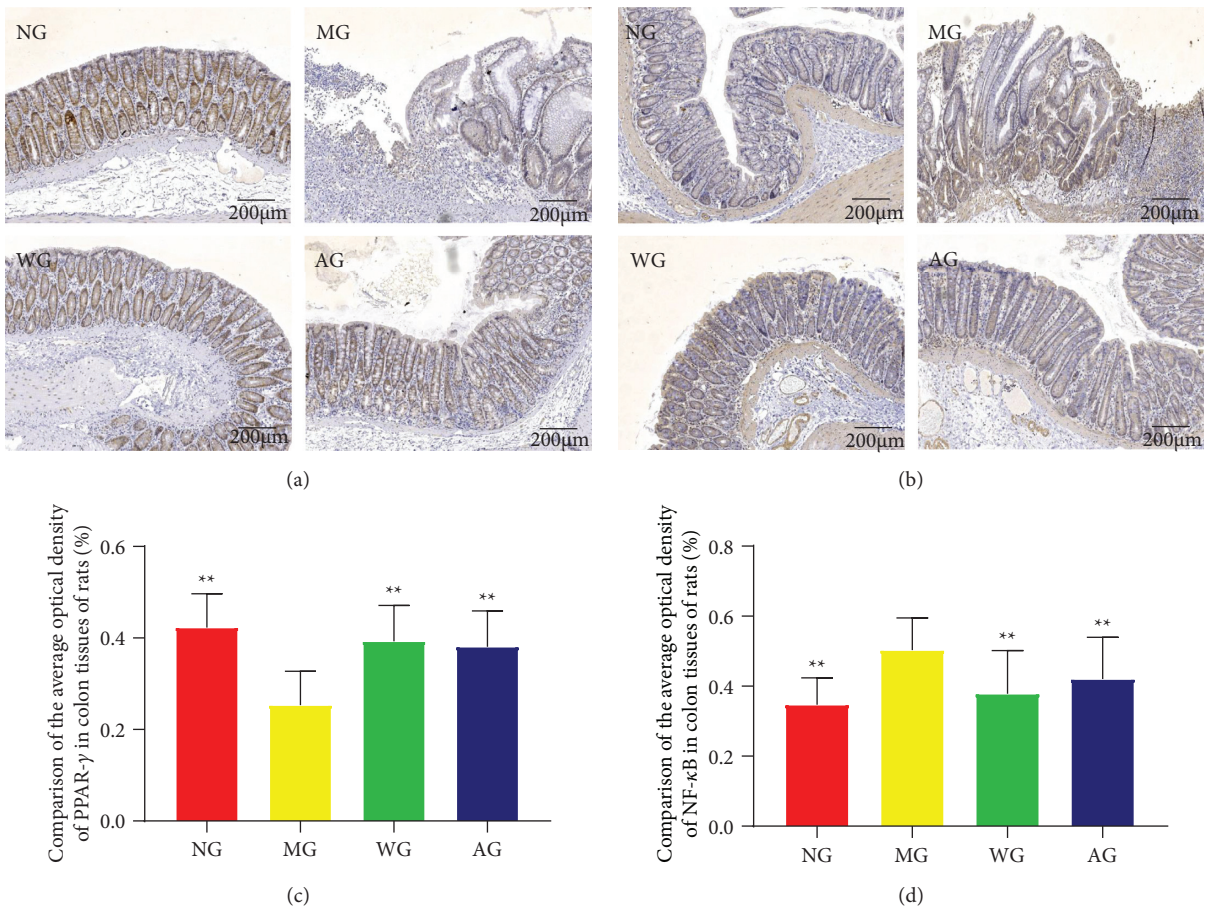

Figure 4: The effect of artemisinin on the expression of PPAR-γ (a) and NF-κB (b) by immunohistochemistry (n = 8 or 10). Quantitative analyses of AOD values of PPAR-γ (c) and NF-κB (d) at 100×magnification. $^{**}P < 0.01$ vs MG.

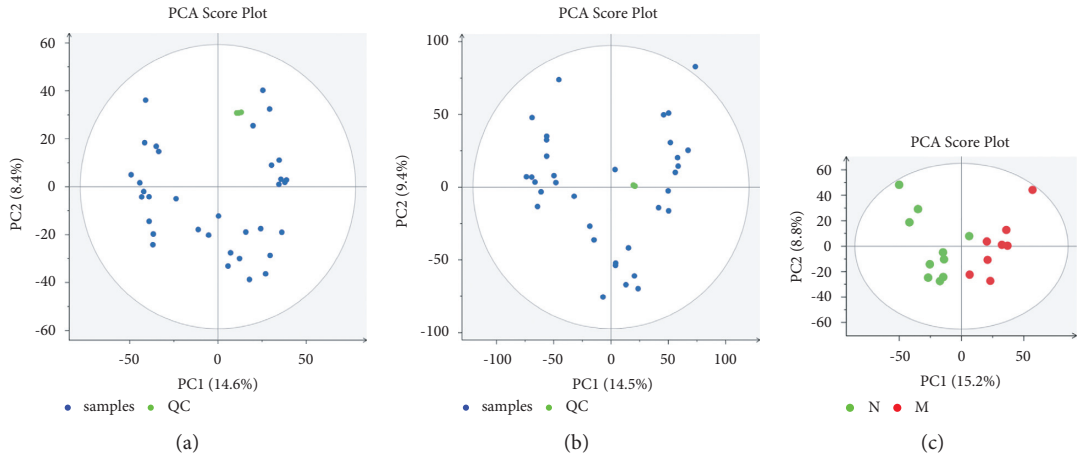

Figure 5: Continued.

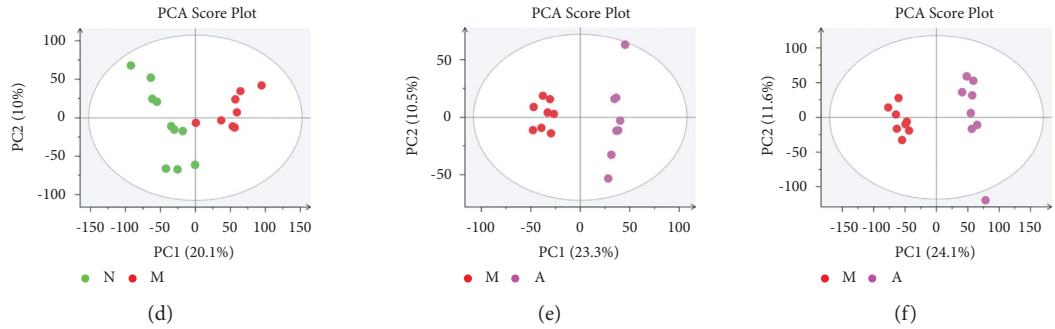

Figure 5: (a) PCA score plots of QC samples in positive ion mode; (b) PCA score plots of QC samples in negative ion mode; (c) PCA model results of NG and MG in positive ion mode; (d) PCA model results of NG and MG in negative ion mode; (e) PCA model results of MG and AG in positive ion mode; (f) PCA model results of MG and AG in negative ion mode.

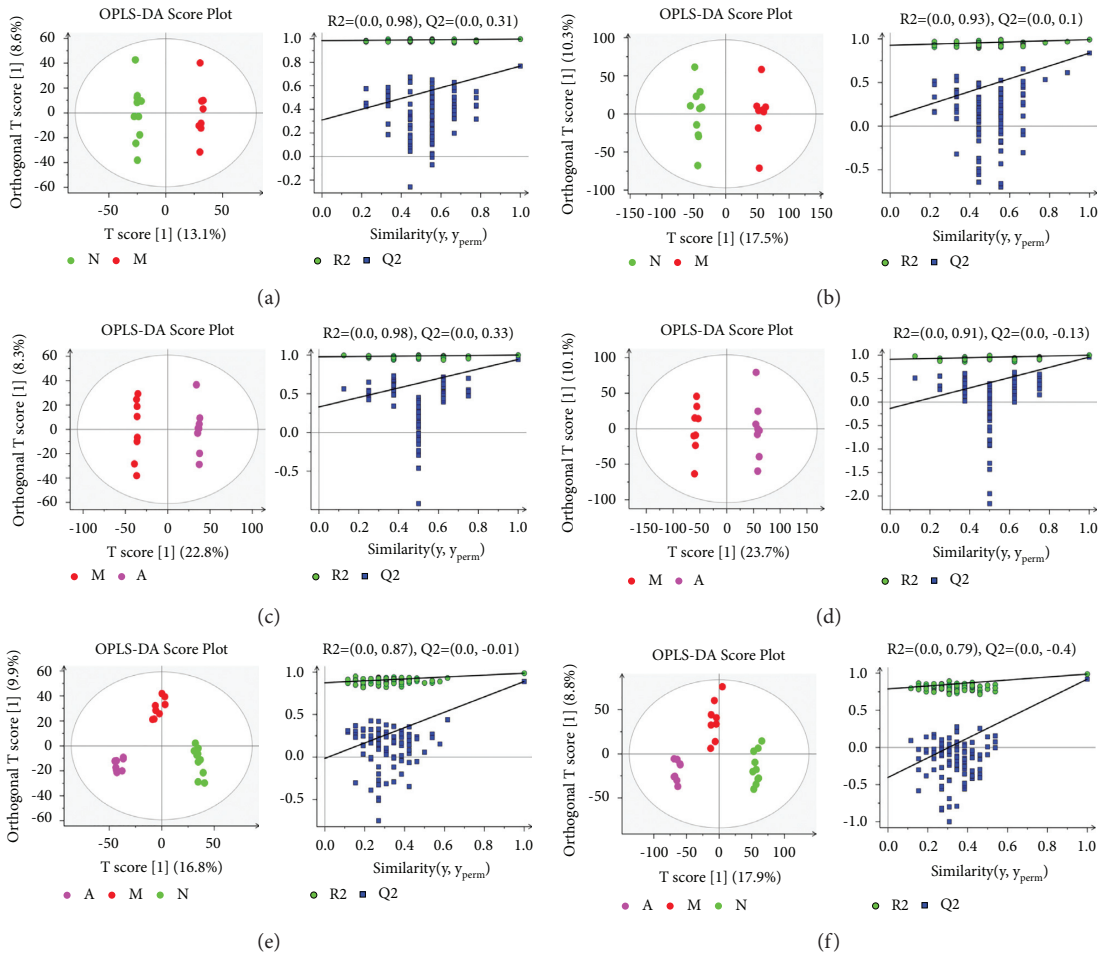

Figure 6: The OPLS-DA score plots and PLS-DA's 100 times permutation tests: (a) NG vs MG scores in positive ion mode; (b) NG vs MG scores in negative ion mode; (c) MG vs AG scores in positive ion mode; (d) MG vs AG scores in negative ion mode; (e) NG, MG and AG scores in positive ion mode; (f) NG, MG and AG scores in negative ion mode (OPLS-DA's model parameters: (a) $R^2Y = 0.997$, $Q^2 = 0.733$; (b) $R^2Y = 0.991$, $Q^2 = 0.831$; (c) $R^2Y = 0.999$, $Q^2 = 0.921$; (d) $R^2Y = 0.998$, $Q^2 = 0.936$; (e) $R^2Y = 0.988$, $Q^2 = 0.909$; (f) $R^2Y = 0.992$, $Q^2 = 0.937$).

4. Discussion

In recent years, with the development of industrialization, the incidence of UC has shown a significant upward trend in the world [21]. Although studies have shown that multiple factors such as genetics, immunity, environment, and intestinal microecology may lead to the occurrence of UC, the specific mechanism of UC is still unclear [22, 23]. Due to the complexity of the pathogenesis of UC and the lack of specific biomarkers, it greatly increases the medical burden and physical and mental discomfort of patients [24]. Bioinformatics methods can help us study and understand the

Table 2: Statistical analysis of potential metabolites of ulcerative colitis rats intervened by artemisinin.

No.	Differential metabolites	Formula	MG vs NG		AG vs MG	
			p value	Up/down	*p* value	Up/down
1	(R)-3-hydroxybutyric acid	C4H8O3	0.0067284	Down	0.023948675	Up
2	Jasmonic acid	C12H18O3	0.001182325	Down	0.007405533	Up
3	Homovanillin	C9H10O3	0.045589156	Down	0.000939106	Up
4	Gentisic acid	C7H6O4	0.002915086	Down	0.001947528	Up
5	Pyrimidodiazepine	C9H11N5O2	0.000862359	Down	0.001947528	Up
6	Cysteine-S-sulfate	C3H7NO5S2	0.036795147	Down	0.003876041	Up
7	1H-indole-3-acetamide	C10H10N2O	0.002915086	Down	0.010081694	Up
8	14,15-DiHETrE	C20H34O4	0.008763529	Down	0.007405533	Up
9	5-methylcytosine	C5H7N3O	0.000448668	Down	0.040568856	Up
10	p-aminobenzoic acid	C7H7NO2	0.036795147	Down	0.031324131	Up
11	Maleic acid	C4H4O4	0.045589156	Down	0.031324131	Up
12	L-aspartic acid	C4H7NO4	0.002915086	Down	0.040568856	Up
13	3-methylthiopropionic acid	C4H8O2S	0.011331976	Down	0.018129008	Up
14	L-proline	C5H9NO2	0.014548024	Down	0.040568856	Up
15	Dimethyl sulfone	C2H6O2S	0.018543313	Down	0.001947528	Up
16	L-methionine	C5H11NO2S	0.023467646	Down	0.00538494	Up
17	Pyrrolidonecarboxylic acid	C5H7NO3	0.000624338	Up	0.031324131	Down
18	L-malic acid	C4H6O5	0.018543313	Up	0.000939106	Down
19	L-carnitine	C7H16NO3	0.002173751	Up	0.023948675	Down
20	Isocitric acid	C6H8O7	0.003880688	Up	0.002761604	Down
21	Indoleglycerol phosphate	C11H14NO6P	0.000862359	Up	0.013587273	Down
22	Dethiobiotin	C10H18N2O3	0.045589156	Up	0.000939106	Down
23	S-lactoylglutathione	C13H21N3O8S	0.014548024	Up	0.002761604	Down
24	3-(3,4-dihydroxyphenyl)pyruvate	C9H7O5	0.008763529	Up	0.031324131	Down
25	Gluconic acid	C6H12O7	0.00512852	Up	0.00538494	Down
26	Phenylacetic acid	C8H8O2	0.001609069	Up	0.001359376	Down
27	Creatinine	C4H7N3O	0.023467646	Up	0.040568856	Down
28	D-glucose	C6H12O6	0.018543313	Up	0.000409933	Down
29	Thymine	C5H6N2O2	0.018543313	Up	0.000409933	Down
30	O-phosphoethanolamine	C2H8NO4P	0.001182325	Up	0.001359376	Down
31	Deoxyuridine	C9H12N2O5	0.0067284	Up	0.007405533	Down
32	Pimelic acid	C7H12O4	0.00512852	Up	0.001947528	Down
33	6-ketoprostaglandin E1	C20H32O6	0.011331976	Up	0.013587273	Down

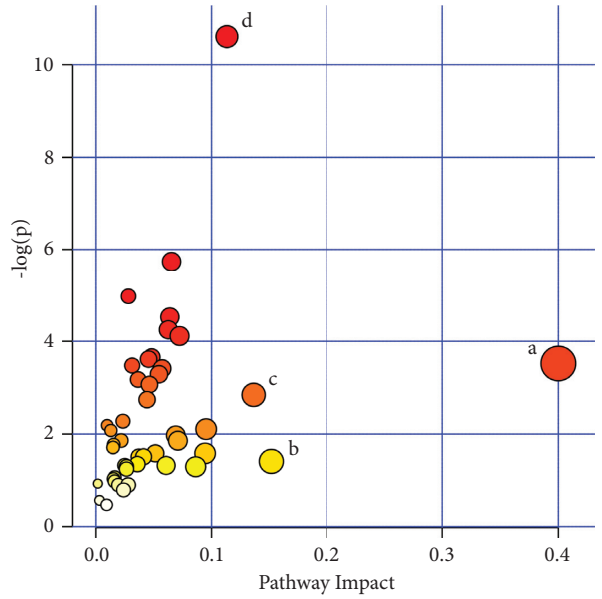

Figure 7: Metabolic pathways involved in potential markers in plasma. (a) Renal cell carcinoma; (b) alanine, aspartate, and glutamate metabolism; (c) synthesis and degradation of ketone bodies; (d) central carbon metabolism in cancer.

underlying mechanism of UC more clearly. To find a solution to this problem, we used the GEO database to screen the datasets and verified the relevant targets.

The GEO database is an international public repository of high-throughput microarray and next-generation sequencing functional genome datasets submitted by the research community [25]. We screened in the GEO database and selected two eligible datasets, GSE36807 and GSE9452. After data analysis, we got 170 overlapping DEGs, including 32 upregulated genes and 138 downregulated genes. Then, we performed GO function and KEGG pathway enrichment analyses on the common DEGs of the two groups of microarray data and found that the pathogenesis of UC was related to inflammation and immune response, mainly enriched in IL-17 signaling pathway and NF-κB signaling pathway, suggesting that inflammation and abnormal activation of the immune system may be the core features of the pathogenesis of UC [26].

Based on the current data, we believed that the IL-17 signaling pathway is more likely to reflect the degree of inflammation in DSS-induced colitis rats. Therefore, we established a UC rat model and verified the IL-17 signaling pathway and inflammation-related indicators.

The IL-17 signaling pathway is one of the important mechanisms affecting the occurrence and development of UC. NF-κB plays a key pivotal role in the pathogenesis of UC, and activated NF-κB can release various cytokines and immune mediators including IL-17 and activate the IL-17 signaling pathway [27]. IL-17 is a specific effector secreted by Th17 cells, which has a strong inflammatory effect. It promotes the production of IL-6, IL-1β, and other inflammatory factors through recruitment, mobilization, and activation of macrophages and neutrophil granulocytes and mediates inflammatory invasion and tissue damage [28]. As a proinflammatory factor, IL-23 is involved in the formation and expansion of IL-17. When the IL-23/IL-17 inflammatory axis is formed, the inflammatory response continues to expand [29]. In addition, Peter et al. found that the IL-33/ST2 axis can aggravate Dss-induced colitis and IL-33 can specifically induce the activation of key pathogenic cytokines including IL-17 and IL-13 and maintain and amplify the inflammatory response of the IL-17 signaling pathway [30]. PPAR-γ is a key receptor for 5-ASA and has a protective effect on mucosal damage induced by the IL-17 signaling pathway by suppressing the activation of NF-κB [31, 32]. The experimental results showed that artemisinin inhibited the expression of proinflammatory cytokines such as IL-17 and IL-1β in the IL-17 signaling pathway and upregulated the expression of PPAR-γ, suggesting that artemisinin can alleviate the inflammatory immune response of UC rats.

Studies have reported that metabolomics may become an important approach for the early diagnosis of UC and provide a tool for exploring the metabolic regulation mechanism of UC. Therefore, for further exploring the therapeutic effect of artemisinin on UC, we used LC-MS to analyze the serum metabolic profiles of DSS rats and artemisinin-treated rats. PCA and PLS-DA analyses showed that 33 different metabolites could be significantly distinguished between artemisinin-treated and DSS-treated rats, mainly involving amino acid metabolism, energy metabolism, and other biochemical processes.

Amino acids play an important role in maintaining intestinal health by acting as substrates for protein synthesis in intestinal mucosal cells and modulators of metabolic pathways [33]. Amino acid metabolism mainly affects the material metabolism, energy supply, and intestinal mucosal barrier of UC [34–36] and is also closely related to the process of cell proliferation, differentiation, and apoptosis [37]. Currently, amino acid supplementation has been explored as a treatment for UC [38, 39]. This search found that DSS-induced colitis rats had significant abnormalities in amino acid metabolism, among which the contents of L-aspartic acid, L-proline, and L-methionine were significantly reduced. L-methionine is an essential amino acid, and Roediger et al. found methionine has a protective effect on sulfide-induced acute oxidative damage in rat colon cells [40]. L-aspartic acid is the synthetic precursor of L-methionine in the body and can be combined with various amino acids to make active drugs such as fatigue recovery agents [41–43]. In addition, Notararigo et al. reported that the levels of L-proline and L-methionine in UC patients were significantly lower than those in healthy controls, which were related to the impaired intestinal mucosal barrier, intestinal microbiota disturbance, and impaired absorption capacity in UC patients [44]. Consistent with the above studies, we showed that the rats in the DSS model group were emaciated, lethargic, and significantly decreased in activity, which may be related to the lower levels of L-aspartic acid and L-methionine, reflecting the insufficient intestinal energy absorption including essential amino acids [38, 45]. Moreover, differential metabolites were mainly involved in alanine, aspartate, and glutamate metabolism. Hong et al. reported that compound sophorae decoction can significantly improve the symptoms of DSS-induced colitis by modulating alanine, aspartate, and glutamate metabolism [46]. Therefore, artemisinin might alleviate the inflammation in UC by alanine, aspartate, and glutamate metabolism.

Creatinine and L-carnitine are involved in the energy supply of mammalian cells [47]. Creatine is an important compound for energy storage and utilization [48], and creatinine is the breakdown product of creatine phosphate in muscles [47]. In this study, creatinine was significantly increased in the MG, indicating that DSS-induced colitis rats have a disordered energy supply. L-carnitine is involved in the metabolism of most mammals, plants, and some bacteria and plays a key role in lipid metabolism and β-oxidation, and it is used to transport long-chain fatty acids into mitochondria to be oxidized for energy production and is an important part of muscle energy metabolism [49]. Studies have reported that under the influence of oxidative stress and weight loss in DSS-induced colitis, carnitine and creatine typically increase during disease development, which may reflect the overall stress state of the animals and further indicates that ATP and fatty acids are required for energy supply during UC [50, 51]. However, this situation was reversed after artemisinin intervention, indicating that artemisinin has positive effects on regulating stress response and energy supply in UC rats.

Synthesis and degradation of ketone bodies are other important pathways for artemisinin to interfere with the occurrence and development of UC. A previous study reported that diet-induced ketolytic metabolism can significantly reduce pain and inflammation [52]. Another study demonstrated that increased ketogenesis can mitigate TNFα-induced intestinal cells apoptosis and inflammation, suggesting that ketogenesis has a protective role in TNFα-induced intestinal pathology [53]. In this study, we showed that artemisinin could alleviate the inflammatory response in UC rats, indicating that artemisinin may play a role in regulating the synthesis and degradation of ketone bodies in UC rats.

In the present study, the expressions of glucose and gluconic acid were upregulated in MG rats, suggesting that DSS-induced colitis rats had an obvious disorder of glucose metabolism, such as decreased glucose decomposition, enhanced gluconeogenesis, and weakened glycolysis. It was reported that UC patients with high endoscopic activity [UCEIS $\geq$ 3] had significantly elevated glucose concentration [38], and high glucose levels were also found in fecal extracts and other biological specimens of UC patients [54]. This indicates that energy-related metabolites in the colon play an important role in maintaining the balance of gut microbiota and intestinal cells [55, 56], and the elevated glucose levels in DSS model rats may be caused by the energy disturbance of the host-microbiome system [57, 58]. Nevertheless, glucose and gluconic acid decreased after artemisinin intervention, demonstrating that the glycolysis pathway and energy metabolism disorders in rats were improved.

5. Conclusion

In this study, we performed a bioinformatics approach to identify DEGs in UC. In order to study the protective effect of artemisinin on DSS-induced colitis, we conducted animal experiments to verify the IL-17 signaling pathway, which is mainly enriched in UC DEGs and preliminarily explored the changes of endogenous metabolites in serum of UC rats after artemisinin intervention. These results demonstrate that artemisinin can regulate the balance of proinflammatory and anti-inflammatory factors, degrade the inflammatory response of UC, and adjust amino acid metabolism and synthesis and degradation of ketone bodies, which are related to energy metabolism and antioxidant capacity. This study aimed to provide a potential new strategy for the treatment of UC.

Data Availability

The datasets used and/or analyzed during the current study are available from the corresponding author on reasonable request.

Ethical Approval

This experiment was approved by the Ethics Committee and Animal Experiment Committee of Hebei Academy of Traditional Chinese Medicine.

Conflicts of Interest

The authors declare that they have no conflicts of interest.

Authors' Contributions

Xuemei Jia, Yunxiao Gao, and Liran Liu contributed equally to this study. Xuemei Jia, Yunxiao Gao, and Liran Liu wrote the manuscript and did the statistical analysis. Yuxi Guo and Jie Wang conducted the experiment. Hongyu Ma and Runyuan Zhao prepared the figures. Qian Yang and Yao Du conceived and designed the project.

Acknowledgments

This study was supported by the Scientific Research Project of Hebei Provincial Administration of Traditional Chinese Medicine (nos. 2020079, 2020080, 2020083, and 2020084).

Supplementary Materials

Table S1: the overlapping differential genes in two databases (GSE36807 and GSE9452) in ulcerative colitis. Table S2: enriched terms in the KEGG pathways for DEGs in ulcerative colitis (top 20). Table S3: main metabolic pathways information of impact >0.1. (*Supplementary Materials*)

References

[1] C. Ma, R. Sedano, A. Almradi et al., "An international consensus to standardize integration of histopathology in ulcerative colitis clinical trials," *Gastroenterology*, vol. 160, no. 7, pp. 2291–2302, 2021.

[2] A. Dal Buono, G. Roda, M. Argollo, K. Paridaens, L. Peyrin-Biroulet, and S. Danese, "Treat to target' in mild to moderate ulcerative colitis: evidence to support this strategy," *Current Drug Targets*, vol. 22, no. 1, pp. 117–125, 2021.

[3] S.-C. Wei, J. Sollano, Y. T. Hui et al., "Epidemiology, burden of disease, and unmet needs in the treatment of ulcerative colitis in Asia," *Expert Review of Gastroenterology & Hepatology*, vol. 15, no. 3, pp. 275–289, 2021.

[4] N. Ishida, S. Onoue, T. Miyazu et al., "Further research on the clinical relevance of the ulcerative colitis colonoscopic index of severity for predicting 5-year relapse," *International Journal of Colorectal Disease*, vol. 36, no. 12, pp. 2661–2670, 2021.

[5] W. Rabbenou and T. A. Ullman, "Risk of colon cancer and recommended surveillance strategies in patients with ulcerative colitis," *Gastroenterology Clinics of North America*, vol. 49, no. 4, pp. 791–807, 2020.

[6] J. Zhang, X. Wang, L. Xu, Z. Zhang, F. Wang, and X. Tang, "Investigation of potential genetic biomarkers and molecular mechanism of ulcerative colitis utilizing bioinformatics analysis," *BioMed Research International*, vol. 2020, Article ID 4921387, 2020.

[7] Z. R. Hu, W. J. Zheng, Q. Yan, W. W. Hu, and X. S. Sun, "[Bioinformatic analysis of differentially expressed genes and Chinese medicine prediction for ulcerative colitis]," *Zhongguo Zhongyao Zazhi*, vol. 45, no. 7, pp. 1684–1690, 2020.

[8] D. Wang, X. Ma, S. Guo et al., "Effect of huangqin tang on urine metabolic profile in rats with ulcerative colitis based on UPLC-Q-exactive orbitrap MS," *Evidence-based*

Complementary and Alternative Medicine: eCAM, vol. 2020, Article ID 1874065, 2020.

[9] N. Ma, Z. Zhang, F. Liao, T. Jiang, and Y. Tu, "The birth of artemisinin," *Pharmacology & Therapeutics*, vol. 216, Article ID 107658, 2020.

[10] B. H. Kiani, W. K. Kayani, A. U. Khayam, E. Dilshad, H. Ismail, and B. Mirza, "Artemisinin and its derivatives: a promising cancer therapy," *Molecular Biology Reports*, vol. 47, no. 8, pp. 6321–6336, 2020.

[11] T. Li, H. Chen, N. Wei et al., "Anti-inflammatory and immunomodulatory mechanisms of artemisinin on contact hypersensitivity," *International Immunopharmacology*, vol. 12, no. 1, pp. 144–150, 2012.

[12] H. G. Kim, J. H. Yang, E. H. Han et al., "Inhibitory effect of dihydroartemisinin against phorbol ester-induced cyclooxygenase-2 expression in macrophages," *Food and Chemical Toxicology*, vol. 56, pp. 93–99, 2013.

[13] A. S. Lee, H. J. Hur, and M. J. Sung, "The effect of artemisinin on inflammation-associated lymphangiogenesis in experimental acute colitis," *International Journal of Molecular Sciences*, vol. 21, no. 21, 2020.

[14] D. Hu, Y. Wang, Z. Chen et al., "Artemisinin protects against dextran sulfate-sodium-induced inflammatory bowel disease, which is associated with activation of the pregnane X receptor," *European Journal of Pharmacology*, vol. 738, pp. 273–284, 2014.

[15] F. Liu, Y. Yao, Z. Lu et al., "5-Hydroxy-4-methoxycanthin-6-one alleviates dextran sodium sulfate-induced colitis in rats via regulation of metabolic profiling and suppression of NF-κB/p65 signaling pathway," *Phytomedicine*, vol. 82, Article ID 153438, 2021.

[16] N. Psychogios, D. D. Hau, J. Peng et al., "The human serum metabolome," *PLoS One*, vol. 6, no. 2, Article ID e16957, 2011.

[17] H. Zhao, Y. Liu, Z. Li et al., "Identification of essential hypertension biomarkers in human urine by non-targeted metabolomics based on UPLC-Q-TOF/MS," *Clinica Chimica Acta*, vol. 486, pp. 192–198, 2018.

[18] H. Chu, A. Zhang, Y. Han et al., "Metabolomics approach to explore the effects of Kai-Xin-San on Alzheimer's disease using UPLC/ESI-Q-TOF mass spectrometry," *Journal of Chromatography B*, vol. 1015-1016, pp. 50–61, 2016.

[19] J. Fritsch, L. Garces, M. A. Quintero et al., "Low-fat, high-fiber diet reduces markers of inflammation and dysbiosis and improves quality of life in patients with ulcerative colitis," *Clinical Gastroenterology and Hepatology*, vol. 19, no. 6, pp. 1189–1199, 2021.

[20] M. Murano, K. Maemura, I. Hirata et al., "Therapeutic effect of intracolonically administered nuclear factor kappa B (p65) antisense oligonucleotide on mouse dextran sulphate sodium (DSS)-induced colitis," *Clinical and Experimental Immunology*, vol. 120, no. 1, pp. 51–58, 2000.

[21] J. Matson, S. Ramamoorthy, and N. E. Lopez, "The role of biomarkers in surgery for ulcerative colitis: a review," *Journal of Clinical Medicine*, vol. 10, no. 15, 2021.

[22] F. Zhu, Y. Ke, Y. Luo et al., "Effects of different treatment of fecal microbiota transplantation techniques on treatment of ulcerative colitis in rats," *Frontiers in Microbiology*, vol. 12, Article ID 683234, 2021.

[23] E. A. Arafat, R. E. Marzouk, S. A. Mostafa, and W. H. E. Hamed, "Identification of the molecular basis of nanocurcumin-induced telocyte preservation within the colon of ulcerative colitis rat model," *Mediators of Inflammation*, vol. 2021, Article ID 7534601, 2021.

[24] L. Shi, X. Han, J.-X. Li et al., "Identification of differentially expressed genes in ulcerative colitis and verification in a colitis mouse model by bioinformatics analyses," *World Journal of Gastroenterology*, vol. 26, no. 39, pp. 5983–5996, 2020.

[25] E. Clough and T. Barrett, "The gene expression Omnibus database," *Methods in Molecular Biology*, vol. 1418, pp. 93–110, 2016.

[26] Q. Zhu, P. Zheng, X. Chen, F. Zhou, Q. He, and Y. Yang, "Andrographolide presents therapeutic effect on ulcerative colitis through the inhibition of IL-23/IL-17 axis," *American Journal of Tourism Research*, vol. 10, no. 2, pp. 465–473, 2018.

[27] X. Zhang, Q.-H. Deng, J.-H. Deng, S.-J. Wang, and Q. Chen, "Lovastatin derivative dehydrolovastatin ameliorates ulcerative colitis in mice by suppressing NF-κB and inflammatory cytokine expression," *Korean Journal of Physiology and Pharmacology*, vol. 24, no. 2, pp. 137–147, 2020.

[28] Y. Ding, M. Chen, Q. Wang et al., "Integrating pharmacology and microbial network analysis with experimental validation to reveal the mechanism of composite Sophora colon-soluble capsule against ulcerative colitis," *Evidence-based Complementary and Alternative Medicine: eCAM*, vol. 2020, Article ID 9521073, 2020.

[29] K. Niu, Q. Li, and Y. Liu, "Molecular targets and mechanisms of scutellariae radix-coptidis rhizoma drug pair for the treatment of ulcerative colitis based on network pharmacology and molecular docking," *Evidence Based Complement Alternative Medicine*, vol. 2021, Article ID 9929093, 2021.

[30] P. N. Pushparaj, D. Li, M. Komai-Koma et al., "Interleukin-33 exacerbates acute colitis via interleukin-4 in mice," *Immunology*, vol. 140, no. 1, pp. 70–77, 2013.

[31] S. C. Ng and M. A. Kamm, "Review article: new drug formulations, chemical entities and therapeutic approaches for the management of ulcerative colitis," *Alimentary Pharmacology & Therapeutics*, vol. 28, no. 7, pp. 815–829, 2008.

[32] Y. Liu, Y. Qu, L. Liu et al., "PPAR-γ agonist pioglitazone protects against IL-17 induced intervertebral disc inflammation and degeneration via suppression of NF-κB signaling pathway," *International Immunopharmacology*, vol. 72, pp. 138–147, 2019.

[33] T. Kanazawa, I. Taneike, R. Akaishi et al., "Amino acids and insulin control autophagic proteolysis through different signaling pathways in relation to mTOR in isolated rat hepatocytes," *Journal of Biological Chemistry*, vol. 279, no. 9, pp. 8452–8459, 2004.

[34] S. A. Scott, J. Fu, and P. V. Chang, "Microbial tryptophan metabolites regulate gut barrier function via the aryl hydrocarbon receptor," *Proceedings of the National Academy of Sciences*, vol. 117, no. 32, pp. 19376–19387, 2020.

[35] S. Nikolaus, B. Schulte, N. Al-Massad et al., "Increased tryptophan metabolism is associated with activity of inflammatory bowel diseases," *Gastroenterology*, vol. 153, no. 6, pp. 1504–1516, 2017.

[36] L. Brencher, F. Petrat, K. Stych, T. Hamburger, and M. Kirsch, "Effect of Glycine, pyruvate, and resveratrol on the regeneration process of postischemic intestinal mucosa," *BioMed Research International*, vol. 2017, Article ID 1072969, 2017.

[37] M. Giris, B. Depboylu, and S. Dogru-Abbasoglu, "Effect of taurine on oxidative stress and apoptosis-related protein expression in trinitrobenzene sulphonic acid-induced colitis," *Clinical and Experimental Immunology*, vol. 152, no. 1, pp. 102–110, 2008.

[38] F. Probert, A. Walsh, M. Jagielowicz et al., "Plasma nuclear magnetic resonance metabolomics discriminates between high and low endoscopic activity and predicts progression in a prospective cohort of patients with ulcerative colitis," *Journal of Crohn's and Colitis*, vol. 12, no. 11, pp. 1326–1337, 2018.

[39] T. Sakata, K. Hana, T. Mikami, T. Yoshida, H. Endou, and I. Okayasu, "Positive correlation of expression of L-type amino-acid transporter 1 with colorectal tumor progression and prognosis: higher expression in sporadic colorectal tumors compared with ulcerative colitis-associated neoplasia," *Pathology, Research & Practice*, vol. 216, no. 6, Article ID 152972, 2020.

[40] W. E. Roediger, W. Babidge, and S. Millard, "Methionine derivatives diminish sulphide damage to colonocytes--implications for ulcerative colitis," *Gut*, vol. 39, no. 1, pp. 77–81, 1996.

[41] H. Benveniste, J. Drejer, A. Schousboe, and N. H. Diemer, "Elevation of the extracellular concentrations of glutamate and aspartate in rat hippocampus during transient cerebral ischemia monitored by intracerebral microdialysis," *Journal of Neurochemistry*, vol. 43, no. 5, pp. 1369–1374, 1984.

[42] G. Xiao, J. Yang, and L. Yan, "Comparison of diagnostic accuracy of aspartate aminotransferase to platelet ratio index and fibrosis-4 index for detecting liver fibrosis in adult patients with chronic hepatitis B virus infection: a systemic review and meta-analysis," *Hepatology*, vol. 61, no. 1, pp. 292–302, 2015.

[43] F. Liu, T. A. Patterson, N. Sadovova et al., "Ketamine-induced neuronal damage and altered N-methyl-D-aspartate receptor function in rat primary forebrain culture," *Toxicological Sciences*, vol. 131, no. 2, pp. 548–557, 2013.

[44] S. Notararigo, M. Martín-Pastor, J. E. Viñuela-Roldán, A. Quiroga, J. E. Dominguez-Munoz, and M. Barreiro-de Acosta, "Targeted 1H NMR metabolomics and immunological phenotyping of human fresh blood and serum samples discriminate between healthy individuals and inflammatory bowel disease patients treated with anti-TNF," *Journal of Molecular Medicine*, vol. 99, no. 9, pp. 1251–1264, 2021.

[45] R. Schicho, R. Shaykhutdinov, J. Ngo et al., "Quantitative metabolomic profiling of serum, plasma, and urine by 1H NMR spectroscopy discriminates between patients with inflammatory bowel disease and healthy individuals," *Journal of Proteome Research*, vol. 11, no. 6, pp. 3344–3357, 2012.

[46] Z. C Hong, Q. Cai, X. Y. Duan et al., "Effect of compound Sophorae decoction in the treatment of ulcerative colitis by tissue extract metabolomics approach," *Journal of traditional Chinese medicine = Chung i tsa chih ying wen pan*, vol. 41, no. 3, pp. 414–423, 2021.

[47] J. L. Izquierdo-Garcia, P. Comella-Del-Barrio, R. Campos-Olivas et al., "Discovery and validation of an NMR-based metabolomic profile in urine as TB biomarker," *Scientific Reports*, vol. 10, no. 1, p. 22317, 2020.

[48] C. Colas, G. Banci, R. Martini, and G. F. Ecker, "Studies of structural determinants of substrate binding in the Creatine Transporter (CreaT, SLC6A8) using molecular models," *Scientific Reports*, vol. 10, no. 1, p. 6241, 2020.

[49] H. Zhang, P. Fu, B. Ke et al., "Metabolomic analysis of biochemical changes in the plasma and urine of collagen-induced arthritis in rats after treatment with Huang-Lian-Jie-Du-Tang," *Journal of Ethnopharmacology*, vol. 154, no. 1, pp. 55–64, 2014.

[50] R. Lee, D. West, S. M. Phillips, and P. Britz-McKibbin, "Differential metabolomics for quantitative assessment of oxidative stress with strenuous exercise and nutritional intervention: thiol-specific regulation of cellular metabolism with N-acetyl-L-cysteine pretreatment," *Analytical Chemistry*, vol. 82, no. 7, pp. 2959–2968, 2010.

[51] S. C. Connor, W. Wu, B. C. Sweatman et al., "Effects of feeding and body weight loss on the1H-NMR-based urine metabolic profiles of male Wistar Han Rats: implications for biomarker discovery," *Biomarkers*, vol. 9, no. 2, pp. 156–179, 2004.

[52] D. N. Ruskin, M. Kawamura, and S. A. Masino, "Reduced pain and inflammation in juvenile and adult rats fed a ketogenic diet," *PLoS One*, vol. 4, no. 12, p. e8349, 2009.

[53] J. T. Kim, D. L. Napier, J. Kim et al., "Ketogenesis alleviates TNFα-induced apoptosis and inflammatory responses in intestinal cells," *Free Radical Biology and Medicine*, vol. 172, pp. 90–100, 2021.

[54] G. Le Gall, S. O. Noor, K. Ridgway et al., "Metabolomics of fecal extracts detects altered metabolic activity of gut microbiota in ulcerative colitis and irritable bowel syndrome," *Journal of Proteome Research*, vol. 10, no. 9, pp. 4208–4218, 2011.

[55] X. Lin, X. Liu, J. Xu et al., "Metabolomics analysis of herb-partitioned moxibustion treatment on rats with diarrhea-predominant irritable bowel syndrome," *Chinese Medicine*, vol. 14, no. 1, p. 18, 2019.

[56] S. R. Jacobs, C. E. Herman, N. J. Maciver et al., "Glucose uptake is limiting in T cell activation and requires CD28-mediated Akt-dependent and independent pathways," *The Journal of Immunology*, vol. 180, no. 7, pp. 4476–4486, 2008.

[57] H. M. I. Abdallah, N. M. Ammar, M. F. Abdelhameed et al., "Protective mechanism of Acacia saligna butanol extract and its nano-formulations against ulcerative colitis in rats as revealed via biochemical and metabolomic assays," *Biology*, vol. 9, no. 8, 2020.

[58] M. A. Farag, A. Abdelwareth, I. E. Sallam et al., "Metabolomics reveals impact of seven functional foods on metabolic pathways in a gut microbiota model," *Journal of Advanced Research*, vol. 23, pp. 47–59, 2020.

Hindawi
Evidence-Based Complementary and Alternative Medicine
Volume 2022, Article ID 6468299, 8 pages
https://doi.org/10.1155/2022/6468299

Research Article

Protective Effects of Interleukin-37 Expression against Acetaminophen-Induced Hepatotoxicity in Mice

Zhiwei Xu,[1,2] **Kan Li**,[2] **Xiuhe Pan**,[2] **Jun Tan**,[3] **Yan Li**,[2] **and Mingcai Li**[2]

[1]*The Affiliated Lihuili Hospital of Ningbo University, Ningbo Medical Center Lihuili Hospital, Ningbo, China*
[2]*School of Medicine, Ningbo University, Ningbo, China*
[3]*HwaMei Hospital, University of Chinese Academy of Sciences, Ningbo, China*

Correspondence should be addressed to Yan Li; liyan@nbu.edu.cn and Mingcai Li; mingcaili@126.com

Received 19 January 2022; Revised 14 March 2022; Accepted 23 March 2022; Published 4 April 2022

Academic Editor: Xiang Liu

Aim. Interleukin (IL)-37 is a new anti-inflammatory cytokine of the IL-1 family. This study aimed to determine the effects of IL-37 on acetaminophen (APAP)-induced liver injury. *Materials and Methods*. IL-37 plasmids were injected into mice via a tail vein hydrodynamics-based gene delivery. *Results*. Our results showed that IL-37 pretreatment significantly decreased serum alanine aminotransferase and aspartate aminotransferase levels, hepatic myeloperoxidase activity, and attenuated the histological liver damage. Compared to the APAP group, IL-37 administration decreased Kupffer cells numbers in the liver of APAP-induced hepatotoxicity in mice. Furthermore, IL-37 pretreatment reduced the expression of proinflammatory cytokines including tumor necrosis factor-α, IL-6, IL-17, and nuclear factor-κB (NF-κB) in APAP-induced mice. *Conclusion*. These results demonstrate that delivery of IL-37 plasmid can ameliorate APAP-induced liver injury by reducing proinflammatory cytokines production and preventing the activation of the NF-κB signaling pathway. IL-37 may be a promising candidate against APAP-induced liver injury.

1. Introduction

Liver is the largest digestive gland and the center of the human energy metabolism, which is closely related to human health. Liver diseases, including viral hepatitis, autoimmune hepatitis, and alcoholic liver disease, represent a significant public health problem, as many can develop into liver failure [1]. Acetaminophen (N-acetyl-p-aminophenol or APAP)-induced hepatotoxicity is also the main cause of acute liver failure. APAP may cause abdominal pain, nausea, and even acute liver failure. APAP antidote N-acetylcysteine is commonly used to treat APAP-induced hepatotoxicity. A better understanding of the mechanism underlying the hepatotoxicity is needed for the generation of more effective therapeutic strategies against the disorder.

Interleukin (IL)-37 (formerly IL-1 family member 7, IL-1F7) is identified as a novel anti-inflammatory cytokine of the IL-1 family, which includes IL-1α, IL-1β, IL-1 receptor antagonist (Ra), IL-18, IL-33, IL-36α, IL-36β, IL-36γ, IL-36Ra, and IL-38 [2]. At present, no mouse homologue has been identified; however, five different isoforms of human IL-37 have been described (IL-37a–e) [3, 4]. It exists in several organs and tissues including the brain, kidney, heart, bone marrow, and testis in specific isoforms. IL-37 is also expressed in peripheral blood mononuclear cells, monocytes, dendritic cells, and epithelial cells, and almost completely inhibits the synthesis of proinflammatory cytokines [5, 6]. Studies have shown that IL-37 is constitutively expressed in tissues from patients with rheumatoid arthritis compared to health subjects [7]. Moreover, some studies indicate that IL-37 has significant anti-inflammatory effects in models of septic shock, dextran sulfate sodium colitis, ischemia-reperfusion injury, obesity-induced inflammation, allergic airway inflammation, and lung fibrosis [7–15]. These findings tend to imply that IL-37 mediates a negative feedback mechanism to suppress excessive inflammation. It has been reported that IL-37 is protective against hepatic ischemia/reperfusion injury [16], and IL-37 can affect concanavalin A (ConA)-induced

hepatitis [17–19]. However, its protective effect on APAP-induced liver injury needs to be elucidated.

In the present study, we found that IL-37 inhibited APAP-induced liver injury in mice. IL-37 treatment exhibited significantly reduced serum alanine aminotransferase (ALT) and aspartate aminotransferase (AST) levels, hepatic myeloperoxidase (MPO) activity, and ameliorated histological liver damage in mice. The protective effect of IL-37 was associated with reduced tumor necrosis factor (TNF)-α, IL-6, and IL-17 production.

2. Materials and Methods

2.1. Reagents and Mice. APAP was purchased from Sigma Chemical Co (St. Louis, MO, USA). Plasmids pcDNA3.1 and pcDNA3.1-IL-37 (6-polyhistidine tag was introduced into the 3′ end of IL-37 cDNA for detection and purification) were preserved in our laboratory. RNAiso Plus reagents were purchased from TaKaRa Bio, Inc (Dalian, China). The HiFiScript 1st strand cDNA synthesis kit was purchased from ComWin Biotech Co., Ltd. (Beijing, China). Radio immunoprecipitation assay (RIPA) lysis buffer was purchased from Beyotime Institute of Biotechnology (Shanghai, China). Bovine serum albumin (BSA) was purchased from Solarbio Science and Technology Co. (Beijing, China).

Six–eight-week-old male BALB/c mice weighing between 18 and 22 g were obtained from the Animal Experimentation Center of Zhejiang Chinese Medical University (Hangzhou, China). Mice were kept with standard laboratory conditions with free access to food and water. The animals were set to adapt to the new environment for seven days before experimental procedures, which was under a protocol approved by the Ethical Committees of Ningbo University School of Medicine.

2.2. Recombinant Plasmid Extraction. E. coli TOP10 carrying pcDNA3.1 and pcDNA3.1-IL-37 were respectively large-scale culture, and then plasmids were extracted by EndoFree Maxi Plasmid kit (Tiangen Biotech, Beijing, China). Finally, the plasmids were stored at −80°C for later experiment.

2.3. Hydrodynamic Plasmid Injection. Plasmid DNA was introduced into mouse liver using hydrodynamic tail vein injection approach as reported [20, 21]. Briefly, 100 μg/mouse of corresponding plasmid DNA was diluted in 2.0 ml of saline (0.1 ml/g bodyweight) and injected into the mouse via tail vein within a time period of 5–10 s. The mice were typically recovered from the injection within 5–10 min.

2.4. Detection of IL-37 mRNA and Protein Expression. Mice were injected with pcDNA3.1-IL-37 plasmids as described above, and then were sacrificed after hydrodynamic procedures at 0, 6, 12, 24, 48, 72, and 96 h. Finally, liver tissues were collected for RNA extraction and the liver homogenates were obtained for enzyme-linked immunosorbent assay (ELISA) at indicated time points. Total RNA from above harvested liver was extracted and the cDNA was synthesized from 4 μg of total RNA using the HiFiScript 1st strand cDNA synthesis kit and amplified by reverse transcription-polymerase chain reaction (RT-PCR). The PCR primers of IL-37 and β-actin (Generay Biotech, Shanghai, China) are given in Table 1. Differences in expression were normalized to the β-actin signal. The cycles for IL-37 PCR were as follows: 98°C for 5 min, 35 cycles of 98°C for 30 s, 62°C for 30 s, 72°C for 30 s, and then 72°C for 10 min. The conditions for β-actin PCR were equal with above, except for annealing temperature of 62.9°C. PCR products were separated by 1.2% agarose gels electrophoresis.

IL-37 concentrations in mouse liver homogenates at 0, 6, 12, 24, 48, 72, and 96 h after hydrodynamic tail vein injection were determined by ELISA kit (CUSABIO, Wuhan, China).

2.5. Experimental Design. Mice liver damage was induced by intraperitoneal injection of APAP (400 mg/kg bodyweight) dissolved in pyrogen-free saline as previously described [22, 23]. The animals were euthanized 24 h after APAP administration. Blood and liver were collected for subsequent analysis.

Mice fasted overnight were randomly divided into three groups: pcDNA3.1/saline group, pcDNA3.1/APAP group, and pcDNA3.1-IL-37/APAP group. To assess the protective effect of IL-37 expression on APAP-induced hepatotoxicity, pcDNA3.1-IL-37 plasmid was administrated via hydrodynamic tail vein injection 24 h prior to treatment with APAP as described above. Meanwhile, the pcDNA3.1 empty plasmid was injected according to the same protocol as a control.

2.6. Assay for Serum Transaminase Activity. Liver enzymes including ALT and AST activities in serum were determined using ALT and AST reagent kits (Nanjing Jiancheng Bioengineering Institute, Nanjing, China) according to the manufacturer's instructions.

2.7. Measurement of Liver MPO Activity. The liver tissues were weighted, and 5% tissue homogenate was prepared; then, the MPO activity in liver samples was measured with commercial kits (Nanjing Jiancheng Bioengineering Institute, Nanjing, China) according to the manufacturer's protocols.

2.8. Analysis of Liver Histopathology. Liver tissues were fixed in 10% buffered formalin for 48 h. The tissues were embedded in paraffin and cut at thicknesses of 4 μm. The tissue sections were stained with hematoxylin and eosin (H&E), and histological examination was performed by a pathologist blinded to the experiment.

2.9. Immunohistochemistry. For immunohistochemical staining, antigen retrieval was performed by incubating the sections using 10 mM citrate buffer, pH 6 for 15 min at 97°C. Activity of endogenous peroxidase was blocked by incubating sections with 3% v/v hydrogen peroxide for 10 min. Sections were then washed with phosphate buffer solution

Table 1: Primer sequences used in this study.

Gene	Gene primers	Amplified fragment length (bp)
IL-37	Forward 5′-CGG GGT ACC ATG TCC TTT GTG GGG GAG-3′ Reverse 5′-GCT CTA GAC TAA TCG CTG ACC TCA CTG-3′	657
TNF-α	Forward 5′-TCT TCT CAT TCC TGC TTG TGG-3′ Reverse 5′-CAC TTG GTG GTT TGC TAC GAC-3′	200
IL-6	Forward 5′-GTG ACA ACC ACG GCC TTC CCT ACT-3′ Reverse 5′-GGT AGC TAT GGT ACT CCA-3′	313
IL-17	Forward 5′-TATCCCTCTGTGATCTGGGAAG-3′ Reverse 5′-ATCTTCTCGACCCTGAAAGTGA-3′	161
β-Actin	Forward 5′-TCC TGT GGC ATC CAT GAA ACT-3′ Reverse 5′-GAA GCA CTT GCG GTG CAC GAT-3′	315

(PBS) three times and blocked with 5% normal blocking serum at 37°C for 20 min. Next, the sections were incubated overnight at 4°C with primary antibodies including anti-mouse F4/80 (Santa Cruz Biotechnology, Shanghai, China, 1 : 50) or anti-His6 mouse primary antibodies (Beyotime, Beijing, China, 1 : 100). On the second day, sections were washed with PBS and incubated with 1 : 200 diluted HRP-conjugated anti-rat IgG secondary antibodies (Bioss Biotech, Beijing, China) for 1 h at 37°C. Color development was induced using 3, 3′-diaminobenzidine (DAB) substrate (Boster, Wuhan, China) during a 10–30 min incubation period. Using this substrate, specific staining was visualized by light microscopy.

2.10. Determination of Cytokine Levels by RT-PCR and ELISA. Total RNA was extracted from the collected liver at 24 h after APAP injection as described earlier. RT-PCR was used to assess the expression levels of inflammatory cytokines in the liver injury. PCR primers (Generay, Shanghai, China) are given in Table 1. PCR products were separated by 1.2% agarose gels electrophoresis. All samples were normalized against the intensity of β-actin. Serum cytokine concentrations of TNF-α, IL-6, and IL-17 were also determined by ELISA kits (ExCell Bio, Shanghai, China) according to the manufacturer's instructions.

2.11. Western Blot. Liver tissues stored at −80°C were minced into small pieces and fully homogenated in 1 ml RIPA lysis buffer with 10 μl phenylmethane-sulfonyl fluoride (PMSF) using a Tissue Tearor (Biospec, Bartlesville, USA). The homogenates were then put on ice for 30 min and centrifuged at 12,000 g at 4°C for 15 min. The concentration of the supernatants was calculated using the bicinchoninic acid (BCA) protein assay (Kaiji, China). The supernatants were then mixed in 4 × loading buffer, boiled for 5 min, and subjected to sodium dodecyl sulfate-polyacrylamide gel electrophoresis (SDS-PAGE). After electrophoresis, proteins were transferred onto polyvinylidene fluoride (PVDF) membranes (Millipore, Bedford, MA, USA). After blocking with 5% BSA in Tris buffered saline with Tween-20 (TBST) (20 mM Tris-HCl, pH 7.5, 500 mM NaCl, and 0.05% Tween-20), membranes were incubated with 1 : 800 diluted nuclear factor-κB (NF-κB), p65, and β-actin antibodies (TransGen, Beijing, China) at 4°C overnight, followed with 1 : 5000 diluted horseradish peroxidase (HRP)-conjugated anti-goat IgG secondary antibodies (Bioss Biotech, Beijing, China). Protein bands were visualized by an enhanced chemiluminescence reaction (ECL) (Amersham Pharmacia Biotech, Piscataway, NJ) and analyzed with a Tanon gel image analysis system (Tanon, Shanghai, China).

2.12. Statistics. Data were expressed as mean ± SD. Student's t-test was used to compare two groups. For multiple comparisons, the one-way ANOVA with Dunnett's method was used. In all analyses, $p < 0.05$ was considered statistically significant.

3. Results

3.1. IL-37 Expression in Mice by Hydrodynamic Gene Delivery of IL-37 Plasmids. To monitor the levels of IL-37 expression in BALB/c mice, the mice were injected with pcDNA3.1-IL-37 plasmids using hydrodynamic tail vein injection [20,21] and sacrificed at 0, 6, 12, 24, 48, 72, and 96 h. Livers were collected for mRNA and protein extraction. We first checked IL-37 mRNA expression in the liver by RT-PCR. It was found that highest levels of IL-37 mRNA were present at 24 h after gene delivery. At the same time, IL-37 mRNA showed a time-dependent decrease (Figure 1(a)).

We then examine IL-37 protein levels in liver homogenate by ELISA to confirm the above results. As shown in Figure 1(b), it was found by ELISA that IL-37 protein was expressed in mouse liver homogenate after hydrodynamic tail vein injection of pcDNA3.1-IL-37 plasmid. Importantly, the levels of IL-37 protein in liver tissue showed similar trend as its mRNA levels described above (Figure 1(b)).

To further demonstrate the expression of IL-37 in mouse livers by hydrodynamic gene delivery of pcDNA3.1-IL-37 plasmid, we detected the expression of exogenous IL-37 protein in mouse livers by immunohistochemical staining. The results showed that we could detect the expression of IL-37 protein only after injection of pcDNA3.1-IL-37 plasmid (Figure 1(d)), while there was no expression of IL-37 after injection of control pcDNA3.1 plasmid (Figure 1(c))

3.2. IL-37 Protects Mice from Liver Injury Induced by APAP. To explore whether IL-37 protein has a protective effect on APAP-induced hepatotoxicity, the experimental liver injury

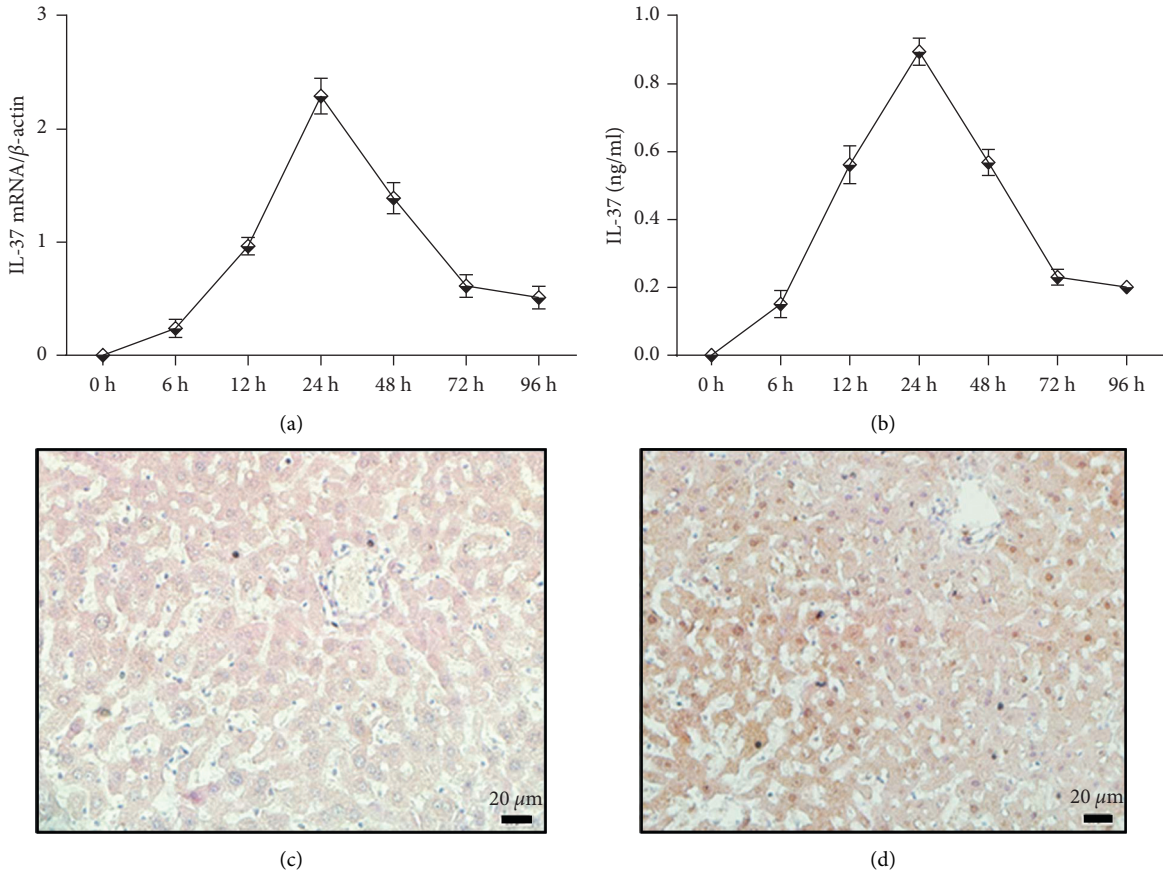

Figure 1: Detection the expression of exogenous IL-37. (a) IL-37 mRNA levels in mouse liver tissues analyzed by RT-PCR at 0, 6, 12, 24, 48, 72, and 96 h after hydrodynamic procedures. Data are expressed as mean ± SD of animals analyzed at each time point ($n = 5$). (b) IL-37 protein levels in liver homogenate analyzed by ELISA at each similar time point. Data are expressed as mean ± SD of animals analyzed at each time point ($n = 5$). IL-37 mRNA and protein levels were normalized with β-actin expression. IL-37 protein expression was detected in mouse livers 24 h after injection of empty pcDNA3.1 (c) and pcDNA3.1-IL-37 (d) plasmids using immunohistochemical staining.

model on BALB/c mice was established. Mice were injected plasmid pcDNA3.1 and pcDNA3.1-IL-37 using hydrodynamic tail vein injection. After 24 h of hydrodynamic procedure, the mice were then intraperitoneally injected APAP (400 mg/kg bodyweight). The mice were sacrificed at 24 h for analysis of liver injury. Blood and liver tissue were obtained at 24 h after APAP injection. As shown in Figure 2(a), serum ALT and AST levels in the pcDNA3.1/APAP group were significantly increased compared with the pcDNA3.1/saline group. Importantly, serum ALT and AST levels in the pcDNA3.1-IL-37/APAP group were lower than those in the pcDNA3.1/APAP group (Figure 2(a)). Hepatic MPO levels were increased in the APAP (400 mg/kg) group than that in the saline group. However, pcDNA3.1-IL-37 injection significantly decreased hepatic MPO levels compared with the pcDNA3.1/APAP group ($p < 0.01$, Figure 2(b)). The result demonstrates that pcDNA3.1-IL-37 treatment reduces neutrophil accumulation and inflammation in the liver.

The protective effect of pcDNA3.1-IL-37 pretreatment was further confirmed by analysis of liver tissue sections after 24 h of APAP injection. Compared with the pcDNA3.1/saline group, the pcDNA3.1/APAP group showed a serious liver injury as manifested by the spotted necrosis at 24 h after APAP induction. However, pcDNA3.1-IL-37/APAP pretreatment showed significant less severity of liver necrosis (Figure 2(c)). This histopathologic liver damage correlated with the elevated serum levels of the liver enzymes.

Kupffer cells, the resident macrophages in the liver, play a critical role in immune-mediated liver injury [24]. Therefore, we investigated the accumulation of Kupffer cells in the liver by immunohistochemistry using anti-F4/80 stain. Liver tissue sections after 24 h of APAP injection were stained with anti-F4/80 for Kupffer cells. In the pcDNA3.1/APAP group, more infiltrating F4/80$^+$ Kupffer cells were observed around hepatic and portal venules and sinusoids in each section in comparison with the pcDNA3.1/saline group. The increase of the infiltrating F4/80$^+$ Kupffer cells population in the pcDNA3.1-IL-37/ConA group was inhibited in comparison with the pcDNA3.1/APAP group (Figure 2(d)). These results indicate that IL-37 expression attenuates liver injury induced by APAP injection.

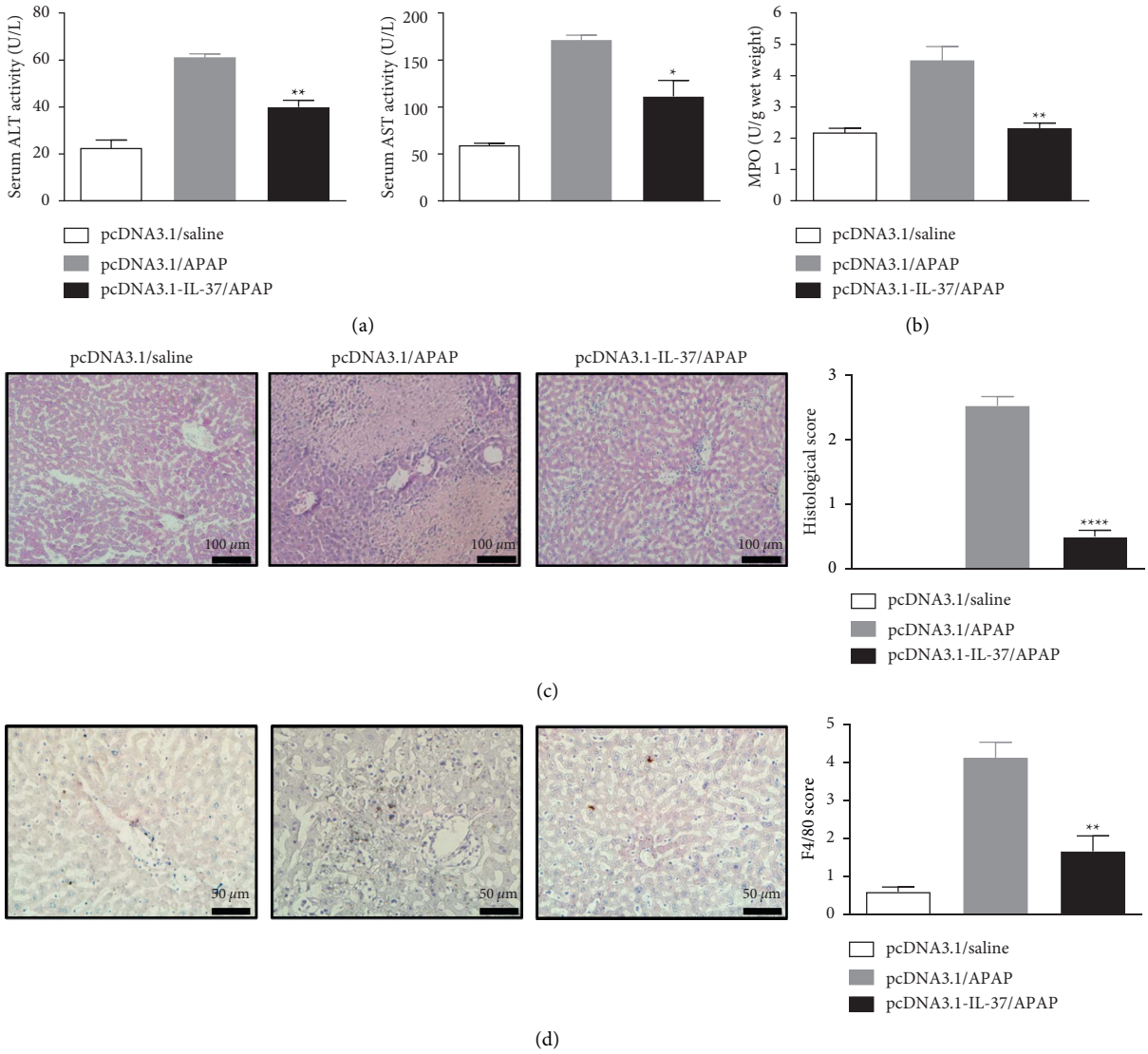

Figure 2: pcDNA3.1-IL-37 pretreatment attenuates APAP-induced liver injury. Mice underwent pretreatment with pcDNA3.1-IL-37 at 24 h before APAP challenge. The serum and liver tissue of animals were collected at 24 h after APAP injection. Liver sections obtained from animals at 24 h after APAP injection were subjected to histological analysis of hepatic necrosis. (a) Serum ALT and AST levels measured in each group. (b) Liver MPO activity. (c) Representative images of H&E staining chosen from each group. Bar graph shows the histopathological scores of inflammatory cells infiltration and liver necrosis. (d) Effect of IL-37 on the liver infiltrating Kupffer cells. Liver tissues were immunostained with anti-F4/80 antibody. Typical images were chosen from each group. Bar graph shows the scores of F4/80$^+$ Kupffer cells. Data are expressed as mean ± SD ($n = 6$–8 per group, $^* p < 0.05$, $^{**} p < 0.01$, and $^{****} p < 0.0001$ vs. the pcDNA3.1/APAP group).

3.3. Effect of IL-37 on Serum Cytokine Levels of APAP-Induced Liver Injury. APAP-induced liver injury is associated with the change of various inflammatory cytokines. To investigate whether IL-37 expression influences the systemic release of inflammatory cytokines, we first checked serum cytokine levels of TNF-α, IL-6, and IL-17 in mice after APAP treatment by ELISA. Proinflammatory cytokines TNF-α, IL-6, and IL-17 in serum from mice after APAP treatment were increased in pcDNA3.1/APAP in comparison with the pcDNA3.1/saline group. In contrast, it was noted that the increased serum cytokine levels of TNF-α, IL-6, and IL-17 were prevented in the pcDNA3.1-IL-37/APAP group (Figure 3).

3.4. Influence of IL-37 on the Expression of Inflammatory Cytokines mRNA and NF-κB p65 Protein in the Liver Tissues. To further confirm the above observations, we then checked mRNA levels of cytokines from the collected liver at 24 h after APAP treatment by RT-PCR. The results showed that the mRNA levels of proinflammatory cytokines TNF-α, IL-6, and IL-17 in the liver tissues of the pcDNA3.1-IL-37/APAP group were significantly decreased in comparison with the pcDNA3.1/APAP group. The data detected by RT-PCR were similar to those detected by ELISA (Figures 4(a)–4(c)). Western blot analysis showed that APAP can upregulate NF-κB p65 protein expression in the liver tissues; however, IL-37 treatment significantly decreased APAP-induced NF-κB p65

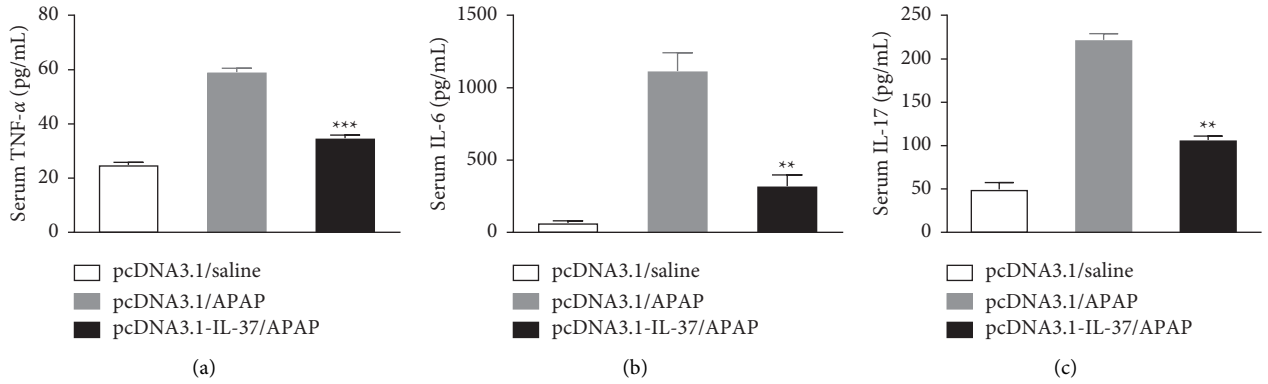

Figure 3: Effect of IL-37 expression on serum cytokine levels of APAP-induced liver injury. Mice were pretreated with pcDNA3.1-IL-37 at 24 h before APAP injection. Serum samples were collected at 24 h after APAP injection for the detection of proinflammatory and anti-inflammatory cytokines. Serum levels of TNF-α (a), IL-6 (b), and IL-17 (c) measured at 24 h after APAP injection by ELISA. Data are expressed as mean ± SD ($n = 6$–8 per group, $^{**}p < 0.01$ 1 and $^{****}p < 0.001$ vs. the pcDNA3.1/APAP group).

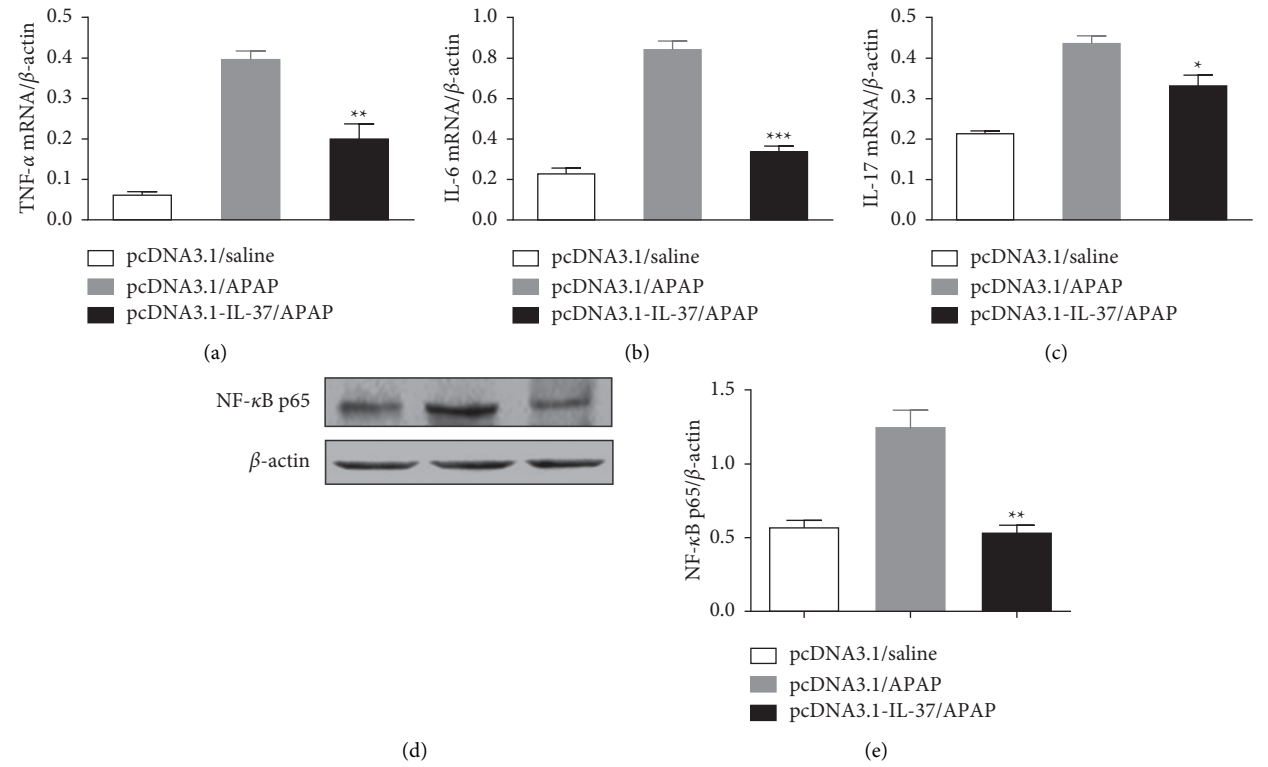

Figure 4: Influence of IL-37 on expression of inflammatory cytokines mRNAs and NF-κB p65 proteins in APAP-induced liver injury. Mice were pretreated with pcDNA3.1-IL-37 at 24 h before APAP injection. Liver tissue samples were collected at 24 h after APAP administration for the detection of TNF-α (a), IL-6 (b), and IL-17 (c) by RT-PCR. Liver tissues were collected at 24 h after APAP administration for Western blot detections (d) and the corresponding densitometry analysis (e) of NF-κB p65. β-Actin was used as an internal control. Data are expressed as mean ± SD ($n = 6$–8 per group, $^{*}p < 0.05$, $^{***}p < 0.001$, and $^{***}p < 0.001$ vs. the pcDNA3.1/APAP group).

activation (Figures 4(d) and 4(e)). The results demonstrated that IL-37 inhibited inflammation by negatively regulating the NF-κB signaling pathway.

4. Discussion

In the present study, we demonstrated that human IL-37 could be expressed in mouse liver by hydrodynamic tail vein injection of pcDNA3.1-IL-37 plasmid. IL-37 expression significantly reduced APAP-induced liver injury, serum ALT and AST levels, MPO activity, and inflammatory cells (neutrophils and macrophages) infiltration in the liver. Moreover, IL-37 expression significantly decreased proinflammatory cytokines (TNF-α, IL-6, and IL-17) levels in serums and liver tissues. These results suggest that IL-37 expression can protect mice from APAP-induced hepatotoxicity.

It has been reported that high levels of foreign gene expression in mouse hepatocytes can be achieved by the rapid

injection of a large volume of naked plasmid DNA solution into the tail vein [25, 26]. Although a mouse homologue of IL-37 has not been reported, human IL-37 is functional in the mouse [8]. Therefore, we introduced a plasmid that expresses human IL-37 into mice using hydrodynamic tail vein injection. Indeed, the hydrodynamic tail vein procedure successfully delivered IL-37 into mouse liver by the detection of IL-37 mRNA and protein in liver tissue. Moreover, it was found that the highest levels of IL-37 mRNA and protein were presented at 24 h after gene delivery (Figure 1). Therefore, APAP was injected into mice at 24 h after gene delivery.

In this study, we demonstrated that IL-37 expression could inhibit APAP-induced liver inflammation and necrosis. Serum ALT and AST activity and liver histopathology are widely used as conventional indicators for the evaluation of liver injury. Our findings revealed that pcDNA3.1-IL-37 plasmids delivery significantly decreased hepatic injury, as judged by reduced serum ALT and AST activity, histopathological changes, and the ratio of necrotic to liver tissue in area (Figure 2).

The migration of neutrophils to mouse liver induced by APAP can be indirectly evaluated by measuring MPO activity [27, 28]. APAP-induced liver injury was accompanied by neutrophil infiltration, which was proved by the increase of MPO activity [29, 30]. Our results showed that pretreatment with pcDNA3.1-IL-37 plasmid significantly reduced APAP-induced MPO activity (Figure 2). Kupffer cells are the resident macrophages in the liver and play a critical role in the innate immune response and produce cytokines and chemokines under activated conditions. Activated Kupffer cells triggered by hepatocyte damage may lead to increased release of proinflammatory cytokines such as TNF-α, IL-6, and IL-17. So, we examined the number of Kupffer cell infiltration in the liver. F4/80 is a representative surface marker of mouse mononuclear phagocytes. It is a stable antigen and is not usually present in other types of leukocytes [31, 32]. Infiltrated Kupffer cells were defined by the expression of F4/80, and we found that IL-37 significantly inhibited the increase of $F4/80^+$ Kupffer cells after APAP injection (Figure 2(d)).

Previous studies showed that the prognosis of patients with APAP-induced liver injury is related to inflammation [33, 34]. Excessive APAP can activate macrophages (Kupffer cells), recruit other inflammatory cells (such as lymphocytes and neutrophils), and lead to downstream inflammatory response [35]. Studies have found that APAP can upregulate NF-κB p65 protein expression and inflammatory cytokines production of including IL-1β, IL-6, IL-17, and TNF-α in the liver tissues [29, 36, 37]. Roh et al. [38] demonstrated that overexpression of IL-17 by hydrodynamic tail vein injection of plasmid pcDNA3.1-IL-17 greatly enhanced the severity of liver injury. In this study, we observed a significant reduction in the TNF-α, IL-6, and IL-17 levels in serum as well as mRNA expression in the liver with treatment by IL-37 (Figures 3 and 4). Moreover, IL-37 treatment reduced NF-κB p65 protein expression levels in the liver tissues of APAP-treated mice (Figure 4). Our findings suggest that the protective effect of IL-37 on APAP-induced liver injury is related to its inhibition of NF-κB signal pathway activation and downregulation of subsequent proinflammatory cytokine expression.

5. Conclusion

To the best of our knowledge, this is the first report on the effect of IL-37 expression in the APAP-induced hepatotoxicity model in mice. The protective effect of IL-37 expression on APAP-induced liver injury is closely related to the inhibition of neutrophil migration and Kupffer cell activation, which results in the decrease of ALT, AST, and proinflammatory cytokines levels. These results indicate that IL-37 is a potential novel hepatoprotective agent.

Data Availability

The datasets used and/or analyzed during the current study are available from the corresponding author upon request.

Conflicts of Interest

The authors declare that there are no conflicts of interest.

Acknowledgments

This study was partially supported by the Huamei Research Foundation (2017HMKY07), Medicine and Health Sciences Research Foundation of Zhejiang Province (2019KY177), and Natural Science Foundation of Ningbo (202003N4115 and 202003N4118).

References

[1] C. Wang, H. Nie, K. Li et al., "Curcumin inhibits HMGB1 releasing and attenuates concanavalin A-induced hepatitis in mice," *European Journal of Pharmacology*, vol. 697, no. 1–3, pp. 152–7, 2012.

[2] A. Mantovani, C. A. Dinarello, M. Molgora, and C. Garlanda, "Interleukin-1 and related cytokines in the regulation of inflammation and immunity," *Immunity*, vol. 50, no. 4, pp. 778–795, 2019.

[3] X. Wang, K. Xu, S. Chen, Y. Li, and M. Li, "Role of interleukin-37 in inflammatory and autoimmune diseases," *Iranian journal of immunology: IJI*, vol. 15, no. 3, pp. 165–174, 2018.

[4] G. Kaplanski, "Interleukin-18: biological properties and role in disease pathogenesis," *Immunological Reviews*, vol. 281, no. 1, pp. 138–153, 2018.

[5] D. Boraschi, D. Lucchesi, S. Hainzl et al., "IL-37: a new anti-inflammatory cytokine of the IL-1 family," *European Cytokine Network*, vol. 22, no. 3, pp. 127–147, 2011.

[6] P. W. Zhao, W. G. Jiang, L. Wang, Z. Y. Jiang, Y. X. Shan, and Y. F. Jiang, "Plasma levels of IL-37 and correlation with TNF-alpha, IL-17A, and disease activity during DMARD treatment of rheumatoid arthritis," *PLoS One*, vol. 9, no. 5, Article ID e95346, 2014.

[7] L. Ye, L. Ji, Z. Wen et al., "IL-37 inhibits the production of inflammatory cytokines in peripheral blood mononuclear cells of patients with systemic lupus erythematosus: its correlation with disease activity," *Journal of Translational Medicine*, vol. 12, no. 1, p. 69, 2014.

[8] C. A. Dinarello and P. Bufler, "Interleukin-37," *Seminars in Immunology*, vol. 25, no. 6, pp. 466–468, 2013.

[9] M. F. Nold, C. A. Nold-Petry, J. A. Zepp, B. E. Palmer, P. Bufler, and C. A. Dinarello, "IL-37 is a fundamental

inhibitor of innate immunity," *Nature Immunology*, vol. 11, no. 11, pp. 1014–1022, 2010.

[10] A. R. Moschen, C. Molnar, B. Enrich, S. Geiger, C. F. Ebenbichler, and H. Tilg, "Adipose and liver expression of interleukin (IL)-1 family members in morbid obesity and effects of weight loss," *Molecular Medicine (Cambridge, Mass.)*, vol. 17, no. 7-8, pp. 840–845, 2011.

[11] M. S. Kim, A. R. Baek, J. H. Lee et al., "IL-37 attenuates lung fibrosis by inducing autophagy and regulating TGF-β1 production in mice," *The Journal of Immunology*, vol. 203, no. 8, pp. 2265–2275, 2019.

[12] J. Wang, Y. Shen, C. Li et al., "IL-37 attenuates allergic process via STAT6/STAT3 pathways in murine allergic rhinitis," *International Immunopharmacology*, vol. 69, pp. 27–33, 2019.

[13] Y. Li, Q. Gao, K. Xu et al., "Interleukin-37 attenuates bleomycin-induced pulmonary inflammation and fibrosis in mice," *Inflammation*, vol. 41, no. 5, pp. 1772–1779, 2018.

[14] L. Lunding, S. Webering, C. Vock et al., "IL-37 requires IL-18Rα and SIGIRR/IL-1R8 to diminish allergic airway inflammation in mice," *Allergy*, vol. 70, no. 4, pp. 366–373, 2015.

[15] J. Lv, Y. Xiong, W. Li et al., "IL-37 inhibits IL-4/IL-13-induced CCL11 production and lung eosinophilia in murine allergic asthma," *Allergy*, vol. 73, no. 8, pp. 1642–1652, 2018.

[16] N. Sakai, H. L. Van Sweringen, R. M. Belizaire et al., "Interleukin-37 reduces liver inflammatory injury via effects on hepatocytes and non-parenchymal cells," *Journal of Gastroenterology and Hepatology*, vol. 27, no. 10, pp. 1609–1616, 2012.

[17] A. M. Bulau, M. Fink, C. Maucksch et al., "In vivo expression of interleukin-37 reduces local and systemic inflammation in concanavalin A-induced hepatitis," *TheScientificWorldJournal*, vol. 11, pp. 2480–90, Article ID 968479, 2011.

[18] X. X. Feng, G. Chi, and H. Wang, "IL-37 suppresses the sustained hepatic IFN-gamma/TNF-alpha production and T cell-dependent liver injury," *International Immunopharmacology*, vol. 69, pp. 184–193.

[19] G. Li, D. Kong, Y. Qin et al., "IL-37 overexpression enhances the therapeutic effect of end ometrial regenerative cells in concanavalin A-induced hepatitis," *Cytotherapy*, vol. 23, no. 7, pp. 617–626, 2021.

[20] H. Sun and D. Liu, "Hydrodynamic delivery of interleukin 15 gene promotes resistance to high fat diet-induced obesity, fatty liver and improves glucose homeostasis," *Gene Therapy*, vol. 22, no. 4, pp. 341–347, 2015.

[21] Y. K. Song, F. Liu, G. Zhang, and D. Liu, "Hydrodynamics-based transfection: simple and efficient method for introducing and expressing transgenes in animals by intravenous injection of DNA," *Methods in Enzymology*, vol. 346, pp. 92–105, 2002.

[22] P. E. Ganey, J. P. Luyendyk, S. W. Newport et al., "Role of the coagulation system in acetaminophen-induced hepatotoxicity in mice," *Hepatology*, vol. 46, no. 4, pp. 1177–1186, 2007.

[23] Z. Zhou, J. Qi, D. Yang et al., "Exogenous activation of toll-like receptor 5 signaling mitigates acetaminophen-induced hepatotoxicity in mice," *Toxicology Letters*, vol. 342, pp. 58–72, 2021.

[24] S. Akai, Y. Uematsu, K. Tsuneyama, S. Oda, and T. Yokoi, "Kupffer cell-mediated exacerbation of methimazole-induced acute liver injury in rats," *Journal of Applied Toxicology*, vol. 36, no. 5, pp. 702–715, 2016.

[25] Y. H. Huang, Y. X. Chen, L. J. Zhang, Z. X. Chen, and X. Z. Wang, "Hydrodynamics-based transfection of rat interleukin-10 gene attenuates porcine serum-induced liver fibrosis in rats by inhibiting the activation of hepatic stellate cells," *International Journal of Molecular Medicine*, vol. 34, no. 3, pp. 677–686, 2014.

[26] F. Andrianaivo, M. Lecocq, S. Wattiaux-De Coninck, R. Wattiaux, and M. Jadot, "Hydrodynamics-based transfection of the liver: entrance into hepatocytes of DNA that causes expression takes place very early after injection," *The Journal of Gene Medicine*, vol. 6, no. 8, pp. 877–883, 2004.

[27] D. G. Souza, G. D. Cassali, S. Poole, and M. M. Teixeira, "Effects of inhibition of PDE4 and TNF-alpha on local and remote injuries following ischaemia and reperfusion injury," *British Journal of Pharmacology*, vol. 134, no. 5, pp. 985–994, 2001.

[28] M. R. Betto, L. F. Lazarotto, T. T. Watanabe, D. Driemeier, C. E. Leite, and M. M. Campos, "Effects of treatment with enalapril on hepatotoxicity induced by acetaminophen in mice," *Naunyn-Schmiedeberg's Archives of Pharmacology*, vol. 385, no. 9, pp. 933–943, 2012.

[29] F. C. Liu, H. P. Yu, A. H. Chou, H. C. Lee, and C. C. Liao, "Corilagin reduces acetaminophen-induced hepatotoxicity through MAPK and NF-kappaB signaling pathway in a mouse model," *American Journal of Translational Research*, vol. 12, no. 9, pp. 5597–5607, 2020.

[30] H. C. Lee, H. P. Yu, C. C. Liao, A. H. Chou, and F. C. Liu, "Escin protects against acetaminophen-induced liver injury in mice via attenuating inflammatory response and inhibiting ERK signaling pathway," *American Journal of Translational Research*, vol. 11, no. 8, pp. 5170–5182, 2019.

[31] J. M. Austyn and S. Gordon, "F4/80, a monoclonal antibody directed specifically against the mouse macrophage," *European Journal of Immunology*, vol. 11, no. 10, pp. 805–815, 1981.

[32] Y. Zhou, K. Chen, and L. He, "The protective effect of resveratrol on concanavalin-A-induced acute hepatic injury in mice," *Gastroenterology Research and Practice*, vol. 2015, Article ID 506390, 11 pages, 2015.

[33] C. G. Antoniades, A. Quaglia, L. S. Taams et al., "Source and characterization of hepatic macrophages in acetaminophen-induced acute liver failure in humans," *Hepatology*, vol. 56, no. 2, pp. 735–746, 2012.

[34] B. M. Stutchfield, D. J. Antoine, A. C. Mackinnon et al., "CSF1 restores innate immunity after liver injury in mice and serum levels indicate outcomes of patients with acute liver failure," *Gastroenterology*, vol. 149, no. 7, pp. 1896–1909 e1814, 2015.

[35] H. Guo, J. Sun, D. Li et al., "Shikonin attenuates acetaminophen-induced acute liver injury via inhibition of oxidative stress and inflammation," *Biomedicine & Pharmacotherapy*, vol. 112, Article ID 108704, 2019.

[36] H. C. Lee, C. C. Liao, Y. J. Day, J. T. Liou, A. H. Li, and F. C. Liu, "IL-17 deficiency attenuates acetaminophen-induced hepatotoxicity in mice," *Toxicology Letters*, vol. 292, pp. 20–30, 2018.

[37] B. L. Woolbright and H. Jaeschke, "Role of the inflammasome in acetaminophen-induced liver injury and acute liver failure," *Journal of Hepatology*, vol. 66, no. 4, pp. 836–848, 2017.

[38] Y. S. Roh, S. Park, C. W. Lim, and B. Kim, "Depletion of Foxp3+ regulatory T cells promotes profibrogenic milieu of cholestasis-induced liver injury," *Digestive Diseases and Sciences*, vol. 60, no. 7, pp. 2009–2018, 2015.

Hindawi
Evidence-Based Complementary and Alternative Medicine
Volume 2022, Article ID 3598856, 13 pages
https://doi.org/10.1155/2022/3598856

Research Article

Mechanism of the Treatment of Irritable Bowel Syndrome with Sini Powder and Tong Xie Yao Fang Decoction Based on Network Pharmacology

Rong Tang[1], **Xiaoqing Peng**[1], **Xiaohong Zhou**[1], **Zhimin Zheng**[1], **Jiayu Yin**[1], **and Hong Liu**[2]

[1]*Department of Pharmacy, Guangzhou First People's Hospital, School of Medicine, South China University of Technology, Panfu Road 1, Guangzhou 510180, Guangdong, China*
[2]*Department of Traditional Chinese Medicine, The First Affiliated Hospital of Guangdong Pharmaceutical University, Gonghexiheng Street 1, Guangzhou 510080, Guangdong, China*

Correspondence should be addressed to Hong Liu; 303280010@qq.com

Received 8 November 2021; Revised 21 February 2022; Accepted 10 March 2022; Published 1 April 2022

Academic Editor: Xiang Liu

This study used a network pharmacology approach to investigate the potential active ingredients of Sini Powder and Tong xie yao fang decoction and the underlying mechanisms in irritable bowel syndrome (IBS) treatment. The potential active ingredients of Sini Powder and Tong xie yao fang decoction were obtained from TCMSP databases, and the potential targets of the active ingredients were predicted and analyzed by using the Swiss Target Prediction database. T Genecard, DisGeNET, and OMIM databases were processed to screen the potential therapeutic targets in IBS. The interaction of overlapped candidates between the potential biotarget of herb extracts and the potential therapeutic target of IBS were analyzed by STRING website and visualized by the Cytoscape V3.8.0 software. Gene ontology (GO) analysis and Kyoto Genomics and Genomics Encyclopedia (KEGG) pathway were processed to categorize and map the potential biofunctions and effects of these candidates by using David database. *Result*. There were 139 predicted active components and 248 related biotargets of Sini Powder and Tong xie yao fang decoction which were involved in IBS treatment, and 522 annotations and 101 related pathways are obtained by enrichment analysis ($P < 0.01$, FDR < 0.05). The underlying mechanisms of Sini Powder and Tong xie yao fang decoction may be related to neuroactive ligand-receptor interaction, calcium, cAMP, and HIF-1 signaling pathways. In conclusion, our results showed that the effect and mechanism of Sini Powder and Tong xie yao fang decoction in IBS treatment were in multi-ingredient, multitargets and multipathways, which would provide several potential and promising strategies for the further research and development of Sini Powder and Tong xie yao fang decoction on IBS treatment.

1. Introduction

Irritable bowel syndrome (IBS) is a dysfunctional gastrointestinal disease, which is characterized by recurrent abdominal pain, and associated with abnormal fecal form and/or abnormal frequency of defecation [1, 2]. The nationwide prevalence of Chinese IBS is 1.4%–11.5% in 2020 [3]. The high-risk factors of IBS at least including high fat, high bioamine, and high carbohydrate diets, or intestinal infection [4, 5]. IBS patients usually suffered from anxiety, depression, and physical discomforts, which largely reduced their life quality [6]. Up to date, the pathophysiological mechanism of IBS remains as a complex context, accumulating evidence have been shown that visceral hypersensitivity, mental disorder, gut dysbiosis, gastrointestinal motility disorders, and intestinal low-grade inflammation contributed to dysfunction of gut-to-brain axis, which in turn played important roles in IBS initiation [7–11]. The therapeutic goals of IBS have so far been confined to ameliorate syndromes and improve patients' life quality. Clinically, IBS treatments

mainly includes diet, lifestyle, medical, mental, and behavioral interventions, besides, individualized management is more important and required [3, 12].

Traditional Chinese medicine has showed promising advantages in IBS treatment [13, 14]. Traditional Chinese medicine theory holds that liver stagnation and spleen deficiency play important roles in pathogeneses of IBS [15]. The combination of Sini Powder and Tong xie yao fang decoction has proven effective and been reported fewer adverse reactions in IBS treatment [16, 17]. Sini powder is derived from the treatise on febrile diseases and is composed of Chinese thorowax root, Radix Paeoniae Alba, trifoliate orange (Fructus Aurantii Immaturus), and Chinese licorice (*Glycyrrhiza uralensis*). Tong xie yao fang decoction is derived from Danxi's Mastery of Medicine and is composed of *Rhizoma Atractylodis*, Radix Paeoniae Alba, Citri Reticulatae Pericarpium (Chenpi), and *Saposhnikovia divaricate* root. Both Sini powder and Tong xie yao fang decoction are based on the principle of reconciling the function of liver and spleen. The combination of two formulas can disperse the stagnated main and collateral channels in liver and spleen, which in turn to restore their normal function to ameliorate diarrhea, abdominal pain, and abdominal distension symptoms in IBS patients [16, 17]. However, the potential active ingredients of Sini powder and Tong xie yao fang decoction and the underlying mechanisms remain largely elusive.

In the present study, we explored the effective components, and then screened the hub targets and the relevant signaling pathways of Sini powder and Tong xie yao fang decoction based on network pharmacology analysis. Thus, our results would provide a theoretical reference for the study of its pharmacological mechanism and its clinical application.

2. Materials and Methods

2.1. Screening of Active Ingredients of Sini Powder and Tong xie yao fang Decoction and Target Prediction. The traditional Chinese medicine systems pharmacology database and analysis platform (TCMSP) (https://tcmspw.com/) was used to retrieve Chinese medicines (Chinese thorowax root, Radix Paeoniae Alba, trifoliate orange Fructus aurantii Immaturus), and Chinese licorice (*Glycyrrhiza uralensis*), *Rhizoma Atractylodis*, Citri Reticulatae Pericarpium (Chenpi), and *Saposhnikovia divaricata* root, which are components of Sini powder and Tong xie yao fang decoction. The active components of these Chinese medicines were collected and screened based on oral bioavailability (OB) ≥ 30% and drug-likeness (DL) ≥ 0.18. The SDFs (structure data files) of the molecular structure of potential active components were obtained through the PubChem database (https://pubchem.ncbi.nlm.nih.gov/), and their potential targets were predicted using the Swiss Target Prediction database (https://www.swisstargetprediction.ch/). Their potential targets were finally subjected to gene standardization through the UniProt database (https://www.UniProt.org/).

2.2. Prediction of IBS-Related Targets. Using "irritable bowel syndrome" as the keyword, searches, and screening were conducted using disease gene databases such as DrugBank (https://www.drugbank.ca/), DisGeNET (https://www.disgenet.org/), Genecards (https://www.genecards.org), OMIM (https://www.omim.org/), and TTD (https://db.idrblab.net/ttd/). The obtained target genes were introduced into the UniProt database for gene standardization.

2.3. Construction of the Active Ingredient-Target Network of the Drugs. The targets obtained in the steps described in "1.1" and "1.2" were imported into the Venny 2.1 website to create a Venn diagram, and the common targets of Sini powder and Tong xie yao fang decoction for IBS were obtained. Cytoscape 3.8.0 software was used to construct a drug active ingredient-potential therapeutic target network. The degree of node connectivity represents the number of edges connected to a certain point. The greater the value is, the greater the importance of the point in the topological structure. The degree of node connectivity was calculated using Cytoscape software, and the important effective ingredients and targets of Sini powder and Tong xie yao fang decoction in the treatment of IBS were clarified.

2.4. Construction of the Protein Interaction Network (PPI). The common targets obtained with the procedure described in "1.3" were imported into the STRING database (https://string-db.org/), the species "homo sapiens" was selected, and the threshold was set to >0.7. Free targets were hidden to obtain PPI networks. The data were imported into Cytoscape 3.8.0 software for visualization, and the core targets in the PPI network were obtained. The Molecular Complex Detection (MCODE) plug-in in Cytoscape 3.8.0 software was used to perform a modular analysis of the core targets of the PPI network. Degree cutoff = 2, degree cutoff > 2, node score cutoff = 0.2, K-Core = 2, and Max.Depth = 100 were set, and the features of the targets were analyzed to select core target modules.

2.5. Functional Annotation of Common Target Genes Using Gene Ontology (GO) and Kyoto Encyclopedia of Genes and Genomes (KEGG) Pathway Enrichment Analysis. The common targets obtained in step "1.3" were imported into the DAVID 6.8 database (https://david.ncifcrf.gov/) for GO and KEGG analysis. The screening conditions were set as $P < 0.01$ and FDR < 0.05. The top 20 enriched results were displayed, the results were visualized using the Image GP tool, and the analysis results were displayed in the form of bubble graphs.

3. Results

3.1. Screening of Active Ingredients of Sini Powder and Tong Xie and Target Prediction. According to the OB and DL parameters and after excluding the compounds that were not included in PubChem or for which the relevant target could

not be predicted by the Swiss Target, the following active ingredients were screened from the TCMSP database: 14 Chinese thorowax root (including 3 duplicate compounds), 11 Radix Paeoniae Alba (including 4 duplicate compounds), 20 Fructus aurantii Immaturus (including 4 duplicate compounds), 87 *Chinese licorice* (including 6 duplicate compounds), 3 *Rhizoma Atractylodis*, 14 *Divaricate Saposhnikovia* root (including 3 duplicate compounds), and 4 Citri Reticulatae Pericarpium (including 3 duplicate compounds). A total of 139 active ingredients were finally obtained (Table 1). Chinese thorowax root, Radix Paeoniae Alba, Fructus aurantii Immaturus, Chinese licorice, *Rhizoma Atractylodis*, *Divaricate Saposhnikovia* root, and Citri Reticulatae Pericarpium are referred to as BR, PRA, AFI, GRER, AMR, SR, and CRP, respectively. The abovementioned 139 active ingredients were retrieved from the PubChem website and the Swiss Target Prediction database to obtain 9,846 targets. After screening and the removal of duplications, a total of 960 targets were obtained.

3.2. Construction of the Active Ingredient-Target Network of the Drugs. Five disease databases—DrugBank, DisGeNET, Genecards, OMIM, and TTD—were searched, and 57, 429, 768, 623, and 27 of target sites were obtained, respectively. After summarizing the abovementioned targets and removing duplicate targets, 1,690 disease targets were finally obtained. A total of 248 common targets were obtained by taking the intersection of the targets obtained in the steps described in sections "2.1" and "2.2" (Figure 1(a)). Cytoscape 3.8.0 software was used to construct a network diagram of traditional Chinese medicine-active ingredient-potential therapeutic targets (Figure 1(b)). The diagram contains a total of 394 nodes and 3,313 edges. The degree of potential therapeutic targets of IBS (i.e., the number of compounds involved in the regulation of this target) was calculated. The top 10 potential targets were cytochrome P450 family 19 subfamily A member 1 (CYP19A1), estrogen receptor beta (ESR2), ESR1, acetylcholinesterase (ACHE), epidermal growth factor receptor (EGFR), adenosine A2A receptor gene (ADORA2A), ATP binding cassette subfamily B member 1 (ABCB1), v-src avian sarcoma (Schmidt-Ruppin A-2), viral oncogene homolog (SRC), monoamine oxidase A (MAOA), and matrix metalloproteinase 9 (MMP9). Additionally, a potential active compound can correspond to multiple potential therapeutic targets, such as obacunone, praeruptorin B, 7-acetoxy-2-methyl isoflavone, alfalfa toxin, poncimarin, licochalcone B, wogonin, and quercetin. This reflects the characteristics of the network structure of a single drug with multiple targets and multiple drugs that have the same target in the active ingredient-target network diagram, indicating that Sini powder and Tong xie yao fang decoction use a multitarget, multipathway, and multistep approach to treat IBS.

3.3. Construction of the PPI Network between the Active Ingredients of Sini Powder and Tong Xie Yao Fang Decoction and IBS. The 248 common targets obtained in the process described in "2.3" were imported into the STRING database to construct the PPI network. After the TSV file was obtained, it was imported into Cytoscape 3.8.0 software for visualization and network topology analysis. The PPI network contained a total of 232 nodes (16 target proteins are not involved in the interaction), and there were 1884 edges. The larger the degree value is, the larger the size of the hexagonal area and the darker the color (Figure 2(a)). The median degree value was 12, and a degree value ≥24 was used as the screening condition to obtain the core target proteins of Sini powder and Tong xie yao fang decoction in the treatment of IBS (Figure 2(b)). Of these, AKT Serine/Threonine Kinase 1 (AKT1, degree = 76); phosphatidylinositol-4, 5-Bisphosphate 3-Kinase Catalytic Subunit Alpha (PIK3CA, degree = 67); phosphoinositide-3-kinase regulatory subunit 1 (PIK3R1, degree = 66); signal transducer and activator of transcription 3 (STAT3, degree = 64); vascular endothelial growth factor (VEGF, degree = 62); mitogen-activated protein kinase 1 (MAPK1, degree = 60); H-Ras Proto-Oncogene; GTPase (HRAS, degree = 57); SRC (degree = 56); EGFR (degree = 54); and C-X-C motif chemokine ligand 8 (CXCL8, degree = 50) were obtained. The larger degree value of the target point reflects the high density of nodes and their surrounding nodes, which play important roles in the network. Therefore, these targets may be keys in the treatment of IBS. The MCODE plug-in of Cytoscape software was used for modular analysis of the screened core target proteins, and their characteristics were analyzed to screen the core target modules (Figure 2(c)). Selected modules have higher information transmission efficiency, and a single target has stronger interactions with other nodes.

3.4. GO Functional Enrichment and KEGG Pathway Enrichment Analysis. When $P < 0.01$ and FDR < 0.05, a total of 522 GO functions were enriched in common targets (including 79 molecular function items, 386 biological process items, and 57 cell component items). In terms of molecular functions, these functions were mainly enriched in protein binding, ATP binding, drug binding, enzyme binding, 5-hydroxytryptamine binding, protein kinase activity, protein serine/threonine kinase activity, protein tyrosine kinase activity, transcription factor binding, etc (Figure 3(a)). In terms of biological process, they were mainly enriched in the transcription of RNA polymerase II promoter, cell proliferation, gene expression, positive regulation of the ERK1 and ERK2 cascade, drug response, negative regulation of apoptosis process, protein phosphorylation, inflammatory response, and protein autophosphorylation, MAPK cascade, etc (Figure 3(b)). In terms of molecular components, they were mainly enriched in the plasma membrane, dendrites, synapses, and neuronal cell bodies (Figure 3(c)). The KEGG pathway enrichment screening resulted in 101 signaling pathways. The results suggest that cancer, neuroactive ligand-receptor interaction, proteoglycan in cancer, calcium ion signal, cAMP, hepatitis B, hypoxia-inducible factor 1-alpha (HIF-1), pancreatic cancer, and other signal pathways may be closely related to the pathogenesis of IBS (Figure 3(d)).

Table 1: List of active components of Sini powder and Tong xie yao fang decoction.

Herb	MOL ID	Molecule name	ID	OB%	DL
Radix bupleuri	MOL001645	Linoleyl acetate	BR1	42.1	0.2
Radix bupleuri	MOL002776	Baicalin	BR2	40.12	0.75
Radix bupleuri	MOL000449	Stigmasterol	BR3	43.83	0.76
Radix bupleuri	MOL000354	Isorhamnetin	A1	49.6	0.31
Radix bupleuri	MOL000422	Kaempferol	B1	41.88	0.24
Radix bupleuri	MOL004598	3, 5, 6, 7-tetramethoxy-2-(3, 4, 5-trimethoxyphenyl) chromone	BR4	31.97	0.59
Radix bupleuri	MOL004609	Areapillin	BR5	48.96	0.41
Radix bupleuri	MOL013187	Cubebin	BR6	57.13	0.64
Radix bupleuri	MOL004644	Sainfuran	BR7	79.91	0.23
Radix bupleuri	MOL004653	(+)-anomalin	BR8	46.06	0.66
Radix bupleuri	MOL004702	Saikosaponin c_qt	BR9	30.5	0.63
Radix bupleuri	MOL004718	α-spinasterol	BR10	42.98	0.76
Radix bupleuri	MOL000490	Petunidin	BR11	30.05	0.31
Radix bupleuri	MOL000098	Quercetin	A2	46.43	0.28
White peony root	MOL001918	Paeoniflorgenone	PRA1	87.59	0.37
White peony root	MOL001919	(3S, 5R, 8R, 9R, 10S, 14S)-3, 17-dihydroxy-4, 4, 8, 10, 14-pentamethyl-2, 3, 5, 6, 7, 9-hexahydro-1H-cyclopenta[a]phenanthrene-15, 16-dione	PRA2	43.56	0.53
White peony root	MOL001921	Lactiflorin	PRA3	49.12	0.8
White peony root	MOL001924	Paeoniflorin	PRA4	53.87	0.79
White peony root	MOL001925	Paeoniflorin_qt	PRA5	68.18	0.4
White peony root	MOL001928	Albiflorin_qt	PRA6	66.64	0.33
White peony root	MOL001930	Benzoyl paeoniflorin	PRA7	31.27	0.75
White peony root	MOL000211	Mairin	A7	55.38	0.78
White peony root	MOL000358	Beta-sitosterol	A6	36.91	0.75
White peony root	MOL000359	Sitosterol	C	36.91	0.75
White peony root	MOL000422	Kaempferol	B1	41.88	0.24
Fructus aurantii immaturus	MOL013276	Poncirin	AFI1	36.55	0.74
Fructus aurantii immaturus	MOL013277	Isosinensetin	AFI2	51.15	0.44
Fructus aurantii immaturus	MOL013279	5, 7, 4′-trimethylapigenin	AFI3	39.83	0.3
Fructus aurantii immaturus	MOL013428	Isosakuranetin-7-rutinoside	AFI4	41.24	0.72
Fructus aurantii immaturus	MOL013430	Prangenin	AFI5	43.6	0.29
Fructus aurantii immaturus	MOL013435	Poncimarin	AFI6	63.62	0.35
Fructus aurantii immaturus	MOL013436	Isoponcimarin	AFI7	63.28	0.31
Fructus aurantii immaturus	MOL013437	6-methoxy aurapten	AFI8	31.24	0.3
Fructus aurantii immaturus	MOL001798	Neohesperidin_qt	AFI9	71.17	0.27
Fructus aurantii immaturus	MOL001803	Sinensetin	AFI10	50.56	0.45
Fructus aurantii immaturus	MOL001941	Ammidin	A5	34.55	0.22
Fructus aurantii immaturus	MOL013352	Obacunone	AFI11	43.29	0.77
Fructus aurantii immaturus	MOL002914	Eriodyctiol (flavanone)	AFI12	41.35	0.24
Fructus aurantii immaturus	MOL004328	Naringenin	B2	59.29	0.21
Fructus aurantii immaturus	MOL005100	5, 7-dihydroxy-2-(3-hydroxy-4-methoxyphenyl) chroman-4-one	A3	47.74	0.27
Fructus aurantii immaturus	MOL005828	Nobiletin	A4	61.67	0.52
Fructus aurantii immaturus	MOL005849	Didymin	AFI13	38.55	0.24

Table 1: Continued.

Herb	MOL ID	Molecule name	ID	OB%	DL
Fructus aurantii immaturus	MOL000006	Luteolin	AFI14	36.16	0.25
Fructus aurantii immaturus	MOL007879	Tetramethoxyluteolin	AFI15	43.68	0.37
Fructus aurantii immaturus	MOL009053	4-((2S, 3R)-5-((E)-3-hydroxyprop-1-enyl)-7-methoxy-3-methylol-2, 3-dihydrobenzofuran-2-yl)-2-methoxy-phenol	AFI16	50.76	0.39
Licorice	MOL001484	Inermine	GRER1	75.18	0.54
Licorice	MOL001792	DFV	GRER2	32.76	0.18
Llicorice	MOL000211	Mairin	A7	55.38	0.78
Licorice	MOL002311	Glycyrol	GRER3	90.78	0.67
Licorice	MOL000239	Jaranol	GRER4	50.83	0.29
Licorice	MOL002565	Medicarpin	GRER5	49.22	0.34
Licorice	MOL000354	Isorhamnetin	A1	49.6	0.31
Licorice	MOL000359	Sitosterol	C	36.91	0.75
Licorice	MOL003656	Lupiwighteone	GRER6	51.64	0.37
Licorice	MOL003896	7-methoxy-2-methyl isoflavone	GRER7	42.56	0.2
Licorice	MOL000392	Formononetin	GRER8	69.67	0.21
Licorice	MOL000417	Calycosin	GRER9	47.75	0.24
Licorice	MOL000422	Kaempferol	B1	41.88	0.24
Licorice	MOL004328	Naringenin	B2	59.29	0.21
Licorice	MOL004805	(2S)-2-[4-hydroxy-3-(3-methylbut-2-enyl)phenyl]-8, 8-dimethyl-2, 3-dihydropyrano[2, 3-f]chromen-4-one	GRER10	31.79	0.72
Licorice	MOL004808	Glyasperin B	GRER11	65.22	0.44
Licorice	MOL004810	Glyasperin F	GRER12	75.84	0.54
Licorice	MOL004811	Glyasperin C	GRER13	45.56	0.4
Licorice	MOL004814	Isotrifoliol	GRER14	31.94	0.42
Licorice	MOL004815	(E)-1-(2, 4-dihydroxyphenyl)-3-(2, 2-dimethylchromen-6-yl)prop-2-en-1-one	GRER15	39.62	0.35
Licorice	MOL004820	Kanzonols W	GRER16	50.48	0.52
Licorice	MOL004824	(2S)-6-(2, 4-dihydroxyphenyl)-2-(2-hydroxypropan-2-yl)-4-methoxy-2, 3-dihydrofuro(3, 2-g)chromen-7-one	GRER17	60.25	0.63
Licorice	MOL004827	Semilicoisoflavone B	GRER18	48.78	0.55
Licorice	MOL004828	Glepidotin A	GRER19	44.72	0.35
Licorice	MOL004833	Phaseolinisoflavan	GRER20	32.01	0.45
Licorice	MOL004835	Glypallichalcone	GRER21	61.6	0.19
Licorice	MOL004838	8-(6-hydroxy-2-benzofuranyl)-2, 2-dimethyl-5-chromenol	GRER22	58.44	0.38
Licorice	MOL004841	Licochalcone B	GRER23	76.76	0.19
Licorice	MOL004848	Licochalcone G	GRER24	49.25	0.32
Licorice	MOL004849	3-(2, 4-dihydroxyphenyl)-8-(1, 1-dimethylprop-2-enyl)-7-hydroxy-5-methoxy-coumarin	GRER25	59.62	0.43
Licorice	MOL004855	Licoricone	GRER26	63.58	0.47
Licorice	MOL004856	Gancaonin A	GRER27	51.08	0.4
Licorice	MOL004857	Gancaonin B	GRER28	48.79	0.45
Licorice	MOL004860	Licorice glycoside E	GRER29	32.89	0.27
Licorice	MOL004863	3-(3, 4-dihydroxyphenyl)-5, 7-dihydroxy-8-(3-methylbut-2-enyl) chromone	GRER30	66.37	0.41
Licorice	MOL004864	5, 7-dihydroxy-3-(4-methoxyphenyl)-8-(3-methylbut-2-enyl)chromone	GRER31	30.49	0.41
Licorice	MOL004866	2-(3, 4-dihydroxyphenyl)-5, 7-dihydroxy-6-(3-methylbut-2-enyl) chromone	GRER32	44.15	0.41
Licorice	MOL004879	Glycyrin	GRER33	52.61	0.47
Licorice	MOL004882	Licocoumarone	GRER34	33.21	0.36
Licorice	MOL004883	Licoisoflavone	GRER35	41.61	0.42
Licorice	MOL004884	Licoisoflavone B	GRER36	38.93	0.55
Licorice	MOL004885	Licoisoflavanone	GRER37	52.47	0.54
Licorice	MOL004891	Shinpterocarpin	GRER38	80.3	0.73
Licorice	MOL004898	(E)-3-(3, 4-dihydroxy-5-(3-methylbut-2-enyl)phenyl)-1-(2, 4-dihydroxyphenyl)prop-2-en-1-one	GRER39	46.27	0.31
Licorice	MOL004903	Liquiritin	GRER40	65.69	0.74
Licorice	MOL004904	Licopyranocoumarin	GRER41	80.36	0.65

Table 1: Continued.

Herb	MOL ID	Molecule name	ID	OB%	DL
Licorice	MOL004905	3, 22-dihydroxy-11-oxo-delta(12)-oleanene-27-alpha-methoxycarbonyl-29-oic acid	GRER42	34.32	0.55
Licorice	MOL004907	Glyzaglabrin	GRER43	61.07	0.35
Licorice	MOL004908	Glabridin	GRER44	53.25	0.47
Licorice	MOL004910	Glabranin	GRER45	52.9	0.31
Licorice	MOL004911	Glabrene	GRER46	46.27	0.44
Licorice	MOL004912	Glabrone	GRER47	52.51	0.5
Licorice	MOL004913	1, 3-dihydroxy-9-methoxy-6-benzofurano(3, 2-c)chromenone	GRER48	48.14	0.43
Licorice	MOL004914	1, 3-dihydroxy-8, 9-dimethoxy-6-benzofurano(3, 2-c)chromenone	GRER49	62.9	0.53
Licorice	MOL004915	Eurycarpin A	GRER50	43.28	0.37
Licorice	MOL004917	Glycyroside	GRER51	37.25	0.79
Licorice	MOL004924	(-)-medicocarpin	GRER52	40.99	0.95
Licorice	MOL004935	Sigmoidin-B	GRER53	34.88	0.41
Licorice	MOL004941	(2R)-7-hydroxy-2-(4-hydroxyphenyl)chroman-4-one	GRER54	71.12	0.18
Licorice	MOL004945	(2S)-7-hydroxy-2-(4-hydroxyphenyl)-8-(3-methylbut-2-enyl)chroman-4-one	GRER55	36.57	0.32
Licorice	MOL004948	Isoglycyrol	GRER56	44.7	0.84
Licorice	MOL004949	Isolicoflavonol	GRER57	45.17	0.42
Licorice	MOL004959	1-methoxyphaseollidin	GRER58	69.98	0.64
Licorice	MOL004961	Quercetin der.	GRER59	46.45	0.33
Licorice	MOL000497	Licochalcone a	GRER60	40.79	0.29
Licorice	MOL004974	3′-methoxyglabridin	GRER61	46.16	0.57
Licorice	MOL004978	2-((3R)-8, 8-dimethyl-3, 4-dihydro-2H-pyrano(6, 5-f)chromen-3-yl)-5-methoxyphenol	GRER62	36.21	0.52
Licorice	MOL004980	Inflacoumarin A	GRER63	39.71	0.33
Licorice	MOL004985	Icos-5-enoic acid	GRER64	30.7	0.2
Licorice	MOL004988	Kanzonol F	GRER65	32.47	0.89
Licorice	MOL004989	6-prenylated eriodictyol	GRER66	39.22	0.41
Licorice	MOL004990	7, 2′, 4′-trihydroxy–5-methoxy-3–arylcoumarin	GRER67	83.71	0.27
Licorice	MOL004991	7-acetoxy-2-methylisoflavone	GRER68	38.92	0.26
Licorice	MOL004993	8-prenylated eriodictyol	GRER69	53.79	0.4
Licorice	MOL004996	Gadelaidic acid	GRER70	30.7	0.2
Licorice	MOL000500	Vestitol	GRER71	74.66	0.21
Licorice	MOL005000	Gancaonin G	GRER72	60.44	0.39
Licorice	MOL005001	Gancaonin H	GRER73	50.1	0.78
Licorice	MOL005003	Licoagrocarpin	GRER74	58.81	0.58
Licorice	MOL005007	Glyasperins M	GRER75	72.67	0.59
Licorice	MOL005008	Glycyrrhiza flavonol A	GRER76	41.28	0.6
Licorice	MOL005012	Licoagroisoflavone	GRER77	57.28	0.49
Licorice	MOL005013	18α-hydroxyglycyrrhetic acid	GRER78	41.16	0.71
Licorice	MOL005016	Odoratin	GRER79	49.95	0.3
Licorice	MOL005017	Phaseol	GRER80	78.77	0.58
Licorice	MOL005018	Xambioona	GRER81	54.85	0.87
Licorice	MOL000098	Quercetin	A2	46.43	0.28
Rhizoma atractylodis macrocephalae	MOL000028	α-amyrin	AMR1	39.51	0.76
Rhizoma atractylodis macrocephalae	MOL000033	(3S, 8S, 9S, 10R, 13R, 14S, 17R)-10, 13-dimethyl-17-((2R, 5S)-5-propan-2-yloctan-2-yl)-2, 3, 4, 7, 8, 9, 11, 12, 14, 15, 16, 17-dodecahydro-1H-cyclopenta[a]phenanthren-3-ol	AMR2	36.23	0.78
Rhizoma atractylodis macrocephalae	MOL000072	8β-ethoxy atractylenolide III	AMR3	35.95	0.21
Radix saposhnikoviae	MOL011732	Anomalin	SR1	59.65	0.66
Radix saposhnikoviae	MOL011737	Divaricatacid	SR2	87	0.32
Radix saposhnikoviae	MOL011740	Divaricatol	SR3	31.65	0.38
Radix saposhnikoviae	MOL001941	Ammidin	A5	34.55	0.22
Radix saposhnikoviae	MOL011747	Ledebouriellol	SR4	32.05	0.51
Radix saposhnikoviae	MOL002644	Phellopterin	SR5	40.19	0.28
Radix saposhnikoviae	MOL000359	Sitosterol	C	36.91	0.75
Radix saposhnikoviae	MOL000173	Wogonin	SR6	30.68	0.23
Radix saposhnikoviae	MOL000358	Beta-sitosterol	A6	36.91	0.75

Table 1: Continued.

Herb	MOL ID	Molecule name	ID	OB%	DL
Radix saposhnikoviae	MOL001494	Mandenol	SR7	42	0.19
Radix saposhnikoviae	MOL001942	Isoimperatorin	SR8	45.46	0.23
Radix saposhnikoviae	MOL003588	Prangenidin	SR9	36.31	0.22
Radix saposhnikoviae	MOL007514	Methyl icosa-11, 14-dienoate	SR10	39.67	0.23
Radix saposhnikoviae	MOL013077	Decursin	SR11	39.27	0.38
Orange peel	MOL000359	Sitosterol	C	36.91	0.75
Orange peel	MOL004328	Naringenin	B2	59.29	0.21
Orange peel	MOL005100	5, 7-dihydroxy-2-(3-hydroxy-4-methoxyphenyl)chroman-4-one	A3	47.74	0.27
Orange peel	MOL005828	Nobiletin	A4	61.67	0.52

4. Discussion

Liver stagnation and spleen deficiency are important pathogenies of IBS in the theory of the traditional Chinese medicine. Sini powder and Tong xie yao fang decoction, which restrict the liver and support the spleen, have good indications and clinical efficacy for IBS [16, 17].

In the present study, the topological properties of the active ingredients-potential target network of Sini powder and Tong xie yao fang decoction were analyzed. We screened and picked up the ingredients with the highest degree value, such as obacunone, praeruptorin B, 7-acetoxy-2-methyl isoflavone, alfalfa toxin, poncimarin, licochalcone B, wogonin, and quercetin for the subsequent analysis. Obacunone is a natural compound that is widely present in plants in the Rutaceae family. It has anti-inflammatory, antitumor, antioxidative, and antipulmonary fibrosis effects. It has been confirmed in animal models that obacunone can inhibit the production of proinflammatory mediators [18]. It also alleviate colitis by improving the abnormal composition of intestinal microbiota and suppressing excessive activation of toll-like receptors (TLRs)/NF-κB signaling cascades to [19]. Licochalcone B can exert anti-inflammatory effects by inhibiting the phosphorylation of nuclear factor kappa B (NF-κB) P65 in the lipopolysaccharides (LPS) signaling pathway [20]. Wogonin is a pure natural flavonoid with a variety of biological activities, such as antiviral, anti-inflammatory, anticancer, neuroprotective, and antianxiety effects [21]. Previous studies have showed that wogonin can be used to treat colitis by inducing the expression of transcription factor HIF-1α through the protein kinase B/glycogen synthase kinase β (AKT/GSK3β) signaling pathway to increase interleukin 10 (IL-10) production [22]. Synergistic treatment using quercetin and 5-aminosalicylic acid improved symptoms and signs in a rat model of IBS after infection and improved the therapeutic effect [23]. As a coumarin-based component, praeruptorin B has been confirmed to have anti-inflammatory, antioxidant, antitumor, and analgesic activities [24, 25]. However, there are few reports on the treatment of IBS using praeruptorin B. In the present study, our results and the others suggest that the ingredients of the Sini powder and Tong xie yao fang decoction mainly served as anti-inflammatory mediators which indicate that the combined decoction might have a promising therapeutic value for the IBS treatment. Moreover, one potential valuable ingredient praeruptorin B was selected in the present study, which might be a promising target for IBS further research and drug discovery.

We next investigate the underlying mechanism of the valuable ingredients in the Sini powder and Tong xie yao fang decoction. Top ten core targets, such as AKT1, PIK3CA, PIK3R1, STAT3, VEGF, MAPK1, HRAS, SRC, EGFR, and CXCL8 were selected and further analysis. Previous studies have showed that overexpression of microRNA495 down-regulated STAT3 to improve intestinal mucosal barrier function in ulcerative colitis [26]. Cell adhesion molecule 1 (CADM1) also would inhibit STAT3 signaling pathway to improve the intestinal barrier function of rats with IBS-D [27]. EGFR is a transmembrane receptor tyrosine kinase in the ErbB family that can promote intestinal development, regulate tight-binding protein expression, inhibit oxidative stress-induced apoptosis, and reduce intestinal epithelial colonization by inducing the autophosphorylation of RTK and the subsequent activation of the Ras/MAPK, PI3K/AKT, and PLC-γ/PKC signaling pathways, and it plays an active role in regulating intestinal permeability and promoting the integrity of the intestinal barrier [28]. VEGF is one of the most important factors in gastrointestinal mucosal remodeling, mucosal defense, and ulcer healing. The anti-ulcer drug sofalcone can prevent gastric mucosal injury through the upregulation of VEGF production mediated by the nuclear factor erythroid-2 related factor 2/hemeoxygenase-1 (Nrf2/HO-1) pathway [29]. Camellia oil can improve ketoprofen-induced gastrointestinal mucosal injury by upregulating HO-1 and VEGF [30]. The ERK/MAPK pathway can increase the expression level of intestinal tight junction proteins to enhance the intestinal barrier function in dogs with splenic asthenia syndrome [31]. Taken these together, the Sini powder and Tong xie yao fang decoction might improve intestinal barrier function, regulate intestinal permeability, exert a protective effect on the gastrointestinal mucosa, and inhibit the inflammatory response in IBS treatment.

Our results further showed that the top ten core genes mainly involved cell proliferation, inflammatory response, protein phosphorylation, ERK1/2 cascade, MAPK cascade, neurons, 5-hydroxytryptamine (5-HT) binding, and protein binding by GO functional enrichment analysis. 5-HT is a neurotransmitter in the intestinal tract that is considered an important signaling molecule. It mainly acts on various

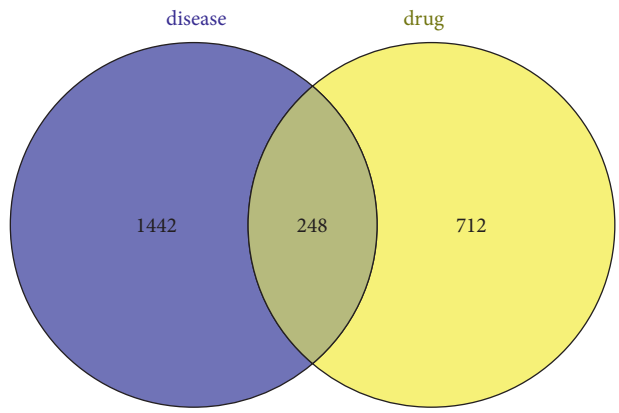

(a)

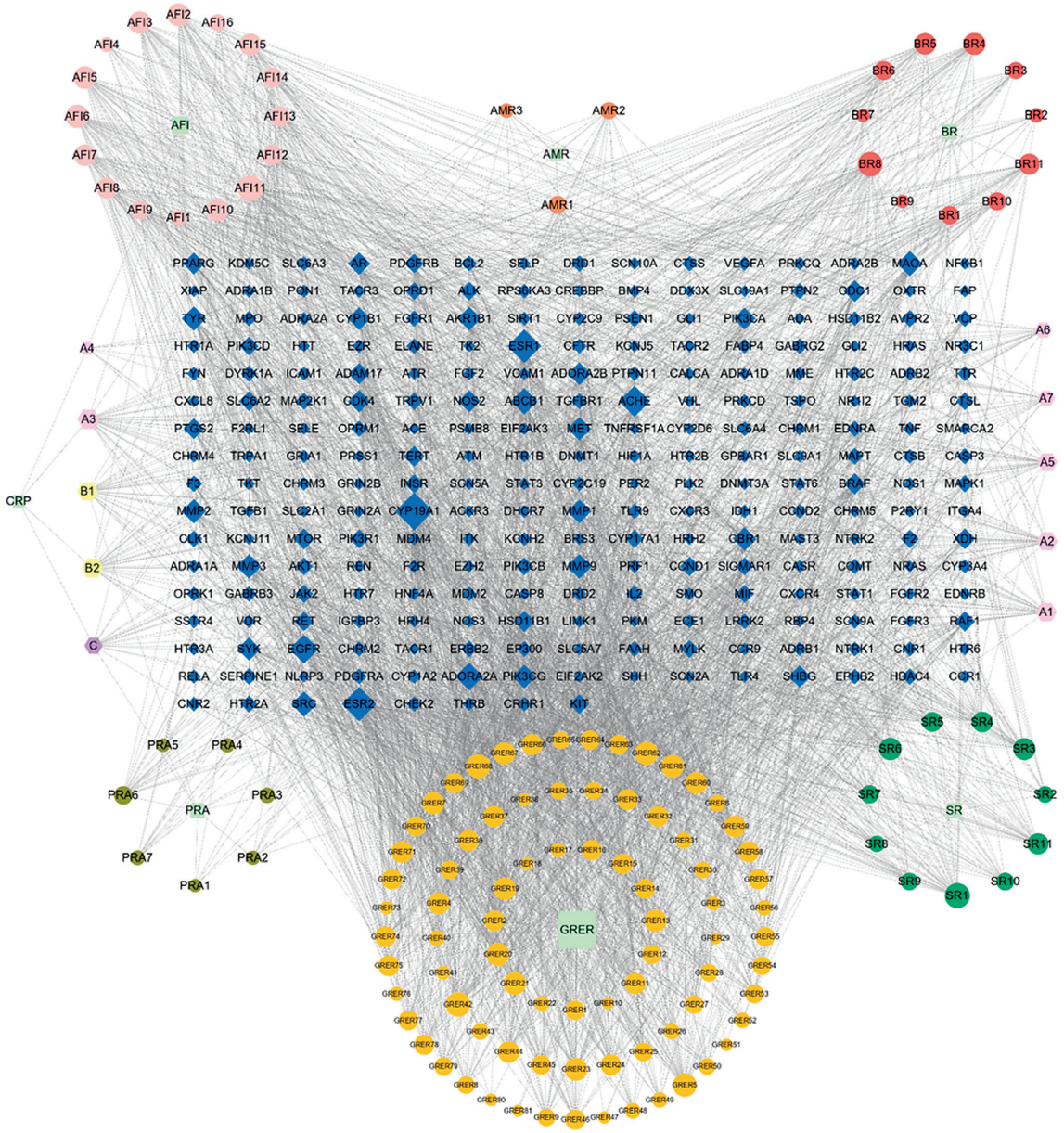

(b)

FIGURE 1: Active ingredient-target network of the drugs. (a) Venn diagram of related targets of active ingredients of Sini powder and Tong xie yao fang decoction in the treatment of irritable bowel syndrome. (b) Drugs-active components-target network diagram of Sini powder and Tong xie yao fang decoction in the treatment of irritable bowel syndrome.

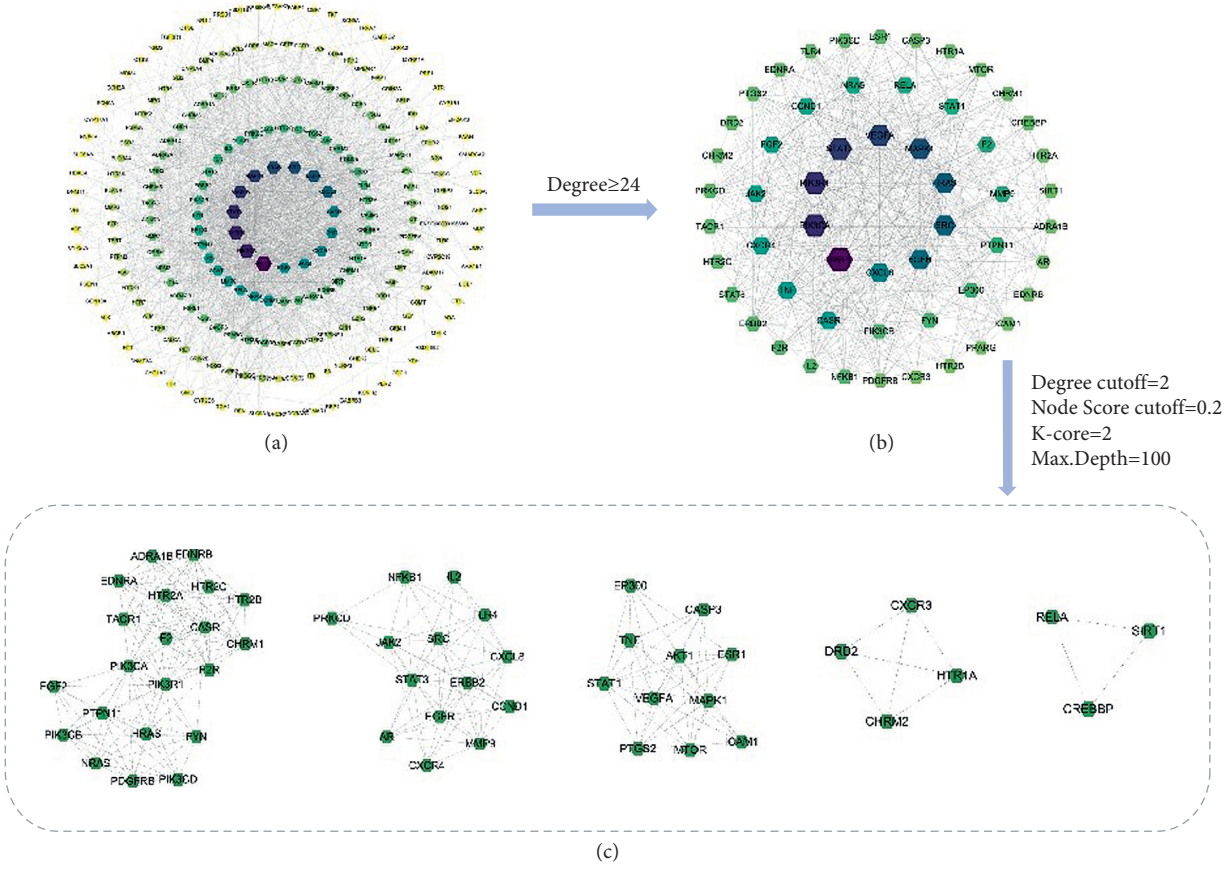

Figure 2: PPI networks of Sini powder and Tong xie yao fang decoction in the treatment of irritable bowel syndrome. (a) Bio-targets of Sini powder and Tong xie yao fang decoction in irritable bowel syndrome treatment. (b) Key biotargets from (a). (c) Modularization analysis of (b).

receptors on smooth muscle, enteric neurons, intestinal cells, and immune cells to regulate various intestinal functions. The symptoms of IBS (such as visceral sensitivity and gastrointestinal motility disturbance) are related to the level of 5-HT in the intestine. Previous studies have showed that an increase in 5-HT levels is correlated with diarrhea-dominant IBS. A decrease in the 5-HT level is correlated with constipation-dominant IBS [32]. The KEGG pathway enrichment analysis showed that the treatment of IBS with Sini Powder and Tong xie yao fang decoction involves multiple signaling pathways, such as cancer, neuroactive ligand-receptor interaction, calcium ion signaling, cAMP, HIF-1, and hepatitis B. The cAMP signaling pathway maintains the stability of the internal and external environment of intestinal cells, improves enteric nerve function, and regulates intestinal secretion and absorption [33]. PKA may mediate SP through cAMP signaling to regulate visceral sensitivity and enhance gastrointestinal motility [34]. In the rat model of diarrhea-dominant IBS, the expression levels of the L-type voltage-gated calcium channels Cav1.2 and Cav1.3 in the colon was found to be elevated to different degrees, suggesting that the increase in the L-type voltage-gated calcium channel may be the molecular basis of colonic motility disorders [35]. The T-type voltage-gated calcium channel Cav3.2 is upregulated in IBS and participates in visceral hypersensitivity, which is closely related to the occurrence and development of IBS [36]. HIF-1α is a sensitive indicator of intestinal hypoxia and is related to the maintenance of the intestinal barrier. Studies have confirmed that intestinal epithelial HIF-1α is an important protective factor against colitis and can effectively alleviate inflammatory colonic injury [37]. Taken these together, the Sini powder and Tong xie yao fang decoction might regulate intestinal nerve function, improve visceral sensitivity and gastrointestinal motility, and maintain intestinal barrier function to treat IBS by integrating these multi-pathways.

In summary, this study investigated the potential material basis and mechanism of action of the Sini powder and Tong xie yao fang decoction in the treatment of IBS through a network pharmacology method. The main mechanism of Sini powder and Tong xie yao fang decoction in the treatment of IBS may be the regulation of intestinal 5-HT levels to improve intestinal nerve function, act on calcium channels to improve visceral sensitivity, maintain intestinal barrier function to provide mucosal protection, and inhibit inflammatory responses. In general, the drug has multi-ingredient, multitarget, and multipathway characteristics and plays a therapeutic role through the synergistic effect of multipathway system regulation. The present study had provided an alternative potential strategy for IBS treatment. However, more evidence from the IBS animal model and IBS patients should be evaluated in the future studies.

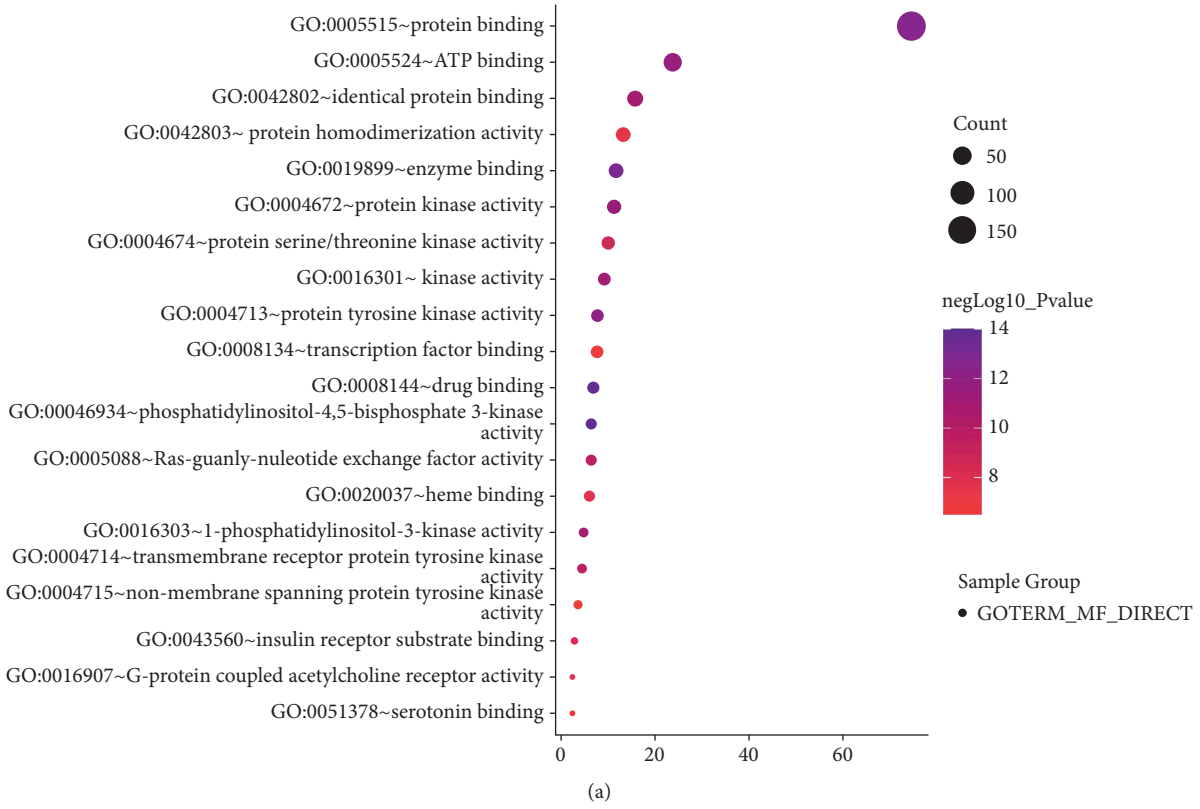

(a)

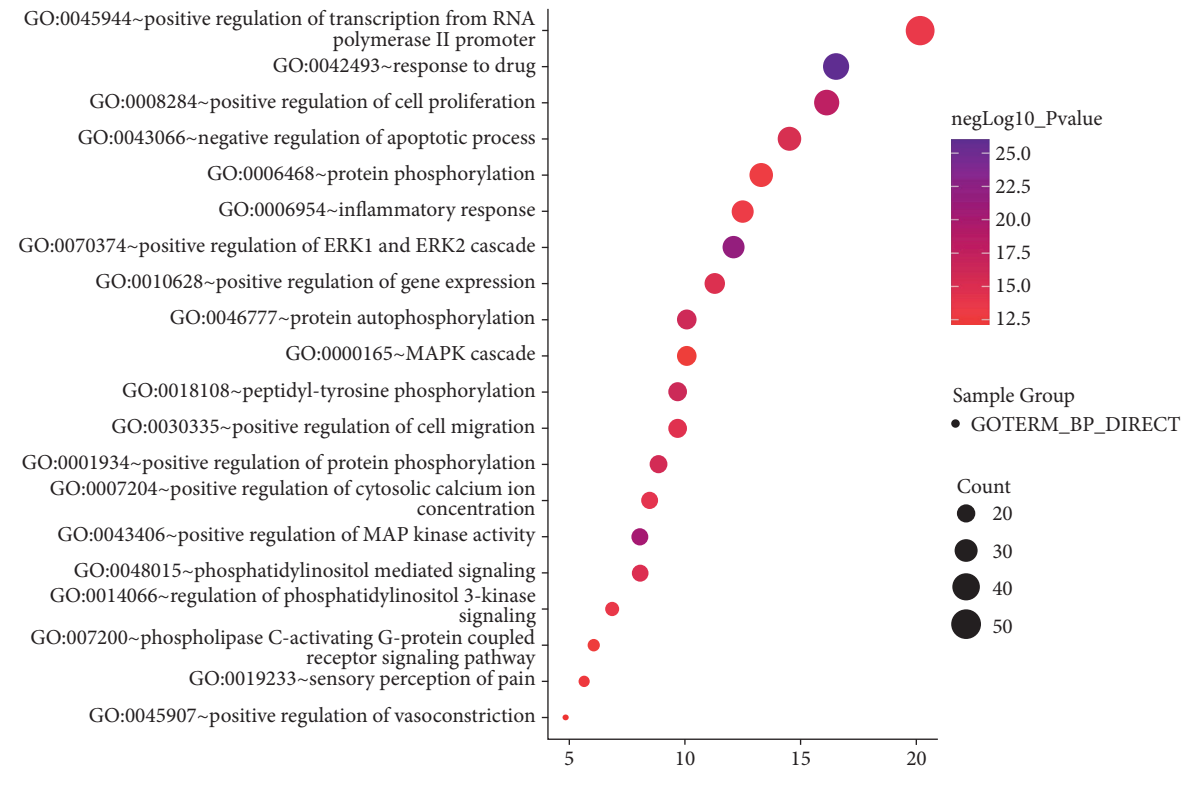

(b)

Figure 3: Continued.

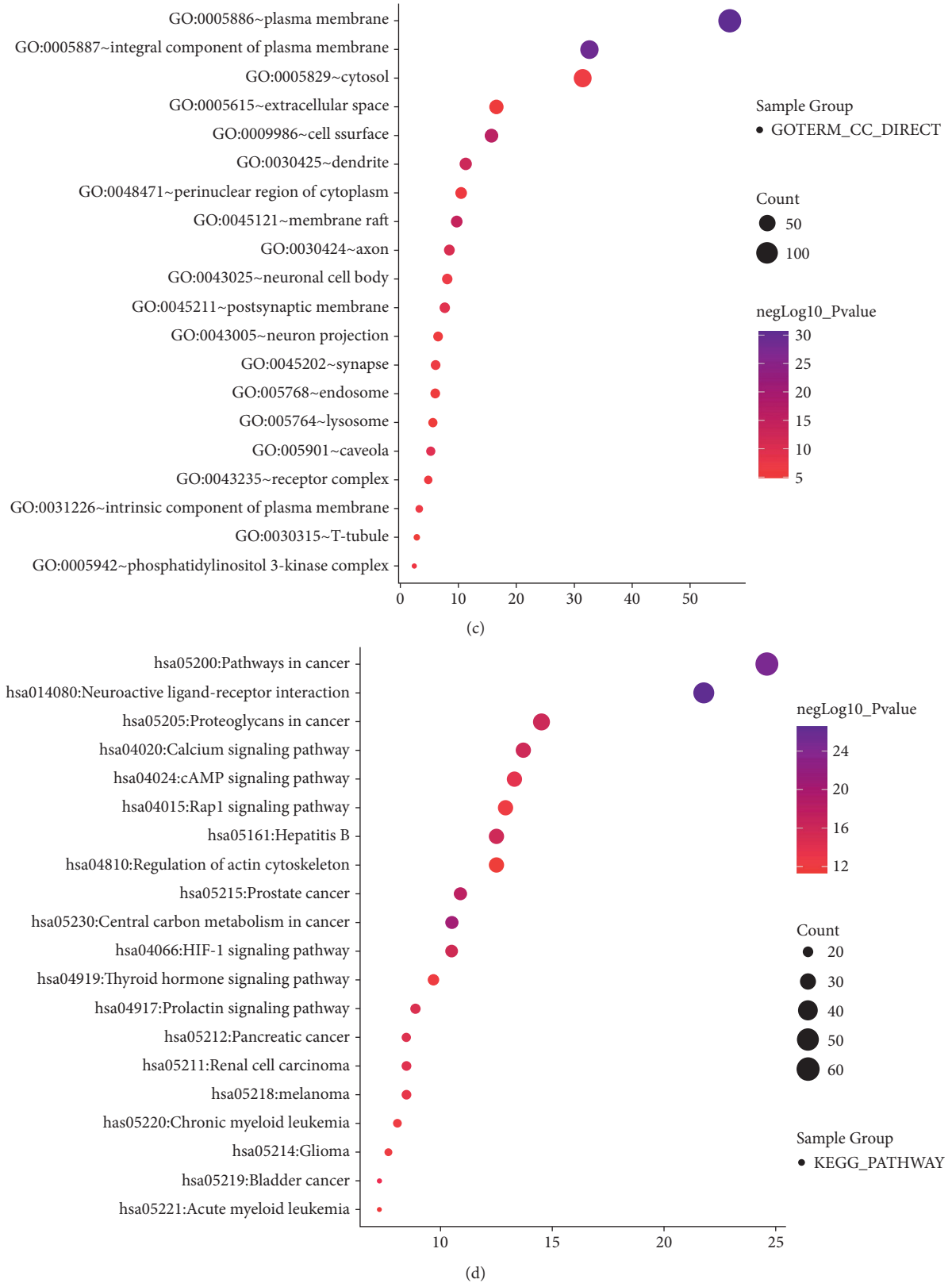

Figure 3: GO and KEGG PATHWAY enrichment analysis for targets of Sini powder and Tong xie yao fang decoction related to IBS. (a) Molecular function. (b) Biological processes. (c) Cellular component. (d) Bubble chart of KEGG pathway analysis. The order of importance was ranked by –log10 (*P* value) and gene number. In terms of *P* values, in ascending order, the top 20 GO functions and KEGG pathways were used to make bubble plots.

Data Availability

The data used to support the findings of this study are available from the corresponding author upon request.

Disclosure

The fund providers had no role in the design of the study; collection, analysis, interpretation of data; writing the manuscript; and the decision to submit the manuscript for publication.

Conflicts of Interest

The authors declare that they have no conflicts of interest.

Authors' Contributions

Hong Liu conceived and designed the study. Rong Tang, Xiaoqing Peng, Xiaohong Zhou, Zhimin Zheng, and Jiayu Yin acquired and analyzed the data. Rong Tang prepared the manuscript. Hong Liu submitted the manuscript. All authors have read and approved the final manuscript.

Acknowledgments

This work was supported by Basic and Applied Basic Research Fund Project of Guangdong Province (2020A1515110615), Medical Research Foundation of Guangdong Province (B2020043).

References

[1] B. Radovanovic-Dinic, S. Tesic-Rajkovic, S. Grgov, G. Petrovic, and V. Zivkovic, "Irritable bowel syndrome—from etiopathogenesis to therapy," *Biomedical Papers of the Medical Faculty of the University Palacky*, vol. 162, no. 1, pp. 1–9, 2018.

[2] A. C. Ford, A. D. Sperber, M. Corsetti, and M. Camilleri, "Irritable bowel syndrome," *The Lancet*, vol. 396, no. 10263, pp. 1675–1688, 2020.

[3] Y.-L. Liu and J.-S. Liu, "Chinese expert consensus of irritable bowel syndrome in 2020," *Chinese Medical Journal*, vol. 40, pp. 803–818, 2021.

[4] H. Zeng, T. Bai, and H. Xh, "Research advances in the pathogenesis of irritable bowel syndrome," *Chinese Journal of Practical Internal Medicine*, vol. 40, pp. 115–118, 2020.

[5] F. Klem, A. Wadhwa, L. J. Prokop et al., "Prevalence, risk factors, and outcomes of irritable bowel syndrome after infectious enteritis: a systematic review and meta-analysis," *Gastroenterology*, vol. 152, no. 5, pp. 1042–1054, 2017.

[6] I. M. Gralnek, R. D. Hays, A. Kilbourne, B. Naliboff, and E. A. Mayer, "The impact of irritable bowel syndrome on health-related quality of life," *Gastroenterology*, vol. 119, no. 3, pp. 654–660, 2000.

[7] M. H. Farzaei, R. Bahramsoltani, M. Abdollahi, and R. Rahimi, "The role of visceral hypersensitivity in irritable bowel syndrome: pharmacological targets and novel treatments," *Journal of Neurogastroenterology and Motility*, vol. 22, no. 4, pp. 558–574, 2016.

[8] X. Zhuang, L. Xiong, L. Li, M. Li, and M. Chen, "Alterations of gut microbiota in patients with irritable bowel syndrome: a systematic review and meta-analysis," *Journal of Gastroenterology and Hepatology*, vol. 32, no. 1, pp. 28–38, 2017.

[9] M. I. Pinto-Sanchez, A. C. Ford, C. A. Avila et al., "Anxiety and depression increase in a stepwise manner in parallel with multiple FGIDs and symptom severity and frequency," *American Journal of Gastroenterology*, vol. 110, no. 7, pp. 1038–1048, 2015.

[10] A. W. DuPont, Z.-D. Jiang, S. A. Harold et al., "Motility abnormalities in irritable bowel syndrome," *Digestion*, vol. 89, no. 2, pp. 119–123, 2014.

[11] K. De Punder and L. Pruimboom, "Stress induces endotoxemia and low-grade inflammation by increasing barrier permeability," *Frontiers in Immunology*, vol. 6, p. 223, 2015.

[12] W. D. Chey, J. Kurlander, and S. Eswaran, "Irritable bowel syndrome," *JAMA*, vol. 313, no. 9, pp. 949–958, 2015.

[13] B. Li, J. Rui, X. Ding, Y. Chen, and X. Yang, "Deciphering the multicomponent synergy mechanisms of SiNiSan prescription on irritable bowel syndrome using a bioinformatics/network topology based strategy," *Phytomedicine*, vol. 63, Article ID 152982, 2019.

[14] H. Fan, L. Zheng, Y. Lai et al., "Tongxie formula reduces symptoms of irritable bowel syndrome," *Clinical Gastroenterology and Hepatology*, vol. 15, no. 11, pp. 1724–1732, 2017.

[15] Y. Wang, H. Fan, X. Qi et al., "Are personalized tongxie formula based on diagnostic analyses more effective in reducing IBS symptoms?-a randomized controlled trial," *Complementary Therapies in Medicine*, vol. 40, pp. 95–105, 2018.

[16] W. Liu, "Clinical study on Sini decoction and tongxie yaofang in treating liver qi and spleen-type irritable bowel syndrome," *Systems Medicine*, vol. 4, pp. 121-122, 2019.

[17] D. Liu, "Clinical study on the treatment of D-IBS by Tong xie yao fang decoction combined with modified Sini powder," *China Journal of Chinese Medicine*, vol. 27, pp. 1341-1342, 2012.

[18] X. Luo, Z. Yu, B. Yue et al., "Obacunone reduces inflammatory signalling and tumour occurrence in mice with chronic inflammation-induced colorectal cancer," *Pharmaceutical Biology*, vol. 58, no. 1, pp. 886–897, 2020.

[19] X. Luo, B. Yue, Z. Yu et al., "Obacunone protects against ulcerative colitis in mice by modulating gut microbiota, attenuating TLR4/NF-κB signaling cascades, and improving disrupted epithelial barriers," *Frontiers in Microbiology*, vol. 11, p. 497, 2020.

[20] J.-I. Furusawa, M. Funakoshi-Tago, T. Mashino et al., "Glycyrrhiza inflata-derived chalcones, licochalcone A, licochalcone B and licochalcone D, inhibit phosphorylation of NF-κB p65 in LPS signaling pathway," *International Immunopharmacology*, vol. 9, no. 4, pp. 499–507, 2009.

[21] D. L. Huynh, T. H. Ngau, N. H. Nguyen, G. B. Tran, and C. T. Nguyen, "Potential therapeutic and pharmacological effects of Wogonin: an updated review," *Molecular Biology Reports*, vol. 47, pp. 9779–9789, 2020.

[22] Q. Wu, S. Xie, Y. Zhu et al., "Wogonin strengthens the therapeutic effects of mesenchymal stem cells in DSS-induced colitis via promoting IL-10 production," *Oxidative Medicine and Cellular Longevity*, vol. 2021, p. 5527935, 2021.

[23] H. K. Huang, J. W. Luo, L. I. Xiao-Ting, J. Y. Wang, Y. W. Luo, and N. N. Dong, "Efficacy of quercetin combined with 5-aminosalicylic acid in collaborative treatment of irritable bowel syndrome rats with infections," *Chinese Journal of Nosocomiology*, vol. 27, 2017.

[24] E. H. M. Hassanein, A. M. Sayed, O. E. Hussein, and A. M. Mahmoud, "Coumarins as modulators of the keap1/

nrf2/ARE signaling pathway," *Oxidative Medicine and Cellular Longevity*, vol. 2020, Article ID 1675957, 25 pages, 2020.

[25] J. Kreiner, E. Pang, G. B. Lenon, and A. W. H. Yang, "Saposhnikoviae divaricata: a phytochemical, pharmacological, and pharmacokinetic review," *Chinese Journal of Natural Medicines*, vol. 15, no. 4, pp. 255–264, 2017.

[26] X.-Q. Chu, J. Wang, G.-X. Chen, G.-Q. Zhang, and C. DeYong, "Overexpression of microRNA-495 improves the intestinal mucosal barrier function by targeting STAT3 via inhibition of the JAK/STAT3 signaling pathway in a mouse Mmodel of ulcerative colitis," *Pathology Research and Practice*, vol. 214, no. 1, pp. 151–162, 2018.

[27] S. Sun, W. Liu, and Y. Li, "CADM1 enhances intestinal barrier function in a rat model of mild inflammatory bowel disease by inhibiting the STAT3 signaling pathway," *Journal of Bioenergetics and Biomembranes*, vol. 52, pp. 343–354, 2020.

[28] X. Tang, H. Liu, S. Yang, Z. Li, J. Zhong, and R. Fang, "Epidermal growth factor and intestinal barrier function," *Mediators of Inflammation*, vol. 2016, Article ID 1927348, 9 pages, 2016.

[29] A. Shibuya, K. Onda, H. Kawahara et al., "Sofalcone, a gastric mucosa protective agent, increases vascular endothelial growth factor via the Nrf2-heme-oxygenase-1 dependent pathway in gastric epithelial cells," *Biochemical and Biophysical Research Communications*, vol. 398, no. 3, pp. 581–584, 2010.

[30] Y.-T. Cheng, S.-L. Wu, C.-Y. Ho, S.-M. Huang, C.-L. Cheng, and G.-C. Yen, "Beneficial effects of camellia oil (camellia oleifera Abel.) on ketoprofen-induced gastrointestinal mucosal damage through upregulation of HO-1 and VEGF," *Journal of Agricultural and Food Chemistry*, vol. 62, no. 3, pp. 642–650, 2014.

[31] F. ShiBin, L. Cheng, H. MengChu, G. Xue'er, W. Xichun, and W. JinJie, "Effect of supplementary Sijunzi decoction on the small intestinal tight junction proteins expression and ERK/MAPK pathway in spleen deficiency canines," *Journal of Yunnan Agricultural University*, vol. 34, no. 6, pp. 971–979, 2019.

[32] S. Banskota, J.-E. Ghia, and W. I. Khan, "Serotonin in the gut: blessing or a curse," *Biochimie*, vol. 161, pp. 56–64, 2019.

[33] Y. Chen, F. Chu, J. Lin et al., "The mechanisms of action of WeiChang'An pill (WCAP) treat diarrhoea-predominant irritable bowel syndrome (IBS-D) using network pharmacology approach and in vivo studies," *Journal of Ethnopharmacology*, vol. 275, Article ID 114119, 2021.

[34] Y. Ma, X. Huang, Y. Chen, J. Fang, F. Pan, and T. Zhang, "PKA dependent cAMP signaling mediated SP regulation of visceral sensitivity and shuganjianpi decoction prevention of irritable bowel syndrome," *Liaoning Journal of Traditional Chinese Medicine*, vol. 44, no. 1, pp. 180–183, 2017.

[35] L. Chunhua, "Progress in study on ion channel and pathogenesis of irritable bowel syndrome," *Chinese Journal of Gastroenterology*, vol. 24, pp. 501–504, 2019.

[36] F. Marger, A. Gelot, A. Alloui et al., "T-type calcium channels contribute to colonic hypersensitivity in a rat model of irritable bowel syndrome," *Proceedings of the National Academy of Sciences of the USA*, vol. 108, no. 27, pp. 11268–11273, 2011.

[37] Z. C. Tang Hanlin, L. Sun, and H. Yang, "Therapeutic effects of IEC-derived HIF-1α in mouse colitis and its mechanism," *Immunological Journal*, vol. 35, pp. 219–224, 2019.

Hindawi
Evidence-Based Complementary and Alternative Medicine
Volume 2022, Article ID 2200662, 9 pages
https://doi.org/10.1155/2022/2200662

Research Article

The Traditional Chinese Medicine Hua Tuo Zai Zao Wan Alleviates Atherosclerosis by Deactivation of Inflammatory Macrophages

Zhihua Yu,[1] Xuanlu Zheng,[2] Chenghui Wang,[2] Chuan Chen,[1] Na Ning,[3] Danting Peng,[3] Te Liu ,[1] and Weidong Pan [2]

[1]*Shanghai Geriatric Institute of Chinese Medicine, Shanghai University of Traditional Chinese Medicine, Shanghai 200031, China*
[2]*Department of Neurology, Shuguang Hospital Affiliated to Shanghai University of Traditional Chinese Medicine, Shanghai 200031, China*
[3]*Guangzhou Baiyunshan Qixing Pharmaceutical Co.,Ltd, Guangzhou 510530, China*

Correspondence should be addressed to Te Liu; liute1979@126.com and Weidong Pan; panwd@medmail.com.cn

Received 18 February 2022; Accepted 8 March 2022; Published 28 March 2022

Academic Editor: Xiang Liu

Introduction. Positive effects have been observed when the traditional Chinese medicine Hua Tuo Zai Zao Wan (HTZZW) has been used for the treatment of atherosclerosis (AS), although with an unclear mechanism. *Methods*. ApoE-/- C57/BALB mice were used to determine the efficacy of HTZZW by blood lipid biochemical analysis and histopathology H&E staining. qPCR and western blot were used to determine the expression of METTL3/14 and NF-κB. *Results*. High-fat diet-fed ApoE-/- mice that consumed HTZZW exhibited significantly smaller plaque areas and significantly decreased unstable collagen areas in the aortic arch as well as significantly lower blood levels of total cholesterol, triglycerides, high-density lipoprotein cholesterol, and low-density lipoprotein cholesterol compared with the control group. Consumption of HTZZW significantly decreased the proportion of Mφ1 in the peripheral blood. HTZZW not only inhibited the expression of m6A methyltransferases METTL14, METTL3, and overall RNA methylation level, but it also decreased the m6A modification level on specific sites of NF-κB mRNA. *Conclusion*. HTZZW significantly alleviated the progression of AS by regulating the expression of the m6A methyltransferases METTL14 and METTL3 in macrophages, eliminating m6A modifications of NF-κB mRNA, influencing the stability of NF-κB mRNA, and ultimately resulting in the deactivation of inflammatory macrophages.

1. Introduction

Atherosclerosis (AS) is a chronic disease characterized by lipid accumulation, apoptosis and necrosis, smooth muscle cell proliferation, and local inflammation [1–4]. It may serve as a key pathological basis for cardiovascular and cerebrovascular diseases such as coronary heart disease and cerebral stroke [5–8]. The pathogenesis of AS is extremely complex, and previous studies have indicated that inflammation and lipid infiltration are closely related to vascular endothelial cell senescence and dysfunction [2, 3, 6, 9]. Reverse cholesterol transport (RCT) plays a pivotal role in plaque and necrotic core development in AS, while cytokines and chemokines can cause damage to endothelial cells and smooth muscle cells, thereby increasing the number of macrophages (Mφ), which has an atherosclerosis-promoting effect. In addition, macrophages also play a role in the regulation of inflammation, which further promotes the development of AS [10, 11].

Many studies have indicated that Chinese herbal medicine significantly affects AS by delaying its onset and progression [1, 7]. The traditional Chinese medicine (TCM) compound formulation Hua Tuo Zai Zao Wan (HTZZW), which effectively promotes blood circulation and eliminates blood stasis, is used in China for the treatment of stroke sequelae such as hemiplegia, facial paralysis, and dysarthria.

Its main constituents include Chuanxiong (the dry rootstock of *Ligusticum chuanxiong* Hort), Wuzhuyu (the nearly ripe, dried fruit of *Evodia rutaecarpa* (Juss.) Benth), and borneol. Although the use of HTZZW for the abovementioned conditions is well documented, its effect on AS and mechanism of action has not been reported in the current literature.

When methylation of the adenosine base at the nitrogen-6 (N-6) position in RNA occurs, N-6 methyladenosine (m6A) is formed. This modification, which is common in the mRNA of most eukaryotes (ranging from yeast, plants, and fruit flies to mammals) and viruses, plays a key regulatory role in posttranscriptional mRNA regulation and metabolism [12–16]. The m6A methyltransferases METTL14 and METTL3 form the stable m6A methyltransferase complex in a 1 : 1 ratio and perform RNA m6A modifications as a "writer" [5, 17–19], while the fat mass and obesity-associated (FTO) protein acts as an "eraser" to eliminate RNA m6A modifications [15, 17–19]. Therefore, RNA m6A modifications are dynamic and reversible enzymatic reactions [15, 17–19]. Some studies have suggested that RNA m6A modifications can enhance the stability, transcriptional activity, and translational activity of mRNA; promote tumorigenesis and tumor invasion; and increase stem cell reprogramming efficiency [16–18, 20, 21]. However, the changes and mechanism of action of RNA m6A modifications during the development of AS have not yet been elucidated.

Based on the evidence previously described, in the present study, we developed a mouse model of acquired AS by feeding $ApoE^{-/-}$ mice with a high-fat diet. We then treated the mice with HTZZW to test the hypothesis that HTZZW alleviates AS progression by regulating m6A modification levels on NF-κB mRNA, thereby influencing NF-κB mRNA stability and decreasing Mφ activity and inflammatory cytokine release.

2. Materials and Methods

All studies were performed in accordance with the Declaration of Helsinki, the Guidelines for Animal Studies of the University of Shanghai University of Traditional Chinese Medicine, and the National Institutes of Health of China. The committee of animal handling of the University of Shanghai University of Traditional Chinese Medicine also approved the experimental procedures used.

2.1. Animal Grouping and Drug Intervention. Forty male apolipoprotein E knockout ($ApoE^{-/-}$) C57/BALB mice (SPF grade, 6–8 weeks old, body mass of 30 ± 5 g) were purchased from the Shanghai Research Center for Model Organisms (License No. SCXK (Shanghai) 2017-0004). HTZZW (License No. 17195) was purchased from Guangzhou Bai Yun Shan Qi Xing Pharmaceutical Co., Ltd. (Guangzhou, China). The $ApoE^{-/-}$ C57/BALB mice were randomly assigned to four groups with 10 mice each after 1 week of acclimatization with normal feed: the blank control group (normal diet), the saline group (high-fat diet + equivalent volume of saline), the moderate-dose HTZZW group (HTZZW (M); high-fat diet + 8 g/kg HTZZW), and the low-dose HTZZW group (HTZZW (L); high-fat diet + 4 g/kg HTZZW). Drug intervention was performed for 12 weeks. The study was approved by the Ethics Committee at the Shanghai Institute of Geriatrics (SHAGESYDW2017008). All experiments were performed in accordance with China National Science and Technology Commission animal laboratory regulations.

2.2. Hematoxylin and Eosin (H & E) Staining. H & E staining was performed to observe the pathological morphology of aortic tissue obtained from the mice. After fixing the aortic tissue of each mouse in 10% formaldehyde, the aortic arch located 0.5 cm away from the aortic root was removed, dehydrated using the standard procedure, embedded in paraffin, and continuously sectioned starting from the aortic root (5-μm thickness). The sections were stained using H & E to observe the pathological morphology under an optical microscope.

2.3. Masson Staining. Paraffin-embedded sections containing atherosclerotic plaques at the aortic root were sectioned, dewaxed, washed with double-distilled water for 5 min, and stained with hematoxylin for 5–10 min for nuclei staining. The stained sections were then thoroughly washed with water, stained with Masson's ponceau-fuchsin solution for 6–10 min, soaked in 2% aqueous glacial acetic acid for 5 s, differentiated in 1% aqueous phosphomolybdic acid for 3–5 min, directly stained with aniline blue for 5 min, soaked in 0.2% aqueous glacial acetic acid for several seconds, cleared with xylene, sealed, and photographed.

2.4. Fluorescence-Based Reverse Transcription Quantitative PCR (qRT-PCR). Total RNA was extracted from the cells of various control and treatment groups using TRIzol reagent (Invitrogen) in accordance with the manufacturer's instructions. After treatment with DNase I (Sigma-Aldrich), the total RNA was quantified and reverse transcribed into cDNA using the ReverTra Ace-α First Strand cDNA Synthesis Kit (Toyobo). qRT-PCR was performed using a RealPlex4 real-time PCR detection system (Eppendorf) with SyBR Green RealTime PCR Master Mix (Toyobo) as the fluorescent dye for nucleic acid amplification. The qRT-PCR conditions were as follows: 40 amplification cycles of denaturation at 95°C for 15 s, annealing at 58°C for 30 s, and extension at 72°C for 42 s. The relative gene expression levels were determined using the $2^{-\Delta\Delta Ct}$ method, with $\Delta Ct = Ct\_genes - Ct\_18sRNA$ and $\Delta\Delta Ct = \Delta Ct\_all\_groups - \Delta Ct\_blankcontrol\_group$. The mRNA expression levels were normalized using 18s rRNA. The primers used during amplification were as follows: mMettl3-F: 5′-GACTCTG GGCACTTGGAT-3′; mMettl3-R: 5′-GTTGTGCTGGGCT TAGGG-3′; mMettl14-F: 5′-GAACCGTGAAGCGAAGCA-3′; mMettl14-R: 5′-AGCCTGGCCTGATAGTGC-3′; mFto-F: 5′-AGGATGAAAGTGAGGACGAG-3′; mFto-R: 5′-T GGTGAAGAGGGATTGTTA-3′; m18SrRNA-F: 5′-AG

GGGAGAGCGGGTAAGAGA-3′; m18SrRNA-R: 5′-GGACAGGACTAGGCGGAACA-3′.

2.5. Western Blotting. Total protein isolated from the various groups was subjected to denaturing electrophoresis using a sodium dodecyl sulfate-polyacrylamide gel electrophoresis (SDS-PAGE) system with a 12% gel and subsequently transferred to a polyvinylidene fluoride (PVDF) membrane (Millipore). After blocking and washing, the membrane was incubated with the primary antibody at 37°C for 45 min. The membrane was then thoroughly washed and incubated with the secondary antibody at 37°C for 45 min. After washing four times with Tris-buffered saline containing Tween-20 (TBST) for 14 min each time at room temperature, the membrane was treated with an enhanced chemiluminescence (ECL) reagent (Pierce Biotechnology) and exposed (Sigma-Aldrich).

2.6. Immunofluorescence Staining. Five mice were randomly selected from each group. From each mouse, a specimen containing plaques at the aortic root was resected, dehydrated, cleared, embedded in paraffin, sectioned, dewaxed, and rehydrated. After treatment with citrate buffer in a boiling water bath for 10 min for antigen retrieval, the specimen was cooled to room temperature, subjected to the same treatment again, and again cooled to room temperature. Blocking was performed at room temperature for 2 h using a 5% bovine serum albumin (BSA) blocking solution. The corresponding goat anti-rabbit polyclonal antibody was diluted to 1 : 500, and blocking was performed for 1 h. After overnight shaking at 4°C, the specimen was washed with phosphate-buffered saline (PBS) for 15 min. Fluorescein isothiocyanate (FITC)-conjugated anti-mouse IgG monoclonal secondary antibody was diluted in a blocking solution at a 1 : 500 ratio. Sections were incubated with a secondary antibody at room temperature for 1 h. After washing with PBS for 45 min, the specimen was mounted using an antifade medium containing 4ingperature for 1 h. The dary antibody was diluted in a blocking solution at the aortic root resected, dehydrated, cleared, and embedded in pa.

2.7. Blood Lipid Testing. Peripheral blood was collected from the mice. Blood samples were incubated at 4°C for 4 h and centrifuged at 10,000 rpm for 10 min at 4°C. The supernatant of each centrifuged sample was collected, and total cholesterol (TC), triglycerides (TG), high-density lipoprotein cholesterol (HDL-C), and low-density lipoprotein cholesterol (LDL-C) in serum were tested in accordance with the instructions provided with the test kit.

2.8. Dot-Blotting. Different doses of genomic DNA from each group were spotted on the Hybond-N+ membrane, and then the spotted DNA was cross-linked to the membrane by the UV crosslinker. The membrane was blocked in 5% BSA and subsequently incubated with anti-5hmC antibody (CST) and horseradish peroxidase (HRP)-conjugated anti-mouse secondary antibody (CST), and finally developed with ECL reagents and exposed to imaging film.

2.9. RNA Immunoprecipitation (RIP)-PCR. RIP experiments were performed using the Magna RIP RNA-Binding Protein Immunoprecipitation Kit (Millipore, Bedford, MA). All the steps of RIP were performed as previously described [22, 23]. In brief, cells from all groups were lysed (500 μL per plate) in a modified cell lysis buffer used for western blotting and IP (20 mM Tris, pH 7.5, 150 mM NaCl, 1% Triton X-100, 1 mM EDTA, sodium pyrophosphate, β-glycerophosphate, Na_3VO_4, and leupeptin) (Beyotime Institute of Biotechnology). After lysis, each sample was centrifuged to clear the insoluble debris and was then preincubated with 20 μg of protein A agarose beads (Beyotime Institute of Biotechnology) by rocking for 30 min at 4°C, followed by centrifugation and transfer to a fresh 1.5 mL tube. The mouse anti-human Ago2 monoclonal antibody (1 : 100; Santa Cruz Biotechnology, CA, USA) was added, and the solution was incubated for 90 min before the readdition of 20 μg of protein A agarose beads to capture the immune complexes. The agarose beads were then washed three times with ice-cold homogenization buffer. The specific primers were designed as follows: NF-κB-m6A-F: 5′-GCTCCTAAGGTGCTGACA-3′; NF-κB-m6A-R: 5′-TCCGAAAGCGAGATAAAG-3′.

2.10. Statistical Analysis. Each experiment was performed at least three times, and the data are shown as the mean-standard error where applicable. Differences were evaluated with a Student's t-test. A P value of less than 0.05 was considered statistically significant.

3. Results

3.1. HTZZW Effectively Alleviates Pathological Manifestations of as in ApoE$^{-/-}$ Mice. H & E staining showed that the aortic roots of the saline group exhibited obvious lipid streak formation and foam cell aggregation, as well as large areas of lipid plaques, with a certain number of plaques being vulnerable, indicating the existence of the atheroma formation stage (Figure 1). However, compared with the saline group, there was a significantly smaller area of AS plaques and significantly reduced lipid deposition for the HTZZW (M) group (Figure 1). The results of Masson staining indicated that the proportion of collagen fibers in plaques at the aortic root of the saline group was significantly increased, while the proportion of unstable collagen fibers in plaques at the aortic root of the HTZZW (M) group was significantly decreased (Figure 1). In addition, the results of blood lipid tests performed on peripheral blood samples indicated that the serum TG, TC, LDL-C, and HDL-C levels of the HTZZW (M) group were significantly decreased compared to those in the blank control group (Figure 1). This indicated that a moderate dose of HTZZW significantly decreased vascular lipid deposition and peripheral blood lipid levels in mice with AS.

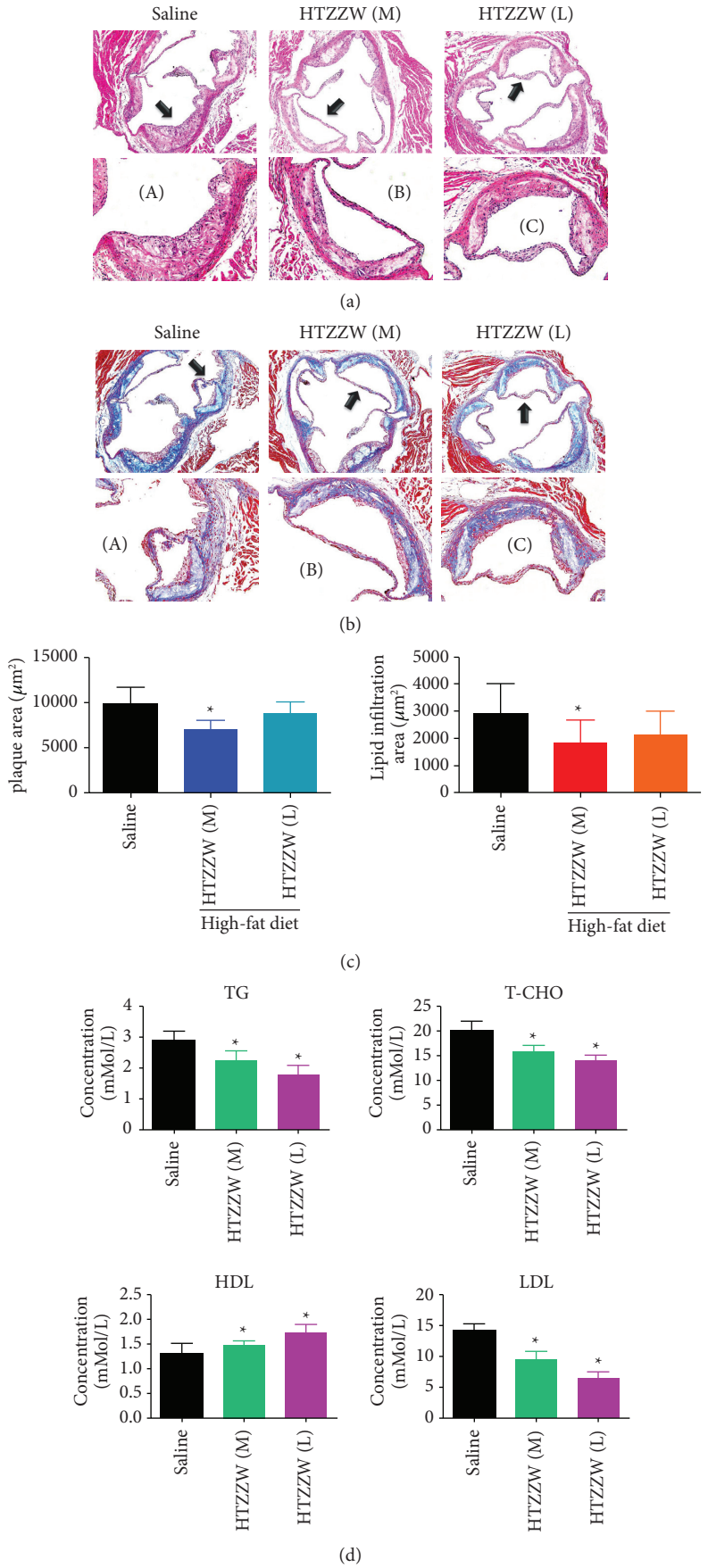

Figure 1: HTZZW effectively alleviated the pathological manifestations of AS in ApoE$^{-/-}$mice. (a) H & E staining of the aortic roots of mice, magnification 100x. (a–c) High-power magnification of the regions indicated by arrows, magnification = 200x. (b) Masson staining of the aortic arch of mice, magnification 100x. (a–c) High-power magnification of the regions indicated by arrows, magnification 200x. (c) Statistical results of the plaque area and lipid infiltration area of the aortic arch in mice. $^{*}P < 0.05$ vs. saline group; t-test; $n = 8$. (d) ELISA results of blood lipid testing. $^{*}P < 0.05$ vs. saline group; t-test; $n = 8$.

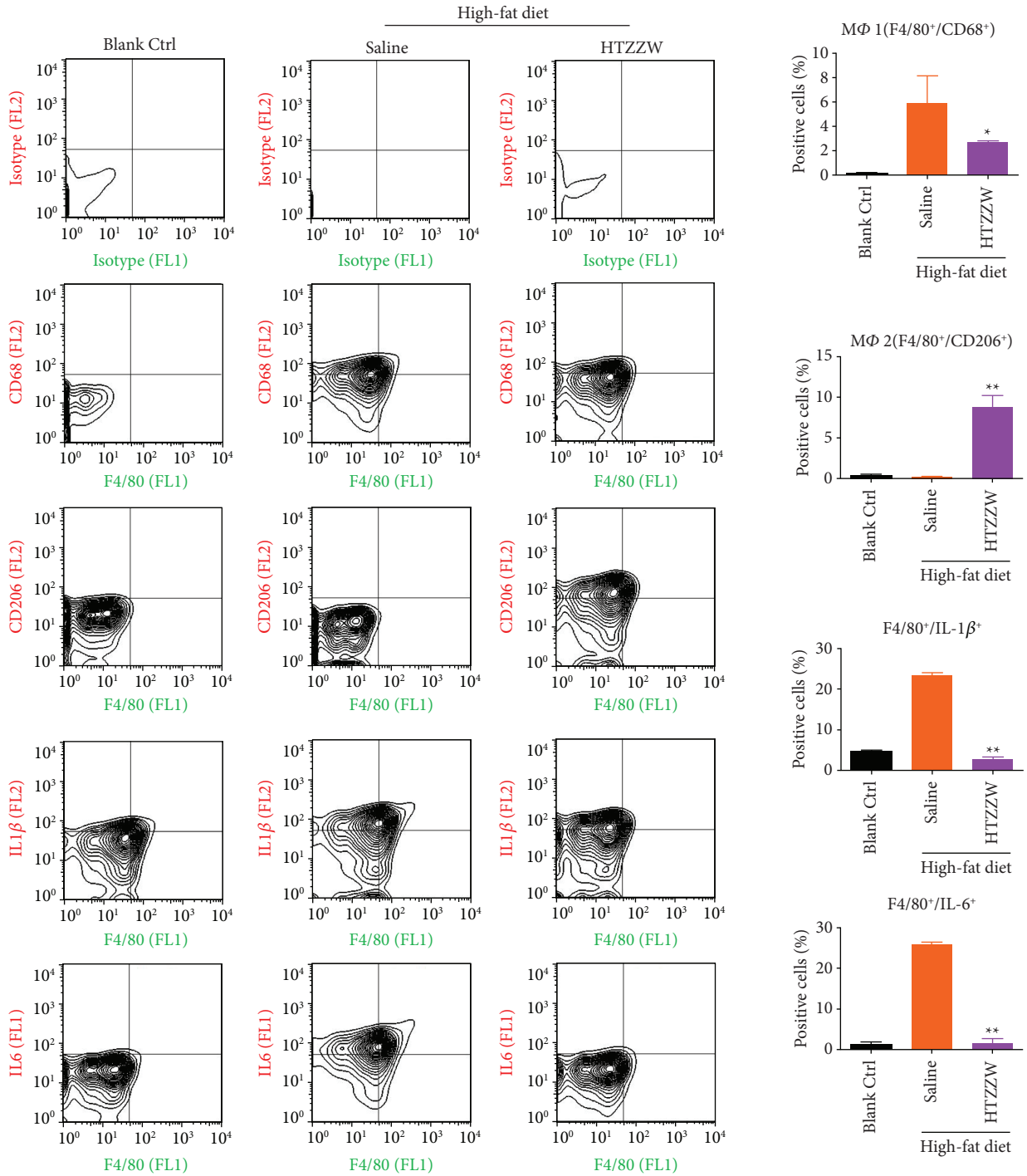

Figure 2: Flow cytometry results. HTZZW inhibited Mφ1 activity and inflammatory cytokine release. $^{**}P < 0.01$ vs. saline group; $^{*}P < 0.05$ vs. saline group; t-test; $n = 8$.

3.2. HTZZW Inhibits Mφ1 Activity and Inflammatory Cytokine Release. Flow cytometry analyses indicated that the proportions of F4/80+/CD68+ (Mφ1) and F4/80+/CD206+ (Mφ2) cells in the peripheral blood of mice from the blank control group were extremely low, while the proportions of the two aforementioned types of cells were significantly increased in the saline group (Figure 2). However, after treatment of the AS mouse model using a moderate dose of HTZZW, the proportion of Mφ1 significantly decreased, while the proportion of Mφ2 significantly increased (Figure 2), indicating that HTZZW can significantly stimulate the conversion of Mφ1 to Mφ2 in AS mice. In addition, the proportions of F4/80+/IL − 1β+ and F4/80+/IL − 6+ significantly decreased after the treatment of AS mice with a

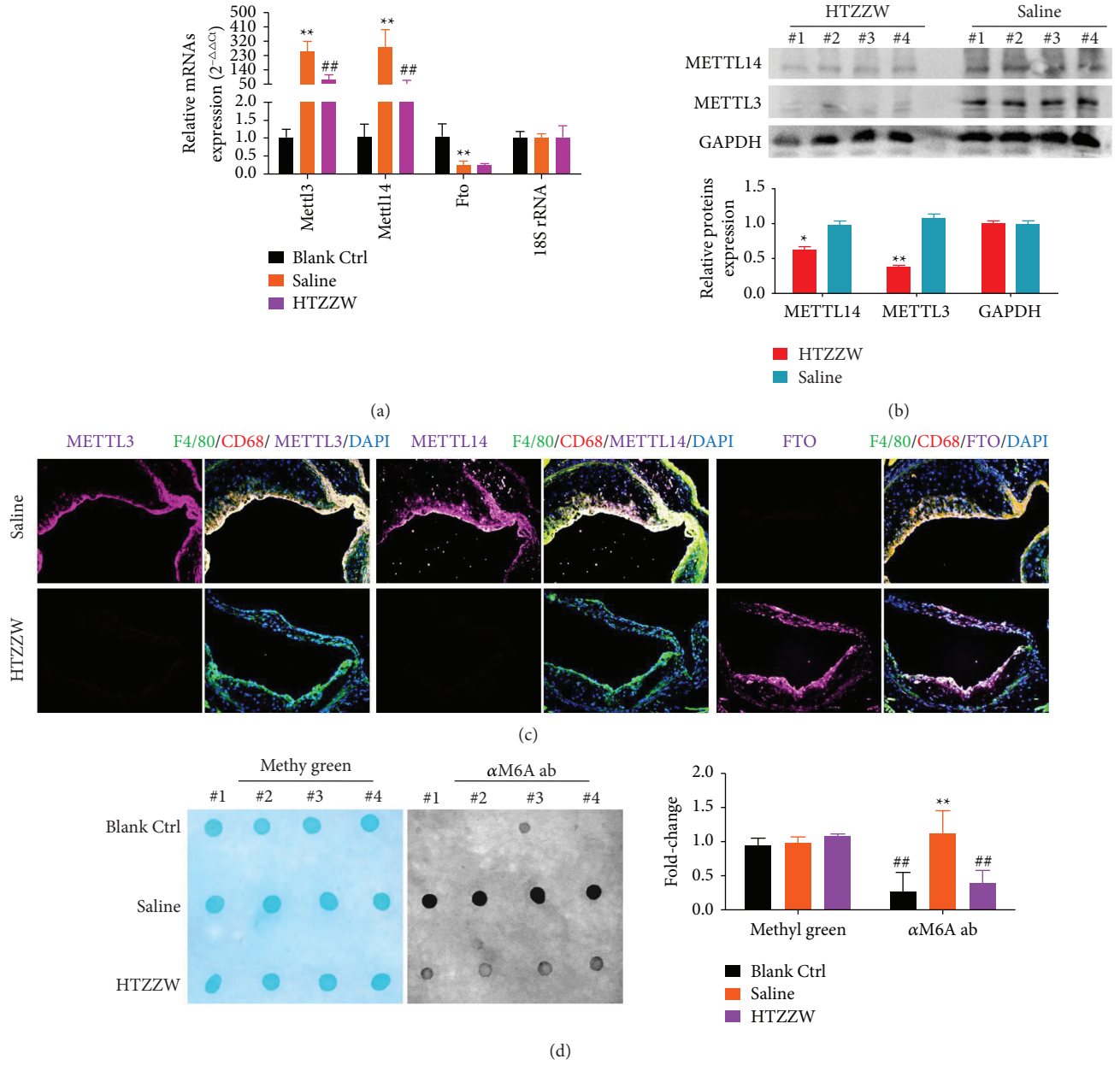

FIGURE 3: HTZZW influenced the expression of m6A methyltransferases and the overall RNA m6A level in the Mφ1 of AS mice. (a) qPCR results of m6A methyltransferase expression levels in mRNA. $^{**}P < 0.01$ vs. blank ctrl group; $^{\#\#}P < 0.01$ vs. saline group; t-test; $n = 8$. (b) Western blotting results of RNA m6A methyltransferase expression levels. (c) Results of immunofluorescence staining of the aortic arch of mice. (d) Dot blot results of the overall RNA m6A level in mice. $^{**}P < 0.01$ vs. blank ctrl group; $^{\#\#}P < 0.01$ vs. saline group; t-test; $n = 4$.

moderate dose of HTZZW (Figure 2). These results suggest that HTZZW can significantly decrease macrophage activity and inflammatory cytokine release in AS mice.

3.3. HTZZW Influences the Overall RNA m6A Level in Mφ1 Cells of as Mice. Changes in expression levels of enzymes that control RNA m6A modifications in the various groups were measured. qPCR and western blotting indicated that Mettle3 and Mettle14 expression levels significantly increased, while the Fto expression level significantly decreased in the Mφ1 cells of mice from the saline group (Figure 3). In contrast, the Mφ1 of the HTZZW (M) group showed a significant decrease in the Mettle3 and Mettle14 expression levels and a significant increase in the Fto expression level (Figure 3), which was opposite to the results of the saline group. The results of immunofluorescence staining were also consistent with the results previously described (Figure 3). In addition, the results of dot blotting indicated that the overall RNA m6A level in the Mφ1 of the HTZZW (M) group was significantly lower than that of the Saline group (Figure 3). These results demonstrated that HTZZW decreased the overall RNA m6A level in the Mφ1 of AS mice by inhibiting the expression of RNA m6A methyltransferases.

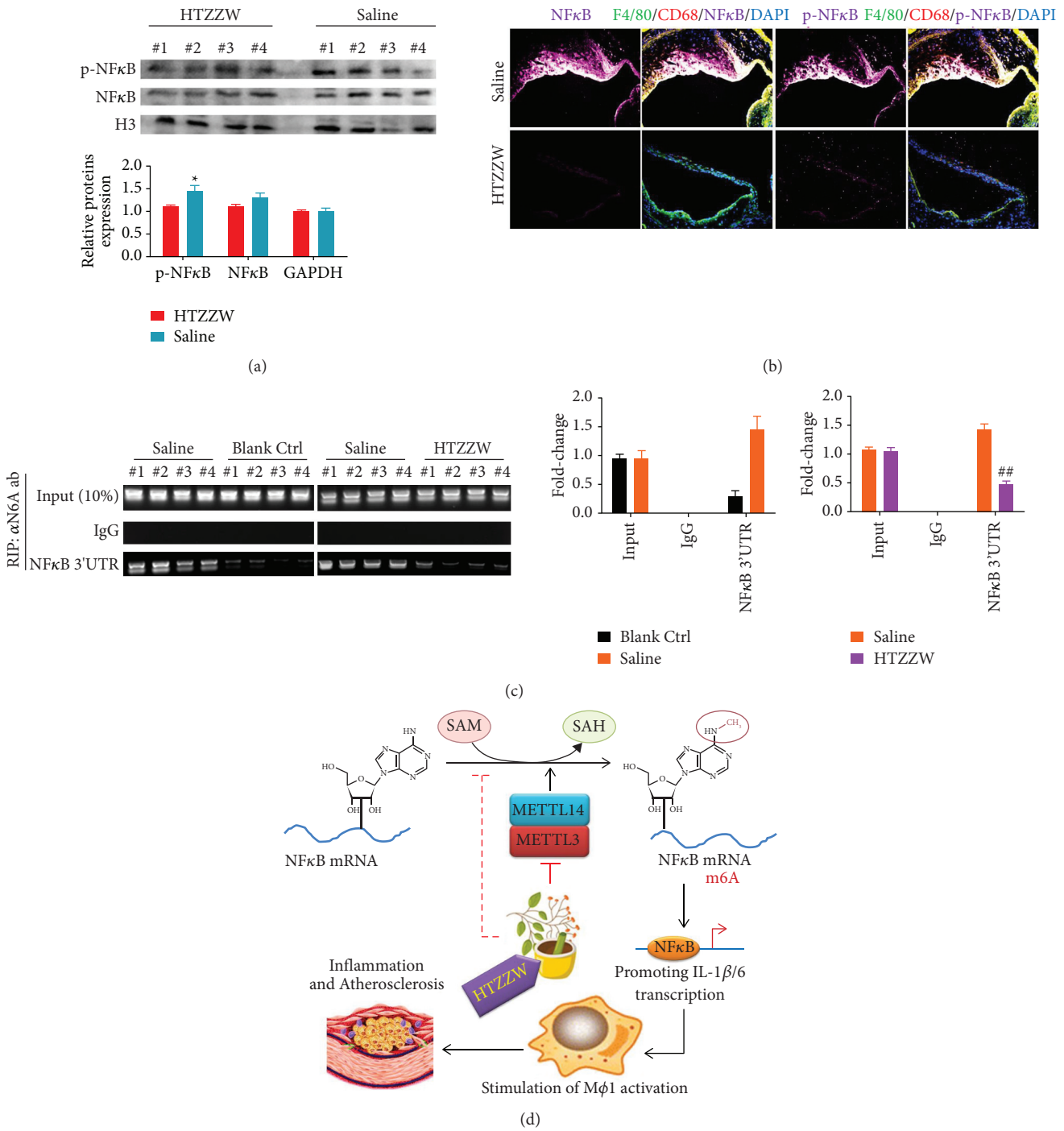

Figure 4: HTZZW inhibited NF-κB RNA m6A modifications and induced a decrease in the expression level of NF-κB RNA. (a) Western blotting results of the expression levels of NF-κB and phosphorylated NF-κB (p-NF-κB) in cell nuclei. $^{**}P < 0.01$ vs. saline group; *t*-test; $n = 4$. (b) Results of immunofluorescence staining of the aortic arch of mice. (c) RIP-PCR results. $^{**}P < 0.01$ vs. blank ctrl group; $^{\#\#}P < 0.01$ vs. saline group; *t*-test; $n = 4$. (d) The mechanism by which HTZZW alleviates inflammation and AS through the inhibition of NF-κB RNA m6A modifications in Mφ1.

3.4. HTZZW Inhibits NF-κB RNA m6A Modifications and Results in Decreased NF-κB RNA Expression. Western blotting results indicated that the protein levels of total NF-κB and phosphorylated NF-κB (p-NF-κB) in Mφ1 nuclei of the saline group were significantly higher than those of the blank control group (Figure 4). However, the protein levels of total NF-κB and p-NF-κB in Mφ1 nuclei of the HTZZW (M) group were significantly decreased (Figure 4). The results of immunofluorescence staining were consistent with the western blotting results (Figure 4). These results revealed that HTZZW inhibited the activation of NF-κB in Mφ1. Subsequently, the RIP-PCR results showed that complexes

cross-linked to the anti-m6A antibody (α m6A ab) in the Mφ1 of the saline group could be amplified to obtain specific products of the 3′ untranslated region (UTR) of NF-κB mRNA (Figure 4). However, amplification of specific NF-κB mRNA 3′-UTR products was not observed for the complexes crossed-linked to α m6A ab in the Mφ1 of the HTZZW (M) group (Figure 4). These results suggested that HTZZW inhibited m6A modifications at specific sites in the 3′-UTR of NF-κB mRNA, which resulted in decreased stability and expression of NF-κB mRNA.

4. Discussion

Inflammation and abnormal lipid metabolism are important triggers of AS [2, 8, 24, 25], and macrophages are the key cells in AS plaques that are involved in lipid metabolism and inflammation [2, 8, 22, 23]. In a previous study, we showed that induction of the conversion of high cholesterol-related Mφ1 to Mφ2 significantly reduced inflammatory cytokine levels and foam cell formation in AS plaques [22]. This indicates that macrophages possessing an inflammatory phenotype aggravate the progression of AS. Further research revealed that the weakening of the polarity of Mφ1 and alleviation of the disease progression of AS could be achieved by promoting the expression of transporters involved in reverse transcription (ATP-binding cassette transporter member 1 and ATP-binding cassette subfamily G member 1) and inhibiting the phosphorylation and activation of NF-κB [22, 24, 25], which suggests that NF-κB may be a potential target for the treatment of AS.

NF-κB, which is pivotal in the regulation of cell responses, can be found in almost all animal cells and participates in cell responses to a variety of external stimuli, including cytokines, radiation, heavy metals, and viruses [22, 24–27]. It also plays a key role in the inflammatory and immune responses of cells [22, 24–27]. NF-κB acts as a first responder to harmful cellular stimuli. There are many known activators of the NF-κB pathway, including tumor necrosis factor-alpha (TNF-α), interleukin (IL)-1β, IL-2, IL-6, IL-8, and IL-12, induced nitric oxide synthase (iNOS), cyclooxygenase-2 (COX-2), chemokines, adhesion molecules, and colony-stimulating factors [22, 24–27].

Continued NF-κB activation indirectly causes the polarization of Mφ1 [22]. Many studies have investigated the activation and stability of NF-κB at the transcriptional and translational levels using cells, including demethylation modifications in promoter regions and phosphorylation/acetylation modifications at certain sites of the NF-κB protein [22, 24–27]. However, there are relatively few reports of methylation modifications in the NF-κB mRNA.

RNAm6A refers to the methylation of the adenosine base at the nitrogen-6 (N-6) position in RNA. This modification, which is common in the mRNA of most eukaryotes (ranging from yeast, plants, and fruit flies to mammals) and viruses, plays a key role in posttranscriptional mRNA regulation and metabolism [12–16]. Meyer et al. and Dominissini et al. employed a method that combined m6A-specific methylated RNA immunoprecipitation with high-throughput sequencing to analyze human and mouse genes for the determination of transcriptome-wide RNA m6A distributions. RNA m6A was mainly distributed near the 3′-UTR of mRNAs and the stop codons of coding sequences (CDS). Furthermore, the distributions of m6A in human and mouse genes were found to be highly conserved. Other studies reported that RNA m6A enhanced mRNA stability [12, 13, 17, 20], and further research showed that m6A peaks were mainly enriched near the stop codons, 3′-UTRs, and long exons of mRNA, with the major conserved sequences being G (m6A) C (70%) and A (m6A) C (30%) [12, 14, 28].

Based on the results previously described, we measured the m6A modifications at specific regions in the 3′-UTR of NF-κB mRNA and found that the m6A level at specific regions in the 3′-UTR of NF-κB mRNA of macrophages of the wild-type (WT) group was extremely low, while the corresponding level was significantly increased in high-fat diet-fed ApoE$^{-/-}$ mice. We deduced that high methylation modification levels at the specific sites in NF-κB mRNA resulted in its stable translation and expression. However, the TCM compound formulation HTZZW eliminated these m6A modifications, with the potential mechanism being the inhibition of the expression of the m6A methyltransferases METTL14 and METTL3 in macrophages. In addition, our experimental results also demonstrated that HTZZW significantly inhibited Mφ1 polarization and significantly reduced the activity of inflammatory cytokine release, plaque area, and unstable collagen accumulation in the aortic arch as well as blood lipid levels in AS mice.

5. Conclusion

From the various aspects of phenotype, pathology, and epigenetics, the present study showed that the TCM compound formulation HTZZW significantly alleviated the progression of AS. Additionally, HTZZW exerted its effect via epigenetic regulation. It could regulate the expression of the m6A methyltransferases METTL14 and METTL3 in macrophages, thereby eliminating m6A modifications at specific regions in the 3′-UTR of NF-κB mRNA, which influences the stability of NF-κB mRNA and ultimately results in the deactivation of inflammatory macrophages.

Data Availability

The data are available from the corresponding author on reasonable request.

Disclosure

Zhihua Yu and Xuanlu Zheng are co-first authors.

Conflicts of Interest

The authors declare that there are no conflicts of interest.

Authors' Contributions

Dr. Zhihua Yu and Xuanlu Zheng participated in the design of the research, performed most of the experiments, and participated in part of the manuscript writing. Dr. Chenghui

Wang, Dr. Chuan Chen, and Na Ning participated in parts of the experimental design and carried out parts of the experiments, and also participated in the manuscript writing. Dr. Danting Peng participated in parts of the experimental design and data collection. Professor Te Liu and Professor Weidong Pan designed the whole experiment, participated in data collection, discussed the experimental results, and completed the manuscript.

Acknowledgments

This work was supported by grants from the National Natural Science Foundation of China (81973899), the Development Fund for Shanghai Talents (2017054), and the Fund for Xinglin Talents of Shanghai University of TCM (201707081).

References

[1] Q. Liu, J. Li, A. Hartstone-Rose et al., "Chinese herbal compounds for the prevention and treatment of atherosclerosis: experimental evidence and mechanisms," *Evidence-Based Complementary and Alternative Medicine*, vol. 2015, Article ID 752610, 15 pages, 2015.

[2] G. F. P. Bories and N. Leitinger, "Macrophage metabolism in atherosclerosis," *FEBS Letters*, vol. 591, 2017.

[3] B. W. Wong, E. Marsch, L. Treps, M. Baes, and P. Carmeliet, "Endothelial cell metabolism in health and disease: impact of hypoxia," *The EMBO Journal*, vol. 36, no. 15, pp. 2187–2203, 2017.

[4] Y. Zhang, P. Ren, Q. Kang et al., "Effect of tetramethylpyrazine on atherosclerosis and SCAP/SREBP-1c signaling pathway in ApoE(-/-) mice fed with a high-fat diet," *Evidence-Based Complementary and Alternative Medicine*, vol. 2017, Article ID 3121989, 8 pages, 2017.

[5] T. A. Seimon, M. J. Nadolski, X. Liao et al., "Atherogenic lipids and lipoproteins trigger CD36-TLR2-dependent apoptosis in macrophages undergoing endoplasmic reticulum stress," *Cell Metabolism*, vol. 12, no. 5, pp. 467–482, 2010.

[6] H. Xu, D. Shi, and K. Chen, "Atherosclerosis: an integrative east-west medicine perspective," *Evidence-Based Complementary and Alternative Medicine*, vol. 2012, Article ID 148413, 4 pages, 2012.

[7] D. Z. Shen, S. L. Xin, C. Chen, and T. Liu, "Effect of atorvastatin on expression of TLR4 and NF-kappaB p65 in atherosclerotic rabbits," *Asian Pacific Journal of Tropical Medicine*, vol. 6, no. 6, pp. 493–496, 2013.

[8] Z. Chen and H. Xu, "Anti-inflammatory and immunomodulatory mechanism of tanshinone IIA for atherosclerosis," *Evidence-Based Complementary and Alternative Medicine*, vol. 2014, Article ID 267976, 6 pages, 2014.

[9] W. Wong, "Protected from atherosclerosis by TFEB," *Science*, vol. 355, no. 6324, p. 490.

[10] E. Favari, A. Chroni, U. J. Tietge, I. Zanotti, J. C. Escola-Gil, and F. Bernini, "Cholesterol efflux and reverse cholesterol transport," *Handbook of Experimental Pharmacology*, vol. 224, pp. 181–206, 2015.

[11] A. Rohatgi, A. Khera, J. D. Berry et al., "HDL cholesterol efflux capacity and incident cardiovascular events," *Northern Engineer*, vol. 371, no. 25, pp. 2383–2393, 2014.

[12] K. D. Meyer, Y. Saletore, P. Zumbo, O. Elemento, C. E. Mason, and S. R. Jaffrey, "Comprehensive analysis of mRNA methylation reveals enrichment in 3′ UTRs and near stop codons," *Cell*, vol. 149, no. 7, pp. 1635–1646, 2012.

[13] D. Dominissini, S. Moshitch-Moshkovitz, S. Schwartz et al., "Topology of the human and mouse m6A RNA methylomes revealed by m6A-seq," *Nature*, vol. 485, no. 7397, pp. 201–206, 2012.

[14] Y. Yue, J. Liu, and C. He, "RNA N6-methyladenosine methylation in post-transcriptional gene expression regulation," *Genes & Development*, vol. 29, no. 13, pp. 1343–1355, 2015.

[15] G. Jia, Y. Fu, X. Zhao et al., "N6-methyladenosine in nuclear RNA is a major substrate of the obesity-associated FTO," *Nature Chemical Biology*, vol. 7, no. 12, pp. 885–887, 2011.

[16] T. Chen, Y. J. Hao, Y. Zhang et al., "m(6)A RNA methylation is regulated by microRNAs and promotes reprogramming to pluripotency," *Cell Stem Cell*, vol. 16, no. 3, pp. 289–301, 2015.

[17] C. Tang, R. Klukovich, H. Peng et al., "ALKBH5-dependent m6A demethylation controls splicing and stability of long 3'-UTR mRNAs in male germ cells," *Proc Natl Acad Sci U S A*, vol. 115, no. 2, pp. E325–E333, 2018.

[18] M. Chen, L. Wei, C. T. Law et al., "RNA N6-methyladenosine methyltransferase-like 3 promotes liver cancer progression through YTHDF2-dependent posttranscriptional silencing of SOCS2," *Hepatology*, vol. 67, no. 6, pp. 2254–2270, 2018.

[19] J. Liu, Y. Yue, D. Han et al., "A METTL3-METTL14 complex mediates mammalian nuclear RNA N6-adenosine methylation," *Nature Chemical Biology*, vol. 10, no. 2, pp. 93–95, 2014.

[20] X. Wang, Z. Lu, A. Gomez et al., "N6-methyladenosine-dependent regulation of messenger RNA stability," *Nature*, vol. 505, no. 7481, pp. 117–120, 2014.

[21] I. Barbieri, K. Tzelepis, L. Pandolfini et al., "Promoter-bound METTL3 maintains myeloid leukaemia by m(6)A-dependent translation control," *Nature*, vol. 552, no. 7683, pp. 126–131, 2017.

[22] F. Dou, J. Chen, H. Cao et al., "Anti-atherosclerotic effects of LXRalpha agonist through induced conversion of M1 macrophage to M2," *American Journal of Translational Research*, vol. 11, no. 6, pp. 3825–3840, 2019.

[23] J. A. VanderBurgh and C. A. Reinhart-King, "The role of age-related intimal remodeling and stiffening in atherosclerosis," *Advances in Pharmacology*, vol. 81, pp. 365–391, 2018.

[24] S. Ghosh and M. Karin, "Missing pieces in the NF-kappaB puzzle," *Cell*, vol. 109, pp. S81–S96, 2002.

[25] J. Napetschnig and H. Wu, "Molecular basis of NF-kappaB signaling," *Annual Review of Biophysics*, vol. 42, pp. 443–468, 2013.

[26] J. Sun, P. Huang, J. Liang et al., "Cooperation of Rel family members in regulating Abeta1-40-mediated pro-inflammatory cytokine secretion by retinal pigment epithelial cells," *Cell Death & Disease*, vol. 8, no. 10, p. e3115, 2017.

[27] Z. Gong, T. Liu, Y. Wan et al., "Decreased c-rel activation contributes to aberrant interleukin-2 expression in CD4(+)T cells of aged rats," *Molecular Immunology*, vol. 61, no. 1, pp. 1–6, 2014.

[28] M. Bartosovic, H. C. Molares, P. Gregorova, D. Hrossova, G. Kudla, and S. Vanacova, "N6-methyladenosine demethylase FTO targets pre-mRNAs and regulates alternative splicing and 3′-end processing," *Nucleic Acids Research*, vol. 45, no. 19, pp. 11356–11370, 2017.

Hindawi
Evidence-Based Complementary and Alternative Medicine
Volume 2022, Article ID 4787643, 20 pages
https://doi.org/10.1155/2022/4787643

Review Article

Activities and Molecular Mechanisms of Diterpenes, Diterpenoids, and Their Derivatives in Rheumatoid Arthritis

Muhammad Torequl Islam,[1] Cristina Quispe,[2] Jesús Herrera-Bravo,[3,4] Md. Mizanur Rahaman,[1] Rajib Hossain,[1] Chandan Sarkar,[1] Md Abdur Raihan,[1] Md. Mashrur Chowdhury,[5] Shaikh Jamal Uddin,[6] Jamil A. Shilpi,[3] João Marcelo de Castro e Sousa,[7] Ana Amélia de Carvalho Melo-Cavalcante,[7] Mohammad S. Mubarak,[8] Javad Sharifi-Rad,[9] and Daniela Calina[10]

[1]*Department of Pharmacy, Life Science Faculty, Bangabandhu Sheikh Mujibur Rahman Science and Technology University, Gopalganj 8100, Bangladesh*
[2]*Facultad de Ciencias de la Salud, Universidad Arturo Prat, Avda. Arturo Prat 2120, Iquique 1110939, Chile*
[3]*Departamento de Ciencias Básicas, Facultad de Ciencias, Universidad Santo Tomas, Santiago, Chile*
[4]*Center of Molecular Biology and Pharmacogenetics, Scientific and Technological Bioresource Nucleus, Universidad de La Frontera, Temuco 4811230, Chile*
[5]*Department of Pharmacy, Southern University Bangladesh, Arefin Nagar 4210, Chattagram, Bangladesh*
[6]*Pharmacy Discipline, Khulna University, Khulna 9208, Bangladesh*
[7]*Postgraduate Program in Pharmaceutical Sciences, Federal University of Piaui, Teresina 64049-550, Brazil*
[8]*Department of Chemistry, The University of Jordan, Amman 11942, Jordan*
[9]*Facultad de Medicina, Universidad del Azuay, Cuenca, Ecuador*
[10]*Department of Clinical Pharmacy, University of Medicine and Pharmacy of Craiova, 200349 Craiova, Romania*

Correspondence should be addressed to Javad Sharifi-Rad; javad.sharifirad@gmail.com and Daniela Calina; calinadaniela@gmail.com

Received 11 October 2021; Revised 11 December 2021; Accepted 2 February 2022; Published 25 March 2022

Academic Editor: Yanhong Zhu

Diterpenes and their derivatives have many biological activities, including anti-inflammatory and immunomodulatory effects. To date, several diterpenes, diterpenoids, and their laboratory-derived products have been demonstrated for antiarthritic activities. This study summarizes the literature about diterpenes and their derivatives acting against rheumatoid arthritis (RA) depending on the database reports until 31 August 2021. For this, we have conducted an extensive search in databases such as PubMed, Science Direct, Google Scholar, and Clinicaltrials.gov using specific relevant keywords. The search yielded 2708 published records, among which 48 have been included in this study. The findings offer several potential diterpenes and their derivatives as anti-RA in various test models. Among the diterpenes and their derivatives, andrographolide, triptolide, and tanshinone IIA have been found to exhibit anti-RA activity through diverse pathways. In addition, some important derivatives of triptolide and tanshinone IIA have also been shown to have anti-RA effects. Overall, findings suggest that these substances could reduce arthritis score, downregulate oxidative, proinflammatory, and inflammatory biomarkers, modulate various arthritis pathways, and improve joint destruction and clinical arthritic conditions, signs, symptoms, and physical functions in humans and numerous experimental animals, mainly through cytokine and chemokine as well as several physiological protein interaction pathways. Taken all together, diterpenes, diterpenoids, and their derivatives may be promising tools for RA management.

1. Introduction

Arthritis is a long-term musculoskeletal illness marked by inflammation of the joints. Rheumatoid arthritis (RA) is one of the most common kinds of arthritis [1]. It is a long-term condition marked by inflammatory synovitis. Joint asymmetry and invasive inflammation are common symptoms of RA, which can lead to joint deformity, dysfunction, and even loss of function. Adults in rich countries have a prevalence of 0.5–1.0%, with 5–50 new cases per 100,000 persons each year. Women and the elderly, on the other hand, are the ones who suffer the most [2]. Although the exact origin of RA is unknown, medicinal therapy is a common and effective treatment option for RA patients.

Treatments for RA include nonsteroidal anti-inflammatory medications (NSAIDs), corticosteroids, disease-modifying antirheumatic medicines (DMARDs), and biological response modifiers [3]. All of these anti-RA drugs, unfortunately, have numerous negative effects. NSAIDs may endanger patients' lives by increasing the risk of upper gastrointestinal (GI) haemorrhage, liver, and kidney damage [4, 5]. Furthermore, headaches, cognitive impairments, and allergic reactions are common reasons for patients to stop taking NSAIDs, limiting their usage. Infection, hypersplenism, hypertension, osteoporosis, and fractures are all possible side effects of long-term corticosteroid usage [6, 7]. Vomiting, diarrhea, rashes, low white blood cell (WBC) counts, and impaired liver and renal function are also side effects of DMARDs [8, 9].

Biological therapies with high pharmacological selectivity and fewer side effects provide novel RA treatment alternatives [10]. Regrettably, these are pricey. As a result, many patients may be unable to afford these drugs [11]. As a result, it is critical to seek out treatments that have a positive therapeutic benefit, few side effects, and are affordable. Many ailments are treated according to conventional medical principles. Many major studies on therapeutic items with natural origins have been conducted by modern scientists.

Plants or their derivatives, marine items, and so forth are examples. These natural items have been discovered as a promising treatment option for RA [12]. Aside from that, several conventional pharmaceutical formulae for RA care have been difficult. Two significant features of this method are the use of nutraceuticals and polyherbal approaches [13, 14]. However, when these preparations are used in combination with other drugs, they may cause health problems. As a consequence, researchers devised a novel strategy for extracting active chemicals from some of these things. Terpenes, flavonoids, catechins, quinones, alkaloids, anthocyanins, and anthoxanthins are just a few of the plant-derived phytochemicals that can alter T cell development, inflammatory signaling pathways, and synoviocyte death. As a result, they can be utilized to treat rheumatoid arthritis [15].

Diterpenes are a diverse group of structurally diverse natural chemicals abundant in nature [16, 17]. These are C20 compounds containing four isoprene (C_5H_8) units that may be found in both terrestrial and marine settings in plants, fungi, bacteria, and animals [18, 19]. Several diterpenes are potential pharmaceutical candidates due to their exceptional pharmacological effect [20–23]. Some diterpenes are considered to be the defining traits of a genus, making them taxonomically significant [24].

Natural diterpenoid compounds come in a wide range of chemical forms and contain many medicinal and economically relevant molecules. All diterpenoids are made from the same substrate, (E, E, E)-geranylgeranyl diphosphate, which is then cyclized into one of the multiple scaffolds by a diterpene synthase [25]. Secondary metabolites with 20 carbon atoms result from the condensation of four isoprene units.

Diterpenoids are divided into approximately 45 distinct categories, and they are also present in marine animals, where their skeletons are fascinating [26]. Based on their skeletal nucleus, diterpenes are classified as linear, bicyclic, tricyclic, tetracyclic, pentacyclic, or macrocyclic. They are usually found in nature polyoxygenated, with keto and hydroxyl groups that are commonly esterified by tiny aliphatic or aromatic acids [27].

Diterpenoids have a variety of biological functions, including antioxidant [23, 28], anti-inflammatory [29, 30], and immune-modulatory action [31]. Given the significance, the goal of this study is to outline the effects of diterpenes, diterpenoids, and their derivatives on RA based on current understanding.

2. Review Methodology

A search with the keywords "Diterpene AND Rheumatoid arthritis," "Diterpenoid AND Rheumatoid arthritis," "Diterpene AND Arthritis," "Diterpenoid AND Arthritis," "Diterpene derivative AND Rheumatoid arthritis," and "Diterpene derivative AND Arthritis" was conducted in the PubMed, Science Direct, Google Scholar, and Clinicaltrials.gov databases. A total of 2708 records were found. After screening, among them, this study used 48 published records that are related to its aim.

This study includes only the records of having antiarthritic or anti-RA along with anti-inflammatory activities of the diterpenes, diterpenoids, and their derivatives obtained from various sources (e.g., medicinal plants and marine origins) on various test systems (e.g., humans), laboratory animals (e.g., mice, rats, and rabbits), and their derivatives (e.g., cells, tissues or organs).

Most of the diterpenes, diterpenoids, and their derivatives have antioxidant and anti-inflammatory properties, and for this reason, this study does not include them. Reports on crude extracts or fractions without chemical characteristics having antiarthritic or anti-RA effects were also excluded in this study.

This study mainly focuses on the anti-RA activities of diterpenes, diterpenoids, and their derivatives. However, it will also focus on the antiarthritic effects of these substances based on updated database records (till 31 August 2021).

3. Physiopathology in RA: A Brief Overview

Since cytokines are directly involved in RA pathogenesis, they have been intensively explored and examined as potential RA targets. Cytokines can be classified as pro or anti-

inflammatory cytokines according to their antigen response activities. TNF-α, interleukins (ILs) (e.g., IL-1β, -6, -7, -15, -17, -18, and -23), interferon-gamma (IFN-γ), and granulocyte-macrophage colony-stimulating factor (GM-CSF) have all been found to limit inflammation in the progression of RA. In the synovium, synovial fluid, serum, and peripheral blood of RA patients, these cytokines were detected in high amounts [32–38].

T cell trafficking and proinflammatory cytokines such as TNF-α, IL-1β, IL-6, and MMPs are reduced when IL-7 is blocked, which lowers joint inflammation [39]. The major cause of IL-23-induced synovial inflammation (RORs) is the activation of Janus kinase (JAK)/signal transducer and activator of transcription (STAT), tyrosine kinase 2, NF-κB, and retinoic acid receptor-related orphan receptors [40].

Macrophages can produce a variety of cytokines such as TNF-α, IL-1β, -6, -7, -15, -18, and -23. In this regard, TNF-α may stimulate fibroblast-like synoviocytes (FLS) and synovial cell proliferation through nuclear factor kappa-B (NF-κB) and extracellular regulated protein kinases (ERK)-1/2-E26 transformation-specific (ETS)-1 regulatory pathways [37]. Consequently, several inflammatory mediators such as IL-6 and matrix metalloproteinases (MMP), MMP-1 and MMP-3, are secreted and increase inflammation [41].

Small molecular metabolites such as PGs, lipoxins (LXs), platelet-activating factor (PAF) and leukotrienes (LTs), nitric oxide (NO), and ROS play important roles in the physiopathology of RA [42]. PG expressions such as PGD2, PGE2, PGF2a, PGI2, PGJ2, and TXA2 are aberrant in RA [42]. LXs derived from arachidonic acids, such as LXA4 and LXB4, possess anti-inflammatory properties. LXA4 can reduce memory B cell response in RA patients' synovial tissues by engaging the lipoxin A4 receptor (ALX)/formyl peptide receptor-2 (FPR-2) and, therefore, reduce inflammation [43, 44]. Circulating platelet activation affects leukocyte activity and contributes to inflammation development in RA patients [45]. TNF-α-regulated pathways are known to control PAF, and TNF-α antagonists decrease platelet activation in active RA [46].

Chemokines have a role in the underlying pathophysiology of RA by attracting leukocytes and influencing angiogenesis. Published research indicated that XC chemokines and their receptors (such as XCL1 and XCR1) and CX3C chemokines and their receptors (e.g., CX3CL1 and CX3CR1) are upregulated in RA patients' mononuclear cells (MNCs) and FLS, respectively [47, 48]. Numerous inflammatory chemokines are mostly generated in the joints of RA patients by synovial macrophages and FLS, while CX3CL1 is produced by synovial endothelial cells. The chemokines XC and CX3C are linked to the recruitment of T lymphocytes and synovial fibroblasts. Furthermore, CX3CL1 and XCL1 stimulate the migration of monocytes and subchondral mesenchymal progenitor cells into the RA synovium, respectively [49]. CC chemokines including CCL2–5, CCL7, CCL13, CCL14, CCL16, CCL18–21, and CCL-25 are differentially expressed in RA plasma and synovium [50]. An upregulated CC chemokine CCL5 is significantly correlated with swollen joints, erythrocyte sedimentation rate (ESR), and c-reactive protein (CRP) in RA patients [51]. On the other hand, CXC chemokines, such as CXCL1, CXCL2, CXCL5, CXCL8, CXCR1, and CXCR2, are generally involved in neutrophil chemotaxis [52]. The chemokine CXCL10 promotes effector T cells into the joint [53].

The expression of peroxisome proliferator-activated receptor-gamma (PPARγ or PPARG) in human monocytes/MDMs may be an indication of disease activity and treatment effectiveness in RA. Several studies have shown that key cell types in the joints [54, 55] express PPARγ at both the mRNA and protein levels.

Long noncoding RNAs (lncRNAs) are more than 200 nucleotides in length and are extensively expressed in many organs of the human body. Several researchers have shown that lncRNA could be used to diagnose RA [56, 57].

In RA patients with active synovitis, osteoprotegerin (OPG) expression on macrophage type synovial lining cells and also endothelial cells is low. As a result, addressing OPG expression in RA patients' inflamed joints may be an essential approach for the treatment of RA in humans [58]. The RANKL/OPG pathway is the connecting factor between bone production and bone resorption in the complicated system of bone remodeling. RANKL promotes the activation and differentiation of preosteoclasts and mature osteoclasts by binding to their receptors (RANK).

Certain hormones, growth factors, and cytokines affect the synthesis of RANKL and OPG by osteoblasts in various ways. Thus, the level of proliferation and activity of osteoclasts are determined by the balance of RANKL and OPG. Bone erosions in RA are caused by osteoclastic bone resorption in synovitis sites, in which RANKL expression is also observed [59].

Currently, available anti-RA agents focus on targeting cytokines, chemokines, and various physiological proteins in humans. Adalimumab is an anti-RA medication that prevents TNF and its receptors from binding, thus lowering cytokines (e.g., MMP-1 and MMP-3)-mediated inflammatory mechanisms and cartilage and bone degradation [41]. On the other hand, (5R)-5-hydroxytriptolide can systemically affect the FLS and, in particular, in the process of immune-related processes at 100 nM concentration through a genome-wide microarray assay in RA patients [60]. IL-1 activates the extracellular signal-regulated kinase (ERK), c-Jun N-terminal kinase (JNK), apetala (AP)-1, and NF-B activating pathways, which stimulate MMP production and leukocyte adhesion to RA FLS [61], whereas oridonin (2–10 M for 24–72 h) suppress RA FLS proliferation in RA [62]. In RA FLS, (5R)-5-hydroxytriptolide (50 and 100 nM) reduced proliferation and invasion, as well as cytokine production (MMP-3, IL-1, and -6) [63]. By stimulating the synthesis of MMPs and NF-κB ligand (RANKL) receptors, IL-6 promotes bone resorption and cartilage degradation [64, 65].

NSAIDs work by reducing the enzymatic activity of the cyclooxygenase (COX) enzymes, which are involved in the production of prostaglandins (PGs). NSAIDs inhibit COX-2, which limits PG synthesis at sites of inflammation; however, inhibiting COX-1 in other tissues (e.g., platelets and mucosa) results in classic NSAID side effects such as bleeding and GI ulcers [66]. Summarized scheme of the physiopathology of RA is shown in Figure 1.

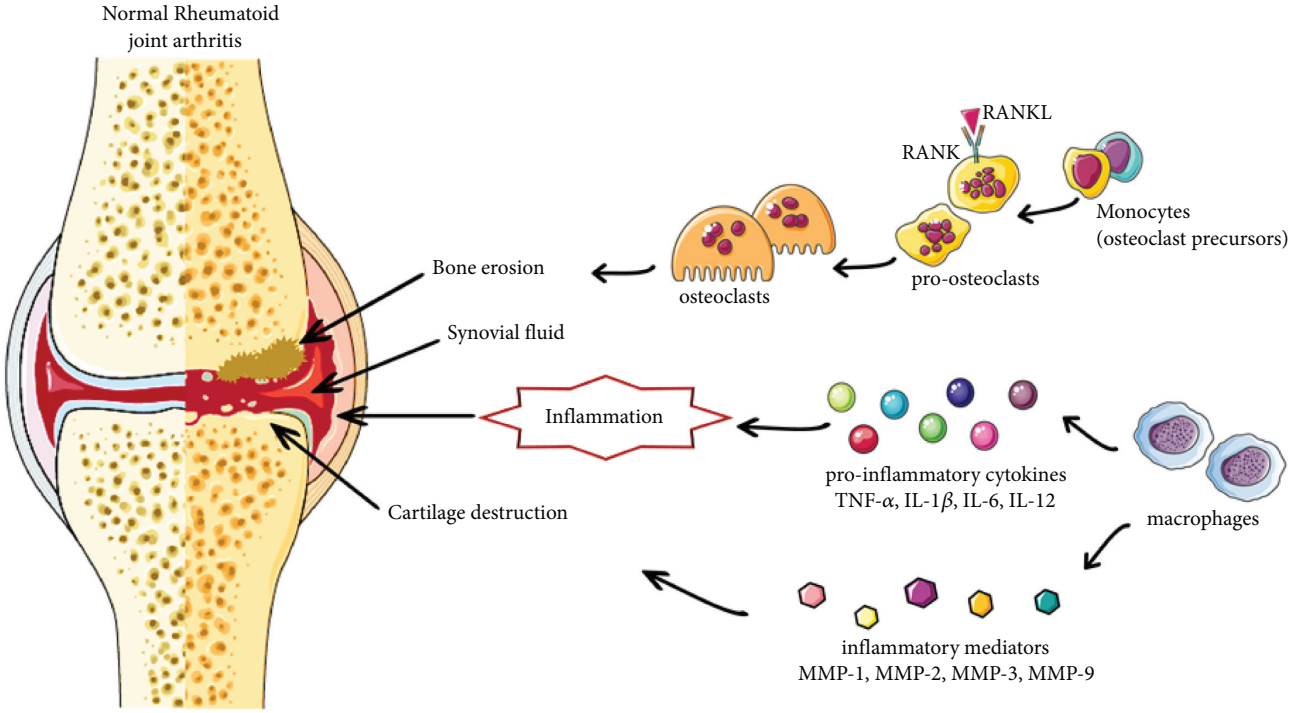

Figure 1: Diagram with the most representative mechanisms of RA pathogenesis.

4. Anti-RA Activities of Diterpenoids: Actions and Molecular Mechanisms

Diterpenoids are the most prominent source of anti-RA agents with potential pharmacological effects.

4.1. Cytokine Targeting Diterpenes and Their Derivatives. A recent study has been claimed that diterpenes isolated from *Caesalpinia minax* (Hance) substantially reduced the change in paw swelling perimeter, arthritic score, and increased bodyweight loss in vivo study [67]. Furthermore, the primary components of the extract were 14 cassane derivatives, such as caesalpins A–H, caesalminaxin A–L, and others, which exhibit a promising effect on the expression of mRNA of the cytokines IL-1β and IL-6 and TNF-α generated by macrophage cells. Moreover, some other diterpenoids (rhodojaponin III, rhodojaponin VI, 2-O-methylrhodojaponin, and 5′-β-D-glucopyranosyloxyjasmonic acid) in *Rhododendron molle* fruits at 0.6 mg/kg dose dramatically reduced RA symptoms in CIA rats [68] by strongly preventing aberrant T and B lymphocyte proliferation and substantially decreased levels of the proinflammatory cytokines IL-1β and IL-6, as well as TNF-α. It has been seen that (5R)-5-hydroxytriptolide can inhibit IL-1β, IL-6, and IL-21 secretion and elevated IL-10 secretion in peripheral blood and synovial fluid of RA patients [69]. Andrographolide in bone marrow macrophages cells and mice inhibited RANKL-stimulated osteoclastogenesis via downregulating NF-κB and ERK/MAPK expression, thereby averting bone loss [70]. Cryptotanshinone at 6 and 18 mg/kg (p.o., for 16 days) in type II collagen-induced arthritis in female Wistar rats, and 5 and 20 μM concentration inhibits the degradation of NF-κB (IκB)-α blocker [71].

Research findings indicated that triptolide (1–4 nM/L) inhibited RANKL-induced NF-κB activation and RANKL and tumor cell-induced osteoclastogenesis [72]. Additionally, a derivative of triptolide (5R)-5-hydroxytriptolide downregulated the expression of (p)-IκB, a major regulator of the RANKL-signaling pathway in RA patients' peripheral blood and synovial fluid [69]. Another study suggested that triptolide (2.5–40 nM) enhanced the inhibitory effects of TREGS on osteoclast differentiation and bone resorption through an increase in the secretion of IL-10 and transforming growth factor-beta 1 (TGF-β1) in mice bone marrow macrophages [73].

Table 1 provides the list of various diterpenes, diterpenoids, and their derivatives, which act in various RA models.

Triptolide in collagen-induced arthritis rats significantly inhibited triggering receptors expressed on myeloid cells (TREM)-1 mRNA and DAP12 mRNA expression and activation of JAK2 and STAT3 in the ankles of test animals and in LPS-stimulated U937 cells [82].

In MH7A cells, retinoic acid-platinum (II) complex (0.25–12 μM) downregulated the activation of the MEK/NF-κB pathway [90], whereas sclareol exhibited anti-RA potential in collagen-induced arthritis in vivo and in vitro models [74]. Furthermore, through inhibiting NF-B translocation and MAPK pathway activation, sclareol inhibited the IL-1β-induced production of TNF-α, MMP-1, and IL-6. Furthermore, sclareol at doses of 5 and 10 mg/kg (i.p.) reduced the number of Th17 cells in mice and improved edema and bone erosion.

In a cytokine-stimulated expression of the major cartilage damaging proteases, MMP-3, MMP-13, and ADAMTS-

Table 1: Diterpenes, diterpenoids, and their derivatives in various rheumatoid arthritis models.

Diterpenes/derivatives	Concentration/dose test system	Results/mechanisms	References
Sclareol	3.125–100/3.125–12.5 μM SW982 human synovial cell lines in vitro	↓TNF-α, ↓IL-6, ↓NF-κB ↓p38, ↓MAPK ↓ERK	[74]
	5–10 mg/kg (i.p., every other day over 21 days) collagen-induced arthritis DBA/1J mice in vivo	↓Swelling in paws, ↓serum anti-CII antibodies ↓IL-1β, ↓IL-6, ↓TNF-α, ↓IL-17 ↓Th17, ↓Th1	
Excavatolide B	10 μM LPS-stimulated RAW 264.7 cells in vitro	↓Multinucleated cell ↓Actin ring formation ↓TRAP, ↓MMP-9, ↓K	[75]
	2.5–5 mg/kg (s.c.) type II collagen-induced arthritis in rats in vivo	↓RA characteristics, ↑histopathological features ↓TRAP-positive multinucleated cells ↓Cathepsin K, ↓MMP-2, ↓MMP-9, ↓CD11b ↓NFATc1, ↓IL-17A, ↓CSF	
Andrographolide	2.5–10 μM bone marrow macrophages (BMM) cells in vitro	↓RANKL ↓NF-κB	[70]
	5–30 mg/kg (i.p., every other day for 8 days) C57/BL6 mice in vivo	↓ERK/MAPK osteoclastogenesis ↓bone loss	
	50 mg/kg/d combined with methotrexate (2 mg/kg/week, i.p. for 35 days) Freund's adjuvant-induced arthritis in Wistar rats in vivo	↑Methotrexate effect hepatoprotective ↓TNF-α, ↓IL-6, ↓IL-1β	[76]
	25 μM LPS-stimulated neutrophils in vitro	↑Apoptosis ↓TRAPs	[77]
	25–50 mg/kg (i.p., for 37 days) adjuvant-induced arthritis C57BL/6 mice in vivo	↓Neutrophil infiltration ↓NETs in the ankle joints ↓Systemic inflammation	

Table 1: Continued.

Diterpenes/derivatives	Concentration/dose test system	Results/mechanisms	References
Triptolide	0.1 mg/kg (p.o., for 28 days) type II collagen-induced arthritis in rats in vivo	Delayed onset of arthritis ↓Arthritis incidence ↓Clinical arthritis severity score ↓Histopathological arthritis severity score ↓Cell-mediated immunity	[78]
	0.01–10 μM RSF cells in vitro	↓Viability, ↓proliferation, ↑apoptosis ↑Caspase-3 ↓PPAR-γ ↑DNA fragmentation	[79]
	SW1353 cells synovial fibroblasts chondrocytes in vitro	↓MMP-3, MMP-13 ↓IL-1, -17 ↓TNF-α	[80]
	11–45 μg/kg/day (i.g., for 28 days) bovine type II collagen-induced arthritis DA rats in vivo HFLS-R cells HUVEC cells in vitro	↓Arthritis scores ↓Density of capillaries, small, medium, and large vessels in the synovial membrane tissues of inflammatory joints ↓Matrigel-induced cell adhesion ↓VEGF, ↓VEGFR, ↓Ang-1, ↓Ang-2, ↓Tie2	[81]
	1–4 nM/L MDA-MB-23 human breast tumor cells U266 multiple myeloma cells PC-3 prostate tumor cells in vitro	↓TNF-α, ↓IL-17, ↓IL-1β, ↓p38, ↓JNK ↓RANKL ↓NF-κB ↓Osteoclastogenesis	[72]
	6.25–200 nM LPS-stimulated U937 cells in vitro	↓TREM-1 ↓JAK2, ↓STAT3 ↓TNF-α, ↓IL-1β, -6	[82]
	9.31–18.62 μg/kg (p.o., for 21 days) collagen-induced arthritis rats in vivo	↓TREM-1/DAP12 ↓JAK2, ↓STAT3 ↓TNF-α, ↓ IL-1β, ↓IL-6	
	2.5–40 nM bone marrow macrophages in vitro male C57BL/6 mice in vivo	↓Osteoclasts development ↓Bone resorption ↑IL-10 ↑TGF-β1 ↓TNF-α	[73]
	10, 30, and 50 nM HFLS-RA cells in vitro	↓JNK ↓Migration	[83]
	100 μg/kg (i.p., 21 days) collagen-induced arthritis in DBA/1 mice *in vivo*	↑Clinical arthritic conditions ↓Joint destruction	
Triptolide (TP) loaded with miR-30-5p inhibitor (MSNs@PCM@TP)	TP 15 mg loaded in nanoformulation. TP 50 μg/kg (i.p.) MSNs@PCM@TP 100 μg/mL (i.p.) collagen-induced arthritis in rats in vivo RA FLS cells in vitro	↓Proliferation ↑Apoptosis ↓Immune system activation in rats	[84]
Triptolide loaded by a poly-γ-glutamic acid-grafted l-phenylalanine ethyl ester copolymer	6.25–200 nM RAW264.7 cells in vitro, 0.5–2 mg/kg (i.p.) mice in vivo	Anti-RA effect ↓Triptolide toxicity on the liver, kidney, and spleen	[85]
Triptolide-loaded poly (d,l-lactic acid) nanoparticles	0.05–0.2 mg/kg (p.o., for 14 days) induced arthritis in rats in vivo	↓Arthritis anti-inflammatory	[86]
	12.5–50 nM peripheral blood and synovial fluid of RA patients in vitro	↑OPG, ↑OPG/RANKL ↓IL-1β, ↓IL-6, ↓IL-21, ↓IL-23 ↑IL-10 ↓p-IκB	[69]
(5R)-5-Hydroxytriptolide	Murine RAW264.7 cells in vitro	↓TRAP-positive cells	
	100 nM/mL genome-wide microarray assay in RA patients	Influenced the FLS especially in the process of immune-related pathways	[60]
	50–100 nM RA FLS cells in vitro	↓MMP-3, ↓IL-1, ↓IL-6, ↓WAKMAR2/miR-4478/E2F1/p53	[63]
Kirenol	100–200 μg/mL RA FLS cells in vitro 7.5–30 mg/kg (i.p., for 21 days) collagen-induced arthritis DBA/1 mice in vivo	↓IL-6, ↓migration, ↓invasion ↓IL-6, ↓synovium hyperplasia, ↓cartilage erosion	[87]

Table 1: Continued.

Diterpenes/derivatives	Concentration/dose test system	Results/mechanisms	References
Ginkgolide B	10, 20, 40 μM (i.p., for 43 days) collagen II-induced arthritis male DBA/1J mice in vivo	↓Arthritis scores, ↓synovial hyperplasia ↓Cartilage and bone destruction ↓IL-1β, ↓IL-6, ↓MCP-1, ↓TNF-α, ↓MMP-3, ↑IL-10	[88]
	5–80 μM LPS-induced FLS cells in vitro	↓Viability ↓Caspase-3, ↓Bax, ↓Bcl-2 ↓MMP, ↓Wnt5a, ↓JNK, ↓p65	
	1, 10, 25, 50 μM LPS-stimulated murine macrophages in vitro	↓iNOS ↓COX-2	
11-epi-Sinulariolide acetate	9 mg/kg (s.c., once every 2 days from day 7 to day 28 postimmunization) adjuvant-induced arthritis in Lewis rats in vivo	↓RA characteristics ↓Cathepsin K ↓MMP-9, ↓TRAP ↓TNF-α	[89]
Retinoic acid-platinum (II) complex	0.25–12 μM MH7A cells in vitro	↓TNF-α ↑Apoptosis, ↑cell cycle arrest ↓MEK/NF-κB	[90]
	2 and 5 mg/kg (i.g.) Sprague-Dawley rats in vivo	↓IL-1β, ↓IL-6, ↓IL-8, ↓MMP-1, ↓MMP-13 ↓iNOS, ↓COX-2 mRNA	
Leflunomide in combination with methotrexate	20 mg once daily in RA patients	↓RA signs and symptoms improved physical function	[91]
Oridonin	2–10 μg/mL, 24–72 h RA HFLS cells in vitro	↓Proliferation ↑Bax, ↓caspase-3, ↓IL-1β ↓GFP-LC3 punctate dots, ↓ATG5, ↓Beclin1	[52]
Tanshinone IIA	30 mg/kg (i.p., for 30 days) adjuvant-induced arthritis C57BL/6 mice in vivo	↓Proinflammatory cytokines ↓Cartilage degradation, ↓neutrophils infiltration ↓IL-6, ↓TNF-α, ↓neutrophil NETosis	[94]
	1–80 μM RA HFLS cells in vitro	↑Cytotoxicity, ↑apoptosis ↑lncRNA GAS5, ↑caspase-3, ↑caspase-9 ↓PI3K/AKT	[93]
Phlomisoside F	5, 10, 20 mg/kg (p.o., for 28 days) adjuvant-induced arthritis Wistar rats in vivo	Markedly offset the bodyweight loss, ↓paw edema, ↓arthritis scores ↓TNF-α, ↓IL-1β, ↓IL-6, ↓COX-2, ↓5-LOX, ↑IL-10	[92]
Phytol	200 μL (injection in tail, for 10 days) DA rats in vivo	Restored oxidative-burst effect induced a strikingly similar IFN-β-dependent pathway. effective against naturally occurring genetic polymorphisms in the Ncf-1 gene that modulate the activity of the NADPH oxidase complex, which is potentially regulated in the severity of arthritis.	[95]
Resiniferatoxin	10 μL of 0.001–0.003% (injection) evoked pain scores arthritic C57BL6 mice in vivo	↓Arthritis ↓Inflammation	[96]
Xylopic acid nanoformulation	200 μg/mL RAW 264.7 cells in vitro, 5 mg/kg (i.v.) adjuvant-induced arthritis in SD rats in vivo	Anti-inflammatory Antirheumatoid	[97]
Cryptotanshinone	6–18 mg/kg (p.o., for 16 days) type II collagen-induced arthritis in Wistar rats in vivo	↓NF-κB ↓IkB-α	[71]
	5–20 μM LPS-induced Raw264.7 macrophages in vitro		
	20–60 mg/kg (p.o., for 6 weeks) adjuvant-induced arthritis in DBA/1 mice in vivo	↓Inflammation and joint destruction ↓p300 ↓STAT3	[98]

Table 1: Continued.

Diterpenes/derivatives	Concentration/dose test system	Results/mechanisms	References
Carnosic acid	30–60 mg/kg (i.p., 4 weeks) collagen-induced arthritis in C57BL/KsJ-db/db mice in vivo, 10 or 20 μM mouse bone marrow cells in vitro	↓Osteoclasts ↓Bone loss ↓Inflammation ↓ROS ↓p38	[99]

↑, increase; ↓, decrease; CSF, macrophage colony-stimulating factor; NETs, neutrophil extracellular traps; HFLS-RA, human fibroblast-like synoviocytes of rheumatoid arthritis; HUVECs, human umbilical vein endothelial cells; TREM-1, triggering receptor expressed on myeloid cells-1; ROS, reactive oxygen species; JAK, Janus kinase; STAT3, signal transducer and activator of transcription 3; RSF, rheumatoid synovial fibroblasts; BMM, bone marrow macrophages; JNK, c-Jun N-terminal kinase; RSF, rheumatoid synovial fibroblasts; RANKL, receptor activator of NF-jB ligand; OPG, osteoprotegerin; IL, interleukin; WAKMAR 2, wound and keratinocyte migration–associated long noncoding RNA 2; NF-κB, nuclear factor-κB; TRAP, tartrate-resistant acid phosphatase; lncRNAs, long noncoding RNAs; GAS5, growth arrest-specific 5; IκBα, nuclear factor of kappa light polypeptide gene enhancer in B cells inhibitor, alpha.

4 in human and bovine chondrocytes, SW1353 cells, and synovial fibroblasts, triptolide inhibited cytokine-induced MMP-3 and MMP-13 gene expression in primary human OA chondrocytes, bovine chondrocytes, SW1353 cells, and human syn [80]. It also prevented MMP-13 production by IL-1 in human and bovine cartilage explants and IL-1, IL-17, and TNF-α induced expression of ADAMTS-4 in bovine chondrocytes.

Triptolide inhibited the IL-1-induced phosphorylation of ERK, p38, and JNK at protein levels in bovine type II collagen-induced arthritis DA rats treated with 11–45 g/kg/day (i.g.) for 28 days and significantly decreased the expression of angiogenic activators such as TNF-α, IL-17, vascular endothelial growth factor (VEGF), VEGF receptor (VEGFR), and Ang-1 [81]. Triptolide also lowered the production of TNF-α, IL-1β, and IL-6 in blood and joints of collagen-induced arthritic rats [82].

Similarly, Kirenol, isolated from *Herba siegesbeckiae*, at 100–200 μg/mL inhibited the migration, invasion, and proinflammatory IL-6 secretion in RA-associated synovial fibroblasts [87]. Moreover, it inhibited the production of proinflammatory cytokines (e.g., IL-6) and synovium hyperplasia and cartilage erosion in a dose-dependent manner in collagen-induced arthritis male DBA/1 mice, whereas tanshinone IIA suppressed IL-6 and TNF-α expression and release in neutrophils and promoted neutrophil apoptosis in adjuvant-induced arthritis in female C57BL/6 mice [94].

Phlomisoside F (5, 10, and 20 mg/kg, p.o., for 28 days) inhibited the expression of TNF-α, IL-1β, IL-6, COX-2, and 5-lipoxygenase (5-LOX), and increased the expression of IL-10 in complete Freund's adjuvant-induced arthritis male Wistar rats [94]. 11-epi-Sinulariolide acetate (9 mg/kg, s.c., once every 2 days from day 7 to day 28 postimmunization) reduced the expression of cathepsin K, MMP-9, TRAP, and TNF-α in ankle tissues in adjuvant-induced RA in female Lewis rats [89].

Research findings indicated that retinoic acid-Pt (II) complex (2 and 5 mg/kg, i.g.) drastically decreased IL-1β, IL-6, IL-8, MMP-1, and MMP-13 levels in synovial fluid dose-dependently in Sprague-Dawley rats [90]. It also significantly inhibited the expression of iNOS and COX-2 mRNA proteins in RA rats. Furthermore, retinoic acid-platinum (II) complex (0.25–12 μM) reduced TNF-α-induced proliferation in a concentration-dependent manner in MH7A cells.

In collagen II-induced arthritis male DBA/1J mice, ginkgolide B (10, 20, and 40 μM, i.p., for 43 days) decreased the serum levels of IL-1β, IL-6, TNF-α, MMP-3, and MMP-13 and increased the anti-inflammatory cytokine IL-10 [99]. The synovial production of monocyte chemoattractant protein-1 (MCP-1) may be crucial in the recruitment of mononuclear phagocytes during RA inflammation [100]. Xie et al. [99] demonstrated that ginkgolide B significantly decreases the serum levels of chemokine MCP-1 in arthritis animals.

In animal studies, WB2086, a human PAF receptor antagonist, reduces PAF-induced platelet aggregation [101]. Findings showed that sclareol exhibits significant anti-inflammatory effects in experimental animals; it inhibits NO production and upregulates inducible nitric oxide synthase (iNOS) and COX-2 expression in lipopolysaccharide (LPS)-stimulated macrophages [102]. It also decreased paw edema and neutrophil infiltration in the λ carrageenan-induced paw edema animal model. On the other hand, aphamines A–C isolated from *Aphanamixis polystachya* exhibited inhibitory effects on NO production (IC_{50}: 6.71–15.36 μmol/L) and reduced the expression of iNOS in LPS-induced RAW 264.7 macrophages [103].

Serralabdanes A–E isolated from the whole plant of *Chloranthus serratus* also showed inhibitory effects on LPS-induced NO production in RAW264.7 cells [104]. Other compounds such as tripterycoside A–C, 11-O-β-d-glucopyranosyl-neotritophenolide, and wilfordoside A at 10 μM exerted substantial inhibition of IL-1β secretion in LPS-induced rat primary synovial fibroblasts [105]. Similarly, researchers found that secoferruginol isolated from the heartwood of *Cryptomeria japonica* modulates human DC function in a fashion that favors Th2 cell polarization [106], whereas songorine, a C_{20} diterpenoid alkaloid and 12-keto analogue of napelline, isolated from *Aconitum soongaricum*, exhibited anti-inflammatory and antiarthritis activities [107].

Some of the important proteins involved in RA include JAK, p38 mitogen-activated protein kinase (MAPK), extracellular receptor kinase (ERK), JNK, IL-1 receptor-associated kinase (IRAK)-4, MMPs, toll-like receptor 4 (TLR-4), G protein-coupled receptor kinase (GRK)-2, Bruton's tyrosine kinase (BTK), CD3, CD11a, CD19, CD20, and CD80. JAK is a component of the JAK/STAT signaling

system, which is constantly active, resulting in increased levels of MMPs and apoptotic chondrocytes in RA synovial joints [108]. Published research showed that excavatolide B (2.5 and 5 mg/kg, s.c.) in adjuvant (AIA) and type II collagen-induced arthritis in rats attenuate the protein expression of CD11b and nuclear factor of activated T cells 1 (NFATc1) in ankle tissues [75]. Giannelli et al. [109] reported that evaluation of synovial fluid concentrations of TIMPs (e.g., TIMP-1 and TIMP-2) is more reliable than that determined in serum when remodeling cartilage ECM proteins, besides MMPs evaluated. These researchers suggested that both TIMPs and MMP inhibitors might be a potential target for novel RA treatments administered directly into the joint area. In this respect, triptolide (10, 30, and 50 nM) in RA FLS from 7 RA patients reduced the TNF-α-induced expression of phosphorylated JNK [83]. Additionally, it has been demonstrated that a JNK-specific inhibitor reduces the migration and invasion of RA FLS.

Research by Zhong and colleagues showed that sclareol exhibits antiosteoarthritic properties in IL-1β-induced rabbit chondrocytes and a rabbit model of osteoarthritis induced by ACLT [110]. Sclareol also inhibited MMP, iNOS, and COX-2 expression and increased TIMP-1 expression and ameliorated cartilage degradation in the test systems. Similarly, 11-epi-sinulariolide acetate significantly inhibited the expression of the proinflammatory proteins iNOS and COX-2 in LPS-stimulated murine macrophages [89]. Moreover, oridonin (2–10 μg/mL for 24–72 h) increased apoptosis, protein levels of Bax, and cleaved caspase-3 in RA FLS. However, it significantly decreased IL-1β levels in the test system [52]. Meanwhile, excavatolide B at 10 μM inhibited multinucleated cell and actin ring formation and also tartrate-resistant acid phosphatase (TRAP or TRAPase), MMP-9, and cathepsin K expression in LPS-stimulated RAW 264.7 cells [75].

Researchers also demonstrated that the soft coral-derived diterpene at 2.5 and 5 mg/kg (s.c.) significantly attenuated the characteristics of RA, improved histopathological features, decreased the number of TRAP-positive multinucleated cells, and attenuated the protein expression of cathepsin K, MMP-2, and MMP-9 in ankle tissues as well as the level of IL-17A and macrophage colony-stimulating factor in adjuvant (AIA) and type II collagen-induced arthritis in rats. Figure 2 shows the possible mechanisms of diterpenes and their derivatives targeting cytokines.

4.2. Chemokines Targeting Diterpenes and Their Derivatives. A clinical trial of E6011 (an anti-CX3CL1 mAb) is currently underway, and it has been shown to have a potential function in active RA patients [111]. In LPS-induced FLS, ginkgolide B (5–80 μM) remarkably inhibited RA FLS viability in a concentration-dependent fashion. It also reduced the apoptotic ratio and enhanced the expression of cleaved caspase-3 and Bax. Furthermore, it reduced Bcl-2 expression in RA FLS, decreased the development of inflammation by regulating inflammatory cytokine secretion and MMP gene expression, and reduced expression levels of Wnt5a, (p)-JNK, and p-P65 in synovial tissues and RA FLS [88].

Other diterpenes, diterpenoids, or their derivatives that inhibit RA FLS include triptolide [79, 83], tanshinone IIA [93], (5R)-5-hydroxytriptolide [60], Kirenol [87], oridonin [52], and triptolide (TP) loaded with miR-30-5p inhibitor [84].

Findings showed that carnosol, carnosic acid, carnosic acid-12-methyl ether, 20-deoxocarnosol, and abieta-8,11,13-triene-11,12,20-triol significantly blunt gene expression levels of iNOS, cytokines/interleukins (IL-1α, IL-6), and chemokines including CCL5/RANTES, CXCL10/IP-10 in murine macrophages (RAW264.7 cells), and human chondrocytes [112].

Figure 3 shows the possible mechanisms of diterpenes and their derivatives targeting chemokines.

4.3. Diterpenes and Their Derivatives Acting on Other Proteins. Triptolide (0.01–10 μM) downregulated PPAR-γ activation and induced DNA fragmentation in RSF in rheumatoid synovial fibroblasts from RA patients [79]. It also decreased arthritis scores and significantly reduced capillaries, small, medium, and large vessel density in the synovial membrane tissues of inflamed joints in bovine type II collagen-induced arthritis DA rats [81]. Moreover, triptolide inhibited Matrigel-induced cell adhesion of HFLS-RA, and HUVEC as well as disrupted tube formation of HUVEC on Matrigel, and suppressed the VEGF-induced chemotactic migration of HFLS-RA and HUVEC, respectively, in arthritis rats.

(5R)-5-Hydroxytriptolide increased the rate of osteoprotegerin (OPG) expression in $CD3^+$ T leukomonocytes in peripheral blood and the ratio of OPG/RANKL in both peripheral blood and synovial fluid in peripheral blood and synovial fluid of RA patients [69]. It also inhibited IL-23 secretion in the supernatants of PBMCs and SFMCs in peripheral blood and synovial fluid of RA patients [69]. It additionally prevented collagen-induced arthritis via inhibiting OPG/RANK/RANKL signaling in osteoclastogenesis and IFN-γ signaling in T cells [113, 114]. Recently, Zhou et al. [63] demonstrated that it exerts an anti-RA effect through the WAKMAR2/miR-4478/E2F1/p53 dependent pathway in RA FLS. MEG3 lncRNA overexpression reduces inflammation by affecting the AKT/mTOR signaling pathway [115].

Tanshinone IIA (1–80 μM) exerted cytotoxically apoptosis effects through upregulating lncRNA GAS5, possibly with an increase in cleaved caspase-3/9 expression and inhibiting the PI3K/AKT signaling pathway in FLS from RA patients [93]. In addition, numerous studies indicated that PGs play an important role in physiological immune responses and in pathological diseases related to inflammation and tissue damage.

In murine macrophages (RAW264.7 cells) and human chondrocytes, carnosol, carnosic acid, carnosic acid-12-methyl ether, 20-deoxocarnosol, and abieta-8,11,13-triene-11,12,20-triol reduced NO and PGE_2 production in a concentration-dependent manner. They also significantly reduced iNOS and cytokine (IL-1α and IL-6) gene expression levels in the test systems [112]. Additionally, these substances altered the expression of catabolic and anabolic

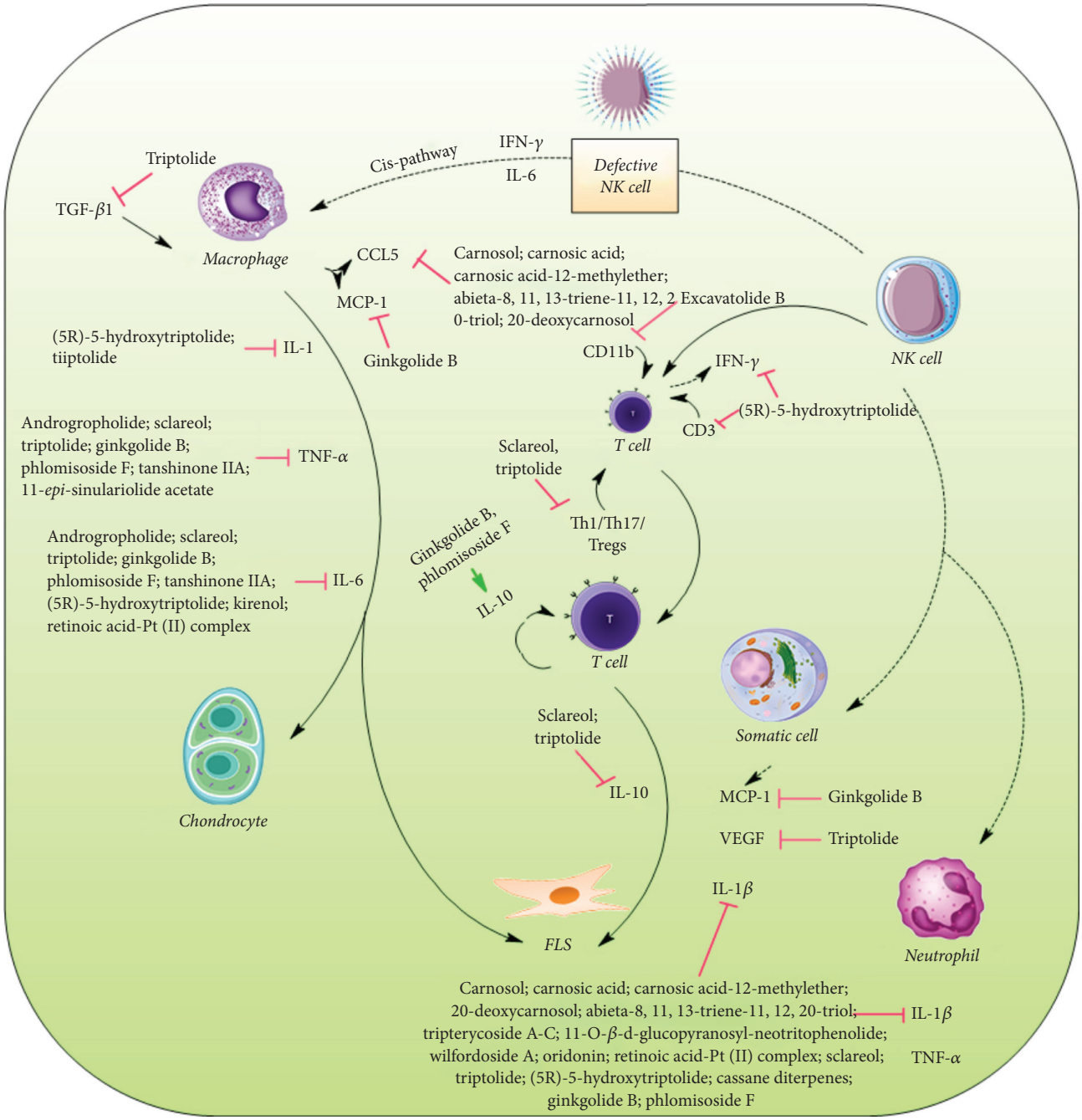

Figure 2: Diterpenes and their derivatives targeting cytokines in RA.

genes in the chondrosarcoma cell line SW1353 and primary human chondrocytes, stimulated by IL-1β, where catabolic genes such as MMP-13 and ADAM metallopeptidase with thrombospondin type 1 motif 4 (ADAMTS-4) that contribute to cartilage erosion were downregulated, whereas anabolic gene expression, particularly Col2A1 and aggrecan, was moved towards prepathophysiological equilibrium. Furthermore, carnosol exhibited the greatest overall impact on inflammatory mediators as well as macrophage and chondrocyte gene expression. It significantly inhibited IL-1β-induced nuclear translocation of NF-κB-p65, suggesting that it is primarily regulated through the NF-κB signaling pathway. Lobolide, a cembrane diterpene, also acts through the NF-κB signaling pathway [116]. Moreover, andrographolide attenuated mouse cortical chemokine levels from the CC and CXC subfamilies in LPS-induced chemokine upregulation in a mouse model [117].

Table 2 provides the list of diterpenes, diterpenoids, and their derivatives that interact with various proteins involved in inflammatory and RA processes.

4.4. Miscellaneous Pathways in RA Treatment. In type II collagen-induced arthritis in rats, triptolide (0.1 mg/kg, p.o.,

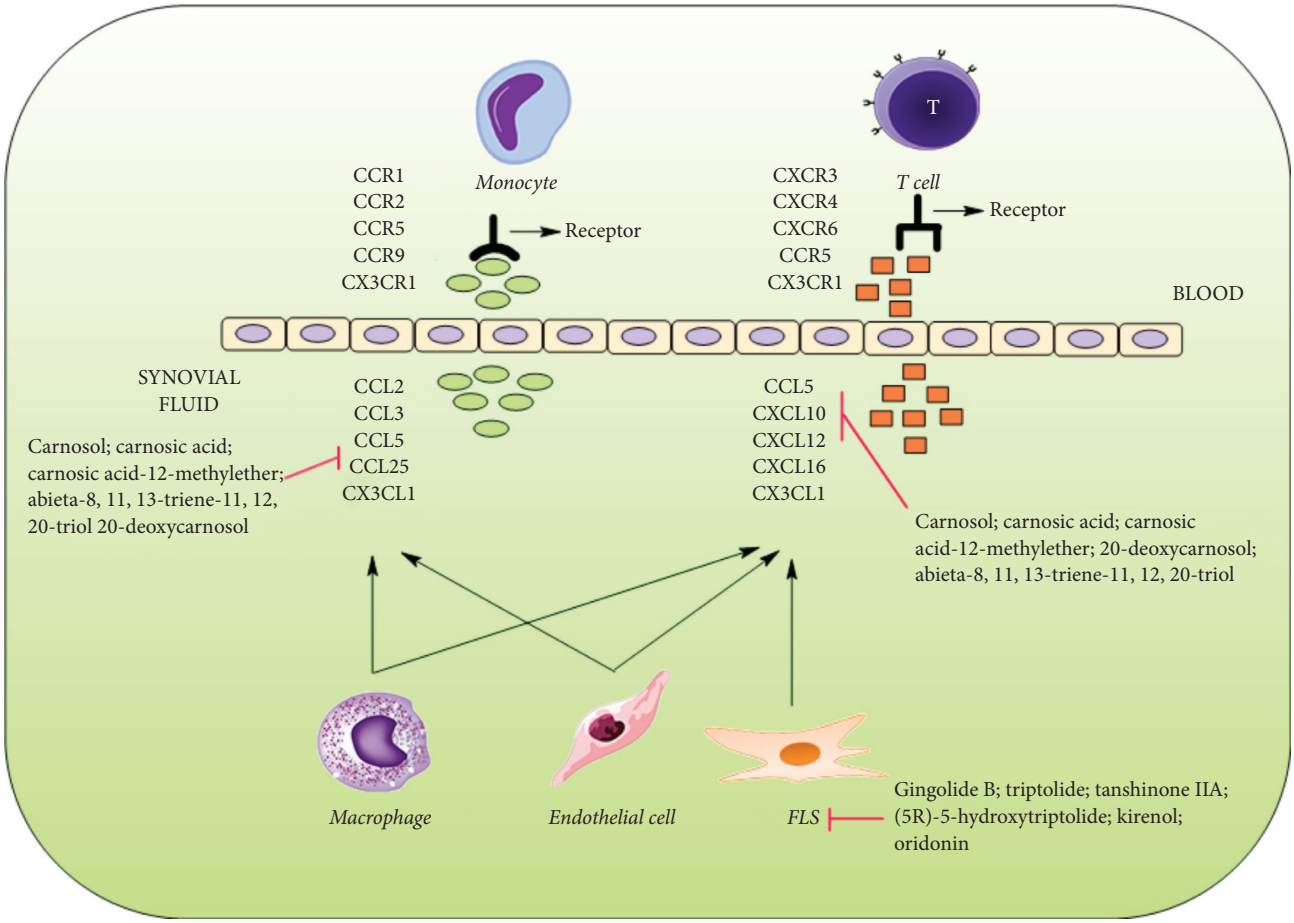

Figure 3: Diterpenes and their derivatives targeting chemokines in RA.

for 28 days) significantly delayed the onset of arthritis. In addition, the arthritis incidence, clinical arthritis severity score, histopathological arthritis severity score, and in vivo cell-mediated immunity to collagen were all reduced [78].

In bovine collagen type II and complete Freund's adjuvant-induced arthritis in DBA/1 mice, cryptotanshinone (20 and 60 mg/kg, p.o., for 6 weeks) ameliorated the inflammation and joint destruction [98]. It also suppressed p300-mediated STAT3 acetylation in test animals. Similarly, carnosic acid at 30 and 60 mg/kg (i.p., 4 weeks) in collagen-induced arthritis in male C57BL/KsJ-db/db mice and at 10 or 20 μM in mouse bone marrow cells reduced osteoclast formation and bone loss through suppression of inflammation by regulating the ROS-dependent p38 pathway [99]. On the other hand, xylopic acid nanoformulation showed anti-inflammatory and anti-RA effects in RAW 264.7 cells and complete Freund's adjuvant-induced arthritis in male Sprague-Dawley rats [97].

Research findings showed that 7β-hydroxycalcaratarin A, a labdane-type diterpenoid derived from *Hedychium coronarium*, inhibits superoxide anion generation by human neutrophils in response to formyl-L-methionyl-L-leucyl-L-phenylalanine/cytochalasin B (fMLP/CB). It also inhibited fMLP/CB-induced elastase release [118]. Chemotherapy with docetaxel (60 mg/m^2) and carboplatin dosed every 3 weeks for 4 cycles to an ovarian carcinoma patient (66-year-old woman) was found to mask RA [119].

Andrographolide (25 μM, for 16 h) in LPS-stimulated neutrophils accelerated apoptosis and inhibited autophagy-dependent extracellular TRAPs formation [77]. It also reduced neutrophil infiltration and NETosis in the ankle joints and relieved the systematic inflammation in adjuvant-induced arthritis C57BL/6 mice. Tanshinone IIA inhibited the NET formation of neutrophils in adjuvant-induced arthritis in female C57BL/6 mice [92]. On the other hand, triptolide (0.01–10 μM) reduced viability and proliferation and induced apoptosis of RSF in a concentration-dependent manner in FLS from RA patients [79]. It also upregulated caspase-3 activity in the test system, whereas retinoic acid-platinum (II) complex (0.25–12 μM) in MH7A cells induced apoptosis and caused the arrest of the cell cycle [90].

4.5. Improvement of Physiological Functions in RA Animals. Andrographolide (50 mg/kg/day) combined with methotrexate (2 mg/kg/week) for 35 days (injection) in complete Freund's adjuvant-induced arthritis in Wistar rats improved the serum marker. This may be attributed to the antioxidant activity of this compound, as evidenced by histological alterations in the liver [76]. Andrographolide when combined with methotrexate in complete Freund's adjuvant-induced arthritis in Wistar rats strengthened the antiarthritic capacity of methotrexate, reduced the inflammatory symptoms

Table 2: Diterpenes and their derivatives targeting other proteins in rheumatoid arthritis.

Target proteins	Diterpenes/diterpenoids or their derivatives	Reference
IL-23	(5R)-5-Hydroxytriptolide	[69]
p38 MAPK	Sclareol	[74]
ERK	Triptolide, andrographolide, sclareol	[70, 74, 81]
NF-κB	Lobolide, andrographolide, carnosol, sclareol, (5R)-5-hydroxytriptolide, retinoic acid-platinum (II) complex	[60, 70, 74, 90, 112, 116]
TRAP	11-epi-Sinulariolide acetate, (5R)-5-hydroxytriptolide, excavatolide B, andrographolide	[69, 75, 89, 115]
MMPs	Triptolide, 11-epi-sinulariolide acetate, excavatolide B, ginkgolide B, retinoic acid-platinum (II) complex	[75, 80, 88–90]
Cathepsin K	11-epi-Sinulariolide acetate, excavatolide B	[75, 89]
CD11b	Excavatolide B	[75]
PPAR-γ	Triptolide	[79]
VEGF, VEGFR, Ang-1, Ang-2, Tie2	Triptolide	[81]
JNK	Triptolide, ginkgolide B	[81, 83, 88]
RANK/RANKL, OPG	Triptolide, andrographolide, (5R)-5-hydroxytriptolide	[69, 70, 72, 113, 114]
p-IκB	(5R)-5-Hydroxytriptolide	[69]
TREM-1	Triptolide	[82]
JAK2		
STAT3	Triptolide, cryptotanshinone	[82, 98]
iNOS	Sclareol, 11-epi-sinulariolide acetate, carnosol, carnosic acid, carnosic acid-12-methylether, 20-deoxocarnosol and abieta-8,11,13-triene-11,12,20-triol, and retinoic acid-platinum (II) complex, aphamines A–C	[89, 90, 102, 103, 110, 112]
COX-2	Sclareol, 11-epi-sinulariolide acetate, retinoic acid-platinum (II) complex	[89, 90, 102, 110]
PI3K/AKT	Tanshinone IIA	[93]
lncRNA GAS5		
5-LOX	Phlomisoside F	[92]
WAKMAR2/miR-4478/E2F1/p53	(5R)-5-Hydroxytriptolide	[63]
ADAMTS-4	Triptolide, carnosol, carnosic acid, carnosic acid-12-methylether, 20-deoxocarnosol, abieta-8,11,13-triene-11,12,20-triol	[80, 112]
PGE2	Carnosol, carnosic acid, carnosic acid-12-methylether, 20-deoxocarnosol, abieta-8,11,13-triene-11,12,20-triol	[112]

in animals, showed hepatoprotective activity, and significantly reduced serum TNF-α, IL-6, and IL-1β levels [76].

Triptolide loaded by a poly-γ-glutamic acid-grafted l-phenylalanine ethyl ester copolymer at 6.25–200 nM reduced the damaging effects on the liver, kidney, and spleen of mice [85]. In addition, triptolide (100 μg/kg, i.p., 21 days) improved clinical arthritic conditions and joint destruction in collagen-induced arthritis in male DBA/1 mice [83], whereas triptolide-loaded poly(D,L-lactic acid) nanoparticles (0.05–0.2 mg/kg, p.o., for 14 days) in complete Freund's adjuvant-induced arthritis in male Wistar rats significantly inhibited arthritis and exerted a preferable anti-inflammatory effect with long-time administration [86].

In another study, triptolide loaded with miR-30-5p inhibitor significantly inhibited RA synovial fibroblast proliferation and increased apoptosis in collagen-induced arthritis female Sprague-Dawley rats [84]. This nanopreparation also downregulated immune system activation in rats.

Phytol (acyclic diterpene alcohol derived from chlorophyll) at 200 μL (injection in the tail, for 10 days) was found to restore the oxidative-burst effect and induce a strikingly similar IFN-β-dependent pathway in DA rats [95].

Researchers suggested that it may be effective against naturally occurring genetic polymorphisms in the Ncf-1 gene that modulated the activity of the NADPH oxidase complex, which is potentially regulated in the severity of arthritis, whereas 11-epi-sinulariolide acetate significantly inhibited RA characteristics in adjuvant-induced arthritis in female Lewis rats [89].

Resiniferatoxin (10 μL of 0.001 or 0.003%, injection) significantly improved arthritis with monoarticular inflammatory arthritis in evoked pain scores in arthritic male C57BL6 mice [96]. Similarly, tanshinone IIA (30 mg/kg, i.p., for 30 days) alleviated cartilage erosion and neutrophil infiltration in the ankle joints and reduced proinflammatory cytokine expression levels in sera in adjuvant-induced arthritis in female C57BL/6 mice [92]. In the complete Freund's adjuvant-induced arthritis rat model, phlomisoside F (5, 10, and 20 mg/kg, p.o., for 28 days) markedly offset the body weight loss, inhibited the paw edema, and reduced the arthritis scores and indices of the thymus and spleen [92]. Leflunomide (20 mg once daily) in combination with methotrexate improved signs, symptoms, and physical function in RA patients [91], while ginkgolide B (10, 20, and 40 μM, i.p., for 43 days) in collagen II-induced arthritis male

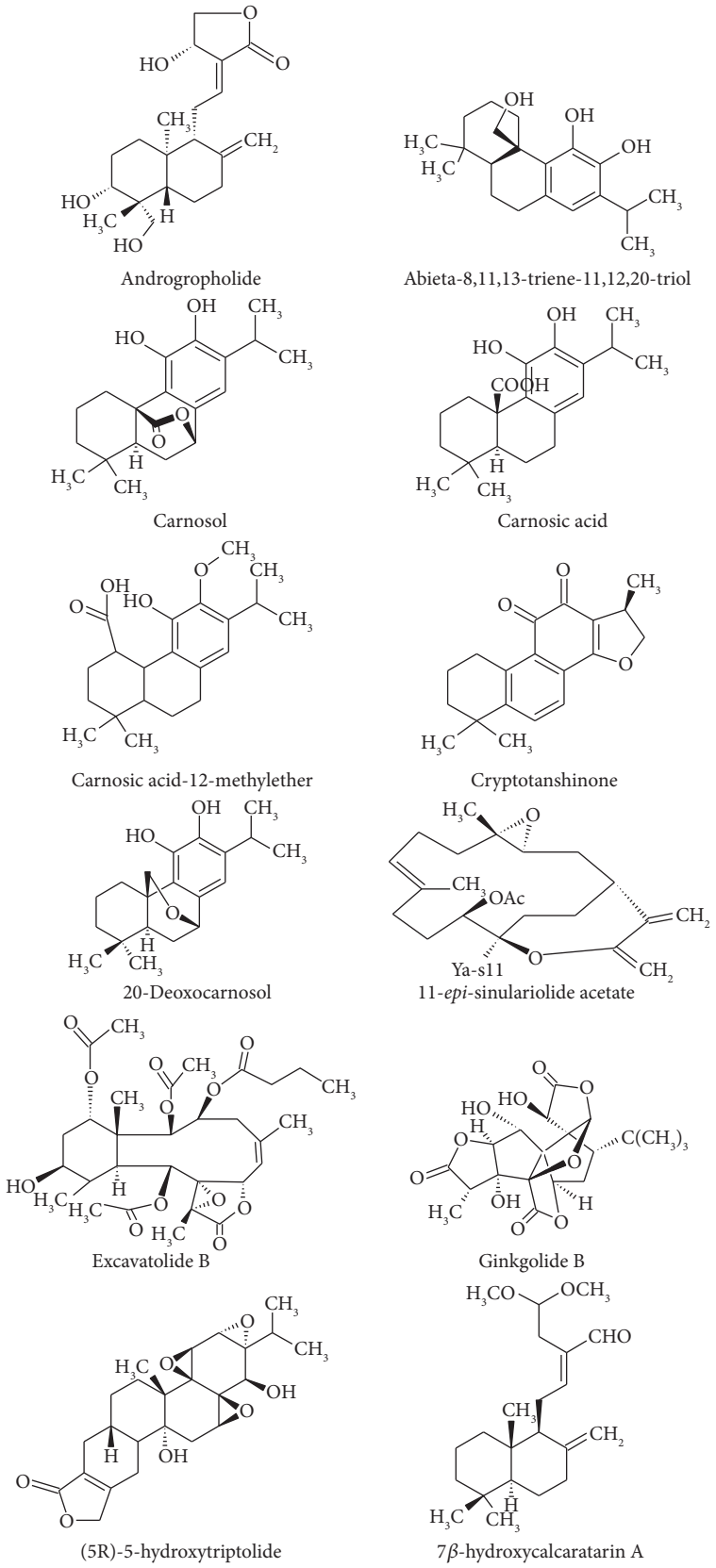

(a)

Figure 4: Continued.

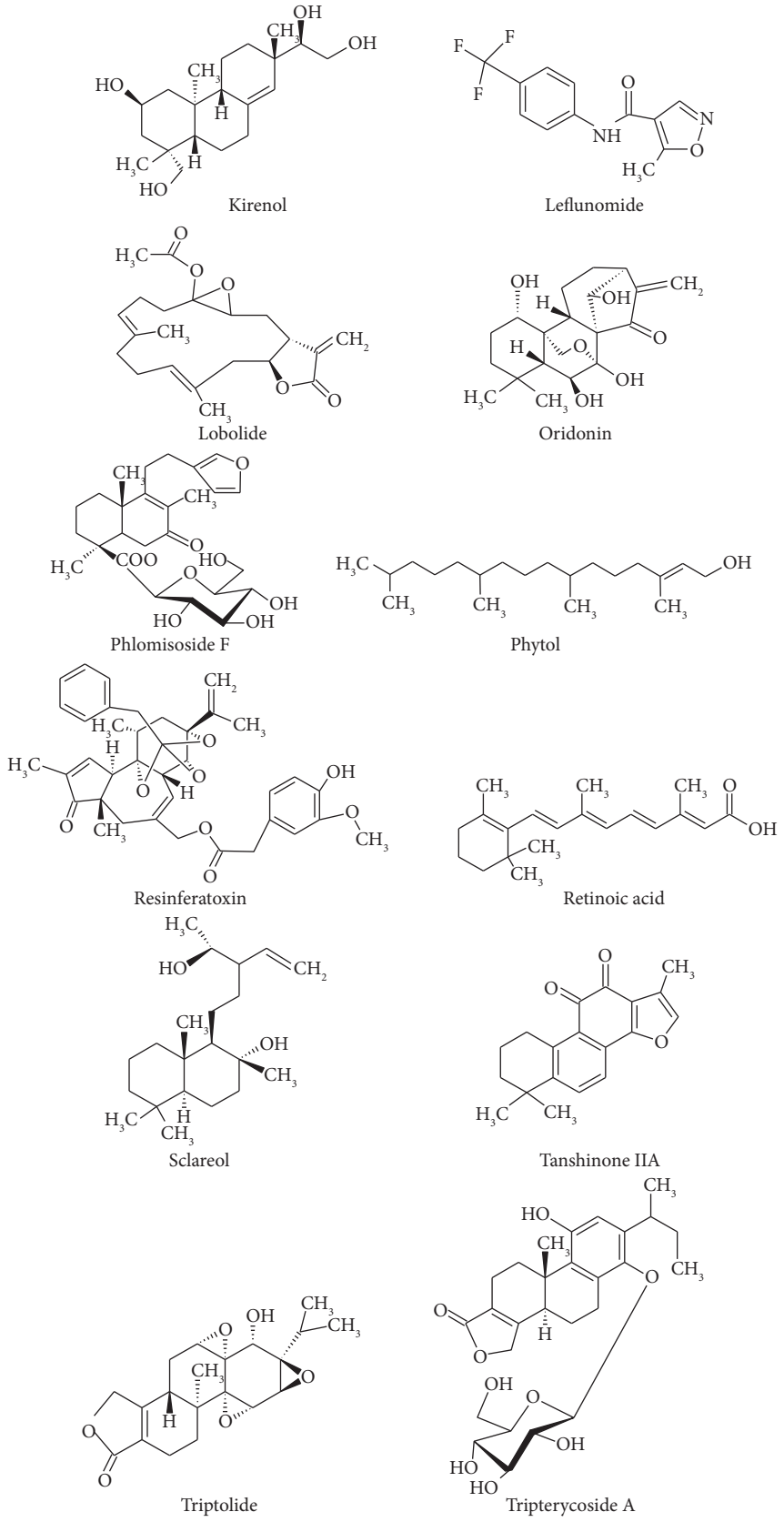

(b)

Figure 4: Continued.

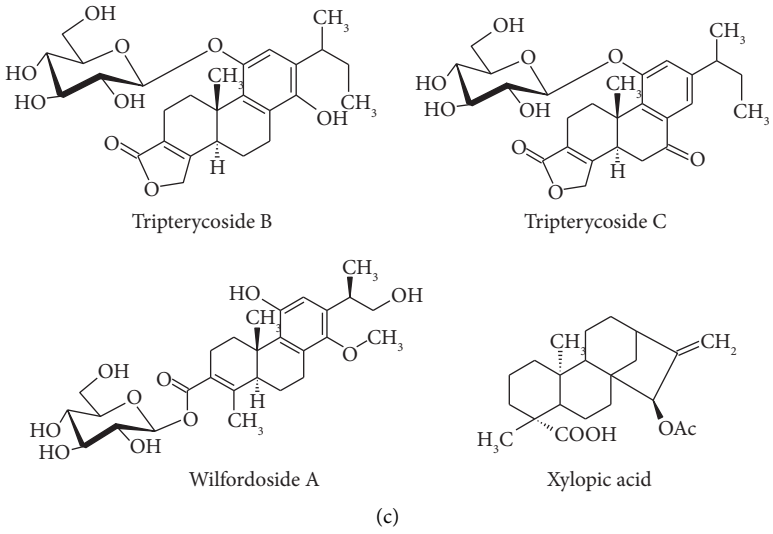

Figure 4: Chemical structures of some important anti-RA diterpenes and their derivatives.

DBA/1J mice significantly decreased arthritis scores, synovial hyperplasia, and cartilage and bone destruction [88].

The chemical structures of some anti-RA diterpenes and their derivatives are shown in Figure 4.

5. Discussion

Diterpenes and their derivatives are gaining popularity due to their intriguing biological and pharmacological properties. Thus far, hundreds of natural diterpene compounds from terrestrial and marine species have been described. Many of these compounds have become clinically effective.

Plants are an important source of diterpenes. Diterpenes can be linear, bicyclic, tricyclic, tetracyclic, pentacyclic, or macrocyclic. They are typically found in nature in a polyoxygenated form with keto and hydroxyl groups, which are frequently esterified by small-sized aliphatic or aromatic acids. For example, the anticancer drug taxol is used as a promising anticancer agent for ovarian, breast, and lung cancers. In addition, many of its synthetic derivatives are also examples of medicinal agents in the management of various diseases in humans. Docetaxel, sold under the brand name Taxotere®, is a taxoid antineoplastic drug used to treat a variety of malignancies, including locally advanced or metastatic breast cancer, metastatic prostate cancer, gastric adenocarcinoma, and head and neck cancer. Moreover, carboplatin, when combined with this drug, was found to mask RA in an ovarian carcinoma patient [119]. Similarly, ginkgolides are other promising diterpenes that have strong and specific antagonistic action against platelet-activating factors rising in shock, burns, ulceration, and inflammatory skin disorders [120]. Additionally, ginkgolide B exhibits multiedge-like anti-RA effects in in vitro and in vivo test models [88]. Meanwhile, the anti-RA diterpene resiniferatoxin (an ultrapotent vanilloid derived from the latex of *Euphorbia resinifera*) is promising for bladder hyperreflexia and diabetic neuropathy [120]. In short, diterpenes, diterpenoids, and their derivatives might be promising tools to manage RA and its consequences.

According to current knowledge [50], the most promising therapeutic targets in RA include the following:

(1) Cytokines: TNF, IL-1, IL-1R, IL-6A, IL-6R, IL-2, IL-10, IL-15, IL-17, IL-17R, IL-18, and IFN-γ

(2) Chemokines: CCL2, CCR9, CX3CL1, CCR1, CCR2, CCR5, CCR7, CXCL10, CXCL12, CXCL13, CXCL16, CXCR1/2, CXCR3, CXCR4, and CXCR7

(3) Other related proteins: BTK, CD3, CD11a, CD19, CD20, CD80, GRK2, GM-CSF, IL-23, IRAK-4, JAK, MEK, MMP-9, p38 MAPK, and TLR-4

(4) Small molecular metabolites: PGD2, PGE2, PGI2, PGJ2, PGF2α, TXA2, LTB4R, CysLT1R, ALX, PAFR, ROS, iNOS, CB2, and FFAH

This review suggests that diterpenes and their derivatives act on the cytokines (IL-1, IL-1α, IL-1β, IL-6, IL-8, IL-10, IL-17, IL-17A, IL-21, IFN-γ, TNF-α, TGF-β1, MMPS (e.g., MMP-1, MMP-2, MMP-3, MMP-9, and MMP-13), and MCP-1), chemokines (CCl5 and CXCL10), and many proteins (IL-23, p38 MAPK, ERK, NF-κB, TRAP, cathepsin K, CD11b, PPAR-γ, VEGF, VEGFR, Ang-1, Ang-2, Tie2, JNK, RANK/RANKL, OPG, p-IκB, TREM-1, JAK2, STAT3, iNOS, COX-2, PI3K/AKT, lncRNA GAS5, 5-LOX, WAKMAR2/miR-4478/E2F1/p53, ADAMTS-4, and PGE2).

It appears that diterpenes and their derivatives have multiedge-like actions on different RA models. These compounds exerted anti-RA effects through the cytokine, chemokine, inflammatory/noninflammatory proteins, and small molecular metabolites pathways. Among the diterpenes, triptolide and its derivative (5R)-5-hydroxytriptolide have been found to display promising anti-RA activity in various test systems.

Other hopeful anti-RA diterpenes and diterpenoids found in this updated review include carnosol and carnosic acid and their derivatives, excavatolide B, Kirenol,

ginkgolide B, 11-epi-sinulariolide acetate, oridonin, phlomisoside F, phytol, retinoic acid, resiniferatoxin, sclareol, and xylopic acid among others.

A novel triptolide derivative (also known as LLDT-8), which exhibited anti-RA therapeutic properties, is currently in phase II clinical studies in China [63]. Diterpenes and their derivatives act through multidimensional pathways in different RA animal models. Moreover, triptolide-loaded nanocomplexes also improved anti-RA potential in experimental modalities. Besides these compounds/formulations, andrographolide, tanshinone IIA, and its derived compound cryptotanshinone also displayed promising anti-RA effects in test systems.

6. Conclusion

To date, many natural products that have the anti-RA capacity, including those obtained from medicinal plants and marine organisms, have been identified. The sources of diterpenes and diterpenoids are widely distributed. Natural products, including medicinal plant-derived chemicals, are a prominent source of semisynthetic and synthetic derivatives. Hence, nature and modern medicinal science are capable of providing new and more effective diterpene derivatives. Diterpenes and their derivatives have been shown to possess promising immunomodulatory properties in various experimental models; therefore, these natural bioactive compounds are a promising adjuvant pharmacotherapy in RA.

Data Availability

The data used to support the findings of this study are available from the corresponding author upon request and are cited within the article as references.

Conflicts of Interest

The authors declare that they have no conflicts of interest.

Authors' Contributions

All authors made a significant contribution to the work reported, whether that is in the conception, study design, execution, acquisition of data, analysis, and interpretation, or in all these areas, that is, revising or critically reviewing the article, giving final approval of the version to be published, agreeing on the journal to which the article has been submitted, and confirming to be accountable for all aspects of the work.

References

[1] K. Almutairi, J. Nossent, D. Preen, H. Keen, and C. Inderjeeth, "The global prevalence of rheumatoid arthritis: a meta-analysis based on a systematic review," *Rheumatology International*, vol. 41, no. 5, pp. 863–877, 2021.

[2] P. Miossec, "Rheumatoid arthritis: still a chronic disease," *Lancet*, vol. 381, no. 9870, pp. 884–886, 2013.

[3] M. I. Koenders and W. B. van den Berg, "Novel therapeutic targets in rheumatoid arthritis," *Trends in Pharmacological Sciences*, vol. 36, no. 4, pp. 189–195, 2015.

[4] R. A. Simon and J. Namazy, "Adverse reactions to aspirin and nonsteroidal antiinflammatory drugs (NSAIDs)," *Clinical Reviews in Allergy & Immunology*, vol. 24, no. 3, pp. 239–252, 2003.

[5] J.-R. Laporte, L. Ibáñez, X. Vidal, L. Vendrell, and R. Leone, "Upper gastrointestinal bleeding associated with the use of NSAIDs: newer versus older agents," *Drug Safety*, vol. 27, no. 6, pp. 411–420, 2004.

[6] A. Ruyssen-Witrand, B. Fautrel, A. Saraux, X. Le-Loët, and T. Pham, "Infections induced by low-dose corticosteroids in rheumatoid arthritis: a systematic literature review," *Joint Bone Spine*, vol. 77, no. 3, pp. 246–251, 2010.

[7] D. Satyanarayanasetty, K. Pawar, P. Nadig, and A. Haran, "Multiple adverse effects of systemic corticosteroids: a case report," *Journal of Clinical and Diagnostic Research*, vol. 9, no. 5, p. FD01, 2015.

[8] S. T. Gilani, D. A. Khan, F. A. Khan, and M. Ahmed, "Adverse effects of low dose methotrexate in rheumatoid arthritis patients," *Journal of the College of Physicians and Surgeons-Pakistan*, vol. 22, no. 2, pp. 101–104, 2012.

[9] E. M. Ruderman, "Overview of safety of non-biologic and biologic DMARDs," *Rheumatology*, vol. 51, no. suppl 6, pp. vi37–vi43, 2012.

[10] G. Murdaca, F. Spanò, and F. Puppo, "Use of leflunomide plus TNF-α inhibitors in rheumatoid arthritis," *Expert Opinion on Drug Safety*, vol. 12, no. 6, pp. 801–804, 2013.

[11] I. Lekander, F. Borgström, J. Lysholm et al., "The cost-effectiveness of TNF-inhibitors for the treatment of rheumatoid arthritis in Swedish clinical practice," *The European Journal of Health Economics*, vol. 14, no. 6, pp. 863–873, 2013.

[12] X. Xia, B. H. May, A. L. Zhang et al., "Chinese herbal medicines for rheumatoid arthritis: text-mining the classical literature for potentially effective natural products," *Evidence-Based Complementary and Alternative Medicine*, vol. 2020, Article ID 7531967, 14 pages, 2020.

[13] C. Gioia, B. Lucchino, M. G. Tarsitano, C. Iannuccelli, and M. Di Franco, "Dietary habits and nutrition in rheumatoid arthritis: can diet influence disease development and clinical manifestations?" *Nutrients*, vol. 12, no. 5, p. 1456, 2020.

[14] I. S. Aswathy, S. Krishnan, J. Peter, V. Sabu, and A. Helen, "Scientific validation of anti-arthritic effect of Kashayams—a polyherbal formulation in collagen induced arthritic rats," *Journal of Ayurveda and Integrative Medicine*, vol. 12, no. 1, pp. 20–27, 2021.

[15] X. Wang, G. Fang, Y. Yang, and Y. Pang, "The newly discovered natural compounds against rheumatoid arthritis—an overview," *Phytochemistry Letters*, vol. 34, pp. 50–58, 2019.

[16] M. Gaysinski, A. Ortalo-Magné, O. P. Thomas, and G. Culioli, "Extraction, purification, and NMR analysis of terpenes from brown algae," in *Natural Products from Marine Algae*, pp. 207–223, Humana Press, New York, NY, USA, 2015.

[17] R. A. Khan, R. Hossain, A. Siyadatpanah et al., "Diterpenes/diterpenoids and their derivatives as potential bioactive leads against dengue virus: a computational and network pharmacology study," *Molecules*, vol. 26, no. 22, p. 6821, 2021.

[18] L.-G. Lin, C. Ung, Z.-L. Feng, L. Huang, and H. Hu, "Naturally occurring diterpenoid dimers: source, biosynthesis, chemistry and bioactivities," *Planta Medica*, vol. 82, no. 15, pp. 1309–1328, 2016.

[19] J. R. Hanson, "Diterpenoids of terrestrial origin," *Natural Product Reports*, vol. 34, no. 10, pp. 1233–1243, 2017.

[20] M. T. Islam, "Diterpenes and their derivatives as potential anticancer agents," *Phytotherapy Research*, vol. 31, no. 5, pp. 691–712, 2017.

[21] M. F. C. J. Paz, M. T. Islam, S. Tabrez et al., "Effect of diterpenes on hepatic system," *Current Pharmaceutical Design*, vol. 24, no. 35, pp. 4093–4100, 2018.

[22] M. T. Islam, S. K. Bardaweel, M. S. Mubarak et al., "Immunomodulatory effects of diterpenes and their derivatives through NLRP3 inflammasome pathway: a review," *Frontiers in Immunology*, vol. 11, Article ID 572136, 2020.

[23] R. Hossain, M. T. Islam, P. Ray et al., "Amentoflavone, new hope against SARS-CoV-2: an outlook through its scientific records and an in silico study," *Pharmacognosy Research*, vol. 13, 2021.

[24] J. De-Paula, L. Bueno, D. Cavalcanti, Y. Yoneshigue-Valentin, and V. Teixeira, "Diterpenes from the brown alga Dictyota crenulata," *Molecules*, vol. 13, no. 6, pp. 1253–1262, 2008.

[25] M. J. Smanski, R. M. Peterson, and B. Shen, "Platensimycin and platencin biosynthesis in Streptomyces platensis, showcasing discovery and characterization of novel bacterial diterpene synthases," in *Natural Product Biosynthesis by Microorganisms and Plants, Part A*, vol. 515, pp. 163–186, Academic Press, Cambridge, MA, USA, 2012.

[26] L. P. Sandjo and V. Kuete, "Diterpenoids from the medicinal plants of Africa," in *Medicinal Plant Research in Africa*, pp. 105–133, Elsevier, Amsterdam, Netherlands, 2013.

[27] A. Ludwiczuk, K. Skalicka-Woźniak, and M. I. Georgiev, "Terpenoids," *Pharmacognosy*, Academic Press, Cambridge, MA, USA, pp. 233–266, 2017.

[28] C. Sy, O. Dangles, P. Borel, and C. Caris-Veyrat, "Interactions between carotenoids from marine bacteria and other micronutrients: impact on stability and antioxidant activity," *Marine Drugs*, vol. 13, no. 11, pp. 7020–7039, 2015.

[29] X. Huang, B. Lv, S. Zhang, Q. Dai, B.-B. Chen, and L.-N. Meng, "Effects of radix curcumae-derived diterpenoid C on *Helicobacter pylori*-induced inflammation and nuclear factor kappa B signal pathways," *World Journal of Gastroenterology*, vol. 19, no. 31, pp. 5085–5093, 2013.

[30] L. Gan, Y. Zheng, L. Deng et al., "Diterpenoid lactones with anti-inflammatory effects from the aerial parts of Andrographis paniculata," *Molecules*, vol. 24, no. 15, p. 2726, 2019.

[31] X. Lu, L. Li, C.-Y. Zhang, H. Schluesener, and Z.-Y. Zhang, "Natural diterpenoid oridonin ameliorates experimental autoimmune neuritis by promoting anti-inflammatory macrophages through blocking notch pathway," *Frontiers in Neuroscience*, vol. 13, p. 272, 2019.

[32] C. A. Dinarello, "Historical insights into cytokines," *European Journal of Immunology*, vol. 37, no. S1, pp. S34–S45, 2007.

[33] V. Goëb, P. Aegerter, R. Parmar et al., "Progression to rheumatoid arthritis in early inflammatory arthritis is associated with low IL-7 serum levels," *Annals of the Rheumatic Diseases*, vol. 72, no. 6, pp. 1032–1036, 2013.

[34] Y. Guo, N. Wang, S. Zhao, L. Hou, Y. Xu, and N. Zhang, "Increased interleukin-23 is associated with increased disease activity in patients with rheumatoid arthritis," *Chinese Medical Journal*, vol. 126, no. 5, pp. 850–854, 2013.

[35] N. J. Gullick, H. S. Abozaid, D. M. Jayaraj et al., "Enhanced and persistent levels of interleukin (IL)-17$^+$ CD4$^+$ T cells and serum IL-17 in patients with early inflammatory arthritis," *Clinical & Experimental Immunology*, vol. 174, no. 2, pp. 292–301, 2013.

[36] H. Radner and D. Aletaha, "Anti-TNF in rheumatoid arthritis: an overview," *Wiener Medizinische Wochenschrift*, vol. 165, no. 1, pp. 3–9, 2015.

[37] A. D. Cook, C. Louis, M. J. Robinson, R. Saleh, M. A. Sleeman, and J. A. Hamilton, "Granulocyte macrophage colony-stimulating factor receptor α expression and its targeting in antigen-induced arthritis and inflammation," *Arthritis Research & Therapy*, vol. 18, no. 1, p. 287, 2016.

[38] I. V. Reyes-Pérez, P. E. Sánchez-Hernández, J. F. Muñoz-Valle et al., "Cytokines (IL-15, IL-21, and IFN-γ) in rheumatoid arthritis: association with positivity to autoantibodies (RF, anti-CCP, anti-MCV, and anti-PADI4) and clinical activity," *Clinical Rheumatology*, vol. 38, no. 11, pp. 3061–3071, 2019.

[39] S. A. Y. Hartgring, C. R. Willis, D. Alcorn et al., "Blockade of the interleukin-7 receptor inhibits collagen-induced arthritis and is associated with reduction of T cell activity and proinflammatory mediators," *Arthritis & Rheumatism*, vol. 62, no. 9, pp. 2716–2725, 2010.

[40] K. A. Knoop, N. Kumar, B. R. Butler et al., "RANKL is necessary and sufficient to initiate development of antigen-sampling M cells in the intestinal epithelium," *The Journal of Immunology*, vol. 183, no. 9, pp. 5738–5747, 2009.

[41] P. J. Mease, "Adalimumab in the treatment of arthritis," *Therapeutics and Clinical Risk Management*, vol. 3, p. 133, 2007.

[42] Q. Cheng, H. Wu, and Y. Du, "The roles of small-molecule inflammatory mediators in rheumatoid arthritis," *Scandinavian Journal of Immunology*, vol. 93, no. 3, Article ID e12982, 2021.

[43] A. Hashimoto, I. Hayashi, Y. Murakami et al., "Antiinflammatory mediator lipoxin A4 and its receptor in synovitis of patients with rheumatoid arthritis," *Journal of Rheumatology*, vol. 34, no. 11, pp. 2144–2153, 2007.

[44] S. Ramon, S. Bancos, C. N. Serhan, and R. P. Phipps, "Lipoxin A_4 modulates adaptive immunity by decreasing memory B-cell responses via an ALX/FPR2-dependent mechanism," *European Journal of Immunology*, vol. 44, no. 2, pp. 357–369, 2014.

[45] A. Zarbock, R. K. Polanowska-Grabowska, and K. Ley, "Platelet-neutrophil-interactions: linking hemostasis and inflammation," *Blood Reviews*, vol. 21, no. 2, pp. 99–111, 2007.

[46] A. A. Manfredi, M. Baldini, M. Camera et al., "Anti-TNFα agents curb platelet activation in patients with rheumatoid arthritis," *Annals of the Rheumatic Diseases*, vol. 75, no. 8, pp. 1511–1520, 2016.

[47] J. Panezai, A. Ali, A. Ghaffar et al., "Upregulation of circulating inflammatory biomarkers under the influence of periodontal disease in rheumatoid arthritis patients," *Cytokine*, vol. 131, Article ID 155117, 2020.

[48] Y. Tian, M. A. Terkawi, T. Onodera et al., "Blockade of XCL1/lymphotactin ameliorates severity of periprosthetic osteolysis triggered by polyethylene-particles," *Frontiers in Immunology*, vol. 11, p. 1720, 2020.

[49] M. Endres, K. Andreas, G. Kalwitz et al., "Chemokine profile of synovial fluid from normal, osteoarthritis and rheumatoid arthritis patients: CCL25, CXCL10 and XCL1 recruit human subchondral mesenchymal progenitor cells," *Osteoarthritis and Cartilage*, vol. 18, no. 11, pp. 1458–1466, 2010.

[50] J. Huang, X. Fu, X. Chen, L. Zheng, Y. Huang, and C. Liang, "Promising therapeutic targets for treatment of rheumatoid arthritis," *Frontiers in Immunology*, vol. 12, Article ID 686155, 2021.

[51] M. Yang, F. Wu, C. Xie et al., "Expression of CC chemokine ligand 5 in patients with rheumatoid arthritis and its correlation with disease activity and medication," *Chinese Medical Sciences Journal*, vol. 24, no. 1, pp. 50–54, 2009.

[52] Y. Miyabe, C. Miyabe, T. T. Murooka et al., "Complement C5a receptor is the key initiator of neutrophil adhesion igniting immune complex-induced arthritis," *Science Immunology*, vol. 2, no. 7, Article ID eaaj2195, 2017.

[53] J.-H. Lee, B. Kim, W. J. Jin, H.-H. Kim, H. Ha, and Z. H. Lee, "Pathogenic roles of CXCL10 signaling through CXCR3 and TLR4 in macrophages and T cells: relevance for arthritis," *Arthritis Research & Therapy*, vol. 19, no. 1, pp. 1–14, 2017.

[54] M. Ricote, A. C. Li, T. M. Willson, C. J. Kelly, and C. K. Glass, "The peroxisome proliferator-activated receptor-γ is a negative regulator of macrophage activation," *Nature*, vol. 391, no. 6662, pp. 79–82, 1998.

[55] C. Giaginis, A. Giagini, and S. Theocharis, "Peroxisome proliferator-activated receptor-γ (PPAR-γ) ligands as potential therapeutic agents to treat arthritis," *Pharmacological Research*, vol. 60, no. 3, pp. 160–169, 2009.

[56] D. Xu, Y. Jiang, Y. Lu et al., "Long noncoding RNAs expression profile and functional networks in rheumatoid arthritis," *Oncotarget*, vol. 8, no. 56, Article ID 95280, 2017.

[57] L. Sun, J. Tu, C. Liu, A. Pan, X. Xia, and X. Chen, "Analysis of lncRNA expression profiles by sequencing reveals that lnc-AL928768.3 and lnc-AC091493.1 are novel biomarkers for disease risk and activity of rheumatoid arthritis," *Inflammopharmacology*, vol. 28, no. 2, pp. 437–450, 2020.

[58] D. R. Haynes, E. Barg, T. N. Crotti et al., "Osteoprotegerin expression in synovial tissue from patients with rheumatoid arthritis, spondyloarthropathies and osteoarthritis and normal controls," *Rheumatology*, vol. 42, no. 1, pp. 123–134, 2003.

[59] P. Geusens, "The role of RANK ligand/osteoprotegerin in rheumatoid arthritis," *Therapeutic Advances in Musculoskeletal Disease*, vol. 4, no. 4, pp. 225–233, 2012.

[60] S. Guo, L. Jia, T. Jiang et al., "(5R)-5-hydroxytriptolide (LLDT-8) induces substantial epigenetic mediated immune response network changes in fibroblast-like synoviocytes from rheumatoid arthritis patients," *Scientific Reports*, vol. 9, no. 1, 2019.

[61] C.-M. Yang, S.-F. Luo, H.-L. Hsieh et al., "Interleukin-1β induces ICAM-1 expression enhancing leukocyte adhesion in human rheumatoid arthritis synovial fibroblasts: involvement of ERK, JNK, AP-1, and NF-κB," *Journal of Cellular Physiology*, vol. 224, no. 2, pp. 516–526, 2010.

[62] S.-D. He, S.-G. Huang, H.-J. Zhu et al., "Oridonin suppresses autophagy and survival in rheumatoid arthritis fibroblast-like synoviocytes," *Pharmaceutical Biology*, vol. 58, no. 1, pp. 146–151, 2020.

[63] X. Zhou, D. Xie, J. Huang et al., "Therapeutic effects of (5R)-5-hydroxytriptolide on fibroblast-like synoviocytes in rheumatoid arthritis via lncRNA WAKMAR2/miR-4478/E2F1/p53 axis," *Frontiers in Immunology*, vol. 12, p. 296, 2021.

[64] P. Oelzner, S. Franke, G. Lehmann, T. Eidner, G. Hein, and G. Wolf, "The balance between soluble receptors regulating IL-6 trans-signaling is predictive for the RANKL/osteoprotegerin ratio in postmenopausal women with rheumatoid arthritis," *Rheumatology International*, vol. 32, no. 1, pp. 199–206, 2012.

[65] C. B. Little, A. Barai, D. Burkhardt et al., "Matrix metalloproteinase 13-deficient mice are resistant to osteoarthritic cartilage erosion but not chondrocyte hypertrophy or osteophyte development," *Arthritis & Rheumatism*, vol. 60, no. 12, pp. 3723–3733, 2009.

[66] L. J. Crofford, "Use of NSAIDs in treating patients with arthritis," *Arthritis Research & Therapy*, vol. 15, no. 3, 2013.

[67] Z. Tong, L. Cheng, J. Song et al., "Therapeutic effects of Caesalpinia minax Hance on complete Freund's adjuvant (CFA)-induced arthritis and the anti-inflammatory activity of cassane diterpenes as main active components," *Journal of Ethnopharmacology*, vol. 226, pp. 90–96, 2018.

[68] Y. He, Y. Yao, Q. Xie, X. Fang, and S. Liang, "Anti-rheumatoid arthritis potential of diterpenoid fraction derived from Rhododendron molle fruits," *Chinese Journal of Natural Medicines*, vol. 19, no. 3, pp. 181–187, 2021.

[69] Y. Shen, T. Jiang, R. Wang et al., "(5R)-5-hydroxytriptolide (LLDT-8) inhibits osteoclastogenesis via RANKL/RANK/OPG signaling pathway," *BMC Complementary and Alternative Medicine*, vol. 15, no. 1, pp. 1–10, 2015.

[70] Z. J. Zhai, H. W. Li, G. W. Liu et al., "Andrographolide suppresses RANKL-induced osteoclastogenesis in vitro and prevents inflammatory bone loss in vivo," *British Journal of Pharmacology*, vol. 171, no. 3, pp. 663–675, 2014.

[71] Y. Wang, S. Wang, Y. Li et al., "Therapeutic effect of cryptotanshinone on collagen-induced arthritis in rats via inhibiting nuclear factor kappa B signaling pathway," *Translational Research*, vol. 165, no. 6, pp. 704–716, 2015.

[72] B. Park, "Triptolide, a diterpene, inhibits osteoclastogenesis, induced by RANKL signaling and human cancer cells," *Biochimie*, vol. 105, pp. 129–136, 2014.

[73] H. Xu, H. Zhao, C. Lu et al., "Triptolide inhibits osteoclast differentiation and bone resorption in vitro via enhancing the production of IL-10 and TGF-β1 by regulatory T cells," *Mediators of Inflammation*, vol. 2016, Article ID 8048170, 10 pages, 2016.

[74] S.-W. Tsai, M.-C. Hsieh, S. Li et al., "Therapeutic potential of sclareol in experimental models of rheumatoid arthritis," *International Journal of Molecular Sciences*, vol. 19, no. 5, p. 1351, 2018.

[75] Y.-Y. Lin, Y.-H. Jean, H.-P. Lee et al., "Excavatolide B attenuates rheumatoid arthritis through the inhibition of osteoclastogenesis," *Marine Drugs*, vol. 15, no. 1, p. 9, 2017.

[76] G. Li, Y. Liu, F. Meng et al., "Tanshinone IIA promotes the apoptosis of fibroblast-like synoviocytes in rheumatoid arthritis by up-regulating lncRNA GAS5," *Bioscience Reports*, vol. 38, no. 5, 2018.

[77] X. Li, K. Yuan, Q. Zhu et al., "Andrographolide ameliorates rheumatoid arthritis by regulating the apoptosis-NETosis balance of neutrophils," *International Journal of Molecular Sciences*, vol. 20, no. 20, p. 5035, 2019.

[78] W.-Z. Gu and S. R. Brandwein, "Inhibition of type II collagen-induced arthritis in rats by triptolide," *International Journal of Immunopharmacology*, vol. 20, no. 8, pp. 389–400, 1998.

[79] N. Kusunoki, R. Yamazaki, and S. Kawai, "Triptolide, an active compound identified in a traditional Chinese herb, induces apoptosis of rheumatoid synovial fibroblasts," *Arthritis Research and Therapy*, vol. 5, no. 3, 2003.

[80] A. Liacini, J. Sylvester, and M. Zafarullah, "Triptolide suppresses proinflammatory cytokine-induced matrix metalloproteinase and aggrecanase-1 gene expression in chondrocytes," *Biochemical and Biophysical Research Communications*, vol. 327, no. 1, pp. 320–327, 2005.

[81] X. Kong, Y. Zhang, C. Liu et al., "Anti-angiogenic effect of triptolide in rheumatoid arthritis by targeting angiogenic cascade," *PLoS One*, vol. 8, no. 10, Article ID e77513, 2013.

[82] D. Fan, X. He, Y. Bian et al., "Triptolide modulates TREM-1 signal pathway to inhibit the inflammatory response in rheumatoid arthritis," *International Journal of Molecular Sciences*, vol. 17, no. 4, p. 498, 2016.

[83] Y. Yang, Y. Ye, Q. Qiu et al., "Triptolide inhibits the migration and invasion of rheumatoid fibroblast-like synoviocytes by blocking the activation of the JNK MAPK pathway," *International Immunopharmacology*, vol. 41, pp. 8–16, 2016.

[84] X. Zhang, X. Zhang, X. Wang et al., "Efficient delivery of triptolide plus a miR-30-5p inhibitor through the use of near infrared laser responsive or CADY modified MSNs for efficacy in rheumatoid arthritis therapeutics," *Frontiers in Bioengineering and Biotechnology*, vol. 8, p. 170, 2020.

[85] L. Zhang, T. Wang, Q. Li et al., "Fabrication of novel vesicles of triptolide for antirheumatoid activity with reduced toxicity in vitro and in vivo," *International Journal of Nanomedicine*, vol. 11, p. 2663, 2016.

[86] M. Liu, J. Dong, Y. Yang, X. Yang, and H. Xu, "Anti-inflammatory effects of triptolide loaded poly (D,L-lactic acid) nanoparticles on adjuvant-induced arthritis in rats," *Journal of Ethnopharmacology*, vol. 97, no. 2, pp. 219–225, 2005.

[87] J. Wu, Q. Li, L. Jin et al., "Kirenol inhibits the function and inflammation of fibroblast-like synoviocytes in rheumatoid arthritis in vitro and in vivo," *Frontiers in Immunology*, vol. 10, p. 1304, 2019.

[88] C. Xie, J. Jiang, J. Liu, G. Yuan, and Z. Zhao, "Ginkgolide B attenuates collagen-induced rheumatoid arthritis and regulates fibroblast-like synoviocytes-mediated apoptosis and inflammation," *Annals of Translational Medicine*, vol. 8, no. 22, 2020.

[89] Y.-Y. Lin, Y.-H. Jean, H.-P. Lee et al., "A soft coral-derived compound, 11-epi-sinulariolide acetate suppresses inflammatory response and bone destruction in adjuvant-induced arthritis," *PLoS One*, vol. 8, no. 5, Article ID e62926, 2013.

[90] Z. Cui, Y. Lin, Y. Liu, L. Cao, and L. Cui, "Retinoic acid-platinum (II) complex [RT-Pt (II)] protects against rheumatoid arthritis in mice via MEK/nuclear factor kappa B (NF-κB) pathway downregulation," *Medical Science Monitor: International Medical Journal of Experimental and Clinical Research*, vol. 26, Article ID e924787, 2020.

[91] J. Wu, X. Chen, L. Yuan et al., "Chinese herbal formula Huayu-Qiangshen-Tongbi decoction compared with leflunomide in combination with methotrexate in patients with active rheumatoid arthritis: an open-label, randomized, controlled, pilot study," *Frontiers of Medicine*, vol. 7, p. 484, 2020.

[92] X. Zhang, Y. Dong, H. Dong, W. Zhang, and F. Li, "Investigation of the effect of phlomisoside F on complete Freund's adjuvant-induced arthritis," *Experimental and Therapeutic Medicine*, vol. 13, no. 2, pp. 710–716, 2017.

[93] F. Li, L. He, S. Luo et al., "Evaluation of the effect of andrographolide and methotrexate combined therapy in complete Freund's adjuvant induced arthritis with reduced hepatotoxicity," *Biomedicine & Pharmacotherapy*, vol. 106, pp. 637–645, 2018.

[94] S. Zhang, G. Huang, K. Yuan et al., "Tanshinone IIA ameliorates chronic arthritis in mice by modulating neutrophil activities," *Clinical & Experimental Immunology*, vol. 190, no. 1, pp. 29–39, 2017.

[95] P. Olofsson, A. Nerstedt, M. Hultqvist et al., "Arthritis suppression by NADPH activation operates through an interferon-β pathway," *BMC Biology*, vol. 5, no. 1, p. 19, 2007.

[96] J. Bert, M. L. Mahowald, S. Frizelle, C. W. Dorman, S. C. Funkenbusch, and H. E. Krug, "The effect of treatment with resiniferatoxin and capsaicin on dynamic weight bearing measures and evoked pain responses in a chronic inflammatory arthritis murine model," *Internal Medicine Review (Washington, DC: Online)*, vol. 2016, no. 6, p. 89, 2016.

[97] R. N. Alolga, Y. Opoku-Damoah, D. A. Alagpulinsa et al., "Metabolomic and transcriptomic analyses of the anti-rheumatoid arthritis potential of xylopic acid in a bioinspired lipoprotein nanoformulation," *Biomaterials*, vol. 268, Article ID 120482, 2021.

[98] Y. Wang, C. Zhou, H. Gao et al., "Therapeutic effect of cryptotanshinone on experimental rheumatoid arthritis through downregulating p300 mediated-STAT3 acetylation," *Biochemical Pharmacology*, vol. 138, pp. 119–129, 2017.

[99] G. Xia, X. Wang, H. Sun, Y. Qin, and M. Fu, "Carnosic acid (CA) attenuates collagen-induced arthritis in db/db mice via inflammation suppression by regulating ROS-dependent p38 pathway," *Free Radical Biology and Medicine*, vol. 108, pp. 418–432, 2017.

[100] A. E. Koch, S. L. Kunkel, L. A. Harlow et al., "Enhanced production of monocyte chemoattractant protein-1 in rheumatoid arthritis," *The Journal of Clinical Investigation*, vol. 90, no. 3, pp. 772–779, 1992.

[101] S. I. Svetlov, J. M. Barton, and M. S. Olson, "The specific binding of the platelet-activating factor (PAF) receptor antagonist WEB 2086 and the benzodiazepine flunitrazepam to rat hepatocytes," *Life Sciences*, vol. 58, no. 5, pp. PL81–PL86, 1995.

[102] G.-J. Huang, C.-H. Pan, and C.-H. Wu, "Sclareol exhibits anti-inflammatory activity in both lipopolysaccharide-stimulated macrophages and the λ-carrageenan-induced paw edema model," *Journal of Natural Products*, vol. 75, no. 1, pp. 54–59, 2012.

[103] P. Zhang, X. Shang, P. Tang et al., "Aphamines A–C, dimeric acyclic diterpene enantiomers from Aphanamixis polystachya," *Chinese Chemical Letters*, vol. 32, no. 4, pp. 1480–1484, 2021.

[104] M. Zhang, J. Wang, J. Luo, P. Wang, C. Guo, and L. Kong, "Labdane diterpenes from Chloranthus serratus," *Fitoterapia*, vol. 91, pp. 95–99, 2013.

[105] J. Liu, Q. Wu, J. Shu, R. Zhang, and L. Liu, "Three new abietane-type diterpene glycosides from the roots of Tripterygium wilfordii," *Fitoterapia*, vol. 120, pp. 126–130, 2017.

[106] M. Takei, A. Umeyama, and S. Arihara, "Diterpenes inhibit IL-12 production by DC and enhance Th2 cells polarization," *Biochemical and Biophysical Research Communications*, vol. 355, no. 3, pp. 603–610, 2007.

[107] H. Khan, S. M. Nabavi, A. Sureda et al., "Therapeutic potential of songorine, a diterpenoid alkaloid of the genus Aconitum," *European Journal of Medicinal Chemistry*, vol. 153, pp. 29–33, 2018.

[108] C. J. Malemud, "The role of the JAK/STAT signal pathway in rheumatoid arthritis," *Therapeutic Advances in Musculoskeletal Disease*, vol. 10, no. 5-6, pp. 117–127, 2018.

[109] G. Giannelli, R. Erriquez, F. Iannone, F. Marinosci, G. Lapadula, and S. Antonaci, "MMP-2, MMP-9, TIMP-1 and TIMP-2 levels in patients with rheumatoid arthritis and psoriatic arthritis," *Clinical & Experimental Rheumatology*, vol. 22, no. 3, pp. 335–338, 2004.

[110] Y. Zhong, Y. Huang, M. B. Santoso, and L.-D. Wu, "Sclareol exerts anti-osteoarthritic activities in interleukin-1β-induced rabbit chondrocytes and a rabbit osteoarthritis model,"

International Journal of Clinical and Experimental Pathology, vol. 8, no. 3, p. 2365, 2015.

[111] Y. Tanaka, T. Takeuchi, H. Yamanaka et al., "A phase 2 study of E6011, an anti-fractalkine monoclonal antibody, in patients with rheumatoid arthritis inadequately responding to biological disease-modifying antirheumatic drugs," *Modern Rheumatology*, vol. 31, no. 4, pp. 783–789, 2021.

[112] J. Schwager, N. Richard, A. Fowler, N. Seifert, and D. Raederstorff, "Carnosol and related substances modulate chemokine and cytokine production in macrophages and chondrocytes," *Molecules*, vol. 21, no. 4, p. 465, 2016.

[113] R. Zhou, W. Tang, Y.-X. Ren et al., "(5R)-5-hydroxytriptolide attenuated collagen-induced arthritis in DBA/1 mice via suppressing interferon-γ production and its related signaling," *Journal of Pharmacology and Experimental Therapeutics*, vol. 318, no. 1, pp. 35–44, 2006.

[114] J.-Z. Zeng, L.-F. Ma, H. Meng, H.-M. Yu, Y.-K. Zhang, and A. Guo, "(5R)-5-hydroxytriptolide (LLDT-8) prevents collagen-induced arthritis through OPG/RANK/RANKL signaling in a rat model of rheumatoid arthritis," *Experimental and Therapeutic Medicine*, vol. 12, no. 5, pp. 3101–3106, 2016.

[115] G. Li, Y. Liu, F. Meng et al., "LncRNA MEG3 inhibits rheumatoid arthritis through miR-141 and inactivation of AKT/mTOR signalling pathway," *Journal of Cellular and Molecular Medicine*, vol. 23, no. 10, pp. 7116–7120, 2019.

[116] X. Lv, S. Chen, J. Li, J. Fang, Y. Guo, and K. Ding, "Lobolide, a diterpene, blockades the NF-κB pathway and p38 and ERK MAPK activity in macrophages in vitro," *Acta Pharmacologica Sinica*, vol. 33, no. 10, pp. 1293–1300, 2012.

[117] S. Y. Wong, M. G. K. T. Tan, W. A. Banks, W. S. F. Wong, P. T.-H. Wong, and M. K. P. Lai, "Andrographolide attenuates LPS-stimulated up-regulation of CC and CXC motif chemokines in rodent cortex and primary astrocytes," *Journal of Neuroinflammation*, vol. 13, no. 1, p. 34, 2016.

[118] J.-J. Chen, C.-W. Ting, Yi-C. Wu et al., "New labdane-type diterpenoids and anti-inflammatory constituents from Hedychium coronarium," *International Journal of Molecular Sciences*, vol. 14, no. 7, pp. 13063–13077, 2013.

[119] M. A. Callender and E. S. Antonarakis, "Rheumatoid arthritis masked by docetaxel chemotherapy in a patient with ovarian carcinoma," *Journal of Clinical Rheumatology: Practical Reports on Rheumatic & Musculoskeletal Diseases*, vol. 14, no. 2, p. 121, 2008.

[120] V. Lanzotti, "Diterpenes for therapeutic use," in *Natural Products*, pp. 3173–3191, Springer, Berlin, Germany, 2013.

Hindawi
Evidence-Based Complementary and Alternative Medicine
Volume 2022, Article ID 2252218, 8 pages
https://doi.org/10.1155/2022/2252218

Research Article

Electroacupuncture Pretreatment Exhibits Lung Protective and Anti-Inflammation Effects in Lipopolysaccharide-Induced Acute Lung Injury via SIRT1-Dependent Pathways

Dan Luo,[1,2] **Li Liu**,[3] **Hai-ming Zhang**,[2,4] **Yu-dian Zhou**,[2] **Min-feng Zhou**,[5] **Jin-xiao Li**,[5] **Zhao-min Yu**,[6] **Qian Tang**,[2] **Shu-rui Yang**,[2] **Rui Chen**,[5] **and Feng-xia Liang**[2]

[1]*Department of Respiratory, Wuhan No. 1 Hospital, Wuhan 430022, China*
[2]*Department of Acupuncture and Moxibustion, Hubei University of Traditional Chinese Medicine, Wuhan 430061, China*
[3]*Department of Pathology, Wuhan No. 1 Hospital, Wuhan 430022, China*
[4]*Department of Oncology, Integrated Traditional Chinese and Western Medicine, The Central Hospital of Wuhan, Tongji Medical College, Huazhong University of Science and Technology, Wuhan 430014, China*
[5]*Department of Integrated Traditional Chinese and Western Medicine, Union Hospital, Tongji Medical College, Huazhong University of Science and Technology, Wuhan 430022, China*
[6]*Department of Oncology, Hubei Province Hospital of Integrated Traditional Chinese and Western Medicine, Wuhan 430015, China*

Correspondence should be addressed to Rui Chen; unioncr@163.com and Feng-xia Liang; fxliang5@hotmail.com

Received 12 December 2021; Revised 15 February 2022; Accepted 25 February 2022; Published 15 March 2022

Academic Editor: Xiang Liu

To investigate the effect of electroacupuncture (EA) on acute lung injury (ALI), a lipopolysaccharide (LPS) induced ALI mouse model was used in this study. Before receiving intratracheal LPS instillation, mice were given EA at ST36 for 7 days as a long-term treatment or one time as a short-term treatment. Lung histopathological examination, lung injury scores, lung wet/dry (W/D) ratio, and inflammatory cytokines included proinflammation factors such as TNF-α, IL-1β, and IL-6 and anti-inflammation factors such as IL-4 and IL-10 in serum and bronchoalveolar lavage fluid (BALF) were detected at the end of experiment. The results show that EA pretreatment ameliorated the lung damage and inflammatory response by LPS. In addition, we found that SIRT1 and its deacetylation of NF-κB were promoted after EA pretreatment in lung tissues. Meanwhile, the expression of angiotensin-converting enzyme 2 (ACE2) is also enhanced by EA pretreatment. Thus, the present findings suggest that EA could be a potential therapy of ALI.

1. Introduction

Acute lung injury (ALI) and acute respiratory distress syndrome (ARDS) are critical diseases with high morbidity and mortality [1]. Clinical statistics show that sepsis is one of the most frequent risk factors for ALI and ARDS [2]. Specific pathogens including human coronaviruses (hCoVs) infection cause uncontrolled massive inflammatory activation which is also known as a cytokine storm resulting in ALI/ARDS [3,4]. Some specific inflammatory cytokines, for example, tumor necrosis factor α (TNF-α), interleukin (IL)-1β, and IL-6, have been identified as biomarkers for the diagnosis and prognosis of ALI/ARDS. Lipopolysaccharide (LPS) which is a major component in Gram-negative bacteria has been widely used to induce ALI/ARDS in animal models. A short exposure of LPS like inhalation will arouse an acute inflammatory response that leads to ALI [5].

Current research studies suggest that SIRT1 plays a major role in ALI [6]. Fu et al. study indicates that SIRT1 has a lung protective function. SIRT1 activator SRT1720 ameliorated LPS-induced ALI but SIRT1 inhibitor EX527 showed the exact opposite results [7]. Other studies found

that the function of SIRT1 on ALI is related to its regulation of inflammatory factor such as NF-IB [8] and TNF-α [9].

The potential of acupuncture to treat inflammatory diseases has been widely studied [10]. A systematic review has discussed whether acupuncture at ST36 might be useful to combat the injuries induced by sepsis [11]. In an ALI model by limb ischemia/reperfusion, electroacupuncture (EA) preconditioning at ST36 and SP6 reduces pulmonary inflammation via the TLR4/NF-κB pathway [12]. Manual acupuncture (MA) at ST36 before LPS instillation also mitigates ALI and pulmonary iNOS/NO expression [13]. Our previous studies have confirmed that EA could be recognized as a feasible sirt1 promoter to modulate inflammation [14]. In this study, we were trying to investigate the therapeutic effects of EA at ST36 on LPS-induced ALI in mice via SIRT1-dependent pathways.

2. Methods

2.1. Animals. 40 male C57BL/6 mice, 8 to 10 weeks old, were purchased from the Beijing Vitong Lihua Experimental Animal Technology Co., Ltd. They were housed in the SPF laboratory animal room. The animals were fed under specific pathogen-free conditions and given standard laboratory chow and water. All experiments involved in this study were approved by the Animal Experimental Committee of Tongji Medical College, Huazhong University of Science and Technology.

2.2. Experimental Design. Animals were randomly divided into four groups: control group ($n = 10$), LPS group ($n = 10$), LPS + EA short-term group (LPS + EA S) ($n = 10$), and LPS + EA long-term group (LPS + EA L) ($n = 10$). After one week of adaptive feeding, the LPS + EA long-term group received EA treatment, ten minutes at a time for seven days, and the LPS + EA short-term group received EA treatment for ten minutes one time before the LPS modeling. In order to simulate ALI, LPS (L2630, Sigma MO, USA) dissolved in 50 μL of sterile saline was given by intratracheal instillation at a dose of 5 mg/kg for 12 h [15]. The control group received no intervention during the experiment. The study protocol was shown in Figure 1.

2.3. EA Delivery. Similar to our previous studies [14], the animals were immobilized using special coats and their lower limbs were exposed. Needles were applied at bilateral ST36 with a depth of 1.5 mm [13]. Needles at bilateral ST36 were inserted into one output of an electrostimulator (LH202H, HANS Electronic Apparatus), using a continuous wave of 2 Hz, 1 mA for 10 min each time.

2.4. Lung Wet/Dry Weight (W/D) Ratio. To assess pulmonary edema, the wet weight (W) of lung tissue was measured immediately when the mice were killed. And the tissue will be heated at 80°C for 24 h to get the dry weight (D). This data were used to calculate the ratio of W/D weight [16].

2.5. Haematoxylin and Eosin (HE) Staining and Immunohistochemistry. Lung tissues were fixed for 24 h in 4% paraformaldehyde. The tissue embedded with paraffin was cut into 4 μm thick sections and part of the tissues were stained with haematoxylin and eosin. Other parts were incubated with monoclonal antibodies against SIRT1 (13161-1-AP, Proteintech, China) and angiotensin-converting enzyme 2 (ACE2) (ab108252, Abcam, United States) overnight at 4°C and then incubated with goat anti-rabbit secondary antibodies (Abcam, USA). 3,3′-diaminobenzidine is used as chromogen. The sections were then dyed using haematoxylin and mounted. The pathological changes of lung tissues and the expression of SIRT1 and ACE2 were observed by an optical microscope (Olympus).

2.6. Lung Injury Scores. Lung injury scores [17] were performed by pathologists, and the category is shown in Table 1.

2.7. Enzyme-Linked Immunosorbent Assay (ELISA). We employed ELISA kits (Meilian Biotechnology, Shanghai, China) to measure TNF-α, IL-1β, and IL-6 concentrations in the serum samples and bronchoalveolar lavage fluid (BALF) samples.

2.8. Western Blotting. Lung tissues were homogenized in radio immunoprecipitation assay (RIPA) lysis buffer. Next, it was centrifuged at 12,000 rpm for 15 min at 4°C to get protein in the supernatants. 10% SDS-PAGE gels were used to separate proteins and then electrophoretically transfer lysates onto PVDF membranes. Membranes were blocked for 1 h with 5% nonfat dry milk and then probed overnight at 4°C with primary antibodies against Sirt1 (13161-1-AP, Proteintech, China), NF-κB (10745-1-AP, Proteintech, China), ac–NF–κB (ab19870, Abcam, UK), and ACE2 (ab108252, Abcam, USA), and then further incubated with an appropriate HRP-conjugated secondary antibody (Proteintech, China) for 2 h at 37°C. The densities of the bands on the membranes were scanned and analyzed by chemiluminescence and quantified with ImageJ software (Rawak Software, Inc., Germany).

2.9. Real-Time Reverse Transcription-Polymerase Chain Reaction. Lung tissue for RNA extraction. The RevertAid First Strand cDNA Synthesis Kit (K1622, Fermentas) was used to reverse-transcribe total RNA into cDNA. The 7900HT real-time system (7900HT Sequence Detector, ABI PRISM) and the SYBR green PCR kit (DRR081 A, TAKARA) were used. The mRNA expression was then quantified by real-time quantitative PCR (RT-qPCR). The $2^{-\Delta\Delta}$Ct method was used to express the gene expression. Specific primers used for PCR are listed in Table 2.

2.10. Statistical Analysis. The data in this work are presented as the mean ± standard. Differences between groups were analyzed by GraphPad Prism 7 software (La Jolla, CA, USA) with one-way analysis of variance (ANOVA) and the student

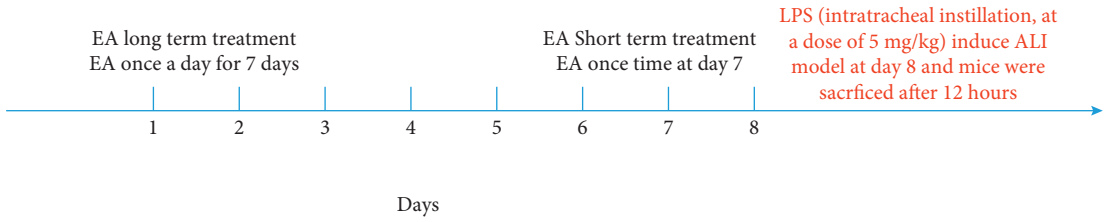

Figure 1: Study protocol.

Table 1: Lung injury score.

Item	Score
Hyperemia	0 minimal damage to 4 maximal damage
Atelectasis	0 minimal damage to 4 maximal damage
Neutrophil infiltration	0 minimal damage to 4 maximal damage
Intraalveolar edema	0 absent to 1 present
Total	0 minimal damage to 13 maximal damage

Table 2: The primer sequences for SIRT1 and ACE2.

SIRT1	Fw 5′-ACGCCTTATCCTCTAGTTCCTGTG-3′
	Rw 5′-CGGTCTGTCAGCATCATCTTCC-3′
ACE2	Fw 5′-TCTGCCACCCCACAGCTT-3′
	Rw 5′-GGCTGTCAAGAAGTTGTCCATTG-3′
Actin	Fw 5′-CTATCGGCAATGAGCGGTTCC-3′
	Rw 5′-TGTGTTGGCATAGAGGTCTTTACG-3′

Newman–Keuls test. A P value of less than 0.05 was considered statistically significant.

3. Results

3.1. EA Pretreatment Alleviated Lung Tissue Damage in LPS-Induced ALI. Pulmonary edema, epithelial and endothelial cell structure damage, inflammatory cell infiltration, and alveolar hemorrhage were observed in mice after intratracheal LPS instillation (Figure 2(a)). LPS significantly increase the lung injury score and lung W/D ratio in both LPS, the LPS + EA short-term group and the LPS + EA long term group. In the LPS + EA long-term group, pathological changes including lung injury score and lung W/D ratio were attenuated compared to those in the LPS group. Although the lung injury score and lung W/D ratio in the LPS + EA short-term group were decreased compared to the LSP group, the difference was not statistically significant (Figures 2(b) and 2(c)).

3.2. EA Pretreatment Attenuated Inflammatory Response in BALF and Serum in LPS-Induced ALI. TNF-α, IL-1β, IL-4, IL-6, and IL-10 were detected in BALF and serum in both groups. After given LPS, it is observed that TNF-α, IL-1β, and IL-6 significantly enhanced. Both EA long-term and short-term pretreatment restrain the inflammatory response promoted by LPS, whereas EA short-term pretreatment has no significant effect on IL-1β and IL-4 in BALF (Figure 3).

3.3. EA Pretreatment Promoted SIRT1 Expression and Reduced the Activation of NF-κB in Lung Tissues in LPS-Induced ALI. The expression of SIRT1 in both groups was tested with immunohistochemistry (Figure 4(a)), western blot (Figures 4(b) and 4(c)), and Rt-PCR (Figure 4(d)). Both EA long-term and short-term pretreatment reversed the inhibition of SIRT1 expression in lung tissues by LPS. Our previous study showed that SIRT1 can regulate the activation of NF-κB through deacetylation. In this study, the levels of both NF-κB (Figures 4(e) and 4(f)) and ac–NF–κB (Figure 4(g) and 4(h)) increased after exposure to LPS. EA long-term pretreatment reversed this progress, but this effect was not repeated in EA short-term pretreatment.

3.4. EA Pretreatment Enhanced ACE2 Expression in Lung Tissues in LP-Induced ALI. ACE2 is confirmed to have a lung protective effect in ALI/ARDS [18]. To better clarify the protective effect of EA, the expression of ACE2 in each group was analyzed by immunohistochemistry (Figure 5(a)), western blot (Figures 5(b) and 5(c)), and Rt-PCR (Figure 5(d)). In ALI produced by LPS, the level of ACE2 is significantly inhibited. Both long-term and short-term EA pretreatment showed enhancement of ACE2 expression.

4. Discussion

In the present study, based on the LPS-induced ALI mouse model, we found that EA pre-treatment presented a lung protective effect. Lung and systemic inflammatory responses aroused by LPS were suppressed by EA. Compared with the EA short-term group, EA pretreatment at ST36 for 7 days is more effective in lung protection and anti-inflammation. The underlying mechanism of EA involves activating SIRT1 and promoting the deacetylation effect of SIRT1 to regulate NF-κB. Meanwhile, the expression of ACE2 is also enhanced after EA pretreatment.

Despite significant advances in management of patients and our understanding of ALI/ARDS during the past decades, the morbidity and mortality from ALI/ARDS remains high [19]. In the pathogenesis of ALI/ARDS [20], the integrity of the capillary endothelium and alveolar epithelium was closed, which enhances edema in lung tissues and forms hyaline membranes. Activated neutrophils and macrophages secrete proinflammatory cytokines such as IL-1, IL-6, and TNF-α. This inflammatory process will destroy the integrity of lung tissue and increase edema.

It is widely accepted that acupuncture could be effective against inflammation in different diseases [21]. Liu et al.

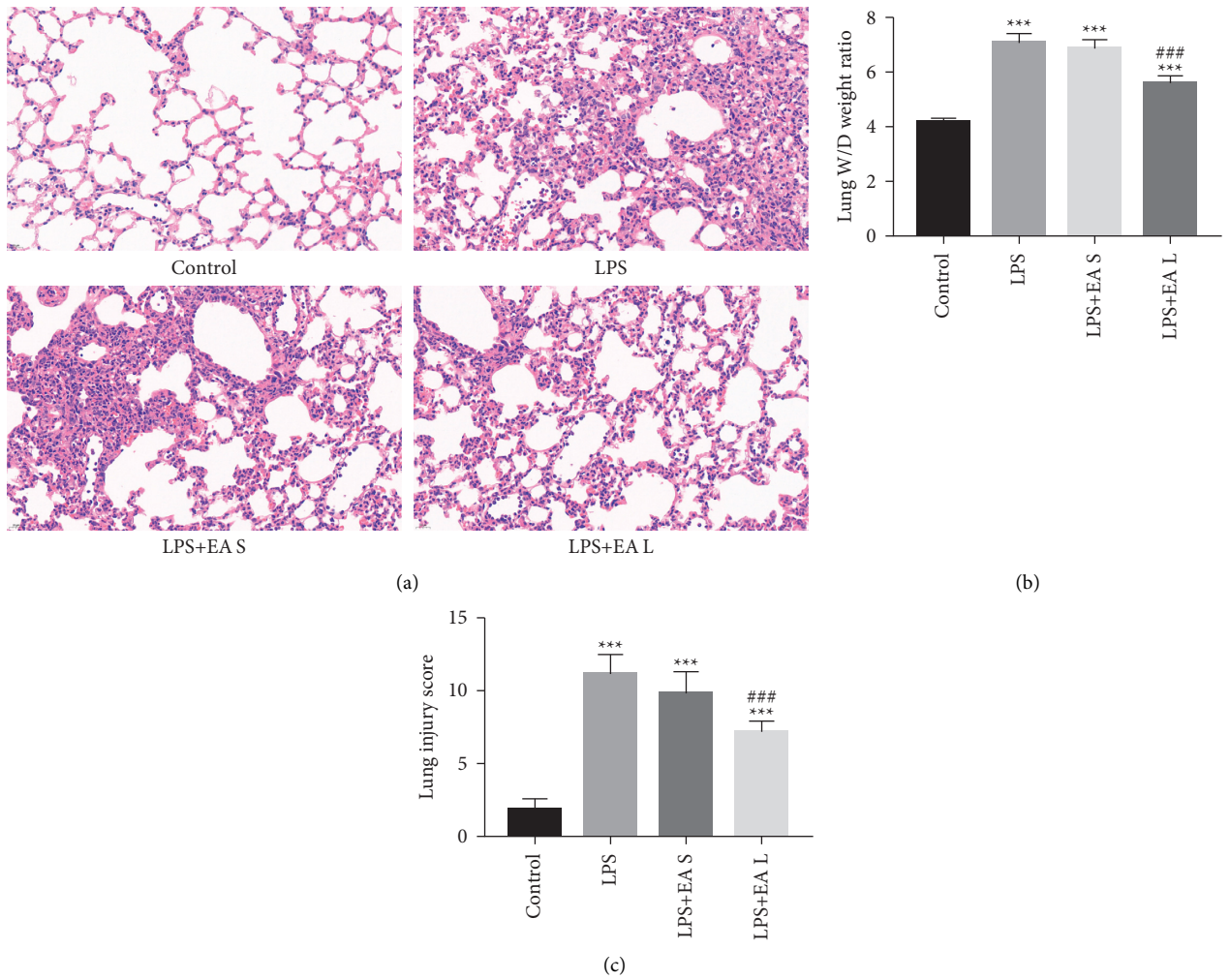

FIGURE 2: EA pretreatment alleviated lung tissue damage in LPS-induced ALI. (a) H&E staining (40×) of different groups. (b) Lung W/D ratios of different groups. (c) Lung injury score of different groups. The data are presented as the mean ± SEM. $^{***}P < 0.001$ versus control group and $^{###}P < 0.001$ versus LPS group.

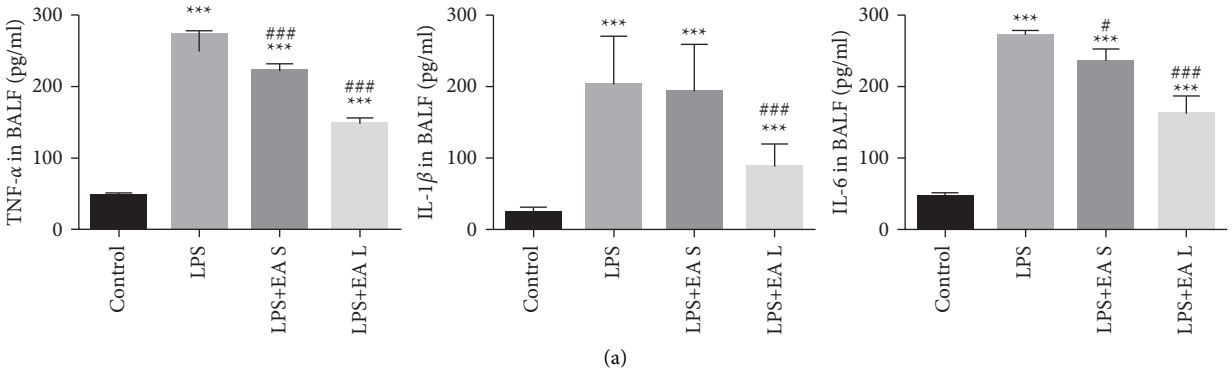

FIGURE 3: Continued.

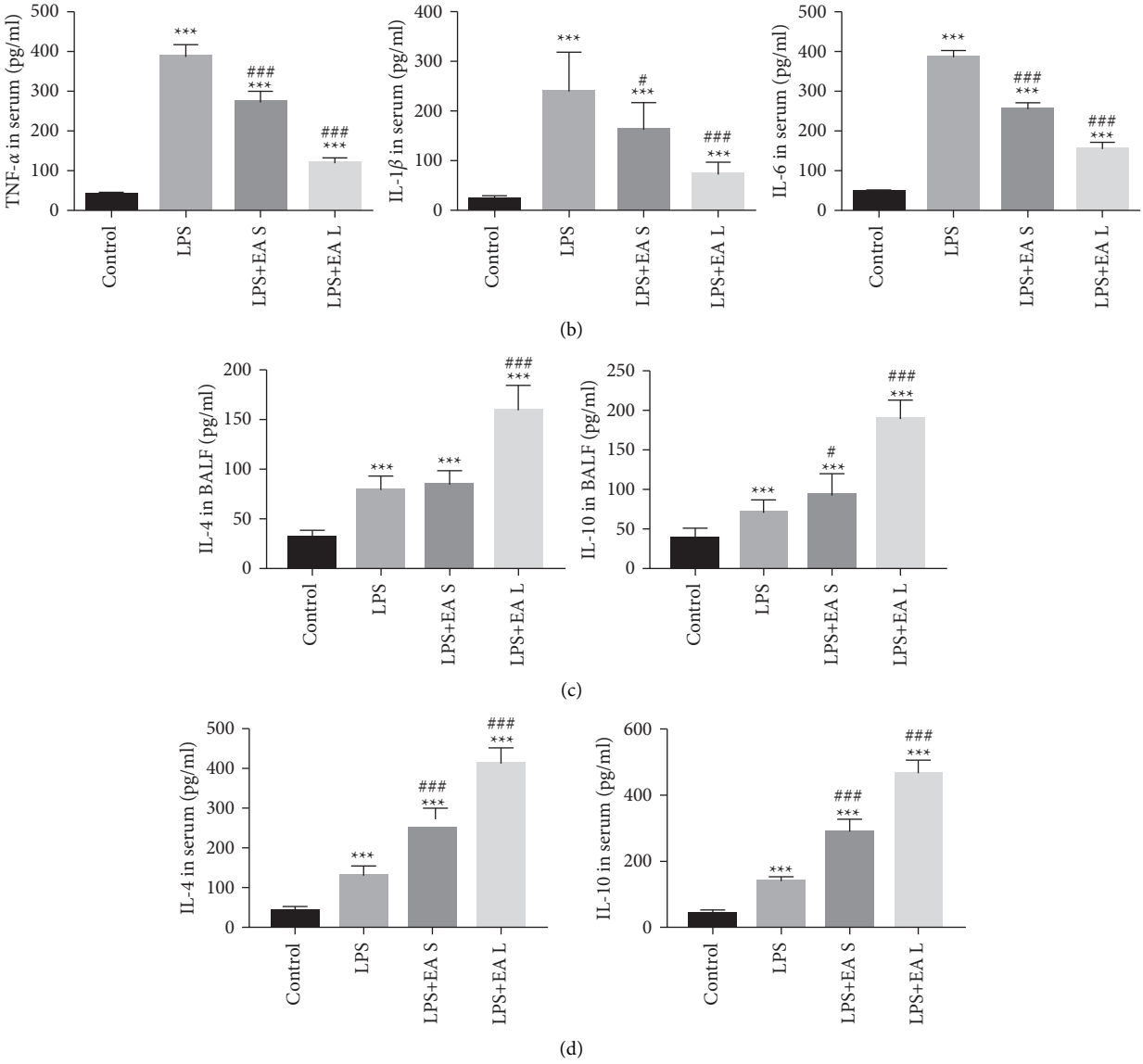

Figure 3: EA pretreatment attenuated inflammatory response in BALF and serum in LPS-induced ALI. (a) Proinflammatory cytokines in BALF. (b) Proinflammatory cytokines in serum. (c) Anti-inflammatory cytokines in BALF. (d) Anti-inflammatory cytokines in serum. The data are presented as the mean ± SEM. $^{***}P < 0.001$ versus control group and $^{\#}P < 0.05$ and $^{\#\#\#}P < 0.001$ versus LPS group.

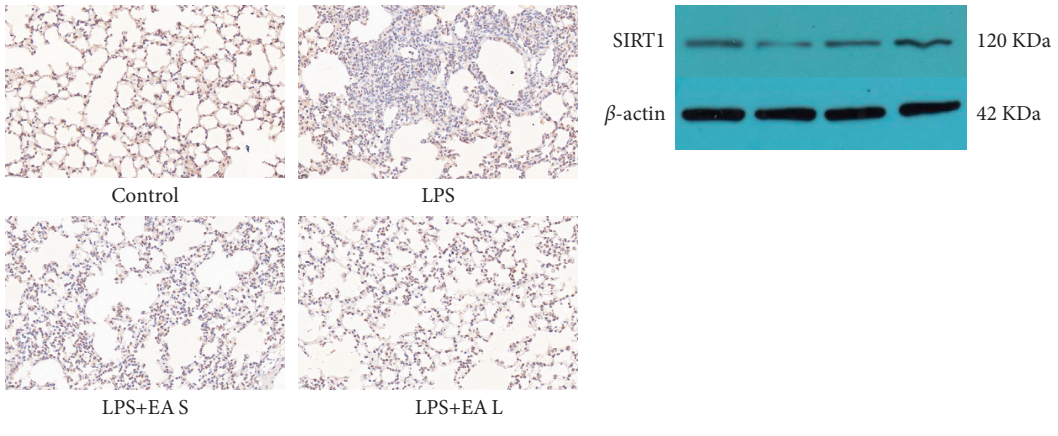

Figure 4: Continued.

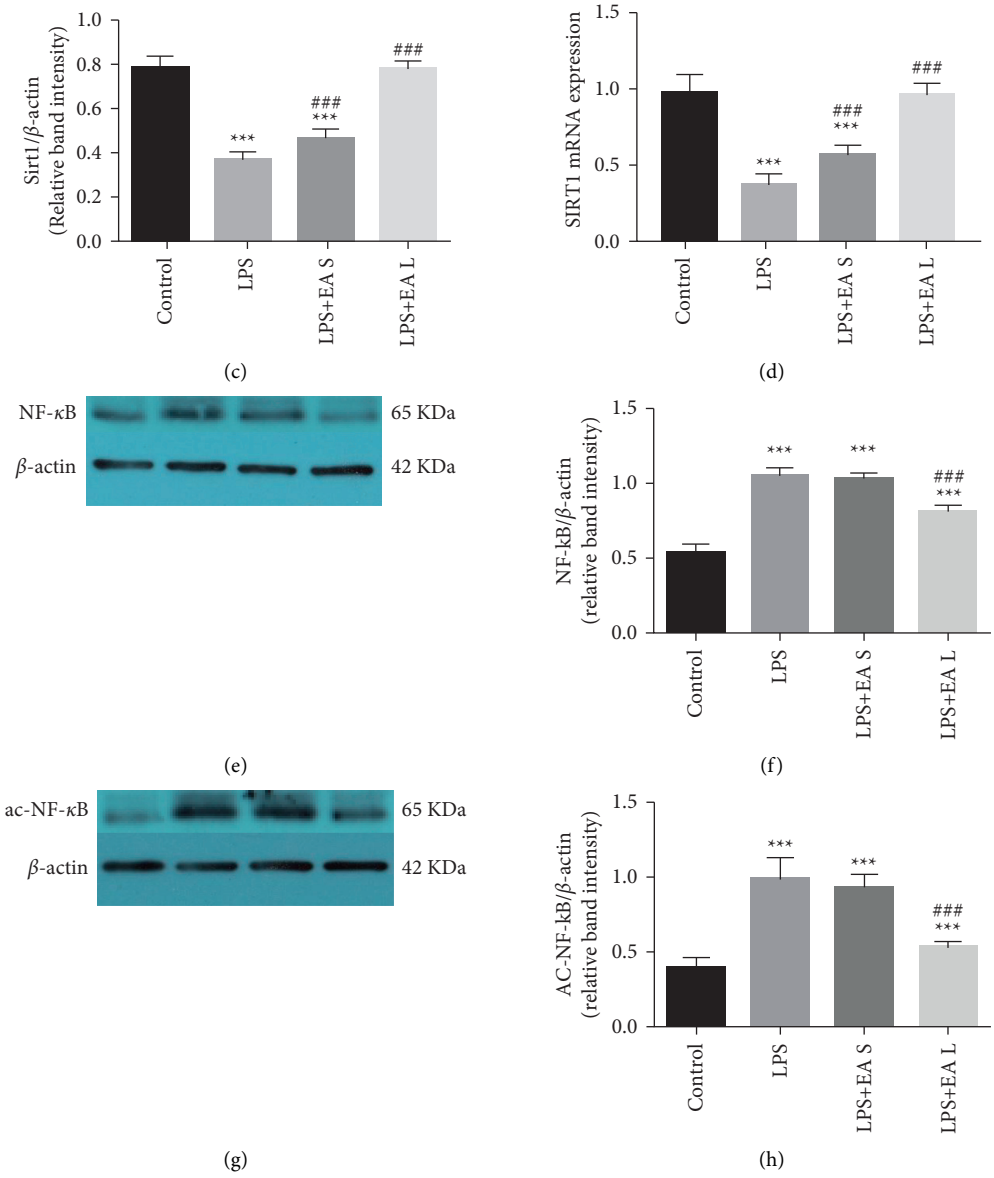

Figure 4: EA pretreatment promoted SIRT1 expression and reduced the activation of NF-κB in lung tissues in LPS-induced ALI. (a) Immunohistochemistry analysis for SIRT1 in mouse lung tissues. (40×) (b–d) Western blot and Rt-PCR analysis for SIRT1 expression. Western blot analysis for NF-κB (e, f) and ac–NF–κB (g, h) expression. The data are presented as the mean ± SEM. $^{***}P < 0.001$ versus control group and $^{\#}P < 0.05$ and $^{\#\#\#}P < 0.001$ versus LPS group.

performed a series of studies about EA in an LPS-induced systemic inflammation mouse model. EA-evoked activation of NPY-expressing sympathetic pathways could present a quick and effective anti-inflammatory action [22]. The effect of EA at different acupoints in suppressing severe systemic inflammation could be attributed to different autonomic nervous systems [23].

There is a strong relationship between SIRT1 and pulmonary epithelial barrier dysfunction. In LPS-induced rats, upregulated expression of SIRT1 could significantly downregulate the expression of NF-κB, TNF-α, MCP-1, IL-1β, MCP-1, and against cell apoptosis [24]. SIRT1 also plays a great role in maintaining the vascular integrity during ALI [7]. Hence, drugs target SIRT1 is believed to a novel therapeutic in patients with acute lung injury [8].

Increasing ACE2 activity has been recognized as a feasible approach for the treatment of ALI in the past decades [25]. ACE2 is a monocarboxypeptidase that plays an important role in maintaining the dynamic balance of the renin-angiotensin system (RAS) which attenuates immunity, inflammation, and other physiological activities [26]. There is evidence showing that SIRT1 is bound to the ACE2 promoter to enhance the expression of ACE2 under conditions of energy stress [27]. More than that, ACE2 could also prevent AT II cells from inflammatory damage via activating the SIRT1-related pathways [28].

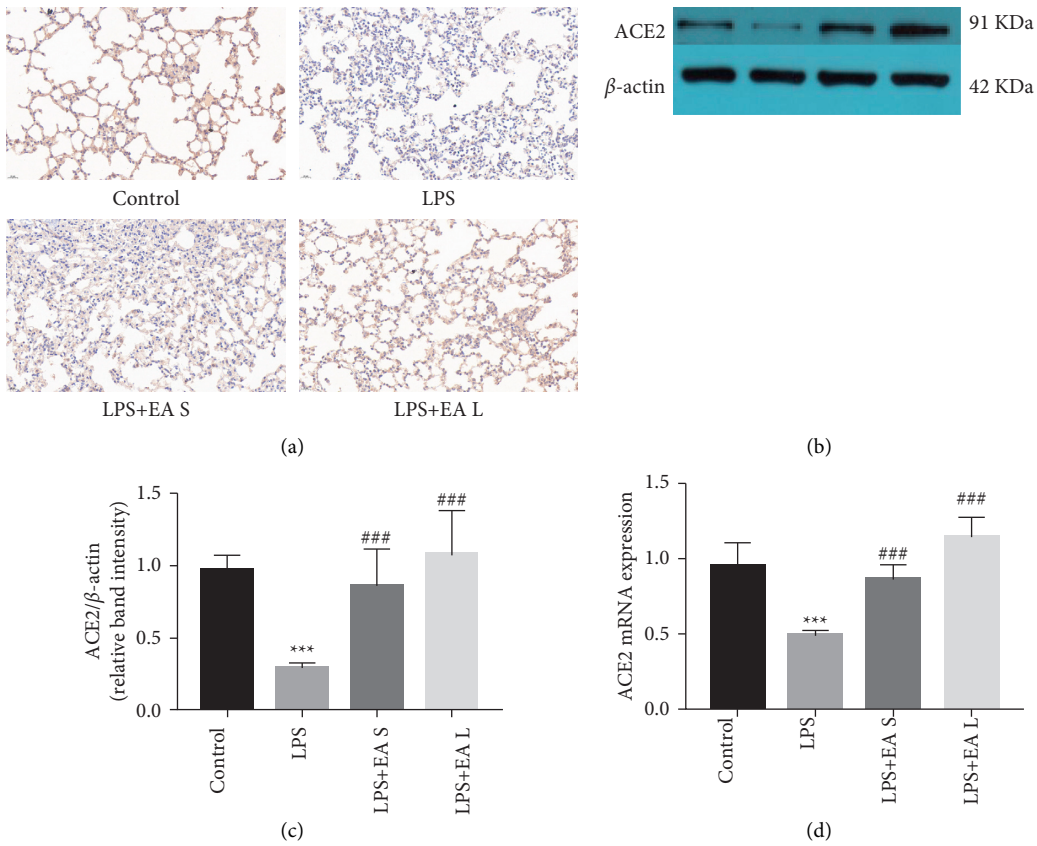

FIGURE 5: EA pretreatment enhanced ACE2 expression in lung tissues in LPS-induced ALI. (a) Immunohistochemistry analysis for ACE2 in mouse lung tissues (40×). (b–d) Western blot and Rt-PCR analysis for ACE2 expression. The data are presented as the mean ± SEM. $^{***}P < 0.001$ versus control group and $^{###}P < 0.001$ versus LPS group.

5. Conclusion

In conclusion, our results showed that EA pretreatment exhibited lung protective and anti-inflammation effects in the LPS-induced ALI mouse model. The mechanisms were based on the regulation of inflammation factors through SIRT1-related pathways. Meanwhile, ACE2 may also play a key role in this progress. All the evidence supports that EA is a potential therapy to ameliorate ALI/ARDS.

Data Availability

The data used to support the findings of this study are available from the corresponding author upon request.

Conflicts of Interest

The authors declare no conflicts of interest.

Authors' Contributions

Dan Luo, Li Liu, and Hai-ming Zhang contributed equally to this work.

Acknowledgments

This research was supported by the National Natural Science Foundation of China (No.81774420, No. 81774401, and No. 82105009), Traditional Chinese Medicine Scientific Research Project of Hubei Provincial Health Commission (ZY2021Q031), and Wuhan Medical Research Project (WX19Y18).

References

[1] I. Vadász and J. I. Sznajder, "Update in acute lung injury and critical care 2010," *American Journal of Respiratory and Critical Care Medicine*, vol. 183, no. 9, pp. 1147–1152, 2011.

[2] V. Kumar, "Pulmonary innate immune response determines the outcome of inflammation during pneumonia and sepsis-associated acute lung injury," *Frontiers in Immunology*, vol. 11, p. 1722, 2020.

[3] Y. Butt, A. Kurdowska, and T. C. Allen, "Acute lung injury: a clinical and molecular review," *Archives of Pathology & Laboratory Medicine*, vol. 140, no. 4, pp. 345–350, 2016.

[4] D. Mokra and P. Kosutova, "Biomarkers in acute lung injury," *Respiratory Physiology & Neurobiology*, vol. 209, pp. 52–58, 2015.

[5] H. Chen, C. Bai, and X. Wang, "The value of the lipopolysaccharide-induced acute lung injury model in respiratory medicine," *Expert Review of Respiratory Medicine*, vol. 4, no. 6, pp. 773–783, 2010.

[6] Y. Liu, H. Guan, J.-L. Zhang et al., "Acute downregulation of miR-199a attenuates sepsis-induced acute lung injury by targeting SIRT1," *American Journal of Physiology - Cell Physiology*, vol. 314, no. 4, pp. C449–C455, 2018.

[7] C. Fu, S. Hao, X. Xu et al., "Activation of SIRT1 ameliorates LPS-induced lung injury in mice via decreasing endothelial tight junction permeability," *Acta Pharmacologica Sinica*, vol. 40, no. 5, pp. 630–641, 2019.

[8] J. Ye, M. Guan, Y. Lu, D. Zhang, C. Li, and C. Zhou, "Arbutin attenuates LPS-induced lung injury via Sirt1/Nrf2/NF-κBp65 pathway," *Pulmonary Pharmacology & Therapeutics*, vol. 54, pp. 53–59, 2019.

[9] T.-H. Chen and J.-J. Wang, "Niacin pretreatment attenuates ischemia and reperfusion of pancreas-induced acute pancreatitis and remote lung injury through suppressing oxidative stress and inflammation and activation of SIRT1," *Transplantation Proceedings*, vol. 50, no. 9, pp. 2860–2863, 2018.

[10] D. Luo, L. Liu, Q. Huang et al., "Crosstalk between acupuncture and NF-κB in inflammatory diseases," *Evid Based Complement Alternat Medicine*, vol. 2020, Article ID 7924985, 7 pages, 2020.

[11] F. Lai, Y. Ren, C. Lai et al., "Acupuncture at zusanli (ST36) for experimental sepsis: a systematic review," *Evidence-Based Complementary and Alternative Medicine: eCAM*, vol. 2020, Article ID 3620741, 16 pages, 2020.

[12] Y. Lou, Q. Yu, K. Xu et al., "Electroacupuncture preconditioning protects from lung injury induced by limb ischemia/reperfusion through TLR4 and NF-κB in rats," *Molecular Medicine Reports*, vol. 22, no. 4, pp. 3225–3232, 2020.

[13] C.-L. Huang, C.-J. Huang, P.-S. Tsai, L.-P. Yan, and H.-Z. Xu, "Acupuncture stimulation of ST-36 (Zusanli) significantly mitigates acute lung injury in lipopolysaccharide-stimulated rats," *Acta Anaesthesiologica Scandinavica*, vol. 50, no. 6, pp. 722–730, 2006.

[14] D. Luo, L. Liu, F. X. Liang, Z. M. Yu, and R. Chen, "Electroacupuncture: a feasible Sirt1 promoter which modulates metainflammation in diet-induced obesity rats," *Evidence-Based Complementary and Alternative Medicine: eCAM*, vol. 2018, Article ID 5302049, 10 pages, 2018.

[15] L. Ning, W. Wei, J. Wenyang, X. Rui, and G. Qing, "Cytosolic DNA-STING-NLRP3 axis is involved in murine acute lung injury induced by lipopolysaccharide," *Clinical and Translational Medicine*, vol. 10, no. 7, p. e228, 2020.

[16] T. Li, G. Xiao, S. Tan et al., "HSF1 attenuates LPS-induced acute lung injury in mice by suppressing macrophage infiltration," *Oxidative Medicine and Cellular Longevity*, vol. 2020, Article ID 1936580, 15 pages, 2020.

[17] C.-M. Chen, L.-F. Wang, B. Su, and H.-H. Hsu, "Methylprednisolone effects on oxygenation and histology in a rat model of acute lung injury," *Pulmonary Pharmacology & Therapeutics*, vol. 16, no. 4, pp. 215–220, 2003.

[18] Y. Imai, K. Kuba, T. Ohto-Nakanishi, and J. M. Penninger, "Angiotensin-converting enzyme 2 (ACE2) in disease pathogenesis," *Circulation Journal*, vol. 74, no. 3, pp. 405–410, 2010.

[19] H. Yadav, B. T. Thompson, and O. Gajic, "Fifty years of research inARDS. Is acute respiratory distress syndrome a preventable disease?" *American Journal of Respiratory and Critical Care Medicine*, vol. 195, no. 6, pp. 725–736, 2017.

[20] N. T. Mowery, W. T. H. Terzian, and A. C. Nelson, "Acute lung injury," *Current Problems in Surgery*, vol. 57, no. 5, Article ID 100777, 2020.

[21] H. Bai, S. Xu, Q. Wu et al., "Clinical events associated with acupuncture intervention for the treatment of chronic inflammation associated disorders," *Mediators of Inflammation*, vol. 2020, Article ID 2675785, 10 pages, 2020.

[22] S. Liu, Z.-F. Wang, Y.-S. Su et al., "Somatotopic organization and intensity dependence in driving distinct NPY-expressing sympathetic pathways by electroacupuncture," *Neuron*, vol. 108, no. 3, pp. 436–450, 2020.

[23] S. Liu, Z. Wang, Y. Su et al., "A neuroanatomical basis for electroacupuncture to drive the vagal-adrenal axis," *Nature*, vol. 598, no. 7882, pp. 641–645, 2021.

[24] X. Li, M. Jamal, P. Guo et al., "Irisin alleviates pulmonary epithelial barrier dysfunction in sepsis-induced acute lung injury via activation of AMPK/SIRT1 pathways," *Biomedicine & Pharmacotherapy*, vol. 118, Article ID 109363, 2019.

[25] K. Kuba, Y. Imai, and J. M. Penninger, "Angiotensin-converting enzyme 2 in lung diseases," *Current Opinion in Pharmacology*, vol. 6, no. 3, pp. 271–276, 2006.

[26] R. Ye and Z. Liu, "ACE2 exhibits protective effects against LPS-induced acute lung injury in mice by inhibiting the LPS-TLR4 pathway," *Experimental and Molecular Pathology*, vol. 113, Article ID 104350, 2020.

[27] N. E. Clarke, N. D. Belyaev, D. W. Lambert, and A. J. Turner, "Epigenetic regulation of angiotensin-converting enzyme 2 (ACE2) by SIRT1 under conditions of cell energy stress," *Clinical Science*, vol. 126, no. 7, pp. 507–516, 2014.

[28] H. Xu and J. Xiao, "ACE2 promotes the Synthesis of pulmonary surfactant to improve at II cell injury via SIRT1/eNOS pathway," *Computational and Mathematical Methods in Medicine*, vol. 2021, Article ID 7710129, 11 pages, 2021.

Hindawi
Evidence-Based Complementary and Alternative Medicine
Volume 2022, Article ID 6741995, 12 pages
https://doi.org/10.1155/2022/6741995

Research Article

Research on the Mechanism of Kaempferol for Treating Senile Osteoporosis by Network Pharmacology and Molecular Docking

Fuyu Tang,[1,2] Peng Zhang,[1,3] Wenhua Zhao,[1,3] Guangye Zhu,[1] Gengyang Shen,[4] Honglin Chen,[1,3,4] Xiang Yu,[4] Zhida Zhang,[4] Qi Shang,[1,3] De Liang,[4] Xiaobing Jiang,[3,4] and Hui Ren[3,4]

[1]*Guangzhou University of Chinese Medicine, Guangzhou 510405, China*
[2]*Liuzhou Hospital of Chinese Medicine (Liuzhou Hospital of Zhuang Medicine), Guangxi Zhuang Autonomous Region, Liuzhou, 545000, China*
[3]*Lingnan Medical Research Center of Guangzhou University of Chinese Medicine, Guangzhou 510405, China*
[4]*The First Affiliated Hospital of Guangzhou University of Chinese Medicine, Guangzhou 510405, China*

Correspondence should be addressed to Xiaobing Jiang; spinedrjxb@sina.com and Hui Ren; renhuispine@163.com

Received 9 December 2021; Accepted 8 January 2022; Published 3 February 2022

Academic Editor: Xiang Liu

Kaempferol (KP), as a natural anti-inflammatory compound, has been reported to have curative effects on alleviating senile osteoporosis (SOP), which is an inflammation-related musculoskeletal disease, but the molecular mechanisms remain unclear due to scanty relevant studies. We predicted the targets of KP and SOP, and the common targets of them were subsequently used to carry out PPI analysis. Moreover, we adopted GO and KEGG enrichment analysis and molecular docking to explore potential mechanisms of KP against SOP. There were totally 152 KP-related targets and 978 SOP-related targets, and their overlapped targets comprised 68 intersection targets. GO enrichment analysis showed 1529 biological processes ($p < 0.05$), which involved regulation of inflammatory response, oxidative stress, regulation of bone resorption and remodeling, osteoblast and osteoclast differentiation, etc. Moreover, KEGG analysis revealed 146 items including 44 signaling pathways ($p < 0.05$), which were closely linked to TNF, IL-17, NF-kappa B, PI3K-Akt, MAPK, estrogen, p53, prolactin, VEGF, and HIF-1 signaling pathways. By means of molecular docking, we found that kaempferol is bound with the key targets' active pockets through some connections such as hydrogen bond, pi-alkyl, pi-sigma, pi-pi Stacked, pi-pi T-shaped, and van der Waals, illustrating that kaempferol has close combination with the key targets. Collectively, various targets and pathways involve in the process of kaempferol treatment against SOP through regulating inflammatory response, oxidative stress, bone homeostasis, etc. Moreover, our study first reported that kaempferol may regulate core targets' expression with involvement of inflammatory response, oxidative stress, and bone homeostasis, thus treating SOP.

1. Introduction

Senile osteoporosis (SOP) is an inflammation-related musculoskeletal disease with serious complications including spine deformation, osteoporotic fracture, and bone pain [1, 2]. Osteoporotic vertebral fracture (OVF) is the worst-affected complication in SOP patients with about 1.8 million vertebral fractures estimated happening every year in China, and the number of vertebral fractures is predicted to increase to 3 million in 2050 [3]. SOP poses serious threats to senior citizens' life and health, which adds to social and family burdens. The treatment of SOP involves the use of drugs inhibiting bone resumption clinically, but long-term use of these drugs can result in some complications, which limit their clinical application [4]. Recently, more and more scholars attach increasing attention to the osteoprotective effect of traditional Chinese medicine on treating SOP [5].

Kaempferol (KP, PubChem CID: 5280863) is a flavonoid identified in various natural products and traditional Chinese medicine like *Drynariae Rhizoma* [6]. KP has been

reported to have the curative effect of treating SOP by acting on both osteoblasts and osteoclasts, which may exert osteogenic and antiosteoclastic effects [7]. The current study has illustrated that KP could influence adipogenesis [8], inflammation [9], oxidative stress [10], osteoblastic apoptosis [11], and osteoclastic apoptosis [12], resulting in osteoprotective effects. Therefore, KP could serve as a complementary and alternative medicine with a good prospect for clinical application on treating SOP.

In our prevent study, we performed bioinformatics analysis including network pharmacology and molecular docking so as to carry out systematic analysis on numerous pathways and targets involved in the function of KP on treating SOP.

2. Materials and Methods

Figure 1 describes the flow chart of study design.

2.1. Obtaining KP-Related Structure and Targets. We obtained the KP-related structure and targets through the following steps: first, we conducted data retrieval on the TCMSP database (https://tcmsp-e.com/) [13], which provides comprehensive information of KP including its structure and target information; second, by searching the PubChem database (https://pubchem.ncbi.nlm.nih.gov/), the KP structure was stored as an "SDF" file, which was imported into the SwissTargetPrediction database (http://new.swisstargetprediction.ch/) [14] to get the targets associated with KP; and third, we adopted the UniProt database (http://www.uniprot.org/uniprot/) to standardize the KP-related target proteins with "popular organisms" limited to humans, which were described as gene symbols.

2.2. SOP-Related Genes and Corresponding Proteins. The key word "Senile Osteoporosis" was searched in the two databases, including GeneCards (https://www.genecards.org/) [15] and Online Mendelian Inheritance in Man (OMIM, https://omim.org/) [16], with the species set as "*Homo sapiens*." The UniProt database was adopted to standardize the corresponding proteins of SOP-related genes.

2.3. Overlapped Target Proteins (OTPs). R (v3.6.1) software was used to take the overlap of KP- and SOP-related target proteins to get OTPs.

2.4. Protein Interaction Analysis of OTPs. The STRING database (https://string-db.org/) [17] was retrieved to get the protein-protein interaction (PPI) data of OTPs. Next, the PPI information of OTPs was input into Cytoscape (v3.7.2) software (https://www.cytoscape.org/) [18] to construct the PPI network and calculate the degrees of targets in the network through network topology analysis. We determined the target proteins with degree above average to be core target proteins. Afterwards, we generated a KP-OTPs-SOP network via Cytoscape.

2.5. GO Enrichment Analysis and KEGG Pathway Analysis. We conducted GO and KEGG analysis of the overlapped targets by means of clusterProfiler package (R3.6.1) and extracted the enrichment results with $p < 0.05$.

2.6. Molecular Docking between Key Targets and KP. The top 5 proteins in terms of degree were chosen for molecular docking, which were considered the key targets in the process of KP treating SOP. In order to explore interaction activity between KP and its key targets, we utilized AutoDock Vina (v1.1.2) software [19] to carry out molecular docking simulations. We searched the PubChem database (https://pubchem.ncbi.nlm.nih.gov/) for the 3D structure of KP. We used AutoDock Tools (v1.5.6) to distribute charge and combine nonpolar hydrogen for KP and converted the results into a PDBQT file. We downloaded the crystal structures of target proteins from the RCSB PDB website (https://www.rcsb.org/). Then, the target protein was separated from its ligand, added polar hydrogen, and distributed charge via AutoDock Tools, which would be subsequently stored as a PDBQT file. AutoDock Tools were also utilized to calculate the center and size of the docking box. Molecular docking simulations among KP and the target proteins were performed with every affinity calculated. Afterwards, Discovery Studio (https://www.3ds.com/products-services/biovia/products/molecular-modeling-simulation/biovia-discovery-studio/) was used to draw and analyze the docking results of KP.

3. Results

3.1. KP-Related Structure and Target Proteins. From TCMSP and SwissTargetPrediction databases, we got 152 targets of KP. With them imported into the UniProt database, we obtained KP-related target proteins called gene symbols. Supplementary Tables S1 and S2 show the KP-related structure and target information.

3.2. Target Information of SOP and Overlapped Target Proteins (OTPs). Through the retrieval of GeneCards and OMIM databases, we obtained a total of 978 target proteins of SOP. We took the overlap of KP- and SOP-related targets as OTPs, which included 68 overlapped targets, as demonstrated in Table 1 and Figure 2(a).

3.3. PPI Network Construction and Core Target Protein Screening. OTPs were imported into the STRING database with the targets having no interactive connections with others hidden. And then we imported the PPI data into Cytoscape (v 3.7.2) to draw PPI network in Figure 2(b). There were 28 target proteins predicted to be the core target proteins (Table 2), whose degrees were above average degree (20.59).

3.4. KP-OTPs-SOP Network Plotting. Figure 2(c) shows the KP-OTPs-SOP network with 70 nodes and 136 edges included. In Figure 2(c), the red circular nodes stand for the overlapped target proteins (OTPs). The orange diamond node stands for "kaempferol." The yellow round rectangle

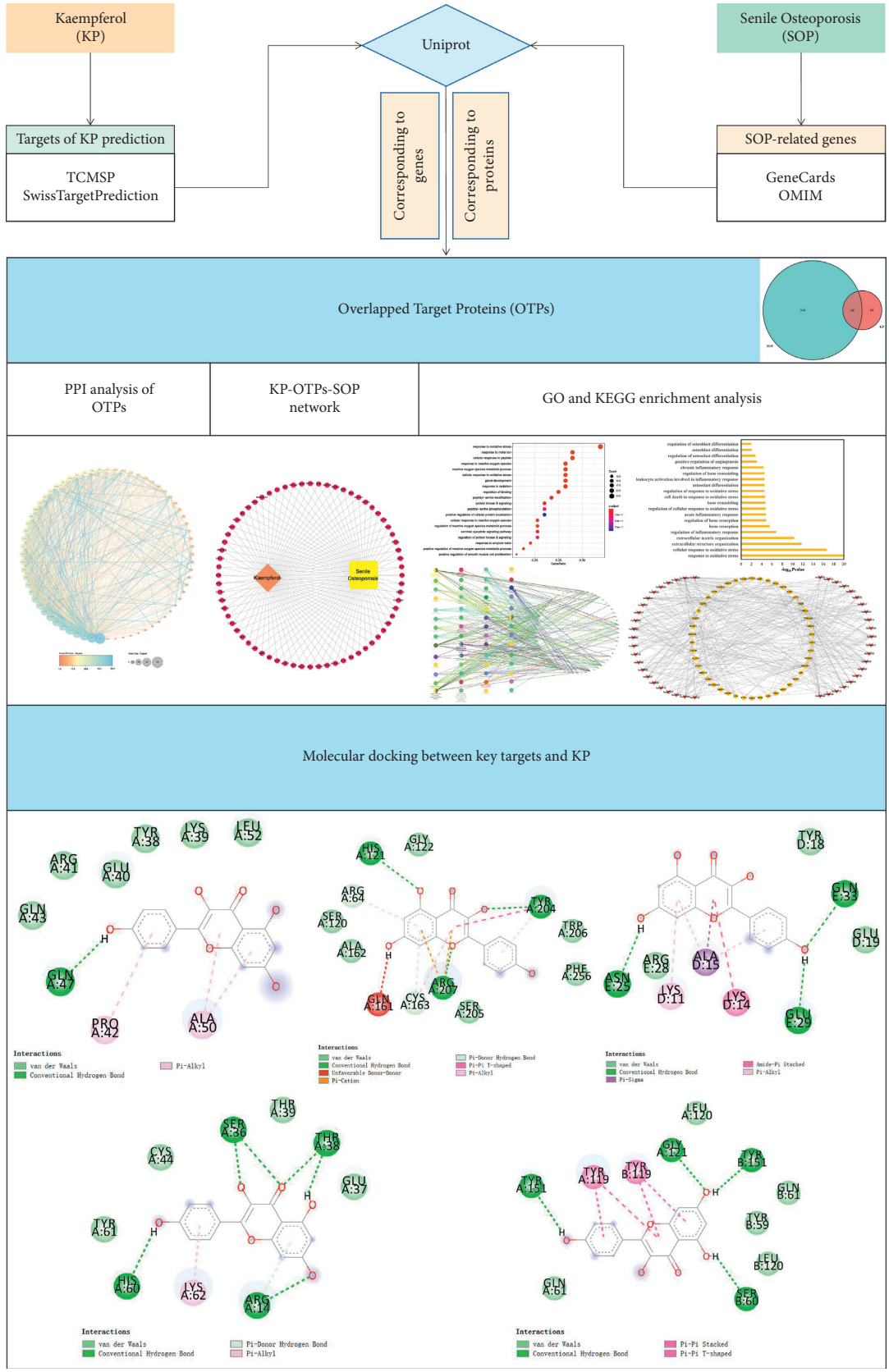

Figure 1: The flowchart of this study.

Table 1: Potential target genes of KP in the treatment of SOP.

Number	Gene
1	NOS2
2	PTGS1
3	AR
4	PPARG
5	PTGS2
6	HSP90AA1
7	PIK3CG
8	PRKACA
9	DPP4
10	PGR
11	F2
12	NOS3
13	RELA
14	AKT1
15	BCL2
16	BAX
17	TNF
18	JUN
19	CASP3
20	MAPK8
21	XDH
22	MMP1
23	STAT1
24	HMOX1
25	CYP3A4
26	CYP1A1
27	ICAM1
28	VCAM1
29	ALOX5
30	AHR
31	INSR
32	GSTM1
33	SLPI
34	NOX4
35	AKR1B1
36	TYR
37	CA2
38	ABCB1
39	GLO1
40	SYK
41	GSK3B
42	MMP9
43	MMP2
44	CDK5
45	CCNB1
46	ESR2
47	TTR
48	CYP19A1
49	EGFR
50	IGF1R
51	MPO
52	PIK3R1
53	CA1
54	SRC
55	PTK2
56	KDR
57	MMP13
58	MMP3
59	MET
60	BACE1
61	AKR1A1
62	APP
63	PARP1
64	MMP12
65	ESR1
66	CFTR
67	TERT
68	MAPT

node stands for "senile osteoporosis." The edges stand for the interactive relationships among kaempferol, senile osteoporosis, and the overlapped targets.

3.5. GO Enrichment Analysis. We got 1529 items of biological process (BP). The top 20 items are shown in Figure 3(a). Noteworthily, we have filtrated 20 entries mainly related to inflammatory response, oxidative stress, angiogenesis, bone remodeling and resorption, and osteoblast and osteoclast differentiation, which have a close association with bone homeostasis as demonstrated in Figure 3(b). Additionally, we input 68 OTPs into Cytoscape for GO.BP enrichment analysis with p value set to 0.00001. Figure 3(c) illustrates the enrichment results mainly involved in the following four aspects: (i) inflammation-associated activities, such as regulation of reactive oxygen species metabolic process, reactive oxygen species biosynthetic process, and cellular response to oxidative stress; (ii) cell cycle, such as negative regulation of apoptotic signaling pathway and negative regulation of extrinsic apoptotic signaling pathway; (iii) angiogenesis, such as regulation of blood vessel endothelial cell migration; and (iv) physiological process, such as female gonad development and mammary gland development.

3.6. KEGG Pathway Analysis. The KEGG enrichment analysis of 68 target genes was performed using R software. We finally got a total of 146 items including the 44 key signaling pathways listed in Table 3. We conducted network visualization via Cytoscape as plotted in Figure 3(d).

3.7. Molecular Docking Analysis. Among 28 core targets, the top 5 target proteins in terms of degree were chosen for molecular docking, including AKT1, TNF, SRC, CASP3, and JUN, which were considered the key targets in the process of KP treating SOP. To verify how KP binds to the key targets, we adopted molecular docking using AutoDock Vina to predict their docking interactions. Table 4 shows the docking results including affinity and interaction information.

According to Figure 4(a), KP combined with AKT1 by forming one hydrogen bond with the residue Gln-47 and six van der Waals interactions with Gln-43, Arg-41, Glu-40, Tyr-38, Lys-39, and Leu-52 (binding affinity: −6.0 kcal/mol). In addition, there were pi-alkyl interactions upon KP with Pro-42 and Ala-50.

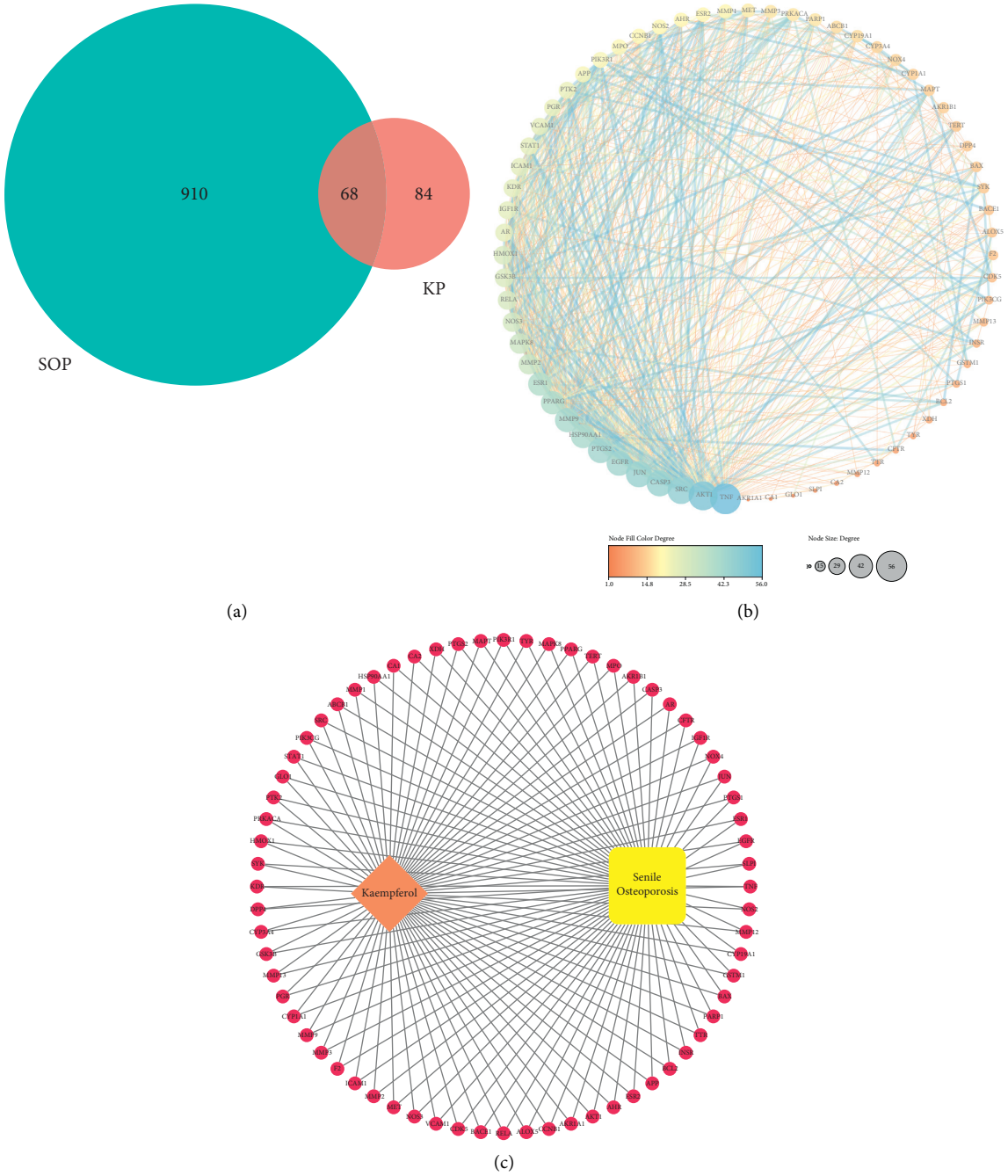

Figure 2: Venn diagram of OTPs (a), PPI network of OTPs (b), and KP-OTPs-SOP network (c).

According to Figure 4(b), the combination affinity of KP on TNF was −7.6 kcal/mol. The residues containing Leu-120, Gln-61, and Tyr-59 interacted with KP by forming 5 van der Waals interactions. Moreover, KP combined with TNF by forming four hydrogen bonds with the residues Gly-121, Ser-60, and Tyr-151. Notably, there were pi-pi stacked and pi-pi T-shaped interactions between KP and Tyr-119.

According to Figure 4(c), the combination affinity of KP on SRC was −5.9 kcal/mol. There existed pi-alkyl interaction and pi-donor hydrogen bond, respectively, provided by the Lys-62 and Arg-14 residues in the interactions with KP. Moreover, KP was bound with the residues Ser-36, Thr-38, Arg-14, and His-60 by hydrogen bonds and Glu-37, Thr-39, Cys-44, and Tyr-61 by van der Waals.

According to Figure 4(d), the combination affinity of KP on CASP3 was −8.4 kcal/mol. There were 6 van der Waals interactions provided by the Gly-122, Ser-120, Ala-162, Ser-205, Phe-256, and Trp-206 residues in the interactions with KP. There existed pi-alkyl interaction and pi-donor hydrogen bonds provided by the Cys-163, Tyr-204, and Arg-64 residues in the interactions with KP. Additionally, KP combined with CASP3 by forming three hydrogen bonds with the residues Arg-207, His-121, and Tyr-204 and an unfavorable donor-donor interaction with Gln-161.

Table 2: Core targets of KP in the treatment of SOP.

Number	Core targets	Degree
1	TNF	56
2	AKT1	52
3	SRC	47
4	CASP3	45
5	JUN	45
6	EGFR	43
7	PTGS2	43
8	HSP90AA1	41
9	MMP9	41
10	ESR1	39
11	PPARG	39
12	MAPK8	32
13	MMP2	32
14	NOS3	30
15	RELA	29
16	HMOX1	28
17	GSK3B	28
18	KDR	26
19	AR	26
20	ICAM1	26
21	IGF1R	26
22	STAT1	25
23	VCAM1	25
24	PGR	24
25	PTK2	24
26	APP	22
27	PIK3R1	22
28	MPO	21

Notably, there were pi-cation and pi-pi T-shaped interactions upon KP with Arg-207 and Tyr-204.

According to Figure 4(e), the combination affinity of KP on JUN was −6.4 kcal/mol. There existed 3 hydrogen bonds provided by the Asn-25, Glu-29, and Gln-33 residues in the interactions with KP. Additionally, there were 3 van der Waals interactions upon KP with Arg-28, Tyr-18, and Glu-19. Notably, KP interacted with the Lys-11, Lys-14, and Ala-15 residues by pi-sigma, pi-alkyl, and amide-pi stacked interactions.

4. Discussion

KP, a flavonoid identified in *Drynariae Rhizoma*, has been revealed to have beneficial effects on SOP via inhibiting osteoclast formation and bone loss [12, 20]. Studies have illustrated that KP exerts the antiosteoporotic function via upregulating microRNA-101 and activating the Wnt/β-catenin pathway, which promotes osteoblast differentiation, proliferation, and migration [21]. To further explore the mechanisms of KP in treating SOP, we carried out a series of bioinformatics analysis to screen potential targets and pathways in the present study.

In our present study, we got 68 overlapped targets between KP and SOP, including 28 core targets listed in Table 2. According to PPI network topology analysis, we noticed that these targets were characteristics of inflammation, oxidative stress, and bone homeostasis-associated proteins. The top five targets ranked by degree are AKT1, TNF, SRC, CASP3, and JUN, which are all bound tightly with KP according to molecular docking results, indicating that they may play a key role in KP treatment for SOP.

AKT1 (RAC-alpha serine/threonine-protein kinase) is identified as a unique signaling intermediate in bone homeostasis that controls the differentiation of osteoblasts and osteoclasts [22]. Some studies have verified that the inhibition of AKT1 expression would enhance bone turnover markers' expression and extracellular matrix mineralization, which consequently suppresses osteoporosis [23]. Moreover, AKT1 plays an important role in the PI3K-Akt signaling pathway, the involvement of which alleviates SOP progression by suppressing inflammatory response and osteoclast formation [24]. Moreover, evidence shows that kaempferol could block AKT1 phosphorylation [25]. Therefore, we speculated that KP could reduce inflammatory response and osteoclast formation by downregulating AKT1 expression levels in patients suffering from SOP, thus exerting therapeutic effects on SOP.

TNF (tumor necrosis factor) is the earliest inflammatory mediator produced in response to oxidative stress and promotes the production of inflammatory mediators and induces the expression of macrophage colony-stimulating factor (M-CSF) [26]. TNF affects SOP healing by activating NF-κB, promoting RANKL-induced osteoclast differentiation, and increasing bone resorption [27]. TNF-α plays a critical role in the development of osteoporosis via regulating oxidative stress, bone homeostasis, and remodeling [28, 29]. Moreover, the existing study reveals that KP could significantly decrease the TNF expression and secretion [30]. Therefore, we speculated that KP could reduce oxidative stress in inflammatory response by downregulating TNF expression in SOP patients, so as to anti-SOP.

SRC (Proto-oncogene tyrosine-protein kinase Src) has been reported to involve in the process of osteoblast differentiation, which plays a vital role in advancing bone maturation [31]. Further studies have revealed that SRC plays a pivotal role in driving osteoblast proliferation and extracellular matrix (ECM) remodeling, which influences bone formation and remodeling [32]. Moreover, SRC is also an osteoclast-specific gene, which is essential for osteoclast function [33]. In general, the involvement of SRC exerts important effects on bone metabolism, which participates in the regulation of osteoblast and osteoclast activities [34]. Notably, sufficient evidence has revealed that KP regulates anti-inflammatory responses by the direct suppression of SRC [35]. However, research is needful to explore whether KP could exert therapeutic effects on SOP by regulating the expression of SRC and thus suppressing inflammatory response.

CASP3 (caspase-3) gets involved in cell apoptosis [36]. Evidence has revealed that the downregulation of CASP3 mRNA can promote SOP healing [37]. Further studies have demonstrated that the upregulation of CASP3 can activate the p53 signaling pathway, destroy osteoblast maturation, and inhibit chondrocyte differentiation, thus restraining SOP healing [38]. It has been verified that CASP3 deletion could alleviate inflammatory response [39]. Moreover, it has been reported that KP treatment could remarkably decrease

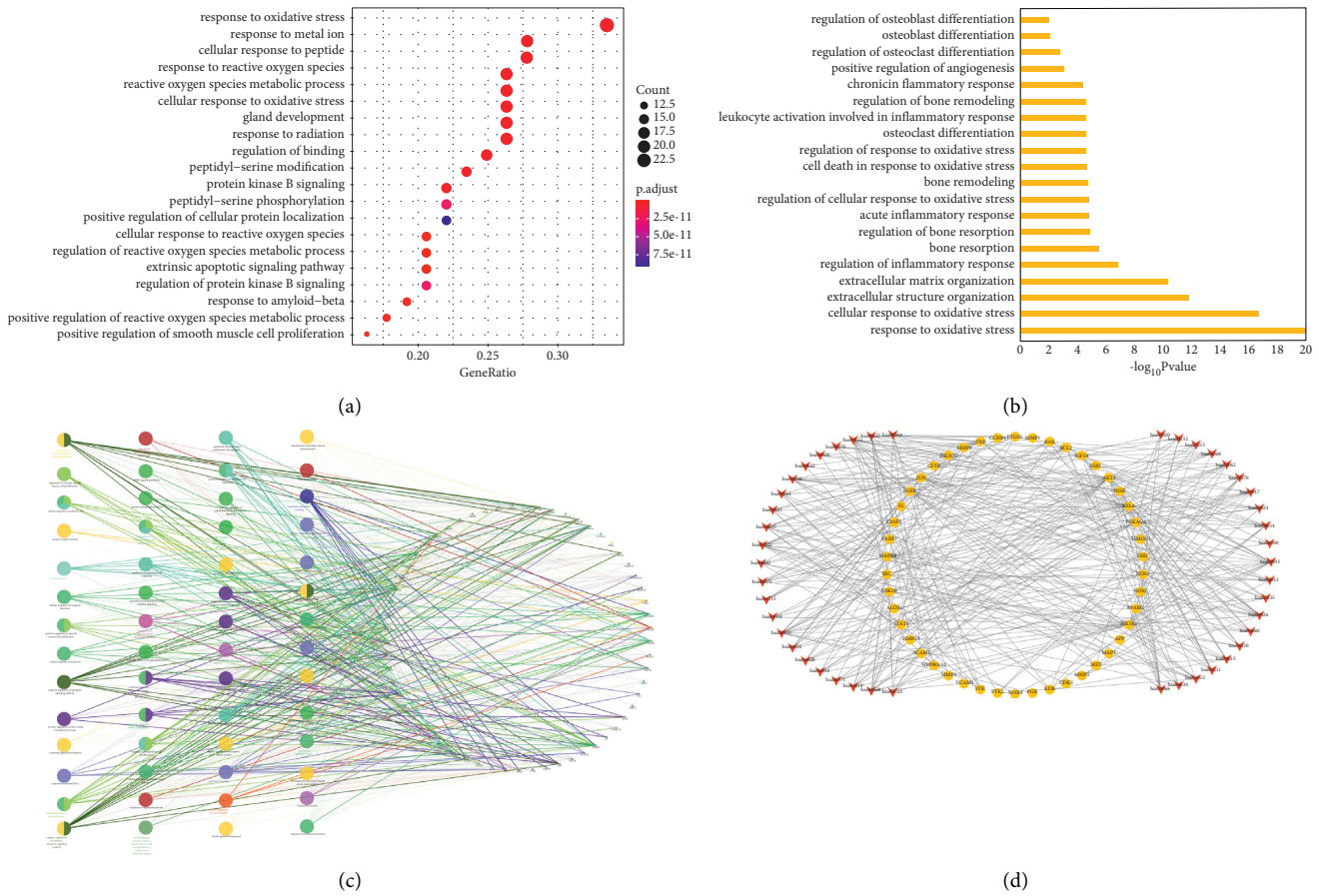

FIGURE 3: GO.BP enrichment analysis (a–c) and pathway-target network (d). (a, b) The top and screened 20 items of biological processes in terms of p value. (c) Different colors represent different biological process groups, and node size stands for term p value, while the edges represent the connections between biological processes and targets. (d) A red V-shaped node represents a signaling pathway, a yellow circular node represents a gene, and an edge represents a relationship between a pathway and a gene.

the CASP3 expression *in vitro* [40]. Nevertheless, there are scanty research projects exploring the regulation of KP on CASP3 expression to alleviate inflammatory response for treating SOP.

JUN is a proinflammatory factor and forms a dimer complex called AP-1 along with FOS, which accelerates the transcription and expression of genes related to bone growth and development containing AP-1 binding sites through multiple mechanisms, thus regulating bone metabolism [41, 42]. Numerous studies have confirmed that the activation of JUN promotes osteoclastogenesis [43]. Moreover, JUN, as a regulatory factor in the JNK signaling pathway, could activate inflammatory response and osteoclast formation [44]. Notably, sufficient evidence has revealed that KP regulates anti-inflammatory responses by the suppression of JUN [45, 46]. Thus, JUN plays a key role in inflammatory response and osteoclastogenesis and KP might treat SOP by suppressing JUN expression.

Similar to PPI analysis, GO enrichment results show consistent results. Additionally, biological processes involving the regulation of inflammatory response, oxidative stress, and bone homeostasis make a key role in KP treating SOP, as demonstrated in Figure 3(b). In recent years, reports have revealed that inflammatory response plays an important role in the pathogenesis of SOP, which could disrupt bone homeostasis by accelerating bone resorption and inhibiting bone formation, thereby triggering SOP [47]. Mounting evidence reveals the role of KP in attenuating inflammatory response by encumbering the expressions of inflammatory mediators in many signaling pathways like MAPK [48]. For example, the MAPK signaling pathway being activated would promote the expressions of inflammatory cytokines TNF-α and IL-1β in inflammatory response, while the presence of KP could suppress this pathway and exert protective effects on SOP [7, 49]. KP, modulating the activities of proinflammatory enzyme, has been reported to inhibit cyclooxygenase expression in numerous inflammatory disorders [50]. KP also suppresses the production of nitric oxide that triggers the activation of TNF-α, thereby inhibiting inflammatory response [51]. There is growing evidence for the role of kaempferol in attenuating inflammatory response mediated by NF-κB, indicating its protective effects on bone loss in postmenopausal osteoporosis by blocking TNF-α-induced nuclear translocation of the NF-κB subunit p65 from the cytoplasm to the nucleus [52]. And KP could suppress age-related NF-κB activation by inhibition of NF-κB subunit p65 translocation so as to restrain inflammatory response [53]. Some

Table 3: KEGG pathway enrichment analysis.

ID	Signaling pathway	Enriched gene number	p value
hsa04933	AGE-RAGE signaling pathway	15	$1.25E-15$
hsa04926	Relaxin signaling pathway	14	$1.24E-12$
hsa04915	Estrogen signaling pathway	14	$3.18E-12$
hsa04657	IL-17 signaling pathway	12	$8.40E-12$
hsa04668	TNF signaling pathway	12	$6.95E-11$
hsa04917	Prolactin signaling pathway	9	$3.91E-09$
hsa04625	C-type lectin receptor signaling pathway	10	$8.98E-09$
hsa04066	HIF-1 signaling pathway	10	$1.42E-08$
hsa04151	PI3K-Akt signaling pathway	15	$1.04E-07$
hsa04012	ErbB signaling pathway	8	$3.64E-07$
hsa04370	VEGF signaling pathway	7	$4.16E-07$
hsa04010	MAPK signaling pathway	13	$5.19E-07$
hsa04211	Longevity regulating pathway	8	$5.21E-07$
hsa04064	NF-kappa B signaling pathway	8	$1.73E-06$
hsa04071	Sphingolipid signaling pathway	8	$4.78E-06$
hsa04722	Neurotrophin signaling pathway	8	$4.78E-06$
hsa04014	Ras signaling pathway	10	$1.56E-05$
hsa04664	Fc epsilon RI signaling pathway	6	$1.70E-05$
hsa04620	Toll-like receptor signaling pathway	7	$1.94E-05$
hsa04660	T cell receptor signaling pathway	7	$1.94E-05$
hsa04062	Chemokine signaling pathway	9	$2.23E-05$
hsa04662	B cell receptor signaling pathway	6	$4.96E-05$
hsa04919	Thyroid hormone signaling pathway	7	$5.18E-05$
hsa05235	PD-L1 expression and PD-1 checkpoint pathway	6	$7.88E-05$
hsa04068	FoxO signaling pathway	7	$8.60E-05$
hsa05022	Pathways of neurodegeneration	13	$9.65E-05$
hsa04912	GnRH signaling pathway	6	0.000100782
hsa04213	Longevity regulating pathway	5	0.000138239
hsa04072	Phospholipase D signaling pathway	7	0.000184632
hsa04921	Oxytocin signaling pathway	7	0.000236022
hsa04015	Rap1 signaling pathway	8	0.000278775
hsa04152	AMPK signaling pathway	6	0.000406963
hsa04621	NOD-like receptor signaling pathway	7	0.000693065
hsa04910	Insulin signaling pathway	6	0.000822176
hsa04150	mTOR signaling pathway	6	0.001558955
hsa04024	cAMP signaling pathway	7	0.002012705
hsa04920	Adipocytokine signaling pathway	4	0.002323
hsa04115	p53 signaling pathway	4	0.002854606
hsa04371	Apelin signaling pathway	5	0.005314536
hsa04630	JAK-STAT signaling pathway	5	0.010013151
hsa04340	Hedgehog signaling pathway	3	0.010486159
hsa04020	Calcium signaling pathway	6	0.01301751
hsa04622	RIG-I-like receptor signaling pathway	3	0.019110112
hsa04550	Signaling pathways regulating pluripotency of stem cells	4	0.028737678

Table 4: Molecular interactions of key targets and KP.

Compound	Target	PDB ID	Affinity (kcal/mol)	Interactions
Kaempferol	AKT1	1UNQ	−6.0	Hydrogen bond, pi-alkyl, van der Waals
Kaempferol	TNF	2AZ5	−7.6	Hydrogen bond, van der Waals, pi-pi stacked, pi-pi T-shaped
Kaempferol	SRC	1O41	−5.9	Hydrogen bond, pi-alkyl, van der Waals
Kaempferol	CASP3	1NMS	−8.4	Hydrogen bond, pi-alkyl, pi-pi T-shaped, pi-cation, unfavorable donor-donor, van der Waals
Kaempferol	JUN	5FV8	−6.4	Hydrogen bond, pi-alkyl, pi-sigma, van der Waals, amide-pi stacked

evidence showed that there was a negative correlation between dietary intake level of KP and serum CRP level, suggesting the key role of KP in reducing the risk of inflammation [54]. It has been verified that oxidative stress makes key functions in SOP-related inflammatory response [55]. Oxidative stress can alter bone homeostasis, accelerate bone resorption, and reduce bone formation, leading to the progression of SOP [56]. And some evidence has illustrated

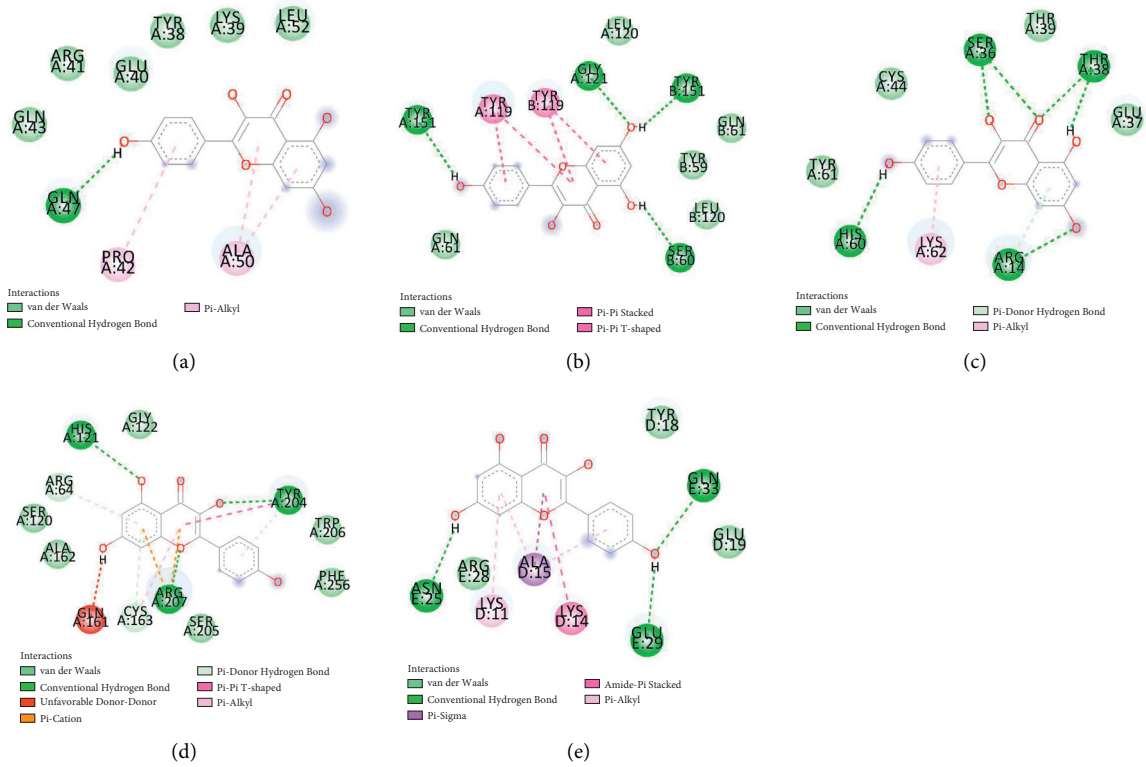

Figure 4: Simulated molecular docking of kaempferol on AKT1 (a), TNF (b), SRC (c), CASP3 (d), and JUN (e).

the therapeutic effects of kaempferol on the damage induced by oxidative stress and inflammation in osteoporosis [7, 57], suggesting that kaempferol is a natural antioxidant for treating osteoporosis. According to our present study, kaempferol may be an antioxidant with a good prospect that helps reduce inflammatory response and oxidative stress, thus improving SOP. Moreover, accumulating studies have revealed that the expressions of core targets, including AKT1 [58], TNF [29], SRC [35], CASP3 [59], JUN [44], etc., make vital functions in regulating inflammatory response and oxidative stress. Therefore, we speculated that KP could regulate core targets' expressions and bone homeostasis by inflammatory response and oxidative stress in SOP patients, so as to anti-SOP.

KEGG enrichment results revealed that PI3K-Akt, MAPK, VEGF, prolactin, HIF-1, TNF, estrogen, IL-17, p53, and NF-kappa B (NF-κB) signaling pathways may exert regulatory functions on kaempferol against SOP.

The involvement of PI3K-Akt signaling pathway alleviates SOP progression by suppressing inflammatory response and osteoclast formation [24]. Moreover, some studies have shown that the PI3K-Akt signaling pathway is involved in the inhibition of osteoporosis through promoting osteoblast proliferation, differentiation, and bone formation [60, 61], Therefore, the PI3K-AKT signaling pathway is essential in bone homeostasis.

Inflammatory pathways including IL-17 [62], TNF [63], and NF-κB [64] signaling pathways participate in regulating osteoclast differentiation. Moreover, the IL-17 signaling pathway can stimulate the synthesis of TNF-α, IL-6, and NF-κB, thereby promoting RANKL-induced osteoclast differentiation [65]. Therefore, IL-17, TNF, and NF-κB signaling pathways are speculated to exert important functions in the process of KP treatment against SOP, which needs further identification.

The estrogen signaling pathway can exert regulatory functions on osteoblasts' and osteoclasts' proliferation, apoptosis, and differentiation [66]. The current study has revealed that KP regulates osteoblastic differentiation via estrogen receptor signaling [67]. Similar to the estrogen signaling pathway, research on the prolactin signaling pathway also indicates that KP has the function of estrogen regulation, which is evidence for kaempferol in treating postmenopausal SOP [68].

Evidence has confirmed that the activation of p53 signaling pathway can disrupt osteoblast maturation and restrain chondrocyte differentiation [38]. The inhibition of MAPK signaling pathway suppresses osteoclastogenesis [69]. The activation of HIF-1/VEGF signaling pathway can accelerate angiogenesis in bone tissues, which gets involved in the pathological evolution of SOP [70, 71].

In summary, our results predict some potential therapeutic targets and pathways, providing reference for future studies on KP treatment against SOP. However, one limitation of this study is that further *in vivo* and *in vitro* experiments are needed to confirm our findings.

5. Conclusion

Collectively, our results first reveal that KP may treat SOP possibly via regulating inflammatory response, oxidative stress, bone homeostasis, etc. These results will provide

theoretical basis for KP treatment against SOP. However, the specific mechanism and material basis still need to be further verified *in vivo* and *in vitro*.

Data Availability

The data sets used and analyzed during the current study are available from the first author on reasonable request.

Conflicts of Interest

The authors declare that there are no conflicts of interest.

Authors' Contributions

All the authors listed participated in study conception, design, data analysis, and drafting the manuscript. All the authors read and approved the submitted manuscript. Fuyu Tang, Peng Zhang, and Wenhua Zhao contributed equally to this work.

Acknowledgments

This project was generously supported by the grants from the National Natural Science Foundation of China (81774338 and 81904225), Guangdong Natural Science Foundation Project (2021A1515011247), Guangxi Natural Science Foundation Project (2020GXNSFAA259082), Guangdong Province Universities and Colleges Pearl River Scholar Funded Scheme (GDUPS 2018), Medical Research Foundation of Guangdong Province (A2021320), Youth Scientific Research Training Project of GZUCM (2019QNPY04), Key Project of Basic Research and Applied Basic Research of Department of Education of Guangdong Province (2018KZDXM021), and Graduate Research Innovation Project of Guangzhou University of Chinese Medicine (A1-2606-21-429-001Z22).

Supplementary Materials

Supplementary Table S1: the structure of kaempferol. Supplementary Table S2: targets of kaempferol. (*Supplementary Materials*)

References

[1] Z. Z. Liu, C. G. Hong, W. B. Hu et al., "Autophagy receptor OPTN (optineurin) regulates mesenchymal stem cell fate and bone-fat balance during aging by clearing FABP3," *Autophagy*, vol. 17, no. 10, pp. 2766–2782, 2021.

[2] Y. Guo, X. Jia, Y. Cui et al., "Sirt3-mediated mitophagy regulates AGEs-induced BMSCs senescence and senile osteoporosis," *Redox Biology*, vol. 41, Article ID 101915, 2021.

[3] L. Si, T. M. Winzenberg, Q. Jiang, M. Chen, and A. J. Palmer, "Projection of osteoporosis-related fractures and costs in China: 2010–2050," *Osteoporosis International*, vol. 26, no. 7, pp. 1929–1937, 2015.

[4] E. F. Eriksen, J. Halse, and M. H. Moen, "New developments in the treatment of osteoporosis," *Acta Obstetricia et Gynecologica Scandinavica*, vol. 92, no. 6, pp. 620–636, 2013.

[5] X.-F. Tang, Z.-T. Ma, Y.-Y. Gao et al., "Systemic osteoprotective effects of *Epimedii Folium* and *Ligustri Lucidi Fructus* in senile osteoporosis rats by promoting the osteoblastogenesis and osteoclastogenesis based on MLP-ANN model," *Chinese Medicine*, vol. 15, no. 1, p. 87, 2020.

[6] Z. L. Xu, M. Y. Xu, H. T. Wang et al., "Pharmacokinetics of eight flavonoids in rats assayed by UPLC-MS/MS after oral administration of *Drynariae rhizoma* extract," *Journal of Analytical Methods in Chemistry*, vol. 2018, Article ID 4789196, 11 pages, 2018.

[7] S. K. Wong, K.-Y. Chin, and S. Ima-Nirwana, "The osteoprotective effects of kaempferol: the evidence from in vivo and in vitro studies," *Drug Design, Development and Therapy*, vol. 13, pp. 3497–3514, 2019.

[8] J. Zhu, H. Tang, Z. Zhang et al., "Kaempferol slows intervertebral disc degeneration by modifying LPS-induced osteogenesis/adipogenesis imbalance and inflammation response in BMSCs," *International Immunopharmacology*, vol. 43, pp. 236–242, 2017.

[9] W.-S. Lee, E.-G. Lee, M.-S. Sung, and W.-H. Yoo, "Kaempferol inhibits IL-1β-stimulated, RANKL-mediated osteoclastogenesis via downregulation of MAPKs, c-fos, and NFATc1," *Inflammation*, vol. 37, no. 4, pp. 1221–1230, 2014.

[10] K. S. Suh, E.-M. Choi, M. Kwon et al., "Kaempferol attenuates 2-deoxy-d-ribose-induced oxidative cell damage in MC3T3-E1 osteoblastic cells," *Biological and Pharmaceutical Bulletin*, vol. 32, no. 4, pp. 746–749, 2009.

[11] I.-R. Kim, S.-E. Kim, H.-S. Baek et al., "The role of kaempferol-induced autophagy on differentiation and mineralization of osteoblastic MC3T3-E1 cells," *BMC Complementary and Alternative Medicine*, vol. 16, no. 1, p. 333, 2016.

[12] C. J. Kim, S. H. Shin, B. J. Kim et al., "The effects of kaempferol-inhibited autophagy on osteoclast formation," *International Journal of Molecular Sciences*, vol. 19, pp. 125–1, 2018.

[13] J. Ru, P. Li, J. Wang et al., "TCMSP: a database of systems pharmacology for drug discovery from herbal medicines," *Journal of Cheminformatics*, vol. 6, no. 1, p. 13, 2014.

[14] D. Gfeller, A. Grosdidier, M. Wirth, A. Daina, O. Michielin, and V. Zoete, "SwissTargetPrediction: a web server for target prediction of bioactive small molecules," *Nucleic Acids Research*, vol. 42, no. W1, pp. W32–W38, 2014.

[15] G. Stelzer, N. Rosen, I. Plaschkes et al., "The GeneCards suite: from gene data mining to disease genome sequence analyses," *Current protocols in bioinformatics*, vol. 54, pp. 1–33, 2016.

[16] J. S. Amberger and A. Hamosh, "Searching online mendelian inheritance in man (OMIM): a knowledgebase of human genes and genetic phenotypes," *Current protocols in bioinformatics*, vol. 58, pp. 1–12, 2017.

[17] C. v. Mering, M. Huynen, D. Jaeggi, S. Schmidt, P. Bork, and B. Snel, "STRING: a database of predicted functional associations between proteins," *Nucleic Acids Research*, vol. 31, no. 1, pp. 258–261, 2003.

[18] P. Shannon, A. Markiel, O. Ozier et al., "Cytoscape: a software environment for integrated models of biomolecular interaction networks," *Genome Research*, vol. 13, no. 11, pp. 2498–2504, 2003.

[19] O. Trott and A. J. Olson, "AutoDock Vina: improving the speed and accuracy of docking with a new scoring function, efficient optimization, and multithreading," *Journal of Computational Chemistry*, vol. 31, no. 2, pp. 455–461, 2010.

[20] B. Nowak, A. Matuszewska, A. Nikodem et al., "Oral administration of kaempferol inhibits bone loss in rat model of ovariectomy-induced osteopenia," *Pharmacological Reports*, vol. 69, no. 5, pp. 1113–1119, 2017.

[21] Y. Wang, H. Chen, and H. Zhang, "Kaempferol promotes proliferation, migration and differentiation of MC3T3-E1 cells via up-regulation of microRNA-101," *Artificial Cells, Nanomedicine, and Biotechnology*, vol. 47, no. 1, pp. 1050–1056, 2019.

[22] A. Mukherjee and P. Rotwein, "Selective signaling by Akt1 controls osteoblast differentiation and osteoblast-mediated osteoclast development," *Molecular and Cellular Biology*, vol. 32, no. 2, pp. 490–500, 2020.

[23] P. Cai, Y. Lu, Z. Yin, X. Wang, X. Zhou, and Z. Li, "Baicalein ameliorates osteoporosis via AKT/FOXO1 signaling," *Aging*, vol. 13, no. 13, pp. 17370–17379, 2021.

[24] L. Zha, L. He, Y. Liang et al., "TNF-α contributes to postmenopausal osteoporosis by synergistically promoting RANKL-induced osteoclast formation," *Biomedicine & Pharmacotherapy*, vol. 102, pp. 369–374, 2018.

[25] E. Jo, S. J. Park, Y. S. Choi, W.-K. Jeon, and B.-C. Kim, "Kaempferol suppresses transforming growth factor-β1-induced epithelial-to-mesenchymal transition and migration of A549 lung cancer cells by inhibiting akt1-mediated phosphorylation of Smad3 at threonine-179," *Neoplasia*, vol. 17, no. 7, pp. 525–537, 2015.

[26] H. Kitaura, P. Zhou, H. J. Kim, D. V. Novack, F. P. Ross, and S. L. Teitelbaum, "M-CSF mediates TNF-induced inflammatory osteolysis," *Journal of Clinical Investigation*, vol. 115, no. 12, pp. 3418–3427, 2005.

[27] R. C. Schulman, A. J. Weiss, and J. I. Mechanick, "Nutrition, bone, and aging: an integrative physiology approach," *Current Osteoporosis Reports*, vol. 9, no. 4, pp. 184–195, 2011.

[28] B. A. Abdel-Wahab and M. E. Metwally, "Clozapine-induced cardiotoxicity: role of oxidative stress, tumour necrosis factor alpha and NF-$\kappa\beta$," *Cardiovascular Toxicology*, vol. 15, no. 4, pp. 355–365, 2015.

[29] C. Sang, Y. Zhang, F. Chen et al., "Tumor necrosis factor alpha suppresses osteogenic differentiation of MSCs by inhibiting semaphorin 3B via Wnt/β-catenin signaling in estrogen-deficiency induced osteoporosis," *Bone*, vol. 84, pp. 78–87, 2016.

[30] M. Palacz-Wrobel, P. Borkowska, M. Paul-Samojedny et al., "Effect of apigenin, kaempferol and resveratrol on the gene expression and protein secretion of tumor necrosis factor alpha (TNF-α) and interleukin-10 (IL-10) in RAW-264.7 macrophages," *Biomedicine & Pharmacotherapy*, vol. 93, pp. 1205–1212, 2017.

[31] G. V. O. Fernandes, A. D. M. Cavagis, C. V. Ferreira et al., "Osteoblast adhesion dynamics: a possible role for ROS and LMW-PTP," *Journal of Cellular Biochemistry*, vol. 115, no. 6, pp. 1063–1069, 2014.

[32] S. M. Barneze Costa, G. da Silva Feltran, V. Namba et al., "Infraphysiological 17β-estradiol (E2) concentration compromises osteoblast differentiation through Src stimulation of cell proliferation and ECM remodeling stimulus," *Molecular and Cellular Endocrinology*, vol. 518, Article ID 111027, 2020.

[33] X. He, L. Zhu, L. An, and J. Zhang, "MiR-143 inhibits osteoclastogenesis by targeting RANK and NF-κB and MAPK signaling pathways," *Current Molecular Pharmacology*, vol. 13, no. 3, pp. 224–232, 2020.

[34] J. H. Kim, K. Kim, I. Kim, S. Seong, and N. Kim, "c-Src-dependent and -independent functions of matk in osteoclasts and osteoblasts," *The Journal of Immunology*, vol. 200, no. 7, pp. 2455–2463, 2018.

[35] S. H. Kim, J. G. Park, J. Lee et al., "The dietary flavonoid Kaempferol mediates anti-inflammatory responses via the Src, Syk, IRAK1, and IRAK4 molecular targets," *Mediators of Inflammation*, vol. 2015, Article ID 904142, 15 pages, 2015.

[36] S. A. Lakhani, A. Masud, K. Kuida et al., "Caspases 3 and 7: key mediators of mitochondrial events of apoptosis," *Science*, vol. 311, no. 5762, pp. 847–851, 2006.

[37] W.-j. Liu, Z.-m. Jiang, Y. Chen et al., "Network pharmacology approach to elucidate possible action mechanisms of Sinomenii Caulis for treating osteoporosis," *Journal of Ethnopharmacology*, vol. 257, Article ID 112871, 2020.

[38] J. Wu, Y. Yang, Y. He et al., "EFTUD2 gene deficiency disrupts osteoblast maturation and inhibits chondrocyte differentiation via activation of the p53 signaling pathway," *Human Genomics*, vol. 13, no. 1, p. 63, 2019.

[39] Y. Li, Y. Yuan, Z.-x. Huang et al., "GSDME-mediated pyroptosis promotes inflammation and fibrosis in obstructive nephropathy," *Cell Death & Differentiation*, vol. 28, no. 8, pp. 2333–2350, 2021.

[40] Y. Ling, H. Xu, N. Ren et al., "Prediction and verification of the major ingredients and molecular targets of tripterygii radix against rheumatoid arthritis," *Frontiers in Pharmacology*, vol. 12, Article ID 639382, 2021.

[41] N. Hannemann, J. Jordan, S. Paul et al., "The AP-1 transcription factor c-jun promotes arthritis by regulating cyclooxygenase-2 and arginase-1 expression in macrophages," *The Journal of Immunology*, vol. 198, no. 9, pp. 3605–3614, 2017.

[42] M. A. Al Mamun, M. M. H. Asim, M. A. Z. Sahin, and M. A. A. Al-Bari, "Flavonoids compounds from *Tridax procumbens* inhibit osteoclast differentiation by down-regulating c-Fos activation," *Journal of Cellular and Molecular Medicine*, vol. 24, no. 4, pp. 2542–2551, 2020.

[43] Q. Zhang, X. Tang, Z. Liu et al., "Hesperetin prevents bone resorption by inhibiting RANKL-induced osteoclastogenesis and jnk mediated irf-3/c-jun activation," *Frontiers in Pharmacology*, vol. 9, Article ID 1028, 2018.

[44] K. M. Lee, C. Y. Lee, G. Zhang, A. Lyu, and K. K. M. Yue, "Methylglyoxal activates osteoclasts through JNK pathway leading to osteoporosis," *Chemico-Biological Interactions*, vol. 308, pp. 147–154, 2019.

[45] T. Behl, K. Mehta, A. Sehgal et al., "Exploring the role of polyphenols in rheumatoid arthritis," *Critical Reviews in Food Science and Nutrition*, pp. 1–22, 2021.

[46] C. Wall, R. Lim, M. Poljak, and M. Lappas, "Dietary flavonoids as therapeutics for preterm birth: luteolin and kaempferol suppress inflammation in human gestational tissues in vitro," *Oxidative Medicine and Cellular Longevity*, vol. 2013, Article ID 485201, 13 pages, 2013.

[47] N. Jiang, J. An, K. Yang et al., "NLRP3 inflammasome: a new target for prevention and control of osteoporosis?" *Frontiers in Endocrinology*, vol. 12, Article ID 752546, 2021.

[48] K. P. Devi, D. S. Malar, S. F. Nabavi et al., "Kaempferol and inflammation: from chemistry to medicine," *Pharmacological Research*, vol. 99, pp. 1–10, 2015.

[49] Z. Sun, Q. Li, R. Hou et al., "Kaempferol-3-O-glucorhamnoside inhibits inflammatory responses via MAPK and NF-κB pathways in vitro and in vivo," *Toxicology and Applied Pharmacology*, vol. 364, pp. 22–28, 2019.

[50] J.-H. Lee and G.-H. Kim, "Evaluation of antioxidant and inhibitory activities for different subclasses flavonoids on enzymes for rheumatoid arthritis," *Journal of Food Science*, vol. 75, no. 7, pp. H212–H217, 2010.

[51] H. S. Rho, A. K. Ghimeray, D. S. Yoo et al., "Kaempferol and kaempferol rhamnosides with depigmenting and anti-inflammatory properties," *Molecules*, vol. 16, no. 4, pp. 3338–3344, 2011.

[52] P. Ramesh, R. Jagadeesan, S. Sekaran, A. Dhanasekaran, and S. Vimalraj, "Flavonoids: classification, function, and

molecular mechanisms involved in bone remodelling," *Frontiers in Endocrinology*, vol. 12, Article ID 779638, 2021.

[53] Y. Qu, X. Li, F. Xu et al., "Kaempferol alleviates murine experimental colitis by restoring gut microbiota and inhibiting the LPS-TLR4-NF-κb Axis," *Frontiers in Immunology*, vol. 12, Article ID 679897, 2021.

[54] O. K. Chun, S.-J. Chung, K. J. Claycombe, and W. O. Song, "Serum C-reactive protein concentrations are inversely associated with dietary flavonoid intake in U.S. adults," *Journal of Nutrition*, vol. 138, no. 4, pp. 753–760, 2008.

[55] S. Zhu, W. Wei, Z. Liu, Y. Yang, and H. Jia, "Tanshinone-IIA attenuates the deleterious effects of oxidative stress in osteoporosis through the NF-κB signaling pathway," *Molecular Medicine Reports*, vol. 17, no. 5, pp. 6969–6976, 2018.

[56] Y. Zhang, Y. Jiang, Y. Luo, and Y. Zeng, "Interference of miR-212 and miR-384 promotes osteogenic differentiation via targeting RUNX2 in osteoporosis," *Experimental and Molecular Pathology*, vol. 113, Article ID 104366, 2020.

[57] H. Yao, J. Sun, J. Wei, X. Zhang, B. Chen, and Y. Lin, "Kaempferol protects blood vessels from damage induced by oxidative stress and inflammation in association with the Nrf2/HO-1 signaling pathway," *Frontiers in Pharmacology*, vol. 11, Article ID 1118, 2020.

[58] C. Lu, L. Liu, S. Chen et al., "Azathioprine pretreatment ameliorates myocardial ischaemia reperfusion injury in diabetic rats by reducing oxidative stress, apoptosis, and inflammation," *Clinical and Experimental Pharmacology and Physiology*, vol. 48, no. 12, pp. 1621–1632, 2021.

[59] Y. Akyuva, M. Nazıroğlu, and K. Yıldızhan, "Selenium prevents interferon-gamma induced activation of TRPM2 channel and inhibits inflammation, mitochondrial oxidative stress, and apoptosis in microglia," *Metabolic Brain Disease*, vol. 36, no. 2, pp. 285–298, 2021.

[60] J.-M. Pan, L.-G. Wu, J.-W. Cai, L.-T. Wu, and M. Liang, "Dexamethasone suppresses osteogenesis of osteoblast via the PI3K/Akt signaling pathway in vitro and in vivo," *Journal of Receptors and Signal Transduction*, vol. 39, no. 1, pp. 80–86, 2019.

[61] J.-C. Xi, H.-Y. Zang, L.-X. Guo et al., "The PI3K/AKT cell signaling pathway is involved in regulation of osteoporosis," *Journal of Receptors and Signal Transduction*, vol. 35, no. 6, pp. 640–645, 2015.

[62] D. Daoussis, A. P. Andonopoulos, and S.-N. C. Liossis, "Wnt pathway and IL-17: novel regulators of joint remodeling in rheumatic diseases. Looking beyond the RANK-RANKL-OPG axis," *Seminars in Arthritis and Rheumatism*, vol. 39, no. 5, pp. 369–383, 2010.

[63] C.-h. Li, Z.-z. Ma, L.-l. Jian et al., "Iguratimod inhibits osteoclastogenesis by modulating the RANKL and TNF-α signaling pathways," *International Immunopharmacology*, vol. 90, Article ID 107219, 2021.

[64] S. Lin, X. l. Zhao, and Z. Wang, "TANK-binding kinase 1 mediates osteoclast differentiation by regulating NF-κB, MAPK and Akt signaling pathways," *Immunology & Cell Biology*, vol. 99, no. 2, pp. 223–233, 2021.

[65] Y. Wang, J. Xu, X. Zhang et al., "TNF-α-induced LRG1 promotes angiogenesis and mesenchymal stem cell migration in the subchondral bone during osteoarthritis," *Cell Death & Disease*, vol. 8, no. 3, Article ID e2715, 2017.

[66] R. Y. Kim, H. J. Yang, Y. M. Song, I. S. Kim, and S. J. Hwang, "Estrogen modulates bone morphogenetic protein-induced sclerostin expression through the Wnt signaling pathway," *Tissue Engineering. Part A*, vol. 21, no. 13-14, pp. 2076–2088, 2015.

[67] A. J. Guo, R. C. Choi, K. Y. Zheng et al., "Kaempferol as a flavonoid induces osteoblastic differentiation via estrogen receptor signaling," *Chinese Medicine*, vol. 7, no. 1, p. 10, 2012.

[68] G. N. Hendy, H. Kaji, H. Sowa, J.-J. Lebrun, and L. Canaff, "Menin and TGF-β superfamily member signaling via the smad pathway in pituitary, parathyroid and osteoblast," *Hormone and Metabolic Research*, vol. 37, no. 6, pp. 375–379, 2005.

[69] X. Li, Y. Wang, L. Li, S. Zhou, and F. Zhao, "Sclareol inhibits RANKL-induced osteoclastogenesis and promotes osteoblastogenesis through promoting CCN1 expression via repressing the MAPK pathway," *Cell Biology and Toxicology*, vol. 37, pp. 849–871, 2021.

[70] H. Zhong, C. Cao, J. Yang, and Q. Huang, "Research on relationship of HIF-1 signaling pathway and postmenstrual osteoporosis," *Sichuan Da Xue Xue Bao Yi Xue Ban*, vol. 48, no. 6, pp. 862–868, 2017.

[71] Y. Chen, B. Zhao, Y. Zhu, H. Zhao, and C. Ma, "HIF-1-VEGF-notch mediates angiogenesis in temporomandibular joint osteoarthritis," *American Journal of Tourism Research*, vol. 11, no. 5, pp. 2969–2982, 2019.

Hindawi
Evidence-Based Complementary and Alternative Medicine
Volume 2022, Article ID 6864195, 14 pages
https://doi.org/10.1155/2022/6864195

Review Article

Moxibustion for Primary Dysmenorrhea: An Adjuvant Therapy for Pain Relief

Sian Pan, Shaohua Wang, Juan Li, Hanyu Yuan, Xiao Xue, Yu Liu, and Zenghui Yue

College of Acupuncture, Massage and Rehabilitation, Hunan University of Chinese Medicine, Changsha 410208, China

Correspondence should be addressed to Yu Liu; luveyu@126.com and Zenghui Yue; yue5381316@126.com

Received 23 November 2021; Revised 25 December 2021; Accepted 30 December 2021; Published 27 January 2022

Academic Editor: Xiang Liu

The latest spectrum of moxibustion disease shows that primary dysmenorrhea is a high-frequency symptom of moxibustion and that it is the dominant clinical disease. In the specific treatment methods, all types of moxibustion methods have been widely used, such as thermal, thunder fire, partitioned, and spreading moxibustion. Moxibustion plays a therapeutic role through its four mechanisms of action: heat, light, moxa smoke, and drug effects. The mechanism of moxibustion treatment for primary dysmenorrhea focuses on adjusting endocrine hormones, regulating immune function and neuro-related factors, and improving uterine microcirculation. In this study, based on the clinical evidence of different moxibustion methods for treating primary dysmenorrhea, the design model, intervention characteristics, and clinical outcomes were analyzed. Meanwhile, the brain effect mechanisms of different imaging methods were summarized from the perspective of neuroimaging. It was pointed out that the left anterior cingulate gyrus, left inferior parietal angular gyrus, and left superior gyrus may be the analgesic brain regions that regulate sensory, emotional, and cognitive aspects. Moreover, the neural circuits involved can be inferred: the frontal cortex-basal ganglia (the pea nucleus)-cerebral cortex, which mediates motivation and emotional drive, and the parietal lobe-basal ganglia-limbic lobe-frontal lobe, which is involved in neurotransmitter transport and emotional regulation and behavioral expression. There are still problems and deficiencies in studies on the mechanism of moxibustion treatment for primary dysmenorrhea. Studies should be strengthened on how moxibustion produces an effect. Attention should be paid to exploring how the spectrum range and peak in the light effect of moxibustion treat primary dysmenorrhea. Studies assessing the mechanisms of moxibustion treatment for primary dysmenorrhea should be conducted to provide an experimental basis and evidence-based medical evidence for clinical treatment.

1. Introduction

Primary dysmenorrhea (PD) is a functional disease characterized by intermittent lower abdominal pain before and after menstruation, without apparent pelvic organic lesions. At the onset of the disease, a patient experiences intermittent pain in the lower abdomen, which can radiate to the lumbosacral portion. Patients with severe PD may experience nausea, vomiting, cold hands and feet, sweating, and even syncope, seriously affecting their quality of life [1]. Reports of the epidemiological prevalence of PD vary widely across studies, ranging from 17% to as high as 90%, with more than half of women describing their pain as moderate to severe. Long-term PD can lead to repression, depression, agony, and other destructive emotions. However, the pathogenesis of PD is complex, and its pathological mechanism remains unclear. Moreover, the current treatment for PD can only alleviate the symptoms in some patients [2]. Currently, nonsteroidal anti-inflammatory drugs (NSAIDs) seem to be effective in treating PD, but their adverse reactions also pose some health risks [3, 4]. Thus, determining a safe and effective therapeutic approach for patients with PD is imperative. Xu et al. [5] performed a meta-analysis involving 20 randomized controlled trials (RCTs) with a sample size of 2134 cases. A comparison of the therapeutic effects of moxibustion, acupuncture, floating eye of the needle, and point application with other treatment methods in the treatment of PD proved that moxibustion combined with point therapy has an overall curative effect on PD. The results of the meta analysis showed that: Firstly,

the total efficacy for the 2 studied interventions was better, with a statistically significant difference from that of the control methods: degrees of freedom (df) = 14, relative risk (RR) = 1.19, 95% confidence interval (95% CI) = (1.14–1.24), $P < 0.000$ for the UTG, and df = 4, RR = 1.15,95% CI (1.02–1.29), $P = 0.03$ for the CDSTG; secondly, the studied interventions were better than the control methods, with statistically significant differences, in relieving the severity of symptoms of PD: df = 3, mean difference (MD) = 3.20, 95% CI (2.36–4.04), $P < 0.000$ for the UTG and df = 1, MD = 2.09, 95% CI (0.16–4.02), $P = 0.03$ for the CDSTG; third, no statistical difference existed between the intervention and control methods groups in the reduction of the level of peripheral blood PGF2α: df = 2, standardized mean difference (SMD) = 0.13, 95% CI (−0.13–0.39), $P = 0.32$. Gou et al. [6] extracted data for studies searched from 10 electronic databases, evaluated the methodological quality of the included studies, and discussed three outcomes: effective rate, pain remission, and prostaglandin F2α (PGF2α) level in serum. Current clinical studies have shown that, compared with nonmoxibustion treatments for PD, moxibustion leads to a higher effective rate and lower level of PGF2α in serum (MD = −4.65,95% CI (−8.42, −0.88), $P = 0.02$). Moreover, research on the disease spectrum and indications of moxibustion therapy based on bibliometric analysis shows that PD is the dominant disease of moxibustion [7, 8].

Moxibustion has a history of thousands of years in China. It originated after humans mastered fire, and countless clinical practices have confirmed its therapeutic effect. Moxibustion treats diseases by burning moxa. The thermal product of burning is an essential factor for producing a therapeutic effect [9]. Additionally, modern medicine believes that hyperthermia has several clinical effects. First, hyperpyrexia can heat local tissues; strengthen metabolism and enzyme reactions; dilate microvessels, thereby strengthening automatic congestion and enhancing phagocytosis; treat local subacute and chronic inflammation. Second, it can reduce the excitability of nerve endings; relieve neuralgia, myalgia, and arthralgia and have antispasticity effects.

Certain bacteria that are not resistant to heat can be reduced, thus achieving the purpose of sterilization. Finally, it can strengthen perspiration, promote metabolism, improve nutrition, and stimulate cell growth and regeneration. More importantly, modern studies on moxibustion have shown that these effects are within the scope of warm moxibustion efficacy. In summary, the thermogenetic effect of moxibustion can not only affect the dynamic distribution of temperature field in biological tissue under moxibustion and the macroscopic energy (thermal energy) migration and change process caused by moxibustion heat but also stimulate the spontaneous infrared spectrum change of thermally sensitive acupoints to produce "resonance." Simultaneously, the combustion products of active ingredients in Folium *Artemisia argyi* can also play an auxiliary therapeutic role. Generally, the organic combination of meridians and acupoints with the physical and chemical effects of moxibustion produces the "comprehensive effect" of moxibustion.

Moxibustion treatment for PD is closely related to central analgesia. A large amount of objective visual evidence provided by neuroimaging indicates that moxibustion treatment of PD is a comprehensive process of treating diseases by stimulating acupoints to regulate the brain network effect [10, 11]. A previous study assessed the central analgesic mechanism of moxibustion in the treatment of PD before and after moxibustion by observing resting-state functional magnetic resonance imaging (rs-fMRI) of the brain [12]. Therefore, this paper will review the mechanism of moxibustion in the treatment of PD and the research progress of moxibustion and neuroimaging for reference.

2. Pathophysiological Studies

The mechanism of moxibustion in the treatment of PD is mainly focused on regulating endocrine hormones, immune function, and nerve factors and improving uterine microcirculation (Figure 1).

2.1. Endocrine Hormones

2.1.1. Prostaglandin E2 and Prostaglandin F2α. Abnormal uterine contractions in patients with PD and nausea, vomiting, and diarrhea in over 60% of patients with PD are associated with prostaglandin (PG). PGE2 and PGF2α are closely related to PD [13]. PGF2α can stimulate the contraction of arcuate vessels and lead to local hypoxia in the endometrial tissue. Endometrial PGF2α can increase the contraction and tension of the uterine smooth muscle. A high concentration of PGF2α acts on the PGF2α receptor on the wall of the spiral arterioles, causing spasmodic contraction of the uterine smooth muscle.

In comparison, a low concentration of PGE2 can inhibit the spontaneous activity of the uterine smooth muscle. The gradual increase in the PGF2α/PGE2 ratio results in excessive contraction of uterine smooth muscle, ischemia, and hypoxia, increasing the sensitivity of peripheral nerves to pain and causing dysmenorrhea [14]. The imbalance of PGE2 and PGF2α secretion is considered the leading cause of PD. Moreover, this process is accompanied by the accumulation of acidic metabolites and a decrease in the pain threshold [15].

Various moxibustion methods have confirmed that the mechanism of moxibustion in the treatment of PD is closely related to the regulation of PGE2 and PGF2α levels [16]. Panbi et al. [17] treated 40 Wistar dysmenorrhea model rats with moxa stick moxibustion, which confirmed that moxa moxibustion could alleviate dysmenorrhea symptoms and downregulate PGF2α content in uterine tissue and improve hemorheology (whole blood viscosity, plasma-specific viscosity, erythrocyte electrophoresis time). Huijuan and Mingxin [18] found in the comparative clinical observation of thunder-fire moxibustion combined with ear points and NSAIDs in 76 patients with PD that the treatment group had significantly reduced PGF2α/PGE2 ratio and that the treatment relieved the clinical symptoms of patients with PD. Sen and Dongfu [19] used moxa stick mild moxibustion at Guanyuan (GV4) point to treat 60 patients with PD and

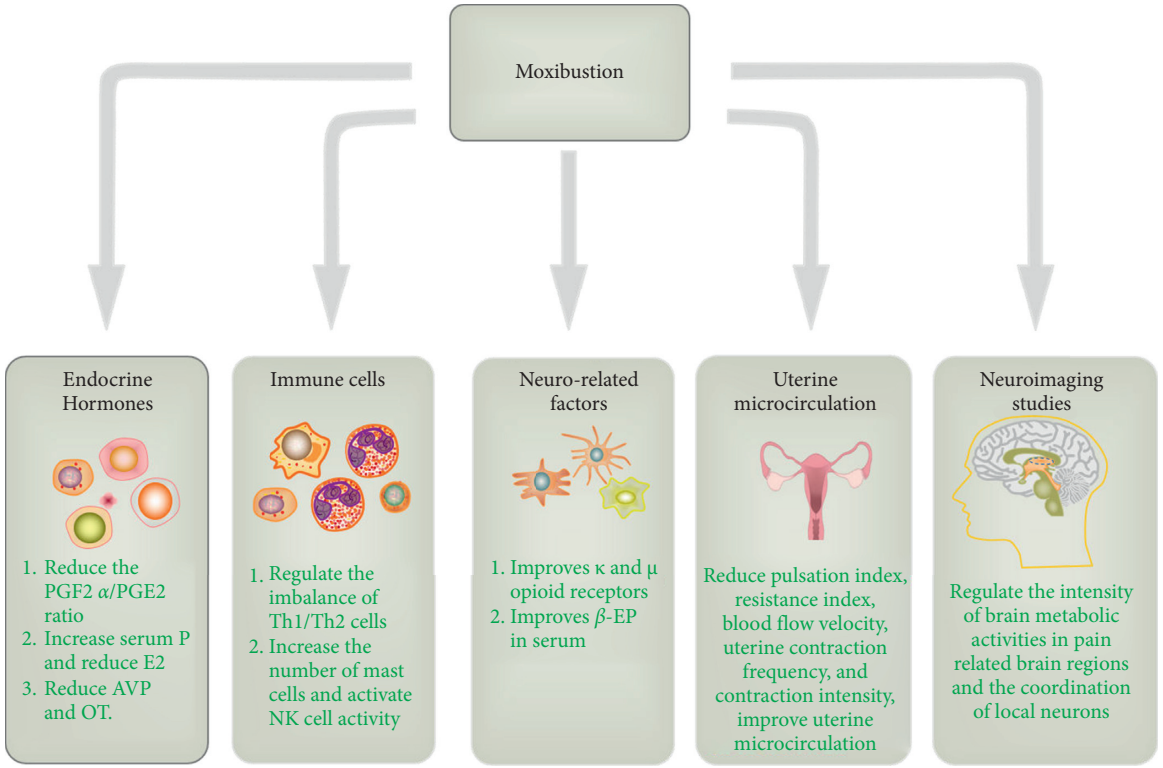

Figure 1: Pharmacological mechanism of moxibustion in the treatment of primary dysmenorrhea. PGE2, prostaglandin E2; PGF2α, prostaglandin F2α; P, progesterone; E2, estradiol; AVP, vasopressin; OT, oxytocin; β-EP, β-endorphin.

confirmed that moxibustion could reduce the serum PGF2α/PGE2 ratio. Limei et al. [20], Xin et al. [21], and Wu [22] treated patients with PD with ginger-partitioned moxibustion and confirmed that it could reduce the serum PGF2α level in patients with PD and relieve clinical symptoms. Jia and Li [23] treated 80 patients with PD with cold coagulation and blood stasis syndrome with thunder-fire moxibustion at the Shenque (CV8) and Guanyuan (GV4) points. It was proven that thunder-fire moxibustion could reduce serum PGF2α level and relieve dysmenorrhea symptoms.

2.1.2. Estradiol and Progesterone. Estradiol (E2) is an estrogen; there are two different peaks of estrogen before and after ovulation, which can increase the PG level in the endometrium before menstruation. In contrast, progesterone (P) can antagonize this effect, reduce the production of PG, and decrease the contraction activity of the uterine smooth muscle to alleviate dysmenorrhea. E2 and P act antagonistically in the uterus. When P level increases, it inhibits the synthesis of PGF2α, promotes blood circulation, stimulates the production and release of analgesic substances (such as β-endorphin [β-EP]), and reduces uterine smooth muscle spasms, thereby relieving dysmenorrhea symptoms. However, when the E2 level increases, it promotes the secretion of PGF2α, aggravates uterine contraction, and causes dysmenorrhea [24].

Moxibustion can effectively treat PD by increasing serum P and decreasing E2 levels. Fan [25] found that partitioned moxibustion increased the expression of P and reduced the expression of E2 in dysmenorrhea rats. Partitioned moxibustion on the umbilicus [26, 27] and electronic moxibustion [28] were selected to treat patients with PD, and the same conclusion was obtained. It was confirmed that partitioned moxibustion on the umbilicus and electronic moxibustion could reduce serum E2 level, increase P level, and relieve dysmenorrhea symptoms. At the same time, it was found that the long-term efficacy of the electronic moxibustion group in the treatment of PD was better than that of the NSAIDs group. A previous study [29] showed that drug-paste-separated moxibustion of Guanyuan (GV4) effectively relieves pain in PD rats, which is probably associated with its effects in downregulating serum E2 level and endometrial ER mRNA expression and upregulating serum P and endometrial PR mRNA expression levels.

2.1.3. Vasopressin and Oxytocin. Vasopressin (AVP) is a hormone secreted by the pituitary gland. Its secretion changes with the concentration of estradiol during the menstrual cycle. The concentration of AVP is lower in the follicular phase and increases during the ovulation phase. AVP acts as a catalyst for PG synthesis, promoting PG synthesis and reducing uterine blood flow caused by pain. AVP may increase uterine contractions and reduce blood flow through the uterus, leading to ischemia and dysmenorrhea [30, 31]. Several researchers have demonstrated the role of AVP in the pathological mechanism of dysmenorrhea [32]. Studies have shown that AVP is a more potent uterine

contraction agent than oxytocin (OT) and strongly stimulates the nonpregnant uterus. OT mainly excites the smooth muscle and uterine artery of the uterus, resulting in the acceleration of uterine contraction; simultaneously, phosphate is activated to stimulate intimal cells to release PGs, which aggravates dysmenorrhea. AVP and OT can contract uterine blood vessels, resulting in temporary uterine ischemia and dysmenorrhea [33].

Moxibustion can alleviate dysmenorrhea symptoms by reducing AVP and OT levels. Ye et al. [34] confirmed that herb-partitioned moxibustion at the Mingmen (GV4) acupoint in treating dysmenorrhea model rats could reduce the expression of OT and AVP ($P < 0.05$) and simultaneously regulate the expressions of PGF2α, PGF2α-R, PGE2, and PGE2-R ($P < 0.05$). Zhenzhen et al. [35] treated dysmenorrhea model rats with moxibustion at Sanyinjiao (SP6). The results showed that moxibustion significantly reduced the peak, mean, and lane values of uterine OT ($P < 0.01$). Wei and Hu [36] used thermal moxibustion at the Guanyuan (CV4) point to treat 117 patients with PD with cold coagulation and dampness stagnation and confirmed that thermal moxibustion could reduce AVP and PGF2α levels in menstrual blood and increase the range of PGE2.

2.2. Immune Function

2.2.1. Th1/Th2 Cell Balance. Th1 and Th2 cells play different roles in immunity and disease. Th1 cells can effectively stimulate and mediate cellular immunity and cytotoxic T cells, activate macrophages, result in delayed hypersensitivity, and eliminate infection caused by intracellular parasitic bacteria. Nevertheless, Th2 cells stimulate humoral immunity. Interleukin-1 (IL-4) secreted by Th2 cells can promote the proliferation of B cells and induce the production of antibodies, especially immunoglobulin E (IgE) [37]. Acupuncture can also regulate the differentiation of different subsets of T cells; that is, it maintains the balance of T cells (Th1/Th2, Th17/Treg) and regulates Th1/Th2 and Th17/Treg to drift to Th2 and Treg, respectively. Thus, this inhibits the production of inflammatory factors (IL-2, IL-12, and interferon [IFN]-γ), increases the expression of anti-inflammatory factors (IL-10), and reduces substances, such as antibody IgE, leukotriene B4, and nitric oxide in serum [38, 39], affecting inflammatory signaling molecules (extracellular signal-related kinase, nuclear factor kappa B, activator protein 1, p38).

Moxibustion can regulate the immune function of patients with PD, reduce the level of Th1 cytokine IFN-γ, promote the expression of serum Th2 cytokines IL-4 and IL-10, regulate the imbalance of Th1/Th2 cells, promote the recovery of immune function, inhibit the production of inflammatory cytokines, continue to play an analgesic role, and relieve the symptoms of dysmenorrhea [40]. Yanna [41] used ginger-partitioned moxibustion to treat 92 patients with PD and found that moxibustion at Sanyinjiao (SP6) could increase the expression of sera IL-4 and IL-10, continuously play an analgesic role, and improve the therapeutic effect. Chen et al. [42] and Le et al. [43] confirmed that medicine-partitioned moxibustion at the Shenque (CV8) point could reduce plasma IFN-γ and increase plasma IL-4 and IL-10 levels to restore the balance of immune function in patients with PD.

2.2.2. Mast Cell and Natural Killer Cell. Early studies have shown mast cell aggregation in small blood vessels, tiny nerves, and nerve endings along the meridian in humans and rats. Acupuncture stimulation can significantly increase the aggregation and degranulation of mast cells along the meridian. Acupuncture and moxibustion can bidirectionally regulate the function of mast cells; that is, it can alleviate the abnormal degranulation of mast cells in the pathological state [44]. Recent studies have shown that substances released by mast cells (adenosine triphosphate, exosomes) can act on local nerve endings and form "synaptic-like" connections with neurons [45, 46]. Small molecule signaling substances (microRNA-155) and cytokines (IL-33) derived from mast cells produce "neuromodulator" effects and regulate "synaptic" functions. Acupuncture and moxibustion alleviate mast cell degranulation and promote "synaptic like" function, which is an essential immune mechanism for the treatment of allergic diseases (asthma) and inflammatory diseases (inflammatory pain) [47, 48]. Natural killer (NK) cells are a class of lymphocytes that lack antigen-specific cell-surface receptors. Acupuncture and moxibustion have bidirectional regulatory effects on NK cells. Acupuncture and moxibustion can increase the number of NK cells, enhance NK cell activity in low immunity (such as chronic stress and fatigue syndrome), and promote the secretion of immune factors by NK cells (such as IFN-γ, IL-10, granulocyte-macrophage stimulating factor) [49, 50]. NK cells are critical immunomodulatory cells in the body and prominent lymphocytes in the endometrial tissue. Studies have shown that activating the activity of NK cells can enhance the pain threshold [51].

Moxibustion can relieve dysmenorrhea symptoms by increasing the number of mast cells and activating NK cell activity. Zhongyin et al. [52] observed the effect of herb-partitioned moxibustion at Guanyuan (CV4) on NK cell activity in rats with PD and confirmed that herb-partitioned moxibustion at Guanyuan (CV4) could increase the activity of uterine NK cells and reduce uterine PGF2α level, and the effect of herb-partitioned moxibustion on NK cell activity in PD rats was better than that of direct moxibustion. Li et al. [53] treated 50 female Wistar dysmenorrhea model rats with cold coagulation and blood stasis by medicine-partitioned moxibustion at the Shenque (CV8) point. The results showed that it could increase the number of mast cells in the Shenque (CV8) point area of dysmenorrhea model rats and promote their degranulation to alleviate the symptoms of dysmenorrhea. Qi et al. [54] found that moxibustion at the Guanyuan (CV4) and Shenque (CV8) points could exert analgesic effects by increasing the activity of NK cells in PD rats.

2.3. Neuro-Related Factors. The effect of moxibustion on PD is closely related to its central analgesic mechanism. Opioid

receptors are widely distributed in the central nervous system and play an essential role in the analgesic effect. Opioid receptors are coupled with G protein, inhibit the activity of adenylate cyclase and calcium channel, activate potassium channel, and prevent the transmission of pain impulse, resulting in analgesic effect. The κ and μ receptors play an important role in central analgesia [33].

Studies have confirmed that the central analgesic mechanism of moxibustion in the treatment of PD may be related to the levels of κ and μ opioid receptors. Zhenzhen et al. [55] found that moxibustion at the Sanyinjiao and Guanyuan points in dysmenorrhea rats with cold coagulation syndrome could increase the expression level of brain κ receptor mRNA, significantly reducing the writhing reaction of dysmenorrhea rats with cold coagulation syndrome, and relieve uterine smooth muscle spasm. Jin et al. [56] confirmed that moxibustion at the Guanyuan point could improve the expression of cold coagulation dysmenorrhea rat spinal cord μ receptors, resulting in an analgesic effect.

Meanwhile, moxibustion can also exert its endogenous analgesic effect by regulating the level of β-EP in serum. Researchers [17, 57] found that herb-partitioned moxibustion on the navel used to treat dysmenorrhea model rats could increase the scope of plasma β-EP and regulate PGF2α and PGE2 levels in uterine tissue, improving the activity of NK cells. In treating patients with PD with moxibustion, prior studies [58, 59] reported that it could increase β-EP levels and regulate serum PGF2α and PGE2 levels, subsequently treating PD.

2.4. Uterine Microcirculation. Improving uterine microcirculation by moxibustion may be one of the mechanisms for relieving PD symptoms. Various moxibustion methods have been confirmed to reduce the pulsation index, resistance index (RI), blood flow velocity, uterine contraction frequency, and contraction intensity; improve uterine microcirculation; relieve dysmenorrhea symptoms [60]. Qin et al. [61] and Liu et al. [62] confirmed that warm acupuncture could significantly reduce the blood flow velocity of uterine arteries at all levels in patients with PD and improve uterine blood flow.

An RCT by Chunxin et al. [63], with a sample size of 101 cases, observed changes in the RI and pulsatility index of the uterine and arcuate arteries before and after treatment, which was detected by color Doppler ultrasound. It is concluded that moxibustion can improve the clinical symptoms of patients with PD with cold dampness stagnation and that the curative effect is better than that of meloxicam tablets. Its product is related to the improvement of the blood supply to the uterus.

Mild moxibustion [64] at the Sanyinjiao (SP6) and Guanyuan(CV4) acupoints may relax uterine microvascular obstacles by reducing PGF2α level in the uterine tissue, improve microcirculation disorder, and alleviate uterine swelling in PD rats. Mild moxibustion can enlarge the microvessels, improve microcirculation disturbance, and relieve uterine swelling in PD rats. During the gentle moxibustion intervention, PGF2α and PGE2 levels in the uterus synchronously increased or decreased, and the changes in PGE2 were noticeable, but the changes in uterine microvasculature and morphology caused by the reduction of PGF2α were more significant than those of PGE2.

In addition, few studies have confirmed that moxibustion can affect the expression of transient receptor potential vanilloid type channel (TRPV) receptors in the uterus, thereby affecting Ca^{2+} channels and alleviating dysmenorrhea symptoms. Chunjing and Ma [65] used umbilical therapy to treat dysmenorrhea model rats with cold coagulation and blood stasis and confirmed that umbilical treatment could reduce the expression of TRPV receptor in the uterus of dysmenorrhea model rats with cold coagulation and blood stasis, thereby inhibiting Ca^{2+} influx caused by mast cell activation, reducing the contraction of uterine smooth muscle, and achieving the therapeutic effect.

3. Neuroimaging Studies

In addition, some studies using rs-fMRI found that moxibustion played a central analgesic mechanism by regulating the intensity of brain metabolic activities in pain-related brain regions and the coordination of local neurons in brain regions.

3.1. Functional Resonance Magnetic Imaging. An RCT [66] with a sample size of 19 cases combined arterial spin labeling and fMRI with clinical efficacy evaluation (visual analog scale [VAS] score). On the first to the third day of the menstrual period, VAS score >4 points, that is, pain scale >40 mm, an immediate (30 min) moxibustion Guanyuan (CV4) or placebo moxibustion Guanyuan intervention was performed. fMRI scanning was performed before and after the intervention, and the VAS scores were recorded before and after treatment. In conclusion, first, moxibustion has a short-term analgesic effect on PD. Second, among the eight brain regions with significantly increased regional cerebral blood flow (CBF) in this study, excluding the activation of the lenticular nucleus, which had no effect on the efficacy of moxibustion in the treatment of PD, the seven brain regions (left anterior cingulate gyrus and collateral cingulate gyrus, left posterior cingulate gyrus, angular gyrus, left inferior parietal angular gyrus, superior marginal gyrus, left medial frontal gyrus, and left middle frontal gyrus) may regulate pain from three different aspects of sensation, emotion, and cognition, which is the possible mechanism of moxibustion for short-term analgesia in the treatment of PD. However, the interaction between activated brain regions requires further study. Third, the brain regions involved in analgesia are the left anterior and paracingulate gyrus, left inferior parietal angular gyrus, and left superior marginal gyrus. Fourth, there are two circuits involved in moxibustion for PD pain relief. The first is the frontal cortex of the basal ganglia cerebral cortex. Among these, the lenticular nucleus is the most critical component. This circuit mediates motivation and emotional drive to promote the expression of goal-directed behavior. The second is the parietal basal ganglia marginal frontal lobe, which is involved in

neurotransmitter transport, emotion regulation, and behavior expression.

An RCT by Zhang [67], with a sample size of 24 cases, performed moxibustion at the Guanyuan (CV4) point as the research object. Seven days before menstruation was selected as the intervention time for moxibustion, and three menstrual cycles were considered a complete course of treatment. The VAS scores of subjects before and after treatment were recorded, and fMRI scans were performed before and after the intervention. First, the results showed that moxibustion had a long-term analgesic effect on PD. Second, moxibustion can alleviate anxiety caused by PD to a certain extent. Third, the brain regions with increased differences in the regional homogeneity (ReHo) values before and after treatment were the right fusiform gyrus, left angular gyrus, and left dorsolateral superior frontal gyrus. The decreased regions were the right paracentral lobule, left superior orbital frontal gyrus, left inferior occipital gyrus, left middle temporal gyrus, and right middle occipital gyrus. Fourth, the brain regions with increased CBF differences before and after treatment were the right middle frontal gyrus, left middle occipital gyrus, anterior cingulate, left paracingulate gyrus, and right precentral gyrus. In contrast, the decreased regions were the right inferior temporal gyrus, right precuneus, right caudate nucleus, left supramarginal gyrus, right superior temporal gyrus, and right superior occipital gyrus. The analysis of ReHo and CBF in the abovementioned pain-related brain areas suggests that this may be the main target of moxibustion in PD treatment.

Dingyi et al. [68] conducted a mechanism study with a sample size of 60 cases. This study performed the moxibustion method using heat-sensitive acupoints, grouped according to whether the heat-sensitive phenomenon occurred at the Guanyuan (CV4) point during moxibustion, and rs-fMRI data were collected before and after moxibustion. DPARSF software and brain functional connectivity analysis with the prefrontal lobe cortex as the seed point were used for postprocessing. Moxibustion at the thermal-sensitive Guanyuan (CV4) point can change the brain operational connection network of patients with PD. The emergence of thermal moxibustion may enhance the connection between the left brainstem and left cerebellum, inhibiting the functional relationship between the left brain white matter area insular lobe and frontal lobe and indirectly affecting the function of other brain areas related to the limbic system.

In conclusion, the application of rs-fMRI technology to study the corresponding mechanism of the brain provides an objective visual basis for clinical application and promotion. From the above, clearly, moxibustion has an analgesic effect in the short term and has an excellent long-term analgesic effect. Moreover, the left anterior and paracingulate gyrus, left inferior parietal marginal angular gyrus, and left superior marginal gyrus were analgesic brain areas and regulated pain from three different aspects: sensation, emotion, and cognition. It provides an objective reference for studying the central analgesic mechanism of moxibustion in the treatment of PD.

3.2. Low-Cost Temperature Transition Mixtures. Yingjie and Ye [69] conducted a mechanism study with a sample size of 60 cases. With the help of TTM technology, the patients were scanned before and after Guanyuan (CV4) point moxibustion. By observing the changes in metabolic heat form and heat radiation value in the local area of the patients, the patients were compared before and after themselves. The results showed an evident decrease in cell metabolic heat in the uterine size of patients with cold cell palace deficiency, and there was no abnormal heat source in the lumbosacral and Shenshu (BL23) points. The results objectively analyzed and explained that moxibustion at the Guanyuan (CV4) point could effectively improve the symptoms of patients with PD with cell palace deficiency and cold syndrome. This provides strong evidence for the application of TTM technology in the evaluation of PD efficacy.

4. Clinical Research

Our previous study showed that moxibustion could adjust the function of the viscera, promote metabolism, and enhance immune function, especially in the treatment of chronic and complex diseases and preventive healthcare. The warm effect generated by moxibustion in treating conditions is the key to achieving a curative effect [70, 71]. The mechanism of moxibustion treatment for PD focuses on adjusting endocrine hormones, regulating immune function and neuro-related factors, and improving uterine microcirculation. In the specific treatment methods, all types of moxibustion methods have been widely used, such as thermal, thunder-fire, partitioned, and spreading moxibustion. Fifty-six RCTs with 5550 patients were included in a systematic review and network meta-analysis, comparing six object-separated moxibustion therapies with acupuncture or oral medicine. Mild moxibustion can not only effectively treat PD but also relieve pain in comparison with ibuprofen, which seems to be an advisable option for PD treatment to relieve symptoms [72].

Moxibustion therapy can reduce the dose of Western medicine and any related adverse reactions. As an adjuvant therapy, moxibustion has a long-term effect on the treatment of PD. The representative clinical studies are presented in Table 1.

5. The Mechanism of Moxibustion

Studies have found that the mechanism of moxibustion is mainly reflected in thermal effect, light effect, moxa smoke, and drug effect. The thermal product is the primary way for moxibustion to play a therapeutic role, and moxa smoke and partition moxibustion also play an essential role in the treatment. However, there is no conclusion on the infrared radiation spectrum range and wave peak in the light effect of moxibustion [83].

5.1. Thermal Effect. The thermal effect is one of the most critical effects of moxibustion [84, 85]. The heat of moxibustion increases the skin's surface temperature at the moxibustion site and simultaneously reaches the muscular

Table 1: Overview of clinical studies of moxibustion.

Intervention method	Number of patients with PD	Experiment method	Observation of efficacy	Result
The herb-partitioned moxibustion [73]	171	Herb-partitioned moxibustion group (A) and starch-partitioned moxibustion group (B) were applied to shenque (CV8) (umbilical every menstrual cycle approximately 2~3 times, until menstruating). Acupuncture group (C) was provided at sanyinjiao (SP6) (started acupuncture 3~5 days before menstruation, once a day until menstruating). Three menstrual cycles are considered a course of treatment.	Clinical efficacy, E2, P, PGF2α	The cured rate in group A was better than those in groups B and C ($P < 0.05$). In group A, E2 and PGF2α levels were decreased, and P level was increased. In groups B and C, PGF2α levels were reduced. The results in group A were better than those in groups B and C ($P < 0.05$).
Heat-sensitive sensation and the conventional warm sensation of moxibustion [74]	189	Heat-sensitive moxibustion and conventional warm sensation groups were applied to guanyuan (GV4) for 40 min beginning 5 days before menstruation. Each menstrual cycle was treated for (7 ± 2) days, and both groups were treated for three periods.	MPQ, CMSS	MPQ and CMSS scores were lower in the treatment group than the control group ($P < 0.01$).
Ginger moxibustion combined with acupuncture and ibuprofen sustained-release capsules [75]	60	The treatment group was treated with ginger moxibustion at shenque (RN8) cooperated with acupuncture at sanyinjiao (SP6), zusanli (ST36), hegu (LI4), and neiguan (PC6) once per day, starting 5 days before menstruation continued for 7 days in each menstrual cycle. The control group took orally two times/day when symptoms of dysmenorrhea occurred. Both groups were treated for three menstrual cycles.	Effective rate, VAS score, PGE2, PGF2α	The instant curative effect, recent curative effect, and long-term curative effect in the treatment group were better than those in the control groups ($P < 0.05$). The long-term VAS score and PGE2 and PGF2a levels in the treatment group were better than those of the control group.
Moxibustion [76]	147	Moxibustion was applied for 20 min at guanyuan (GV4) once daily, seven times in total. Staring 5 days before menstruation, continued for 7 days for three consecutive menstrual cycles, followed up for three menstrual cycles.	The practical clinical rate, TCM symptoms, VAS score, CMSS score, persistent pain time, usage of painkillers, and QOL	The total effective rate was 44.89%, the total score of the symptoms, VAS score, CMSS score, pain persistent time, and usage rate of painkillers were reduced ($P < 0.01$). The scores in the perceptive field, mental field, QOL were all increased ($P < 0.01$).

Table 1: Continued.

Intervention method	Number of patients with PD	Experiment method	Observation of efficacy	Result
Thunder-fire moxibustion combined with wenjing zhitong decoction [77]	116	The treatment group was treated with thunder-fire moxibustion combined with wenjing zhitong decoction once per day, starting 7 days before menstruation until the end of menstruation. The control group took orally two times/day. Both groups were treated for three menstrual cycles.	Clinical efficacy, TCM symptoms, VAS score	Clinical efficacy, TCM symptoms, and VAS score in the treatment group were better than those in control group ($P < 0.05$).
Drug-spreading moxibustion and oral administration of meloxicam [78]	101	Drug-spreading moxibustion was used on the lumbosacral acupoints area and then around the lower abdominal 5 days before menstruation until the third day of menstruation, once 3 days. Meloxicam was prescribed one day before menstruation 7.5 mg at a time once a day and continuously for 3 days.	Clinical efficacy, RI, and PI	The effective rate was 92.3% in the treatment group, which was better than that in the control group ($P < 0.05$). RI and PI in the treatment group were decreased than those in the control group ($P < 0.05$).
Thunder-fire moxibustion combined with ear points and ibuprofen sustained-release capsules [79]	76	The thunder-fire moxibustion selected zhongwan (CV12), guanyuan (CV4), and double sides of zusanli (ST36) points, 30 min per point each time, once a day for 3 consecutive days. Auricular points are selected from the uterus, endocrine, shenmen (TF4), liver, and kidney. For 3 days, oral ibuprofen sustained-release capsules 0.3 g/time, once in the morning and in the evening. Both groups were treated for three menstrual cycles.	VAS score, CMSS score, PGF2α, and PGE2	The VAS scores and CMSS scores of the treatment group were reduced than those in the control group ($P < 0.05$). Serum PGF2α level was decreased, and serum PGE2 level was increased in both groups ($P < 0.05$), and the effect of the treatment group was better than that of the western medicine group ($P < 0.05$).
Herb-partitioned moxibustion at the umbilicus combined with abdominal acupuncture [80]	82	The treatment group was intervened by herb-partitioned moxibustion at the umbilicus plus abdominal acupuncture, and the control group was treated with abdominal acupuncture alone, once per day, starting 7 days before menstruation for 3 consecutive days.	Clinical efficacy, PGE2, PGF2α, PI, and RI	The clinical efficacy rate in the treatment group was higher than that in the control group ($P < 0.05$). Serum PGF2α level, PI, and RI were decreased, and serum PGE2 level was increased in both groups ($P < 0.05$), and the effect of the treatment group was better than that of the western medicine group ($P < 0.05$).

Table 1: Continued.

Intervention method	Number of patients with PD	Experiment method	Observation of efficacy	Result
Moxibustion combined with warm needling [81]	120	In the control group, warm needling was used at guanyuan (CV4) and sanyinjiao (SP6). In the treatment group, besides the same treatment as the control group, moxibustion was added at shenque (CV8). The first menstrual cycle started one day before menstruation, whereas menstrual cycles 2, 3, and 4, started 3 days before menstruation, once a day for 3 days until menstruation.	The score of the severity and the score of the total frequency in the retrospective scale of dysmenorrhea symptoms, VAS score, and the safety of the two therapeutic methods.	The score of severity, score of total frequency, and VAS score of menstrual pain were all reduced, and the effect of the treatment group was better than that of the control group ($P < 0.05$). The safety evaluation was not significant between the two groups ($P > 0.05$).
Baixiao moxibustion and ibuprofen sustained-release capsules [82]	202	Patients in group A received baixiao moxibustion for 30 min; group B received baixiao moxibustion for 15 min; group C was prescribed with ibuprofen sustained-release capsules. Groups A and B were used at guanyuan (CV4), sanyinjiao (SP6), and mingmen (GV4), once per day, starting 10 days before menstruation for 7 consecutive days. Both groups were treated for three menstrual cycles.	The real-time, short-term, and long-term VAS score, RI, PI, PSV, EDV, and PGF2α	The treatment group's real-time, short-term, and long-term efficacy were better than those of the control group ($P < 0.05$). The VAS score, RI, PI, and PGF2α levels were decreased, and PSV and EDV were increased after treatment in the three groups. Both the effects of the treatment group were better than those of the control group ($P < 0.05$).

PGE2, prostaglandin E2; PGF2α, prostaglandin F2 α; P, progesterone; E2, estradiol; VAS, visual analog scale; CMSS, cox menstrual symptom scale; TCM symptoms, traditional Chinese medicine syndrome factors; MPQ, mcgill pain questionnaire; QOL, quality of life. Uterine-artery hemodynamic indexes: resistance index (RI), pulsatility index (PI), peak systolic velocity (PSV), end diastolic velocity (EDV).

layer under the skin. The local temperature of the moxibustion acupoint is increased, and the specific receptors, heat-sensitive immune cells, and heat shock proteins (HSPs) in the acupoint are activated to initiate the warming effect of moxibustion and induce a variety of local effects. Through the nerve and body fluid pathways, the warm and heat stimulation signals and subsequent consequences of moxibustion are transmitted to remote organs and the whole body, causing the following effects of distant specific target organs [86]. TRPV mediates thermal pain, in which TRPV1 can be activated by moxibustion temperature above 43°C, which exists in primary sensory afferent nerve endings, endothelial cells, mast cells, and skin keratinocytes and produces a cascade reaction of biological effects through the nerve fiber pathway [87, 88]. TRPV2 can be activated by moxibustion temperature above 52°C to promote the production of active substances, such as growth factors and inflammatory regulatory factors, to produce subsequent effects [89]. When the moxibustion temperature exceeds 45°C, noxious stimulation will occur, and the harmful sensor of C fiber is activated, resulting in local thermal pain, burning pain, and other sensations and inducing a local burning reaction [90, 91]. At this time, the activation of dorsal reticular nucleus neurons in the medulla oblongata related to analgesia was suddenly strengthened, and the analgesic effect of thermal moxibustion was exerted [87]. Heat stimulation of local moxibustion can change the morphology and quantity of heat-sensitive immune cells and produce an immune response. In addition, studies have confirmed that heat stress can activate HSP and increase HSP expression. HSP is believed to be a local initiation mechanism involved in the warming effect of moxibustion, and it may be an essential substance linking the local and overall effects of moxibustion [90]. The activation of HSP70 expression may be one of the reasons for its analgesic effect [92]. More importantly, the analgesic effect caused by the activation of temperature receptors and nociceptors and the increase in HSP expression may be one of the reasons why moxibustion plays a role in the treatment of PD.

5.2. Light Effect. In addition to the thermal effect, moxibustion also plays a role through the light effect. Although the spectral range and wave peak produced by moxibustion combustion have not been determined, they are considered to be mainly infrared radiation [93, 94]. Far-infrared radiation provides a nondrug alternative therapy to reduce inflammation with PG and cyclooxygenase as targets, especially in the 4–14 m bands [95]. Infrared radiation is an invisible electromagnetic wave that is adjacent to the visible

light region. Infrared radiation is divided into near-infrared radiation (0.8~1.5 m), medium infrared radiation (1.5~5.6 m), and far-infrared radiation (5.6~1000 m) [96]. Some researchers [97] believe that the spectrum of moxibustion is mainly the far-infrared spectrum close to the near-infrared region, but others [98] believe that it belongs to the near-infrared radiation with strong penetration and can penetrate deep tissue below the *epidermis*. In addition, the understanding of the moxibustion radiation spectrum is inconsistent. Generally, the peak value is 0.8~5.6 m. Some researchers believe that moxibustion can produce infrared radiation energy that penetrates the skin, reaches the muscle tissue, and resonates with human acupoints, which may be one of the mechanisms of moxibustion. Therefore, attention should be paid to the spectral range of the light effect and the mechanism of wave peak in the treatment of dysmenorrhea to provide the experimental basis for the target of moxibustion in the treatment of PD [99, 100].

5.3. Moxa Smoke. Moxa smoke produced by moxibustion contains more than 200 chemical components [101]. Moxa smoke has anti-inflammatory effects, promotes blood lipid metabolism, improves immune function, has antibacterial and antitumor effects, and has a particular analgesic effect, which may be one of the mechanisms of moxibustion in the treatment of PD. From the 3-year-old *A. argyi* Ci-li et al., certain analgesic biological substances in it could have a beneficial effect on the human body [102]. Meizhen et al. [103] found that *A. argyi* leaves were rich in flavonoids, which had a sound effect on analgesia, promoted blood circulation, and had immunosuppression effects. The analgesic substances contained in moxa smoke may be related to their effect on pain in PD treatment.

5.4. Drug Effect. Wormwood leaves are warm in nature, can warm meridians, disperse cold and relieve pain, and enhance immunity, hemostasis, and anticoagulants, activating complement, antibacterial, anti-inflammatory, antiviral, and antioxygen free radicals [104]. Partitioned moxibustion adds ginger, garlic, or traditional Chinese medicine based on moxibustion to play the role of warming meridians and dispersing cold and conventional Chinese medicine. Ginger, garlic, or traditional Chinese medicine is placed on human acupoints with thin cuticles. Under the action of moxibustion heat, material-partitioned moxibustion absorbs the drugs into the human body through the skin and capillaries at a specific rate to play the role of drugs [105].

6. Summary and Outlook

In summary, PD is the dominant disease in moxibustion. Various moxibustion methods have been widely used in specific treatment methods, such as thermal, thunder-fire, partitioned, and spreading moxibustion. This paper expounds on the mechanisms of heat effect, light effect, moxa smoke, and drug effect of moxibustion and research on the treatment of PD by moxibustion by regulating endocrine hormones, improving immune function, regulating nerve factors, and improving uterine microcirculation. The above mechanism has been preliminarily clarified, but there are still problems that need to be further studied. The objective visual research evidence provided by neuroimaging suggests that moxibustion can not only have an analgesic effect in the short term but also have an excellent long-term analgesic effect in the treatment of PD. The brain regions that might be analgesia included the right fusiform gyrus, left horn gyrus, left dorsal lateral superior frontal gyrus, right middle frontal gyrus, left middle occipital gyrus, anterior cingulate gyrus, left lateral cingulate gyrus, and right anterior central gyrus. There are two possible circuits for moxibustion to relieve pain in PD: the frontal cortex basal ganglia cerebral cortex, with the lenticular nucleus as the critical component. The second is the parietal basal ganglia marginal frontal lobe. Both pathways can promote the expression of goal-directed behavior through emotional regulation.

Previous studies have the following limitations. First, moxibustion is effective in treating PD, but it is not clear which mechanism is effective for moxibustion. Second, there have been few studies on the spectral range and wave peak of moxibustion in recent years, and there is no unified conclusion. Third, studies on the mechanism of moxibustion for PD mainly focus on endocrine factors, whereas studies on other mechanisms are relatively few. Finally, the application of neuroimaging technology is lacking or single, and there is a lack of relevant research evidence. The number of research samples is small, which requires more experimental data as support. The analysis angle is mostly one or two types of low-frequency amplitude, local consistency, and brain function connection, but there is a lack of systematic and comprehensive data discussion.

7. Future Research Suggestions

The research direction of moxibustion in the treatment of PD should first clarify the relationship between the efficacy of moxibustion in the treatment of PD and related factors, such as acupoint moxibustion duration, moxibustion volume, and drug selection. To determine the effective radiation spectrum range and wave peak of moxibustion in the treatment of PD to provide an experimental basis for selecting radiation materials for the research and development of wearable devices for PD treatment, positron emission tomography/X-ray computed tomography, transcranial magnetic stimulation, electroencephalogram, magnetoencephalography, and other neuroimaging methods should be used. The study's sample size needs to be increased to ensure that the evidence is more objective, and the angle of data analysis should include low-frequency amplitude, local consistency, and brain function connection. Future studies should focus on multimodal neuroimaging technology and improve the brain response mechanism of moxibustion in the treatment of PD as soon as possible.

Data Availability

The data used to support the findings of this study are included within the article.

Conflicts of Interest

The authors declare that they have no conflicts of interest regarding the publication of this paper.

Authors' Contributions

Sian Pan and Yu Liu designed the study. Shaohua Wang, Juan Li, Hanyu Yuan, and Xiao Xue reviewed the research and drafted the manuscript. Sian Pan and Zenghui Yue critically revised the figures and manuscript. All authors approved the final version of the manuscript.

Acknowledgments

This work was supported by the National Natural Science Foundation of China (no. 82004490) and the Innovation Platform Open Fund project of the Hunan Education Department (no. 20K091).

References

[1] K. A. Kho and J. K. Shields, "Diagnosis and management of primary dysmenorrhea," *JAMA*, vol. 323, no. 3, pp. 268-269, 2020.

[2] E. Ferries-Rowe, E. Corey, and J. S. Archer, "Primary dysmenorrhea," *Obstetrics & Gynecology*, vol. 136, no. 5, pp. 1047–1058, 2020.

[3] J. Marjoribanks, R. O. Ayeleke, C. Farquhar, and M. Proctor, "Nonsteroidal anti-inflammatory drugs for dysmenorrhoea," *Cochrane Database of Systematic Reviews*, vol. 2015, no. 7, Article ID CD001751, 2015.

[4] N. K. Ghamry, A. S. Ali, M. A. Shareef et al., "Efficacy and safety of intravenous tramadol versus intravenous paracetamol for relief of acute pain of primary dysmenorrhea: a randomized controlled trial," *Gynecologic and Obstetric Investigation*, vol. 85, no. 5, pp. 388–395, 2020.

[5] T. Xu, L. Hui, Y. L. Juan, S. G. Min, and W. T. Hua, "Effects of moxibustion or acupoint therapy for the treatment of primary dysmenorrhea: a meta-analysis," *Alternative Therapies in Health & Medicine*, vol. 20, no. 4, pp. 33–42, 2014.

[6] C. Q. Gou, J. Gao, C. X. Wu et al., "Moxibustion for primary dysmenorrhea at different interventional times: a systematic review and meta-analysis," *Evidence-Based Complementary and Alternative Medicine: eCAM*, vol. 2016, Article ID 6706901, 8 pages, 2016.

[7] Q. F. Huang, C. Xie, H. G. Wu et al., "[Spectrum and indications of acupuncture and moxibustion therapy based on bibliometric analysis]," *Zhongguo Zhen Jiu = Chinese Acupuncture & Moxibustion*, vol. 41, no. 9, pp. 1055–1059, 2021.

[8] M. X. Yang, L. Zhao, J. Yang, X. X. Cao, Z. N. Yu, and F. R. Liang, "[Bibliometrics analysis on researches of illness spectrum for acu-moxibustion therapy and prospect]," *Zhen Ci Yan Jiu = Acupuncture Research*, vol. 39, no. 3, pp. 247–251, 2014.

[9] L. L. X. J. G. Jing, "Advances of the mechanism of moxibustion," *Chinese Archives of Traditional Chinese Medicine*, vol. 29, no. 12, pp. 2616–2620, 2011.

[10] H. Hu, B. Li, T. Hu, C. Wang, and H. Gao, "[Analysis on the dominant diseases treated with spreading moxibustion therapy based on randomized controlled trials]," *Zhongguo Zhen Jiu = Chinese Acupuncture and Moxibustion*, vol. 39, no. 5, pp. 557–561, 2019.

[11] H. Z. Y. Tao, L. Z. S. Ruirui, L. L. L. Siyi, and Z. F. H. Jian, "Application and prospect of machine learning in acupuncture research," *Chinese Acupuncture & Moxibustion*, vol. 40, no. 12, pp. 1383–1386, 2020.

[12] R.-L. Cai, G.-M. Shen, H. Wang, and Y.-Y. Guan, "Brain functional connectivity network studies of acupuncture: a systematic review on resting-state fMRI," *Journal of Integrative Medicine*, vol. 16, no. 1, pp. 26–33, 2018.

[13] L. Jiang, Y. Yan, Z. Liu, and Y. Wang, "Inflammation and endometriosis," *Frontiers in Bioscience*, vol. 21, pp. 941–948, 2016.

[14] J. A. Maybin, H. O. D. Critchley, and H. N. Jabbour, "Inflammatory pathways in endometrial disorders," *Molecular and Cellular Endocrinology*, vol. 335, no. 1, pp. 42–51, 2011.

[15] P. Kannan, K.-K. Cheung, and B. W.-M. Lau, "Does aerobic exercise induced-analgesia occur through hormone and inflammatory cytokine-mediated mechanisms in primary dysmenorrhea?" *Medical Hypotheses*, vol. 123, pp. 50–54, 2019.

[16] Y. X. Ma, X. Y. Yang, G. Guo, D. Du, Y. Yu, and S. Gao, "Research of herb-partitioned moxibustion for primary dysmenorrhea patients based on the LC-MS metabonomics," *Evidence-Based Complementary and Alternative Medicine: eCAM*, vol. 2015, Article ID 621490, 7 pages, 2015.

[17] Y. X. C. Panbi, Y. Z. W. Xinggui, and X. J. F. Lin, "Effects of moxibustion on hemorheology and uterine PGF_(2α) content in primary dysmenorrhea rats," *Chinese Journal of Preventive Medicine*, vol. 21, no. 11, pp. 826–829, 2015.

[18] S. F. Z. Huijuan and W. Y. S. Mingxin, "Curative effect observation on treatment of primary dysmenorrhea of qi and blood deficiency with thunder-fire moxibustion and ear points," *China Journal of Traditional Chinese Medicine*, vol. 36, no. 4, pp. 2408–2411, 2021.

[19] Z. F. L. Sen and C. L. L. Dongfu, "Clinical research on effects of the treatment of primary dysmenorrhea with moxibustion in different times," *China Health Standard Management*, vol. 8, no. 24, pp. 92-93, 2017.

[20] Z. Z. X. Limei, W. Y. M. Juntao, and H. Chen, "Clinical effect and immediate analgesic effect of traditional Chinese medicine moxibustion nursing intervention on primary dysmenorrhea," *Practical Clinical Nursing Electronic Magazine*, vol. 2, no. 17, pp. 106–114, 2017.

[21] S. K. Z. Xin, L. Y. L. Mingjun, and M. Wu, "Observation on the curative effect of ginger-partitioned moxibustion based on meridian characteristics on patients with primary dysmenorrhea and the influence of serum PGF (2α)/PGE 2," *Shi Zhen Traditional Chinese Medicine*, vol. 25, no. 1, pp. 115-116, 2014.

[22] S.-w. Wu, "Clinical efficacy observation on treatment of primary dysmenorrhea with ginger-partitioned moxibustion at zigong (EX-CA 1)," *Journal of Acupuncture and Tuina Science*, vol. 15, no. 6, pp. 446–450, 2017.

[23] Z. W. Y. Jia and N. Li, "Effect of time-related moxibustion on PFG (2α) content in serum of primary dysmenorrhea of cold coagulation and blood stasis type," *Journal of Liaoning University of Traditional Chinese Medicine*, vol. 19, no. 12, pp. 118–120, 2017.

[24] J. Evans and L. A. Salamonsen, "Inflammation, leukocytes and menstruation," *Reviews in Endocrine & Metabolic Disorders*, vol. 13, no. 4, pp. 277–288, 2012.

[25] G. B. F. Yu-Shan and M. F. L. Yong-Xiu, "Effect of moxibustion at mingmen point on expression of PR and ER in endometrium of dysmenorrhea model rats," *Asia-Pacific Traditional Medicine*, vol. 12, no. 2, pp. 7–9, 2016.

[26] Z. Xue, C. Z. Liu, S. Z. Gao, and Y. X. Ma, "[The herbal-partitioned moxibustion for primary dysmenorrhea and impact on reproductive endocrinal function of patients]," *Zhongguo Zhen Jiu = Chinese Acupuncture and Moxibustion*, vol. 34, no. 3, pp. 209–212, 2014.

[27] K. Lu, "Effect of umbilical therapy on serum estradiol and progesterone content in patients with primary dysmenorrhea," *Journal of Heze Medical College*, vol. 30, no. 2, pp. 58-59, 2018.

[28] W. Wanzhen, *Clinical Study on Treatment of Primary Dysmenorrhea with Congealing Cold and Blood Stasis Using Acupuncture*, FuZhou; College of Acupuncture and Massage, Fujian University of Traditional Chinese Medicine, Fuzhou, China, 2019.

[29] Y. S. Fan, F. R. Miao, A. N. Liao, and F. Xu, "[Effect of drug-paste separated moxibustion on expression of estrogen, progestogen and their endometrial receptor mRNA in rats with primary dysmenorrhea]," *Zhen Ci Yan Jiu = Acupuncture Research*, vol. 38, no. 5, pp. 352–357, 2013.

[30] M. L. Forsling, M. ÅKerlund, and P. StröMberg, "Variations in plasma concentrations of vasopressin during the menstrual cycle," *Journal of Endocrinology*, vol. 89, no. 2, pp. 263–266, 1981.

[31] P. Strömberg, M. Akerlund, M. L. Forsling, E. Granström, and H. Kindahl, "Vasopressin and prostaglandins in premenstrual pain and primary dysmenorrhea," *Acta Obstetricia et Gynecologica Scandinavica*, vol. 63, no. 6, pp. 533–538, 1984.

[32] R. Liedman, S. R. Hansson, D. Howe, S. Igidbashian, R. J. Russell, and M. Åkerlund, "Endometrial expression of vasopressin, oxytocin and their receptors in patients with primary dysmenorrhoea and healthy volunteers at ovulation," *European Journal of Obstetrics & Gynecology and Reproductive Biology*, vol. 137, no. 2, pp. 189–192, 2008.

[33] M. G. G. Li and Y. W. Liu, "Research advances in the mechanism of action of moxibustion treatment on primary dysmenorrhea," *Shanghai Journal of Acupuncture and Moxibustion*, vol. 39, no. 4, pp. 508–513, 2020.

[34] P. Z. Z. Ye, Y. L. J. Wang, and F. M. X. Chen, "Effect of moxibustion on dysmenorrhea model rats," *Hunan Journal of Traditional Chinese Medicine*, vol. 32, no. 5, pp. 174–176, 2016.

[35] Z. M. L. Zhenzhen, Z. J. Q. Dandan, Z. Q. C. Xiao et al., "Effect of moxibustion sanyinjiao and guanyuan on uterine contraction strength and OTR in cold coagulation dysmenorrhea rats," *Guiding Journal of Traditional Chinese Medicine and Pharmacology*, vol. 21, no. 9, pp. 33–36, 2015.

[36] L. H. Z. Wei and J. Hu, "Study on the correlation between moxibustion sensation and moxibustion effect of heat sensitive moxibustion "guanyuan" point in the treatment of primary dysmenorrhea," *Lishizhen Medicine and Materia Medica Research*, vol. 25, no. 5, pp. 1148–1150, 2014.

[37] S. Romagnani, "Human TH1 and TH2 subsets: doubt no more," *Immunology Today*, vol. 12, no. 8, pp. 256-257, 1991.

[38] Y. M. Liu, X. J. Liu, S. S. Bai et al., "The effect of electroacupuncture on T cell responses in rats with experimental autoimmune encephalitis," *Journal of Neuroimmunology*, vol. 220, no. 1-2, pp. 25–33, 2010.

[39] Y. Liu, H. Wang, X. Wang et al., "The mechanism of effective electroacupuncture on T cell response in rats with experimental autoimmune encephalomyelitis," *PLoS One*, vol. 8, no. 1, Article ID e51573, 2013.

[40] J. N. He and M. F. Luo, "[Progress in the study on the relationship between effects of acu-moxibustion and mast cells in acupoints]," *Zhen Ci Yan Jiu = Acupuncture Research*, vol. 32, no. 3, pp. 214–216, 2007.

[41] X. Y. F. Yanna, "Analysis of analgesic effect of moxibustion and acupuncture on primary dysmenorrhea," *Journal of Sichuan of Traditional Chinese Medicine*, vol. 34, no. 10, pp. 166–168, 2016.

[42] N. L. R. Chen, L. Z. C. Du, F. M. L. Ji, and Y. Z. G. Zhou, "Effect of moxibustion on expression of cytokines in primary dysmenorrhea," *Journal of Sichuan of Traditional Chinese Medicine*, vol. 32, no. 4, pp. 150–153, 2014.

[43] C. R. J. Le, L. N. Z. Lijing, and Z. Y. Z. Guangjun, "Effects of different moxibustion amount on IL-4, IL-10 and IFN-γ in cold dysmenorrhea," *Journal of Clinical Acupuncture and Moxibustion*, vol. 30, no. 9, pp. 4–7, 2014.

[44] L. I. L. H. Tian-Feng and C. Yun-Fei, "Advances of the study on correlativity between acupuncture moxibustion and mast cells," *World Journal of Acupuncture-Moxibustion*, vol. 19, no. 4, pp. 43–50, 2009.

[45] B. Chen, M.-Y. Li, Y. Guo, X. Zhao, and H.-M. C. Lim, "Mast cell-derived exosomes at the stimulated acupoints activating the neuro-immune regulation," *Chinese Journal of Integrative Medicine*, vol. 23, no. 11, pp. 878–880, 2017.

[46] T. Chen, W. W. Zhang, Y. X. Chu, and Y. Q. Wang, "Acupuncture for pain management: molecular mechanisms of action," *The American Journal of Chinese Medicine*, vol. 48, no. 4, pp. 793–811, 2020.

[47] N. Yin, H. Yang, W. Yao, Y. Xia, and G. Ding, "Mast cells and nerve signal conduction in acupuncture," *Evidence-Based Complementary and Alternative Medicine: eCAM*, vol. 2018, Article ID 3524279, 9 pages, 2018.

[48] Y. Gong, N. Li, Z. Lv et al., "The neuro-immune microenvironment of acupoints-initiation of acupuncture effectiveness," *Journal of Leukocyte Biology*, vol. 108, no. 1, pp. 189–198, 2020.

[49] T. Sato, Y. Yu, S. Y. Guo, T. Kasahara, and T. Hisamitsu, "Acupuncture stimulation enhances splenic natural killer cell cytotoxicity in rats," *The Japanese Journal of Physiology*, vol. 46, no. 2, pp. 131–136, 1996.

[50] S. K. Kim and H. Bae, "Acupuncture and immune modulation," *Autonomic Neuroscience: Basic & Clinical*, vol. 157, no. 1-2, pp. 38–41, 2010.

[51] I. Manaster, S. Mizrahi, D. Goldman-Wohl et al., "Endometrial NK cells are special immature cells that await pregnancy," *The Journal of Immunology*, vol. 181, no. 3, pp. 1869–1876, 2008.

[52] C. P. Q. Zhongyin, J. L. Y. Wenwen, Z. Y. J. T. Xuyun, and T. Hou, "Effects of moxibustion at guanyuan point on pain response and activity of serum β-EP, uterine PGE2/PGF2α and spleen NK cells in primary dysmenorrhea rats," *Journal of Emergency in Traditional Chinese Medicine*, vol. 30, no. 10, pp. 1701–1704, 2021.

[53] X. Z. S. Li, M. S. F. Ma, and Y. M. S. Gao, "Effect of umbilical cord therapy on mast cells in shenque acupoint area of cold coagulation and blood stasis dysmenorrhea rats," *Lishizhen Medicine and Materia Medica Research*, vol. 28, no. 9, pp. 2288–2290, 2017.

[54] P. B. C. S. S. Qi, H. Y. J. Huang, and H. Lei, "Effect of moxibustion at different acupoints on NK cell activity in primary dysmenorrhea rat model," *Asia-Pacific Traditional Medicine*, vol. 13, no. 15, pp. 4–7, 2017.

[55] Z. M. L. Zhenzhen, Q. I. D. Z. Qingqing, G. M. R. Xiaoxuan, Z. Y. L. Xiaohong, and Z. J. Z. Lufen, "Effects of moxibustion at different acupoints on pain response and κ receptor mRNA expression in central dysmenorrhea rats with cold

coagulation syndrome," *Liaoning Journal of Traditional Chinese Medicine*, vol. 42, no. 6, pp. 1352–1355, 2015.

[56] C. X. Z. Jin, Q. I. D. Z. Lufen, G. M. Z. Mei, and L. X. R. Xiaoxuan, "Effect of different moxibustion stimulus on pain reaction and μopioid receptor mRNA expression in spinal cord of dysmenorrheal rats with cold stagnation syndrome," *Chinese Archives of Traditional Chinese Medicine*, vol. 35, no. 5, pp. 1199–1201, 2017.

[57] P. B. Chen, S. S. Qi, J. Cui et al., "[Herbal-cake-partitioned moxibustion of "shenque" (CV8) has a relative specific effect in relieving abdominal pain and in regulating neuroendocrine-immune network in primary dysmenorrhea rats]," *Zhen Ci Yan Jiu = Acupuncture Research*, vol. 44, no. 2, pp. 120–124, 2019.

[58] M. R. L. Yu and L. Qian, "Effect of moxibustion duration on treatment of primary dysmenorrhea," *China Modern Doctor*, vol. 56, no. 7, pp. 49–52, 2018.

[59] M. Z. W. Jun and Y. Alimu, "Clinical study on primary dysmenorrhea with different moxibustion duration," *Journal of Clinical Acupuncture and Moxibustion*, vol. 33, no. 1, pp. 1–4, 2017.

[60] C. Ruan, S. Lin, X. Chen, Z. Lu, and M. Kong, "[Effect of drug-spreading moxibustion for primary dysmenorrheal with cold-damp stagnation and its uterine artery blood flow]," *Zhongguo Zhen Jiu = Chinese Acupuncture and Moxibustion*, vol. 36, no. 8, pp. 827–830, 2016.

[61] Z. L. X. Qin, R. X. X. Gao, and M. H. X. Tian, "Treatment of 40 cases of primary dysmenorrhea with qi stagnation and blood stasis by warm acupuncture," *Traditional Chinese Medicinal Research*, vol. 30, no. 10, pp. 56–59, 2017.

[62] Q. Liu, X. Li, K. Ren, and S. Yang, "[Effects of mild moxibustion on the uterine microcirculation in patients of primary dysmenorrhea]," *Zhongguo Zhen Jiu = Chinese Acupuncture and Moxibustion*, vol. 38, no. 7, pp. 717–720, 2018.

[63] L. S. R. Chunxin, L. Z. C. Xingkui, and M. Kong, "Treatment of primary dysmenorrhea with cold, dampness and stagnation with moxibustion and its effect on uterine artery blood flow," *Chinese Acupuncture & Moxibustion*, vol. 36, no. 8, pp. 827–830, 2016.

[64] X. Li, S. Guo, Z. Chen et al., "Regulation of mild moxibustion on uterine vascular and prostaglandin contents in primary dysmenorrhea rat model," *Evidence-Based Complementary and Alternative Medicine: eCAM*, vol. 2021, Article ID 9949642, 12 pages, 2021.

[65] Z. X. L. Chunjing and Y. Ma, "Effect of umbilical therapy on TRPV receptor expression in uterus of cold coagulation and blood stasis dysmenorrhea rats," *China Journal of Traditional Chinese Medicine and Pharmacy*, vol. 33, no. 3, pp. 1085–1088, 2018.

[66] Z. Y. Chen, *Study on Central Analgesic Mechanism of Moxibustion Therapy for Primary Dysmenorrhea Based on Arterial Spin Label Functional Magnetic Resonance Imaging*, College of Acupuncture and Massage, Beijing University of Traditional Chinese Medicine, Beijing, China, 2017.

[67] B. Zhang, *Study on the Influence Mechanism of Brain Function of Moxibustion at Guanyuan Point for Primary Dysmenorrhea Based on ASL-FMRI Technology*, College of Acupuncture and Massage, Beijing University of Traditional Chinese Medicine, Beijing, China, 2019.

[68] Z. M. X. Dingyi, C. R. L. Qiaolin, X. S. X. Hongwu, and X. Huang, "Effect of moxibustion on brain functional network in patients with primary dysmenorrhea," *World Chinese Medicine*, vol. 14, no. 8, pp. 1922–1935, 2019.

[69] W. S. Z. Yingjie and M. X. Z. Ye, "Application of TTM in moxibustion at guanyuan point for dysmenorrhea," *Shandong Journal of Traditional Chinese Medicine*, vol. 32, no. 9, pp. 651–653, 2013.

[70] Y. J. W. Huan-Gan, X. U. B. Y. Shu-Guang, M. A. X. C. Xiao-Rong, and L. H. M. Jing-Ping, "Research current situation and development trend of of moxibustion therapy," *Shanghai Journal of Acupuncture and Moxibustion*, vol. 28, no. 1, pp. 1–6, 2009.

[71] A. V. O. Freire, G. C. M. Sugai, M. M. Blanco, A. Tabosa, Y. Yamamura, and L. E. N. A. M. Mello, "Effect of moxibustion at acupoints Ren-12 (zhongwan), St-25 (tianshu), and St-36 (zuzanli) in the prevention of gastric lesions induced by indomethacin in wistar rats," *Digestive Diseases and Sciences*, vol. 50, no. 2, pp. 366–374, 2005.

[72] Z.-X. Wu, M.-J. Cai, P.-D. Huang, J.-Y. Chen, Z.-H. Lv, and X.-Y. Huang, "Comparative efficacy and dysmenorrhea score of 6 object-separated moxibustions for the treatment of Chinese patients with dysmenorrhea," *Medicine*, vol. 100, no. 26, Article ID e26185, 2021.

[73] L. C. X. Zhe and M. Y. G. Shuzhong, "Herb-partitioned moxibustion for primary dysmenorrhea and its effect on reproductive endocrine," *Chinese Acupuncture & Moxibustion*, vol. 34, no. 3, pp. 209–212, 2014.

[74] Z. W. X. Jun, C. Z. J. Lin, X. D. F. Yong, and R. Chen, "To explore the effect of different moxibustion sensations on the efficacy of moxibustion for primary dysmenorrhea based on propensity score: a prospective cohort study," *Acupuncture Research*, vol. 40, no. 6, pp. 465–469, 2015.

[75] W. X. H. Cangcang, "Therapeutic effect of acupuncture on primary dysmenorrhea of cold coagulation and blood stasis type," *Chinese Archives of Traditional Chinese Medicine*, vol. 36, no. 3, pp. 659–662, 2018.

[76] W. X. L. Yinghua, "Clinical observation of moxibustion in the treatment of 147 patients with primary dysmenorrhea of cold coagulation and blood stasis syndrome," *World Journal of Integrated Traditional and Western Medicine*, vol. 14, no. 9, pp. 1316–1318, 2019.

[77] L. Y. L. Jing, "Clinical observation of thunder fire moxibustion combined with self-made wenjing zhitong decoction in the treatment of 55 cases of primary dysmenorrhea," *Journal of Basic Chinese Medicine*, vol. 22, no. 7, pp. 958-959, 2016.

[78] L. S. R. Chunxin, L. Z. C. Xingkui, and M. Kong, "Medicinal moxibustion for cold-dampness stagnation type of primary dysmenorrhea and its effect on uterine artery blood flow in patients," *Chinese Acupuncture & Moxibustion*, vol. 36, no. 8, pp. 827–830, 2016.

[79] S. F. Z. Huijuan and W. Y. S. Mingxin, "Observation on curative effect of thunder fire moxibustion combined with auricular point on primary dysmenorrhea of qi and blood deficiency type," *China Journal of Traditional Chinese Medicine and Pharmacy*, vol. 36, no. 4, pp. 2408–2411, 2021.

[80] F. J. G. Xuejing, "Observation on the efficacy of herb-partitioned moxibustion on navel combined with abdominal acupuncture in the treatment of primary dysmenorrhea," *Shanghai Journal of Acupuncture and Moxibustion*, vol. 38, no. 7, pp. 754–757, 2019.

[81] L. Y. '. e, Z. C. P. Zhimou, H. J. L. Chao, and R. Zhu, "Observation on curative effect of moxibustion at shenque combined with warm acupuncture at guanyuan and sanyinjiao on primary dysmenorrhea," *Chinese Acupuncture and Moxibustion*, vol. 39, no. 4, pp. 367–370, 2019.

[82] Z. J. S. H. I. Lingjia, "Therapeutic observation of baixiao moxibustion for primary dyemenorrhea," *Shanghai Journal of Acupuncture and Moxibustion*, vol. 38, no. 11, pp. 1243–1247, 2019.

[83] Y. J. Y. Li and Z. B. L. Liang, "Research status and analysis of moxibustion mechanism," *Guangming Journal of Chinese Medicine*, vol. 25, no. 5, pp. 900-901, 2010.

[84] B. B. Zhang, "Relationship between COX-2 laser moxibustion and traditional moxibustion mechanism," *World Latest Medicine Information*, vol. 17, no. A1, pp. 151-152, 2017.

[85] Y. Li, C. Sun, J. Kuang et al., "An in vitro and numerical study of moxibustion therapy on biological tissue," *IEEE Transactions on Biomedical Engineering*, vol. 65, no. 4, pp. 779–788, 2018.

[86] L. S. H. Kaiyu and Z. J. S. Zheng, "Analysis on the starting mechanism of moxibustion warm passage effect," *Chinese Acupuncture & Moxibustion*, vol. 37, no. 9, pp. 1023–1026, 2017.

[87] J. Xin, Y. Su, Z. Yang et al., "Distinct roles of ASIC3 and TRPV1 receptors in electroacupuncture-induced segmental and systemic analgesia," *Frontiers of Medicine*, vol. 10, no. 4, pp. 465–472, 2016.

[88] T. Huang, S.-H. Lin, N. M. Malewicz et al., "Identifying the pathways required for coping behaviours associated with sustained pain," *Nature*, vol. 565, no. 7737, pp. 86–90, 2019.

[89] J. Jiang, X. Wang, X. Wu, and Z. Yu, "Analysis of factors influencing moxibustion efficacy by affecting heat-activated transient receptor potential vanilloid channels," *Journal of Traditional Chinese medicine = Chung I Tsa Chih Ying Wen Pan*, vol. 36, no. 2, pp. 255–260, 2016.

[90] W. Zou, H. Lin, W. Liu et al., "Moxibustion relieves visceral hyperalgesia via inhibition of transient receptor potential vanilloid 1 (TRPV1) and heat shock protein (HSP) 70 expression in rat bone marrow cells," *Acupuncture in Medicine*, vol. 34, no. 2, pp. 114–119, 2016.

[91] L. Cheng, P. Li, Y. Patel et al., "Moxibustion modulates sympathoexcitatory cardiovascular reflex responses through paraventricular nucleus," *Frontiers in Neuroscience*, vol. 12, p. 1057, 2018.

[92] Y. W. Li, J. M. Zhao, and L. Chen, "[Effect of electroacupuncture and moxibustion on visceral pain and expression of VR 1 and HSP 70 of "tianshu" (ST 25) region in colorectal distension-induced visceral hypersensitivity rats]," *Zhen Ci Yan Jiu = Acupuncture Research*, vol. 41, no. 4, pp. 291–297, 2016.

[93] Y. Zheng, "Research and application progress of the infrared effects of moxibustion," *Journal of Chinese Integrative Medicine*, vol. 10, no. 2, pp. 135–140, 2012.

[94] L. Lin, K. Cheng, M. T. Tan et al., "Comparison of the effects of 10.6 μm infrared laser and traditional moxibustion in the treatment of knee osteoarthritis," *Lasers in Medical Science*, vol. 35, no. 4, pp. 823–832, 2020.

[95] H. Deng and X. Shen, "The mechanism of moxibustion: ancient theory and modern research," *Evidence-Based Complementary and Alternative Medicine: eCAM*, vol. 2013, Article ID 379291, 7 pages, 2013.

[96] X. Shen, G. Ding, J. Wei et al., "An infrared radiation study of the biophysical characteristics of traditional moxibustion," *Complementary Therapies in Medicine*, vol. 14, no. 3, pp. 213–219, 2006.

[97] X. Wang, S. Zhou, W. Yao et al., "Effects of moxibustion stimulation on the intensity of infrared radiation of tianshu (ST25) acupoints in rats with ulcerative colitis," *Evidence-Based Complementary and Alternative Medicine: eCAM*, vol. 2012, Article ID 704584, 13 pages, 2012.

[98] H. Wenxue, J. Jun, S. Jialin, X. Yonghong, and C. Jianhong, "Research on the measuring and duplication techniques of spectrum of the moxibustion in traditional chinese medicine," in *Proceedings of the 2005 IEEE Engineering in Medicine and Biology 27th Annual Conference*, pp. 4267–4270, Shanghai, China, January 2006.

[99] X. J. Song, S. Y. Wang, Y. L. Li, and D. Zhang, "Analysis of the spectral characteristics of pure moxa stick burning by hyperspectral imaging and Fourier transform infrared spectroscopy," *Evidence-Based Complementary and Alternative Medicine: eCAM*, vol. 2016, Article ID 1057878, 8 pages, 2016.

[100] X. Zhao, M. Gao, Y. M. Zhang, and X. L. Tang, "[Design of a mini-infrared moxibustion instrument based on carbon fiber]," *Zhongguo Zhen Jiu = Chinese Acupuncture and Moxibustion*, vol. 40, no. 1, pp. 109–111, 2020.

[101] T. R. Z. Tingting, L. Q. L. Guohui, H. H. S. Qinglin, and G. Sun, "Research progress on effective components of artemisia argyi leaf and its combustion products," *China Journal of Traditional Chinese Medicine and Pharmacy*, vol. 34, no. 1, pp. 241–244, 2019.

[102] T. L. Z. Ci-li, M. X. W. Xiao-Mei, Q. X. Q. Li, and W. U. H. L. Hui-Rong, "Study on the biological effects and influencing factors of the chemical constituents of artemisia argyi," *Shanghai Journal of Acupuncture and Moxibustion*, vol. 29, no. 2, pp. 74–76, 2010.

[103] H. G. Y. Meizhen, Y. X. S. Zhenhong, and J. Wang, "Effects of artemisia argyi polysaccharide on secretion of cytokines and their activity in mouse immune cells," *Lishizhen Medicine and Materia Medica Research*, vol. 24, no. 7, pp. 1610-1611, 2013.

[104] R. He and B. X. Zhao, "[Progress of researches on mechanisms of needling and moxibustion sensations and their related sensation transmission]," *Zhen Ci Yan Jiu = Acupuncture Research*, vol. 44, no. 4, pp. 307–311, 2019.

[105] Y. Gong, Z. Yu, Y. Wang et al., "Effect of moxibustion on HIF-1α and VEGF levels in patients with rheumatoid arthritis," *Pain Research and Management*, vol. 2019, Article ID 4705247, 9 pages, 2019.

Hindawi
Evidence-Based Complementary and Alternative Medicine
Volume 2021, Article ID 2209574, 13 pages
https://doi.org/10.1155/2021/2209574

Research Article

Huanglian Jiedu Decoction Exerts Antipyretic Effect by Inhibiting MAPK Signaling Pathway

Xing Li,[1,2] **Shizhang Wei**,[2] **Xiao Ma**,[3] **Haotian Li**,[2] **Manyi Jing**,[2] **Honghong Liu**,[4] **Shengqi Niu**,[2,5] **Yuling Tong**,[2,3] **Lisheng Chen**,[2,6] **Ying Wei**,[2,3] **Sichen Ren**,[2,3] **and Yanling Zhao**[1,2]

[1]*School of Traditional Chinese Medicine, Southern Medical University, Guangzhou, China*
[2]*Department of Pharmacy, The Fifth Medical Center of Chinese PLA General Hospital, Beijing, China*
[3]*College of Pharmacy, Chengdu University of Traditional Chinese Medicine, Chengdu, China*
[4]*Integrated TCM and Western Medicine Department, The Fifth Medical Center of Chinese PLA General Hospital, Beijing, China*
[5]*Department of Pharmacy, Medical Supplies Centre of PLA General Hospital, Beijing, China*
[6]*Department of Pharmacy, Hebei North University, Zhangjiakou, China*

Correspondence should be addressed to Yanling Zhao; zhaoyl2855@126.com

Received 17 November 2021; Accepted 15 December 2021; Published 31 December 2021

Academic Editor: Xiang Liu

Aim. The aim of this study was to explore the antipyretic effect and potential mechanism of Huanglian Jiedu Decoction (HLJDD) on LPS-induced fever in rats. *Materials and Methods*. The fever rat model was established by LPS. Anal temperature of rats was measured every 1 hour after modeling. TNF-α, IL-6, PGE_2, and cAMP in rat serum or hypothalamus tissue were detected by ELISA kit. In order to explore the potential active ingredients and mechanism of antipyretic effect of HLJDD, we predicted the underlying antipyretic mechanism by using network pharmacology and then verified its mechanism by Western Blotting. *Results*. The results showed that HLJDD can alleviate LPS-induced fever in rats. The expression levels of TNF-α, IL-6, PGE_2, and cAMP in the treatment group were significantly lower than those in the model group. Western Blotting results showed that the protein expression of p-ERK, p-JNK, and p-P38 was significantly inhibited. *Conclusion*. The findings suggest that HLJDD has a good antipyretic effect on LPS-induced fever in rats, which may be closely related to the inhibition of MAPK signaling pathway.

1. Introduction

Fever is a complex physiological stress response characterized by a regulatory rise in body temperature in response to inflammation or infectious disease [1]. Normally, the body maintains a dynamic balance between heat production and heat loss. When this balance is upset, the body temperature becomes abnormal. Fever is a controlled increase in body temperature, a hypothalamic-mediated response caused by pathogenic injury or invasion [2, 3]. This reaction promotes the synthesis of endogenous heat-producing factors, such as TNF-α, IL-6, PGE_2, and cAMP, which will cause a series of biochemical and physiological changes in the body and eventually lead to elevated body temperature [4–7]. Hyperthermia is a treatment method that heats the temperature of a specific part of the body or the whole body to above the normal body temperature, so as to achieve the therapeutic effect. Traditional Chinese medicine (TCM) has heat therapy, such as sweat steaming, moxibustion, and cupping. Modern research shows that the combination of hyperthermia and chemotherapy is more effective than chemotherapy alone in the treatment of cancer diseases [8]. Studies have also found that increased body temperature regulation may be beneficial to the improvement of human immunity and reduce the sensitivity to infectious diseases [9]. However, in addition to being good for the body, fever can also be harmful [10]. For example, uncontrolled fever is associated with worse outcomes in patients with sepsis or neuronal damage [11].

TCM is a great treasure house, and it has unique advantages in the treatment of fever diseases. Chinese medicine

classifies fever into two categories: fever due to external sensation and fever due to internal injury. External fever is caused by the feeling of external evil. Internal fever is caused by the imbalance of Yin, Yang, Qi, and blood in the internal organs. In external fever, the onset is rapid and the duration is short. In internal fever, the onset is slow and the duration is long, from weeks and months to years. According to the principles of TCM diagnosis and treatment, TCM treatment of fever includes the method of relieving symptoms and reducing fever, the method of dispelling dampness and reducing fever, and the method of nourishing Yin and reducing fever. Huanglian Jiedu Decoction (HLJDD), which originated from *Medical Secrets of an Official* (*Wai Tai Mi Yao* as named in Chinese) in the Tang Dynasty, was created by Tao Wang, a famous medical scientist in the Tang Dynasty. The original prescription of HLJDD is composed of *Coptidis Rhizoma*, *Scutellariae Radix*, *Phellodendri Chinensis Cortex*, and *Gardeniae Fructus* in the ratio of 3 : 2 : 2 : 3, which has the effect of clearing heat and removing toxicity. Clinical evidence suggests that HLJDD can be used in the treatment of a variety of diseases, which can relieve symptoms with a good clinical effect [12]. Pharmacological studies show that HLJDD has significant anti-inflammatory, antibacterial, and antiendotoxin activities [13, 14]. It can be used to treat high fever in children [15], sepsis, and other diseases [16].

Lipopolysaccharide (LPS), commonly known as endotoxin, is an important cell wall component of Gram-negative bacteria [17]. The proinflammatory effects of LPS play an important role in inhibiting bacterial infection. However, dysregulation of the host response to LPS may lead to systemic inflammation, such as sepsis [18]. In recent years, LPS is often used to establish animal models of fever [19–21]. Studies have shown that MAPK signaling pathway plays a key role in regulation of the production of proinflammatory mediators in LPS-induced inflammatory responses [22–24]. However, the effects of HLJDD in LPS-induced fever and the relationship between HLJDD and MAPK signaling pathways are still unclear.

TCM has multicomponent, multitarget, and multipathway characteristics. The therapeutic mechanisms and material basis of many herbal medicines have not been elucidated. With the rapid development of bioinformatics and various medical databases, network pharmacology has strongly contributed to the understanding of the molecular mechanisms of TCM from a holistic and systemic perspective [25]. Meanwhile, it has great advantages in predicting the target of TCM components, discovering multitarget drugs and providing new insights for the study of TCM [26]. HLJDD is a classical Chinese medicine formula for relieving fever and is also commonly used in Chinese medicine clinics. Its antipyretic effect is remarkable, but its antipyretic mechanism has not been completely elucidated. In order to initially explore this problem, this study was conducted to comprehensively evaluate the antipyretic effect of HLJDD by establishing an animal model of fever, combined with modern bioinformatics technology, aiming to provide ideas for the development of new drugs for the efficient, safe, and rapid treatment of fever symptoms. Meanwhile, it aimed to provide reasonable dosing guidance and lay an experimental foundation for the clinical application of HLJDD.

2. Materials and Methods

2.1. Drugs and Reagents. *Coptidis Rhizoma* (batch number: 20121701), *Scutellariae Radix* (batch number: 19101501), *Phellodendri Chinensis Cortex* (batch number: 19120601), and *Gardeniae Fructus* (batch number: 18091101) were purchased from Beijing Lvye Pharmaceutical Co., Ltd. (Beijing, China), and chemically authenticated by thin layer chromatography (TLC) in accordance with the instructions of Chinese Pharmacopoeia. The content was determined by high performance liquid chromatography (HPLC). The product inspection report numbers are CP-20-12-20, CP-19-10-07, CP-19-12-05, and CP-18-09-09, respectively. All detection results show that the quality of *Coptidis Rhizoma*, *Scutellariae Radix*, *Phellodendri Chinensis Cortex*, and *Gardeniae Fructus* is in full compliance with the regulations of the Chinese Pharmacopoeia version 2015. LPS from *Escherichia coli* 0111:B4 purified by phenol extraction was purchased from Sigma (batch number: 000010267).

2.2. Preparation of HLJDD. Weigh *Coptidis Rhizoma*, *Scutellariae Radix*, *Phellodendri Chinensis Cortex*, and *Gardeniae Fructus* at 3 : 2 : 2 : 3 and soak 30 min in pure water (1/10, w/v). Then it was extracted twice by heating (1 h at a time) [27]. After filtering and drying, the yield of HLJDD was 17.90%.

2.3. Ethics Statement. This study was carried out in accordance with the recommendations of the Guidelines for the Care and Use of Laboratory Animals of the Ministry of Science and Technology of China. All operations related to animal experiment are examined and approved by the Animal Ethics and Experimental Committee of the Fifth Medical Center of the PLA General Hospital (Approval ID: IACUC-2019-004).

2.4. Animals. 50 male Sprague-Dawley rats (weighing 180 g–200 g) were purchased from Spiffy Biotechnology Co., Ltd. (Beijing, China, Permission No. SCXK-(Jing) 2019-0010). They were fed adaptively for 7 days under the conditions of temperature 25 ± 0.5°C, relative humidity 55 ± 5%, and alternating light (12 h light/dark cycle) and with free access to sufficient food and water. The anal temperature of rats was measured for 3 consecutive days, and the average value was taken as the baseline temperature of rats.

2.5. Establishment of LPS-Induced Fever Model and Drug Administration. The animals were randomly divided into 5 groups ($n = 10$), including control group, LPS-induced fever model group (100 μg/kg, i.p.), HLJDD low dose group (1.58 g/kg), HLJDD medium dose group (3.15 g/kg), and HLJDD high dose group (6.30 g/kg). The administered medium dose of HLJDD was determined based on the

recommended human dose (30 g/60 kg/day). The HLJDD groups were orally given different doses of HLJDD 1 h before the injection of LPS. At the same time, the control group were orally given with the same volume of normal saline. 1 hour after drug administration, the model group and each HLJDD group were intraperitoneally injected LPS (100 μg/kg) to establish fever rat model. Then the anal temperature of the rats was measured every 1 hour. The last anal temperature was measured at 7 hours, the rats were euthanized and blood was taken through the abdominal aorta, and then the hypothalamus tissue was collected for subsequent studies.

2.6. Measurement of the Serum and Hypothalamus Tissue Levels of Biochemical Indexes. The ELISA kit (enzyme linked biology, Shanghai, China) was used for the detection of serum or hypothalamus tissue levels of TNF-α, IL-6, PGE_2, and cAMP in accordance with the manufacturer's instructions.

2.7. Mechanism Prediction of HLJDD against Fever

2.7.1. Identification Targets of HLJDD and Fever. Traditional Chinese Medicine Systems Pharmacology Database (TCMSP, https://old.tcmsp-e.com/tcmsp.php) was searched to collect the chemical components of the four herbs contained in HLJDD. The screening strategy used for potential active ingredients was oral bioavailability (OB) ≥30% and drug-likeness (DL) ≥0.18. Fever targets were collected from the GeneCard database (https://www.genecards.org/). The intersection targets of HLJDD and fever were obtained from Venn database (http://www.bioinformatics.com.cn/static/others/jvenn/example.html).

2.7.2. Construction of Compound-Target Network. After the components and their corresponding target data were collected, the chemical components and potential targets of the abovementioned drugs in HLJDD were uploaded to Cytoscape3.8.0 to construct the Compound-Target network.

2.7.3. Construction and Analysis of PPI Network. The intersection targets of HLJDD components and fever were uploaded to STRING database (https://string-db.org/), and the screening conditions were with confidence score ≥0.7, so as to establish PPI interaction network. Then, the interacting proteins screened by STRING were imported into Cytoscape3.8.0 to collect the topological parameter values of each interaction target in PPI network, and then the core targets were screened and collected.

2.7.4. GO Enrichment and KEGG Pathway Analysis. The database (DAVID) (https://david.ncifcrf.gov/) has annotation, visualization, and integrated discovery capabilities. We therefore applied the DAVID database for gene ontology (GO) analysis and Kyoto Encyclopedia of Genes and Genomes (KEGG) pathway enrichment analysis.

2.8. Experimental Verification on the Mechanism of HLJDD against LPS-Induced Fever

2.8.1. Western Blotting Analysis for Protein Expression. The total protein in the hypothalamus tissue was extracted by using high-efficiency RIPA lysis buffer supplemented with protease inhibitor and phosphatase inhibitor. The hypothalamus tissue homogenate was centrifuged at 4°C and 12000 g for 10 min. Protein concentration was determined by BCA Protein Assay Kit (Solarbio, Beijing, China). The protein samples were separated by 10% SDS-PAGE of gel at 80 V for 30 min and 120 V for 1 h and then transferred to polyvinylidene fluoride (PVDF) membrane (Millipore, MA, USA). After transmembrane, the PVDF membrane was removed and placed in Tris-buffered saline (TBS) containing 5% skim milk powder, which was sealed at room temperature for 2 h, and then incubated with primary antibodies at 4°C overnight; the detailed information is as illustrated in Table 1. After primary antibody incubation, wash with TBS-0.1% Tween 20 (TBST) buffer solution at room temperature for 3 times, 5 min each time. Then the PVDF membrane was placed into the secondary antibody solution and incubated at room temperature for 1 h. GAPDH was used as internal reference. ImageJ software was used for quantitative analysis.

2.9. Statistics Analysis. All data was presented as mean ± standard deviation ($\bar{X} \pm SD$). The differences between the group means were calculated by one-way ANOVA and Duncan's multirange test with the SPSS computer program (version 26.0). GraphPad Prism software (version 8.2.1) was used to visualize the results. $P < 0.05$ was considered statistically significant and $P < 0.01$ was highly significant.

3. Results

3.1. Effect of HLJDD on LPS-Induced Fever in Rats. As shown in Figure 1, after LPS injection, the anal temperature increased in both model and HLJDD groups and reached the highest temperature at 6 h after LPS injection. The anal temperature of rats in each HLJDD treated group was lower than that of model group. The results showed that HLJDD had a certain antipyretic effect on LPS-induced rat fever.

3.2. Expression of Biochemical Indexes in Fever Rats. In order to explore the antipyretic effect of HLJDD on LPS-induced fever in rats, we detected the expression levels of TNF-α and IL-6 in the serum and PGE_2 and cAMP in the hypothalamus tissue of fever rats (Figure 2). The expression of TNF-α, IL-6, PGE_2, and cAMP in model group was significantly higher than that in control group ($P < 0.01$). It was shown that fever in the LPS-induced fever model in rats was closely associated with elevated levels of these indicators. Compared with model group, the expression of biochemical indexes in HLJDD intervention groups was significantly decreased ($P < 0.05$). Among them, HLJDD groups could significantly reduce the expression levels of PGE_2 and cAMP in a concentration dependent manner (Figures 2(c) and 2(d)).

Table 1: Antibodies information.

Antibodies	Dilution	Manufacturers	Cat. No.
Rabbit anti- Erk1/2	1 : 1000	Cell Signaling Technology	4695
Rabbit anti-p-Erk1/2	1 : 2000	Cell Signaling Technology	4370
Rabbit anti- JNK	1 : 1000	Cell Signaling Technology	9252
Rabbit anti- p-JNK	1 : 1000	Cell Signaling Technology	4668
Rabbit anti- p38	1 : 1000	Cell Signaling Technology	8690
Rabbit anti- p-p38	1 : 1000	Cell Signaling Technology	4511
Rabbit anti-GAPDH	1 : 10000	Proteintech	10494-1-AP
Goat anti-Rabbit IgG (H&L)	1 : 10000	ZENBIO	511203

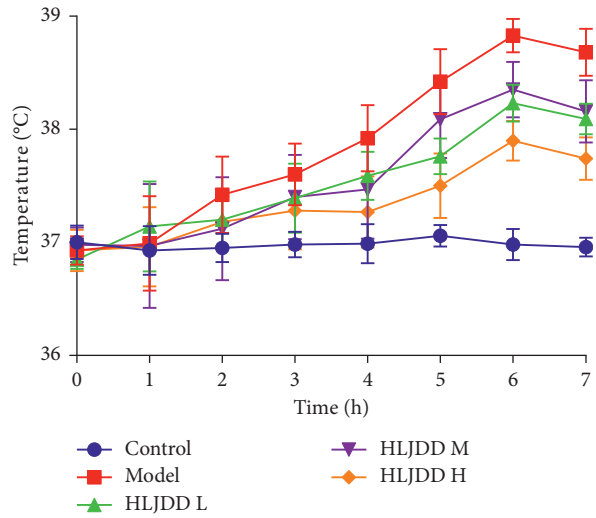

Figure 1: Changes of anal temperature in each group. The temperature at 0 h was the baseline temperature of rats, and the anal temperature was measured every 1 hour after LPS modeling. Control: as a blank control group; Model: intraperitoneal injection of LPS 100 μg/kg; HLJDD L: HLJDD low dose group (1.58 g/kg); HLJDD M: HLJDD medium dose group (3.15 g/kg); HLJDD H: HLJDD high dose group (6.30 g/kg).

3.3. Prediction Results of Antipyretic Effect of HLJDD

3.3.1. Compound-Target Network and Analysis. Due to the characteristics of multiple components and multiple targets, TCM compounds show a variety of pharmacological activities. Therefore, we constructed a network to study the potential mechanism of TCM compounds treating diseases. As shown in Figure 3, there are 257 nodes with 792 edges. Among these active components, we screened 20 components with high degree value, such as quercetin (MOL000098, degree = 127), kaempferol (MOL000422, degree = 50), wogonin (MOL000173, degree = 37), and baicalein (MOL002714, Degree = 29). These components with high degree value in the network are likely to be the main active components of HLJDD (Table 2).

3.3.2. The PPI Network Construction of the Underlying Antipyretic Targets. A total of 64 chemical ingredients and 193 targets of HLJDD were collected and 939 targets of fever were obtained from GeneCard database (Figure 4(a)). These 70 intersection targets may be potential targets of antipyretic effect of HLJDD. The intersection targets were imported into STRING database. After that, PPI network of the underlying antipyretic targets was constructed by Cytoscape3.8.0 with 63 nodes and 455 edges (Figure 4(b)).

3.3.3. GO Enrichment and KEGG Pathway Analysis. The top 10 significantly enriched terms in biological process (BP), cellular component (CC), and molecular function (MF) categories are shown in Figure 5, which indicated that HLJDD may exert its antipyretic effect by regulating positive regulation of nitric oxide biosynthetic process, cellular response to organic cyclic compound, extracellular space, and identical protein binding. In order to explore the potential pathways involved in the antipyretic effect of HLJDD, we conducted KEGG pathway analysis, as shown in Figure 6, with 15 top signaling pathways. Among these 15 signaling pathways, MAPK signaling pathway plays a crucial role.

3.4. Experimental Verification on the Mechanism of HLJDD against LPS-Induced Fever.

To further evaluate the underlying antipyretic mechanism of HLJDD, MAPK signaling pathway was determined. As shown in Figure 7, the expression of ERK, p-ERK, JNK, p-JNK, P38, and p-P38 was detected and the results of Western Blotting were quantified by ImageJ. The results showed that, compared with the control group, the protein expression levels of p-ERK, p-JNK, and p-P38 were significantly increased after LPS injection ($P < 0.05$ or $P < 0.01$). HLJDD could downregulate their protein expression levels, which indicated that HLJDD has antipyretic effect on LPS-induced fever in rats through MAPK signaling pathway suppressing.

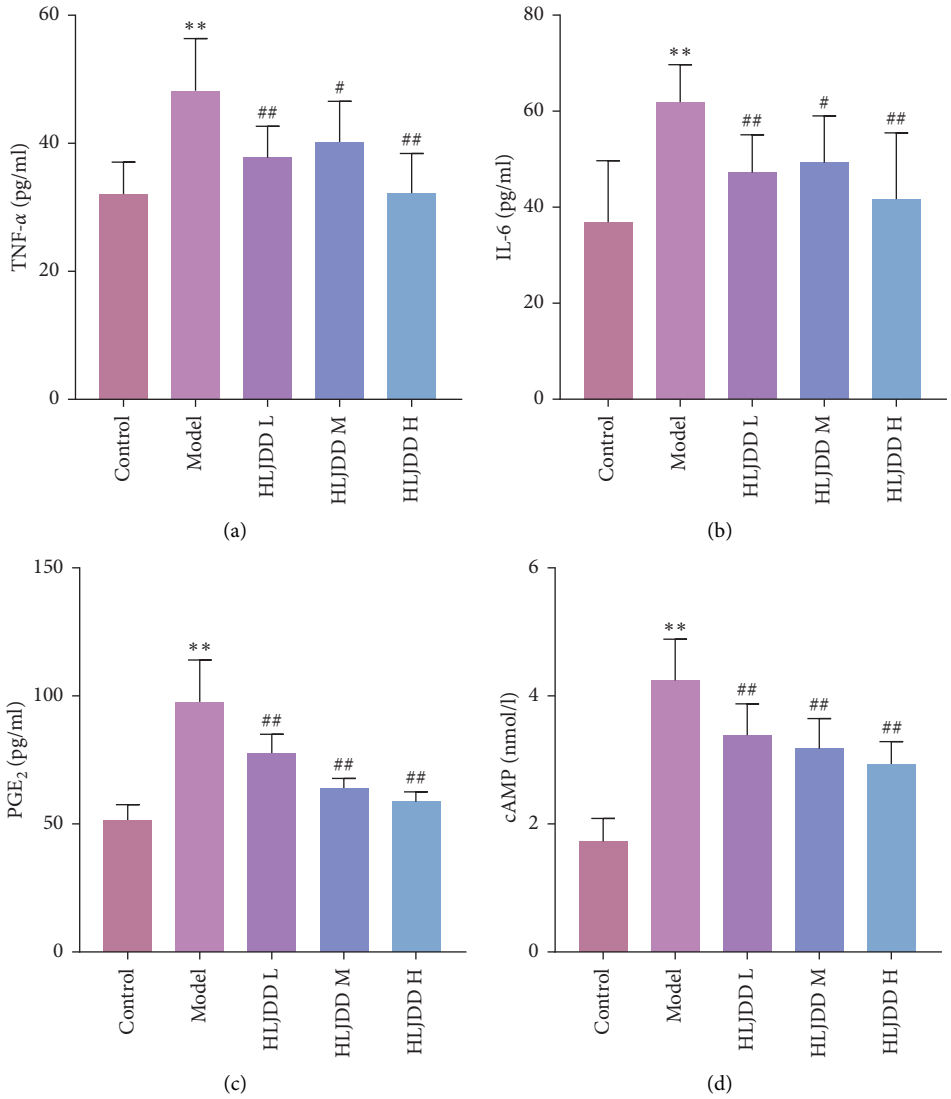

Figure 2: Effect of HLJDD on serum and hypothalamus tissue biochemical indexes of fever rats. (a-b) Expression of TNF-α and IL-6 in serum of fever rats. (c-d) Expression of PGE_2 and cAMP in hypothalamus tissue of fever rats. **<0.01 versus control group. $^{\#\#}$<0.01 versus model group, $^{\#}$<0.05 versus model group. Control: as a blank control group; Model: intraperitoneal injection of LPS 100 μg/kg; HLJDD L: HLJDD low dose group (1.58 g/kg); HLJDD M: HLJDD medium dose group (3.15 g/kg); HLJDD H: HLJDD high dose group (6.30 g/kg).

4. Discussion

Our study shows that HLJDD has a good antipyretic effect on LPS-induced fever in rats, and this effect may be carried out by inhibiting the MAPK signaling pathway.

HLJDD is a classic Chinese medicine prescription for clearing heat and detoxifying [28]. Previous studies have shown that HLJDD significantly reduces the levels of inflammatory factors such as IL-2, TNF-α, and IFN-γ and inflammatory mediators such as PGE_2 and NO and suppresses immune and inflammatory responses [29, 30]. We studied the pharmacological effects of HLJDD (composed of *Coptidis Rhizoma*, *Scutellariae Radix*, *Phellodendri Chinensis Cortex*, and *Gardeniae Fructus* at 3 : 2 : 2 : 3) on LPS-induced fever in rats. At present, there are many methods to replicate the rat model of fever; the common ones are dry yeast, 2,4-dinitrophenol, and lipopolysaccharide. LPS, the outer membrane of Gram-negative bacteria, is a common febrifuge in animal experiments and stimulates macrophages and neutrophils to produce the endogenous pyrogens [31]. In this experiment, the rat fever model was established by intraperitoneal injection of LPS (100 μg/kg). After the administration of HLJDD, it was found that different doses of HLJDD could reduce the temperature rise of rats, and the antipyretic effect was obvious. The biochemical indexes of inflammation were detected by enzyme-linked immunoassay kit, and HLJDD was found to reduce the secretion of LPS-induced inflammatory factors TNF-α, IL-6, PGE_2, and cAMP. This finding suggests that HLJDD reduces body temperature, possibly by reducing proinflammatory cytokines and by inhibiting PGE_2 and CAMP synthesis. This study is the first to investigate the antipyretic activity of HLJDD.

The multicomponent, multitarget nature of Chinese medicine makes its pharmacodynamic mechanism more

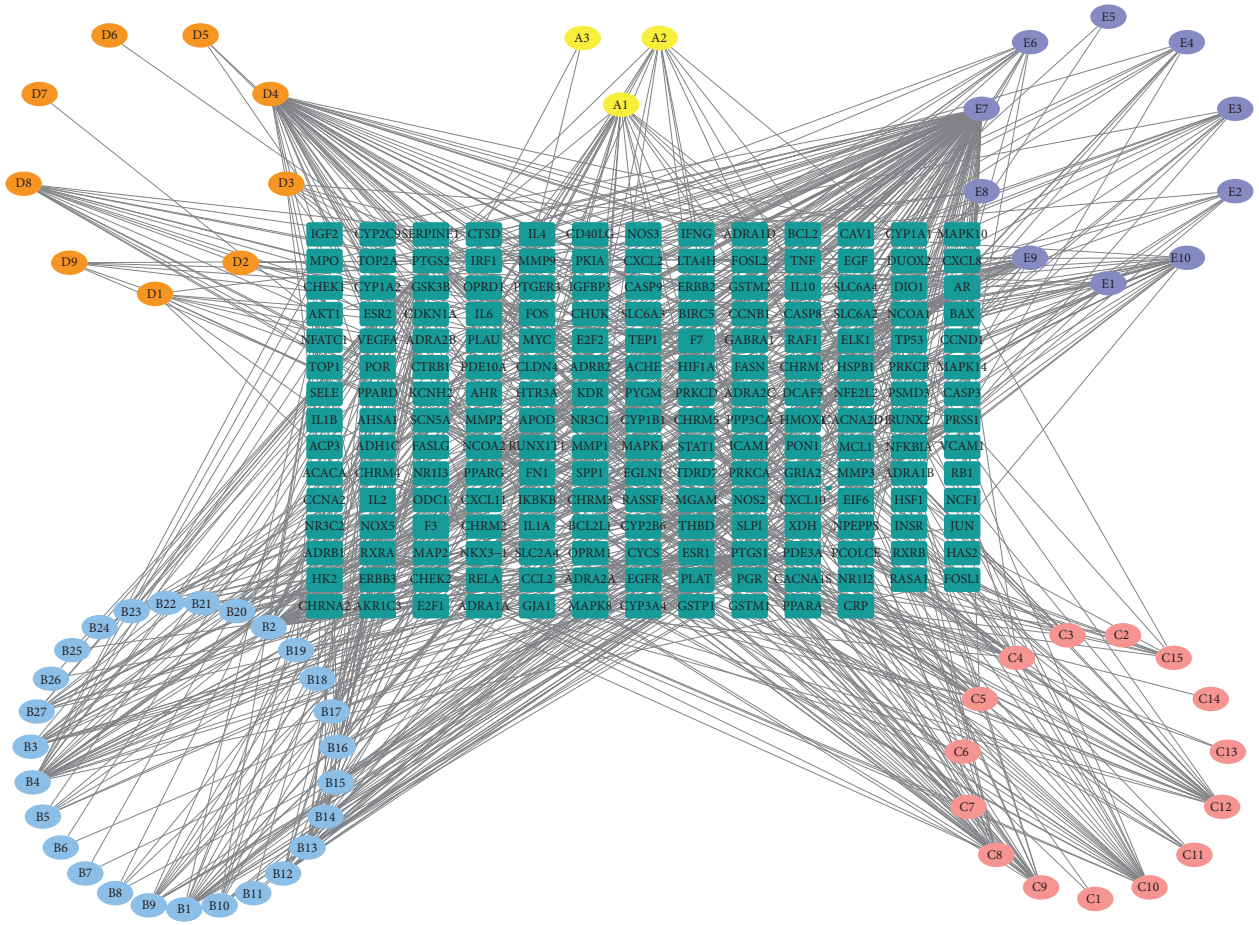

Figure 3: Herb-compound-target network of HLJDD (the ellipses represent components of HLJDD, the 3 yellow ellipses represent *Coptidis Rhizoma* components, the 27 blue ellipses represent *Scutellariae Radix* components, the 15 pink ellipses represent *Phellodendri Chinensis Cortex* components, the 9 orange ellipses represent *Gardeniae Fructus* components, the 10 purple ellipses represent the shared components in the four herbs of HLJDD, and the green round rectangles represent the 193 potential targets of HLJDD).

complex. Therefore, with the help of modern science and technology, we combined network pharmacology to predict the main pharmacodynamic components of HLJDD, further predict the targets corresponding to the components, construct a component target network, and then screen the core targets and predict the possible pathways. Through network pharmacology analysis, we found that quercetin, kaempferol, wogonin, and baicalein might be the main pharmacodynamic components of HLJDD. Baicalin and its aglycone, baicalein, are the main components in *Scutellariae Radix*. The antioxidant and anti-inflammatory effects of baicalein have been demonstrated in a variety of disease models, including cardiovascular disease, inflammatory bowel disease, gout and rheumatoid arthritis, asthma, neurodegenerative diseases, liver and kidney diseases, and cancer [32]. For future research, we plan to select a compound from the prediction results of network pharmacology and explore the antipyretic effect and mechanism of a compound in HLJDD.

MAPK signaling pathway widely exists in all kinds of animal cells and participates in the regulation of cell proliferation, differentiation, transformation, and apoptosis through phosphorylated nuclear transcription factors, cytoskeleton proteins and enzymes, and is closely related to the occurrence of many diseases such as inflammation and tumor [33]. The MAPK pathway has four major branching routes, including ERK, JNK, p38/MAPK, and ERK5. Each MAPK signaling pathway has a relatively independent function. An important role of MAPK signaling pathway is to regulate cellular responses in response to changes in the extracellular environment. ERK pathway is mainly involved in cell proliferation and differentiation, while JNK pathway and p38MAPK pathway are mainly involved in cellular inflammatory response, stress response, and apoptosis [34]. Since MAPK signaling pathway is a classical inflammatory pathway, in addition, we referred to the predicted results of this network pharmacology and selected MAPK signaling pathway, using WB experiments as experimental validation. It was found that the administration of HLJDD reduced the expression levels of phosphorylated proteins of ERK, JNK, and p38 in different dose groups. In particular, the high dose group of HLJDD significantly inhibited the expression of related proteins in MAPK signaling pathway. In summary, HLJDD inhibits the protein expression level in MAPK signaling pathway, thus playing the role of antipyretic and relieving inflammation.

Table 2: Information for candidate bioactive components of HLJDD.

Molecule ID	Molecule name	OB (%)	DL	Degree	Molecule structure	Herb
MOL000098	Quercetin	46.43	0.28	127	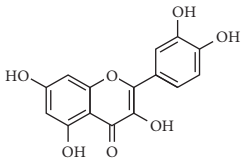	*Coptidis Rhizoma*, *Scutellariae Radix*, *Phellodendri Chinensis Cortex*, *Gardeniae Fructus*
MOL000422	Kaempferol	41.88	0.24	50	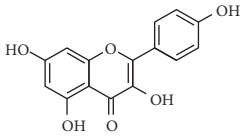	*Gardeniae Fructus*
MOL000173	Wogonin	30.68	0.23	37	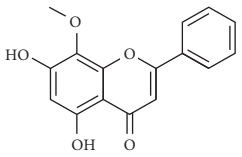	*Scutellariae Radix*
MOL002714	Baicalein	33.52	0.21	29	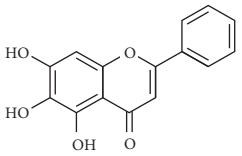	*Scutellariae Radix*
MOL000358	Beta-sitosterol	36.91	0.75	27	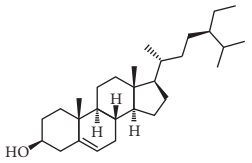	*Coptidis Rhizoma*, *Scutellariae Radix*, *Phellodendri Chinensis Cortex*, *Gardeniae Fructus*
MOL000790	Isocorypalmine	35.77	0.59	24	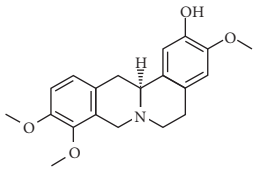	*Phellodendri Chinensis Cortex*
MOL000449	Stigmasterol	43.83	0.76	23	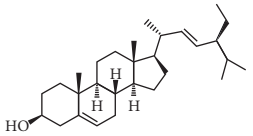	*Coptidis Rhizoma*, *Scutellariae Radix*, *Phellodendri Chinensis Cortex*, *Gardeniae Fructus*
MOL001455	(S)-Canadine	53.83	0.77	23	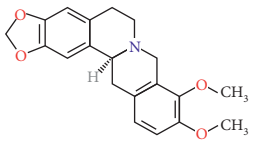	*Phellodendri Chinensis Cortex*
MOL002903	(R)-Canadine	55.37	0.77	22	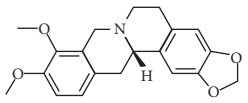	*Coptidis Rhizoma*
MOL002670	Cavidine	35.64	0.81	21	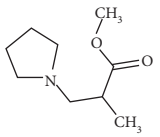	*Phellodendri Chinensis Cortex*

Table 2: Continued.

Molecule ID	Molecule name	OB (%)	DL	Degree	Molecule structure	Herb
MOL000787	Fumarine	59.26	0.83	20	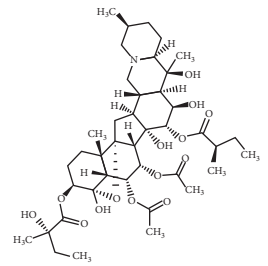	*Phellodendri Chinensis Cortex*
MOL002928	Oroxylin A	41.37	0.23	19	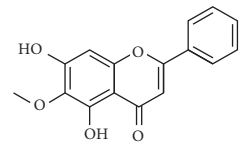	*Scutellariae Radix*
MOL001689	Acacetin	34.97	0.24	19	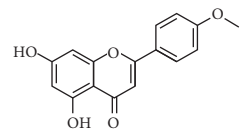	*Scutellariae Radix*
MOL003095	5-Hydroxy-7-methoxy-2-(3,4,5-trimethoxyphenyl)chromone	51.96	0.41	16	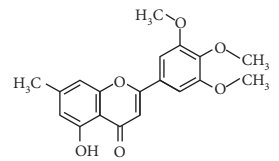	*Gardeniae Fructus*
MOL002651	Dihydrotanshinone II A	43.76	0.4	15	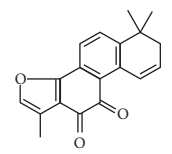	*Phellodendri Chinensis Cortex*
MOL008206	Moslosooflavone	44.09	0.25	15	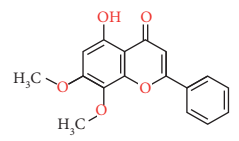	*Scutellariae Radix*
MOL000228	Alpinetin	55.23	0.2	15	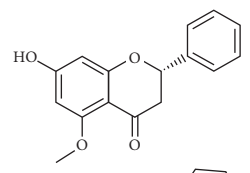	*Scutellariae Radix*
MOL002662	Rutaecarpine	40.3	0.6	14	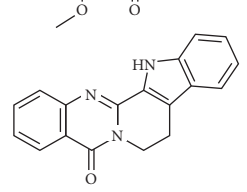	*Phellodendri Chinensis Cortex*
MOL002904	Berlambine	36.68	0.82	14	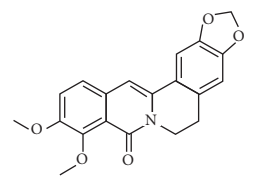	*Coptidis Rhizoma*
MOL000785	Palmatine	64.6	0.65	13	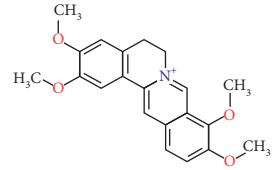	*Coptidis Rhizoma*, *Scutellariae Radix*, *Phellodendri Chinensis Cortex*, *Gardeniae Fructus*

Table 2: Continued.

Molecule ID	Molecule name	OB (%)	DL	Degree	Molecule structure	Herb
MOL012266	Rivularin	37.94	0.37	13	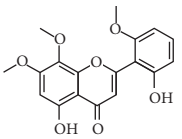	*Scutellariae Radix*
MOL002934	Neobaicalein	104.34	0.44	13	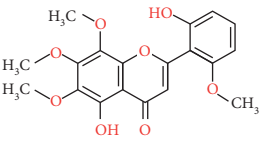	*Scutellariae Radix*
MOL001454	Berberine	36.86	0.78	12	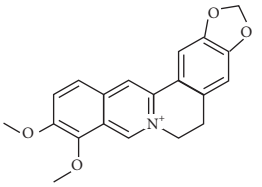	*Coptidis Rhizoma*, *Scutellariae Radix*, *Phellodendri Chinensis Cortex*, *Gardeniae Fructus*
MOL000552	5,2'-Dihydroxy-6,7,8-trimethoxyflavone	31.71	0.35	12	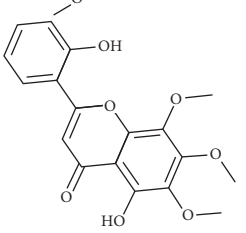	*Scutellariae Radix*
MOL002927	Skullcapflavone II	69.51	0.44	12	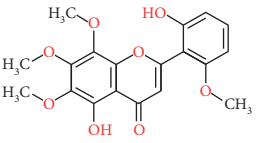	*Scutellariae Radix*

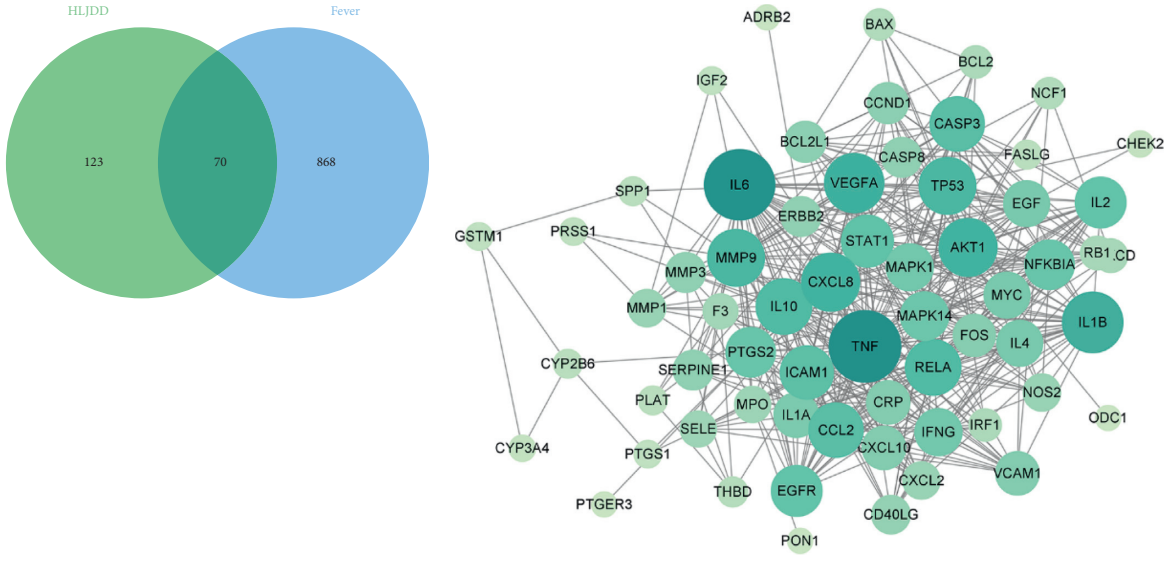

(a) (b)

Figure 4: The network and analysis. (a) Distribution of HLJDD targets and the disease targets. (b) The PPI network. The higher the degree value is, the darker and larger the nodes in the graph will be.

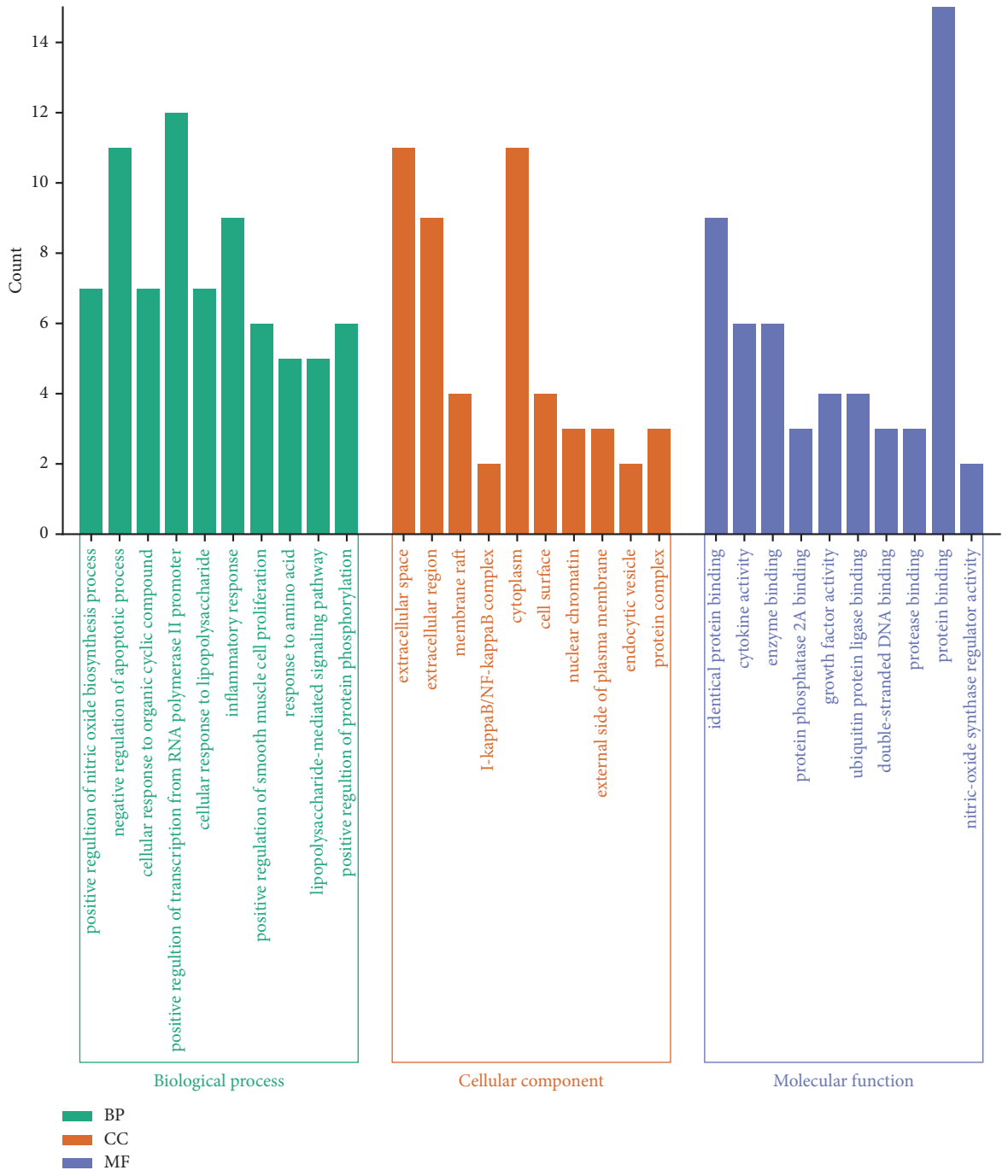

Figure 5: Top 10 GO terms of hub genes.

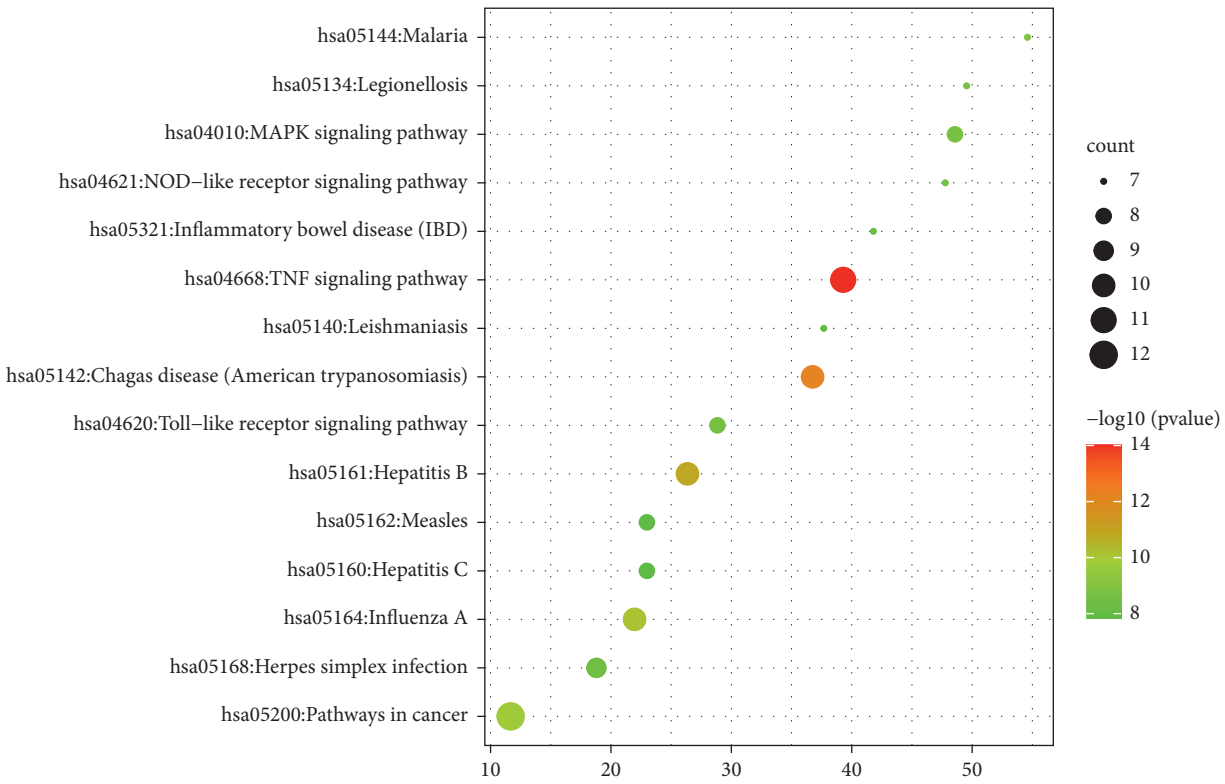

Figure 6: Top 15 KEGG pathway of hub genes.

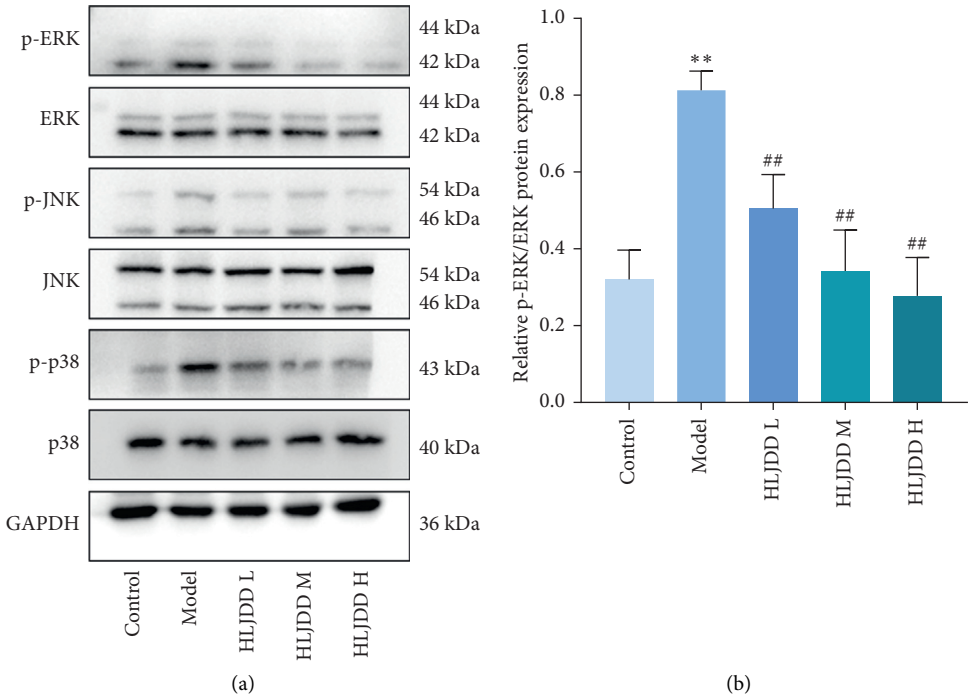

Figure 7: Continued.

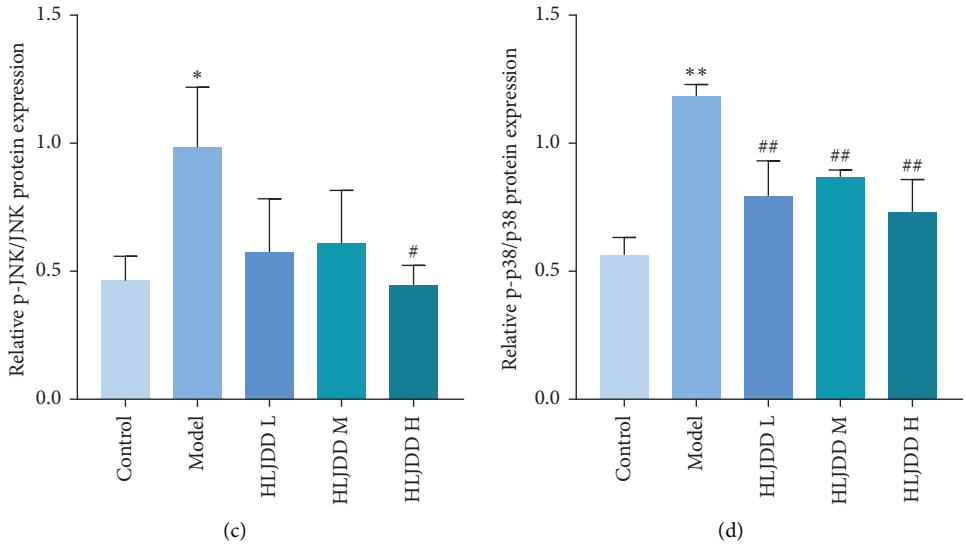

Figure 7: HLJDD suppresses the expression of MAPK signaling pathway. (a) Western Blotting images of ERK, p-ERK, JNK, p-JNK, P38, p-P38, and GAPDH. (b) Relative p-ERK protein expression in hypothalamus tissue. (c) Relative p-JNK protein expression in hypothalamus tissue. (d) Relative p-P38 protein expression in hypothalamus tissue. **<0.01 versus control group. $^{\#\#}$<0.01 versus model group. *<0.05 versus control group. $^{\#}$<0.05 versus model group. Control: as a blank control group; model: intraperitoneal injection of LPS 100 μg/kg; HLJDD L: HLJDD low dose group (1.58 g/kg); HLJDD M: HLJDD medium dose group (3.15 g/kg); HLJDD H: HLJDD high dose group (6.30 g/kg).

5. Conclusion

In this study, we investigated the antipyretic effects of HLJDD at the overall animal level by constructing a febrile rat model and combined with network pharmacology techniques to detect the serum levels of the pyrogenic factors IL-6 and TNF-α and the biochemical indicators PGE_2 and cAMP in the hypothalamus of the model animals. The expression of ERK, p-ERK, JNK, p-JNK, P38, and p-P38, which are related proteins of MAPK signaling pathway, was analyzed in the hypothalamus. The results of this study suggest that HLJDD has antipyretic effect on LPS-induced fever in rats, and its potential mechanism may be related to the inhibition of MAPK signaling pathway. This study lays a theoretical foundation for further study of HLJDD in the treatment of fever.

Data Availability

The data used to support the findings of this study are available from the corresponding author upon reasonable request.

Conflicts of Interest

The authors declare that there are no conflicts of interest.

Acknowledgments

This study was financially supported by the Major Scientific Problems and Medical Technical Challenges of China Medicine Education Association in 2020 (2020KTZ002).

References

[1] A. R. Zampronio, D. M. Soares, and G. E. P. Souza, "Central mediators involved in the febrile response: effects of antipyretic drugs," *Temperature*, vol. 2, no. 4, pp. 506–521, 2015.

[2] J. Roth and G. E. P. De Souza, "Fever induction pathways: evidence from responses to systemic or local cytokine formation," *Brazilian Journal of Medical and Biological Research*, vol. 34, no. 3, pp. 301–314, 2001.

[3] K. Nakamura, "Central circuitries for body temperature regulation and fever," *American Journal of Physiology-Regulatory, Integrative and Comparative Physiology*, vol. 301, no. 5, pp. R1207–R1228, 2011.

[4] B. Conti, I. Tabarean, C. Andrei, and T. Bartfai, "Cytokines and fever," *Frontiers in Bioscience*, vol. 9, no. 1-3, pp. 1433–1449, 2004.

[5] E.-M. Harré, J. Roth, U. Pehl, M. Kueth, R. Gerstberger, and T. Hübschle, "Selected contribution: role of IL-6 in LPS-induced nuclear STAT3 translocation in sensory circumventricular organs during fever in rats," *Journal of Applied Physiology*, vol. 92, no. 6, pp. 2657–2666, 2002.

[6] C. M. Blatteis, S. Li, Z. Li, C. Feleder, and V. Perlik, "Cytokines, PGE2 and endotoxic fever: a re-assessment," *Prostaglandins & Other Lipid Mediators*, vol. 76, no. 1-4, pp. 1–18, 2005.

[7] T. Nguyen, X. Chen, J. Chai et al., "Antipyretic, anti-inflammatory and analgesic activities of Periplaneta americana extract and underlying mechanisms," *Biomedicine & Pharmacotherapy*, vol. 123, Article ID 109753, 2020.

[8] S. Toraya-Brown and S. Fiering, "Local tumour hyperthermia as immunotherapy for metastatic cancer," *International Journal of Hyperthermia*, vol. 30, no. 8, pp. 531–539, 2014.

[9] S. S. Evans, E. A. Repasky, and D. T. Fisher, "Fever and the thermal regulation of immunity: the immune system feels the

heat," *Nature Reviews Immunology*, vol. 15, no. 6, pp. 335–349, 2015.

[10] L. M. Harden, S. Kent, Q. J. Pittman, and J. Roth, "Fever and sickness behavior: friend or foe?" *Brain, Behavior, and Immunity*, vol. 50, pp. 322–333, 2015.

[11] B. H. Lee, B. Lee, D. Inui et al., "Association of body temperature and antipyretic treatments with mortality of critically ill patients with and without sepsis: multi-centered prospective observational study," *Critical Care*, vol. 16, no. 1, p. R33, 2012.

[12] Y. Li, "Modern clinical research progress of huanglian jiedu decoction," *Chinese Medicine Modern Distance Education of China*, vol. 16, no. 24, pp. 158–160, 2018.

[13] J. Zhou, X. Gu, X. Fan et al., "Anti-inflammatory and regulatory effects of huanglian jiedu decoction on lipid homeostasis and the TLR4/MyD88 signaling pathway in LPS-induced zebrafish," *Frontiers in Physiology*, vol. 10, p. 1241, 2019.

[14] G. Chen, Y. Xu, J. Jing et al., "The anti-sepsis activity of the components of Huanglian Jiedu Decoction with high lipid A-binding affinity," *International Immunopharmacology*, vol. 46, pp. 87–96, 2017.

[15] L. Y. Gao, "Clinical effect of Huanglian Jiedu Decoction on children with high fever [J]," *World Latest Medicine Information*, vol. 17, no. 90, p. 101, 2017.

[16] T.-T. Fan, B.-L. Cheng, X.-M. Fang, Y.-C. Chen, and F. Su, "Application of Chinese medicine in the management of critical conditions: a review on sepsis," *The American Journal of Chinese Medicine*, vol. 48, no. 6, pp. 1315–1330, 2020.

[17] D. Megrian, N. Taib, J. Witwinowski, C. Beloin, and S. Gribaldo, "One or two membranes? Diderm Firmicutes challenge the Gram-positive/Gram-negative divide," *Molecular Microbiology*, vol. 113, no. 3, pp. 659–671, 2020.

[18] A. Płóciennikowska, A. Hromada-Judycka, K. Borzęcka, and K. Kwiatkowska, "Co-operation of TLR4 and raft proteins in LPS-induced pro-inflammatory signaling," *Cellular and Molecular Life Sciences*, vol. 72, no. 3, pp. 557–581, 2015.

[19] E. A. Saramago, G. S. Borges, C. G. Singolani-Jr Jr et al., "Molecular hydrogen potentiates hypothermia and prevents hypotension and fever in LPS-induced systemic inflammation," *Brain, Behavior, and Immunity*, vol. 75, pp. 119–128, 2019.

[20] L. H. Yamashiro, G. E. P. de Souza, and D. de Melo Soares, "Role of CINC-1 and CXCR2 receptors on LPS-induced fever in rats," *Pfluegers Archiv European Journal of Physiology*, vol. 471, no. 2, pp. 301–311, 2019.

[21] D. d. M. Soares, D. R. Santos, C. Rummel et al., "The relevance of kalikrein-kinin system via activation of B 2 receptor in LPS-induced fever in rats," *Neuropharmacology*, vol. 126, pp. 84–96, 2017.

[22] H. N. Kim, J. D. Kim, J. H. Yeo et al., "Heracleum moellendorffii roots inhibit the production of pro-inflammatory mediators through the inhibition of NF-κB and MAPK signaling, and activation of ROS/Nrf2/HO-1 signaling in LPS-stimulated RAW264.7 cells," *BMC Complementary and Alternative Medicine*, vol. 19, no. 1, p. 310, 2019.

[23] M. Guha and N. Mackman, "LPS induction of gene expression in human monocytes," *Cellular Signalling*, vol. 13, no. 2, pp. 85–94, 2001.

[24] S. Y. Park, G.-y. Park, W. S. Ko, and Y. Kim, "Dichroa febrifuga Lour. inhibits the production of IL-1β and IL-6 through blocking NF-κB, MAPK and Akt activation in macrophages," *Journal of Ethnopharmacology*, vol. 125, no. 2, pp. 246–251, 2009.

[25] T.-t. Luo, Y. Lu, S.-k. Yan, X. Xiao, X.-l. Rong, and J. Guo, "Network pharmacology in research of Chinese medicine formula: methodology, application and prospective," *Chinese Journal of Integrative Medicine*, vol. 26, no. 1, pp. 72–80, 2020.

[26] R. Zhang, X. Zhu, H. Bai, and K. Ning, "Network pharmacology databases for traditional Chinese medicine: review and assessment," *Frontiers in Pharmacology*, vol. 10, p. 123, 2019.

[27] Y. Tong, R. Wang, X. Liu et al., "Zuojin Pill ameliorates chronic atrophic gastritis induced by MNNG through TGF-β1/PI3K/Akt axis," *Journal of Ethnopharmacology*, vol. 271, Article ID 113893, 2021.

[28] Y. Yang, H.-J. Wang, J. Yang et al., "Chemical profiling and quantification of Chinese medicinal formula huang-lian-jie-du decoction, a systematic quality control strategy using ultra high performance liquid chromatography combined with hybrid quadrupole-orbitrap and triple quadrupole mass spectrometers," *Journal of Chromatography A*, vol. 1321, pp. 88–99, 2013.

[29] L. J. Wang and Q. Xu, "Study on anti-inflammatory mechanism of huanglian jiedu decoction," *China Journal of Chinese Materia Medica*, vol. 20, pp. 493–495, 2000.

[30] Q. Fang, X. P. Zhan, J. L. Mo, and M. Sun, "Therapeutic effect of huanglian jiedu decoction on AD rats and its effect on cytokine content," *China Journal of Chinese Materia Medica*, vol. 29, pp. 575–578, 2004.

[31] J. Roth and C. M. Blatteis, "Mechanisms of fever production and lysis: lessons from experimental LPS fever," *Comprehensive Physiology*, vol. 4, no. 4, pp. 1563–1604, 2014.

[32] B. Dinda, S. Dinda, S. DasSharma, R. Banik, A. Chakraborty, and M. Dinda, "Therapeutic potentials of baicalin and its aglycone, baicalein against inflammatory disorders," *European Journal of Medicinal Chemistry*, vol. 131, pp. 68–80, 2017.

[33] Q. Shi, W. Lang, S. Wang et al., "Echinacea polysaccharide attenuates lipopolysaccharide-induced acute kidney injury via inhibiting inflammation, oxidative stress and the MAPK signaling pathway," *International Journal of Molecular Medicine*, vol. 47, no. 1, pp. 243–255, 2021.

[34] Y.-H. Kim, M.-K. Kang, E.-J. Lee et al., "Astragalin inhibits cigarette smoke-induced pulmonary thrombosis and alveolar inflammation and disrupts PAR activation and oxidative stress-responsive MAPK-signaling," *International Journal of Molecular Sciences*, vol. 22, no. 7, p. 3692, 2021.